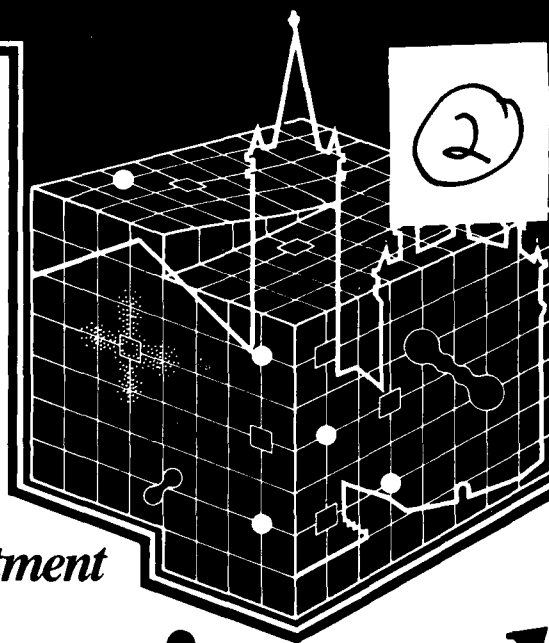


DTIC FILE COPY

AD-A206 030

ICDIC  
PARMA  
88

Physics Department



# *International Conference on Defects in Insulating Crystals*

University of Parma  
August 29<sup>th</sup>  
September 2<sup>nd</sup>, 1988

DTIC  
ELECTE  
MAR 15 1989

DISTRIBUTION STATEMENT A

Approved for public release  
Distribution Unlimited

89 3 15 027

ICDIC  
PARMA  
88

*Physics Department*  
*University of Parma*

***International  
Conference on  
Defects in  
Insulating  
Crystals***

*Parma August 29<sup>th</sup> September 2<sup>nd</sup>, 1988*

### ACKNOWLEDGEMENTS

The International Conference on Defects in Insulating Crystals is being held under the patronage of the **European Physical Society**.

The Local Organizing Committee gratefully acknowledges financial support from the following organizations:

- University of Parma
- Consiglio Nazionale delle Ricerche (C.N.R.)
- Gruppo Nazionale di Struttura della Materia (G.N.S.M.)
- Centro Interuniversitario di Struttura della Materia (C.I.S.M.)
- Commission of the European Communities
- I.B.M. - Italia
- International Union of Crystallography (I.U.Cr.)
- Ente Nazionale Energie Alternative (E.N.E.A.)
- Cassa di Risparmio di Parma
- Eastman Kodak Co., Research Laboratories, Rochester, USA
- Siemens Aktiengesellschaft, Munich, F.R.G.
- Comune di Parma
- Unione Parmense degli Industriali
- Gordon and Breach, Science Publishers, Inc., New York
- U.S. Army, European Research Office, London
- Jasco s.r.l. Cremella (Como)
- RIAL S.p.A., Parma
- Amministrazione Provinciale di Parma
- Telettra S.p.A., Milano
- Barilla S.p.A., Parma
- Chiesi Farmaceutici S.p.A., Parma
- Varian S.p.A., Milano

III

Accession For	
1975-07-20	✓
1975-07-20	✓
per form 50	
A-1	

#### **INTERNATIONAL ADVISORY COMMITTEE**

F. AGULLÓ LÓPEZ - Madrid - Spain  
R. CAPELLETTI - Parma - Italy  
J. CASTAING - CNRS Meudon - France  
A. V. CHADWICK - Canterbury - United Kingdom  
J. CORISH - Dublin - Ireland  
J. Z. DAMM - Wroclaw - Poland  
H. W. DEN HARTOG - Groningen - The Netherlands  
M. DE SOUZA - São Carlos - Brazil  
D. FENG - Nanjing - China  
W. B. FOWLER - Lehigh - U.S.A.  
K. FUNKE - Münster - F.R.G.  
M. HIRAI - Sendai - Japan  
L. W. HOBBS - MIT Cambridge - U.S.A.  
N. ITOH - Nagoya - Japan  
P. W. M. JACOBS - London Canada  
A. A. KAPLYIANSKI - Leningrad - U.S.S.R.  
A. B. LIDIARD - Harwell - United Kingdom  
F. LÚTY - Salt Lake City - U.S.A.  
J. RUBIO - Iztapalapa - Mexico  
D. SCHOEMAKER - Antwerp - Belgium  
J. M. SPAETH - Paderborn - F.R.G.

#### **PROGRAM COMMITTEE**

F. AGULLÓ LÓPEZ - Madrid - Spain  
R. CAPELLETTI - Parma - Italy  
J. CORISH - Dublin - Ireland  
F. FERMI - Parma - Italy  
U. M. GRASSANO - Roma - Italy  
M. MANFREDI - Parma - Italy  
C. PARACCHINI - Parma - Italy  
J. M. SPAETH - Paderborn - F.R.G.

**DOMESTIC ADVISORY COMMITTEE**

F. BASSANI - Pisa  
C. BUCCI - Parma  
G. CHIAROTTI - Roma  
R. FIESCHI - Parma  
M. FONTANA - Parma  
F. FUMI - Genova  
U. M. GRASSANO - Roma  
V. GRASSO - Messina  
P. MAZZOLDI - Padova  
A. RANFAGNI - Firenze  
G. SPINOLO - Milano  
N. TERZI - Milano  
M. P. TOSI - Trieste  
G. VILIANI - Trento

**LOCAL ORGANIZING COMMITTEE**

R. CAPELLETTI - Conference Chairman  
F. FERMI - Conference Secretary  
A. GAINOTTI - Member  
M. MANFREDI - Treasurer  
C. PARACCHINI - Member

## FOREWORD

The 1988 Parma Conference carries on the tradition of International Conferences, which originated as a meeting on "Color Centers in Alkali Halides" in 1956. Over the years the meeting has developed into the International Conference on Defects in Insulating Crystals.

This year it will focus on the current state of knowledge of defects and defect processes in a wide range of materials. It will bring together scientists from both academic institutions and industry and will present a unique opportunity for discussion of the role of defects in modern material technology. The Conference will stress the value of a fundamental scientific understanding of defects in the design and application of materials for specific purposes. *defects research (m-p)* ←

The contributions made by the International, Domestic, and Program Advisory Committee to the planning and selection of the scientific program and invited speakers was of singular importance. The scientific program will consist of 22 invited lectures, plus oral contributions and poster presentations.

The sponsorship and the financial support from a variety of organizations and industries are gratefully acknowledged. Both types of institutions have expressed and demonstrated strong interest in the objectives of the Conference.

The Conference has been organized in the context of the Physics Department of the University of Parma: the colleagues of the Local Organizing Committee and all those people actively involved in the difficult task of organizing an International Conference are deeply acknowledged.

The Conference will be held in Parma, a historic town in northern Italy. The lively atmosphere of an old Italian town should provide warm hospitality and a relaxing time for all the participants, who are heartily welcome.

Rosanna Capelletti  
Conference Chairman

TIME-TABLE

MONDAY 29	TUESDAY 30	WEDNESDAY 31	THURSDAY 1	FRIDAY 2
9:00 - 9:45 WELCOME	9:00 - 10:30 LECTURES 3 - L1 and 3 - L2	9:00 - 10:45 LECTURES 5 - L1, 5 - L2 and 5 - L3	9:00 - 10:30 LECTURES 6 - L1 and 6 - L2	9:00 - 10:30 LECTURES 8 - L1 and 8 - L2
9:45 - 10:30 LECTURE 1 - L1	10:30 - 11:00 COFFEE	10:45 - 11:05 COFFEE	10:30 - 11:00 COFFEE	10:30 - 11:00 COFFEE
10:30 - 11:20 COFFEE	11:00 - 13:00	11:05 - 12:15 LECTURES 5 - L4 and 5 - L5	11:00 - 13:00	11:00 - 13:00
11:20 - 13:00 ORAL SESSION 1A	ORAL SESSION 3A	ORAL SESSION 3B	ORAL SESSION 9A	ORAL SESSION 8A
ORAL SESSION 1B	ORAL SESSION 3B	ORAL SESSION 3B	ORAL SESSION 9B	ORAL SESSION 8B
LUNCH	LUNCH	LUNCH	LUNCH	LUNCH
13:00 - 15:35 LECTURE 2A - L1	15:00 - 16:10	EXCURSION	15:00 - 16:10	15:00 - 16:40
15:35 - 16:15 ORAL SESSION 2A	LECTURES 4A - L1 4A - L2 4B - L1 4B - L2		LECTURES 7A - L1 7A - L2 7B - L1 7B - L2	ORAL SESSION 9A
16:15 - 16:45 COFFEE	16:10 - 16:40 COFFEE		10:10 - 16:40 COFFEE	16:40 - 17:00 COFFEE
16:45 - 18:05 ORAL SESSION 2A	10:40 - 19:00 POSTER SESSION 1		16:40 - 19:00 POSTER SESSION II	17:00 CLOSING
COCKTAIL	DINNER		CONFERENCE BANQUET	DINNER
	CONCERT			

## CONTENTS

XIV

### SESSION 1

- 1 - L1 COUPLING AND ENERGY TRANSFER BETWEEN F CENTERS AND MOLECULAR DEFECTS  
Fang Rong, Yihong Yang, and Fritz Lüty

#### SESSION 1A - F-Aggregate centers

- 1A - O1 OPTICAL AND THERMAL BISTABILITY OF TWO  $F_H(OH^-)$  CENTER CONFIGURATIONS IN KBr AND KI  
G.Baldacchini, S.Botti, U.M.Grassano, L.Gomes, and F.Lüty
- 1A - O2 MICROSCOPIC STRUCTURE AND BISTABILITY OF  $F_H^-$  CENTRES IN ALKALI HALIDES  
M.Jordan, H.Söthe, J.-M.Spaeth, and F.Lüty
- 1A - O3 SPIN-ORBIT COUPLING OF  $F_H(OH^-)$ -CENTERS IN CESIUM HALIDES  
V.Dierolf, H.J.Paus, and F.Lüty
- 1A - O4 MAGNETO-OPTICAL PROPERTIES OF  $F_2^+$  CENTERS IN KCl CRYSTAL  
D.A.Donatti, M.A.Aegerter, and T.Iida
- 1A - O5 ON SPECTRORADIOMETRIC STUDY OF KCl CRYSTALS DURING ELECTROLYTIC COLOURATION  
P.Rearinne and P.Ketolainen

#### SESSION 1B - Clustering and relaxation

- 1B - O1 AGGREGATION PROCESSES OF  $Pb^{2+}$  IN IONIC CRYSTALS  
S.Benci, A.Chiari, and F.Fermi
- 1B - O2 RESONANCE FLUORESCENCE OF NONMETALLIC SILVER CLUSTERS IN SILVER HALIDES  
E.Schreiber, H.Stolz, and W. von der Osten
- 1B - O3 ELECTRICAL RELAXATION IN SODIUM BETA' ALUMINA AND BETA' ALUMINA CONTAINING RARE EARTH IONS  
M.C.Wintersgill, J.J.Fontanella, B.Dunn, D.L.Yang, and C.G.Andeen
- 1B - O4 ION MASS EFFECTS IN ION-IMPLANTED LiF  
A.T.Davidson, J.D.Comins, and T.E.Derry

- 1B - O5 LATTICE DISTORTIONS, ORIENTATIONAL CORRELATIONS AND LATTICE RELAXATION IN  $(\text{KBr})_{1-x}(\text{KCN})_x$   
P.Wochner, E.Burkel, and J.Peisl

SESSION 2A - Laser active centers and picosecond dynamical effects

- 2A - L1 MODERN DEVELOPMENTS IN COLOR CENTER LASERS AND LUMINESCENCE  
Giuseppe Baldacchini
- 2A - O1 CHALCOGEN-VACANCY DEFECTS AS BUILDING BLOCKS FOR  $\text{F}_2$ -LIKE STABLE COLOR CENTER LASERS IN ALKALI HALIDES  
Bing-Kun Yu and W.Gellermann
- 2A - O2 OPTICAL, ODES, AND ODENDOR INVESTIGATIONS ON  $\text{Pb}^+(1)$  AND RELATED CENTRES IN ALKALINE EARTH FLUORIDES AND  $\text{KMgF}_3$   
M.Fockele, F.Lohse, J.M.Spaeth, and R.H.Bartram
- 2A - O3 SUBPICOSECOND SPECTROSCOPY OF SELF-TRAPPING AND DEFECT FORMATION IN ALKALI HALIDES  
R.T.Williams and G.P.Williams, Jr.
- 2A - O4 PICOSECOND RADIATIONLESS DECAY OF EXCITED ELECTRONIC STATES OF DEFECTS IN  $\text{KCl}$  AND  $\text{NaBr}$   
M.Lebians, C.Sieren, W.Joosen, and D.Schoemaker
- 2A - O5 SUBPICOSECOND LATTICE RELAXATION FOLLOWING ULTRA-FAST LASER EXCITATION OF LOCAL CENTERS IN SOLIDS: A COHERENT PHONON DESCRIPTION  
G.Consolati and N.Terzi

SESSION 2B - Transport and dipolar relaxations

- 2B - L1 GRAIN-BOUNDARY MASS TRANSPORT IN CERAMIC OXIDES  
C. Monty
- 2B - O1 DIPOLE-DEFECT INTERACTION EFFECTS IN  $\text{CaF}_2:\text{Ce}$ ,  $\text{Mn}$   
S.W.S.McKeever and B.Jassemnejad
- 2B - O2 THE INFLUENCE OF PHASE BOUNDARIES ON THE HALL-MOBILITY OF PHOTOELECTRONS IN  $\text{AgBr}_2\text{I}_{1-x}$  - CRYSTALS  
B.Finkernagel and F.Granzer

- 2B - O3 HIGH FREQUENCY IONIC CONDUCTIVITY AND PERMITTIVITY OF  $\text{Sr}_{1-x}\text{Ce}_x\text{F}_{2+x}$  MEASURED BY MEANS OF TIME DOMAIN REFLECTOMETRY  
P. Dorembo and H.W. den Hartog
- 2B - O4 ELECTRIC-FIELD ASSISTED PROTON DIFFUSION IN  $\text{LiNbO}_3$   
N.Schmidt, K.Betzler, M.Grabs, and S.Kapphan
- 2B - O5 DIELECTRIC RELAXATION AND COMPUTER SIMULATION STUDIES OF RUTILE-STRUCTURED  $\text{MnF}_2$  DOPED WITH TRIVALENT CATIONS  
S.Ling, A.S.Nowick, A.N.Cormack, and C.R.A.Catlow
- 2B - O6 THERMALLY STIMULATED DEPOLARIZATION STUDIES OF CLUSTERING IN RARE EARTH DOPED ALKALINE EARTH FLUORIDES  
G.E.Matthews, Jr., P.Steed, and M.Dameron

### SESSION 3

- 3 - L1 ADVANCES IN THE COMPUTER SIMULATION OF DEFECTIVE MATERIALS  
J.H. Harding
- 3 - L2  $\text{O}_2$  DEFECTS: THE FIRST SOLID STATE MODEL SYSTEM FOR SUPERFLUORESCENCE  
D.Schmid, L.O.Schwan, and A.Schiller

### SESSION 3A - Excitons

- 3A - O1 THREE-PHOTON SPECTROSCOPY OF EXCITONS AND POLARITONS IN ALKALI HALIDES  
F.Beerwerth, D.Fröhlich, and P.Köhler
- 3A - O2 RELAXATION OF SELF-TRAPPED EXCITONS IN ALKALI CHLORIDE CRYSTALS STUDIED BY TIME DELAYED DOUBLE EXCITATION IN PICOSECOND RANGE  
Y.Suzuki, H.Abe, and M.Hirai
- 3A - O3 RADIATIVE AND NON-RADIATIVE DE-EXCITATION PROCESSES OF LOCALIZED EXCITONS IN  $\text{KCl:Br}$   
K.Tanaka, H.Kosaka, O.Arimoto, K.Kan'no, and Y.Nakai

- 3A - 04 A THEORETICAL BASIS FOR THE RABIN-KLICK CRITERION IN TERMS OF OFF-CENTER SELF-TRAPPED EXCITON RELAXATION  
K.S.Song, C.H.Leung, and R.T.Williams
- 3A - 05 OPTICAL AND SPIN DEPHASING OF THE PHOSPHORESCENT  $O_2$  DEFECT IN CALCIUM OXIDE  
P.A. van Leeuwen and M.Glasbeek
- 3A - 06  $(MoO_4)$  COMPLEXES IN  $CaWO_4$  - RESULTS OF ODMR AND ESR INVESTIGATIONS  
R.Grasser, A.Hofstaetter, A.Scharmann, F.Schoen, P.G.Baranov, V.V.Diakonov, and N.G.Romanov

#### **SESSION 3B - Lattice defect calculations**

- 3B - 01 CALCULATION OF IONIC MOBILITY IN SILVER HALIDES USING THREE-BODY POTENTIAL  
C.R.A.Catlow, F.M.Healy, J.Corish, P.W.M.Jacobs, M.Leslie, Y.Tan, and R.C.Baetzold
- 3B - 02 DEFECTS AND IMPURITY STATES IN TITANATES  
R.A.Jackson, S.M.Tomlinson, M.J.Akhtar, and C.R.A.Catlow
- 3B - 03 NON-STOICHIOMETRY IN ALKALINE EARTH EXCESS ALKALINE EARTH TITANATES  
A.N.Cormack and K.R.Udayakumar
- 3B - 04 EMBEDDED QUANTUM CLUSTER CALCULATIONS ON DEFECTS IN BINARY OXIDES  
R.W.Grimes, C.R.A.Catlow, and A.M.Stoneham
- 3B - 05 LATTICE POTENTIAL ENERGY CALCULATIONS OF POTASSIUM CYANIDE-POTASSIUM HALIDE MIXED CRYSTALS AND RELATION TO ORDER-DISORDER PHASE TRANSITIONS  
P.Bourson, G.Gorczyca, and D.Durand
- 3B - 06 PAIRING OF OFF-CENTER DEFECTS IN IONIC CRYSTALS DUE TO VIBRONIC VAN DER WAALS BINDING: PRECURSOR TO NEW PHASE FORMATION  
M.Georgiev and M.Borisov

#### SESSION 4A

- 4A - L1 ANOMALY CHARGE PHOTO-TRANSFER IN DOPED INSULATORS  
A.A. Kaplyanski
- 4A - L2 DYNAMICAL PROCESSES ASSOCIATED WITH SELF-TRAPPED EXCITONS IN INSULATORS: DE-EXCITATION AND DEFECT FORMATION AT HIGHLY EXCITED STATES  
Noriaki Itoh, Katsumi Tanimura, and Chihiro Itoh

#### SESSION 4B

- 4B - L1 CALCULATION OF THE ENTROPIES OF POINT DEFECTS IN INSULATING CRYSTALS  
P.W.M. Jacobs
- 4B - L2 THEORY OF DISPERSED IONIC CONDUCTORS  
Armin Bunde

#### POSTER SESSION I - TUESDAY

- TU - P1 THE EFFECT OF IONIC IMPLANTATION AND ADDITIVE COLOURING ON THE ELECTRON CENTERS IN  $\text{RbAg}_4\text{I}_5$  SUPERIONIC CRYSTALS  
S.I.Bredikhin, N.N.Kovaleva, N.V.Lichkova, and I.Sh.Khasanov
- TU - P2 ELECTRON EMISSION IN SUPERIONIC  $\text{RbAg}_4\text{I}_5$  CRYSTALS STIMULATED BY PHASE TRANSITIONS  
S.I.Bredikhin, N.N.Kovaleva, S.Z.Shmurak, and A.B.Poletaev
- TU - P3 SPECTRAL COMPOSITION AND DECAY KINETICS OF UF EMISSION FROM  $\text{KCl}_{1-x}\text{Br}_x\text{:Pb}^{2+}$  CRYSTALS  
K.Polák, M.Manfredi, and M.Nikl
- TU - P4 LUMINESCENCE DECAY TIME OF  $\text{Ti}^{3+}$  IN PHOSPHATE GLASSES  
L.E.Bausá, G.Lifante, J.García-Solé, and A.Durán
- TU - P5 TIME RESOLVED STUDY OF SECONDARY EMISSION IN  $\text{KI:Se}_2^-$   
H.Murata, T.Kishigami, and R.Kato
- TU - P6 OPTICAL PROPERTIES OF  $\text{Ho}^{3+}$  IN  $\text{KCaF}_3$  CRYSTALS  
M.A.Mondragon, J.García M., and W.A.Sibley

- TU - P7 OPTICAL STUDIES ON  $\text{KCaF}_3\text{:Mn:Eu}$ ,  $\text{RbCdF}_3\text{:Mn:Eu}$  AND  $\text{RbCaF}_3\text{:Mn:Eu}$  CRYSTALS  
J.García M., W.A.Sibley, and J.M.Spaeth
- TU - P8 THE INFLUENCE OF HIGH EXTERNAL ELECTRIC FIELDS ON THE CUBIC  $\text{Eu}^{2+}$  CENTERS IN  $\text{CaF}_2$  SINGLE CRYSTALS  
N.Gouskos
- TU - P9 RAMAN- AND IR-SPECTRA OF THE OH(OD)-STRETCH MODES IN  $\text{LiTaO}_3$   
H.P.Winkler, A.Jovanović, M.Wöhlecke, and S.Kapphan
- TU - P10 MAGNETO OPTICAL STUDIES OF F CENTER/MOLECULAR DEFECT PAIRS IN ALKALI HALIDE CRYSTALS  
G.Baldacchini, S.Botti, U.M.Grassano, and F.Lüty
- TU - P11  $\text{OH}^-$  ISOTOPE EFFECTS ON VIBRATIONAL AND ELECTRICAL ANHARMONICITIES AS A PROBE OF THE DEFECT ENVIRONMENT  
W. Beall Fowler and R. Capelletti
- TU - P12  $\text{F}_A$  AND F-AGGREGATE CENTRES IN  $\text{RbCl:Li}^+$   
G.Baldacchini, E.Giovenale, F. De Matteis, A.Scacco, F.Somma, and U.M.Grassano
- TU - P13 MEASUREMENT OF THE ANGULAR SHIFT OF THE  $\text{Li}^+$  ION IN  $\text{F}_A(\text{Li}^+)$  CENTER CRYSTALS  
M.May, S.Debrus, J.P.Hong, B.Quernet, E.Rzepka, and A.Bouazi
- TU - P14 THE ROLE OF  $\text{OH}^-$  IONS IN THE CHARGE COMPENSATION OF IMPURITIES IN  $\text{ZnWO}_4$  SINGLE CRYSTALS  
I.Földvári, R.Capelletti, L.A. Kappers, and A.Watterich
- TU - P15 AN INFRARED ABSORPTION BAND CAUSED BY  $\text{OH}^-$  IONS IN  $\text{LiNbO}_3\text{:Mg}$ , Cr CRYSTALS  
L.Kovács, I.Földvári, I.Cravero, K.Polgár, and R.Capelletti
- TU - P16 RESONANT ELECTRONIC RAMAN SCATTERING OF THE  $\text{Sm}^{++}$  - CATION VACANCY COMPLEX IN KCl  
B.Cocquyt, W. Joosen, and D.Schoemaker
- TU - P17 PRODUCTION OF A PARAMAGNETIC  $\text{Bi}^0$  CENTER IN X-IRRADIATED  $\text{KCl:Bi}$  CRYSTALS  
S.V.Nistor, E.Goovaerts, I.Ursu, and D.Schoemaker
- TU - P18 ESR OF NON-CUBIC  $\text{Fe}^{3+}$  CENTERS IN  $\text{LiCl}$  CRYSTALS  
S.V.Nistor, D.P.Lazar, and M.Velter-Stefanescu

- TU - P19 THE EPR STUDY OF  $\text{Co}^{2+}$  CENTERS IN  $\text{PbCl}_2$  SINGLE CRYSTALS  
J.Rosa, A.G.Badalyan, P.G.Baranov, and V.A.Khramtsov
- TU - P20 STUDY OF VANADYL CENTERS IN LITHIUM POTASSIUM SULPHATE SINGLE CRYSTALS: BY EPR  
N.Sathyanarayana and S.Radhakrishna
- TU - P21  $\text{F}(\text{Br}^-)$ -CENTRES IN  $\text{BaFBr}$   
F.K.Koschnick, H.Söthe, and J.M.Spaeth
- TU - P22 AN ESR STUDY OF VANADIUM IMPURITY IONS IN SINGLE-CRYSTAL ZINC TUNGSTATE  
G.J.Edwards, O.R.Gilliam, R.H.Bartram, L.A.Kappers, A.Watterich, and I.Földvári
- TU - P23 EFFECT OF HYDROSTATIC PRESSURE ON THE  $\text{Ag}^+$  OFF-CENTER MOTION IN  $\text{RbCl}$   
M.Fricke, O.Kanert, and R.Küchler
- TU - P24 NUCLEAR MAGNETIC RESONANCE STUDY OF SINGLE-CRYSTAL RUTILE  
O.Kanert and H.Kolem
- TU - P25 CALCULATIONS OF SOME SIMPLE DEFECTS IN PURE AND DOPED  $\text{CaF}_2$  AND  $\text{SrF}_2$  CRYSTALS WITH ALKALI IMPURITIES  
A.Amara, G.Cremer, F.Martin-Brunetiere, and M.Thuau
- TU - P26 CALCULATION OF THE  $\text{F}_2^+$  LINEAR CENTRE IN  $\text{CaF}_2$   
A.Amara and M.Thuau
- TU - P27 EFFECT OF PRESSURE ON INTRA-d TRANSITIONS  
M.J.Caldas, M.R.Sardela Jr., and A.Fazzio
- TU - P28 THEORETICAL STUDY ON  $\text{Ni}^+$  IN FLUORIDE LATTICES  
M.T. Barriuso, J. Aramburu, and M. Moreno
- TU - P29 DEPENDENCE OF THE COVALENCY OF THE  $(\text{MnF}_6)^{4-}$  COMPLEX ION UPON THE  $\text{Mn}^{2+} - \text{F}^-$  DISTANCE  
M.T.Barriuso, J.A.Aramburu, M.Moreno, M.Flórez, G.Fernández Rodrigo, and L.Pueyo
- TU - P30 INFLUENCE OF OXYGEN OCTAHEDRON SIZE ON THE ELECTRONIC STRUCTURE OF  $\text{Co}^{2+}$  DOPED PEROVSKITE  
P. Moretti
- TU - P31 CRYSTAL-FIELD MODEL OF A  $\text{Pb}^{II}(2)$  CENTRE IN  $\text{SrF}_2$   
R.H.Bartram, M.Fockele, L.Lohse, and J.-M.Spaeth

- TU - P32 TERM ENERGY CALCULATIONS AND OPTICAL SPECTRA IN  $\text{Cr}^{3+}$  -  
DOPED SPINEL - LIKE COMPOUNDS  
F.M. Michel-Calendini, C.Linarès, W.Nie, and G.Boulon
- TU - P33 CORRECTION TO THE CONTINUUM APPROXIMATION FOR THE  
LARGE POLARON BOUND TO A DEFECT: THE GROUND STATE EN-  
ERGY  
Y.Frongillo and Y.Lepine
- TU - P34 A COMPUTER SIMULATION STUDY OF THE  $V_k$  CENTER IN ALKALI  
HALIDES USING HARTREE-FOCK CLUSTERS  
A.B.Kunz and Ravindra Pandey
- TU - P35 ANNIHILATION ON PERCOLATION CLUSTER: SMOLUCHOVSKI THE-  
ORY AND NUMERICAL EXPERIMENT  
A.G.Vitukhnovsky, B.L.Pyttel, and I.M.Sokolov
- TU - P36 THEORETICAL SIMULATIONS OF TRIPLET SELF-TRAPPED EXCI-  
TONS IN  $\text{SiO}_2$  AND KCl CRYSTALS  
A.L.Shluger and E.K. Shidlovskaya
- TU - P37 SHORT-LIVING FRENKEL-TYPE DEFECTS IN  $\text{TlCl}$   
D.K.Millers, L.G.Grigorjeva, and A.V.Nomojev
- TU - P38 SELF-TRAPPING OF HOLES AND EXCITONS IN  $\text{Al}_2\text{O}_3$  CRYSTAL  
P.Kulis, Z.Rachko, M.Springis, I.Tale, and J.Jansons
- TU - P39 OPTICAL PROPERTIES OF TWOFOLD COORDINATED Si, Ge, AND  
Sn ATOMS IN AMORPHOUS SILICON DIOXIDE  
L. N. Skuja
- TU - P40 MAGNETIC FIELD EFFECT ON THE DECAY PROCESSES OF TRIPLET  
LOCALIZED EXCITONS IN  $\text{KBr:I}$   
T.Mukai, K.Kan'no, and Y.Nakai
- TU - P41 RED EMISSION AND TRAPPED-HOLE CENTERS PRODUCED BY DE-  
EXCITATION OF LOCALIZED EXCITONS IN  $\text{KCl:I}$  AND  $\text{RbCl:I}$   
K.Kan'no, K.Tanaka, and Y.Nakai
- TU - P42 COLOR CENTERS IN SUPER IONIC CONDUCTORS  $\text{RbAg}_4\text{I}_5$  AND  
 $\text{KAg}_4\text{I}_5$   
T.Awano and M.Ikezawa
- TU - P43 OPTICAL PROPERTIES AND COLORATION OF ALKALI SILVER  
HALIDES  
M.Ikezawa, T.Awano, K.Edamatsu, T.Nanba, T.Matsuyama, and H.Yamaoka

- TU - P44 EFFECTS OF TWO-DIMENSIONAL DEFECTS ON EXCITONS IN BISMUTH IODIDE CRYSTALS  
T.Komatsu, T.Karasawa, K.Watanabe, T.Higashimura, T.Iida, I. Kaizu, and Y.Kaifu
- TU - P45 EPR STUDY OF HOLE TRAPPING AT CATION VACANCIES IN SILVER HALIDES  
C.T.Kao, L.G.Rowan, and L.M.Slifkin
- TU - P46 NONRADIATIVE DECAY OF EXCITATIONS IN DEFECTS (A PHONON TRANSPORT APPROACH)  
M.Wagner and J.Vázquez-Márquez
- TU - P47 SPECTRAL DEPENDENCE OF THE ODMR TRANSITIONS OF THE BROMINE-BOUND STE IN AgCl  
J.P.Spoonhower and F.J.Ahlers
- TU - P48 ROLE OF THE CATION ON THE FORMATION OF HALOGEN AGGREGATES IN X-IRRADIATED ALKALI HALIDES CRYSTALS  
M.Bernard, E.Rzepka, and S.Lefrant
- TU - P49 STUDIES OF COLOUR CENTRES IN LiYF<sub>4</sub> CRYSTALS  
Fang Shugan and Le Zhiqiang
- TU - P50 THE FORMATION OF VACANCIES DURING THERMAL DECOMPOSITION OF ALKALINE EARTH HYDROXIDES  
L.I.Barsova and T.K.Yurik
- TU - P51 LUMINESCENCE OF NON RELAXED IODINE BOUND EXCITONS IN AgBr ?  
W.Czaja and Y.Burki
- TU - P52 PHOTOLUMINESCENCE, PHOTOCONDUCTIVITY AND THERMOLUMINESCENCE IN Eu<sup>2+</sup> DOPED ALKALI HALIDES  
I.Aguirre de Cárcer, F. Cussó, and F. Jaque
- TU - P53 ON THE NATURE OF THE BROAD OPTICAL ABSORPTION BAND IN LiNbO<sub>3</sub>  
F.Agulló López and E.R.Hodgson
- TU - P54 EFFECTS OF VARIABLE TL SPECTRA ON TL DOSIMETRY  
H.M.Rendell and P.D.Townsend
- TU - P55 RADIATION-INDUCED DEFECT CENTRES IN  $\alpha$ -Al<sub>2</sub>O<sub>3</sub>  
R.A.Wood
- TU - P56 RADIATION DAMAGE IN NaCl: STORED ENERGY AND MODEL CALCULATIONS  
J.C.Groote, J.R.W.Weerkamp, J.Beersma, and H.W.den Hartog

- TU - P57 RADIATION-INDUCED ABSORPTION BANDS DUE TO CHLORINE-RELATED DEFECTS IN  $\alpha$ -SiO<sub>2</sub>  
H.Takada, Y.Suzuki, H.Kimura, and M.Hirai
- TU - P58 AN EPR STUDY OF X-RADIATION DAMAGE IN Eu<sup>2+</sup>-DOPED BaFBr  
R.S.Eachus and R.H.D.Nuttall
- TU - P59 NONLINEAR POLARIZATION SPECTROSCOPY OF F<sub>2</sub>-CENTERS IN KCl  
S.A.Boiko, A.M.Brodin, M.I.Dykman, M.P.Lisitsa, G.G.Tarasov, R. Voska, and I.Földvári
- TU - P60 INVESTIGATION OF IMPURITIES IN CUBIC CRYSTALS BY MEANS OF NONLINEAR POLARIZATION SPECTROSCOPY  
S.A.Boiko, A.M.Brodin, M.Ya.Valakh, M.I.Dykman, M.P.Lisitsa, G.G.Tarasov, A.M.Shpak
- TU - P61 MAGNETO-OPTICAL EFFECTS BY NONEQUILIBRIUM SPIN POLARIZATION INDUCED IN THE F-CENTER BY MODULATED AND SATURATED PUMPING  
N.Akiyama, Y.Mori, and H.Ohkura
- TU - P62 LASER EMISSION AND CONCENTRATION QUENCHING OF THE F<sub>A</sub>(II) CENTERS IN KCl:Li  
G.Baldacchini, E.Giovenale, U.M.Grassano, M.Meucci, A.Scacco, and M.Tonelli
- TU - P63 OPTICAL PROPERTIES OF LASING COLOR CENTERS IN FLUORIDES  
G. Hörsch and H.J.Paus
- TU - P64 ON THE TEMPERATURE DEPENDENCE OF THE REFRACTIVE INDEX OF A LASER ACTIVE KCl:Li CRYSTAL  
K.-E. Peiponen, P.Silfsten and K.Karttunen
- TU - P65 OPTICAL STUDIES OF ELASTIC ORDER-DISORDER TRANSFORMATIONS IN DOUBLE-MIXED ALKALI-HALIDE-CYANIDE CRYSTALS  
J.Ortiz-Lopez and F.Lüty
- TU - P66 SPECTRAL HOLE-BURNING IN THE SECOND HARMONIC ABSORPTION OF ROTATIONALLY LOCALIZED CN<sup>-</sup> DEFECTS IN ALKALI HALIDES  
M.Schrempel, W.Gellermann, and F.Lüty
- TU - P67 TUNABLE COLOUR CENTRE LASERS IN THE RANGE 150-800 nm  
P.Fabeni, G.P.Pazzi, R.Linari, A.Ranfagni, and L.Salvini

- TU - P68 FAR INFRARED REFLECTIVITY SPECTRA AND LATTICE DYNAMIC OF LOW TEMPERATURE PHASES OF NaCN  
G.Gorczyca, P.Bourson, and D.Durand
- TU - P69 DOUBLE BRIDGING IMPURITY STRUCTURES AND HYPERVALENT STATE OF MOLECULAR CHLORINE IN VITREOUS SILICON DIOXIDE  
E.M.Dianov, V.O.Sokolov, and V.B.Sulimov
- TU - P70 OH<sup>-</sup> DISPLACEMENT IN CsCl AT LOW TEMPERATURES CALCULATED FROM THE FREQUENCY SHIFT ASSOCIATED WITH THE F<sub>H</sub>(OH<sup>-</sup>) CENTER  
Philip W. Gash
- TU - P71 DEFECT STRUCTURES AND IONIC TRANSPORT IN LITHIUM OXIDE  
A.V.Chadwick, K.W.Flack, J.H.Strange, and J.H.Harding
- TU - P72 MOLECULAR DYNAMICS SIMULATIONS OF ALKALI BORATE GLASSES  
W.Soppe and H.W. den Hartog
- TU - P73 DEFECT STRUCTURE AND ENERGETICS IN CALCIA STABILIZED ZIRCONIA  
A.Dwivedi and A.N.Cormack
- TU - P74 STATIC SIMULATION STUDIES OF HIGH T. SUPERCONDUCTORS  
S.M.Tomlinson, C.R.A.Catlow, M.S.Islam, and M.Leslie
- TU - P75 EXTENDED X-RAY ABSORPTION AND COMPUTER SIMULATION STUDIES OF ELECTRO-OPTIC MATERIALS  
S.M.Tomlinson, C.R.A. Catlow, A.V.Chadwick, J.Jones, and H.Donnerburg
- TU - P76 SUBSTRUCTURES IN IONIC CRYSTALS ACCORDING TO THE SELF-CONSISTED LIDIARD-DEBYE-HUECKEL THEORY  
D.Ouroushev
- TU - P77 ATOMISTIC CALCULATIONS AND EXAFS OF HALIDE IMPURITIES IN AgBr  
Y.T.Tan, R.C.Baetzold, and K.J.Lushington
- TU - P78 DEFORMATION AND CHARGE TRANSFER EFFECTS ON DEFECTS PROPERTIES OF IONIC SOLIDS  
Sankar P. Sanyal and R.K.Singh
- TU - P79 EFFECT OF PLASTIC DEFORMATION AND THERMAL TREATMENTS ON THE ITC SPECTRA OF Ba<sub>1-x</sub>La<sub>x</sub>F<sub>2+x</sub>.  
N.Suarez, M.Puma, and F.Lorenzo

- TU - P80 DIELECTRIC LOSS IN BERLINITE  
J.J.Fontanella, M.C.Wintersgill, R.D.Shannon, G.R.Rossman, and B.H.T.Chai
- TU - P81 DIELECTRIC LOSS OF OH<sup>-</sup> IONS IN ALKALI HALIDES  
L.Gomes and F.Lüty
- TU - P82 THERMOLUMINESCENCE AND IONIC THERMOCURRENT IN CALCITE  
J.F. de Lima, E.M.Yoshimura, and E.Okuno
- TU - P83 IONIC THERMOCURRENTS IN NATURAL CaF<sub>2</sub>  
M.E.G.Valerio, E.Okuno, and A.R.Blak
- TU - P84 DIELECTRIC RELAXATIONS ASSOCIATED WITH RADIATION INDUCED POINT DEFECT DIPOLES IN ELECTRICALLY INSULATING CERAMICS  
S.N.Buckley and P.Agnew
- TU - P85 THERMALLY STIMULATED DEPOLARIZATION CURRENTS IN MgAl<sub>2</sub>O<sub>4</sub>  
A.Ibarra, R.Vila, and M.Jiménez de Castro
- TU - P86 THE EVOLUTION OF DIELECTRIC PROPERTIES INDUCED BY ANNEALING OF NEUTRON DAMAGE IN Al<sub>2</sub>O<sub>3</sub>  
R.Heidinger and F.Königer
- TU - P87 DIELECTRIC MEASUREMENTS OF IMPURITY INDUCED DYNAMICS IN Fe DOPED BaTiO<sub>3</sub>  
M.Maglione, R.Böhmer, A.Loidl, and G.Godefroy
- TU - P88 DIELECTRIC PROPERTIES OF CONDENSED FLUOROCARBON MIXTURES  
R.Böhmer and A.Loidl
- TU - P89 ITC - SPECTRA OF NaCl - CRYSTAL CONTAINING Cr<sup>3+</sup> - IONS  
M.Suszyńska and R.Capelletti
- TU - P90 CHARACTERISTIC FEATURES OF THE BISMUTH CENTRES IN ALKALI HALIDE CRYSTALS  
M.Suszyńska and R.Capelletti
- TU - P91 KINETICS OF AGGREGATION AND PRECIPITATION IN NaCl CRYSTALS DOPED WITH Eu<sup>2+</sup>  
A.Gubański, M.Suszyńska, and D.Nowak-Woźny

- TU - P92 ELECTRON TRAPPING IN  $H^2$  DEFECTS DURING THE PHOTO-CONVERSION OF ANION VACANCES IN THERMOCHEMICALLY REDUCED CaO CRYSTALS  
V.M.Orera and Y.Chen
- TU - P93 AGGREGATION KINETICS OF I.V. DIPOLES IN NaCl:Eu<sup>2+</sup> CRYSTALS  
B.Macalik and J.Pożniak
- TU - P94 ABOUT THE ORIGIN OF TL PEAK 2 IN THE LiF: Mg, Ti SYSTEM  
A.Petö
- TU - P95 AGGREGATION PROCESSES IN NaCl:Eu<sup>2+</sup> SYSTEM  
R.Capelletti, R. Cywinski, M.Manfredi, and H. Opyrchal
- TU - P96 THE ROLES OF DEFECTS IN STRUCTURAL PHASE TRANSITIONS OF COMPLEX OXIDE CRYSTALS  
Feng Duan
- TU - P97 THERMAL AND DYNAMICAL PROPERTIES OF MIXED LEAD HALIDES  $PbCl_{2x}Br_{2(1-x)}$   
M.Lumbreras and C.Carabatos-Nédelec
- TU - P98 INVESTIGATION OF THERMALLY INDUCED Li<sup>+</sup> ION DISORDER IN Li<sub>2</sub>O USING NEUTRON DIFFRACTION  
T.W.D.Farley, W.Hayes, S.Hull, M.T.Hutchings, and M.Vrtis
- TU - P99 XES CHARACTERIZATION AND DEFECT STRUCTURE OF TmBa<sub>2</sub>Cu<sub>3</sub>O<sub>x</sub> SINGLE CRYSTALS  
G.Jasiolek and A.Pajaczkowska
- TU - P100 OPTICAL AND THERMODYNAMIC PROPERTIES OF FERROELECTRICS WITH HYDROGEN BONDS IN THE PRESENCE OF DEFECTS  
I.V.Stasyuk, R.Y.Stetsiv, and A.L.Ivankiv

#### SESSION 5

- 5 - L1 X-RAY STORAGE PHOSPHORS: PHYSICAL MECHANISM AND APPLICATIONS  
Heinz von Seggern
- 5 - L2 ION IMPLANTATION IN ELECTRO-OPTIC MATERIALS  
Peter D. Townsend
- 5 - L3 SURFACE DEFECTS EXPLOITED FOR GAS SENSING  
Wolfgang Göpel

- 5 - L4 THE ROLE OF IONIC DEFECTS IN THE RADIATION PHYSICS OF  
THE SILVER HALIDES, AND THEIR EXPLOITATION IN PHOTOGRAPHY  
R.S.Eachus and Myra T. Olm
- 5 - L5 HIGH TEMPERATURE ELECTRON IRRADIATION OF FUSION MATERIALS  
E.R. Hodgson

#### SESSION 6

- 6 - L1 DEFECTS AND STRUCTURAL CHANGES IN PEROVSKITE SYSTEMS: FROM INSULATORS TO SUPERCONDUCTORS  
D.M. Smyth
- 6 - L2 IMPURITIES AND DEFECTS IN FLUORIDE GLASSES  
Marcel Poulain

#### SESSION 6A - Impurities I

- 6A - O1 OPTICAL PROPERTIES OF COLOR CENTERS IN GADOLINIUM GALLIUM GARNET CRYSTALS  
L.S.Cain, G.J.Pogatschnik, and Y.Chen
- 6A - O2 COMPUTER MODELLING OF PRESSURE-DEPENDENT CHROMIUM PHOTOLUMINESCENCE  
R.H.Bartram, J.C.Charpie, A.M.Woods, and R.S.Sinkovits
- 6A - O3 THEORETICAL IMPURITY LEVELS OF Ni AND V IONS IN THE BaTiO<sub>3</sub> PEROVSKITE HOST  
P. Moretti, and F.M. Michel-Calendini
- 6A - O4 SELF-TRAPPED ELECTRON CENTERS IN ELECTRON-IRRADIATED ZINC TUNGSTATE SINGLE CRYSTALS  
A.Watterich, G.J.Edwards, O.R.Gilliam, R.H.Bartram, Á.Péter, and R.Voszka
- 6A - O5 PHOTOIONIZATION, TRAPPED EXCITONS AND LUMINESCENCE OF Eu<sup>2+</sup> AND Yb<sup>2+</sup> RARE EARTH IONS IN CRYSTALS OF ALKALINE EARTH FLUORIDES  
B.Moine, B.Courtois, C.Pedrini, and D.S.McClure

- 6A - O6 THERMOCHEMICAL REDUCTION AND RADIATION EFFECTS IN LANTHANUM MAGNESIUM ALUMINATE CRYSTALS  
Y.Chen, M.M.Abraham, M.R.Kotka, G.J.Pogatschnik, L.S.Cain, J.L.Park, and C.Y.Chen

SESSION 6B - Transport and non stoichiometry

- 6B - O1 CALCULATED LATTICE AND DEFECT PROPERTIES OF  $M_2CuO_4$  ( $M = La, Y, Nd, Pr, Al$ ) RELATED TO HIGH  $T_c$  SUPERCONDUCTIVITY  
N.L.Allan and W.C.Mackrodt
- 6B - O2 EXTENDED DEFECTS IN  $YBa_2Cu_3O_{7-x}$  AND RELATED PEROVSKITES  
T.E.Mitchell and T.Roy
- 6B - O3 THE INFLUENCE OF LOCAL ELECTRIC FIELD AND OF CORRELATION IN THE ELECTRONIC TRANSPORT: THE CASE OF  $CdF_2$   
V.Dallacasa and C.Paracchini
- 6B - O4 MOLECULAR DYNAMICS OF THE FAST-ION CONDUCTOR  $\delta$ -BISMUTH OXIDE: EFFECT OF CRYSTAL POTENTIAL AND NUMBER OF PARTICLES  
D.A. Mac Dónaill, P.W.M.Jacobs, and Z.A. Rycerz
- 6B - O5 DEFECT STRUCTURE AND TRANSPORT PROPERTIES OF MIXED IRON - MANGANESE - OXIDES  
R.Dieckmann and P.Franke
- 6B - O6 STRUCTURAL AND DYNAMIC PROPERTIES OF MIXED CATION FLUORIDE CONDUCTORS  
P.A.Cox and C.R.A.Catlow

SESSION 7A

- 7A - L1 LOCAL STRUCTURE AROUND IMPURITIES INFERRED FROM OPTICAL AND E.P.R. SPECTROSCOPY  
M. Moreno
- 7A - L2 APPLICATION OF MAGNETIC MULTIPLE RESONANCES TO STUDY DEFECTS IN III-V COMPOUNDS  
J.-M. Spaeth

### SESSION 7B

- 7B - L1 THE PHYSICS OF LATTICE DEFECTS IN THE SILVER HALIDES  
L.M. Slifkin
- 7B - L2 IMPURITY AGGREGATION IN IONIC CRYSTALS  
M.Manfredi

### POSTER SESSION II - THURSDAY

- TH - P1 OPTICAL PROPERTIES OF IMPURITY PERTURBED COLOR CENTERS IN INSULATING OXIDE CRYSTALS  
G.J.Pogatschnik and Y. Chen
- TH - P2 OPTICAL AND EPR INVESTIGATION ON AS GROWN NaBr:Mn<sup>2+</sup> AND LiCl:Mn<sup>2+</sup> SINGLE CRYSTALS  
C.Marco de Lucas, F.Rodríguez, and M.Moreno
- TH - P3 OPTICAL INVESTIGATIONS ON NH<sub>4</sub>Br:Cu<sup>2+</sup> AND NH<sub>4</sub>Cl:Cu<sup>2+</sup>  
A.G.Breñosa, F.Rodríguez, and M.Moreno
- TH - P4 DEPENDENCE OF CRYSTAL-FIELD SPECTRUM OF RbMnF<sub>3</sub> AND KMnF<sub>3</sub> WITH TEMPERATURE IN THE 14-600 K RANGE  
F.Rodríguez, M.Moreno, J.M.Dance, and A.Tressaud
- TH - P5 EVOLUTION OF THE F AGGREGATE CENTERS UNDER F LIGHT BLEACHING: A SIMPLE MODEL  
V.D.Rodríguez and E.Pérez
- TH - P6 THERMAL AND OPTICAL BLEACHING OF ABSORPTION SPECTRA IN REDUCED LiNbO<sub>3</sub>  
A.García-Cabañes, E.Diéguez, J.M.Cabrera, and F.Agulló-López
- TH - P7 THE RELAXATION DYNAMICS OF OPTICALLY EXCITED F CENTERS IN ALKALI HALIDES  
Y.Mori and H.Ohkura
- TH - P8 EFFECT OF IONIZING RADIATIONS ON CsCdBr<sub>3</sub> CRYSTALS  
C.Andraud, F.Pellé, O.Pilla, J.P.Denis, and B.Blanzat
- TH - P9 SPECTROSCOPIC PROPERTIES OF EXCHANGE COUPLED PAIRS OF Cr<sup>3+</sup> IN THE UNIDIMENSIONAL CRYSTAL CsCdBr<sub>3</sub>  
F.Pellé, J.P.Denis, O.Pilla, and B.Blanzat

- TH - P10 HIGH PRESSURE AND LOW TEMPERATURE PHOTOLUMINESCENCE OF  $\text{Cr}^{3+}$  IN  $\text{Na}_3\text{In}_2\text{Li}_3\text{F}_{12}$   
D.de Viry, F.Pellé, N.Tercier, J.P.Denis, and B.Blanzat
- TH - P11 ZERO-PHONON LINE AND PHONON-SIDEBAND OF  $\text{Sm}^{2+}$ -DOPED  $\text{CaF}_2$ : MIXING EFFECT OF THE  $f^6$  AND  $f^6 d$  ELECTRON CONFIGURATIONS  
T.Tsuboi
- TH - P12 LUMINESCENCE OF F AND  $\text{F}^+$  CENTERS IN MAGNESIUM OXIDE  
G.P.Williams, Jr., G.H.Rosenblatt, R.T.Williams, and Y.Chen
- TH - P13 STOKES AND ANTI-STOKES RESONANT RAMAN SCATTERING OF  $\text{F}_H(\text{CN}^-)$  DEFECTS IN CsBr  
G.Cachei, H.Stolz, W. von der Osten, and F.Lüty
- TH - P14 MECHANISM FOR THE PHOTOREFRACTIVE EFFECT IN PLZT 9/65/35  
J.P.Spoonhower, R.S.Eachus, and J.A.Agostinelli
- TH - P15 TIME-RESOLVED SPECTROSCOPY OF  $\text{BaFBr}/\text{Eu}^{2+}$   
J.P.Spoonhower and M.S.Burberry
- TH - P16 RESONANT RAMAN SCATTERING OF THE  $\text{F}_A(\text{Li}^+)$  CENTER IN KBr  
M.Lebians, W.Joosen, E.Goovaerts, and D.Schoemaker
- TH - P17 EQUILIBRIUM ORIENTATIONS OF DIATOMIC MOLECULAR IMPURITIES IN CUBIC CRYSTALS DETERMINED BY A POLARIZED RAMAN STUDY OF THE STRETCHING MODE  
H.Fleurent, W.Joosen, and D.Schoemaker
- TH - P18 PHOTOINDUCED REORIENTATION OF  $\text{F}_A$  CENTRES IN ALKALI HALIDES  
G.Baldacchini, E.Giovenale, F.De Matteis, A.Scacco, F.Somma, and U.M.Grassano
- TH - P19 SUBBAND GAP EXCITATION SPECTRA OF SILVER HALIDES  
A.Marchetti and M.Burberry
- TH - P20 OFF-CENTER DIRECTION OF  $\text{Cu}^+$  ION IN NaBr  
S.Emura, T.Murata, H.Maeda, H.Ito, and M.Ishiguro
- TH - P21  $\text{Ni}^+$  CENTERS IN  $\text{RbCaF}_3$ : A PARAMAGNETIC PROBE FOR STUDYING THE 195 K STRUCTURAL PHASE TRANSITION  
R.Alcalá, E.Zorita, and P.J.Alonso

- TH - P22 INFLUENCE OF  $Mn^{2+}$  IMPURITIES ON HIDROLYSIS PROCESSES INDUCED IN  $SrF_2$  BY HIGH TEMPERATURE ANNEALING  
P.J.Alonso, J.I.Peña, and R.Alcalá
- TH - P23 ZEEMAN EFFECT AND MAGNETIC CIRCULAR DICHROISM OF ANISOTROPIC CENTRES IN CUBIC CRYSTALS  
W.A.Runciman and N.B.Manson
- TH - P24 ON THE DEFECT EQUILIBRIUM IN THE  $Ba_{1-x}Gd_xF_{2+x}$  SOLID SOLUTIONS: A STUDY BY EPR AND ITC  
E.Laredo, A.Bello, and M.E.Galavis
- TH - P25  $Mn^{2+}$  ON Li-SITE IN  $LiNbO_3$  : AN ENDOR INVESTIGATION  
G.Corradi, H.Söthe, J.-M.Spaeth, and K.Polgár
- TH - P26  $Ag^{++}$  AND  $Ag^{++}-Ag^+$  CENTRES IN  $Na_xAg_{1-x}Cl$  AN ENDOR INVESTIGATION  
J.R.Niklas, U.Leonhardt, and J.-M.Spaeth
- TH - P27 EPR SPECTROSCOPY OF  $KDP:Cr^{3+}$   
D.Bravo, F.J.López, E.Diéguez, and J.M.Cabrera
- TH - P28 EPR AND ITC OF THE SUPERIONIC CONDUCTOR SYSTEM  $PbF_2-GdF_3$   
I.V.Murin, S.V.Chernov, W. Gunsser, and J.Henning
- TH - P29 THE ROLE OF IMPURITY METAL-VACANCY COMPLEXES IN THE PHOTOCHEMISTRY OF THE SILVER HALIDES  
M.T.Olm, R.S.Eachus, and R.C.Baetzold
- TH - P30 LUMINESCENT PROPERTIES OF ALKALI-EARTH ZIRCONATES DOPED BY Ti and Eu  
A.N.Belskiy, I.A.Kamenskikh, V.V.Mikhailin, A.N.Vasili'ev, I.Davoli, and S.Stizza
- TH - P31 QUANTUM EFFICIENCY OF  $Eu^{2+}$  PHOTOLUMINESCENCE IN NaCl CRYSTALS  
I. Mugeńska and R.Cywiński
- TH - P32 EFFECT OF AGGREGATION AND ENERGY TRANSFER ON OPTICAL PROPERTIES OF  $Mn^{2+}$  IONS IN NaCl:Eu, Mn AND KCl:Eu, Mn SYSTEMS  
R.Cywiński and E.Mugeński
- TH - P33 A NEW TYPE OF COLOR CENTER IN CESIUM HALIDES: F CENTER ASSOCIATED TO A PAIR OF  $OH^-$  DEFECTS  
M.Krantz, F.Lüty, V.Dierolf, and H.J.Paus

- TH - P34 NATURE OF ENERGY TRANSFER IN F CENTER/ $\text{OH}^-$  DEFECT PAIRS IN KCl TESTED WITH ANTI-STOKES RESONANCE RAMAN SCATTERING  
G.Halama, K.T.Tsen, and F. Lüty
- TH - P35 Q-SWITCHING OF A Nd:YLF PULSED LASER USING  $\text{F}_2^-$  COLOR CENTER IN LiF  
N.D.Vieira Jr., F.E.da Costa, W.de Rossi, S.L.Balochi, and S.P.Morato
- TH - P36 SENSITIZED LUMINESCENCE OF DOPED  $\text{NaNO}_2$  SINGLE CRYSTALS  
T.Schmidt, J.Köhler, and D.Schmid
- TH - P37 KINETICS OF NON-STEADY-STATE DIFFUSION CONTROLLED TUNNELING RECOMBINATION OF DEFECTS IN  $\text{KCl}, \alpha\text{-Al}_2\text{O}_3$ , DNA  
E. Kotomin, I. Tale, V. Tale, P. Butlers, and P. Kulis
- TH - P38 THE EFFECT OF DYNAMICAL DISORDERING UPON THERMOSTIMULATED PROCESSES IN IONIC CRYSTALS  
I.A.Tale, and V.G. Tale
- TH - P39 CATHODOLUMINESCENCE AND THERMOLUMINESCENCE SPECTRA OF QUARTZ  
B.J.Luff, A.C.Cox, and P.D.Townsend
- TH - P40 GENERATION-RECOMBINATION AGGREGATION OF RADIATION DEFECTS: VOLUME AND SURFACE EFFECTS IN SOLIDS  
F.Pirogov
- TH - P41 LASER DAMAGE MECHANISM REVEALED BY THE MORPHOLOGY OF DAMAGED REGIONS  
L.C.Nistor, V.Teodorescu, and S.V.Nistor
- TH - P42 RADIATION-INDUCED DEFECTS IN QUARTZ: RELEVANCE TO THE PRE-DOSE EFFECT IN THERMOLUMINESCENCE DOSIMETRY  
S.W.S.McKeever, X.H.Yang, and R.Chen
- TH - P43 THERMALLY STIMULATED CONDUCTIVITY AND LUMINESCENCE IN FLUOROPEROVSKITES  
N.Kristianpoller, B.Trieman, R.Chen, and Y.Kirsh
- TH - P44 RADIATION DEFECTS IN A  $\text{KTiPO}_4$  SINGLE CRYSTAL  
L.G.Karaseva, B.V.Andreev, and V.V.Gromov
- TH - P45 THERMOLUMINESCENCE OF  $\text{Eu}^{3+}$  AGGREGATES IN  $\text{CdF}_2$  CRYSTALS  
S.Benci, F.Fermi, and A.Nagornyj

- TH - P46 DEFECT LUMINESCENCE IN UNDOPED YAG  
G.Wu, A.Wu, R.P.Shafer, G.P.Williams,Jr., R.T.Williams, C.Y.Chen, and Y.Chen
- TH - P47 STUDY OF THRESHOLD EFFECT IN Mg-DOPED LITHIUM NIOBATE CRYSTAL  
Fengxiqi, Ying Jifong, Liu Jingchen, and Zhang Qiren
- TH - P48 EFFECT OF TEMPERATURE ON  $\gamma$ -RADIATION INDUCED I.V. DIPOLES AGGREGATION IN  $\text{KCl:Eu}^{2+}$  CRYSTALS  
H.Opyrchal, K.D.Nierzewski, B.Macalik, and M.Manfredi
- TH - P49 THERMOLUMINESCENCE AND OPTICAL ABSORPTION IN CALCIUM ALUMINATE GLASSES  
R.Verzini and A.R.Blak
- TH - P50 NUMERICAL INTEGRATION METHOD APPLIED TO THE STUDY OF ATOMIC HYDROGEN IN  $\alpha\text{-Si}:(\text{H},\text{O},\text{N})$  AND NATURAL BERYL DECAY KINETICS  
W.W.Furtado, S.Isotani, R.Antonini, A.R.Blak, and W.M.Pontuschka
- TH - P51 CHARACTERISATION OF PLANAR OPTICAL WAVEGUIDES IN ION-IMPLANTED QUARTZ  
L.Zhang, P.J.Chandler, P.D.Townsend, and F.L.Lama
- TH - P52 LUMINESCENCE OF  $\text{Al}_2\text{O}_3$  DURING ION IMPLANTATION  
A.A.AlGhamdi and P.D.Townsend
- TH - P53 CHARACTERIZATION OF SILVERIODO-SILVEROXYSALT METAL OXIDES AND A MODEL OF STRUCTURAL DEFECTS  
A.N.Durga Rani, P.Sathya Sainath Prasad, and S.Radhakrishna
- TH - P54 IR, RAMAN AND OPTICAL PROPERTIES OF  $\text{R}_2\text{MX}_4$  FERROELECTRIC CRYSTALS FOR APPLICATION IN HOLOGRAPHIC RECORDERS AS OPTICAL STORAGE ELEMENTS  
P.S.Sainath Prasad and S.Radhakrishna
- TH - P55 PHOTOTHERMAL IMAGING BY F- $\text{Z}_2$  CONVERSION IN  $\text{KCl:Gd}^{2+}$   
C.Vijayan and Y.V.G.S. Murti
- TH - P56 POINT DEFECTS IN SILICA-BASED OPTICAL FIBERS: EFFECTS ON OPTICAL PROPERTIES  
B.Poumellec, H.Février, J.M.Gabriagues, G.Lavanant, and P.Ledoux
- TH - P57 LIGHT SCATTERING AND ABSORPTION IN POLYCRYSTALLINE FIBERS  
L.N. Butvina and E.M. Dianov

- TH - P58 THEORY OF FLUORESCENCE AND AMPLIFICATION OF LIGHT BY LOCALIZED VIBRATIONS  
M.I.Dykman and V.N.Smelyanski
- TH - P59 HOLE NARROWING IN INHOMOGENEOUS SPECTRA OF DEFECTS ON BURNING BY TWO TIME-DELAYED PULSES  
I.Rebane
- TH - P60 SUM RULES OF NONLINEAR SUSCEPTIBILITIES OF MATERIAL CONTAINING DEFECTS  
K. E. Peiponen
- TH - P61 DEFECT STRUCTURE AND ELECTRICAL CONDUCTIVITY IN  $\text{LiNbO}_3$   
A.Mehta, E.K.Chang, and D.M.Smyth
- TH - P62 CATION INTERDIFFUSION IN ALKALI EARTH TITANATES  
E.P.Butler, H.Jain, and D.M.Smyth
- TH - P63 HIGH TEMPERATURE TREATED INCLUSION COMPLEXES OF ZEOLITE A AS FAST IONIC CONDUCTORS  
N.Petranović and D.Minić
- TH - P64 THE INFLUENCE OF STRUCTURE DEFECTS ON THE SPECIFIC HEAT, OPTICAL AND ELECTRICAL PROPERTIES OF  $\text{PbF}_2$ -TYPE SUPERIONIC CRYSTALS  
I.Kosacki, A.P.Litvinchuk, and M.Ya.Valakh
- TH - P65 THERMAL CONDUCTIVITY OF NEUTRON IRRADIATED OXIDES  
B.Salce and A.M. de Goer
- TH - P66 IRRADIATION EFFECTS ON DIFFUSION IN GLASSES  
P.Calmon, Y.Serruys, and G.Brebec
- TH - P67 HIGH TEMPERATURE STUDIES OF RARE EARTH FLUORIDES USING BRILLOUIN SCATTERING  
P.E.Ngoepe and J.D.Comins
- TH - P68 VISUAL OBSERVATION OF FAST CHEMICAL DIFFUSION IN STABILIZED ZIRCONIA  
E.Fredj and D.S.Tannhauser
- TH - P69 THE CHARGE SEPARATING AND RECTIFYING BEHAVIOUR OF PHASE BOUNDARIES IN SILVER HALIDE MIXED CRYSTALS  
F.Granzer, R.Kricsanowits, Th.Müssig, J.Niklas, and B.Pischel
- TH - P70 TRANSFER OF PHOTOGENERATED ELECTRONS AND HOLES THROUGH PHASE BOUNDARIES BETWEEN DIFFERENT SILVER HALIDES  
R.Alhäuser and F.Granzer

- TH - P71 SHALLOW DONOR IMPACT IONIZATION IN SEMIINSULATING GaAs  
C.Paracchini
- TH - P72 INJECTION OF CHARGE CARRIERS IN DEFECT INDUCED ALKALI HALIDES  
K.Goswami and A.K. Maiti
- TH - P73 HIGH TEMPERATURE MÖSSBAUER STUDIES OF DIFFUSION IN THE IRON OXIDES  
K.D.Becker, and V. v. Wurmb
- TH - P74 DEFECT PARAMETERS FOR SODIUM CHLORIDE FROM IONIC CONDUCTIVITY MEASUREMENTS  
I.E.Hooton and P.W.J.Jacobs
- TH - P75 EFFECT OF FRENKEL DEFECTS ON IONIC CONDUCTION AND BULK MODULUS OF  $\text{SrCl}_2$  AND  $\text{PbF}_2$   
S.Ghosh and M.Makur
- TH - P76 CALCULATED DEFECT PROPERTIES AND SUPER-IONIC TRANSITION IN  $\text{Li}_2\text{O}$   
N.L.Allan, W.C.Mackrodt, and S.Rimmington
- TH - P77 CALCULATED TEMPERATURE-DEPENDENCE OF LATTICE AND IMPURITY MIGRATION IN  $\text{MgO}$   
J.C.G.Carrol, J.Corish, and W.C.Mackrodt
- TH - P78 COHERENT NEGATIVE PHOTOVOLTAIC CURRENT AND POLAR DOMAIN INSTABILITY IN DOPED INSULATORS  
N.Kristoffel
- TH - P79 LOW-TEMPERATURE ANOMALY OF DISLOCATION MOBILITY IN PURE AND DOPED ALKALI HALIDE CRYSTALS  
Yu.S.Boyarskaya, D.Z.Grabko, and R.P.Zhitau
- TH - P80 THE CHARGE IN THE DEFECT STRUCTURE AND MECHANICAL PROPERTIES OF  $\text{LiF}$  CRYSTALS IN THE PROCESS OF POSTRADIATION ANNEALING  
M.V. Galustashvili, D.G.Driyaev, and Z.K.Saralidze
- TH - P81 MICROINDENTATION STUDIES OF SOME CHALCOGENIDE GLASSES  
D.Arivuoli, F.D.Gnanam, and P.Ramasamy
- TH - P82 FORMATION OF DEPRESSED MACROSPIRALS IN THE FLUX GROWN YAG CRYSTALS  
M.Thirumavalavan, J.Kumar, F.D.Gnanam, and P.Ramasamy

- TH - P83 STRAIN-AGEING EFFECTS IN PURE AND DOPED SILVER HALIDE CRYSTALS  
J.A.Bellis and M.T.Sprackling
- TH - P84 CRACKS AND PLASTIC DEFORMATION IN AN INDENTATION IN MgO  
M.R.Dalmau Garcia
- TH - P85 MICROSTRUCTURE AND PHYSICAL PROPERTIES OF YTTRIA-STABILIZED  $ZrO_2$ (YSZ) DOPED WITH  $WO_3$   
M.Hartmanová, F.Hanic, A.A.Urusovskaya, I.Travěnek, E.Morháčová, and G.G.Knab
- TH - P86 SEM, EDS & DISLOCATION ETCHING STUDIES ON FLUX GROWN SUBSTRATE CRYSTALS FOR LIQUID PHASE EPITAXIAL GROWTH OF HEXAFERRITE FILMS  
P.N.Kotru, F.Licci, and G.Salviati
- TH - P87 MICROHARDNESS MEASUREMENTS ON FLUX GROWN PURE, DOPED AND MIXED RARE EARTH ALUMINATE AND ORTHOCHROMITE CRYSTALS  
P.N.Kotru, A.K.Razdan, and B.M.Wanklyn
- TH - P88 TWO-PARAMETERS DESCRIPTION OF  $Eu^{2+}$  DISTRIBUTION IN KCl SINGLE CRYSTAL  
M.Czapelski and T.Morawska-Koval
- TH - P89 GROWTH DEFECTS IN BARIUM-STRONTIUM NIOBATE CRYSTALS  
Yu.S. Kuz'minov, L.I. Ivleva, and N.M. Polozkov
- TH - P90 TIN OXIDES IN THIN FILMS  
D.D.Nihtianova, S.K.Peneva, and L.L.Petrov
- TH - P91 PHASE AND CHEMICAL INHOMOGENEITY OF  $PbMoO_4$  SINGLE CRYSTALS  
M.P.Tarasov, D.D.Nihtianova, and M.N.Maleev
- TH - P92 OXYGEN VACANCY ORDERING IN THE  $BaFeO_{3-y}$  AND  $Ba_xLa_{1-x}FeO_{3-y}$  SYSTEMS  
J-C Grenier, M.Parras, J.M.Gonzales-Calbet, M.Vallet-Regi, and M.Pouchard
- TH - P93 INHOMOGENEITIES AND THE SPURIOUS MODES IN  $GaYIG$   
E.Beregi, L.Fetter, G.Nagy, and E.Pál
- TH - P94 NONSTOICHIOMETRY DEFECTS IN  $A^2B_2C_6$  COMPOUND  
S.I. Radautsan, I.M. Tiginyanu, and Yu.O. Derid

- TH - P95 SOME CONNECTIONS BETWEEN LUMINESCENCE PROPERTIES AND LATTICE POINT DEFECTS IN  $\text{Y}_2\text{SiO}_5:\text{Tb}^{3+}$   
R.Morlotti, A.Viglienzoni, S.Kemmler-Sack, and J.Reichardt
- TH - P96 NEAR-ELECTRODE REGIONS IN AN ELECTROCHEMICAL CELL OF  $\text{Ag}/\text{RbAg}_4\text{J}_6/\text{Me}$  TYPE AS STUDIED BY OPTICAL METHODS  
A.V.Boris, S.I.Bredikhin, N.N.Kovaleva, and N.V.Lichkova
- TH - P97 THE ELECTRICAL AND STRUCTURAL PROPERTIES OF TIN OXIDE  
A.V.Chadwick, R.M.Geatches, J.M.Steele, J.D.Wright, S.J.Peacock, and S.M.Tomlinson
- TH - P98 A MODEL OF NEAR-UV-PHOTOEMISSION FROM CATION-VACANCY-BONDED  $\text{H}_2\text{O}$  ON ALKALI FLUORIDE (100) FACES  
L.Ernst
- TH - P99 PHOTOINDUCED PROCESSES IN ARSENIC AND ANTIMONY CHALCOGENIDES  
V.Pashkevich, V.Gerbreder, and A.Cvetkov
- TH - P100 LOW FREQUENCY RAMAN SCATTERING FROM METAL COLLOIDS IN  $\text{NaCl}$   
G.Mariotto, M.Montagna, G.Viliani, E.Duval, and C.Maï

#### SESSION 8

- 8 - L1 SYNCHROTRON RADIATION STUDIES OF DEFECTS IN SOLIDS  
A.V. Chadwick
- 8 - L2 QUASIELASTIC DIFFUSE NEUTRON SCATTERING TO STUDY DEFECTS AND DISORDER IN IONIC MATERIALS  
M.T. Hutchings

#### SESSION 8A - Applications

- 8A - O1 INFRARED CHARACTERIZATION OF TRITIUM IN  $\text{LiNbO}_3$  SINGLE CRYSTALS  
R.González, C.Ballesteros, Y.Chen, and M.M.Abraham
- 8A - O2 COMPUTED PROPERTIES OF CHARGED DEFECTS IN ALKALINE - EARTH FLUOROHALIDE CRYSTALS  
R.C. Baetzold

- 8A - O3 ISOTOPE AND ANHARMONICITY EFFECTS ON OH<sup>-</sup> DIPOLES PERTURBED BY Mg-INDUCED DEFECTS IN LiF AND NaF  
R.Capelletti, W.Beall Fowler, I.Földvári, and L.Kovács
- 8A - O4 MICROSCOPIC PROBING OF THE DYNAMICS OF Ti IONS IN BaTiO<sub>3</sub> BY NMR  
A.Hackmann, O.Kanert, H.Kolem, H.Schulz, K.A.Müller, and J.Albers
- 8A - O5 COLOR CENTERS WAVEGUIDES ON ALKALI HALIDES: FIRST MEASUREMENTS OF THE INSERTION LOSS  
H.J.Kalinowski, L.C.Scavarda do Carmo, R.A.Nunes, and S. Paciornik
- 8A - O6 INTRINSIC DEFECT IN SiO<sub>2</sub> GLASSES AND CRYSTALS  
A.R.Silin

#### SESSION 8B - Radiation damage and ion implantation

- 8B - O1 RADIATION DEFECT BEHAVIOR IN UO<sub>2</sub> - A CHANNELING STUDY  
A.Turos, Hj.Matzke, and S.Fritz
- 8B - O2 V<sub>k</sub> CENTERS IN TETRAHALIDES  
A. Martín, and F.J. López
- 8B - O3 ANNEALING BEHAVIOUR OF THE LOW TEMPERATURE PROPERTIES OF NEUTRON-IRRADIATED QUARTZ CRYSTALS  
L.Michiels, N.Vanreyten, and I.Mangelschots
- 8B - O4 LOW TEMPERATURE THERMOLUMINESCENCE AND PHOSPHORESCENCE OF X-IRRADIATED Ge-DOPED QUARTZ  
A.Halperin
- 8B - O5 A SELF TRAPPED HOLE IN ALKALI SILVER HALIDE CRYSTALS  
T.Awano, T.Nanba, M.Ikezawa, T.Matsuyama, and H.Yamaoka
- 8B - O6 Nd:YAG LASER STIMULATED LUMINESCENCE AT ROOM TEMPERATURE IN THERMOCHEMICALLY REDUCED AND IN NEUTRON IRRADIATED MgO  
K.Chakrabarti, V.K.Mathur, and G.P.Summers

#### SESSION 9A - Impurities II

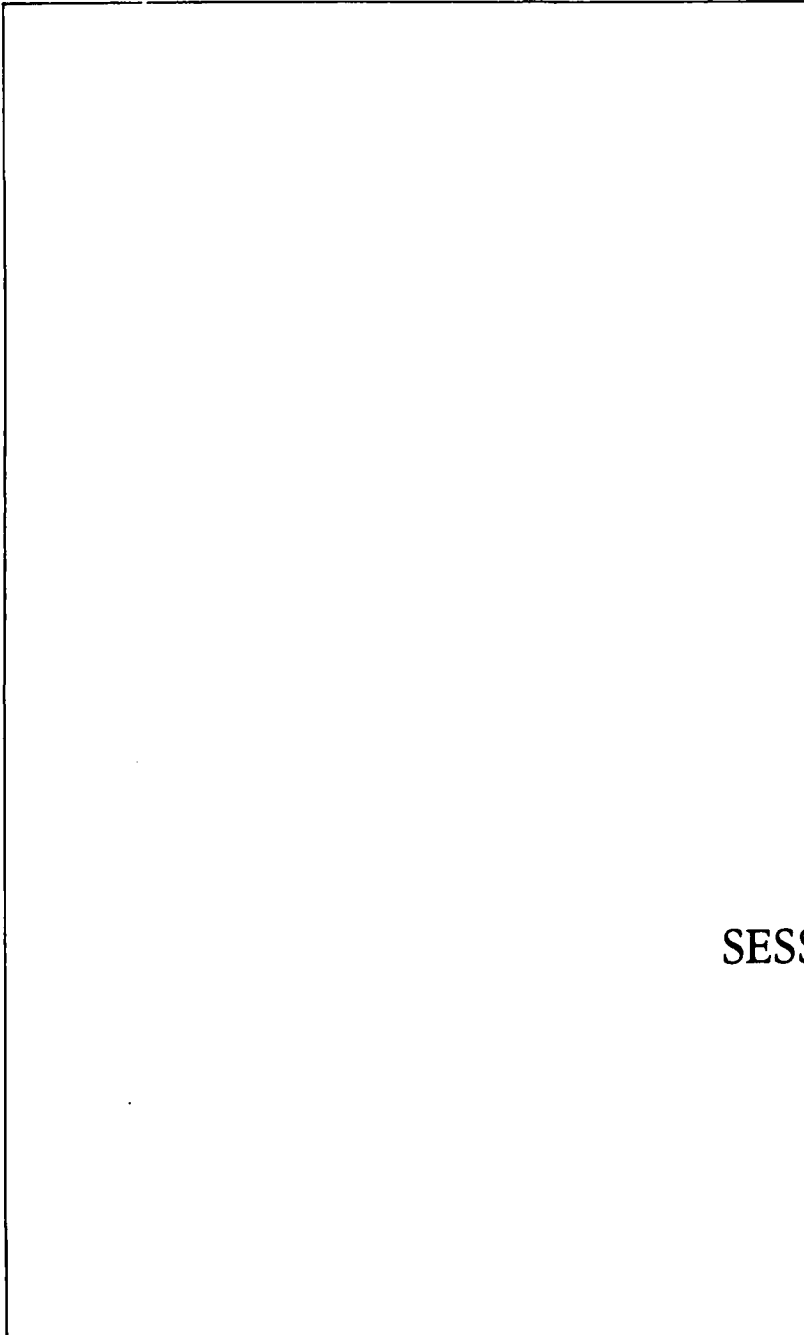
- 9A - O1 THEORY OF DEFECTS IN SILICON DIOXIDE: E' CENTERS NEAR THE SiO<sub>2</sub>-Si INTERFACE  
Andrew X. Chu and W. Beall Fowler

- 9A - 02 EVIDENCE FOR A TEMPERATURE DEPENDENT TUNNELING PARAMETER  
F.Bridges and M.Jost
- 9A - 03 TWO-PHOTON SPECTROSCOPY IN  $\text{Ag}^+$  DOPED ALKALI HALIDES  
M.Casalboni, R.Francini, U.M.Grassano, and F.G.Lohmeier
- 9A - 04 EPR STUDY OF JAHN-TELLER EFFECT IN  $\text{Ag}^{2+}:\text{KLiSO}_4$  CRYSTALS  
Y.Ravi Sekhar and H.Bill
- 9A - 05 SIMULATION OF F-TYPE CENTERS AND HYDROGEN ANIONS IN  $\text{MgO}$   
R. Pandey and J.M.Vail

SESSION 9B - Dislocations and diffusion

- 9B - 01 PLASTIC ANISOTROPY IN  $\text{CoO}$  SINGLE CRYSTALS  
F.Guiberteau, A.Dominguez-Rodriguez, and J.Castaing
- 9B - 02 ATOMISTIC CALCULATION OF POINT DEFECT INTERACTION WITH DISLOCATION IN  $\text{NiO}$   
J.Rabier, J.Soullard, and M.P.Puls
- 9B - 03 A DIRECT EVIDENCE OF DISLOCATION DISSOCIATION IN THE  $\text{NaCl}$ -STRUCTURE  
A.Foitzik, W.Skrotzki, and P.Haasen
- 9B - 04 DISLOCATION INTERSECTION IN  $\text{NaCl}$  SINGLE CRYSTALS  
F.Appel
- 9B - 05 DIFFUSION OF  $\text{Zn}^{2+}$  IN  $\text{AgBr}$  AND  $\text{AgCl}$  - EVIDENCE FOR NONLINEAR TEMPERATURE DEPENDENCE OF GIBBS FREE ENERGY FOR DEFECT FORMATION, ASSOCIATION AND MOTION  
A.L. Laskar, S. Betarbet, and J. Laskar

ABSTRACTS



SESSION 1

COUPLING AND ENERGY TRANSFER BETWEEN F CENTERS AND MOLECULAR DEFECTS\*Fang Rong, Yihong Yang<sup>†</sup> and Fritz Luty

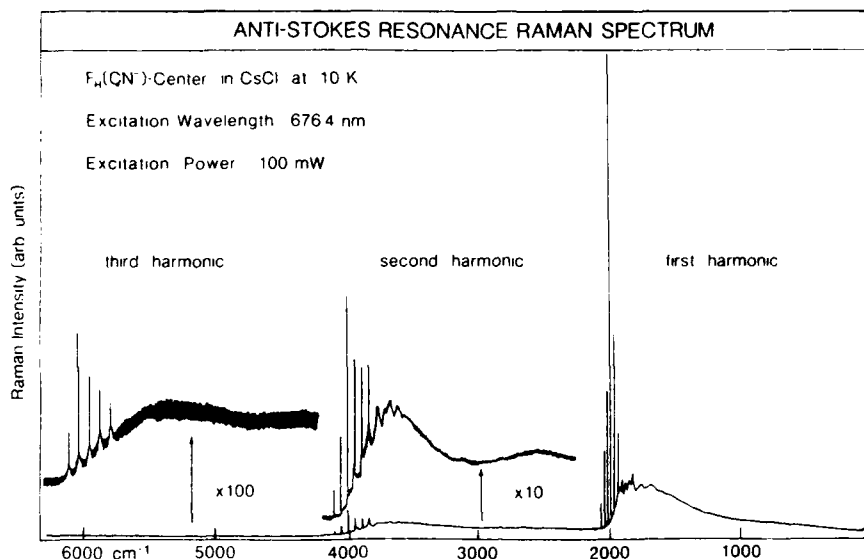
Physics Department, University of Utah, Salt Lake City, Utah 84112, USA

Association of the most simple electronic (e) and vibrational (v) "model-defects" in alkali-halides--F centers and molecular ions--has created a new class of defect pairs, characterized by unusual (e - v) energy transfer as well as (e) and (v) radiative and non-radiative relaxation processes on totally different time-scales. Besides mentioning some essential results on F centers associated to other molecular partners (like OH<sup>-</sup>, OD<sup>-</sup>...), we concentrate in this survey on the F center-CN<sup>-</sup> pair ("F<sub>H</sub>(CN<sup>-</sup>) center"), most extensively studied with optical absorption, (e) and (v) fluorescence, and Stokes and anti-Stokes resonance Raman scattering techniques.

The electronic absorption of the F<sub>H</sub>(CN<sup>-</sup>) defects covers a wide range of behavior under host material variation between two extremes: from only slightly broadened and red-shifted F<sub>H</sub>-absorption (compared to the F band) in KCl--to a distinct splitting<sub>H</sub> into separated F<sub>H</sub>(1) and F<sub>H</sub>(2) bands, polarized || and ⊥ to the <100> pair axis in CsCl. Fluorescence behavior covers a similar wide range: small reduction of the electronic F<sub>H</sub> emission and weak vibrational CN<sup>-</sup> emission only between its lowest v = 1 → 0 states in KCl--in contrast to total electronic emission quenching under appearance of a cascade of emission-transitions between the 7 lowest CN<sup>-</sup> v-states in CsCl. These results indicate a strong variation in (e - v) energy transfer strength between the excited F<sub>H</sub> electron and CN<sup>-</sup> ion--from a very weak one in KCl to the strongest one in CsCl (with an abrupt jump between hosts of NaCl and CsCl structure). Besides this not yet understood variation, the most basic question remains unanswered: How, at what stage, and in what time-scale of the "optical cycle" does the e - v transfer occur?

A powerful technique to approach these questions are Raman measurements, in which the CN<sup>-</sup> attached F center is used in a two-step way: By pumping with the same laser beam, one can both populate by (e - v) energy transfer non-equilibrium CN<sup>-</sup> vibrational states, and probe their existence and physical properties<sup>1,2</sup> by anti-Stokes resonance Raman scattering. Recent first experiments<sup>1,2</sup> with this technique on F<sub>H</sub> centers in CsCl<sub>1</sub> and CsBr, were restricted to the narrow spectral region around 2000 cm<sup>-1</sup>, where the first harmonic CN<sup>-</sup> stretching modes occur, thus missing significant parts and important features of the Raman behavior.

As one example from measurements in many hosts of CsCl and NaCl structure, Fig. 1 shows a survey-picture of our anti-Stokes<sub>1</sub> resonance Raman results on F<sub>H</sub>(CN<sup>-</sup>) in CsCl, covering the total 0 - 6400 cm<sup>-1</sup> energy region. Obviously we observe anti-Stokes resonance Raman transitions between CN<sup>-</sup> vibrational levels in first, second, and even third harmonic, with a relative reduction factor between successive harmonics as small as ~20. Probably the most unexpected new result is the observation of a broad and unsymmetric anti-Stokes band starting abruptly at the first sharp CN<sup>-</sup> vibrational transition in each harmonic and expanding far beyond all the sharp lines towards the low energy side. The total intensity of the broad band is in each harmonic at least one order of magnitude higher than the sum of all sharp CN<sup>-</sup> lines. Obviously the anti-Stokes Raman process, triggered by resonance excitation of the coupled F center, occurs (in contrast to vibrational emission) only to a small fraction in sharp purely CN<sup>-</sup> vibrational Δv = 1,2,3 transition in the different harmonics, while its major part appears as quasi-continuous transitions apparently involving rotational and/or phonon states between the CN<sup>-</sup> vibrational levels.



Besides different selection rules for ir fluorescence and resonance Raman transitions, their time-scale is very different: spontaneous  $CN^-$  ir fluorescence occurs in the msec range, while the average time between pumping and Raman-probing of each  $F_H(CN^-)$  defect is  $\sim 0.1 - 1 \mu\text{sec}$  in our experiments. This can play important roles in determining the relative population of different excited v-states of  $CN^-$  with both experiments: while the "slow" ir fluorescence shows in hosts of the NaCl structure (e.g. KCl) only transitions from the  $v = 1$  state, the "quick" Raman-probe shows (in KCl, RbCl and KBr) occupation of states up to  $v = 5$ , with maximum population at  $v = 3$ . Obviously rapid relaxation processes depopulate these higher states, before slow vibrational emission can occur. In contrast to this, both ir and Raman data show in CsCl the same v-state population with a maximum at  $v = 4$ , indicating that after e - v transfer all relaxation processes occur slowly and as a cascade of fluorescence. Additional measurements of the "upward"  $\Delta v$  Raman Stokes-transitions allow us to determine also the population of the ( $v=0$ ) ground state relative to the excited v-states. After the  $\sim \mu\text{sec}$  pump/Raman-probe delay-time we find almost 100% of the  $CN^-$  still in excited states for CsCl--but only  $\sim 25\%$  for KCl. While in CsCl  $F_H(1)$  and  $F_H(2)$  band excitation produces similar (e-v) transfer effects both in ir and Raman, excitation variation across the inhomogeneously broadened  $F_H$  band in KCl show that the e-v transfer efficiency (measured in Raman and ir emission strength) is much stronger on the low energy side of the band, showing the existence of unresolved but differently directed and (e-v) coupled 2p states in this system. Our attempts to interpret these extended results consistently in a model leave basic questions still open as a challenge for further experimental and theoretical approaches.

\*Supported by NSF grant DMR 87-06416

†Yihong Yang died tragically from a severe disease February 3, 1988.

1) K.T. Tsen, G. Halama, F. Luty, Phys. Rev. **36**, 9247 (1987).

2) G. Cachei, H. Stolz, W. von der Osten, F. Luty (paper in this meeting).



SESSION 1A

OPTICAL AND THERMAL BISTABILITY OF TWO  $F_H(OH^-)$  CENTER CONFIGURATIONS  
IN KBr and KI

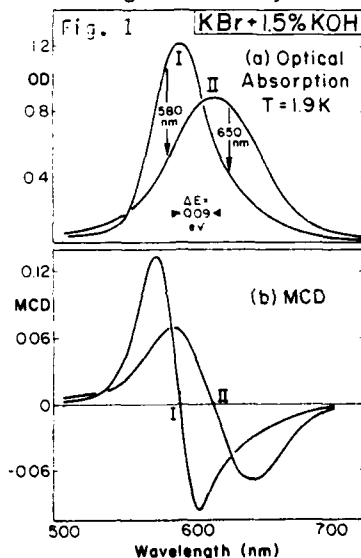
G. Baldacchini, S. Botti, U.M. Grassano  
ENEA CRE Frascati-00044 Frascati (Italy)

and

Laercio Gomes and Fritz Luty\*

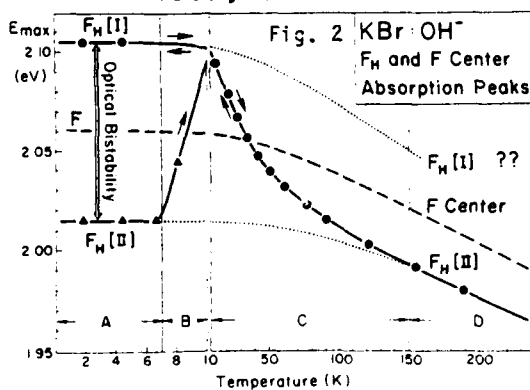
Physics Department, University of Utah, Salt Lake City Utah U.S.A.

Optical and magneto-optical (MCD) studies of  $F_H(OH^-)$  centers in KBr (using the same technique as in the previous paper) led to the discovery of an interesting bistability for this defect pair. After optical association of



$F$  centers with  $OH^-$  defects, the  $F_H(OH^-)$  pairs show at 1.9 K an absorption band (peak at 588 nm) and a related MCD spectrum as shown under "I" in Fig. 1. Weak optical irradiation at ~580 nm converts these spectra into red-shifted and broadened absorption- and MCD-spectra marked "II". As indicated in Fig. 1 optical irradiation at 650 nm reconverts the spectra II back into the spectra I. This bi-directional conversion of high quantum-efficiency obviously creates two different configurations I and II of the  $F$  center/ $OH^-$  pair, both characterized by essentially the same spin-orbit parameter and high thermal stability at  $T \leq 4.2$  K. (The partial overlap of their absorptions prevents total optical conversion and exact measurement of the "pure"  $F_H[I]$  and  $F_H[II]$  center spectra).

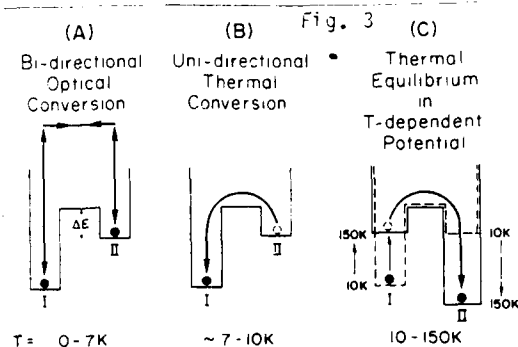
The question for the thermal development of the bistability is addressed in Fig. 2, showing the measured  $F_H$  absorption peak position--compared to the  $F$  band peak--in KBr under cooling. Above ~150 K (range "D") the



$F_H$  peak is located on the red side of the  $F$  band and follows closely its "normal" temperature variation (partially produced by thermal lattice expansion). Cooling below 150 K (range "C") produces an abnormally strong blue-shift of the  $F_H$  band, intersecting the  $F$  band position and placing it on the high energy side of  $F$  at its final 2.105 eV low temperature value. Only in the  $T < 7$  K range "A" bistability works and optical conversion into the strongly red-shifted band II can be achieved. If heating beyond  $T = 7$  K is done with the

$F_H$  center in the blue-shifted state I, the peak position follows exactly the cooling curve. However, if started from the red  $F_H[II]$  state, thermal conversion from II to I occurs in the narrow range B ( $7-10$  K), so that under further heating above  $10$  K the same  $E_{\max}(T)$  behavior is obtained as under cooling.

A tentative interpretation is illustrated in Fig. 3 using a simple box-potential model with unequal energies  $E(I) < E(II)$  for the two configurations, remaining unchanged up to  $\sim 10$  K. In range "A" ( $T < 7$  K) the energy barrier height  $\Delta E$  from well II is  $\Delta E > kT$  such that no thermal exchange but bi-directional optical conversion can take place. For  $T > 7$  K (range B)  $\Delta E \approx kT$  and uni-directional thermal  $II \rightarrow I$  conversion into the deeper well occurs. Above



$10$  K it is reasonable that temperature effects (e.g. lattice expansion) start to produce changes in the unequal well potential. We assume that the  $10$  K situation  $E(I) < E(II)$  with thermal equilibrium  $n(I) > n(II)$  changes gradually under temperature increase into the opposite one, such that  $n(II) > n(I)$  is obtained at  $\sim 150$  K and for even higher temperature (range D) essentially only the configuration II is occupied. This is supported by the fact that for  $T > 150$  K the "normal F-center-type"  $E_{\max}(T)$  behavior is observed; extrapolation of this normal T-dependence (lower pointed curve in Fig. 2) through range C leads at low temperature into the optically produced stable  $F_H[II]$  configuration. Similarly a thermal persistence of the pure  $F_H[I]$  system when heating from low temperature into range C could lead to the upper dotted line extrapolation in Fig. 2.

An important question remains open so far: what is the microscopic structure of the two  $F/OH^-$  pair configurations I and II? The fact that their low temperature absorptions lie blue- or red-shifted nearly symmetrically (by  $\pm 0.045$  eV) from the F band, suggest in a simple Ivey law picture a contraction or expansion of the effective vacancy volume by about  $\pm 3\%$  due to two different arrangements of the neighboring  $OH^-$  molecule. Tentative models, involving various positional shifts, dipole orientations or lattice site changes of the  $OH^-$  defect relative to the F center will be discussed. Any model must account for the fact that  $I \leftrightarrow II$  exchange occurs with small thermal activation above  $7$  K without light excitation, i.e. in the electronic ground state of the defect pair. Conclusive evidence about the microscopic structure of the two configurations are expected to be obtained from optically detected ENDOR studies. Results applying this powerful technique are reported in a separate paper on this meeting<sup>1</sup>.

It should be mentioned at least, that we obtained similar results about bistability of two  $F_H(OH^-)$  configurations in  $KI:OH^-$ . Details about this system will be reported.

\*Supported by NSF grant DMR 87-06416

(1) M. Jordan, H. Söthe, J.M. Spaeth and F. Lüty (see abstract in Proceedings of this Conference).

# MICROSCOPIC STRUCTURE AND BISTABILITY OF $F_H^-$ CENTRES IN ALKALI HALIDES

M. Jordan, H. Söthe, J.-M. Spaeth and F. Lüty\*

University of Paderborn, Fachbereich Physik, Warburger Str. 100 A, 4790 Paderborn, FRG

\*Physics Department, University of Utah, Salt Lake City, Utah 84112, USA

$F_H^-$ -centres are formed by associating F-centres to defect anions or defect molecules in alkali halides. Especially the  $F_H(OH^-)$ - and  $F_H(CN^-)$ -centres are very interesting in view of laser activity in the infrared. While an optical pumping of the  $CN^-$  vibration via the F-centre excitation has been observed /1/, the  $OH^-$  as dopant only quenches the F-centre emission /2/.

To determine the structure of these  $F_H^-$ -centres, both the  $F_H(OH^-)$ - and the  $F_H(CN^-)$ -centres in KCl were investigated by ENDOR. After associating the F-centres to  $F_H^-$ -centres new ENDOR lines appear in the spectrum superimposed to the ENDOR lines of the remaining F-centres ( $\approx 50\%$ ). The ESR spectrum does not show any difference after the  $F_H^-$ -formation.

The  $F_H(OH^-)$ -centre is a F-centre with the  $OH^-$  defect molecule in a [200]-position and has tetragonal symmetry. Because of the presence of the  $OH^-$  the nearest  $K^+$ -neighbours are split into three types with different superhyperfine interactions. One of them is shifted from the F-centre towards the  $OH^-$  by about 9%. From the temperature dependence of the shf interactions it could be concluded that both- this distorted  $K^+$  neighbour and the  $OH^-$ -vibrate in an anharmonic potential. This result is very similar to that of previous measurements on the  $F_H(F^-)$ -centres in KCl /3,4/.

Contrary to the  $F_H(OH^-)$ -centre the  $F_H(CN^-)$ -centre has [110]-symmetry, the  $CN^-$ -molecule occupying a nearest neighbour  $Cl^-$  vacancy. Because of the nearly equal ion size of  $CN^-$  and  $Cl^-$  the lattice distortion in the neighbourhood of this centre is much smaller. The ENDOR lines of  $^{13}C$ , in  $^{13}CN^-$  doped crystals, are split into a dublett, due to the different [111]-orientations of the  $CN^-$  defect molecule in the crystal. This splitting and the superhyperfine interaction itself depend on the temperature and change strongly between

30K and 50K. The  $\text{CN}^-$  molecule is situated such that C is not on the centre position of the  $\text{Cl}^-$  vacancy /5/.

A novel feature is found for  $\text{F}_\text{H}(\text{OH}^-)$ -centres in KBr. They show for temperatures below 4.2K a bistability. By bleaching the  $\text{F}_\text{H}$ -absorption band in the high energy part, a new band at lower energy appears. This bleaching can be reversed reproducibly from the 'blue' band into the 'red' one and vice versa. ENDOR measurements were performed by optical detection using the magnetic circular dichroism (MCD) of the absorption /6/. The ENDOR lines of the 2<sup>nd</sup> shell  $\text{Br}^-$  neighbours have a lower symmetry in both centres compared to F-centres and are markedly different from each other. From a preliminary analysis of the ENDOR angular dependencies it is concluded that the  $\text{OH}^-$  occupies different sites in both centres. In the 'red'  $\text{F}_\text{H}(\text{OH}^-)$ -centre it is on a [200]-position, while in the 'blue' centre it is on a nearest [110]-position. The details of structures are discussed.

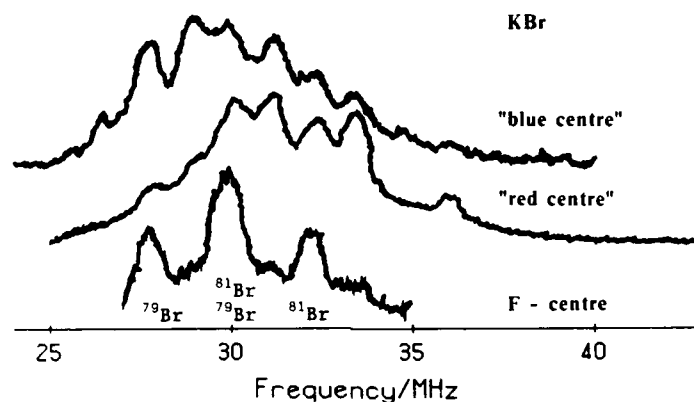


Fig. 1 ODENDOR lines of second shell  $\text{Br}^-$  neighbours,  $B_0 // [100]$ ,  $T = 1.6\text{K}$ ,  $\nu_{\text{ESR}} = 24\text{GHz}$ . The spectra were digitally filtered.

- /1/ Y. Yang and F. Lüty, Phys. Rev. Lett. 51, 419 (1983).
- /2/ L. Gomes and F. Lüty, Phys. Rev. B30, 7194 (1984).
- /3/ H. Söthe, P. Studzinski and J.-M. Spaeth, phys. stat. sol. (b) 130, 339 (1985).
- /4/ H. Söthe, P. Studzinski and J.-M. Spaeth, International conference on DEFECTS IN INSULATING CRYSTALS; Utah, Salt Lake City (1984)
- /5/ M. Jordan, Diplomarbeit Paderborn (1987)
- /6/ D.M. Hofmann, B.K. Meyer, F. Lohse and J.-M. Spaeth, Phys. Ref. Lett., 53, 1187 (1984)

SPIN-ORBIT COUPLING OF  $F_H(OH^-)$ -CENTERS IN CESIUM HALIDES

V. Dierolf and H.J. Paus

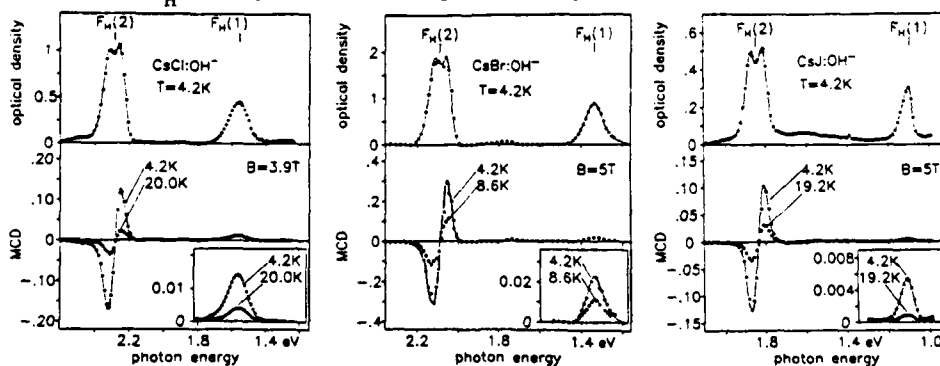
Physikalisches Institut, Universität Stuttgart, D-7000 Stuttgart W.-Germany

Fritz Luty \*

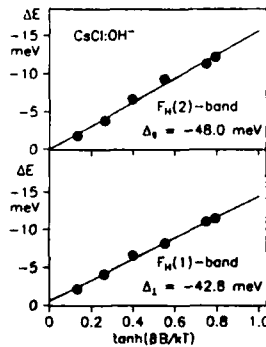
Physics Department, University of Utah, Salt Lake City, Utah USA 84112

$F$  centers with n.n. cationic impurity neighbors in hosts with fcc (NaCl) structure form  $F_A$  centers of tetragonal  $C_{4v}$  symmetry, characterized by splitting of the  $F$  band into two  $F_A(1)$  and  $F_A(2)$  absorptions polarized  $\parallel$  and  $\perp$  to the  $\langle 100 \rangle$  axis of the defect pair. The splitting  $\Delta E$  never exceeds 0.28 eV, and the typical negative and anisotropic spin orbit energies have been measured by MCD and satisfactorily explained theoretically<sup>1,2</sup>.

In cesium halides, only n.n.n. anionic defects can produce defect pairs (" $F_H$  centers") of the same  $C_{4v}$  symmetry. Recent investigations on the interesting  $F_H(CN^-)$  and  $F_H(OH^-)$  defects have shown<sup>3</sup> that the presence of a n.n.n.  $OH^-$  defect produces an unusually large ( $\sim 0.7$  eV) splitting of the  $F$  band. These spectral properties make  $F_H(OH^-)$  defects in cesium halides a very interesting subject for spin orbit investigations of their non-relaxed excited states with MCD techniques; particularly they are model cases to test the validity of the established theories under extension to this extreme case of very wide splitting. Fig. 1 illustrates for  $F_H(OH^-)$  defects in the 3 cesium-halides the  $F_H(1)$  and  $F_H(2)$  absorption and MCD spectra; the latter consist of large (derivative-shaped)  $F_H(2)$  signals, and very small  $F_H(1)$  signals (following spectrally the band).



Taking into account that no preferential alignment of defect orientations occur, we used two treatments for analysis and interpretation of the MCD data. The HSS moment method<sup>2</sup> allows us to determine the SO parameters  $\Delta_{\perp}$  and  $\Delta_{\parallel}$  from the measured B/T dependence of the  $F_H(1)$  and  $F_H(2)$  band MCD effect (Fig. 2). On the other hand, a simple atomic SO model used with tetragonal crystal field in perturbation theory, yields only one isotropic SO parameter  $\Delta$  related directly to the observed splitting of the  $F_H(2)$  band. All these calculated data, obtained from MCD measurements of  $F_H$  and F centers (in the same crystal and apparatus), are listed in table I.



	$F_H(OH^-)$ -Center			F-Center Moment Analysis
	Moment Analysis $\Delta_{\parallel}$	Atomic Model $\Delta_{\perp}$	$\Delta$	
CsCl	-48.0 meV	-42.8 meV	-99 meV	-43.6 meV
CsBr	-50.8 meV	-47.6 meV	-100 meV	-48.2 meV
CsI	-57.0 meV	-53.5 meV	-91 meV	-55.2 meV

The difference in the  $\Delta$  results obtained from the simple atomic model and the more exact HSS moment analysis suggests that besides spin-orbit interaction, coupling with lattice vibrations contributes additionally to the splitting of the  $F_H(2)$  band--similar as shown for the F center in Cs-halides<sup>4</sup>. The SO anisotropy (difference between  $\Delta_{\parallel}$  and  $\Delta_{\perp}$ ) was well explained for the  $F_A$ -centers. This interpretation can be easily transferred to the case of  $F_H(OH^-)$  defects and yields good agreement with the measurements if one regards that the influence on SO coupling by an  $OH^-$  impurity is smaller than that of the replaced host anion ( $Cl^-$ ,  $Br^-$ ,  $I^-$ ).

\* Supported by NSF Grant DMR 87-06416

1. H.J. Paus, D.Y. Smith, Intern. Conf. on Defects in Insulating Crystals, Salt Lake City, pg. 361 (1984).
2. Ch. Henry, St. E. Schnatterly, C.H. Slichter, Phys. Rev. **137**(2), A 583 (1965).
3. M. Krantz and F. Luty, Phys. Rev. **B37**, May 15 edit. (1988).
4. P.R. Moran, Phys. Rev. **137**(3) A 1016 (1965).

# MAGNETO-OPTICAL PROPERTIES OF $F_2^+$ CENTERS IN KCL CRYSTAL

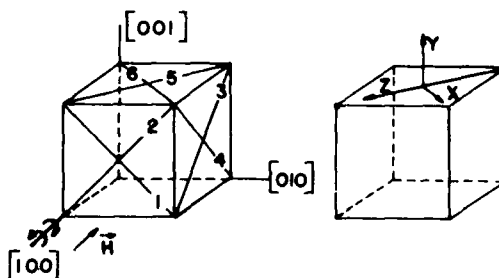
D.A. Donatti and M.A. Aegerter, Instituto de Física e Química de São Carlos, University of São Paulo, Caixa Postal 369, 13560 São Carlos, SP (Brasil).

T.Iida, Department of Physics, Osaka City University, 558 OSAKA (Japan)

The formation and the optical properties of  $F_2^+$  center in ionic crystals, an electron bound to the double well potential of two  $[110]$  nearest neighbors anionic vacancies, have been studied by Aegerter et al <sup>(1)</sup>. The presence of other active defects such as  $F$ ,  $F^-$  and  $F_2$  centers had always impeded further optical studies. A process developed by Gellermann et al <sup>(2,3)</sup> for KCL :  $SH^-$  or  $OH^-$  give the possibility to obtain systems of pure  $F_2^+$  centers allowing for the first time a complete study of the magneto-optical properties of these prototype  $H_2^+$  like molecular-ion.

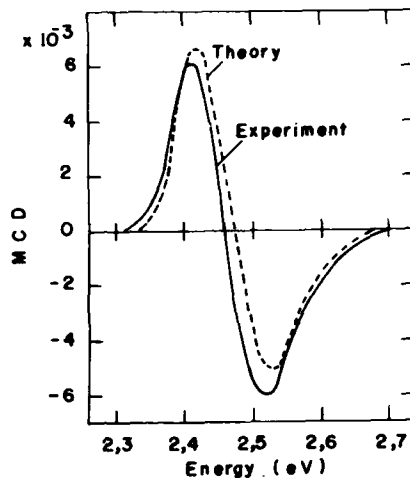
The Magnetic Circular Dichroism (MCD) has been studied between 1,5 and 300K and for field up to 5T <sup>(4,5)</sup>. In absorption the MCD has been only observed in the  $1s\sigma_g \rightarrow 2p_y\pi_u$  and  $1s\sigma_g \rightarrow 2p_x\pi_u$  transitions at 493 and 509 nm respectively. No dichroism has been observed in the infra-red transition  $1s\sigma_g \rightarrow 2p\sigma_u$  at 1,4  $\mu m$  and in both emissions  $2p\sigma_u^* \rightarrow 1s\sigma_g^*$  and  $2p\pi_u^* \rightarrow 1s\sigma_g^*$  within our detection limit ( $2 \cdot 10^{-4}$ ). In the configuration shown in figure 1 we found that only the defects lying in the directions 3,4,5 and 6 present a MCD.

Fig.1 - Scheme of the position, direction of light and field and representation of the electrical dipole transition of  $F_2^+$  centers in a typical experiment.



The spectral variation of the MCD has been calculated using the perturbation theory at first order with a hamiltonian including a spin-orbit interaction in the  $2p\pi_u$  levels and molecular orbital wave functions obtained as a linear combination of atomic orbital of the  $1s$  and  $2p$  type. Figure 2 shows a comparison of the experimental and theoretical results obtained for a spin orbit coupling  $\zeta_z = 3,6$  meV.

Fig. 2 - Experimental and theoretical DCM spectra of the  $1s\sigma_g \rightarrow 2p\pi_u$  transition.  $T=4.2K$ ,  $H=1.97T$ ,  $\int_{-t} = 3.6meV$



The  $F_2^+$  ground state EPR has been detected optically (X-band). Only one band has been observed with  $\vec{H} \parallel [100]$  and  $[110]$  giving an isotropic  $g=1.965 \pm 0.007$  and a half width of  $80 \pm 5$  Gauss. The spin-lattice relaxation time measured at 3.2KG was found to obey a direct process  $T_1^{-1} = 4,3 \cdot 10^{-2} \cotgh(g\beta H/2kT)$  for  $3 < T < 11K$ .

#### Acknowledgements:

The authors are grateful to Prof. F. Lüty for kindly providing the  $KCL:SH^-$  crystals and to FAPESP, CNPq and FINEP (Brasil) for the financial support of this work.

#### References:

1. M.A. Aegerter and F. Lüty, Phys. Stat. Sol. (6) 43, 227 and 245 (1971).
2. W. Gellermann, F. Lüty, K.P. Koch and H. Welling, Optics Communications, 35, 430 (1980).
3. W. Gellermann, F. Lüty, K.P. Koch and G. Litfin, Phys. Stat. Sol. (a), 57, 411 (1980).
4. D.A. Donatti, Ph.D. thesis, University of São Paulo (1987).
5. D.A. Donatti, M.A. Aegerter and T.Iida, to be published..

ON SPECTRORADIOMETRIC STUDY OF KCl CRYSTALS  
DURING ELECTROLYTIC COLOURATION

P. Raerinne and P. Ketolainen

Väisälä Laboratory, Department of Physics, University of Joensuu,  
P.O. Box 111, SF-80101 Joensuu, Finland

Electrolytic colouration is one of the methods to produce colour centres into alkali halide crystals. Although the method is known from the 1930s, no spectroscopic studies simultaneously with the colouration process has been carried out. The process is, especially at higher temperatures, so quick that one can not use conventional spectrographic methods to record the absorption spectrum of the coloured crystal. Nowadays high-speed scanning spectroradiometers offer an excellent tool for this purpose. Based to a photodiode array and containing no moving gratings or mirrors they can measure the whole spectrum simultaneously within few seconds.

We have used a spectroradiometer to record and store spectra of undoped KCl crystals during the electrolytic colouration at different temperatures. Measurements were carried out by projecting an enlarged picture of the crystal onto a transparent screen and focusing the optical head of the spectroradiometer to the back side of the screen. The spectrum of the light going through the crystal before and during the colouration was measured and stored by the radiometer. The absorption spectrum of the crystal was then computed and different absorption bands separated using a microcomputer connected with the radiometer.

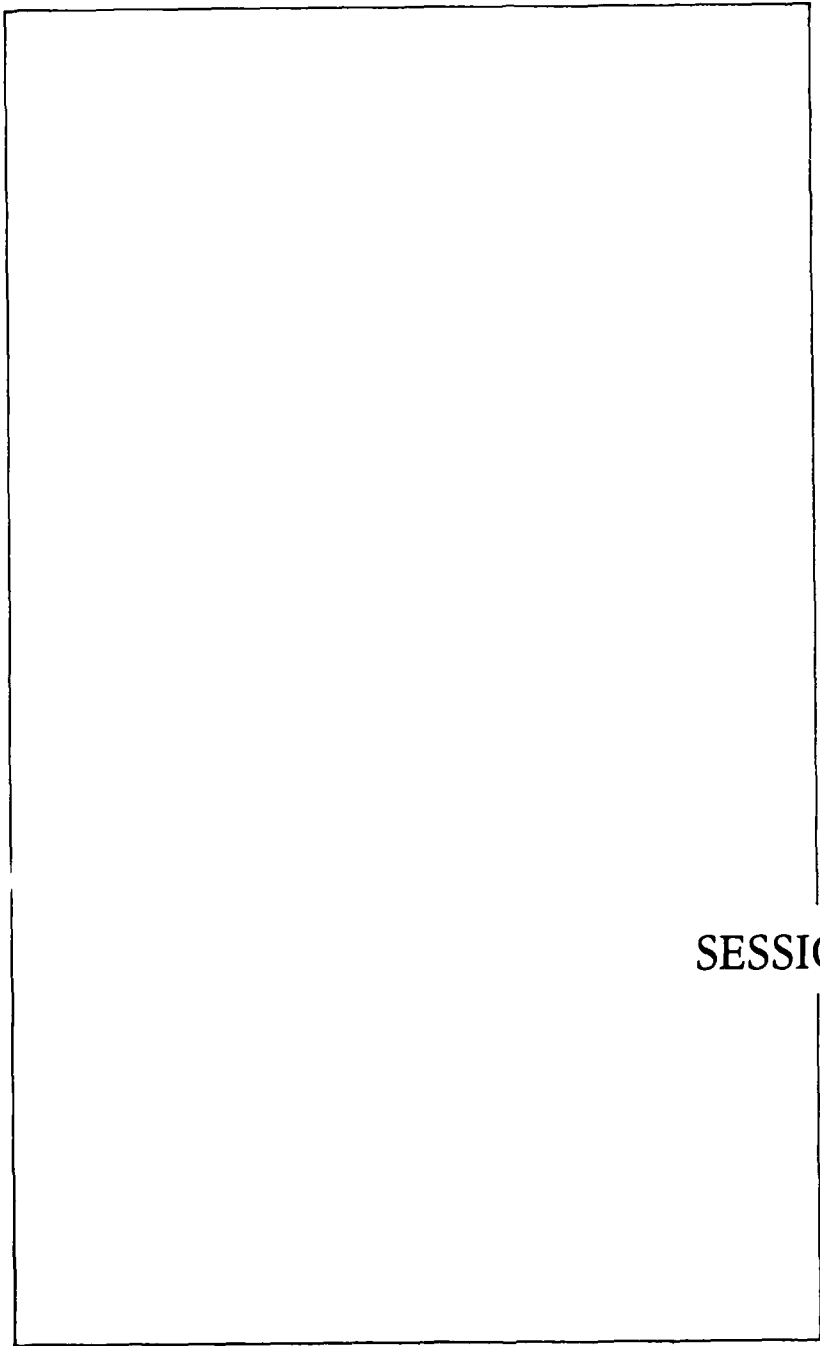
When the colour cloud begins to spread into the crystal, it contains at first only F-centres, but soon new absorption bands appear on both sides of the original F-band. These bands shift farther from the F-band during the colouration process and so the

colour becomes darker, although the maximum absorption does not increase remarkably. The noticeable broadening of the spectrum begins between the temperatures 500 C and 550 C. We explain this phenomenon to be related with the thermal dissociation of F-centres, when F-centre electrons have enough energy to shift directly into the conduction band.

We conclude that the long wavelength band is of colloidal origin. During the colouration F-centres coagulate, loose their electrons to potassium ions and alkali metal colloids are formed. The shifting of the band towards longer wavelengths means that the size of the colloidal particles increases. In the so called third stage of the electrolytic colouration, when colour seems to saturate there exists a dynamic equilibrium between F-centres and colloidal centres.

Switching off the electric field has no effect on the spectrum. When the electric field is reversed, the colour cloud moves towards the cathode without any change in the spectrum and so colloidal and F-centres migrate together in the electric field. Because colloidal centres are electrically neutral, they must be destroyed by loosing electrons, which are then captured by the anion vacancies, and new F-centres are generated. The speed of this process determines the speed of F-centre migration.

The experimental set-up was similar to those used generally for studying F-centre migration. The role of the light used to project the picture of the crystal may be significant to create colloids, because an effective light is indispensable to keep the measuring times as short as possible.



SESSION 1B

AGGREGATION PROCESSES OF  $Pb^{2+}$  IN IONIC CRYSTALS\*<sup>\*</sup> S.Benci, A.Chiari<sup>++\*</sup> and F.Fermi<sup>++\*</sup><sup>+</sup> Istituto di Scienze Fisiche - Univ. degli Studi di Parma<sup>++</sup> Dipartimento di Fisica - Univ. degli Studi di Parma<sup>\*</sup> Unità di Parma, Centro Interuniversitario di Struttura della Materia del Ministero della Pubblica Istruzione - 43100 Parma, Italy and Gruppo Nazionale di Struttura della Materia del C.N.R. - 43100 Parma Italy

Luminescence polarization measurements has been performed on KCl and NaCl crystals doped with  $Pb^{2+}$  in order to obtain direct informations on the symmetry of  $Pb^{2+}$  aggregate centers and to follow and to clarify the steps of the aggregation processes of impurities in ionic crystals. The experimental approach has been carried out by means of luminescence polarization of samples with different concentrations of impurities aged at high temperature for different times. The theoretical analysis of the aggregation processes has been performed by means of the calculated results of Bannon et al. (1) while the calculations on the polarization experimental results, in order to realize the symmetry of the emitting centers, have been carried out following the Feofilov's theory (2).

The polarization spectra of  $NaCl:Pb^{2+}$  and  $KCl:Pb^{2+}$  have been measured at 80 K and 300 K. The samples were quenched for 500°C to RT in order to obtain samples with homogeneously dispersed impurities before the annealing procedure.

The  $KCl:Pb^{2+}$  samples, doped with lead concentration ranging from 10 to 40 ppm, were annealed at 215°C to obtain aggregates with increasing size and complexity, while the  $NaCl:Pb^{2+}$  samples were annealed at 300 K.

The absorption spectra of  $KCl:Pb^{2+}$  crystals show two absorption bands at  $\lambda = 264$  nm and  $\lambda = 280$  nm, that grow during the isothermal annealings. The emission spectra for excitation in the range  $\lambda = 264$  nm -  $\lambda = 285$  nm of samples with different thermal treatments show a large emission band ( $\Delta E = 0.6$  eV) that shifts to low energies for  $\lambda_{exc} = 285$  nm.

The polarization spectra at  $\alpha = 0^\circ$  and  $\alpha = 45^\circ$  ( $\alpha$  is the azimuthal angle) for the emission at 580 nm show low polarization degree for all the samples and for different annealing times, assuming significant values only for  $\lambda_{exc} > 280$  nm. These polarization results do not allow to resolve the symmetries of the emitting centers.

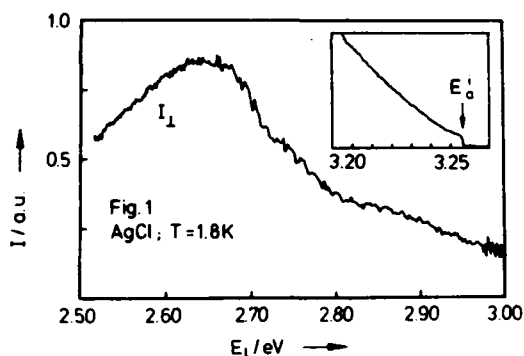
The analysis of the aggregation processes, performed following the Bannon et al. calculations (1), explains the low polarization degree found for the emitting levels involved in the luminescence processes. The possible aggregates expected in our samples have symmetry axes and planes coincident with those of the lattice and the emissions are due to a set of transitions with a quasi-cubic symmetry giving, as a whole, low values of the luminescence polarization degree, as experimentally found. So, the theoretical and experimental picture for  $\text{Pb}^{2+}$  in KCl crystals can account for the first aggregation steps of I.V. dipoles and the Suzuki phase formation. As stressed before in KCl: $\text{Pb}^{2+}$  samples annealed at 215°C, the polarization measurements do not supply useful information about the symmetry of the dipolar complexes, however, the agreement between theoretical and experimental approaches has been a stimulus to further work on other crystals. We have undertaken the analysis of the experimental results obtained for NaCl: $\text{Pb}^{2+}$ , that give clear information about the symmetries of the  $\text{Pb}^{2+}$  emitting centers (3). The analysis of the aggregation processes following the quoted work of Bannon et al. (1) is in progress.

- 1) N.M.Bannon, J.Corish and P.M.Jacobs, Phil.Mag. A51, 797 (1985).
- 2) P.P.Feofilov, The Physical Basis of Polarized Emission, Consultants Bureau, New York (1961).
- 3) S.Benci, F.Fermi and R.Reverberi, Phys.stat.sol.(b) 109, 543 (1982).

RESONANCE FLUORESCENCE OF NONMETALLIC SILVER CLUSTERS  
IN SILVER HALIDES

E. Schreiber, H. Stolz and W. von der Osten  
 Fachbereich Physik, Universität-GH, 4790 Paderborn, FRG

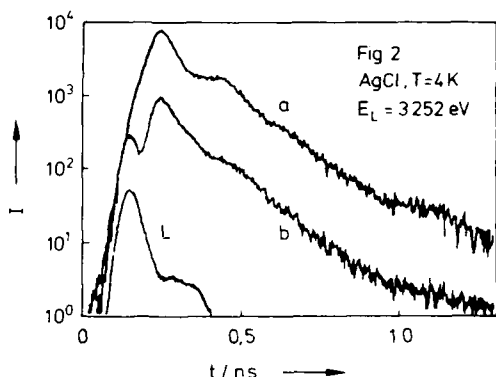
In the silver halides AgCl and AgBr, elemental silver in different form and stages of aggregation is known to exist. In irradiated small emulsion grains it can occur as latent-image specks consisting of a small number of silver atoms. For larger single crystals, depending on the temperature, it has been suggested that under light irradiation aggregates of different size may be produced leading finally, at sufficiently high intensities, to the formation of photolytic silver [1].



In AgCl and AgBr single crystals at low temperatures, we recently have discovered resonance fluorescence (RF) with substantial intensity that we attribute to nonmetallic silver clusters embedded in the crystalline matrix [2]. This fluorescence is sample dependent and originates from radiative deexcitation of discrete electronic states of the clusters which, due to their small concentration, do not give rise to measurable absorption. The RF occurs at excitation energies  $E_L$  below the indirect absorption edge  $E_a^1$  where no intrinsic absorption is to be expected. Its excitation spectrum with a peak and structure extends over a broad range of energies (Fig. 1 for AgCl). At  $E_a^1$  it shows a steep decrease of intensity. Polarized excitation results in a strong depolarized component  $I_{\perp}$  of RF.

Employing picosecond spectroscopy, we measured decay times of 100 - 500 ps and depolarization times of the order of 30 ps. As displayed in

Fig. 2 (curve b), the time resolution of our experiments allows to discriminate Rayleigh scattering that instantaneously follows the exciting laser



pulse (L) from the delayed RF.

Our results are well described in terms of an electron-in-a-box model by taking into account energy- and cross-relaxation between nearly degenerate excited cluster states. In particular, a sudden drop in energy-relaxation time at  $E_a^i$  is obtained that parallels the observed decrease of RF intensity under cw excitation. This drop in intensity and

relaxation times indicates an additional relaxation mechanism at  $E_a^i$  which we attribute to resonant energy transfer between the electronic states of the clusters and the lowest exciton state by dipole-dipole interaction. This Förster-type process, in which excitons are resonantly created by the oscillating electric field of the dipole transition, accounts for the observed energy and temperature dependence and enables us to estimate an average sample dependent cluster size of about  $10 \text{ \AA}$  diameter.

Our interpretation gets strong support by results in differently treated crystals. For instance, by annealing in halogen atmosphere the emitted intensity is considerably reduced while the decay times increase (Fig. 2, a+b), which nicely corresponds to the expected reduction in size and number of silver clusters. Presently, spectral holeburning experiments are attempted to reveal the inhomogeneous broadening of the spectra caused by the distribution in cluster size and to give further support to our interpretation.

- [1] R.S. Eachus in: The Physics of Latent Image Formation in Silver Halides, World Scient. 1984, p.249 and ref. therein
- [2] E. Schreiber, H. Stolz and W. von der Osten  
Solid State Commun. 62, 27 (1987)

ELECTRICAL RELAXATION IN SODIUM BETA" ALUMINA AND  
BETA" ALUMINA CONTAINING RARE EARTH IONS\*

M. C. Wintersgill and J. J. Fontanella  
Physics Department  
U.S. Naval Academy  
Annapolis, MD 21402-5026

B. Dunn and D. L. Yang  
Department of Material Science  
University of California, Los Angeles  
Los Angeles, CA 20024

C. G. Andeen  
Physics Department  
Case Western Reserve University  
Cleveland, OH 44106

The lanthanide beta" aluminas represent a new class of optically interesting materials. Materials containing neodymium and sodium, for example, exhibit rather high values of optical gain, and laser action at 1.06 micro-m has been observed in small platelet crystals.(1) These compositions possess two intriguing properties; anomalously strong absorption at 580 nm and a fluorescence lifetime which is substantially larger than that of neodymium in YAG.

In order to probe the structure of these materials, complex impedance studies have been carried out over the temperature range 0.01-380K both parallel and perpendicular to the optic axis for both sodium beta" alumina and sodium beta" alumina containing various amounts of rare earth ions.

At very low temperatures, dielectric loss in sodium beta" alumina is found which is analogous to the tunneling system known to exist in sodium beta alumina. The influence of rare earth ions on the two-level tunneling system is described.

At intermediate temperatures, various relaxations are found. The influence of thermal treatment along with the effect of rare earth ions on these relaxations is given.

1. M. Jansen, A. Alfrey, O. M. Stafsudd, B. Dunn, D. L. Yang, and G. C. Farrington, Optics Letters, 9, 119 (1984).

\*This work was supported in part by the Office of Naval Research.

ION MASS EFFECTS IN ION-IMPLANTED LiFA.T. Davidson<sup>o</sup>, J.D. Comins<sup>+</sup> and T.E. Derry<sup>\*</sup><sup>o</sup>Physics Department, University of Zululand, Kwa Dlangezwa  
3886, South Africa<sup>+</sup>Department of Physics, University of the Witwatersrand, Johannesburg  
P.O.Wits 2050 South Africa<sup>\*</sup>Wits-CSIR Schonland Research Centre for Nuclear Sciences,  
University of the Witwatersrand, Johannesburg, P.O. Wits 2050,  
South Africa.

Simulations of the ion-implantation process in LiF have been carried out using the TRIM-86, Version 2.0 computer programme (1). This follows the trajectories of individual ions and recoils, including both electronic and nuclear stopping. Hence range and damage distributions can be determined and energy loss mechanisms investigated.

Calculations with 100 keV rare gas ions show that the potential contribution of the displacement damage on the fluorine sublattice, i.e. vacancies, to the total F-centre concentration is low and is consistent with previous observations that direct displacement damage after ion-implantation is difficult to identify. In contrast with high energy implantations where the electronic stopping of the incident ions is the dominant factor throughout the damage profile, the calculations show that for lower energies the ionization loss associated with collision-induced damage can play a more important role, especially for heavy ions. These effects are illustrated in Fig.1 for Ne<sup>+</sup> and Kr<sup>+</sup> in LiF.

Comparisons of F- and F<sub>2</sub>-centre production using different ions at the same dose levels have been carried out. In figure 2 it is seen that when LiF is implanted with 100keV rare gas ions to a dose of 10<sup>16</sup> cm<sup>-2</sup>, the heavier ions Kr<sup>+</sup> and Xe<sup>+</sup> are significantly less efficient in producing these defects than Ne<sup>+</sup> and Ar<sup>+</sup>. On the basis of the total ionization loss (incident ions and recoils) being considerably smaller for the heavier ions (Fig 1) it would appear that for the rare gas implants the excitonic mechanism of

defect production can account satisfactorily for these observed ion-mass effects.

Fig.2 also shows the results for LiF implanted with 100 keV  $\text{Mg}^+$  ions to a dose of  $10^{16} \text{ cm}^{-2}$ . Comparison with the results for  $\text{Ne}^+$ , an ion of similar mass shows that  $\text{Mg}^+$  implantation results in significant enhancements of the F- and  $\text{F}_2$ -centre concentration. Since this difference does not seem to be related to the electronic or nuclear stopping power, it is suggested that secondary reactions such as H-centre stabilization by the implanted magnesium and an inhibition of vacancy-interstitial recombination are involved.

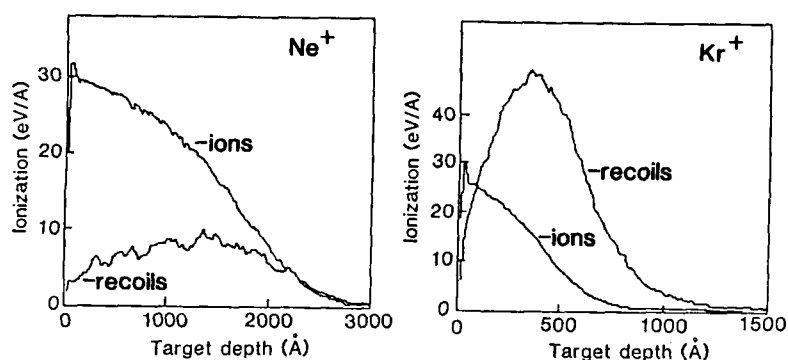


Fig.1

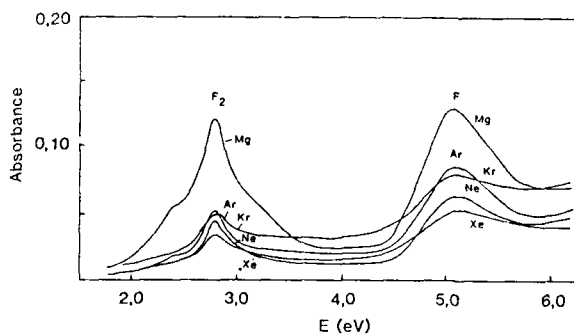


Fig.2

- (1) J.F. Ziegler, J.P. Biersack and U. Littmark: The Stopping and Range of Ions in Solids, Pergamon, 1985.

LATTICE DISTORTIONS, ORIENTATIONAL CORRELATIONS AND LATTICE  
RELAXATION IN  $(\text{KBr})_{1-x}(\text{KCN})_x$

P. Wochner, E. Burkel and J. Peisl

Sektion Physik der Ludwig-Maximilians-Universität, D-8000 München, F.R.G.

During the last decade, enormous experimental and theoretical efforts have been undertaken to understand the formation and the static and dynamical properties of the orientational glass state in  $(\text{KBr})_{1-x}(\text{KCN})_x$ <sup>1-6</sup>. But until now there are a lot of questions discussed in controversy like the nature of the two level systems<sup>2,7</sup> or the nature of the mechanisms responsible for the glass formation<sup>3,4</sup>, all lacking in detailed information about the local structure and the distorted environment of the CN dumb-bells.

Therefore we investigated the coherent quasielastic diffuse scattering of thermal neutrons from  $(\text{KBr})_{1-x}(\text{KCN})_x$  single crystals with  $x=0.07, 0.17$  and  $0.32$ <sup>8</sup>. We proved that the diffuse scattering in the vicinity of the Bragg-peaks, strongly increasing below the freezing temperature, is Huang diffuse scattering caused by the lattice distortions around the CN<sup>-</sup> defects in the KBr matrix. Fig. 1 shows the characteristic feature of the Huang diffuse scattering, a  $\xi^{-2}$  dependence of the

symmetric part of this intensity,  $I_{\text{sym}}(\xi) = 1/2 (I(+\xi) + I(-\xi))$ , and a  $\xi^{-1}$  behaviour of the asymmetric part  $I_{\text{as}}(\xi) = 1/2 (I(+\xi) - I(-\xi))$ . The quantitative analysis provides a detailed picture of the relaxation behaviour of the displacement field of the CN<sup>-</sup> defects and their orientational correlations: At the lowest temperatures the CN ions are frozen preferably in  $[111]$  directions. The orientational pair correlation function of the CN<sup>-</sup> shows parallel (or antiparallel) alignment. Therefore, the common assumption of a random distribution of the CN orientations in the glassy state of  $(\text{KBr})_{1-x}(\text{KCN})_x$  is not justified. With increasing temperature the orientational correlations decay ending up in uncorrelated single  $[111]$  defects. This behaviour is confirmed by

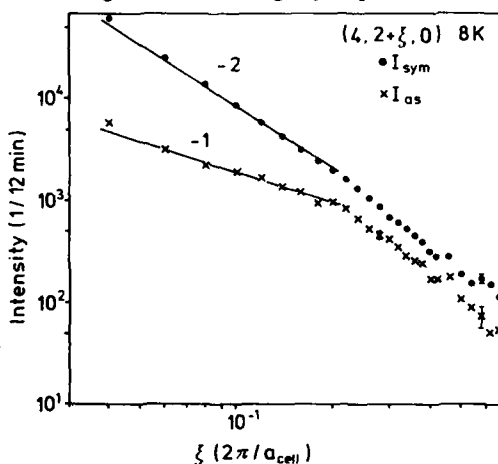


Fig.1 Distortion-induced diffuse scattering intensity of  $(\text{KBr})_{0.68}(\text{KCN})_{0.32}$  at 8 K close to (420) in the  $[010]$  direction,  $I_{\text{sym}}(\xi)$  (•) and  $I_{\text{as}}(\xi)$  (x)

ized by the intensity due to uncorrelated defects is shown. At temperatures higher than the freezing temperature relaxation time effects of the distortion field due to the rapid reorientation of the defect are obvious, which result in a decrease of the shear distortions of the defect. They show up in Fig. 2 in the decrease of the diffuse intensity below the intensity of uncorrelated single defects. Due to the limited lifetime of the distortion field of the mobile defects in this temperature range, a quasielastic broadening of this coherent diffuse scattering is observed in contradiction to the hitherto<sup>3</sup> reported measurements.

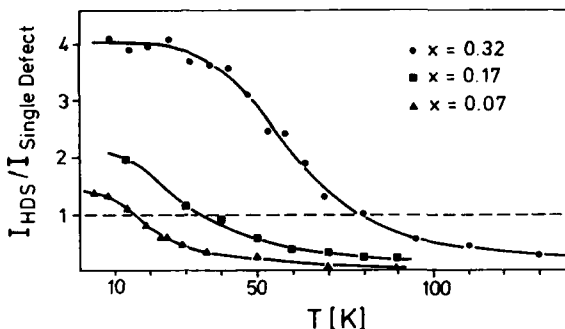


Fig.4 Diffuse scattering intensity at (4 2.16 0) for the different concentrations, normalized by the intensity due to randomly correlated defects.

Our picture of the relaxational behaviour of the displacement field of the CN defects and their orientational correlations is in close analogy to the new selfconsistent mode coupling theories of the glass transition<sup>9,10</sup>. On approaching the freezing temperature the orientational fluctuations of the CN molecules slows down, leading to an increase of the shear distortions. Because the interaction of the CN dumb-bells is mediated by lattice strains, these shear distortions are coupled via a certain feedback mechanism to the slowly decaying orientational correlations. Therefore the alignment between the CN ions increases and consequently the shear distortions.

#### References:

- 1) I.I. De Yoreo, W. Knaak, M. Meissner, R.O. Pohl, Phys. Rev. B **34**, 8828 (1986)
- 2) J.P. Sethna, K.S. Chow, Phase Transitions **5**, 317 (1985)
- 3) K.H. Michel, J.M. Rowe, Phys. Rev. B **22**, 1417 (1980)
- 4) K.H. Michel, Phys. Rev. B **35**, 1405 and 1414 (1987)
- 5) A. Loidl, R. Feile, K. Knorr, Phys. Rev. Lett. **48**, 1263 (1982)
- 6) F. Lüty, J. Ortiz-Lopez, Phys. Rev. Lett. **50**, 1289 (1983)
- 7) C.I. Nicholls, L.N. Yadon, D.G. Haase, M.S. Conradi, Phys. Rev. Lett. **59**, 1317 (1987)
- 8) P. Wochner, E. Burkel, J. Peisl, G. Eckold, submitted to Phys. Rev. Lett.
- 9) U. Bengtzelius, W. Götze and A. Sjölander, J. Phys. C **17**, 5915 (1984)
- 10) K.H. Michel, preprint (1987)

SESSION 2A

MODERN DEVELOPMENTS IN COLOR CENTER LASERS AND LUMINESCENCE

G. Baldacchini

ENEA, Dip. TIB, U.S. Fisica Applicata, P.O. Box 65,  
00044 Frascati (Rome), Italy

Soon after the first realization of a c.w. tunable laser based on  $F_A(II)$  centers /1/, extensive research has been carried out in order to investigate the potential usefulness of several types of F aggregate centers in alkali halide crystals as active laser materials. As a result of this effort it is today possible, by using different kinds of color centers, to cover entirely the spectral range between 0.8 and 4  $\mu m$  /2/, and also to have a modest but important laser emission at about 5  $\mu m$  /3/.

However, almost all the color centers suitable for lasing have one or more drawbacks which pose troublesome burdens on their use. The crystal preparation with the right impurity and their coloration can be difficult, some aggregate centers are stable only at temperatures well below 0°C, other centers need auxiliary light pumping and still others deteriorate while lasing /2,4/. Only the small class of  $F_A(II)$  and  $F_B(II)$  centers are immune from the previous problems. They are easily produced and are stable both during laser operation and during room temperature storage. It is amazing to note that they were the first to be discovered and they are still the best, as far as the power output is not concerned. However, in spite of their success as lasing materials and their well known optical cycle, recent experiments, especially aimed at the study of the emission properties, have shown new and sometimes unexpected results, which will be summarized in the present work.

It is well known that the  $F_A$  center axis undergoes reorientational processes under optical pumping of appropriate polarization state and wavelength /5/. As a consequence the geometry of the pumping light with respect to the crystal axes has to be properly chosen, in order to reduce orientational bleaching in laser operation. However, also the small off-axis angle of the  $F_A(II)$  center plays a role in this respect. In order to measure this parameter we have devised a simple technique by revealing the luminescence under appropriate geometrical conditions /6/. Moreover, also the overlapping of the two  $F_A$  absorption bands can be determined. Data will be presented for KCl:Li and RbCl:Li, while measurements on other systems are under way.

The luminescence efficiency of the  $F_A(II)$  centers decreases rather quickly by increasing the centers concentration above  $\sim 10^{-17}$  F/cm<sup>3</sup>, and this effect is of some consequences for the

efficiency of laser emission /7,4/. The concentration quenching is a well known phenomenon in the F center, while it is not so in  $F_A$  center. We investigated a few samples of KCl:Li containing high concentration of  $F_A$ (II) centers by using magneto-optical techniques. The results of the experiments, which show an origin of the quenching mechanism different from the one found for F centers /8/, will be discussed together with suggestion for future investigations.

Luminescence in  $F_A$ (II) centers in RbCl:Li is well known /5/ and used in a laser working in the range 2.5-3.65  $\mu\text{m}$  /2/. However, the laser operates at liquid nitrogen temperature as most of the optical experiments performed on this system. Recently we have found that the luminescence peaking at  $\sim 2.9 \mu\text{m}$  decreases with temperature, while at the same time a new emission appears at  $\sim 1.5 \mu\text{m}$ , which is completely dominant at liquid helium temperature. The experimental evidence collected up-to-now strongly supports the idea of the  $F_A$ (I) center at the origin of the new emission band. This unexpected result will be discussed within the frame of the more interesting and broad field of the  $F_A$  classification in type I and type II center.

#### References

- /1/ L.F. Mollenauer and D.H. Olson: Appl.Phys.Lett. 24, 386 (1984)
- /2/ L.F. Mollenauer in "Tunable Laser", vol. 59, ed. L.F. Mollenauer and J.C. White (Springer-Verlag, Berlin, 1987), chap.6 and references therein cited
- /3/ W. Gellerman, Y. Yang and F. Luty: Opt.Comm. 57, 196 (1986)
- /4/ K.R. German: J.Opt.Soc.Am. B3, 149 (1986)
- /5/ F. Luty in "Physics of Color Centers", ed. W.B. Fowler (Academic Press, London, 1968), chap.3
- /6/ G. Baldacchini et al.: Phys.Rev. B33, 4273 (1986)
- /7/ G. Baldacchini et al.: Rev.Phys.Appl. 18, 301 (1983)
- /8/ F. Porret and F. Luty: Phys.Rev.Lett. 26, 843 (1971).

CHALCOGEN-VACANCY DEFECTS AS BUILDING BLOCKS FOR  $F_2^+$ -LIKE  
STABLE COLOR CENTER LASERS IN ALKALI HALIDES

Bing-Kun Yu and Werner Gellermann  
 Physics Department, University of Utah  
 Salt Lake City, Utah 84112

We report on the detailed formation kinetics and latest laser results of  $F_2^+$  centers attached to a double negatively charged chalcogen ion ( $X^{--} = O^{--}, S^{--}, Se^{--}$ ) on a neighboring halide lattice site. These systems have the potential to supply stable color center lasers tunable in the near IR from  $-0.8$  to  $4\mu m$ .<sup>1,2</sup> As building blocks of these " $(F_2^+)_H$  centers" we identified --in  $OH^-$ -contamination-free crystals--

- a) a chalcogen-vacancy defect pair, consisting of a double negatively charged chalcogen ion,  $X^{--}$ , and a charge-compensating  $\langle 110 \rangle$  neighboring anion vacancy,  $\square$ , and
- b) an F center.

If the chalcogen-vacancy defect pair,  $X^{--}\square$ , becomes associated with an F center during light-induced F center aggregation the laser-active  $(F_2^+)_H$  center is formed along with several other possible chalcogen-vacancy/F center configurations. So far  $(F_2^+)_H$  centers could be produced in high concentrations in NaCl, KCl, KBr, and RbCl hosts.

For chalcogen-vacancy defect pair production in these hosts we used  $O_2^{--}$ ,  $S_2^{--}$  or  $Se_2^{--}$  doping impurities and reduced the latter with F centers. The reaction<sup>3</sup> for this process is  $X_2^{--} + 3F \rightarrow 2[X^{--}\square]$ .

The nearly complete transformation of  $O_2^{--}$  impurities into  $O^{--}\square$  defects in the case of KCl can be seen from the UV absorption bands in Fig. 1a.

For the host NaCl doping with  $OH^-$  impurities is possible as an alternative;  $O^{--}\square$  defects are produced in this case, again by a reducing reaction<sup>3</sup> with F centers, according to  $OH^- + 2F \rightarrow [O^{--}\square] + H^-$ .

Isolated F centers, needed as  $[X^{--}\square]$ -aggregation partners for  $(F_2^+)_H$  center formation, are provided by the additive coloration process simply if they are produced in excess quantities to those needed for the  $X^{--}\square$  defect generation. A related further group of laser-active  $F_2^+$  like defects with shifted optical transitions can be produced in which the  $F_2^+$  center is attached, besides to a chalcogen ion on a halide lattice site, to an additional metal impurity on a neighboring alkali lattice site. Using  $Na^+$  co-doping impurities we could produce these " $(F_2^+)_{AH}$  centers" so far in  $KCl:Na^+:O_2^{--}$  and  $KBr:Na^+:O_2^{--}$  crystals. The center formation is similar to that for  $(F_2^+)_H$  center production. It's first step is again a reducing

reaction with F centers.

As seen from the UV absorption spectra for the case of  $\text{KCl}:\text{Na}^+:\text{O}_2^-$  in Fig. 1b, however, a new  $\text{Na}^+:\text{O}^{2-}-\square$  defect complex with shifted spectral transition is now obtained. Obviously this defect complex is formed in higher than statistical proportions, thus making it possible

to produce, under subsequent F center association, favorable high concentrations of  $(\text{F}_2^+)_{\text{AH}}$ -centers.

The current total laser tuning range with  $(\text{F}_2^+)_{\text{H}}$  and  $(\text{F}_2^+)_{\text{AH}}$  center laser systems extends from 1.44 to 2.15  $\mu\text{m}$  using  $\text{NaCl}:\text{OH}^-$  or  $\text{NaCl}:\text{O}_2^-$ ,  $\text{KCl}:\text{Na}^+:\text{O}_2^-$  and  $\text{KBr}:\text{Na}^+:\text{O}_2^-$  crystals. The Table lists their main characteristics:

Crystal	$\text{NaCl}:\text{O}_2^-$	$\text{KCl}:\text{Na}^+:\text{O}_2^-$	$\text{KBr}:\text{Na}^+:\text{O}_2^-$
Tuning Range	1.44 - 1.74	1.69 - 2.02	1.98 - 2.15
Peak Output Power	3.6 W	750 mW	10 mW
Pump laser	Nd:YAG	Nd:YAG	$\text{KCl}:\text{Ti}^+$

Experiments are in progress to use chalcogen-vacancy defect pairs as building blocks for the production of new laser-active stable  $(\text{F}_2^+)_{\text{H}}$  centers in  $\text{LiF}$  and  $\text{NaF}$  and  $(\text{F}_2^+)_{\text{AH}}$  centers in  $\text{KCl}:\text{Li}^+$ .

This work was supported by NSF grant DMR-8706416

and ONR contract N0014-86-K-0258.

#### References:

1. J. Pinto et al., Opt. Lett. **11**, 519 (1986); E. Georgiou et al., Phys. Rev. B **35**, 7636 (1987); 2. D. Wandt et al. J. Appl. Phys. **61**, 864 (1987); Opt. Comm. **61**, 405 (1987); 3. F. Fischer, Naturwissenschaften, 54. Jg., Heft 12 (1967).

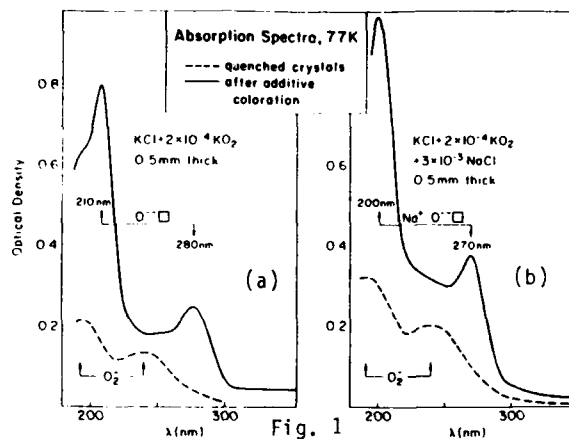


Fig. 1

OPTICAL, ODES, AND ODENDOR INVESTIGATIONS ON  $Pb^{+}(1)$  AND RELATED  
CENTRES IN ALKALINE EARTH FLUORIDES AND  $KMgF_3$

M. Fockele, F. Lohse, J.-M. Spaeth, and R.H. Bartram\*

University of Paderborn, Fachbereich Physik, Warburger Str. 100, D 4790 Paderborn, F.R.G.

\*Department of Physics and Institute of Materials Sciences, University of Connecticut,  
Storrs, CT 06268, U.S.A.

Because of its favorable lasing properties  $Tl^0(1)$  centres attracted great interest [1]. These centres consist of a  $Tl^0$  atom with its 6p electron in the crystal field of an anion vacancy [2,3]. It was shown, that the specific interplay of a large spin-orbit interaction and crystal field favors the  $Tl^0$  laser action while the analogous  $Ga^0$  and  $In^0$  defects do not lase because of small spin-orbit interaction [4]. Also  $Pb^+$  has a large spin-orbit interaction. The analogous  $Pb^{+}(1)$  centres in alkaline earth fluoride crystals (Fig.1) have better thermal stability compared to alkali halides. There is also no need of charge compensation in these divalent crystals for the  $Pb^{+}(1)$  centre [5]. Lead centers in  $KMgF_3$  were already shown to be laser active [6].

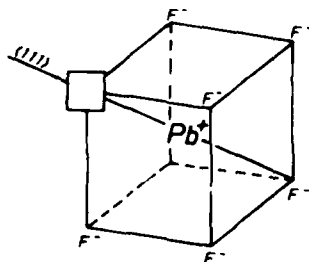


Fig. 1  $Pb^{+}(1)$  centre model.

Although the  $Pb^{+}(1)$  centres in alkaline earth fluorides were already identified, the assignment of their optical bands was not clear because of overlapping optical excitation and emissions bands (Fig.2). We report on new ODES measurements via the MCPE of the  $Pb^{+}(1)$  emission to separate the bands. The other two observed emission bands are assigned to a diamagnetic  $Pb^0(2)$  centre [7] and a Pb dimer centre analogous to the  $Tl^0_2(1)$  dimer

centre in alkali halides [8]. These related lead centres can degrade the efficiency of a  $Pb^{+}(1)$  laser due to overlapping of absorption and emission bands.

ODENDOR investigations via MCD confirm the "laser active structure" with an anion vacancy in the crystal field of the 6p electron of  $Pb^{+}$  on alkaline earth site (Fig.1). The superhyperfine parameters of the four nearest neighbor shells are presented and discussed.

We report also on ODMR measurements on the lasing lead centre in  $KMgF_3$ . The symmetry and the structure model is discussed.

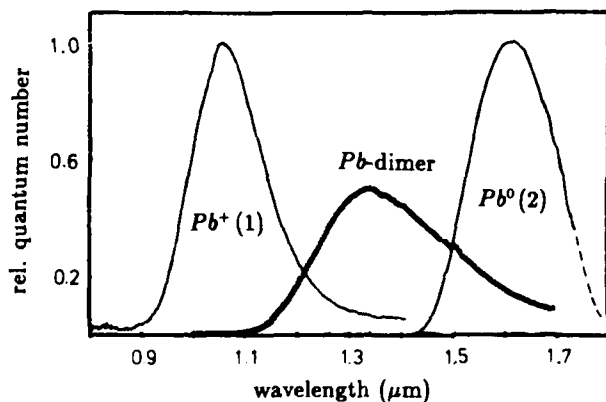


Fig. 2 Optical emissions of  $Pb^{+}(1)$ ,  $Pb^0(2)$ , and  $Pb$  dimer centres in  $SrF_2$  at 10K. Excitation at 660nm, 1020nm, and 740nm resp.

- 1 W. Gellerman, F. Lütty, and C.R. Pollock, *Optics Commun.* **39**, 391 (1981).
- 2 E. Goovaerts, J. Andriessen, S.V. Nistor, and D. Schoemaker, *Phys. Rev. B* **24**, 29 (1981).
- 3 F.J. Ahlers, F. Lohse, J.-M. Spaeth, and L.F. Mollenauer, *Phys. Rev. B* **29**, 1249 (1983).
- 4 M. Fockele, F.J. Ahlers, F. Lohse, J.-M. Spaeth, and R.H. Bartram, *J. Phys. C: Solid State Phys.* **18**, 1963 (1985).
- 5 F. Lohse, M. Fockele and J.-M. Spaeth, *Cryst. Latt. Def.* **16**, 275 (1987).
- 6 G. Hörsch, and H.J. Paus, *Opt. Commun.* **60**, 69 (1987).
- 7 R.H. Bartram, M. Fockele, F. Lohse, and J.-M. Spaeth, *Intern. Conf. on Defects in Insulating Crystals*, Parma (1988).
- 8 F.J. Ahlers, F. Lohse, and J.-M. Spaeth, *J. Phys. C: Solid State Phys.* **18**, 3881 (1985).

SUBPICOSECOND SPECTROSCOPY OF SELF-TRAPPING AND DEFECT FORMATION  
IN ALKALI HALIDES

R. T. Williams and G. P. Williams, Jr.  
Department of Physics  
Wake Forest University  
Winston-Salem, NC 27109 USA

Time-resolved spectroscopy with short pulses derived from mode-locked lasers has provided our earliest available views of the electronic and ionic relaxations involved in self-trapping of holes and excitons and in creation of lattice defects in alkali halides. Up to this time, such investigations in the alkali halides have been done with Nd:YAG<sup>1,2</sup> or ruby<sup>3-5</sup> lasers having pulse widths of 30 to 40 picoseconds. By careful deconvolution assuming simple growth functions, rise-time information has been obtained with estimated delay uncertainties as small as one-tenth of the laser pulse width, i.e. a few picoseconds. However, when there are overlapping components and complex evolution of band shapes, there is information lost due to effective averaging during the pulse. While processes involving thermal activation have been amenable to detailed study in the range of tens to hundreds of picoseconds by these methods,<sup>2-5</sup> many important "prompt" processes are really faster than can be studied with 30 picosecond pulses.

We have assembled a short-pulse laser system for the study of defect formation processes on time scales up to 100 times faster than in previous studies. The goal is to resolve hole/exciton relaxation and defect formation on the scale of optical phonon periods, i.e. about 300 femtoseconds. An actively mode-locked Nd:YAG laser synchronously pumps a dye laser producing a train of 3 ps pulses. Pulse compression in a fiber/grating pair compressor can reduce the pulse width to the order of 300 fs. Amplification provides sufficient ultraviolet energy for excitation of optically significant numbers of electron-hole pairs and enables generation of a white-light probe pulse.

Preliminary data obtained in KBr have demonstrated the feasibility of these experiments. We will report more complete data on hole self-trapping, exciton self-trapping, and defect formation in a number of alkali halides.

Acknowledgment: This work was supported by National Science Foundation Grant No. DMR-8600010.

References:

1. J. N. Bradford, R. T. Williams, and W. L. Faust, Phys. Rev. Lett. 35, 300 (1975).
2. R. T. Williams, B. B. Craig, and W. L. Faust, Phys. Rev. Lett. 52, 1709 (1984).
3. Y. Suzuki, M. Okumura, and M. Hirai, J. Phys. Soc. Japan 47, 184 (1979).
4. J. D'hertoghe and G. Jacobs, Phys. Stat. Sol. (b) 95, 291 (1979).
5. M. Hirai, Y. Suzuki, H. Hattori, T. Ehara, and E. Kitamura, J. Phys. Soc. Japan 56, 2948 (1987).

# **PICOSECOND RADIATIONLESS DECAY OF EXCITED ELECTRONIC STATES OF DEFECTS IN KCl AND NaBr**

M. Leblans, C. Sierens, W. Joosen, and D. Schoemaker

Physics Department, University of Antwerp (UIA)

Universiteitsplein 1, B-2610 Wilrijk (Antwerp), Belgium

The relaxation behavior of the F-center in NaBr and of the  $\text{Ga}^0(1)$  and  $\text{In}^0(1)$  defects in KCl is investigated with picosecond (ps) optical pulses. An experimental set up is used with two synchronously pumped Rhodamine 6G dye lasers emitting pump and probe pulses of 7 ps duration with frequencies, which are tuned at resonance with a particular electronic transition of the point defect. After excitation by the pump, an automatically delayed probe interrogates the recovery of the population of the ground state. The double-modulation detection scheme has a sensitivity of  $10^{-7}$  (Ref.1).

In NaBr crystals doped with  $\text{OH}^-$  we could produce F-centers by x-irradiation. The low energy region of the F-band was excited at 580 nm in the pump-probe experiment. At low temperatures, the decay time  $\tau$  is too long to be determined with an optical delay stage providing a maximum retardation of the probe of 1.6 nanoseconds (ns), however, an upper bound for  $\tau$  of 10 ns is clearly established. Above 70K the process becomes thermally activated with  $\tau$  decreasing from 1170 ps to 40 ps at 160K. Some typical decay spectra are shown in Fig.1. This ps relaxation time is believed to characterize the radiationless electronic transition between the excited p-like state and the ground state of the F-center in NaBr. The observed relaxation time is very different from the F-center luminescence lifetime as measured in the near infrared with single photon counting.<sup>2</sup> Our data are in agreement with the estimated decay time by Baldacchini et al. starting from the temperature dependence of the F-F' conversion efficiency<sup>3</sup> and they also support the Dexter-Klick-Russell rule<sup>4</sup> as a useful empirical criterion to predict fast non-radiative relaxation.

The heavy metal impurity defects  $\text{M}^0(1)$  ( $\text{M} = \text{Ga}, \text{In}, \text{Tl}$ ) in KCl with the laser-active type structure were excited in their third optical band, which corresponds to the lowest allowed np-ns transition of the free  $\text{M}^0$  atom. Subnanosecond relaxation was observed for  $\text{Ga}^0(1)$  and  $\text{In}^0(1)$  with characteristic times of 260 ps and 90 ps at 7K, respectively.<sup>5</sup> The low temperature  $\text{Tl}^0(1)$  decay time is longer than 1 ns. Analysis of the temperature dependence of the  $\text{Ga}^0(1)$  decay time yields an activation energy of  $60 \text{ cm}^{-1}$ . This small barrier and the fast deexcitation of the third excited state cannot be explained within the defect model of a neutral atom

$M^0$  perturbed by an anion vacancy along (100). This relaxation behavior suggests that in the third excited state, the impurity atom is relaxed more towards the anion vacancy, in comparison with the two lowest electronic states of the defect. The radiationless decay of  $Ga^0(1)$  and  $In^0(1)$  is believed to be promoted by the low frequency motion of the  $M^0$  atom, which can be observed in resonant Raman scattering.<sup>5,6</sup>

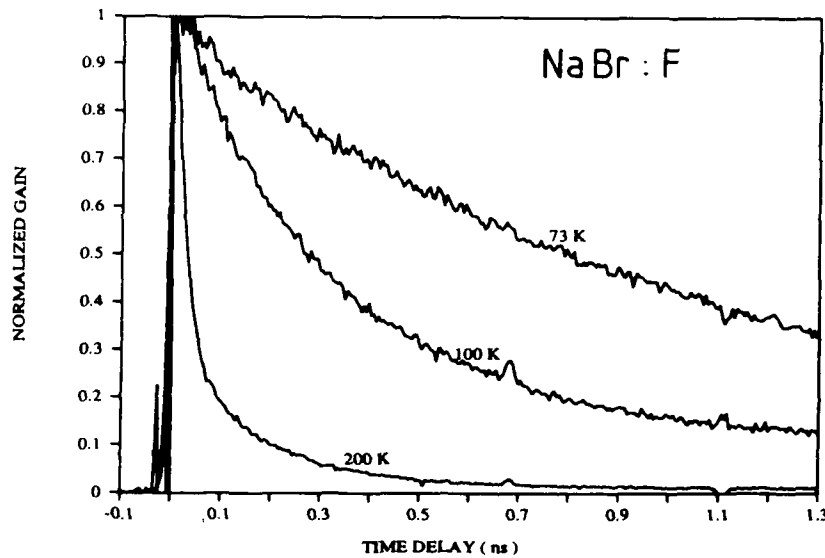


Fig.1 Time-resolved gain spectra in x-irradiated NaBr:OH<sup>-</sup> showing the ground state recovery of the F-center at different temperatures, measured with parallel polarizations of pump and probe.

1. M. De Mazière and D. Schoemaker, J. Applied Phys. **58**, 1439 (1985).
2. L. Bosi, A. Longoni, and M. Nimis, Phys. Stat. Sol.B **89**, 221 (1978).
3. G. Baldacchini, D.S. Pan, and F. Lüty, Phys. Rev.B **24**, 2174 (1981).
4. See, e.g., R.H. Bartram and A.M. Stoneham, Solid State Comm. **17**, 1593 (1975).
5. C. Sierens, W. Joosen, and D. Schoemaker, Phys. Rev.B **37**, xxxx (1988).
6. W. Joosen, C. Sierens, and D. Schoemaker, Solid State Comm. **63**, 69 (1987).

SUBPICOSECOND LATTICE RELAXATION FOLLOWING ULTRAFAST LASER EXCITATION OF  
LOCAL CENTERS IN SOLIDS: A COHERENT PHONON DESCRIPTION

G. CONSOLATI, Istituto di Fisica, Politecnico di Milano  
Piazza Leonardo da Vinci 32, 20133 Milano and  
N. TERZI, Dipartimento di Fisica, Università di Milano  
via Celoria 16, 20133 Milano, Italy.

The short time relaxation process in molecules and crystals, following excitation with ultrashort laser pulses, reveals fundamental aspects of the electron and phonon dynamics and of their coupling. The increasing number of experimental data allows a comparison of the existing theories. In the present work we refer to recent experiments, where a femtosecond pulsed laser is used to study how ions relax around color centers in insulating crystals.<sup>(1,2)</sup> In particular, the transient dynamics of  $F_2^+$ -centre in LiF show that the n.n. relaxation time is shorter than the period of any relevant frequency of the host crystal.<sup>(2)</sup> This seems to disagree with the c.c. model. On the other hand, it could corroborate a recent theory proposing that coherent phonons are generated during the very fast excitation process preceeding the relaxation<sup>(3)</sup>.

Here we report on numerical applications of the coherent phonon theory. We have adopted the following model for the centre. i) The impurity centre, embedded in a harmonic ionic crystal, undergoes a dipole allowed ultrafast transition between two electronic levels, whose energy lies in the forbidden gap. ii) No other energy level exists in the proximity of the excited state: the electronic energy transfer does not compete with the phonon energy relaxation. iii) The change in the electron-phonon (EP) interaction is linear in the phonon coordinates and short range. iv) The coherent phonon wavepacket (wp), generated at  $t=0$  by the light absorption, propagates at further times in a harmonic crystal at  $T=0$  (here described by using the breathing shell model). The time-dependent positions of the ions is identified with the expectation value of the ionic variables on the evolving coherent wp at different times.

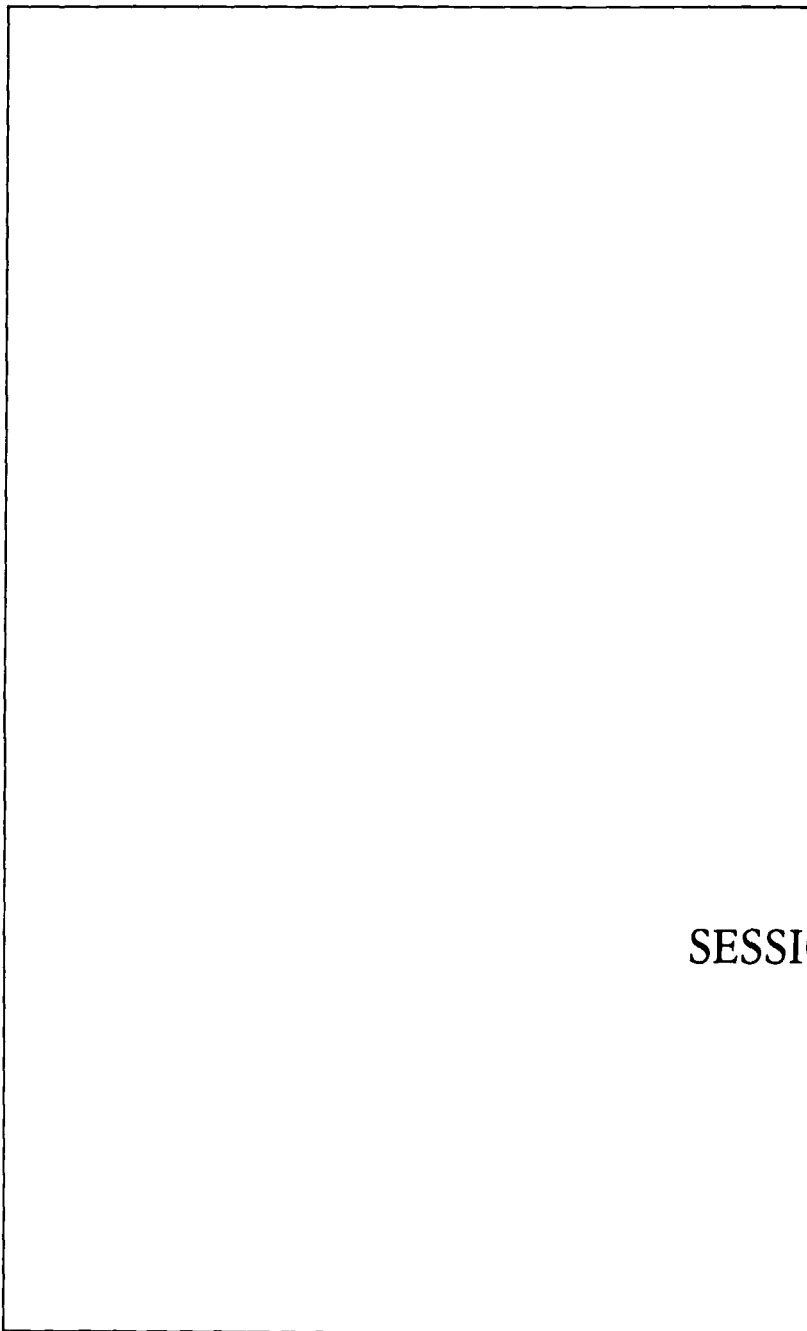
We do not comment the assumptions i)-iii), as they are usually adopted in

dealing with the EP coupling in excited color centres. With regard to the point iv), the non linear EP coupling and the anharmonicity play certainly an important role in modifying the wp during the relaxation process. However, their effect is probably limited at  $T=0$  and on the time scale of fractions of picoseconds, here studied, even in the strong EP coupling limit.

Instead of the experimentally known  $\text{LiF:F}_2^+$ ,<sup>(2)</sup> we have evaluated at the moment the time-dependent relaxation around a substitutional impurity. We have chosen  $\text{Tl}^+$ -doped potassium halides, because we know the EP couplings (included the Jahn-Teller active ones) for A and C-transitions, and the ground-state perturbed lattice dynamics.<sup>(4)</sup> The ion relaxation up to the eighth neighbours has been evaluated at intervals of 10 fs.

Our results can be summarized as follows. The n.n. of the impurity move towards new relaxed equilibrium positions in a strongly damped oscillatory way. However, the ions perform at least one complete large oscillation, a less damped motion than that of the ions surrounding the  $\text{F}_2^+$  centre in LiF. This first short transient (100 fs) is followed by aperiodic oscillations of very small amplitude. The further neighbours are reached by the phonon wp at delayed times, depending on the wp group velocity and therefore on the wp initial composition (strength of the different symmetry components). Their oscillations are also damped but always of smaller amplitude than the motion of the n.n., according to a 3-dim propagation scheme for the phonon wp.

1. W.H.Knox, L.F.Mollenauer and R.L.Fork, Proc. Conf. "Ultrafast Phenomena" held at Snowmass (USA, 1986), unpublished.
2. J.Wiesenfeld, L.F.Mollenauer and E.P.Ippen, P.R.Lett. 47, 1668 (1981).
3. A.Giorgetti and N.Terzi, Solid State Comm. 39, 635 (1981) and N.Terzi, J. Lumin. 31/32, 194 (1984)
4. G.Benedek and N.Terzi, Phys. Rev. B 8, 1746 (1973)



SESSION 2B

GRAIN-BOUNDARY MASS TRANSPORT IN CERAMIC OXIDES

C. MONTY

CNRS, Laboratoire de Physique des Matériaux  
1, Place A. Briand, 92190 MEUDON, France

The study of properties related to grain-boundaries (GBs) has been one of the most active fields of the last ten years in Materials Science. Important applications of ceramics (thermomechanical ceramics, "electro-ceramics", ...) led researchers to prepare polycrystalline materials, sometimes bicrystals, with well controlled GB properties to know more about the characteristics and the role of these extended defects. Some results are now available in oxides and it is possible to extract some specific tendencies. We shall focus this review on mass transport properties (diffusion) in oxide GBs bearing in mind the relations between energy, segregation, structure and diffusion.

After recalling the phenomenology of GB diffusion, we shall present some important results obtained using classical techniques, i.e. the isoconcentration profiles measured using an electron microprobe (EMA) or the average concentration of a radiotracer as a function of depth using mechanical sectioning. Beautiful results have been obtained recently using these methods in  $\text{MgO}$ ,  $\text{Al}_2\text{O}_3$  and Spinel bicrystals by OSENBACH and STUBICAN in Pennstate, USA. Progress in studying GB diffusion in oxides have been nevertheless essentially related to new techniques able to determine small penetration profiles : nuclear reactions analysis (NRA), microsectioning using ion sputtering coupled with radioactive tracers or mass spectrometry analysis (SIMS) or Auger electron analysis (AEA). We shall show results obtained by A. ATKINSON and his staff in Harwell who studied GB selfdiffusion and GB impurity diffusion in  $\text{NiO}$ . We shall discuss finally some results of GB diffusion in  $\text{NiO}$  we have obtained in collaboration and recent work in  $\text{Cu}_2\text{O}$  in which we have been able to determine the nature and charge state of the point defects ( $\text{O}_i^x$ ) involved in GB oxygen selfdiffusion (F. PERINET, Thèse d'Etat, Orsay Sept. 1987).

A general discussion of the data available on GB diffusion in oxides will give ideas on the tendencies observed in these compounds.

DIPOLE-DEFECT INTERACTION EFFECTS IN  $\text{CaF}_2:\text{Ce,Mn}$   
 S.W.S.McKeever and B.Jassemneiad, Department of Physics,  
 Oklahoma State University, OK 74078-0444, USA.

We present data on the concentration and dipole relaxation parameters associated with  $\text{Ce}^{3+}-\text{F}_{\text{int}}^-$  ( $\text{C}_{4v}$  symmetry) complexes in  $\text{CaF}_2$  singly-doped with Ce and doubly-doped with Ce and Mn. The data have been obtained using optical absorption and ionic thermocurrents (ITC). Several samples were studied in this work, each of differing impurity content. The impurity levels ranged from 0.01 mol percent to 2.0 mol percent for Ce, and 0.001 mol percent to 2.0 mol percent for the Mn dopings. (All nominal levels added to the melt.)

The 4f-5d transition in the  $\text{Ce}^{3+}$  ions within the  $\text{C}_{4v}$  complexes gives rise to a prominent absorption band at  $\sim 300$  nm and using the known oscillator strength for the transition ( $4.8 \times 10^{-3}$ ) one can determine the concentration of these centers independently from the polarization measurements. The ITC signal from the reorientation of the  $\text{C}_{4v}$  dipoles consists of a single peak at  $\sim 148$  K. When analysed using the conventional monoenergetic model of dipole rotation, the activation enthalpy so-determined is found to be dependent upon the Ce concentration in a manner which is not expected from this model. These effects manifest themselves in a broadening of the ITC peak as the Ce level is increased. However, the broadening can be successfully accounted for by adopting a Gaussian distribution for the activation enthalpy, of mean value  $E_0$  and of width  $p$ .  $E_0$  was found to be independent of dipole concentration, while  $p$  increased with increasing dipole concentration. The experimental data are fitted to the following equation:<sup>1</sup>

$$J^*(T) = J(T)F(E_0, \tau_0, p, T) \quad (1)$$

where  $F(E_0, \tau_0, p, T)$  is a correction term due to the Gaussian distribution. Here,  $T$  is temperature,  $E$  is energy,  $\tau_0$  is the dipole rotation time constant and  $J(T)$  is the normal ITC curve shape that one obtains from the monoenergetic model.<sup>2</sup>

The experimental data are consistent with a perturbation of the dipole relaxation parameters due to interactions between the dipoles and other defects within the system. However, the strength of the observed effects is very difficult to explain using electrostatic dipole-dipole interactions only. We believe that significant monopole-dipole interactions are also present, the monopoles being non-locally-compensated  $\text{Ce}^{3+}$  ions in  $\text{O}_h$  symmetry. Furthermore, since significant clustering of the dipoles into higher-order clusters (of unknown structure) can be detected in the optical measurements, we suspect that significant elastic interactions may also be affecting the dipole relaxation parameters. This may help to explain the rather large dipole-defect interaction lengths calculated from the data (ie.  $\sim 12$  lattice sites).

When large interaction effects are noted it is unwise to estimate the dipole concentration from the ITC data. However, when the interaction effects are absent (at low Ce levels) we are able to use the ITC data to calculate a dipole moment of  $3.12 \times 10^{-29}$  Cm for the  $\text{Ce}^{3+}\text{-F}_{\text{int}}^-$  complexes.

When Mn is added to the system we note that both the height of the ITC peak and the width parameter  $p$  decrease as more Mn is added. This unexpected behavior is a clear indication that the dipole rotation parameters are very sensitive to the surrounding crystal environment. The optical absorption curve shows no such decrease due to the partial shielding of the 4f electrons by the outer shell electrons causing little or no change in oscillator strength. The behavior of the ITC data can be satisfactorily explained by a reduction in the  $\text{Ce}^{3+}\text{-F}_{\text{int}}^-$  dipole moment. This in turn will cause a reduction in the strength of the electrostatic interaction components, namely the dipole-dipole and the dipole-monopole terms. The dipole moment reduction may be a result of the lattice relaxation that occurs when Mn substitutes for Ca. The Ca-F distance in  $\text{CaF}_2$  is 2.366 Å, whereas the Mn-F distance is 2.265 Å.

We conclude that the dipole relaxation parameters for  $\text{Ce}^{3+}\text{-F}_{\text{int}}^-$  dipoles in  $\text{CaF}_2$  are sensitive functions of the surrounding crystal environment. Interaction effects (both electrostatic and elastic) can cause alterations in these parameters which manifest themselves by a change in the shape of the ITC curve. Such perturbations of the ITC signal may therefore be used as a probe of the lattice defect structure surrounding the dipole.

#### References

1. W. van Weperen and H.W. den Hartog, Phys. Rev. B, **18**, 2857 (1978).
2. C. Bucci and R. Fieschi, Phys. Rev. Letts. **12**, 16 (1964).

THE INFLUENCE OF PHASE BOUNDARIES ON THE HALL-MOBILITY OF  
PHOTOELECTRONS IN  $\text{AgBr}_x\text{I}_{1-x}$ -CRYSTALS

B. Finkernagel and F. Granzer  
Institut Angewandte Physik, Universität D-6000 Frankfurt/Main  
Robert-Mayer-Str. 2-4

The advantages of the large, tabular like silver halide microcrystals, (T-grains), of contemporary high speed photographic emulsions can be fully utilized only if the diffusion length of the photoelectrons is adjusted to the diameter of these grains. In homogeneously composed AgBr-grains the diffusion length  $L$  of electrons, given by:  $L = C \cdot (\tau \cdot \mu_D)^x$  is about 1  $\mu\text{m}$  and thus far below the mean diameter of T-grains, ranging between 3 and 10  $\mu\text{m}$ .  $C$  is a constant,  $\tau$  and  $\mu_D$  is the lifetime and the drift mobility of the photoelectrons respectively, and the exponent  $x$ , depending on the specific model used to calculate  $L$ , takes on the values  $\frac{1}{2}$  or  $\frac{1}{3}$ .

One way to increase the length  $L$  of the diffusion path of the photoelectrons is the augmentation of their lifetime  $\tau$ . This has already been achieved by replacing the pure AgBr crystals by  $\text{AgBr}_x\text{I}_{1-x}$ -mixed crystals. As evidenced by ESR-spectroscopic investigations the recombination of the photogenerated electrons and holes is impeded and therefore the lifetime of the electrons considerably enhanced by the charge separating fields of the phase boundaries in decomposed  $\text{AgBr}_x\text{I}_{1-x}$ -crystals. [1]

There remains, however, the question whether the advantageous influence of phase boundaries on the lifetime  $\tau$  of photoelectrons is partly reduced with regard to their drift mobility  $\mu_D$ . To get an answer on this question which, evidently, is of vital interest for the practical photography, we started measurements of the Hall-mobility - which of course is related to the drift mobility  $\mu$  - of photoelectrons in  $\text{AgBr}_x\text{I}_{1-x}$ -crystals. Sheet crystals with a thickness of 200  $\mu\text{m}$ , an area of about  $2,5 \times 1,5 \text{ cm}^2$  and with compositions ranging from  $0 \leq x \leq 0,5$  were carefully prepared and contacted as

sketched in Fig. 1. The crystals, being insulators in the dark, are exposed to the light of an Osram-UV-Lamp (Ultravitalux) in order to generate the photoelectrons. With the notations of Fig. 1 the Hall-mobility  $\nu_H$  is given by:

$$\nu_H = \frac{U_H \cdot l}{U_L \cdot b \cdot B}$$

All the measurements were performed in a cryostat at 77 K in order to freeze in the movement of interstitial silver ions, thus avoiding photolysis of the crystals.

The results of our Hall-Effekt-measurements performed - in our opinion for the first time ! - on  $\text{AgBr}_x\text{I}_{1-x}$ -crystals are shown in Fig. 2, where the Hall-mobility  $\nu_H$  is plotted vs. the composition  $x$  of the  $\text{AgBr}_x\text{I}_{1-x}$ -crystals.

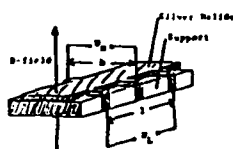


Fig. 1

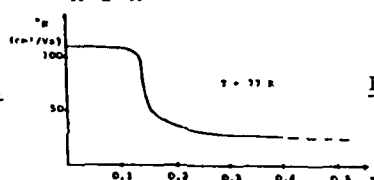


Fig. 2

From the  $\text{AgBr}/\text{AgI}$ -phase diagram [2] it is known, that the homogeneous  $\text{AgBr}_x\text{I}_{1-x}$ -mixed crystals if cooled down below  $120^\circ \text{C}$  starts to decompose into a bromine rich phase ( $\text{NaCl}$ -structure) and an iodine rich phase (Wurtzit-structure) if the iodine content exceeds 15 Mol %. Therefore, the drastic drop of the Hall-mobility at  $x = 0,15$ , has to be attributed to the occurrence of phase boundaries in the  $\text{AgBr}_x\text{I}_{1-x}$ -crystals. This result, indicating an unfavourable influence of phase boundaries on the Hall-mobility - and consequently also on the drift mobility and the diffusion length  $l$  - of photoelectrons must be further substantiated by repeating the experiments at different temperatures with an appropriate puls technique.

- [1] F. Granzer, R. Kricsanowits and Th. Müssig: Proc. ICPS Cologne, 273 (1986)
- [2] Y. Xu, R. Kricsanowits, E. Palm and F. Granzer: Proc. ICPS Cologne, 323 (1986)

HIGH FREQUENCY IONIC CONDUCTIVITY AND PERMITTIVITY OF  $\text{Sr}_{1-x}\text{Ce}_x\text{F}_{2+x}$   
MEASURED BY MEANS OF TIME DOMAIN REFLECTOMETRY

P. Dorenbos and H.W. den Hartog  
 Solid State Physics Laboratory  
 University of Groningen  
 1 Melkweg  
 9718EP Groningen

During the past few years we have studied the ionic conductivity and the permittivity of single crystals  $\text{Sr}_{1-x}\text{Ce}_x\text{F}_{2+x}$  ( $10^{-4} < x < 0.4$ ) extensively by means of ionic thermocurrents and AC-impedance techniques<sup>1-2</sup>. It appears that the  $\text{Ce}^{3+}$  ions distribute randomly over the  $\text{Sr}^{2+}$  host lattice sites. This property together with a high mobility of interstitial fluoride ions in regions of the crystal near  $\text{Ce}^{3+}$  impurities is responsible for percolation type conduction phenomena observed for these crystals.

With the above mentioned techniques, results have been obtained for frequencies ranging from  $\approx 0$  to 30 kHz. In order to obtain information for frequencies between 10 MHz and 10 GHz, a time domain reflectometry (TDR) set-up has been constructed<sup>3</sup>. The TDR experiments can be performed at temperatures between 295 K and 1300 K. Figure 1 shows some characteristic results obtained for a  $\text{SrF}_2$  crystal doped with 2 mol%  $\text{CeF}_3$ . The conductivity has been plotted as an Arrhenius plot with the frequency as a parameter. The frequency dependence of the conductivity can be written as,

$$\sigma(\omega) = A(T) \omega^{n(T)},$$

where  $\omega$  is the angular frequency,  $A(T)$  a proportionality constant, and the power  $n(T)$  is in the range 0 to 1. This equation is known as the Curie-von Schweidler law<sup>4</sup>.

Three conductivity regions can be distinguished in figure 1. In region I, the power  $n(T)$  is close to 1 which is known as the universal dielectric response. In region II,  $n(T)$  is in the range 0.5 to 0.9 which is known as anomalous strong low frequency dispersion. Finally, in region III,  $n=0$  and Arrhenius type DC-ionic conductivity is observed. The conductivity in region I is attributed to the response of the host lattice, whereas the

conductivity observed in region II and III is caused by hopping of interstitial fluoride ions. Percolation type conduction phenomena can be observed for these two regions.

The frequency, the temperature, and the concentration dependence of the conductivity has recently been explained by percolation theory of diffusion in random barrier networks<sup>5</sup>.

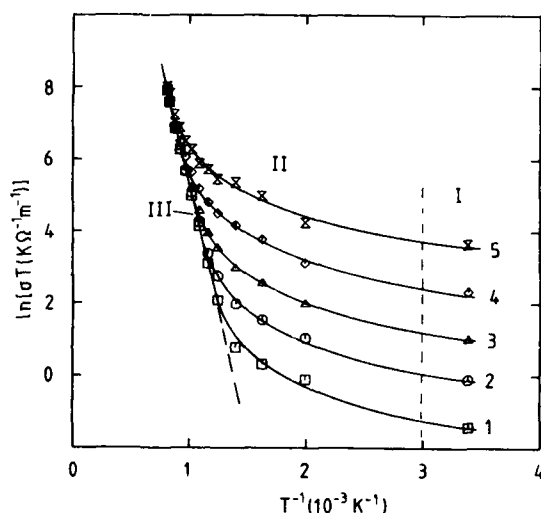


Figure 1. High frequency conductivity of  $\text{SrF}_2:2\text{mol}\%\text{CeF}_3$  measured with time domain reflectometry. Curve 1, 11 MHz; 2, 56 MHz; 3, 222 MHz; 4, 1.2 GHz; 5, 6.1 GHz.

#### REFERENCES

- [1] P. Dorenbos, S. Vrind, J. Dolfing, H.W. den Hartog, *Phys. Rev. B* **35**, 5766 (1987).
- [2] P. Dorenbos, H.W. den Hartog, R. Kruizinga, S. vrind, *Phys. Rev. B* **35**, 5774 (1987).
- [3] P. Dorenbos, H.W. den Hartog, *J. Phys. E: Scient. Instr.*, in press.
- [4] A.K. Jonscher, *Dielectric relaxations in solids* (Chelsea Dielectric Press, London, 1983).
- [5] P. Dorenbos, *Mechanisms of ionic transport in rare earth doped alkaline earth fluorides* (Thesis University of Groningen, 1988).

ELECTRIC-FIELD ASSISTED PROTON DIFFUSION IN  $\text{LiNbO}_3$ 

N. SCHMIDT, K. BETZLER, M. GRABS, AND S. KAPPHAN

Universität Osnabrück, Fachbereich Physik, Postfach 4469, D 4500 Osnabrück

*Doping profiles generated by proton diffusion in  $\text{LiNbO}_3$  are investigated by spatially resolved absorption and second harmonic generation measurements. It is shown that protons are the only mobile ions under the experimental conditions applied (600 °C, 100 V/cm). Lithium ions do not move under these conditions. The resulting refractive index changes can be correlated directly with the local proton density.*

In  $\text{LiNbO}_3$  volume phase holograms — which are usually not stable against readout — can be stabilized by thermal fixing [1]. It has been shown that ion migration — mainly that of protons [2] — plays an important role in this fixing process. Our measurements were performed to answer two questions:

- (1) are besides protons also Li-ions mobile under conditions similar to thermal fixing,
- (2) which refractive index change can be correlated with the proton doping?

Both the Li/Nb ratio and proton doping affect the refractive indices in  $\text{LiNbO}_3$ . The variation of the corresponding phase matching temperature (PMT) can be measured by spatially resolved second harmonic generation (SRSHG) [3]. Congruent  $\text{LiNbO}_3$  samples were doped with protons by heating them to about 600 °C in humid atmosphere with an applied electric field of about 100 V/cm. A typical PMT profile as measured by spatially resolved second harmonic generation (SRSHG) is shown in fig. 1 (dashed line). After this field treatment the sample was cut into two pieces which were annealed at 850 °C in dry atmosphere to equilibrate the sample. Under these annealing conditions hydrogen will leave the crystal rapidly. Remaining variations of the PMT should therefore be due to field induced concentration changes of Li-ions. However, after annealing, both pieces did show the same constant phase matching temperature nearly identical to that of the sample in the as-grown state. This means that the local Li/Nb ratio was not changed by the above treatments. From this fact it can be concluded that the measured PMT profile is due to a variation of the proton concentration and that only protons are mobile under our experimental conditions.

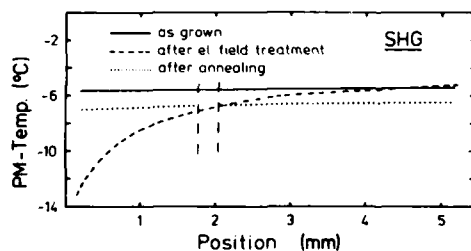


Fig. 1: Spatially resolved measurement of the phase matching temperature in  $\text{LiNbO}_3$  (full line: as grown, dashed line: after field assisted proton diffusion, dotted line: after cutting at the vertical dashed lines and annealing the sample).

To determine the refractive index change induced by protons, SRSHG measurements were combined with spatially resolved absorption measurements (fig. 2). The resulting variation of the phase matching temperature with the OH absorption is given by

$$\frac{\Delta T_{PM}}{\Delta \alpha} = 0.51 \text{ K/cm}^{-1}$$

From the change in the phase matching temperature the index change can be calculated [4]. Using the absorptions strength of OH in  $\text{TiO}_2$  [5] the proton content can be derived. The evaluation yields a proton induced refractive index change of

$$\frac{\Delta n}{\Delta [\text{OH}]} = 5.7 \cdot 10^{-23} \text{ cm}^3$$

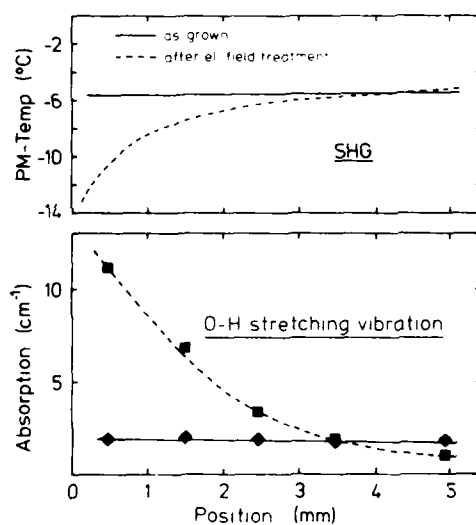


Fig. 2: Spatially resolved measurements of phase matching temperature (upper) and absorption in the OH-stretching vibration line (lower) before (full line) and after field doping with protons (dashed line).

This work is supported by the Deutsche Forschungsgemeinschaft (SFB 225 / B1).

1. J. J. Amodoi, D. L. Staebler, Appl. Phys. Letters **18** (1971), p. 540.
2. H. Vormann, G. Weber, S. Kapphan, E. Krätzig, Sol. State Commun. **40** (1981), p. 543.
3. N. Schmidt, K. Betzler, S. Kapphan, Cryst. Lattice Defects Amorphous Mater. **15** (1987), p. 103.
4. J. Noda, M. Fukuma, Y. Ito, J. Appl. Phys. **51** (1980), p. 1379.
5. O. W. Johnson, J. DeFord, J. W. Shaner, J. Appl. Phys. **44** (1973), p. 3008.

DIELECTRIC RELAXATION AND COMPUTER SIMULATION STUDIES OF  
RUTILE-STRUCTURED  $\text{MnF}_2$  DOPED WITH TRIVALENT CATIONS\*

S. Ling<sup>†</sup> and A.S. Nowick  
School of Mines, Columbia University, New York, NY 10027 USA

A.N. Cormack  
College of Ceramics, Alfred University, Alfred NY 14802, USA

and

C.R.A. Catlow  
Department of Chemistry, University of Keele, Staffs. ST5 5BG, UK

The fluorides that have the tetragonal rutile structure, e.g.  $\text{MgF}_2$ ,  $\text{MnF}_2$  and  $\text{ZnF}_2$ , probably constitute the simplest ionic crystals which have a uniaxial structure, and therefore display anisotropy in their second-rank tensor properties (e.g., diffusion, dielectric constant and electrical conductivity). Nevertheless, the nature of the dominant intrinsic defect in such materials has not been well established, both Schottky and anion Frenkel defects having been proposed.<sup>1,2</sup>

The present experiments involve low-temperature dielectric relaxation measurements on  $\text{Er}^{3+}$ - and  $\text{Y}^{3+}$ -doped  $\text{MnF}_2$ . Unexpectedly, dielectric loss peaks were observed at cryogenic temperatures involving very low activation energies,  $E$ . For both dopants, a prominent peak is observed for samples oriented parallel to the  $c$ -axis with  $E \sim 2$  meV. Both samples also show peaks in perpendicular orientations with  $E = 37$  meV for  $\text{Er}^{3+}$  and 46 meV for  $\text{Y}^{3+}$  doping. Such low  $E$ -values are probably too small to be controlled by lattice migration of a defect. Rather, we expect that they are due to very low symmetry configurations which allows a flip-flop motion involving a low  $E$  to produce reorientation.

Computer simulation calculations have been carried out which are much improved over early studies of this system.<sup>3</sup> In earlier studies, which employed the HABES-II code designed for cubic crystals and used different interatomic potentials, predicted a preference for the cation defect over the anion Frenkel. The present work uses a improved code (CASCAPE) and better F-F and anion-anion potentials. The results have

the previous prediction, with an energy per defect for the anion Frenkel of only 1.53 eV as against 1.99 eV for Schottky. (Similar results apply to  $\text{MgF}_2$  as well.) It was also shown that the fluorine interstitial,  $\text{F}_i$ , adopts a complex structure of the split-interstitial type. This defect is found to associate strongly with trivalent dopants (association energies being 0.80 eV for  $\text{Y-F}_i$  and 0.94 eV for  $\text{Er-F}_i$  in  $\text{MnF}_2$ ). Further, this association gives rise to low symmetry dipolar structures with the necessary off-symmetry configurations to explain the experimental findings.

Since there is no alternative way to explain these low-temperature relaxations in terms of impurity association with Mn vacancies, as would be predicted from a Schottky model, we may conclude that these experiments serve to establish the nature of the intrinsic defect in  $\text{MnF}_2$  as anion Frenkel.

\*Work supported in part by the United State Department of Energy.

+ Now at: Exxon Research and Engineering Laboratory, Annandale, NJ 08801.

1. D.S. Park and A.S. Nowick, J. Phys. Chem. Solids 37 (1976) 607.

2. C.R.A. Catlow, R. James and M.J. Norgett, J. de Physique 37 (1976) C7-443.

THERMALLY STIMULATED DEPOLARIZATION STUDIES OF  
CLUSTERING IN RARE EARTH DOPED ALKALINE EARTH FLUORIDES

G. E. Matthews, Jr., Pam Steed, and Martha Dameron

Wake Forest University

Winston-Salem, NC 27109

We have used thermally stimulated depolarization (TSD) measurements as a probe of the nature of clusters of rare earth dopants in alkaline earth fluorides. There have long been indications of clustering of rare earth impurities in calcium fluoride containing a few tenths of an atomic per cent dopant.<sup>1</sup> Evidence indicates that the " $R_{IV}$ " relaxation observed in calcium fluoride is associated with a cluster of rare earths, probably a dimer.<sup>2</sup> Defect structure calculations predict several possible structures of small clusters in fluorite crystals<sup>3</sup>, but confirmation by experiment is difficult.

While TSD spectra provide no information regarding the symmetry of a center, defect-defect interactions broaden TSD peaks. The degree of broadening of ESR lines is quite sensitive to the nature of defect clusters in the surrounding crystal<sup>4</sup>. Similarly, broadening of TSD peaks is strongly affected by the types of clusters present<sup>5,6</sup>. Thus, TSD line shapes provide a probe of the structure of those centers found near the defect whose relaxation is monitored.

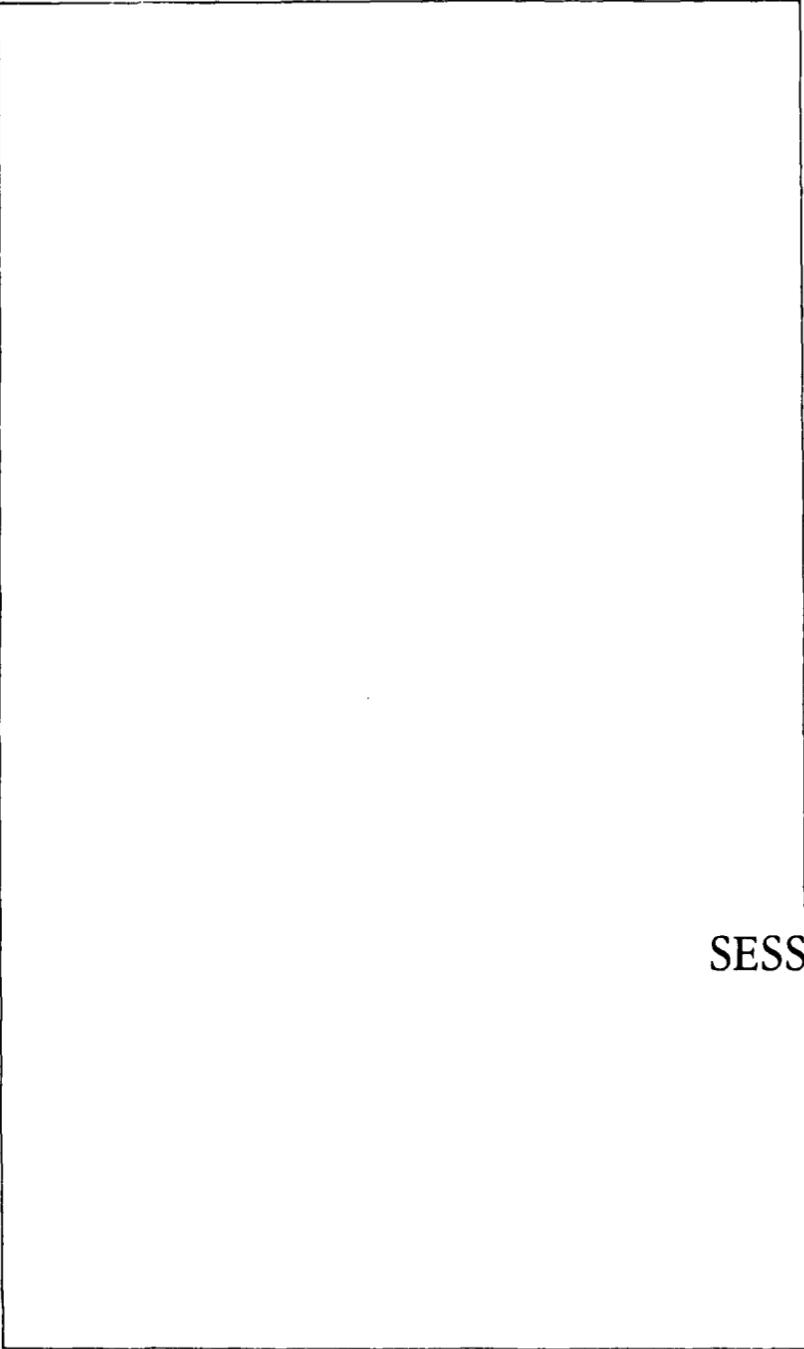
In crystals with small dopant concentrations, each TSD peak is well described in terms of what would be expected from a simple Arrhenius relaxation with a single activation energy. However, at higher concentrations, interactions among defects become significant. To include the effects of defect-defect interactions in the theory of TSD relaxations, we assume a distribution of activation energies for defects of each species. The width of the distribution of activation energies is determined by a least squares fit of the TSD peak using an expression for the measured current that reflects a distribution of activation energies.

The width of the distribution of activation energies does not uniquely determine the structure of the surrounding defects. Instead, computer

simulations of crystals are generated containing plausible combinations of various defect species randomly placed. Coulombic interaction between defects is used to calculate the shift in the activation energy of each dipolar defect. The distribution of activation energies for a defect species in these simulated crystals is compared against the experimentally measured distribution. In this manner, many possible defect configurations can be ruled out.

Our computer model indicates that the degree of broadening of TSD peaks is strongly affected by the monopole and dipole moments of defects present. Our measurements of as  $\text{CaF}_2\text{:Gd}$  indicate excellent agreement between experiment and computer model when the  $R_{IV}$  relaxation is assigned to the "gettered" dimer<sup>7</sup>. At concentrations up to 0.1 mole %, monomers and gettered dimers account for most impurities present. However, at a concentration of 0.5 mole %, most of the gadolinium present must be associated with clusters of more than two dopant ions. Further, we have found that the width and the shape of the distribution of activation energies depends on the number and type of defects present.

1. R. Capelletti, E. O. Kuno, G. E. Matthews, Jr., and J. H. Crawford, Jr., *Phys. Status Solidi* A47, 617 (1978).
2. C. Andeen, G. Eric Matthews, Jr., M. K. Smith, and J. Fontanella, *Phys. Rev.* B19, 5293.
3. J. Corish, C. R. A. Catlow, P. W. M. Jacobs, S. H. Ong, *Phys. Rev.* B25, 6425 (1982).
4. H. W. den Hartog, *Phys. Rev.* B27, 20 (1983).
5. E. Laredo, M. Puma, N. Suarez, and D. R. Figueroa, *Phys. Rev.* B23, 3009 (1981).
6. W. Van Weperen, B. P. M. Lenting, E. J. Bijvank, and H. W. den Hartog, *Phys. Rev.* B16, 2953 (1977).
7. C. G. Andeen, J. J. Fontanella, M. C. Wintersgill, P. J. Welcher, R. J. Kimble, Jr., G. E. Matthews, Jr., *J. Phys.* C14, 3557 (1981).



SESSION 3

ADVANCES IN THE COMPUTER SIMULATION OF DEFECTIVE MATERIALS

J. H. Harding

Theoretical Physics Division,  
Harwell Laboratory, Didcot OX11 0RA, U.K.

Many of the properties of insulating crystals are controlled by defects. Over the last twenty years, methods have been developed to calculate the energies of defect processes and so understand the properties controlled by them. General purpose codes have been written to make such calculations a matter of routine provided a model of the crystal forces is available. The early calculations were of defects in the bulk. However, the presence of surfaces, grain boundaries and dislocations has a profound effect on the defect population. This affects such properties as sintering, catalysis and heterogeneous reactions. Calculations here are more difficult because of the low symmetry of the problem. This is especially true for dislocations. Two problems must be solved. It is first necessary to calculate the relaxation of the crystal due to the presence of the interface. Only when this has been done is it possible to consider the effect of such interfaces on point defects.

IN this lecture, we shall discuss the physics behind the methods used, paying particular attention to the importance of correctly including the relaxation and polarisation of the lattice caused by the defects. The importance of ensuring that an adequate model of the crystal forces has been obtained will also be stressed. Examples will be given to show the kinds of result that atomistic simulation can give.

In the past, calculations have obtained the internal energy for the defect in a static lattice. However, it is clear that if comparison is to be made with experiment, what is required is the enthalpy at finite temperature. In the past, it has often been assumed that the calculated internal energy may be identified with this quantity. With the advent of methods of calculating entropies, this assumption may be tested. The calculation of entropies also permits the direct evaluation of such quantities as defect

concentrations and hopping rates. Jacobs, in his lecture, discusses the methods of calculating entropies in more detail.

The discussion of temperature effects leads on to the question of the relationship of the methods discussed here to molecular dynamics. In a few special cases, direct comparisons can be made, but the processes for which these methods are most useful are too slow for molecular dynamics to simulate them easily.

Progress in this field has been rapid in the last few years; however there is still much to do. Examples of where more work is needed are the effect of temperature on surfaces and interfaces, the effect of high defect concentrations and obtaining adequate potential models to study complex materials.

O<sub>2</sub><sup>-</sup> DEFECTS: THE FIRST SOLID STATE MODEL SYSTEM FOR SUPERFLUORESCENCE

D. SCHMID, L.O. SCHWAN and A. SCHILLER

Physik der kondensierten Materie, Festkörperspektroskopie,  
Universität Düsseldorf, D-4000 Düsseldorf 1, W-Germany

Superfluorescence is the spontaneous collective emission of coherent light from an ensemble of two-level systems which are initially all in the excited state. It was predicted in 1954 by Dicke /1/ but is was not observed until 1973 /2/. In this contribution we report on experiments with O<sub>2</sub><sup>-</sup> centers in KCl and emphasize a number of novel experimental observations such as multicolor superfluorescence, transverse mode structure and superfluorescence-brightened laser activity. In order to account for the observations, Dicke's model had to be expanded and some of its restrictions had to be released:

(1) In Dicke's model the two-level atoms are assumed to be indistinguishable and to be confined in a volume with linear dimensions small compared to  $\lambda$ , the wavelength of the emitted radiation. In optical experiments this condition is usually not fulfilled. The linear dimensions are not small compared to  $\lambda$ . Most experiments have been performed with thin pencil-shaped excitation volumes of length  $l \gg \lambda$  and with cross section  $A$ , which is characterized by a Fresnel number  $F = A/l\lambda$  in the order of unity. We will report on experiments with excitation volumes described by Fresnel numbers large compared to one. If the exciting pump-pulse is adjusted properly, the emitted superfluorescence beam exhibits characteristic interference patterns indicating that, apart from the temporal coherence of the superfluorescence, also spatial coherence builds up via self-organization in the inverted ensemble. This observation is not due to unintended laser activity with transverse mode structure. The latter can be ruled out, since it is possible to observe laser activity and superfluorescence simultaneously with spectral and spatial features that are quite different from each other. We will present results of computer simulations based on very simple model assumptions, which reflect the self-organization to a spatially coherent state of the ensemble very similar to the state created externally in a distributed feed-back laser.

(2) Dicke's model does not consider the starting process which initiates the self-organization of the inverted ensemble to a coherently emitting entity. This process is a very subtle problem of quantum electronics and has been treated theoretically by many authors /4/. We will compare the theoretical results qualitatively to the experimental results obtained on a pencil-shaped excitation volume /5/. In spite of the fair overall agreement, there is one major discrepancy between theory and experiment. In our experiments the pulses obtained in forward and backward direction are strictly correlated (time of origin, polarization, wavelength and coherence length). The existing theories, however, predict statistical fluctuations of these quantities with respect to each other.

(3) The two-level model is an oversimplification even for the simplest atomic system. Superfluorescence of  $O_2^-$  centers can be observed simultaneously at up to four different wavelengths. To explain these observations the theoretical description had to be expanded to multi-level systems /6 - 8/. The results of these theories are in qualitative agreement with the experimental observations.

#### References

- /1/ R.H. Dicke, Phys. Rev. 93, 99 (1954)
- /2/ See for instance: Q.H.F. Vrehen and H.M. Gibbs in: Dissipative Systems in Quantum Optics, Topics in Current Physics 27, 111 (1982)
- /3/ A. Schiller, L.O. Schwan and D. Schmid, J. Lumin. 38, 243 (1987)
- /4/ F. Haake, H. King, G. Schröder, J.W. Haus and R.J. Glauber, Phys. Rev. A 20, 2047 (1979); A 23, 1322 (1981)
- /5/ R. Florian, L.O. Schwan and D. Schmid, Phys. Rev. A 29, 2709 (1984)
- /6/ F. Haake and R. Reibold, Phys. Rev. A 29, 3208 (1984)
- /7/ P. Schwendimann, Optica Acta 31, 107 (1984)
- /8/ P. Schwendimann and E. Sigmund, Solid State Commun. 50, 379 (1984).



SESSION 3A

# THREE-PHOTON SPECTROSCOPY OF EXCITONS AND POLARITONS IN ALKALI HALIDES

F. Beerwerth, D. Fröhlich, and P. Köhler, Institut für Physik, Universität Dortmund,  
4600 Dortmund 50, Federal Republic of Germany

Nonlinear optical methods like two-photon absorption (TPA) are widely used to study electronic parameters in solids. Although the first TPA experiments were done in alkali halides<sup>1</sup>, there was much more interest in semiconductors like  $\text{Cu}_2\text{O}$ <sup>2</sup> and  $\text{ZnSe}$ <sup>3</sup>. In these materials pronounced structures are resolved in TPA experiments. Details of the electronic bandstructure as effective mass parameters and  $g$  values are determined with high accuracy by two-photon magnetooptics<sup>4</sup>. In crystals without inversion center as  $\text{CuCl}$  the polariton structure was studied by TPA<sup>4</sup>. In alkali halides the pronounced polariton structure of the lowest  $S$  exciton can not be studied by TPA, because alkali halides have a center of inversion. In three-photon spectroscopy (TPS), however, transitions to the transverse polariton (TP) and even the longitudinal exciton (LE) are dipole allowed. Three-photon processes are expected to be very weak, because they are described by third-order perturbation theory. We succeeded to measure three-photon spectra of  $\text{KI}$  and  $\text{CsI}$  by excitation spectroscopy<sup>5</sup>. We have extended these measurements to other alkali halides, including alkali bromides and  $\text{NaCl}$ . As an example we show the polariton structure of  $\text{RbI}$  in Fig. 1. The experimental results are described by a two-oscillator dispersion formula as discussed for  $\text{KI}$  in Ref.5 :

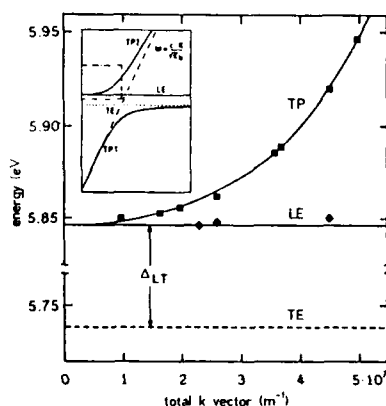


Fig. 1: Resonances on the upper polariton branch (TP) and on the longitudinal exciton (LE) as a function of the total  $k$  vector; inset: schematic diagram of polariton dispersion, indicated square shows region of experimental results.

$$\frac{\hbar^2 c^2 k^2}{E^2} = \epsilon_b \cdot \frac{E_{1L}^2 - E^2}{E_{1T}^2 - E^2} \cdot \frac{E_{2L}^2 - E^2}{E_{2T}^2 - E^2} \quad (1)$$

We get for the fit parameters the following values:  $E_{1T} = 5.738$  eV,  $E_{1L} = 5.846$  eV,  $E_{2T} = 6.47$  eV,  $E_{2L} = 7.28$  eV, and  $\epsilon_b = 2.04$ .

Due to the large oscillator strength of the  $1S$  exciton in alkali halides one gets a rather large longitudinal transverse splitting ( $\Delta_{LT} = 108$  meV) as compared to  $\text{CuCl}$ <sup>4</sup> ( $\Delta_{LT} = 5.4$  meV) and  $\text{GaAs}$ <sup>6</sup> ( $\Delta_{LT} = 0.08$  meV). Two resonances on the upper polariton branch are shown in Fig. 2. The high energy resonance corresponds to a maximum  $k$  vector ( $k_{\max} = 3 \cdot k_{\text{dye}}$ ) whereas the lower resonance corresponds to a minimum  $k$  vector ( $k_{\min} = k_{\text{dye}}$ ).

In high magnetic fields a new very narrow and very weak resonance is resolved at lower energy. This line is interpreted as transition to the paraexciton. From a  $\Gamma_8^-$  ( $j_v = 3/2$ ) valence band and a  $\Gamma_6^+$  ( $j_c = 1/2$ ) conduction band one derives a threefold

orthoexciton ( $F=1$ ,  $\Gamma_4^-$  symmetry) and a fivefold paraexciton ( $F=2$ ,  $\Gamma_1^+$ ,  $\Gamma_5^-$  symmetry). The dipole forbidden paraexciton gets allowed by field induced mixing of ortho- and paraexcitons. Since the paraexciton is extremely narrow, the splitting can easily be resolved. From the magnetic field dependence one gets for the  $g$  value of the paraexciton  $g_p = 1.33 \pm 0.05$  (Fig. 3).

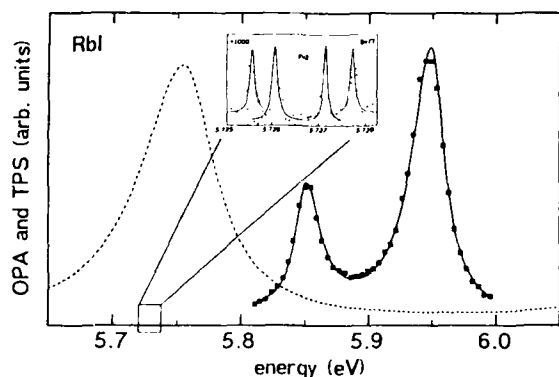


Figure 2

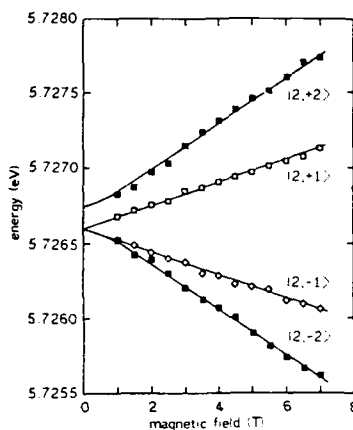


Figure 3

Fig. 2. Three-photon spectra of the lowest exciton structure of RbI at 4.5 K. One-photon absorption (dashed line) from Ref. 7. The inset shows the narrow structure of the  $F=2$  paraexciton components  $M_F = \pm 2, \pm 1$  in a magnetic field of 7T. Note the enlarged scale of the inset.

Fig. 3. Field-dependent splitting of the  $F=2$  paraexciton. Open squares and closed squares show the  $M_F = \pm 1$  and  $M_F = \pm 2$  components, respectively. Solid lines represent a least-squares fit with parameters given in the text.

Another interesting parameter is the exchange interaction which can be derived from the energy values of the paraexciton ( $E_p = 5.7266 \text{ eV} \pm 0.2 \text{ meV}$ ) and the transverse exciton ( $E_{1T} = 5.738 \text{ eV} \pm 3 \text{ meV}$ ). We get for  $\Delta_{ex} = 3/2 (E_{1T} - E_p) = (17 \pm 4) \text{ meV}$ . For the definition of  $\Delta_{ex}$  we refer to Onodera and Toyozawa<sup>8</sup>.

#### References:

- <sup>1</sup> J.J. Hopfield and J.M. Worlock, Phys. Rev. **137**, A 1455 (1965);
- D. Fröhlich and B. Stagninus, Phys. Rev. Lett. **19**, 496 (1967).
- <sup>2</sup> Ch. Uihlein, D. Fröhlich, and R. Kenkies, Phys. Rev. **B 23**, 2731 (1981).
- <sup>3</sup> H.W. Hölscher, A. Nöthe, and Ch. Uihlein, Phys. Rev. **B 31**, 2379 (1985).
- <sup>4</sup> D. Fröhlich, E. Mohler, and P. Wiesner, Phys. Rev. Lett. **26**, 554 (1971);
- D. Fröhlich, E. Mohler, and Ch. Uihlein, Phys. Stat. Sol. (b) **55**, 175 (1973).
- <sup>5</sup> F. Beerwerth and D. Fröhlich, Phys. Rev. Lett. **55**, 2603 (1985).
- <sup>6</sup> R.G. Ulbrich and C. Weisbuch, Phys. Rev. Lett. **38**, 865 (1977).
- <sup>7</sup> K. Teegarden and G. Baldini, Phys. Rev. **155**, 896 (1967).
- <sup>8</sup> Y. Onodera and Y. Toyozawa, J. Phys. Soc. Jpn. **22**, 833 (1967).

RELAXATION OF SELF-TRAPPED EXCITONS IN ALKALI CHLORIDE CRYSTALS  
STUDIED BY TIME DELAYED DOUBLE EXCITATION IN PICOSECOND RANGE

Yoshiro SUZUKI, Hidetoshi ABE and Masamitsu HIRAI

Department of Applied Physics, Faculty of Engineering,  
 Tohoku University, Aramaki-Aoba, Sendai, 980 JAPAN

The conversion of the self-trapped excitons (STE's) at  $2p\sigma_u$  (or  $2p\pi_u$ ) to the F centers in NaCl, KCl and RbCl crystals has been investigated in the picosecond range. The crystals were excited first by a pulsed KrF excimer laser (pulse duration of  $\sim 20$ ns) to create STE's at the lowest triplet state ( $1s\sigma_g$ ). Then, the crystals were excited secondarily to excite STE's from  $1s\sigma_g$  to  $2p\sigma_u$  by a pulsed ruby laser (pulse duration of  $\sim 40$ ps) at  $\sim 100\mu$ s after the first excitation.

Figure 1 presents absorption spectra of NaCl at 14K before and after the second excitation. The lowest dotted curve evidences the formation of STE's at  $1s\sigma_g$  by the first excitation. By the second excitation, the STE absorption band (STE in the figure) starts to decrease, while the F band grows as shown by curves from -25ps to 208ps. In Fig.2 is illustrated the temporal variation of the optical density at representative photon energies at 2.00eV and 2.77eV in the STE and F bands. Experimental points (open circles) for the F band growth at 2.77eV can be followed by a convolution analysis with assuming the stepwise growth. This result makes it clear that the conversion from the STE at  $1s\sigma_g$  to F centers via  $2p\sigma_u$  (or  $2p\pi_u$ ) takes very short period which is out of our time resolution.

Another notable result is the almost complete conversion of STE's to F centers as seen by curves at -25ps and 208ps in Fig.1. The curve at -25ps implies that the first excitation by the KrF laser produces mostly STE's at  $1s\sigma_g$ . In other words, STE's at  $2p\sigma_u$  (or  $2p\pi_u$ ) relax down efficiently to  $1s\sigma_g$ , but inefficiently to F centers. Nevertheless, the second excitation by the ruby laser to excite STE's from  $1s\sigma_g$  to  $2p\sigma_u$  (or  $2p\pi_u$ ) converts almost completely STE's to F centers as shown by curves at -25ps and 208ps. Since the conversion from STE's at  $2p\sigma_u$  (or  $2p\pi_u$ ) to F centers is inefficient, the almost complete conversion may come from repetition cycles of excitations and relaxations between  $1s\sigma_g$  and  $2p\sigma_u$  (or  $2p\pi_u$ ) during the second excitation with the pulse duration of  $\sim 40$ ps. By assuming the branching ratio of  $k_2$  and  $k_3$  for the relaxation of STE from  $2p\sigma_u$  (or  $2p\pi_u$ ) to  $1s\sigma_g$  and for the conversion to F centers, the ratio of  $k_3/k_2$  was determined to be 1/15. This value was confirmed by observing the excitation power dependence of the secondarily induced F band height. Since  $k_3$  is  $\sim 7\%$  of  $k_2$ , the cycle must be repeated by  $\sim 20$  times or more during  $\sim 40$ ps for the complete conversion of STE's to F centers.

Naturally,  $\sim 2$ ps or shorter duration in one cycle is expected. Thus, the relaxation time for the final process going back to  $1s\sigma_g$  or

going to F centers from  $2p\sigma_u$  (or  $2p\pi_u$ ) was estimated by distinguishing it from the total relaxation time obtained by the conventional time-resolved spectroscopy with single excitation.

KCl and RbCl crystals exhibited also similar results as NaCl crystals.

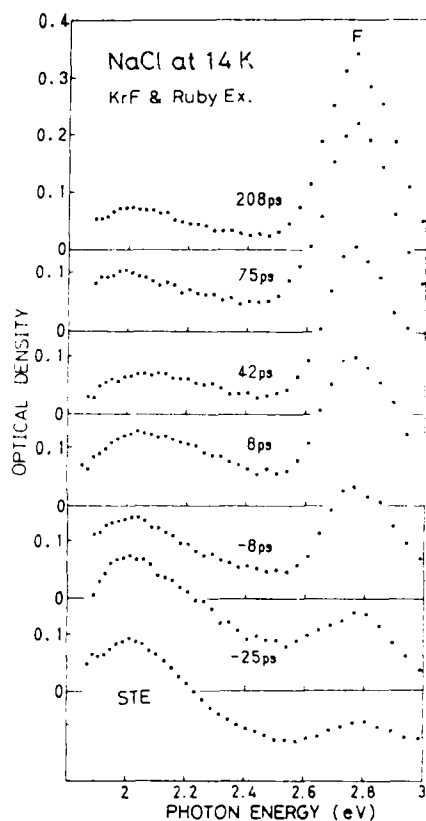


Fig.1 Temporal variation of absorption spectra before and after the second excitation on a NaCl crystal by a ruby laser.

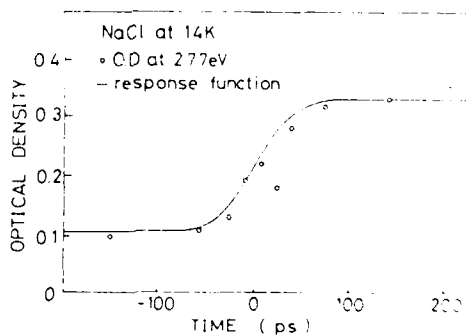
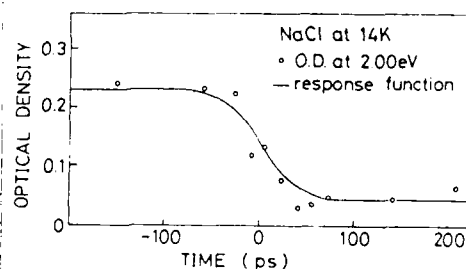


Fig.2 Temporal variation of the optical density at 2.00 eV for STE and at 2.77 eV for F bands in NaCl under the second excitation by a ruby laser.

RADIATIVE AND NON-RADIATIVE DE-EXCITATION PROCESSES  
OF LOCALIZED EXCITONS IN KCl:Br

Koichiro TANAKA, Hideo KOSAKA, Osamu ARIMOTO<sup>\*)</sup>, Ken-ichi KAN'NO  
 and Yoshio NAKAI

*Department of Physics, Kyoto University, Kyoto 606, JAPAN*

KCl:Br crystal is a typical system in which several experiments were made concerned with the Frenkel defect (FD) formation from relaxed excitons: Keller and Patten<sup>1)</sup> detected the creation of H-centers as a result of electrons recombining with  $\text{ClBr}^-$  hetero- $V_K$  centers. The production of F-centers was confirmed under one-photon and two-photon excitation into the  $\text{Br}^-$  absorption band by Maki et al.<sup>2)</sup> and Itoh et al.<sup>3)</sup> In the present work, experiments were made on the luminescence processes due to  $\text{Br}^-$  localized excitons, which will be complementary for the FD formation.

Excitation into the absorption band due to an isolated  $\text{Br}^-$  ion, which is known to locate at 7.46 eV<sup>4)</sup> ( the arrow in the Fig.1 ), does not give any definite emission band at the temperature from 2 K to 78 K. However, excitation into the low energy side of  $\text{Br}^-$  band gives rise to two distinct emission bands at 3.60 eV and 4.88 eV, as shown in Fig.1. These emission bands have been also observed by Wakita and Hirai<sup>5)</sup> under X-ray irradiation. They assigned tentatively these emission bands to originate from localized excitons created at isolated  $\text{Br}^-$  ions. However, the fact that these emission bands are both stimulated strongly at the low energy tail of the impurity band suggests that they originate from impurity dimer centers<sup>6)</sup>. Moreover, it was confirmed that their intensities are both proportional to the square of  $\text{Br}^-$  contents over two orders of magnitude in the low concentration region. This gives a clear evidence that both emission bands derive from bromine dimers. The same situation was confirmed in RbCl:Br crystals.

The initial states responsible for these emission bands have been clarified from their decay characteristics by means of a time-correlated single photon counting method under the single bunch operation of UVSOR, Okazaki, JAPAN. The interval of successive SR light pulses was 177.6 ns and an

-----  
 \*) Present address: Department of Physics, Okayama University, Okayama.

apparent time duration of the exciting light was 550 ps including the time response of the apparatus. In Fig.2 is shown the decay behavior of the 4.88 eV emission (dots), along with a pulse shape of exciting light at 7.25 eV (broken curve). By a convolution analysis it was definitely determined that the emission decay obeys a single exponential function with the time constant 1.2 ns (solid curve). This reveals that the 4.88 eV emission is the fluorescence from a singlet state. On the other hand, the 3.60 eV emission should be attributed to the phosphorescence from a triplet state because its lifetime is too long ( of the order of  $\mu\text{s}$  ) to be determined by the present measurements. On the analogy of  $\pi$  and  $\sigma$  emission from self-trapped excitons in pure alkali halides, it is supposed that the 3.60 eV emission originates from the lowest triplet state and the 4.88 eV emission from the higher singlet state of the  $[\text{Br}_2^-(V_K) + e]$ -relaxed excitons in the matrix of KCl.

It is noteworthy that excitons created at isolated  $\text{Br}^-$  ions in KCl:Br and RbCl:Br decay non-radiatively even at LHeT, unlike any other halogen impurity systems. The FD formation processes mentioned above will be a possible candidate for the non-radiative decay channel.

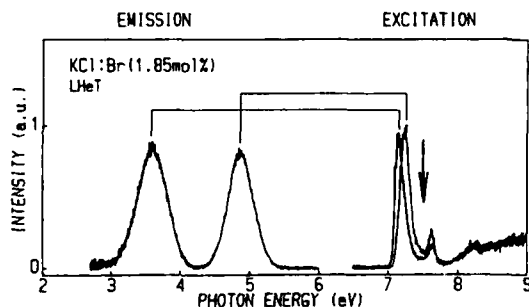


Fig.1. Emission (left side) and excitation (right side) spectra of KCl:Br.

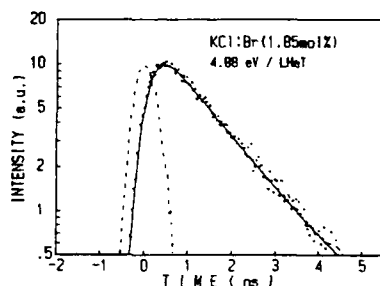


Fig.2. Decay curve of the 4.88 eV emission of KCl:Br.

- 1) F.J.Keller and F.W.Patten: Solid State Commun. 7 (1969), 1603.
- 2) M.Maki, N.Nagasawa and M.Hirai: Solid State Commun. 17 (1975), 1409.
- 3) M.Itoh, K.Kan'no and Y.Nakai: Solid State Commun. 26 (1978), 929.
- 4) D.Hinks and S.Susman: Phys.stat.sol. (b) 52 (1972), K53.
- 5) S.Wakita and M.Hirai: J. Phys. Soc. Jpn. 24 (1972), 1177.
- 6) H.Nakagawa, M.Itoh and Y.Nakai: J. Phys. Soc. Jpn. 32 (1972), 1037.

A THEORETICAL BASIS FOR THE RABIN-KLICK CRITERION  
IN TERMS OF OFF-CENTER SELF-TRAPPED EXCITON RELAXATION

- \* Song, K.S., Department of Physics, University of Ottawa, Ottawa, Canada
- \* Leung, C.H., Division of Sciences, University of New Brunswick, Saint John, Canada
- # Williams, R.T., Department of Physics, Wake Forest University, Winston-Salem, NC, U.S.A.

In 1960, Rabin and Klick<sup>(1)</sup> plotted the X-ray dose per F center created at 4.2 K in various alkali halides versus a parameter S/D, the space between adjacent halide ions along a  $\langle 110 \rangle$  row divided by the diameter of the halogen atom. In crystals with  $S/D > 0.45$ , i.e. KBr, LiF, KCl and NaF in their study, F center formation proceeds with high efficiency at low temperature. In crystals with  $S/D < 0.45$ , i.e. NaCl, KI and NaBr in their study, the F center production efficiency at 4.2 K drops sharply with decreasing S/D, falling to a value for NaBr three orders of magnitude smaller than for the high efficiency crystals.

Rabin and Klick proposed the S/D parameter as a geometric measure of space available for insertion of an interstitial halogen atom to form an H center. It seemed straightforward to suppose that with less space available to receive the H center, F center formation would be strongly discouraged. This is then the geometrical or static rationale for the Rabin Klick criterion. Later, Townsend<sup>(2)</sup> has reconfirmed the trend after adding accumulated data on more alkali halides. However, with quite modest amounts of thermal energy, i.e. activation energies of order 100 meV, the crystals with  $S/D < 0.45$  form F centers with high efficiency also. Furthermore, the crystals with  $S/D > 0.45$  have similar thermally activated stages of F center formation, with roughly the same activation energies, in addition to the low temperature process. It has thus been suggested that the thermally-activated process is universal in alkali halides, and that the group with  $S/D > 0.45$  have an additional temperature-independent channel. The available space argument of Rabin and Klick should inhibit thermally-activated defect formation in crystals with  $S/D < 0.45$ , but it evidently does not. What seems to be inhibited is only the low-temperature process, which in any of the current models is driven by at least 1 eV of self-trapped exciton (STE) relaxation energy, and thus should be even less affected by 'available space' than the thermal activation process.

In this work, we present energy curves representing the potential surface along which the STE relaxes from "on-center" to "off-center" configurations. These curves were calculated using a method developed earlier by us<sup>(3)</sup>. As shown in Figs. 1 and 2 for KCl and NaCl, the relaxation is divided among two configuration coordinates.  $Q_2$  is the odd-parity relaxation of ions surrounding the  $X_2^-$  core, while the  $X_2^-$  is artificially held in the "on-center"  $V_k$  position. Then  $Q_2$  is the coordinate representing off-center motion of the  $X_2^-$  core toward the  $\pi$

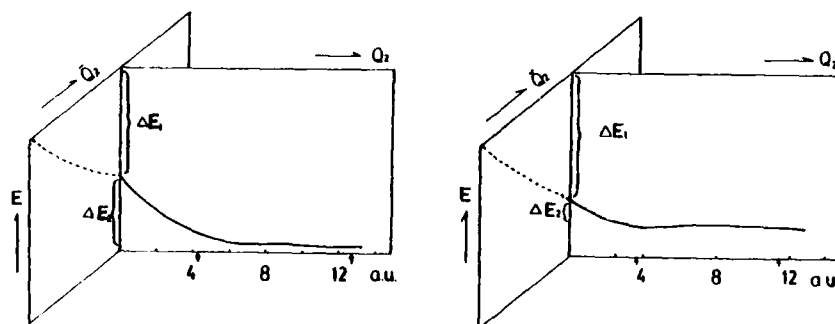
luminescent STE and/or F-H pair. The energy drop associated with relaxation along  $\tilde{Q}_2$  is denoted  $\Delta E_1$ , while the energy drop associated with relaxation along  $Q_2$  is denoted  $\Delta E_2$ . As described in Ref.(4), the energy  $\Delta E_2$  can be transferred to kinetic energy of motion toward larger  $Q_2$ , i.e. larger F-H separation. According to this mechanism for low-temperature F center formation, Figs. 1 and 2 show that much more energy is available in the "productive" channel  $\Delta E_2$  in KCl than in NaCl. Similar computation to be shown for other alkali halides establish quite generally that the ratio  $\Delta E_2/(\Delta E_1 + \Delta E_2)$  increases as S/D increases. The calculated curves also verify that the barrier against thermal diffusion of the H center away from the F center site (i.e. thermally activated defect formation) remain quite small, of the order 100 meV in all the crystals regardless of S/D. Both of these aspects are in quite good agreement with data. It should be noted that the H center is a  $X_2^-$  occupying a halogen site, and its diffusion along a  $\langle 110 \rangle$  axis proceeds by a sequence of "bond-switching". The essential point is the way in which ion-sizes (S/D) influence the dynamical relaxation path of the STE, i.e. division of energy between the "productive" mode  $Q_2$  and the "non-productive" mode  $\tilde{Q}_2$ , rather than simply the available space in a static lattice to receive the H center.

\* Supported by grants from NSERC.

# Supported by NSF grants No. DMR-8600010.

#### Reference

- (1) H. Rabin and C.C. Klick, Phys. Rev. 117, 1005 (1960).
- (2) P.D. Townsend, J. Phys. C 6, 961 (1973).
- (3) C.H. Leung, G. Brunet and K.S. Song, J. Phys. C 18, 4459 (1985).
- (4) R.T. Williams, K.S. Song, W.L. Faust and C.H. Leung, Phys. Rev. B33, 7232 (1986).



Calculated energy surface along  $\tilde{Q}_2$  and  $Q_2$  coordinates  
 Fig 1 for KCl                      Fig 2 for NaCl  
 (full vertical scale: 2.5 eV)

# OPTICAL AND SPIN DEPHASING OF THE PHOSPHORESCENT $O_2^-$ DEFECT IN CALCIUM OXIDE

P.A. van Leeuwen and M. Glasbeek  
 Laboratory for Physical Chemistry, University of Amsterdam,  
 Nieuwe Achtergracht 127, 1018 WS Amsterdam, The Netherlands

Optical and spin relaxation in the photo-excited phosphorescent quartet state of the  $F-O_2^-$  pair center in solid calcium oxide has been studied. The defect gives rise to a zero-phonon line (ZPL) emission peaking at 657 nm [1,2]. The line width of the ZPL has been measured as a function of temperature. In the range from 4.2 K up to 80 K a significant broadening and a shift in the position of the no-phonon line is observed. Fitting of the ZPL shape to a Voigt profile (i.e. a Lorentzian convoluted with a Gaussian) yielded the temperature dependence of the homogeneous line width. The applicability of current theories of optical dephasing in explaining the results is discussed. Deviations from the predictions of the nonperturbative theory by Hsu and Skinner are reported. The data are best interpreted on the basis of a simple perturbative theory for pseudo-local phonons with a frequency of  $160\text{ cm}^{-1}$ .

Spin-lattice relaxation in the excited quartet state of the  $F-O_2^-$  defect is also studied. Analysis of the kinetics of the phosphorescence decay yields the spin-lattice relaxation time ( $T_1$ ) at zero-field. From the temperature dependence of  $T_1$  an Orbach-type spin-lattice relaxation mechanism is inferred, the activation energy being  $60\text{ cm}^{-1}$ . In conclusion, from the above experiments the existence of a number of pseudo-localized mode states becomes apparent.

## References

1. P.A. van Leeuwen, R. Vreeker, and M. Glasbeek, Phys.Rev. B 34, 3483 (1986)
2. M. Glasbeek and P.A. van Leeuwen, J.Lum. 38, 204 (1987)

(MoO<sub>4</sub>) COMPLEXES IN CaWO<sub>4</sub> - RESULTS OF ODMR AND ESR  
INVESTIGATIONS

R. Grasser, A. Hofstaetter, A. Scharmann, F. Schön  
 (1.Phys. Inst. Univ. Giessen, FRG)

and

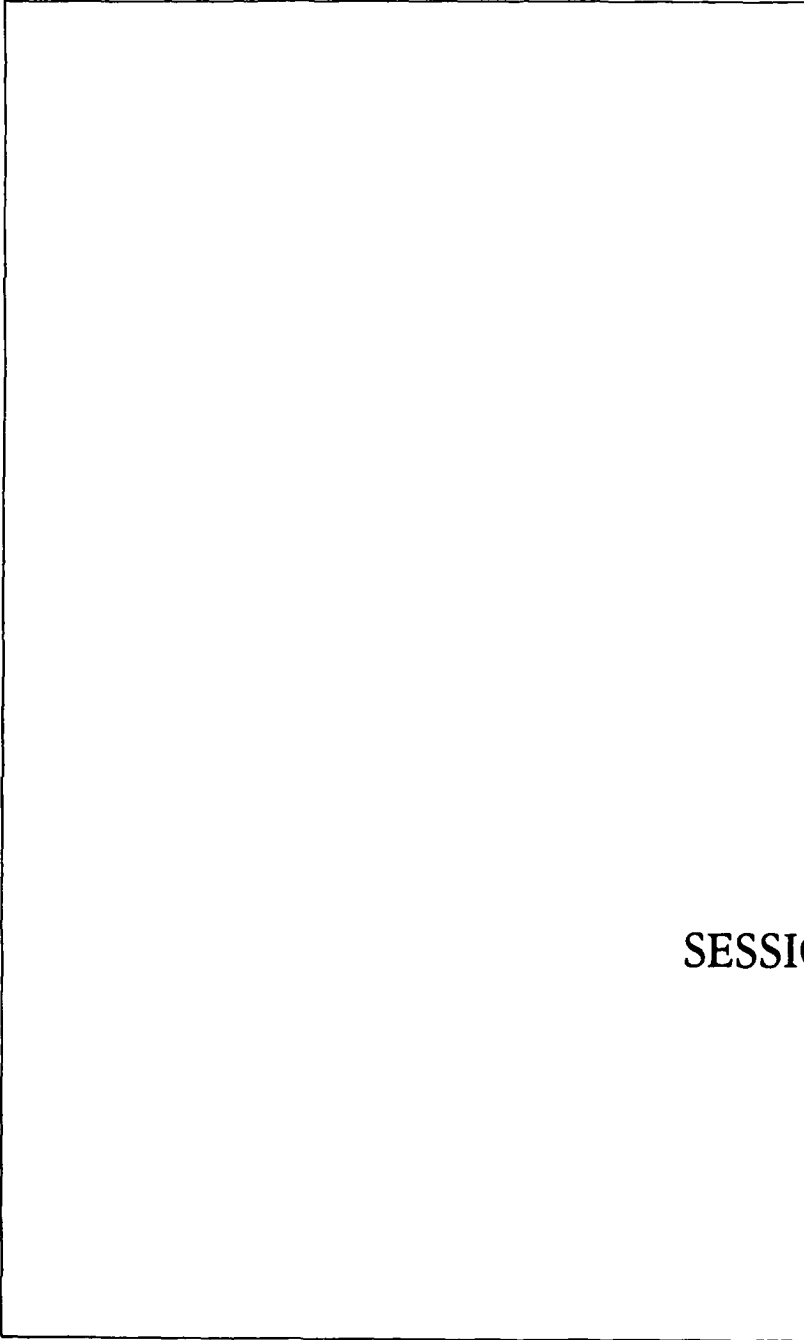
P.G. Baranov, V.V. Djakonov, N.G. Romanov  
 (A.F. Ioffe Phys.-Tech. Institute, Leningrad, USSR)

Due to nearly identical (scheelite) structure of CaMoO<sub>4</sub> and CaWO<sub>4</sub> (MoO<sub>4</sub>) groups can easily be incorporated in the latter compound. Doping CaWO<sub>4</sub> with  $5 \times 10^{-4}$  CaMoO<sub>4</sub> leads to an intense green luminescence in addition to the usual blue tungstate emission. This extra band was studied by ODMR at 1,6 K and 35 GHz. For certain orientations of the magnetic field relative to the crystal axes (B about perpendicular to a W-O bond and in an O-W-O plane) we found a resonance signal with a strong angular dependence. The spectral behaviour of this ODMR line with respect to excitation and emission coincides well with that of the green luminescence. On the other hand it is - beside somewhat differing fine structure parameters - very similar to one of two ODMR signals we found under the same conditions in pure CaMoO<sub>4</sub>. The resonance position of these two lines and their angular dependence again are well described by the data determined by van der Waals 1) for the photo-excited triplet state of CaMoO<sub>4</sub> in ODMR experiments using 75 GHz. From that we suppose the green luminescence observed in this doped CaWO<sub>4</sub> sample to originate from metastable spin triplets of (MoO<sub>4</sub>) complexes, too. This is supported to some extent by the existence of a partially resolved structure on the ODMR line in CaWO<sub>4</sub> : Mo probably due the hyperfine interaction with the nuclei of the odd molybdenum isotopes.

As a result of either X-irradiation at LNT or vacuum reduction the (MoO<sub>4</sub>) groups capture an electron and form a (MoO<sub>4</sub>)<sup>3-</sup> centre. Due to the molecular structure of the complex this additional electron is accommodated in an a<sub>1</sub> orbital stemming from an e orbital split by the symmetry reduction from T<sub>d</sub> to D<sub>2d</sub> (since the tetrahedra are compressed along the crystallographic c-axis). This e (and a<sub>1</sub>) orbital is made up from molybdenum d- and oxygen p-functions resulting in a covalent reduction in the g-shift and the hyperfine

splitting compared to those of a pure  $d_1$  electron. When studying the  $(\text{MoO}_4)^{3-}$  centre in a  $\text{CaWO}_4$  crystal enriched with about 10 %  $^{17}\text{O}$  this covalent contribution shows up in an additional ligand hyperfine structure. We evaluated the  $^{17}\text{O}$  HFS tensor and from that were able to calculate the electronic and geometrical structure of this centre in detail. The results to be presented reveal the regular axial symmetry of the Mo (resp. W) site to be preserved, even in the reduced sample.

- 1) W. Barendswaard, J.H. van der Waals; Mol. Phys. 59, no. 2, p. 337 - 353 (1986)



SESSION 3B

CALCULATION OF IONIC MOBILITY IN SILVER HALIDES USING THREE-BODY POTENTIALS

C.R.A. Catlow and F.M. Healy

Department of Chemistry, University of Keele, Staffordshire ST5 5BG,  
England

J. Corish

Department of Chemistry, Trinity College, Dublin 2, Ireland

P.W.M. Jacobs

Department of Chemistry, The University of Western Ontario, London N6A 5B7  
Canada

M. Leslie

Science and Engineering Research Council, Daresbury Laboratory, Warrington  
WA4 4AD, England

and Y. Tan and R.C. Baetzold

Research Laboratories, Eastman Kodak Company, Rochester, New York,  
New York 14670, U.S.A.

Previous calculations of defect energies for silver halides using two-body potentials yielded Frenkel defect energies that accounted quantitatively for the measured temperature dependence of the ionic conductivity and for silver ion diffusion, but led to results for host anion diffusion that were too low by several orders of magnitude (1 - 4). This was shown to be due to the fact that although the calculated Frenkel defect energies were in good agreement with experiment, the Schottky defect energies were far higher than values inferred from the known diffusivities of  $\text{Cl}^-$  in  $\text{AgCl}$  and of  $\text{Br}^-$  in  $\text{AgBr}$  (5).

It is shown here that this unsatisfactory feature of the two-body potentials can be removed by the inclusion of three-body interactions in either of two forms: a bond-bending model, or the well-known triple dipole model. The parameters in these potentials were determined by fitting to the lattice constant, cohesive energy, elastic constants, dielectric constants, and the frequency of the transverse optic mode. It is impossible to account for the observed values of the elastic constants  $C_{12}$  and  $C_{44}$  in the silver halides with two-body potentials but this can be achieved by introducing three-body terms in either of the above formalisms. However, the triple-dipole model is to be preferred since defect calcul-

ations are more stable than with the bond-bending model.

However, in spite of these substantial improvements, the calculations of silver ion mobility with the triple-dipole model suffer from the same deficiency as did the earlier calculations with two-body potentials, namely that the calculated values are much too large. It is shown that the quadrupolar deformation of the  $\text{Ag}^+$  ion at low symmetry sites is a necessary feature if the low activation energies observed for the  $\text{Ag}^+$  ion motion are to be accounted for in the calculations. These simulations are of the static lattice. For the vibrating crystal, calculations of phonon dispersion show little improvement over results with two-body potentials, thus emphasizing that the silver ion deformation introduced by Kleppmann and Bilz (6) and Kleppmann and Weber (7) is also an essential feature of the vibrating lattice.

#### References

1. C.R.A. Catlow, J. Corish and P.W.M. Jacobs, J. Phys. C., 12, 3433 (1979).
2. P.W.M. Jacobs, J. Corish and C.R.A. Catlow, J. Phys. C., 13, 1977 (1980).
3. P.W.M. Jacobs, J. Corish and B.A. Devlin, Photo. Sci. and Eng., 26, 50 (1982).
4. B.A. Devlin and J. Corish, J. Phys. C., 20, 705 (1987).
5. A.P. Batra and L.M. Slifkin, J. Phys. C., 9, 947 (1976).
6. W.G. Kleppmann and H. Bilz, Commun. Phys., 1, 105 (1976).
7. W.G. Kleppmann and W. Weber, Phys. Rev. B, 20, 1699 (1979).

DEFECTS AND IMPURITY STATES IN TITANATES

R. A. Jackson, S. M. Tomlinson, M. J. Akhtar and C. R. A. Catlow

Department of Chemistry, University of Keele, Keele, Staffs. ST5 5BG, U.K.

The titanates  $\text{BaTiO}_3$ ,  $\text{SrTiO}_3$  and  $\text{PbTiO}_3$  have important applications as materials for semiconductor applications. In particular,  $\text{BaTiO}_3$  exhibits the PTCR effect, and  $\text{PbTiO}_3$  is the prototype for a range of electro-optic devices. This paper will present the results of calculations of the structural and defect properties of these materials, and in the case of  $\text{BaTiO}_3$ , comparisons will be made with the results of EXAFS experiments.

Atomistic simulation techniques for calculating the structural and defect properties of ionic solids are well-established[1]. These techniques have been applied to the calculation of substitution energies for a range of dopant cations in  $\text{BaTiO}_3$ , including Mn, La and Y. Substitution energies at both Ba- and Ti- sites have been calculated; the semiconductor properties will be determined by which site is preferentially occupied by a given ion. EXAFS experiments can provide information about the sites occupied by dopant ions, and results of these experiments are compared with the calculations.

Potential models have been developed for  $\text{SrTiO}_3$  and  $\text{PbTiO}_3$ , and results of defect and lattice dynamical calculations will be presented for  $\text{SrTiO}_3$ . Preliminary structural and defect calculations will be presented for  $\text{PbTiO}_3$ .

References

1. C.R.A.Catlow and W.C.Mackrodt, in 'Computer Simulation of Solids' (Lecture Notes in Physics No. 166), Springer-verlag, Berlin, 1982.

NON-STOICHIOMETRY IN ALKALINE EARTH EXCESS ALKALINE EARTH TITANATES

A.N. Cormack and K.R. Udayakumar  
NYS College of Ceramics  
Alfred University  
Alfred, NY 14802 USA

Materials with the perovskite structure, or a derivative thereof, show a fascinating range of behavior whose origin may be ascribed to the versatility of this particular crystal structure. The defect chemistry of these materials, in general, is no exception to this statement. The diversity of the defect chemistry may be exemplified by the different ways that the alkaline earth titanates accommodate excess alkaline earth; this diversity is the topic of the present paper.

A number of detailed experimental studies [1], have shown that each of  $\text{BaTiO}_3$ ,  $\text{SrTiO}_3$  and  $\text{CaTiO}_3$  have quite different ranges of cation non-stoichiometry. In particular,  $\text{BaTiO}_3$  seems to accommodate very little excess BaO;  $\text{SrTiO}_3$  has a small range of excess SrO but then forms planar defects, known as Ruddlesden - Popper layers [2]; the data on  $\text{CaTiO}_3$  appears to be controversial, with different groups finding apparently conflicting results. By analogy to Ca doped  $\text{BaTiO}_3$ , Han et al [1] suggested  $\text{Ca}_{-1}$  defects to account for their change in electrical conductivity data, although Balachandran and Eror [3] suggested the formulation of Ruddlesden - Popper layers within this system instead.

In order to uncover the reasons for this differing behavior in these related systems and, perhaps, to provide some additional insight into the  $\text{CaTiO}_3$  problem, we undertook a computer simulation study of the energetics of defect formation in these alkaline earth titanates. For each compound, we calculated the defect formation energies and hence were able to obtain energies of solution. In addition to the point defect behavior, we also calculated the energetics of Ruddlesden - Popper layer formation, by considering a homologous series of superlattice phases, the end members of which are  $\text{ATiO}_3$  and  $\text{A}_2\text{TiO}_4$ .

We find that for  $\text{BaTiO}_3$ , defect energies prohibit almost any excess BaO

and that the  $\text{Ba}_2\text{TiO}_4$  prefers to adopt the  $\text{K}_2\text{SO}_4$  structure rather than the  $\text{K}_2\text{NiF}_4$  structure, so Ruddlesden - Popper layer formation will not occur. For  $\text{SrTiO}_3$  we find that  $\text{Sr}_{\text{T}_i}$  defects will be present for a small amount of  $\text{SrO}$  excess, but then Ruddlesden - Popper layers will form. In the case of  $\text{CaTiO}_3$  we find that  $\text{Ca}_{\text{T}_i}$  defects are highly energetic and are not expected to be present. However, the formation energy of the  $\text{Ca}_2\text{TiO}_4$  phase is low enough to suggest that extended defects, in the form of Ruddlesden - Popper layers may be formed in this system.

1. Y.H. Han, M.P. Harmer, Y.H. Hu and D.M. Smyth, in: Transport in Nonstoichiometric Compounds, eds Simkovich and Stubican, Plenum Press NY, 1984.
2. (a) S.N. Ruddlesden and P. Popper, *Acta. Cryst.* 10, 538 (1957)  
(b) R.J.D. Tilley, *J. Solid State Chem.* 21, 293, (1977).
3. U. Balachandran and N.G. Eror, *Mater. Sci. and Engineering* 54, 221 (1982).

EMBEDDED QUANTUM CLUSTER CALCULATIONS ON DEFECTS IN BINARY  
OXIDES

R. W. Grimes<sup>(1)</sup>, C. R. A. Catlow<sup>(1)</sup> and A. M. Stoneham<sup>(2)</sup>

(1) Department of Chemistry, University of Keele, Staffs. ST5 5BG, U.K.

(2) Theoretical Physics Division, AERE Harwell, Didcot, Oxon. OX11 0RA,  
U.K.

With recent growth in computer power, it is now possible to perform accurate calculations of defect energies in insulating solids, using quantum mechanical cluster methods. This paper will present recent applications to relatively simple systems, e.g. MgO, and to the much more complex defect problems posed by fission products in UO<sub>2</sub>.

Restricted Hartree-Fock self-consistent-field calculations on metal oxide cluster embedded in point-charge arrays were undertaken. Calculations were performed on both electronic and atomic defects. Particular attention was given to calculating relative stabilities of different defect charge states, for example, the comparative stability of Xe<sup>0</sup> and Xe<sup>+</sup> substituted at a uranium site in UO<sub>2</sub>.

In the calculations, relaxed coordinates are obtained from simulation techniques based on the Mott-Littleton methodology. These can be used to reduce basis set superposition errors. The simulation method is also used to provide the relaxation energy associated with ions outside the quantum cluster. This has been found to be critical in calculating hole and electron trapping energies in MgO.

**LATTICE POTENTIAL ENERGY CALCULATIONS OF POTASSIUM CYANIDE-POTASSIUM HALIDE MIXED CRYSTALS AND RELATION TO ORDER-DISORDER PHASE TRANSITIONS.**

P. Bourson, G. Gorczyca and D. Durand  
Centre Lorrain d'Optique et Electronique du Solide  
Université de Metz - Supelec - 2, rue E. Belin  
57078 Metz Cedex 03 - (France)

Alkali cyanide-alkali halide mixed crystals exhibit order-disorder phase transitions with various ferroelastically ordered structures under cooling. Phase diagrams analysis of  $(\text{KCN})_x(\text{KCl})_{1-x}$ ,  $(\text{KCN})_x(\text{KBr})_{1-x}$  and  $(\text{KCN})_x(\text{KI})_{1-x}$  systems shows basically a competition between two ordered phases (monoclinic and orthorhombic) when the substitutional halide ion X ( $X = \text{Cl}^-$ ,  $\text{Br}^-$ ,  $\text{I}^-$ ) gradually replaces the  $\text{CN}^-$  dumbbell in the pure KCN crystal (1).

In this work, we tentatively try to understand this phenomenon by calculating the lattice energy potential  $\Phi$  of the mixed systems, under the light of a rigid ion shell model.

The lattice potential energy of the pure materials KCN and KX is first calculated in the cubic phase as a function of temperature, taking into account short range (SR) and long range (LR) interactions.

At the usual Coulomb (LR) interaction, a three body interaction (TBI) (2) is added in order to take account of both the large Cauchy discrepancy ( $C_{12}-C_{44}$ ) and the softening of  $C_{44}$  elastic constant close to the order-disorder phase transition observed in pure KCN (3).

On the other hand, the (SR) interaction potential includes contributions of Van der Waals dipole-dipole and dipole-quadrupole attractions and of Hafemeister-Flygare (HF) type overlap repulsions (4). The strength (b) and the hardness ( $\rho$ ) input parameters of the HF repulsion part of the potential are fitted, as a function of temperature, using the bulk modulus and the equilibrium anion-cation distance  $r_0$  of the pure materials.

In a second step the lattice potential energy of the mixed systems is

calculated according to the general equation :

$$\Phi = x\Phi_{KCN} + (1-x)\Phi_{KX}$$

This potential is minimized against  $r_0$  of the mixture, keeping  $\rho_{KCN}$  and  $\rho_{KX}$  constant, as a function of temperature. The strength parameter (b) of the mixture, obtained from that procedure, gives the relative ratio of the repulsive and attractive parts of the potential energy of the mixed systems.

All the results will be discussed in terms of dipole-dipole and dipole-quadrupole Van der Waals interactions as a function of type and concentration of substitutional halide, transition temperature and structures of the ordered phase in the mixed systems.

- 1) P. Bourson, G. Gorczyca, D. Durand. "Cryst. Latt. Def. and Amorph. Mat.", 16, 311-317 (1987)
- 2) R.K. Singh, N. Kumar, G.B. Varshney. Phys. Stat. Sol. B136, 457-465 (1986)
- 3) D.W. Hafemeister, W.H. Flygare. J. Chem. Phys. 43, 795 (1965)
- 4) H. Haussühl. Solid State Commun., 13, 147-151 (1973)

PAIRING OF OFF-CENTER DEFECTS IN IONIC CRYSTALS DUE TO VIBRONIC  
VAN DER WAALS BINDING: PRECURSOR TO NEW PHASE FORMATION

M. Georgiev and M. Borissov

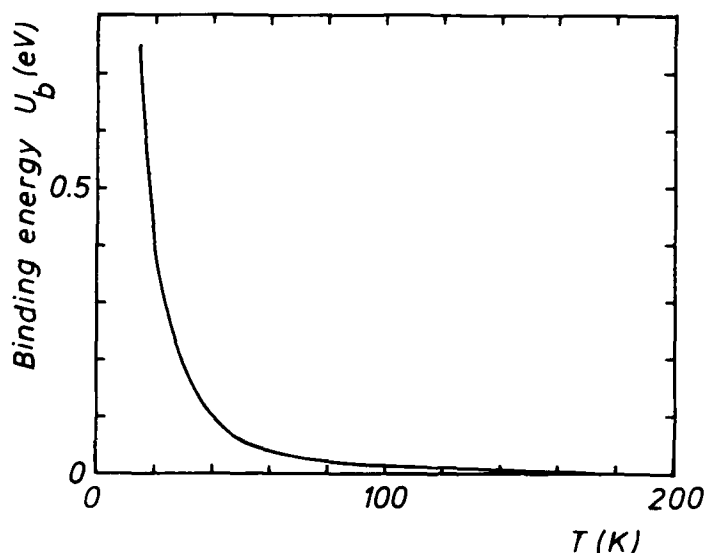
Institute of Solid State Physics, Bulgarian Academy of Sciences  
72 Lenin Boulevard, 1784 Sofia, Bulgaria

Off-center defects, such as univalent impurity dipoles, self-trapped excitons (incipient Frenkel pairs), and small polarons, have focused considerable experimental and theoretical attention because of their effect on the electrical, optical, radiation, and glassy behavior of crystals. In particular, cooperative effects of impurity dipoles give rise to a dipole-glassy state, while formation of STE biexcitons may play a role under a high-intensity excitation. A long standing problem relates to the nature of the binding that holds together off-center partners to form a dimer, the simplest aggregate.

An off-center configurational instability occurs as a result of the mixing of two nearly-degenerate different-parity electronic states  $|g\rangle$  and  $|u\rangle$  at the defect site by an odd vibrational mode. The original on-center conformation is often centrosymmetric; now, the off-center instability gives rise to an electric dipole. For any given spatial orientation of the species, there usually is an equivalent opposite orientation. Consequently, the average off-center dipole of a species is often vanishing because of tunneling transitions between equidipolar sites. Nevertheless, the species is polarizable in an electric field. We have recently proposed that neighboring entities may bind through the universal Van der Waals force to form "vibronic molecules".<sup>1</sup>

Vibronic off-center polarizabilities  $\alpha$  have been derived by Bersuker et al.<sup>2</sup> For a four-site defect type, e.g.

$$\alpha = (p_0^2/3k_B T) (\exp(-\delta/k_B T) + (k_B T/\delta) \sinh(\delta/k_B T)) / (\exp(-\delta/k_B T) + \cosh(\delta/k_B T)) . \quad (1)$$



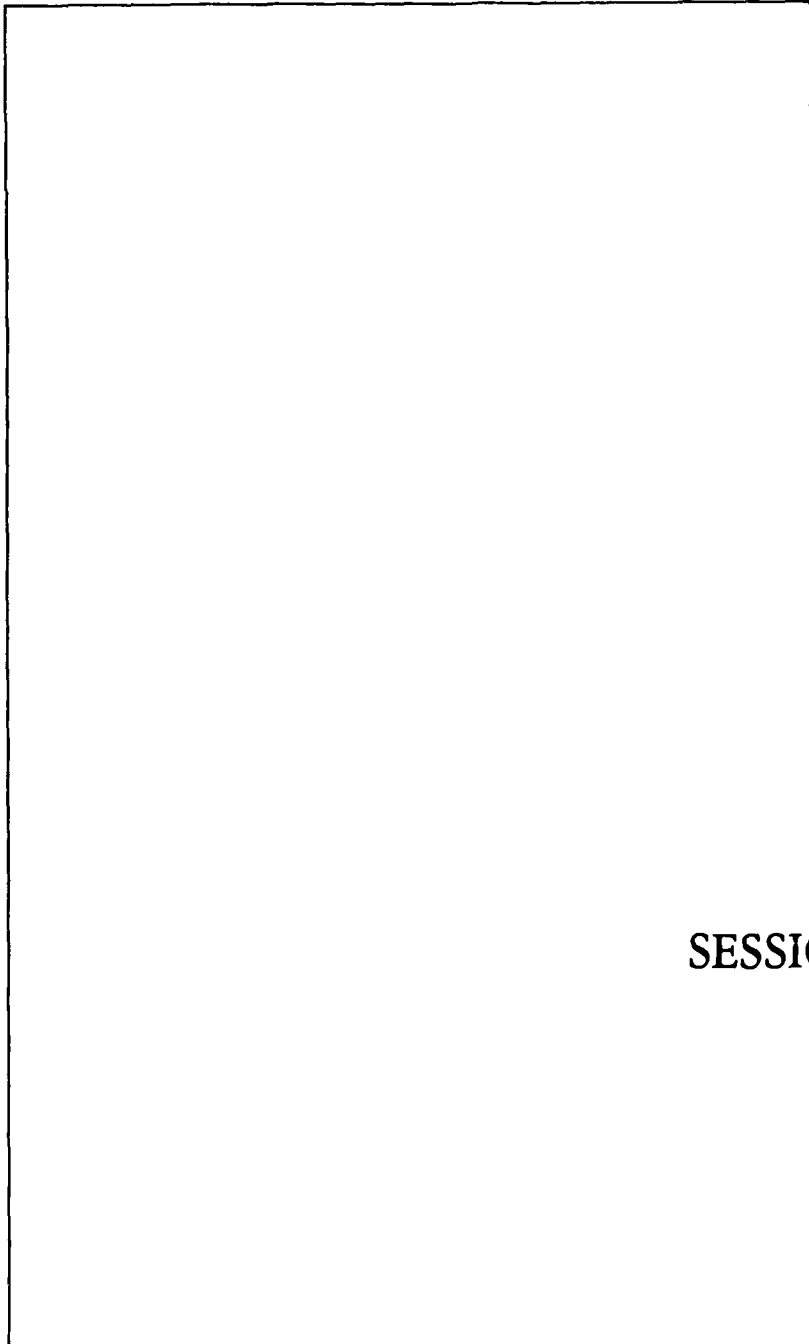
$$p_0 = e \langle u|z|g \rangle ((4E_{JT}/E_{gu})^2 - 1)^{1/2} / (4E_{JT}/E_{gu}) \quad (2)$$

is the magnitude of the off-center dipole moment associated with any spatial orientation of the species<sup>1</sup> ( $E_{JT}$  - the Jahn-Teller energy,  $E_{gu}$  - the energy gap between  $|g\rangle$  and  $|u\rangle$ , while  $\delta$  is the zero-field tunneling splitting. Following F. London's simple arguments, the dimer binding energy is

$$U_b = (\delta/2)(\alpha/kR^3)^2, \quad (3)$$

retaining only the dipole-dipole terms in the multipole expansion. Here  $R$  is the interdefect separation, while  $k$  is an appropriate dielectric constant. Because of (1), eq.(3) predicts a temperature-dependent  $U_b$ . A numerical calculation reported elsewhere<sup>1</sup> for two-site small polarons in superconducting perovskites is shown in the Figure. It displays a number of features with far-reaching consequences.<sup>1</sup>

1. M. Borissov and M. Georgiev, Z. Physik (submitted).
2. I.B. Bersuker, Effekt Yana-Tellera i vibronnie vzaimodeystviya v sovremennoi khimii (Moskva, Nauka, 1987), p. 193.



SESSION 4A

**ANOMALOUS CHARGE PHOTO-TRANSFER IN DOPED INSULATORS****A.A.Kaplyanskii**Ioffe Physico-Technical Institute of the Soviet Academy of Sciences -  
Leningrad - U.S.S.R.

A review is given of experimental studies of photocurrent in ruby crystals  $\text{Al}_2\text{O}_3:\text{Cr}^{3+}$ , namely of the dependencies on applied electric field, pump light frequency, temperature, Cr concentration and of current studies kinetics.

The principal anomaly consists in the observation with the variation of either electric field or light frequency of the stationary photocurrent of both positive and negative (against the applied field) sign.

The photocurrent is interpreted as created due to direct charge exchange between the  $\text{Cr}^{3+}$  ions and Cr ions in unusual charge state ( $\text{Cr}^{4+}$  or  $\text{Cr}^{2+}$ ) which occurs when  $\text{Cr}^{3+}$  is optically excited to the metastable state.

The photoelectric anomalies in ruby are discussed in the frame of the general problem of charge phototransfer in doped insulators.

1) A.A.Kaplyanskii, S.A.Pasul, S.P.Feofilov, J. of Luminesc. **38**, 120-124 (1987) and references quoted there.

DYNAMICAL PROCESSES ASSOCIATED WITH SELF-TRAPPED EXCITONS  
IN INSULATORS: DE-EXCITATION AND DEFECT FORMATION AT HIGHLY  
EXCITED STATES

Noriaki Itoh, Katsumi Tanimura and Chihiro Itoh

Department of Physics, Faculty of Science,  
Nagoya University,  
Furocho, Chikusa, Nagoya 464, Japan

Self-trapped excitons and F-H pairs are isomers. The dynamical processes associated with the self-trapped excitons are of primary importance in understanding the defect processes induced by electronic excitation. In this paper we discuss the conversion from the self-trapped excitons to F-H pairs from several excited states of the self-trapped excitons, electron-excited and hole-excited states of a self-trapped exciton and an exciton perturbed by a self-trapped exciton, in several insulators.

Excitation of the hole of a self-trapped exciton in  $\text{CaF}_2$  was found to create an F-H pair at a relatively high probability. Similar experimental results have been obtained for  $\text{MgF}_2$ . We also found generation of stable F-H pairs quadratic to the density of excitation under excimer-laser irradiation of RbI and attributed to the F-H pair generation due to interaction between self-trapped excitons and free excitons. These results indicate that both the hole excitation and generation of a free exciton in the proximity of a self-trapped exciton generates stable F-H pairs in crystals in which no stable F-H pair is created by

The excited states described above have an energy

higher than the ionization energy  $I_{STE}$  of a self-trapped exciton, and hence cannot be reached after a  $V_k$  center traps an electron and probably not in the process of relaxation of an exciton. Generation of stable F-H pairs from these highly excited states may occur under dense-electronic excitation and account for the laser damage and the damage induced by energetic heavy ions.

Electron-excited states of a self-trapped exciton and hole-excited states with energies less than  $I_{STE}$  can be reached after an electron is trapped by a  $V_k$  center or in the process of exciton relaxation. Thus, even though F-H pairs are known to be generated by electron excitation of self-trapped excitons, it is still controversial whether the branching to an F-H pair occurs after an exciton or  $(V_k + e)$  is relaxed to the lowest excited state or at an excited state with an energy less than  $I_{STE}$ . This problem is reviewed critically.

Self-trapped excitons in amorphous  $SiO_2$  exhibit features which are specific to amorphous. The decay is not exponential and the luminescence peak energy shifts to higher energy with increasing delay. Generation of interstitial-vacancy pairs are observed in amorphous but not in crystals. The correlation between the multiple structure of the self-trapped excitons in amorphous and the defect generation is also discussed.

SESSION 4B

## CALCULATION OF THE ENTROPIES OF POINT DEFECTS IN INSULATING CRYSTALS

P.W.M. Jacobs

Department of Chemistry  
 The University of Western Ontario  
 London, Ontario Canada N6A 5B7

The objective of the computer simulation of an insulating crystal is generally the calculation of the Gibbs energy of the formation, migration or clustering of point defects. The determination of the Gibbs energy change  $g^P$  for any particular defect process is accomplished by calculating the energy change  $u^V$  and entropy change  $s^V$  at constant volume (strictly, constant lattice parameter,  $a$ ) and making use of the thermodynamic relation  $g^P = f^V = u^V - Ts^V$ , where  $f^V$  is the Helmholtz energy change at constant volume and  $T$  is the thermodynamic temperature corresponding to  $a(T)$ . Thus two separate calculations, for  $u^V$  and for  $s^V$ , are required. The calculation of  $u^V$  by a simulation of the crystal in a computer was first achieved in a general and readily applicable fashion by Norgett<sup>1</sup>, although the procedures are based on a strategy developed almost 40 years previously by Mott and Littleton<sup>2</sup>. The calculation of  $s^V$  offers both conceptual and practical difficulties beyond those involved in the calculation of  $u^V$  and the development of a practical code has been achieved only relatively recently (Harding<sup>3</sup>). The calculation of  $s^V$  involves three steps, the first two of which are common to the calculation of  $u^V$ . (a) A crystal potential must be developed and tested. (b) The relaxed positions of the  $N$  ions in a region ( $I$ ) around the defect must be found. (c) The normal-mode vibrational frequencies  $\omega_i$  of the  $N$  ions in  $I$  must be calculated. Current techniques are limited to the quasiharmonic approximation. The formulae are simpler in the high-temperature approximation, in which case the vibrational entropy change accompanying a specified defect process is

$$s^V = -k_B \ln \left[ \frac{\prod_{i=1}^{3N'} \omega_i'}{\prod_{i=1}^{3N} \omega_i} \right] + 3 k_B (N' - N) (1 - \ln (\hbar/k_B T)) \quad (1)$$

where the primed and unprimed symbols refer to the final and initial defect states. Three methods of calculating  $s^V$  have been developed: these are the Green-function method<sup>4,5</sup>; the supercell method<sup>6</sup>; and the large crystallite method<sup>3</sup>. Of these the large crystallite method is the easiest to apply and it is the only method that has been developed so far into a practical code (SHEOL<sup>3</sup>). The Green-function method is the most elegant and gives the best convergence with respect to region size, but it is somewhat cumbersome and the accuracy of the Green functions must be assessed carefully<sup>5</sup>. The supercell method suffered initially from two disadvantages: it requires a computer with a large central memory and at first it was limited to neutral defects, such as a Frenkel pair or a Schottky pair. The first problem has been overcome by the rapid developments in mainframe computers. The second problem, that of dealing with charged defects, has been solved recently by Leslie and Gillan<sup>7</sup>. The only method currently available for routine application is the large crystallite method<sup>3</sup>. In all three methods spurious terms arise from the interaction of the long-range distortion field of the defect with the rigid boundary to Region I. This interaction leads to oscillations in the variation of the entropy of a charged defect with region size, so that it is necessary to determine and apply a correction for this effect.

1. M.J. Norgett, AERE Harwell Report 7650, 1974.
2. N.F. Mott and M.J. Littleton, Trans. Faraday Soc., 34, 485 (1938).
3. J.H. Harding, Physica B, 131, 13 (1985).
4. P.W.M. Jacobs, M.A. Nerenberg and J. Govindarajan in *Computer Simulation of Solids*, ed. C.R.A. Catlow and W.C. Mackrodt, Springer-Verlag, Berlin, 1982.
5. M.J. Gillan and P.W.M. Jacobs, Phys. Rev. B 28, 759 (1983).
6. J.H. Harding and A.M. Stoneham, Phil. Mag. B 42, 705 (1981).
7. M. Leslie and M.J. Gillan, J. Physics C 18, 973 (1985).

## Theory of Dispersed Ionic Conductors

Armin Bunde

I. Institut für Theoretische Physik, Universität Hamburg  
Jungiusstrasse 9, D-2000 Hamburg 36, W. Germany

Mixtures of solid ionic conductors (e.g.  $\beta - AgI$  or  $LiI$ ) with fine particles of an insulating second phase (e.g.  $Al_2O_3$  or  $SiO_2$ ) can show a marked increase in conductivity as compared to the pure homogeneous system. The ionic conductivity first increases strongly with the concentration  $p$  of the dispersed insulating phase. After passing its maximum, the conductivity drops rapidly and seems to extrapolate to zero at some threshold concentration. The discovery of this remarkable phenomenon is due to Liang,<sup>1</sup> who observed an enhancement by 3 orders of magnitude in the  $Li$  conductivity of  $LiI$  after addition of  $Al_2O_3$  particles.

It has been shown experimentally for sandwich arrangements of the  $LiI - SiO_2$  system,<sup>2</sup> that the interface conductivity between the two phases is strongly enhanced. The reason for this enhancement is not completely understood, it might be due to the formation of a space charge layer along the internal interface between the two phases.<sup>3</sup>

In this talk I want to discuss mainly purely macroscopic aspects of the conductance properties of such heterogeneous systems. I want to review a percolation model for dispersed ionic conductors which has been recently developed<sup>4</sup> and which is able to describe correctly the change of conductivity with insulator concentration and various other features of dispersed ionic conductors as well: (1) the decrease of the conductivity enhancement in the  $LiI - Al_2O_3$  when the temperature is increased,<sup>5</sup> (2) the change of the activation energy with insulator concentration  $p$ ,<sup>6</sup> (3) the dependence of the ionic conductivity on the size of the dispersed particles,<sup>7</sup> and (4) the decrease of conductivity with  $p$  if the ionic conductor is in its high conducting  $\alpha$ -phase.

In the percolation model, dispersed ionic conductors are considered as three component systems. The system consists of a matrix of bonds which can be normally conducting (representing the ionic conductor), nonconducting (representing the interior of the insulating particles) or highly conducting (representing the interface between the two phases). The bonds are distributed in space according to a random distribution of insulating material in a normally conducting matrix with a highly conducting interface

in between. A special feature of the model is the existence of two threshold concentrations  $p'_c$  and  $p''_c$ . Near  $p'_c$  (which is less than 0.1), the conductivity behaves similar as in random conductor-superconductor mixtures at the critical concentration, while near  $p''_c$  (which is above 0.9) the conductivity behaves as in random conductor-insulator networks. The combined properties of both networks are essential for the understanding of dispersed ionic conductors.

- <sup>1</sup> C. C. Liang, J. Electrochem. Soc. **120**, 1289 (1973).
- <sup>2</sup> J. B. Phipps and D. H. Whitmore, Solid State Ionics **9/10**, 123 (1983)
- <sup>3</sup> T. Jow and J. B. Wagner, Jr., J. Electrochem. Soc. **126**, 163 (1979); J. Maier, Phys. Status Solidi **B 123**, K89 (1984)
- <sup>4</sup> A. Bunde, W. Dieterich, and E. Roman, Phys. Rev. Lett. **55**, 5 (1985); H. E. Roman, A. Bunde, and W. Dieterich, Phys. Rev. **B34**, 3439 (1986); H. E. Roman and M. Yussouff, Phys. Rev. **B36**, 7285 (1987); R. Blender and W. Dieterich, J. Phys. C **20**, 6113 (1987).
- <sup>5</sup> F. W. Poulsen, N. Hessel Andersen, B. Kinde, and J. Schoonman, Solid State Ionics **9/10**, 119 (1983); R. Dupree, J. R. Mowells, A. Hooper, and F. W. Poulsen, *ibid.* **9/10**, 131 (1983).
- <sup>6</sup> Chen Li-Quan, Zhao Zong-Yuan, Wang Chao-Ying, and Li Zi-Rong, Acta Phys. Sin. **34**, 1027 (1985)
- <sup>7</sup> O. Nakamura and J. B. Goodenough, Solid State Ionics, **7**, 119 (1982); M. R.-W. Chang, K. Shahi, and J. B. Wagner, Jr., J. Electrochem. Soc. **131**, 1213 (1984).

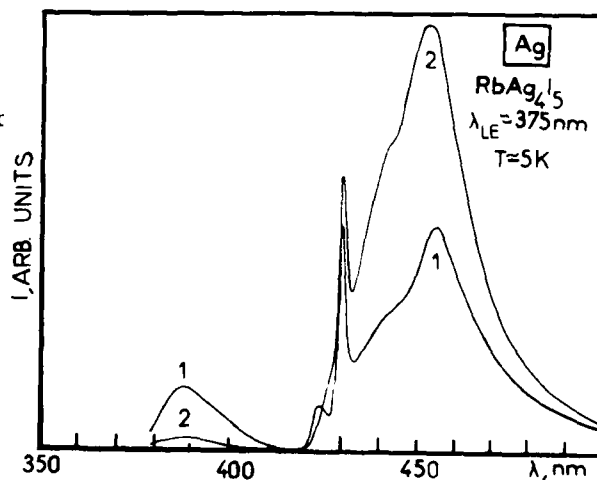
POSTER SESSION I  
TUESDAY

THE EFFECT OF IONIC IMPLANTATION AND ADDITIVE COLOURING  
ON THE ELECTRON CENTERS IN  $\text{RbAg}_4\text{J}_5$  SUPERIONIC CRYSTALS

S.I. Bredikhin, N.N. Kovaleva, N.V. Lichkova, I.Sh. Khasanov  
Institute of Solid State Physics USSR Academy of Sciences,  
Chernogolovka, Moscow district, 142432, USSR

Earlier we have studied the low-temperature  $\gamma$ -phase luminescence spectra of  $\text{RbAg}_4\text{J}_5$  superionic crystals [1]. The luminescence has been shown to be of the center origin and an energy model of these centers has been proposed.

In the present paper is investigated the effect of dissolution of silver films on the  $\text{RbAg}_4\text{J}_5$  crystals photoluminescence (PL) for determining the structure of optically-active centers and elucidating the mechanisms of silver contact and solid electrolyte interaction. A VUP-2 installation was used to deposit a silver film on the cleaved surface. With the film thickness of about 1000 Å the surface of the sample acquired metal glitter. But already in 10-15 hrs the silver film dissolved completely. It turned out that dissolution of a silver film brings about some irreversible modifications in the spectrum of photoluminescence. Fig.1 presents photoluminescence spectra of a primary  $\text{RbAg}_4\text{J}_5$  sample (curve 1) and of the same sample when a 1000 Å thick silver film has been dissolved in its volume (curve 2). It can be seen that the intensities of  $\lambda_{\text{ph}2}=437$  nm and  $\lambda_{\text{ph}3}=455$  nm bands increase. The intensity of the  $\lambda_{\text{ph}1}=390$  nm



band diminishes noticeably and in some cases this band vanishes. This irreversible modification of a PL spectrum is associated with variation in the concentration of different optically-active centers in the  $\text{RbAg}_4\text{J}_5$  crystals under investigation. Indeed, dissolution of a silver film in the sample volume causes an excess concentration of interstitial silver ions in the low-temperature  $\gamma$ -phase. The radiation of  $\lambda_{\text{phl}_2} = 437$  nm and  $\lambda_{\text{phl}_3} = 455$  nm bands can thus be related to the centers which involve interstitial silver, and the radiation of a  $\lambda_{\text{phl}_1} = 390$  nm is conditioned by the centers with silver vacancies. These results well agree with the effect of additive iodine colouring on the structure of the  $\gamma$ -phase luminescence centers of  $\text{RbAg}_4\text{J}_5$  crystals, the effect being discovered and described in the present paper. The influence of ionic implantation on optical characteristics of  $\text{RbAg}_4\text{J}_5$  crystals has been analyzed. Positively charged ions of  $\text{Kr}^+$  and  $\text{Ne}^+$  noble gases were implanted on the surface of the samples. With the radiation dose,  $D \approx 10^{14} - 10^{15} \text{ cm}^{-2}$ , and the energy of implanted ions,  $E = 160 - 180 \text{ keV}$ , the surface of the samples acquired a stable red-orange colour. The absorption spectra of ion-implanted  $\text{RbAg}_4\text{J}_5$  crystals were studied in the 10-300 K temperature range. At  $T = 10 \text{ K}$  the absorption band associated with colouring centers turned out to have the halfwidth  $\Delta E \approx 0.88 \text{ eV}$  and maximum at  $E = 2.5 \text{ eV}$ . The parameters of this absorption band are practically independent of temperature and do not vary under 209 K and 122 K phase transitions. Therefore, colouring centers responsible for this absorption band are not sensitive to the degree of the cation sublattice disordering. So, these colouring centers involve defects of the "rigid" sublattice of a  $\text{RbAg}_4\text{J}_5$  crystal.

1. S.I. Bredikhin, N.N. Kovaleva, N.V. Lichkova, Fiz.Tverd.Tela, 1986, v.28, No.9, p.2813-2818.

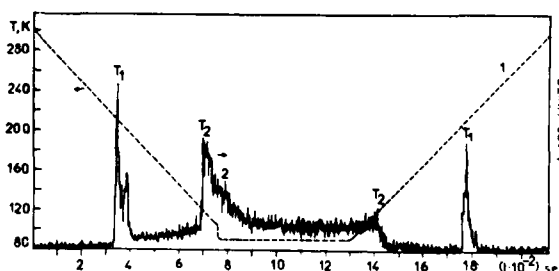
Electron Emission in superionic  $\text{RbAg}_4\text{I}_5$   
crystals stimulated by phase transitions

S.I.Bredikhin, N.N.Kovaleva, S.Z.Shmurak and  
A.B.Poletaev

Institute of Solid State Physics, Academy of Sciences  
of the USSR, Chernogolovka USSR

Electron emission is a highly sensitive effect accompanying various physical processes in crystals. The main goal of this work was to apply the electron emission method for the observation of phase transitions and to study characteristic features of the electron emission as a function of the temperature and the phase state. Fig.1 gives a graphic representation of the experimental results with the signal intensity and the temperature plotted as ordinate and the time scanning as abscissa. From curve 1 - cooling-heating- one can determine the sample temperature at any instant of time, and from curve 2 the electron emission intensity corresponding to this temperature.

It is seen that the intensive electron emission arises in the  $\text{RbAg}_4\text{I}_5$  crystals at the phase transition  $T_1=209\text{K}$  between the superionic  $\alpha$  and  $\beta$  phases, and at the phase transition  $T_2=122\text{K}$  between the  $\beta$ -phase and the non-superionic  $\gamma$ -phase- the emission relaxing slowly with time. It should be pointed out that electron emission arises in the absence of external effects on the sample and it is only caused by temperature variations that is as a result of internal processes occurring in the crystals. The present work deals with various mechanisms of the



electron emission occurrence at the phase transitions in  $\text{RbAg}_4\text{I}_5$  superionic crystals. The electron emission relaxing slowly with time ( $\tau \sim 2 \cdot 10^2$  sec) as a consequence of superionic  $\beta$ -phase-nonsuperionic  $\gamma$ -phase transition is explained in terms of the model of the vacancy-diffusional electron emission mechanism [1].

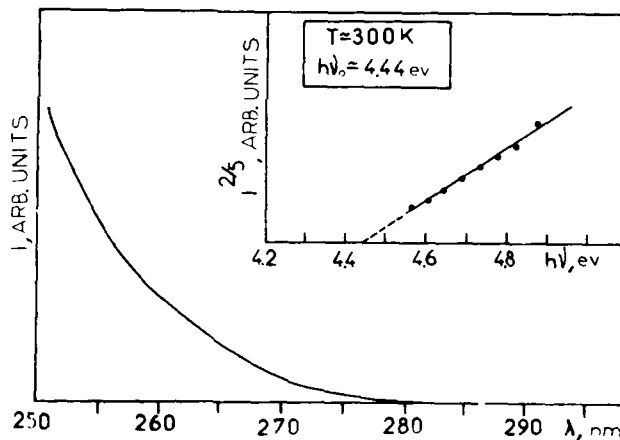
In order to determine the value of the photoelectron work function and to study the influence of the phase state on it, we investigated the photoelectron emission from the cleaved surface of  $\text{RbAg}_4\text{I}_5$  crystals. The investigations were performed within the temperature interval from 300 to 85 K. Fig.2 illustrates the photoelectron emission intensity vs the wavelength of the exciting light at  $T=300$  K. The investigations in question indicate that dependence of the photoeffect intensity on the exciting

quanta energy near the red edge of the photoeffect is described in  $\text{RbAg}_4\text{I}_5$

crystals by the power law

$I = (h\nu - A_{\text{pE}})^{5/2}$ , and the photoeffect threshold value

equals  $A_{\text{pE}} \approx 4.440$  eV, being independent of the crystals phase state.



1. Von Voss W.D., Brotzen F.R. J. Appl. Phys., 1959, vol.30, N 11, p.1639-1645.

SPECTRAL COMPOSITION AND DECAY KINETICS OF UV EMISSION FROM  
 $\text{KCl}_{1-x}\text{Br}_x:\text{Pb}^{2+}$  CRYSTALS

K. Polák, M. Manfredi<sup>\*)</sup>, M. Nikl

Institute of Physics ČSAV, Na Slovance 2, 180 40 Prague 8, ČSSR  
<sup>\*)</sup>Istituto di Fisica, Università degli Studi di Parma, Via delle Scienze,  
 43020 Fontanini - Parma, Italy.

The characteristics of the  $\text{Pb}^{2+}$  ultraviolet emission belonging to  $(^3\text{T}_{1u}, ^3\text{A}_{1u}) \rightarrow ^1\text{A}_{1g}$  transition are mainly governed by the relative strengths of crystal field, spin-orbit interaction and Jahn-Teller effect. The influence of compensating vacancy leads to a splitting of  $^3\text{T}_{1u}$  state and the stabilization of some of J-T minima. This is manifested by two component decay of nanosecond UV emission for both KCl and KBr crystals doped with divalent lead /1, 2/.

We systematically studied the emission properties of mixed  $\text{KCl}_{1-x}\text{Br}_x$  crystals doped with  $\text{Pb}^{2+}$  for  $x = 0.05, 0.2, 0.8, 0.95$  and at temperatures from liquid helium to room temperature. The change in the type of ligand from chlorine to bromine ions causes a stepwise shift both in the position of the A absorption band /3/ and in the maximum of related emission band. By decomposing the observed emission bands into Gaussians we determined four main components with peaks and half-widths as follows:  $\bar{\lambda}_0 = 3.685, 3.585, 3.46$  and  $3.415$  eV with  $\bar{\Delta}_{1/2} = 0.28, 0.30, 0.24$  and  $0.26$  eV resp. The first and last pairs of values belong to the pure  $(\text{PbCl}_6)^{4-}$  and  $(\text{PbBr}_6)^{4-}$  centres.

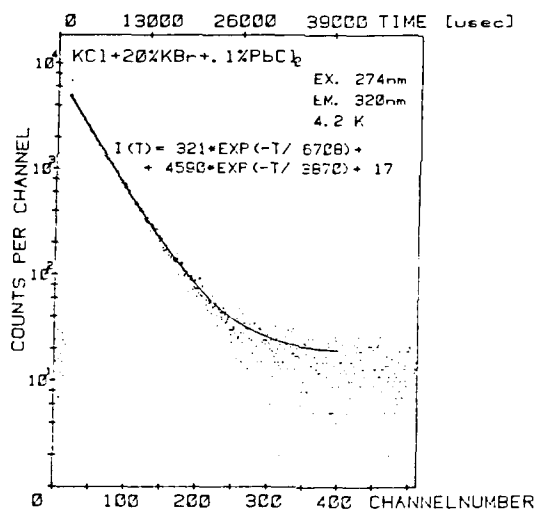
The emission kinetics in the studied spectral range is generally composed by fast and slow contributions. The build-in bromine ions in the vicinity of  $\text{Pb}^{2+}$  give rise to the appearance of a slower part in the decay curve for millisecond time range at LHeT. The one of the real decay curves for  $\text{KCl}_{0.8}\text{Br}_{0.2}:\text{Pb}^{2+}$  crystal is shown in fig. 1. The limit value of  $\tau_s$  for  $\text{KBr}:\text{Pb}^{2+}$  is  $\approx 7$  msec.

The fast decay of A band excited luminescence obeys for  $\text{KCl}:\text{Pb}^{2+}$  the published two-exponential behaviour with  $\tau_f = 10.3$  and  $17.1$  nsec at LHeT. The presence of Br ligand in luminescence centres results again in the appearance of a slower component with the decay time between 30 and 40 nsec.

It is known that the oscillator strength of the A absorption band of  $\text{Pb}^{2+}$

ions is nearly the same for both KCl and KBr crystals ( $f = 0.11$  and  $0.12$  resp. /4,5/. However, our results show that the substitution of a ligand in the vicinity of  $Pb^{2+}$  ions has a strong influence on their emission characteristics. Therefore, it is plausible to assume that the wavefunctions of both ground and excited states have remarkable contributions from neighbouring anions.

- /1/ J.C. Kang, F. Cusso, T.F. Belliveau and D.J. Simkin, 1985, J.Phys.C: Sol. St. Phys. 18, 4753.
- /2/ K. Schmitt, V.S. Sivasankar and P.W.M. Jacobs, 1982, J.Lumin. 27, 313.  
J.G. Kang, T.F. Belliveau and D.J. Simkin, 1983, Chem.Phys.Lett.101,381.
- /3/ A. Bohun, V. Piskackova and J. Trnka, 1966, Czech.J.Phys. B16, 898.
- /4/ W.A. Sibley, E. Sonder and C.T. Butler, 1964, Phys.Rev. 136, A537.
- /5/ P.R. Collins and W.J. Fredericks, 1986, J.Phys.Chem.Solids 47, 529.



LUMINESCENCE DECAY TIME OF  $Ti^{3+}$  IN PHOSPHATE GLASSES

L.E. Bausá, G. Lifante, and J. García-Solé

Departamento de Física Aplicada, Universidad Autónoma de Madrid,  
Cantoblanco, 28049 Madrid (Spain)

and

A. Durán

Instituto de Cerámica y Vidrio, C.S.I.C., Arganda del Rey,  
Madrid (Spain)

The interest in studying the optical properties of  $Ti^{3+}$  ion in different kinds of materials stems from the possibility of this ion as an active laser impurity, as reported for the tunable solid state lasers  $Ti^{3+}:Al_2O_3$  (1) and  $Ti^{3+}:YAG$  (2).

The authors have recently reported that  $Ti^{3+}$ , in glasses of composition  $P_2O_5-Na_2O-Al_2O_3$ , showed a broad emission band centred at 860 nm when excited at the  $T_{2g} \rightarrow E_g$  transition of the  $d^1$  configuration (3).

In this work, photoluminescence decay time measurements of this system were obtained as a function of temperature and impurity concentration (range 0.1% - 2% wt of  $TiO_2$  in the melt).

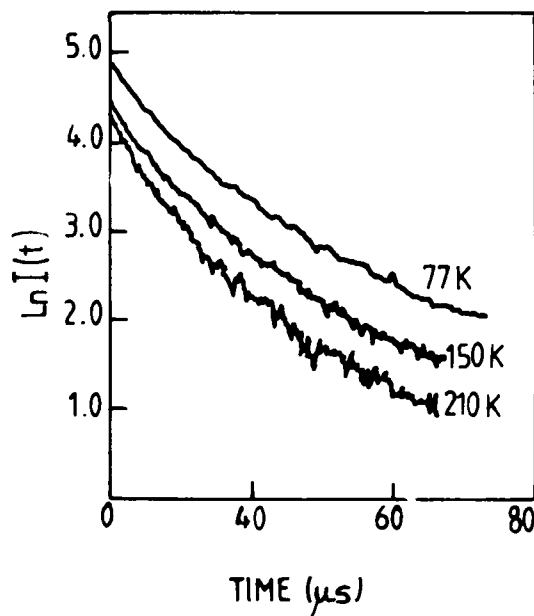


Figure 1.- Decay curves at different temperatures.

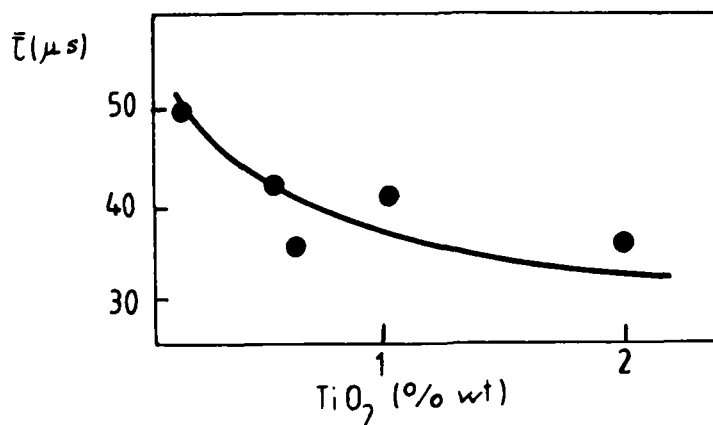


Figure 2.- Dependence of  $\bar{\tau}$  on Ti-concentration.

The shape of the decay curves is not exponential for the different concentrations of the samples investigated in the temperature range 10 to 300K.

Figure 1 shows, for example, the decay plot observed at three different temperatures for a 0.5% TiO<sub>2</sub> doped sample, excited at 660 nm with a N<sub>2</sub> pumped dye laser.

The dependence of the average lifetime,  $\bar{\tau}$ , on Ti<sup>3+</sup> concentration shows a decrease of  $\bar{\tau}$  of about 70% with increasing concentration from 0.1% to 2% of TiO<sub>2</sub> in the melt. This behaviour appears to be consistent with concentration quenching of emitted light.

#### REFERENCES

1. P.F. Moulton, Opt. News, 8 (1982) 9.
2. T.A. Discoll, M. Peressini, R.E. Stone, G. Hansen and H.J. Hoffman, Digest of Technical Papers, Conference on Lasers and Electro Optics, San Francisco, California (1986), p.106.
3. L.E. Bausá, F. Jaque, J. García-Solé and A. Durán, J. Mat. Sci., in press.

# TIME RESOLVED STUDY OF SECONDARY EMISSION IN KI:Se<sub>2</sub><sup>-</sup>

Hiroshi MURATA, Toru KISHIGAMI, and Riso KATO

Department of Physics, Kyoto University

Kyoto 606, Japan

It is known that O<sub>2</sub><sup>-</sup>, S<sub>2</sub><sup>-</sup> and Se<sub>2</sub><sup>-</sup> molecules doped in alkali halides show the strong ordinary luminescence (OL) with vibronic structures at low temperature.<sup>1)</sup> In addition to OL, KI:Se<sub>2</sub><sup>-</sup> shows multiple-order Raman scattering and so-called weak "hot luminescence (HL)" in the higher energy region of the 0-0 line of OL<sup>2)</sup> as shown in Fig.1. In the present study the relaxation process of the optically excited <sup>2</sup>Π<sub>u</sub> state of Se<sub>2</sub><sup>-</sup> in KI is investigated by the time-resolved measurement of the secondary emission.

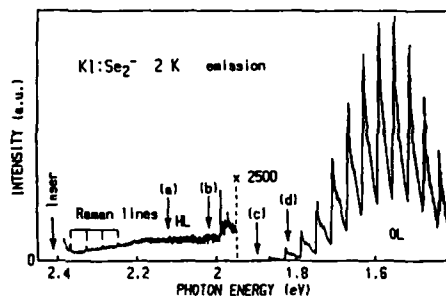


Fig.1. Emission spectrum of KI:Se<sub>2</sub><sup>-</sup> at 2 K excited with the 514.5 nm line of an Ar<sup>+</sup> laser.

Samples were prepared by heating KI single crystals in the selenium vapor.<sup>3)</sup> For the measurement of the time response in the nanosecond range a tunable N<sub>2</sub>-dye laser system and a boxcar integrator were used. In the picosecond range, a synchronously pumped dye laser and a single photon counting system in the Instrument Center, the Institute for Molecular Science at Okazaki, were used. The pulse widths were about 5 nsec and 100 psec, respectively.

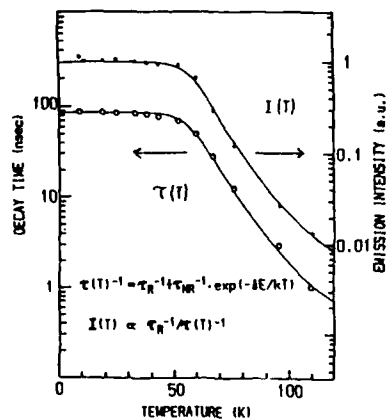


Figure 2 shows the temperature variation of the decay time and time-integrated intensity of OL. These values are almost constant up to 50 K and show a

Fig.2. Temperature dependence of the decay time (left scale) and intensity (right scale) of OL.

similar decrease as temperature rises. This behavior is interpreted in terms of a thermally activated non-radiative decay process at the relaxed excited state of  $\text{Se}_2^-$  as described by the equations in Fig.2. By the curve fitting analysis, we get  $\Delta E = 53 \text{ meV}$ ,  $\tau_R = 85 \text{ nsec}$ , and  $\tau_{NR} = 4.3 \times 10^{-12} \text{ sec}$ .

In Fig.3 are shown the transient behavior of the emission at about 80 K under the excitation at 546 nm with the picosecond laser. Curves (a) and (b) were observed in the higher energy region of OL as indicated by arrows in Fig.1. These curves consist of a fast component with the decay time  $\tau_f \leq 50 \text{ psec}$  and a slow component with  $\tau_s = 2 \text{ nsec}$ . Curves (c) and (d) observed in the energy region of OL show a slow OL component with  $\tau_{OL} = 7 \text{ nsec}$  and the fast component. The latter merges into the strong OL in the lower energy region.

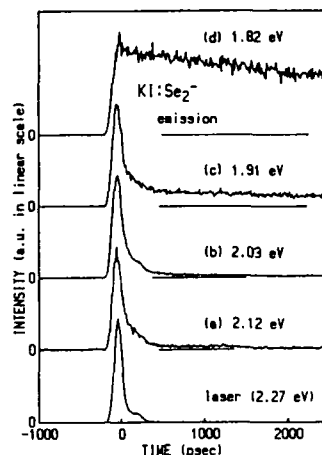


Fig.3. Time responses of the emission at 80 K observed at the positions shown by arrows in Fig.1.

The decay times of the fast components of curves (a)-(d) are the same within the experimental error. The time resolution of the present experiment is not so good enough to reveal the details of the vibrational relaxation of the excited state as in the recent study on  $\text{O}_2^-$  in alkali halides.<sup>4)</sup> We can say, however, that the fast component is really the hot luminescence because it is detectable in the higher energy region of OL, and the vibrational relaxation of the optically excited state proceeds with the time constant less than 50 psec at 80 K.

The intensity of the slow component with  $\tau_s = 2 \text{ nsec}$  differs from sample to sample. Its origin is not clear but it may be due to some other impurities or surface contaminations.

- 
- 1) M.Ikezawa and J.Rolfe: J.Chem.Phys. 58 (1973) 2024.
  - 2) L.A.Rebane and T.Yu.Khaldre: JETP Lett. 26 (1977) 515.
  - 3) L.E.Vannotti and J.R.Morton: J.Chem.Phys. 47 (1967) 4210.
  - 4) W.H.Knox and K.J.Teegarden: J.Lumines. 31/32 (1984) 39.

OPTICAL PROPERTIES OF  $\text{Ho}^{3+}$  IN  $\text{KCaF}_3$  CRYSTALS

M. A. Mondragon

Departamento de Física, UAM-I P. O. Box 55-534  
Deleg. Iztapalapa, 09340 México, D. F.

J. García M.

Instituto de Física, U.N.A.M., P. O. Box 20-364  
Deleg. Alvaro Obregón, 01000 México, D.F.

W. A. Sibley

Physics Department, Oklahoma State  
University, Stillwater, OK 74078

The optical absorption, emission and excitation spectra are reported for  $\text{KCaF}_3:\text{Ho}^{3+}$  crystals. The  $\text{Ho}^{3+}$  ions were found to easily enter this lattice and occupy only one site. The energy level diagram was built according to the optical data.

The measured oscillator strengths for several transitions are compared with the values calculated by the Judd-Ofelt theory. The calculated radiative rates are also reported and the branching ratios suggest that a number of laser transitions are possible.

The temperature dependence of the lifetimes revealed that energy transfer occurs between  $\text{Ho}^{3+}$  ions, which are likely to go into the lattice as pairs.

OPTICAL STUDIES ON  $\text{KCaF}_3\text{:Mn:Eu}$ ,  $\text{RbCdF}_3\text{:Mn:Eu}$   
AND  $\text{RbCaF}_3\text{:Mn:Eu}$  CRYSTALS

J. García M.

Instituto de Física, U.N.A.M., P. O. Box 20-364  
 Deleg. Alvaro Obregón, 01000 México, D. F.

W. A. Sibley

Physics Department, Oklahoma State University  
 Stillwater, 74078

J. M. Spaeth

Gesamthochschule, Paderborn  
 4790 Paderborn, Germany.

Optical transitions of  $\text{Eu}^{2+}$ ,  $\text{Eu}^{3+}$  and  $\text{Mn}^{2+}$  have been investigated for the fluoroperovskites  $\text{KCaF}_3\text{:Mn:Eu}$ ,  $\text{RbCdF}_3\text{:Mn:Eu}$  and  $\text{RbCaF}_3\text{:Mn:Eu}$ .  $\text{Eu}^{2+}$  is present only in  $\text{KCaF}_3$  and  $\text{RbCaF}_3$  although the lattice parameter is quite similar for the three cubic crystals (4.38 Å for  $\text{KCaF}_3^{(1)}$ , 4.45 Å for  $\text{RbCaF}_3^{(1)}$  and 4.40 Å for  $\text{RbCdF}_3^{(2)}$ ). In these crystals  $\text{Eu}^{2+}$  is characterized by two well resolved optical absorption bands due to transitions from the  $8S_{7/2}$  ground state to the excited  $4f^65d(t_{2g})$  and  $4f^65d(e_g)$  states. This optical absorption is common for the  $\text{Eu}^{2+}$  ions in alkali halides and fluorite type crystals<sup>(3)</sup>, but not for  $\text{KMgF}_3$  and  $\text{RbMgF}_3$  where the  $\text{Eu}^{2+}$  ions are in  $\text{K}^+$  or  $\text{Rb}^+$  sites<sup>(4,5)</sup>. The absorption spectrum implies that the divalent europium is in the  $\text{Ca}^{2+}$  site in  $\text{KCaF}_3$  and  $\text{RbCaF}_3$ . The energy levels for  $\text{Eu}^{2+}$ ,  $\text{Eu}^{3+}$  and  $\text{Mn}^{2+}$  and the crystal field value for  $\text{Mn}^{2+}$  in the crystals were obtained.

Energy transfer has been observed between  $\text{Eu}^{2+}$ ,  $\text{Mn}^{2+}$  and  $\text{Eu}^{3+}$  ions. Effective transfer is observed even at low concentrations of  $\text{Mn}^{2+}$ . This suggests that the  $\text{Eu}^{2+}$  and the  $\text{Eu}^{3+}$  ions preferentially cluster around the  $\text{Mn}^{2+}$  ions. The presence of clusters is not unexpected since the  $\text{Mn}^{2+}$  ions (radius 0.80 Å) are smaller than the  $\text{Ca}^{2+}$  ions (0.99 Å) for which they substitute and the  $\text{Eu}^{2+}$  (1.10 Å) ions are larger. The elastic strain when they enter the lattice can be reduced by clustering.

#### References

1. W. L. W. Ludekens and A. J. E. Welch, Acta Cryst. 5, 841 (1952).
2. M. Rosseau, J. Y. Gesland, J. Julliard and J. Novet, Phys. Rev. B12, 1579 (1975).
3. H. Murrieta, J. Hernández and J. Rubio, Kinam 5, 75 (1983).
4. D. K. Sardar, W. A. Sibley and R. Alcala, J. Lumin. 27, 401 (1982).
5. R. Alcala, D. K. Sardar and W. A. Sibley, J. Lumin. 27, 273 (1982).

**THE INFLUENCE OF HIGH EXTERNAL ELECTRIC FIELDS ON  
THE CUBIC  $\text{Eu}^{2+}$  CENTERS IN  $\text{CaF}_2$  SINGLE CRYSTALS**

N.Gouskos

Solid State Section - Physics Department - University of Athens  
104 Salinos Street - Athens 10680 - Greece

In recent years there has been considerable interest [1-5] in studying, using EPR techniques, the influence of very high external electric fields, in excess of  $300 \text{ kV cm}^{-1}$ , on cubic  $\text{Gd}^{3+}$  centres in  $\text{MF}_2$  crystals, where  $\text{M}=\text{Ca}, \text{Cd}, \text{Sr}$  and  $\text{Ba}$ . In the present paper the electric field parameter,  $K$ , is determined for single crystals of  $\text{CaF}_2$  doped with  $\text{Eu}^{2+}$  ions. This parameter was interpreted following the superposition model introduced by Newman [6]. The changes in the positions of the fluoride ions around  $\text{Gd}^{3+}$ , which resulted from the applied field, were calculated using the quasimolecular model of Arkhipov and Malkin [7]. The external electric field, with a maximum intensity of  $400 \text{ kV cm}^{-1}$ , was applied along the [111] direction and the electric field parameter for the  $\text{CaF}_2:\text{Eu}^{2+}$  single crystal was determined as

$$K = [-5.6 \pm 3.0] \times 10^{-12} \text{ cm}^{-1} \text{ kV}^{-2}$$

The large experimental error resulted from the small size of the sample and the fact that the EPR was weaker than that observed for the  $\text{Gd}^{3+}$  ions. From the superposition model of Newman [6] the following relationship for the  $K$  parameter is obtained:

$$K = B_2\{2(t_2^2 - t_2)\Delta'R_{\parallel}^2 + [2(t_2^2 - t_2) + 4|\Delta''R_{\perp}^2 + [4(t_2^2 - t_2) + 2|\Delta''R_{\parallel}^2]\}$$

The parameters  $B_2$  and low power  $t_2$  were determined from the spin-lattice parameters [8].  $B_2$  was  $-147.3 \times 10^{-4} \text{ cm}^{-1}$  and  $t_2$  was 7.4. The displacements  $\Delta'R_{\parallel}$ ,  $\Delta''R_{\perp}^2$  and  $\Delta''R_{\parallel}$  were calculated in the quasimolecular model of Arkhipov and Malkin [7]. The superposition model of Newman gave a value for the electric field parameter for  $\text{CaF}_2:\text{Eu}^{2+}$  of

$$K = -7.4 \times 10^{-12} \text{ cm}^{-1} \text{ kV}^{-2}$$

which is in good agreement with the experimental result.

- 1) N.Gouskos, I.Kh.Salikov and S.N.Arkhipov, Sov.Phys.-Solid State **22**, 3366 (1982)
- 2) N.Gouskos, J.Kuriata and I.Kh.Salikov, J.Phys.C **17**, 2175 (1985)
- 3) N.Gouskos, I.Kh.Salikov and S.N.Arkhipov, Proc.RAMIS-85, Ed.University of Poznam (Poland), Poznan 1985.
- 4) N.Gouskos, Phys.Stat.Sol. (b) (Dec.) (1987)
- 5) N.Gouskos, to be published
- 6) D.J.Newman and W.Urban, Adv.Phys.**24**, 973 (1985)
- 7) S.M.Arkhipov and B.Z.Malkin, Sov.Phys. - Solid State **22**, 1471 (1980)
- 8) D.Zadunajsky de Basch, G.E.Barberis and R.Calvo, Solid State Comm. **18**, 1439 (1978)

RAMAN- AND IR-SPECTRA OF THE OH(OD)-STRETCH MODES IN  $\text{LiTaO}_3$ 

H.P. WINKLER, A. JOVANOVIĆ, M. WÖHLECKE, S. KAPPHAN

Fachbereich Physik der Universität  
Barbarastraße 7, D-4500 Osnabrück, Fed.Rep.Germany

*The temperature dependence of the OH- and OD-stretch modes in  $\text{LiTaO}_3$  has been measured with Raman scattering and Fourier-IR-spectroscopy. The elements of the Ramantensor of a single dipole are derived from those of the ensemble. The pronounced change of the spectra with rising temperature has been used to determine the model parameter of the contributing oscillators.*

In the past the OH-stretching vibration in  $\text{LiNbO}_3$  has been the subject of several investigations. Corresponding detailed research has not been reported for  $\text{LiTaO}_3$ , although  $\text{LiTaO}_3$  is a promising candidate for electro-optic applications and may serve as a model compound of the  $\text{LiNbO}_3$ -family, because of its low phase transition temperature. It is the aim of this contribution to report on some features of the OH- and OD-stretch modes in  $\text{LiTaO}_3$ .

The infrared (ir) and Raman spectra of the OH- and OD-stretching vibrations in  $\text{LiTaO}_3$ , centered at  $\nu_{\text{OH}} = 3478 \text{ cm}^{-1}$  and  $\nu_{\text{OD}} = 2569 \text{ cm}^{-1}$ , respectively, show some structure even for congruent samples. At the low energy side and center part of the spectrum two transitions are visible, while a third transition shows up as a shoulder on the high energy wing. Such structure has been seen in  $\text{LiNbO}_3$  in almost stoichiometric samples only [1]. The OH ir-absorption is polarized perpendicular to the c-axis in  $\text{LiTaO}_3$  as well as in  $\text{LiNbO}_3$ . The first overtones of the OH- and OD-stretch modes have been observed for the first time in  $\text{LiTaO}_3$ . Both the spectral structure and the polarization of the fundamental mode is reflected in the overtone. The anharmonicity is rather small, similar to that in  $\text{LiNbO}_3$ .

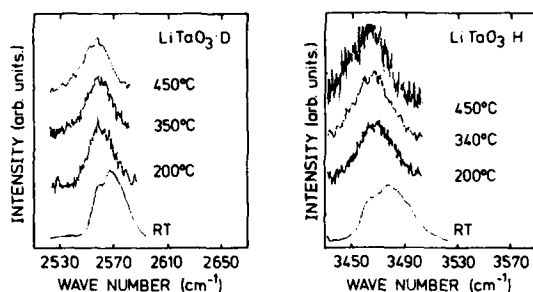


Fig.1 Temperature dependence for the Raman intensity of the OH- and OD-stretching vibration in  $\text{LiTaO}_3$

Raman spectra in the XX or YY configuration exhibit the spectral behaviour of the ir-absorption. These diagonal tensorelements are the strongest and are equal for as grown and moderately doped crystals. Considerable scattering intensities are also observed for ZZ and XY components, while the remaining component are very weak. We have used our model calculation first applied to  $\text{LiNbO}_3$  [2] to calculate the tensorelements of a single dipole from those of the ensemble. The result is a polarizability tensor with minor off-diagonal elements and a ratio close to three for the  $\alpha_{zz}$  to  $\alpha_{xx}$  or

$\alpha_{yy}$  components. This is comparable to the results in  $\text{LiNbO}_3$  and alkali halides like NaCl, KCl and KBr [3,4], reflecting the strongly screened influence of the host on the stretch mode.

The temperature dependence of both the Raman and ir-spectra is yielding information about the composition of the spectrum. Fig. 1 shows the XX Raman spectrum. The strong decrease of the center and high energy transition with increasing temperature is obvious. The low energy transition broadens and the integral scattering intensity (or absorption) is diminished. On cooling the sample down to room temperature, the original spectrum is obtained. This shows that hydrogen or deuterium is not leaving the crystal during the thermal treatment. The fact that the frequency of the low energy transition is almost independent of the temperature allows a well justified decomposition of the spectrum in three transitions of different halfwidth. In Fig. 2 we present an example for such a decomposition.

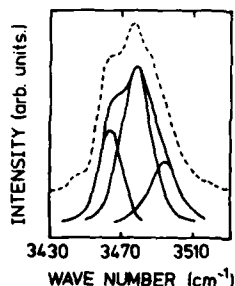


Fig.2 Decomposition of the Raman spectrum of the OH-stretch mode (at RT) into three components

For a best fit the transitions have been described by products of lines with Gauß and Cauchy profile. The results of the procedure can be stated as follows: (i) the frequencies of the transitions contributing to the spectra are separated by  $15 \text{ cm}^{-1}$  for OH and  $10 \text{ cm}^{-1}$  for OD and are within experimental error independent of the temperature. (ii) On the other hand, with the exception of the low energy transition, the intensity of the transitions vary strongly with temperature. Similar trends have been observed in  $\text{LiNbO}_3\text{:H}$  for temperatures up to  $150^\circ\text{C}$  [5].

The above mentioned results may be interpreted by an ensemble of OH (OD) anharmonic oscillators, which are located in the oxygen planes perpendicular to the c-axis. We have to introduce at least two different binding energies to account for the very different temperature behaviour. These results shed new light on the processes involved in the thermal fixing of holograms.

#### Acknowledgement.

This work is supported by the Deutsche Forschungsgemeinschaft ( SFB 225 / C1 ).

#### REFERENCES

1. L. Kovács, V. Szalay, R. Capelletti, *Sol. State Commun.* **52** (1984), p. 1029.
2. A. Jovanović, S. Kapphan, M. Wöhlecke, *Cryst. Latt. Def. and Amorph. Mat.* **15** (1987), p. 137.
3. J.G. Peascoe, M.V. Klein, *J. Chem. Phys.* **59** (1973), p. 2394.
4. J.G. Peascoe, W.R. Fenner, M.V. Klein, *J. Chem. Phys.* **60** (1975), p. 138.
5. Kovács, K. Polgár, R. Capelletti, *Cryst. Latt. Def. and Amorph. Mat.* **15** (1987), p. 115.

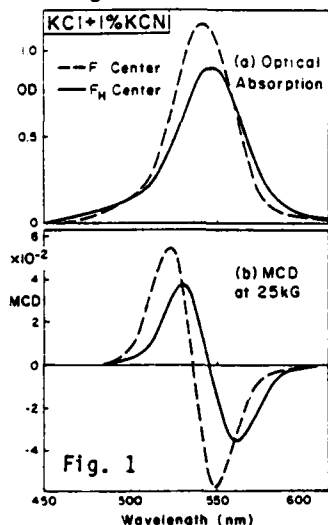
MAGNETO OPTICAL STUDIES OF F CENTER/MOLECULAR DEFECT PAIRS  
IN ALKALI HALIDE CRYSTALS

G. Baldacchini, S. Botti, U.M. Grassano<sup>+</sup> and F. Lüty<sup>\*</sup>

ENEA CRE Frascati -00044 Frascati (Italy)

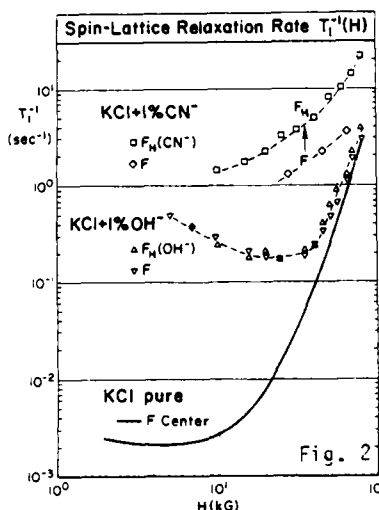
Recently, great scientific interest has developed in the optical properties of F center/molecular ion pairs in various hosts. Association of F centers with molecular defects ("F<sub>H</sub> centers") produces energy transfer between the electronic excitation energy of the F center and the vibrational states of the neighboring molecule. Details of this interaction, however, vary strongly with both the molecule and the crystal structure of the host. The presence of neighboring OH<sup>-</sup> ions produces--at least in NaCl structure hosts--quenching of the F emission without creating OH<sup>-</sup> vibrational emission at 2.7 μm, indicating efficient non-radiative relaxation channels.<sup>1</sup> In contrast to this, F<sub>H</sub>(CN<sup>-</sup>) centers produce under electronic excitation CN<sup>-</sup> vibrational emission at 4.8 μm. The low efficiency of the latter, observed in KCl<sup>2</sup>, rises in CsCl hosts to very high values, allowing the operation of the first visible-light pumped vibrational laser.<sup>3</sup>

The mechanism of interaction between F center and molecular ion is not yet well understood. As one approach to this unsolved problem, we asked in this work the question: to what extent does coupling and energy exchange with the molecular neighbor affect the spin-properties of the F



electron? Using F(OH<sup>-</sup>) centers in KCl, KBr, KI, and F(CN<sup>-</sup>) centers in KCl, CsCl, CsBr, we measured the magnetic circular dichroism (MCD), the ground state spin-lattice relaxation time  $T_1$ , and the spin memory  $\epsilon$  of the electron during the optical cycle. All experiments were performed at -2K on crystals before and after optical association of F centers and molecular ions. The results obtained can be summarized as follows: (a) Typical MCD results are illustrated in Fig. 1 for one example (KCl doped with 1% CN). Rapid quenching produces the pure F absorption and its MCD spectrum, while F center association with the CN<sup>-</sup> defects produces the red-shifted and broadened F<sub>H</sub>(CN<sup>-</sup>) absorption and its related MCD

spectrum. From spectra of this type we learn that the  $F_H$  spin orbit parameter  $\Delta$  is almost the same as that of F centers before aggregation--only slightly decreasing in  $KCl:OH^-$  and  $CN^-$ , while about 20% increasing by  $F_H(OH^-)$  formation in KBr and KI. In the two latter cases an optical bistability was discovered, reported in the following paper.



(b) Fig. 2 illustrates inverse spin lattice relaxation time  $T_1(H)$  for  $OH^-$  and  $CN^-$  doped KCl before and after  $F \rightarrow F_H$  conversion in comparison to F centers in pure KCl. In the low field range the presence of both molecules shortens considerably  $T_1$  (already before and--in most cases even farther--after  $F \rightarrow F_H$  conversion). Towards high fields  $T_1(H)$  approximates the pure F center behavior--closer for  $OH^-$  and less close for  $CN^-$  doped crystals, as seen in Fig. 2.

(c) The spin-memory loss during optical cycle determines the spin-mixing parameter  $\epsilon$  for the F and  $F_H$  centers. Aggregation to  $OH^-$  defects slightly decreases  $\epsilon$ , while association to  $CN^-$  ions produces strong increases of  $\epsilon$ . This latter part is particularly important because both spin-memory loss and electron-molecular energy transfer occurs during the optical excitation/de-excitation cycle. The exchange from electronic into vibrational emission, observed only for  $F_H(CN^-)$  defects, appears to be related in its strength to that of the spin-memory loss: most extreme is the effect for the laser-active  $F_H(CN^-)$  system in CsCl with highest energy transfer and strongest spin-memory loss in the optical cycle.

<sup>+</sup>Dipartimento di Fisica, Università di Tor Vergata, Roma, Italy.

<sup>\*</sup>Physics Department, University of Utah, Salt Lake City, Utah 84112, U.S.A.  
Supported by NSF grant DMR 87-06416

- (1) L. Gomes and F. Luty, Phys. Rev. B 30, 7194 (1984).
- (2) Y. Yang and F. Luty, Phys. Rev. Lett. 51, 419 (1983).
- (3) W. Gellermann, Y. Yang, and F. Luty, Optics Commun. 57, 186 (1986).

OH<sup>-</sup> ISOTOPE EFFECTS ON VIBRATIONAL AND ELECTRICAL ANHARMONICITIES  
AS A PROBE OF THE DEFECT ENVIRONMENT\*

W. Beall Fowler\*\*

Physics Department and Sherman Fairchild Laboratory  
Lehigh University  
Bethlehem, PA 18015 U. S. A.

R. Capelletti

Dipartimento di Fisica dell'Universita  
Parma, Italy

Study of the infrared properties of hydrogen-related defects in semiconductors and insulators has been a significant tool in obtaining information about the structures and properties of such defects. Hydrogen is a particularly important defect constituent because of its small size and mass, the existence of several isotopes, and its ability to form several types of chemical bonds. In many crystals hydrogen-related defect modes lie well above the vibrational bands of the host, thus making them amenable to conventional IR spectroscopic techniques.

In this paper we investigate some of the theoretical aspects of the IR spectra of H-related defects, using OH<sup>-</sup> as an example. We show that it is possible to extract considerable information from IR stretch modes, if one can vary the isotope and the temperature, and if the positions and strengths of vibrational overtones can be measured. Although such information may not be sufficient to determine defect models with certainty, it should allow certain defect models to be discarded.

The classic example of this type of analysis is the paper of Bates and Perkins<sup>1</sup> (BP) on OH<sup>-</sup> in TiO<sub>2</sub>. BP measured the IR spectra of OH<sup>-</sup>,

OD<sup>-</sup>, and OT<sup>-</sup> at temperatures ranging from 8K to 300K. They analyzed their measured isotopic frequency shifts and intensities on the basis of two models, a diatomic anharmonic oscillator model and a harmonic hydrogen-bonded model. Based on this analysis, they concluded that the hydrogen-bonded model was inconsistent with experiment.

We have extended the BP model and have applied<sup>2</sup> our version to data obtained for Ti- and Mg-related OH<sup>-</sup> and OD<sup>-</sup> centers in LiF. Here, too, the anharmonic oscillator model seems basically correct. However, there is striking evidence for electrical anharmonicity (nonlinearity of the electric dipole moment with O-H separation), in addition to mechanical anharmonicity, in certain of the defects studied. This electrical anharmonicity may indicate strong defect-host interactions not previously considered.

In this paper the theoretical aspects of the approach used to analyze the data of Ref. 2 will be discussed. The importance of the coupling of the defect molecule to the lattice through the O atom, and its effect on isotope shifts, is demonstrated. Further analysis of the data of BP<sup>1</sup> suggests an anomalously large anharmonic contribution to the internal OH<sup>-</sup> stretching mode, which at the present time cannot be explained. The effects of electrical anharmonicity are considered in detail, as are the expected experimental consequences of weak hydrogen bonding.

\*Much of this analysis was carried out while WBF was visiting the Dipartimento di Fisica dell'Universita, Parma, Italy.

\*\*Research at Lehigh University supported in part by the Electronic and Solid State Science Program of the U. S. Office of Naval Research.

1. J. B. Bates and R. A. Perkins, Phys. Rev. B 16, 3713 (1977).
2. R. Capelletti, W. Beall Fowler, G. Ruani, and L. Kovacs, Cryst. Latt. Def. and Amorph. Mat. 16, 189 (1987).

F<sub>A</sub> AND F-AGGREGATE CENTRES IN RbCl:Li<sup>+</sup>

G. Baldacchini and E. Giovenale  
 ENEA, Dipartimento TIB, Divisione Fisica Applicata  
 Centro Ricerche Energia Frascati, C.P. 65, 00044 Frascati, Italy

F. De Matteis, A. Scacco, and F. Somma  
 Dipartimento di Fisica, Università "La Sapienza", P.le A. Moro 2, 00185 Roma, Italy

U.M. Grassano  
 Dipartimento di Fisica, Università di Roma - Tor Vergata  
 V. Orazio Raimondo, 00173 Roma, Italy

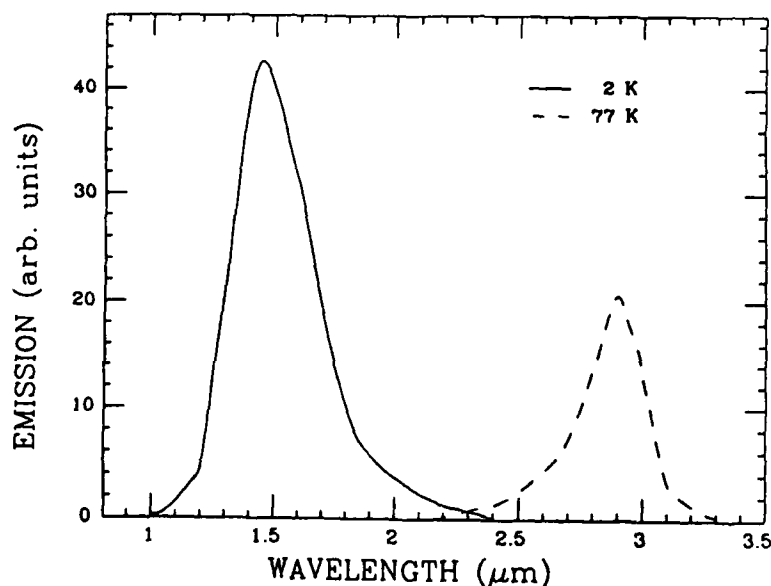
Despite many years of investigation on the properties of the colour centres in ionic crystals, some defects are not yet sufficiently known and more careful studies can reveal new fundamental aspects which are of paramount interest for applications. In particular, the use of a few kinds of point defects in laser technology fostered recent studies on the structure and the optical properties of aggregate and associate colour centres. Indeed the association of one (or more than one) F centre with impurity ions leads to the formation of associate defects, which constitute a numerous class of active media for obtaining laser action [1]. In general, the aggregation and the association of simple defects into more complex centres, due to the vacancy mobility, is obtained by appropriate optical irradiation. In this way, it is likely to create several types of defects, which frequently coexist in the same crystal. The most studied aggregate centres are the F<sub>2</sub> and F<sub>3</sub> complexes, and the best known associate centres are the F<sub>A</sub> and (F<sub>2</sub>)<sub>A</sub> defects (if the impurity is a cation) and the F<sub>H</sub> defects (if the impurity is a halide ion).

We have studied the optical behaviour of associate colour centres in RbCl:Li<sup>+</sup> at different temperatures. Besides the known F<sub>A</sub> centres, (F<sub>2</sub>)<sub>A</sub> defects have been created by irradiation in suitable conditions and observed for the first time. Their I.R. absorption and emission have been measured at 2 K and 77 K, and the peak parameters are reported in the table:

T(K)	E <sub>A</sub> (eV)	W <sub>A</sub> (eV)	E <sub>E</sub> (eV)	W <sub>E</sub> (eV)
2	1.29	0.05	1.03	0.17
77	1.28	0.06	1.01	0.17

The dichroism of the centres and the kinetics of their formation, in strong connection with that of the  $F_2$  centres, have been deduced by absorption measurements. Excitation spectra of the  $(F_2)_A$  luminescence showed the position of the centre absorption band also in the visible range. Our results confirm and clarify previous unexplained observations. However, we have found the  $F_2$  emission bandwidth slightly narrower than that reported earlier [2].

Moreover, a peculiar and up to now not reported behaviour of  $F_A$  centres has been observed. Their luminescence shows unexpected dramatic changes with temperature. The known typical emission of  $F_A(II)$  centres, peaking at about  $2.9 \mu\text{m}$  with a halfwidth of  $0.06 \text{ eV}$ , is clearly observed in the range  $50\text{--}80 \text{ K}$ . However, it practically disappears at  $2 \text{ K}$ , giving rise to a completely different emission band, centered at about  $1.46 \mu\text{m}$  and having a halfwidth of  $0.21 \text{ eV}$ . These band parameters are usually typical of the emission of  $F_A(I)$  centres, which is not predicted for  $\text{RbCl}:\text{Li}^+$  [3]. In the Figure we report the luminescence excited with a He-Ne laser at  $2 \text{ K}$  and  $77 \text{ K}$ . Such a behaviour, whose interpretation is not clear at present, requires more detailed investigations which are under way.



#### References

1. L. Mollenauer and D.H. Olson, *J. Appl. Phys.* **46**, 3109 (1975); I. Schneider and C.R. Pollock, *J. Appl. Phys.* **54**, 6193 (1983).
2. Y. Brada, *J. Chem. Phys.* **58**, 3959 (1973).
3. A.Y.S. Kung and J.M. Vail, *Phys. Stat. Solidi (b)* **79**, 663 (1977).

# MEASUREMENT OF THE ANGULAR SHIFT OF THE $\text{Li}^+$ ION IN $\text{F}_\text{A}$ ( $\text{Li}^+$ ) CENTER CRYSTALS

Marie MAY, Solange DEBRUS, J.P. HONG, Bruno QUERNET  
*Laboratoire d'Optique (U.A. 154 du CNRS)*  
*Université P. et M. CURIE, 4 Place Jussieu, F 75252 Paris Cedex 05.*

Edouard RZEPKA, Abderrahman BOUAZI  
*Laboratoire de Physique Cristalline (U.A. 802 du CNRS)*  
*Université de Nantes, 2 rue de la Houssinière, 44072 Nantes Cedex*

$\text{F}_\text{A}(\text{I})$  type centers created in alkali halides are of  $\text{C}_{4v}$  symmetry. On the other hand,  $\text{F}_\text{A}(\text{II})$  type centers formed in crystals doped with lithium have a lower symmetry since the  $\text{Li}^+$  ions occupy four equivalent positions around a cationic site, lying in the  $\{100\}$  planes. A tunneling motion occurs between these positions, which are slightly shifted in the  $\langle 110 \rangle$  directions with respect to the lattice cationic site. All the properties of  $\text{F}_\text{A}(\text{II})$  centers as well in optical emission (1) and absorption (2) as in Raman spectroscopy (3) are interpreted by considering a  $\text{C}_s$  symmetry. Under these conditions, the  $\text{F}_{\text{A}1}$  and  $\text{F}_{\text{A}2}$  transitions are not parallel to the crystallographic axes of the crystal and the reorientation of the centers under a linearly polarized optical excitation is limited. Moreover the probability of reorientation is temperature independent and gratings have been recorded in such crystals at nitrogen liquid temperature (4).

We present here a theoretical investigation of the anisotropy photoinduced at saturation in an  $\text{F}_\text{A}$  ( $\text{Li}^+$ ) center crystal. It is shown that the angular shift  $\theta$  of the  $\text{Li}^+$  ion may be deduced from the values, for a given wavelength, of dichroism and birefringence photoinduced by an optical excitation in the  $\text{F}_{\text{A}1}$  band on the one hand and by an optical excitation in the  $\text{F}_{\text{A}2}$  band on the other hand. This method presents the advantage to remove the influence of the remaining F centers in the

crystal since it only concerns the photoinduced anisotropy. The experimental results are valid only if the exciting  $F_{A2}$  wavelength does not belong to the K band and if there is no interaction between the centers.

The measurements give  $\theta = 17^\circ$  for a crystal of  $F_A(II)$  KCl:Li and  $\theta = 21^\circ$  for a crystal of  $F_A(II)$  RbCl:Li, at liquid nitrogen temperature.

### References

- (1) G. BALDACCHINI, G.P. GALLERANO, U.M. GRASSANO, A. LANCIANO, A. SCACCO, F. SOMMA, M. MEUCCI, M. TONELLI, Phys. Rev. B **33**, 4273-4282 (1986).
- (2) M. MAY, E. RZEPKA, S. DEBRUS, J.P. HONG, Opt. Commun. **61**, 325-331 (1987).
- (3) M. LEBLANS, W. JOOSEN, E. GOOVAERTS, D. SCHOEMAKER, Phys. Rev. B **35**, 2405-2412 (1987).
- (4) M. MAY, J.P. HONG, S. DEBRUS, E. RZEPKA, J. Appl. Phys. **61**, 852-858 (1987).
- (5) A. BOUAZI, D.E.A. Report, University of Nantes (1987).

THE ROLE OF OH<sup>-</sup> IONS IN THE CHARGE COMPENSATION OF IMPURITIES IN ZnWO<sub>4</sub>  
SINGLE CRYSTALS

<sup>x</sup>I.Földvári, <sup>xx</sup>R.Capelletti, <sup>xxx</sup>L.A.Kappers, <sup>x</sup>A.Watterich.

<sup>x</sup> Research Laboratory for Crystal Physics, 1502, Budapest 112 Pf.132  
 Hungary

<sup>xx</sup> Department of Physics, University of Parma, Parma, Italy

<sup>xxx</sup> Physics Department University of Connecticut, Storrs, CT USA

ZnWO<sub>4</sub> is a well known scintillator material the application of which is influenced by its colour due to impurities. Cation impurities are expected to substitute for either Zn<sup>2+</sup> or W<sup>6+</sup> ions depending on their valence state and ionic radii. The excess charge of the impurities may be compensated either by the cation side (e.g. 3<sup>+</sup>-5<sup>+</sup> pairs instead of the 2<sup>+</sup>-6<sup>+</sup> pairs of the host lattice) or by anionic defects (e.g. OH<sup>-</sup> ions). In our earlier papers /1,2/ the incorporation of iron was studied and interstitial OH<sup>-</sup> was found compensating the extra charge of Fe<sup>3+</sup> ions in Zn<sup>2+</sup> sites.

In the present work we showed that Cr<sup>3+</sup> and Al<sup>3+</sup> have no similar affinity to OH<sup>-</sup> ions. Their charge compensation may happen by the intrinsic W<sup>5+</sup> defects or an unclarified way.

Characteristic OH<sup>-</sup> bands were observed in the spectra of ZnWO<sub>4</sub>:Sb and ZnWO<sub>4</sub>:V crystals with well resolved fine structure at 10 K. The half-width ( 20-30 cm<sup>-1</sup> at RT) and the structure of these bands indicate a strong coupling of OH<sup>-</sup> vibration with the phonon structure of the crystals. The OD - OH exchange in ZnWO<sub>4</sub>:Sb was faster and more effective than in the case of ZnWO<sub>4</sub>:Fe crystals. All these facts support the assumption that the charge compensation of Sb or V ions is given by OH<sup>-</sup> ions substituting O<sup>2-</sup> positions. 5<sup>+</sup>-3<sup>+</sup> cations pairs were shown in a double doped crystal (ZnWO<sub>4</sub>:Sb,Fe) and their role in the decolouration of the crystals has been pointed out in an earlier paper /3/. The OH<sup>-</sup> bands in ZnWO<sub>4</sub> showed strong angular dependence on the polarization of the incident IR light supporting the idea of oriented metal ion - OH<sup>-</sup> complexes.

References:

- 1./ I.Földvári, R.Capelletti, Á.Péter, I.Cravero, A.Watterich:  
Spectroscopic properties of  $\text{ZnWO}_4\text{:Fe}$  single crystals.  
Solid State Comm. 59, 855 (1986).
- 2./ I.Földvári, R.Capelletti, Á.Péter, F.Schmidt: The infrared absorption of  $\text{OH}^-$  in  $\text{ZnWO}_4$  and  $\text{ZnWO}_4\text{:Fe}$  single crystals.  
Solid State Comm. 63, 787 (1987).
- 3./ I.Földvári, Á.Péter, S.Keszthelyi-Ládori, R.Capelletti, I.Cravero, F.Schmidt: Improvement of the quality of  $\text{ZnWO}_4$  single crystals for scintillation applications.  
J.Crystals Growth 79, 714 (1986).

AN INFRARED ABSORPTION BAND CAUSED BY OH<sup>-</sup> IONS  
IN LiNbO<sub>3</sub>:Mg,Cr CRYSTAL

L.Kovács, I.Földvári, I.Cravero, K.Polgár  
Research Laboratory for Crystal Physics, Hungarian Academy  
of Sciences, 1502 Budapest, P.O.Box 132, Hungary

R.Capelletti  
Department of Physics, University of Parma, Parma, Italy

Among the practical applications of LiNbO<sub>3</sub> single crystals one of the most important is the utilization of the photorefractive properties in hologram recording. The photorefractive process is strongly dependent on transition metal impurities (e.g. Fe, Cr) and has been studied extensively [1]. On the other hand, Mg doping above a threshold level increases the resistance of the crystal to laser-damage [2]. Even the OH<sup>-</sup> ions which are always present in air grown LiNbO<sub>3</sub> are assumed to affect the photorefractive behaviour [3]. In the present work we studied a LiNbO<sub>3</sub> crystal containing Mg, Cr, and OH<sup>-</sup> ions simultaneously. Visible and infrared absorption spectra were measured in order to obtain some information about the defect structure of the crystal.

A new infrared absorption band caused by OH<sup>-</sup> ions was found at  $\approx 3506\text{ cm}^{-1}$  in LiNbO<sub>3</sub>:Mg,Cr which distinctly differs from that in pure or chromium doped ( $3485\text{ cm}^{-1}$ ) and heavily magnesium doped ( $3540\text{ cm}^{-1}$ ) crystals. The crystal was grown in air by the Czochralski method. The Li/Nb ratio was adjusted to 1.1, the concentration of Mg and Cr in the melt was  $4 \cdot 10^{-2}$  and  $3.5 \cdot 10^{-4}$  mole/mole respectively. The visible colour of the crystal was found to be rather inhomogeneous along the pulling axis. The upper and lower parts of the boule were greenish and violet respectively with a continuous transition range between them.

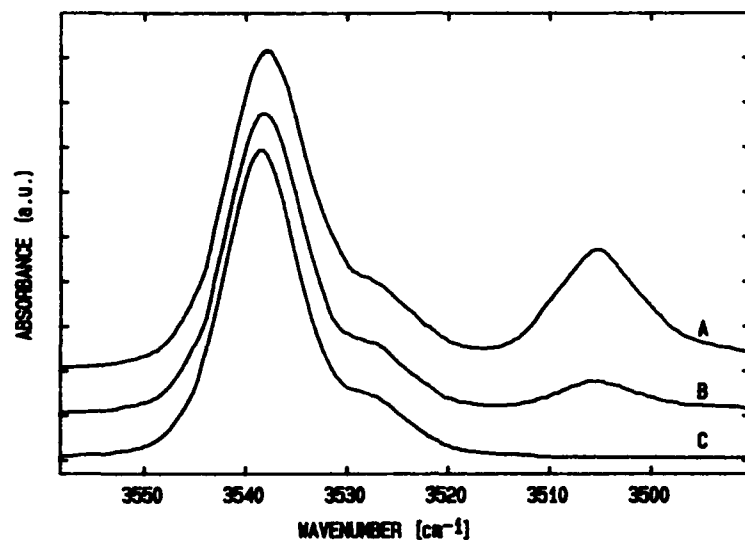


Figure 1. Infrared absorption spectra of  $\text{OH}^-$  ions in  $\text{LiNbO}_3:\text{Mg,Cr}$  at RT. Curve A belongs to the upper part, B to the lower part of the crystal boule. Curve C represents  $\text{LiNbO}_3:\text{Mg}$  crystal.

The experimental results suggest that both  $\text{Cr}^{3+}$  and  $\text{Cr}^{4+}$  ions are present in the crystal. The vibrating hydroxyl ion in a  $\text{Cr}^{3+}_{\text{Nb}}--\text{Mg}^{2+}_{\text{Li}}--\text{OH}^-_{\text{O}}$  complex may be responsible for the appearance of the new absorption band at  $\approx 3506 \text{ cm}^{-1}$  mainly in the greenish upper part of the boule.  $\text{Cr}^{4+}_{\text{Nb}}--\text{Mg}^{2+}_{\text{Li}}$  pairs which are neutral without  $\text{OH}^-$  ions are assumed to be dominant in the violet lower part of the crystal where the absorption at  $\approx 3506 \text{ cm}^{-1}$  is rather weak.

#### References

- [1] A.Räuber, in Current Topics in Mat. Science, Vol.1, p 481, ed. by E.Kaldis, North-Holland Publ. Comp. 1978
- [2] D.A.Bryan, Robert Gerson and H.E.Tomaschke, Appl.Phys. Lett. 44,847,1984
- [3] R.G.Smith, D.B.Fraser, R.T.Denton and T.C.Rich, J.Appl. Phys. 39,4600,1968

# RESONANT ELECTRONIC RAMAN SCATTERING OF THE $\text{Sm}^{++}$ -CATION VACANCY COMPLEX IN KCl

Bas Cocquyt, Wim Joosen, and Dirk Schoemaker  
Physics Department, University of Antwerp (UIA)  
B-2610 Wilrijk (Antwerp), Belgium

The Raman scattering of the  $\text{Sm}^{++}$  ion in KCl is resonantly excited in the  $4f^6 - 4f^55d$  optical transition centered at 540 nm. Six peaks (width  $\approx 5 \text{ cm}^{-1}$ ) are observed between  $240 \text{ cm}^{-1}$  and  $340 \text{ cm}^{-1}$  (Fig.1). According to the polarization properties of the emission upon 632.8-nm excitation they belong to electronic transitions between the  $^7F_0$  and  $^7F_1$  terms in the  $4f^6$  configuration.<sup>1</sup> In the KCl host the threefold degeneracy of the  $^7F_1$  term is lifted: The crystal field splitting depends on the site symmetry of the  $\text{Sm}^{++}$  ion.<sup>2</sup> The signals at  $255 \text{ cm}^{-1}$ ,  $288 \text{ cm}^{-1}$ , and  $321 \text{ cm}^{-1}$  are attributed to the site with  $C_{2v}$  symmetry in agreement with Refs.1 and 2. In this complex the charge compensating cation vacancy is located in a next nearest neighbor (n.n.n.) position along  $\langle 110 \rangle$ . Thermal annealing above 500 C favors a high concentration of this complex. However, the Raman spectrum in Fig.1 shows that other  $\text{Sm}^{++}$ -vacancy complexes or aggregates were not completely annealed.

We have investigated the polarized Raman properties of these electronic transitions. Analysis by means of the extended Behavior Type (BT) method for resonant Raman scattering<sup>3,4</sup> provides independent evidence for the final states being  $J=1$  levels. Measurements in a  $\langle 100 \rangle$  cleaved crystal reveal that the observed transitions are all *completely depolarized*, i.e., they correspond to Raman tensors the diagonal components of which are zero. Additional experiments on a  $\langle 110 \rangle$  polished sample establish within an experimental error of 5 % that the off-diagonal elements are equal in magnitude and opposite in sign. Consequently, the observed Raman transitions transform according to the  $T_{1g}$  representation of the cubic group  $O_h$ , which is compatible with a  $J=0 \rightarrow J=1$  transition between states of equal parity.

In the  $C_{2v}\langle 110 \rangle$  point group the  $T_{1g}$  representation of  $O_h$  reduces to  $B_1$ ,  $B_2$ , and  $A_2$ , for the Raman peaks at  $255 \text{ cm}^{-1}$ ,  $288 \text{ cm}^{-1}$ , and  $321 \text{ cm}^{-1}$ , respectively.<sup>1</sup> The latter representations possess a *non-symmetric* Raman tensor in contrast with the  $T_{1g}$  representation of  $O_h$  the Raman tensor of which is *anti-symmetric*. We conclude that the cation vacancy in a n.n.n. position of the  $\text{Sm}^{++}$  ion does not influence the polarized Raman spectra and, consequently, that the breakdown of cubic site symmetry of  $\text{Sm}^{++}$  is only reflected in the different

energies of the  $J=1$  levels. In order to identify the site symmetries associated with the signals at  $263\text{ cm}^{-1}$ ,  $273\text{ cm}^{-1}$ , and  $298\text{ cm}^{-1}$ , the influence of different thermal treatments and excitation frequencies on the relative Raman intensities of these transitions will be investigated.

1. W.E. Bron and W.R. Heller, Phys. Rev. **136**, A1433 (1964).
2. A.J. Ramponi and J.C. Wright, Phys. Rev.B **31**, 3965 (1985).
3. M. Leblans, W. Joosen, E. Goovaerts, and D. Schoemaker, Phys. Rev.B **35**, 2405 (1987).
4. W. Joosen, E. Goovaerts, and D. Schoemaker, Phys. Rev.B **35**, 8215 (1987).

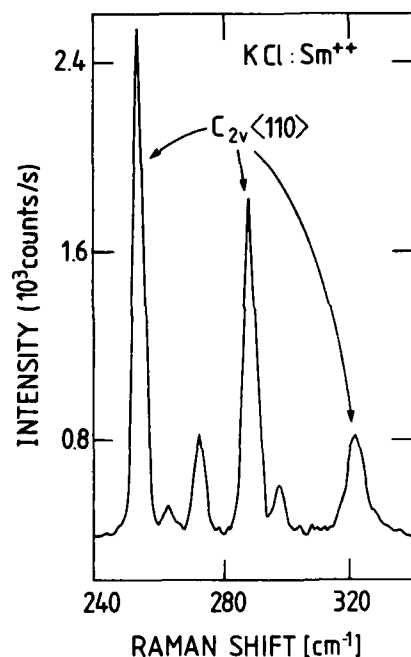


Fig.1 Depolarized Raman spectrum (recorded at 10K) of a  $\langle 100 \rangle$  KCl:Sm<sup>++</sup> sample (1 wt% of SmCl<sub>2</sub> added to the melt) under 514.5-nm excitation. The crystal was quenched at 600 C for 30 minutes.

PRODUCTION OF A PARAMAGNETIC  $\text{Bi}^{\circ}$  CENTER IN X - IRRADIATED  $\text{KCl} \cdot \text{Bi}$  CRYSTALS

S.V. Nistor, E. Goovaerts\*, I. Ursu, and D. Schoemaker\*  
 Central Institute of Physics, POB MG-6 Magurele, Bucuresti  
 Romania 76900

\*University of Antwerp (U.I.A.), Physics Department  
 B-2610 Wilrijk - Antwerpen, Belgium

Since the discovery of laser-active  $\text{Tl}^{\circ}(1)$  centers in  $\text{KCl}$  /1-3/ the interest in the np-type impurity defects has greatly increased. Such irradiation defects have been obtained only in alkali halides doped with  $ns^2$  type cations of the III B and IV B groups of the periodic table.

We report the properties of a paramagnetic center in  $\text{KCl} \cdot \text{Bi}$  crystals, with a  $\text{Bi}^{\circ}(6p^3)$  basical structure. The ESR spectra attributed to such centers can be produced after X-irradiation in the 77-210 K temperature range and subsequent warm - up to, or by direct X-irradiation at  $T > 220$  K, only in samples previously annealed at high temperature. The ESR transitions originate from defects involving a single Bi nucleus, as shown by the pattern of 10 lines of equal intensity resulting from the hyperfine (hf) interaction with a single  $I = 9/2$  nucleus, corresponding to the  $^{209}\text{Bi}$  isotope (natural abundance 100%). The ESR spectrum is described by the spin Hamiltonian with tetragonal symmetry along a  $\langle 100 \rangle$  axis (usual notations /4/):

$$\frac{1}{g_0 \beta} \mathcal{H}_z = \frac{1}{g_0} \bar{H} \hat{g}^{zz} \bar{S}' + \bar{S}' \hat{A}^{zz} \bar{I}$$

where  $S' = \frac{1}{2}$  and  $I = \frac{9}{2}$ .

The spin Hamiltonian parameters are given in the table, together with the corresponding values for the previously studied isoelectronic species  $\text{Sn}^-$  /5/ and  $\text{Pb}^-$  /6/.

Center	T(K)	$g_{  }^{eff}$	$g_{\perp}^{eff}$	$A_{  }^{eff}(mT)$	$A_{\perp}^{eff}(mT)$
Sn <sup>-</sup> (tetrag)	10	1.987 $\pm 0.001$	3.931 $\pm 0.001$	9.7 $\pm 0.2$	15.2 $\pm 0.1$
Pb <sup>-</sup> (1)	15	1.151 $\pm 0.001$	2.560 $\pm 0.004$	25 $\pm 0.1$	21.4 $\pm 0.1$
Bi <sup>0</sup>	8	1.109 $\pm 0.002$	2.712 $\pm 0.003$	23 $\pm 0.2$	22.2 $\pm 0.2$

Due to the large spin-orbit coupling, a quantitative estimation of the observed g-values has been performed by a full diagonalization of the crystal-field, spin-orbit and coulomb repulsion terms between the 20 states of the  $p^3$  configuration. Based on ESR pulse-annealing and optical bleaching data, together with earlier results an isoelectronic Sn<sup>-</sup> and Pb<sup>-</sup> centers /5,6/, possible structural models and production sequences of the Bi<sup>0</sup> center are discussed.

- /1/ D. SCHOEMAKER, E. GOOVAERTS and S.V. NISTOR, Bull. Am. Phys. Soc. 23 200 (1978)
- /2/ E. GOOVAERTS, J. ANDRIESSEN, S.V. NISTOR and D. SCHOEMAKER Phys. Rev. B24, 29 (1981)
- /3/ W. GELLERMAN, F. LUTY and C.R. POLLOCK, Opt. Comm. 39, 381, (1981)
- /4/ I. URSU, La Resonance Paramagnetique Electronique, Dunod, Paris, 1968
- /5/ F. VAN STEEN and D. SCHOEMAKER, Phys. Rev. B19, 59 (1979)
- /6/ E. GOOVAERTS, S.V. NISTOR and D. SCHOEMAKER, Phys. Rev. B25, 83 (1982)

ESR OF NON-CUBIC  $\text{Fe}^{3+}$  CENTERS IN  $\text{LiCl}$  CRYSTALS

S.V. Nistor, D.P. Lazar and M. Velter-Stefanescu

Central Institute of Physics, POB MG-6 Magurele, Bucuresti,  
Romania 76900

It has been shown by ESR spectroscopy that  $\text{Fe}^{2+}$  ions in the  $\text{LiCl}$  lattice act as both electron and hole trapping centers. Substitutional  $\text{Fe}^+$  centers at lattice sites with various symmetries /1/, as well as cubic interstitial  $\text{Fe}_{\text{cub}}^{3+}$  centers /2/, were produced by X-irradiation at 77 K, respectively at room temperature (RT).

We report here the identification in  $\text{LiCl.Fe}$  crystals, X-irradiated at 77 K and subsequently pulse-annealed at higher temperatures, of some non-cubic  $\text{Fe}^{3+}$  centers subjected to extremely strong crystal-fields, which we believe to be the precursors of the  $\text{Fe}_{\text{cub}}^{3+}$  centers.

Details concerning the preparation of the crystals and irradiation procedures were given elsewhere /1/. The ESR measurements were performed in the 35 GHz microwave band in a Varian E12 spectrometer equipped with a  $\text{N}_2$  gas flow attachment.

Three types of orthorhombic non-cubic  $\text{Fe}^{3+}$  centers with local axes  $x||\langle 110 \rangle$ ,  $y||\langle 1\bar{1}0 \rangle$  and  $z||\langle 001 \rangle$ , denoted  $\text{Fe}^{3+}(\text{I})$ ,  $\text{Fe}^{3+}(\text{II})$  and  $\text{Fe}^{3+}(\text{III})$ , have been identified. The local  $z$  axis of the  $\text{Fe}^{3+}(\text{III})$  center is tilted by  $4^\circ$  in a  $\{110\}$  plane. The ESR spectrum is described by the spin Hamiltonian /3/:

$$\mathcal{H}_s = g\beta\bar{H}\bar{S} + B_2^0 O_2^0 + B_2^2 O_2^2 + B_4^0 O_4^0 + B_4^2 O_4^2 + B_4^4 O_4^4$$

where  $S = 5/2$ . The resulting parameters, determined by a computer fitting procedure with experimental data along the main axes, are given in the table.

Center	g	$B_2^0$ (mT)	$B_2^2$ (mT)	$B_4^0$ (mT)	$B_4^2$ (mT)	$B_4^4$ (mT)
$Fe^{3+}(I)$	2.001	50.6	16.7	0.013	0.006	0.138
	$\pm 0.002$	$\pm 0.5$	$\pm 0.5$	$\pm 0.004$	$\pm 0.003$	$\pm 0.004$
$Fe^{3+}(II)$	2.011	49.3	9.9	0.015	0.071	0.394
	$\pm 0.002$	$\pm 0.5$	$\pm 0.1$	$\pm 0.004$	$\pm 0.004$	$\pm 0.004$
$Fe^{3+}(III)$	2.008	16	15			
	$\pm 0.002$	$\pm 0.5$	$\pm 1$			

Pulse annealing experiments on samples X-irradiated at 77 K have shown that the initial small concentration of  $Fe^{3+}(I)$  centers increases more than tenfold in the temperature range  $100\text{ K} \leq T \leq 120\text{ K}$ , where the  $V_K$  centers decay. It means that a precursor  $Fe^{2+}(I)$  center is produced by X-irradiation. Above 140 K the  $Fe^{3+}(I)$  centers decay and the  $Fe^{3+}(II)$  and  $Fe^{3+}(III)$  centers are produced. Above 250 K both centers decay and the  $Fe_{cub}^{3+}$  centers are produced.

The structural models for these centers are based on two possible structures of the precursor  $Fe^{2+}(I)$  i.e., either an interstitial  $Fe^{2+}$ , or a substitutional  $Fe^{2+}$  ion which has trapped an  $Cl_i^-$  by X-irradiation.

- /1/ S.V. NISTOR, I. URSU and M. VELTER-STEFANESCU, Phys. Rev. **B35**, 4595 (1987)
- /2/ S.V. NISTOR and M. VELTER-STEFANESCU, Phys. Stat. Sol. **b138**, 331 (1986)
- /3/ I. URSU, La Resonance Paramagnetique Electronique, Paris, Dunod, 1968

THE EPR STUDY OF  $\text{Co}^{2+}$  CENTERS IN  $\text{PbCl}_2$  SINGLE CRYSTALSJ. Rosa, A.G. Badalyan<sup>\*</sup>), P.G. Baranov<sup>\*</sup>), V.A. Khramtsov<sup>\*</sup>)

Institute of Physics, Czech. Acad. of Sci., 180 40 Prague 8, Na Slovance 2, Czechoslovakia

<sup>\*</sup>)A.F. Ioffe Physics-Technical Institute Acad.of the USSR, Lening ad, USSR

The x-band EPR has been studied at 20 K in single crystals of  $\text{PbCl}_2\text{:Co}$ , the symmetry group of which is  $D_{2h}^{16}$ , with the lattice parameters  $a = 0.7608$ ,  $b = 0.4525$  and  $c = 0.9030 \text{ nm}$  /1/.

$\text{Co}^{2+}$  belongs to the transition metal ions group with unfilled  $3d^7$  orbital. In distorted octahedral field the splitting of the ground state  $^4F$  occurs and the lowest state seems to be the Cramers doublet. Since the only naturally occurring nuclide is  $^{59}\text{Co}$  with  $I=7/2$ , a hyperfine octet is usually resolved with markedly anisotropic g-factor. The spin Hamiltonian with the effective spin  $S'=1/2$  and nuclear spin  $I=7/2$  can be expressed as follows:

$$\hat{\mathcal{H}} = \beta H \bar{g} \hat{S}' + \hat{S}' \bar{A} \hat{I}. \quad (1)$$

The EPR spectrum in the  $a \parallel H$  (fig. 1) or  $c \parallel H$  orientations, respectively consists of two octets, in more general orientation there is the strong dependence of the HFS constants on the magnetic field as well as new lines appear due to forbidden transitions. Spectrum shows strong anisotropic properties both g-factor and HFS constants also. The spectrum can be described by the Hamiltonian (1) where the parameters are given in Tab. 1.

direction	$A^I$			$A^{II}$		
	$g^I$	MHz	$10^{-4} \text{ cm}^{-1}$	$g^{II}$	MHz	$10^{-4} \text{ cm}^{-1}$
c	2.657	659	220	3.262	478	159
a	4.887	855	287	3.684	443	148
b	6.104	2281	394	6.273	991	331

Tab. 1 g-factors and HFS constants of two  $\text{Co}^{2+}$  centers in  $\text{PbCl}_2$

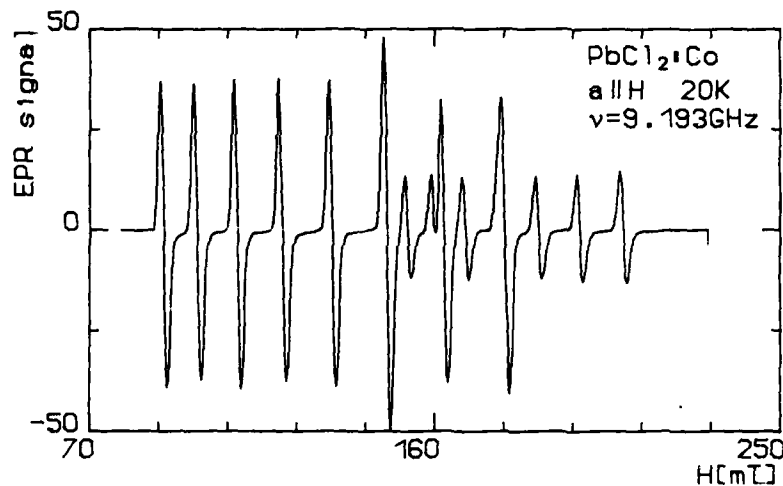


Fig. 1 The EPR spectrum of  $\text{Co}^{2+}$  centers in  $\text{PbCl}_2:\text{Co}$  crystal.  
 $H \parallel a, H \perp b, c; T = 20 \text{ K}; \nu = 9.193 \text{ GHz}.$

By means of symmetry properties of angle dependences of the EPR spectrum, which shows the same symmetry as  $\text{Pb}^{2+}$  site ( $c_1$  and reflection through the  $a$  and  $c$  axes, respectively) we can conclude, that paramagnetic centers responsible for the spectrum are incorporated in the  $\text{PbCl}_2$  lattice on the  $\text{Pb}^{2+}$  sites.

From the above facts it can be deduced that the  $\text{Co}^{2+}$ -ions can play the role of the forementioned centers, incorporated in two different surroundings I and II of  $\text{Pb}^{2+}$  sites.

/1/ Ju.Z. Nozik, L.E. Fykin, L.A. Muradyan, *Kristallografia* 21, 76 (1976).

STUDY OF VANADYL CENTERS IN LITHIUM POTASSIUM SULPHATE  
SINGLE CRYSTALS: BY EPR

N.Sathyanaarayana<sup>1</sup> and S.Radhakrishna<sup>2</sup>

1. Dept. of Physics, Central University of Pondicherry,  
JIPMER Campus, Pondicherry, India-605 006.

2. Dept. of Physics, Indian Institute of Technology,  
Madras, India-600 036.

The 3d transition metal ions are used effectively as impurity probes to find out the local symmetry of the crystalline fields in various environments and also used for detecting the phase transitions occurring in crystalline solids.<sup>1,2</sup> Among the 3d transition metal ions, vanadyl ion is found to be the most stable molecular cation and it can exist in different complexes.<sup>3</sup> Hence, we have undertaken the EPR studies of  $\text{VO}^{2+}$  ions doped Lithium Potassium Sulphate (LPS) single crystals to study the structure of the Lattice. Pure and vanadyl doped LPS crystals are grown isothermally at  $42^\circ\text{C}$  from the aqueous solution made up of equimolar quantities of  $\text{K}_2\text{SO}_4$  and  $\text{Li}_2\text{SO}_4$ . A small amount (0.5 to 2.0 Mol.wt.%) of Vanadyl Sulphate was added to the LPS solution. Vanadyl doped crystals are sea-blue in color and the crystallographic axes are identified by X-ray diffraction. ESR spectra are recorded at 300 K on a varian E-4 spectrometer.

LPS single crystals belong to hexagonal system with bimolecular unit cell of dimensions  $a=5.145 \text{ \AA}$  and  $c=8.629 \text{ \AA}$ . Figure 1 shows the EPR spectrum of  $\text{VO}^{2+}$  ion in LPS crystal recorded when the magnetic field (H) is parallel to the a-axis. As can be seen from the figure, there are two prominent sets of eight lines and each set of lines arises due to the interaction of a single unpaired electron with the vanadium nuclear spin ( $I=7/2$ ).

EPR spectra are recorded in every  $10^\circ$  of rotation in all three planes and the principal  $g$  and  $A$  (hyperfine) parameters<sup>are</sup>/calculated for all the orientations of the spectra. To know the complete behaviour of the spectra, some of the  $VO^{2+}$  ion-doped crystals are crushed into a fine powder and the EPR spectrum is recorded which is shown in Figure 2. This figure indicates that there are two chemically distinguishable  $VO^{2+}$  sites existing in the lattice. The EPR spectra of both the poly and single crystals of  $VO^{2+}$  in LPS system are analysed and the detailed results will be discussed.

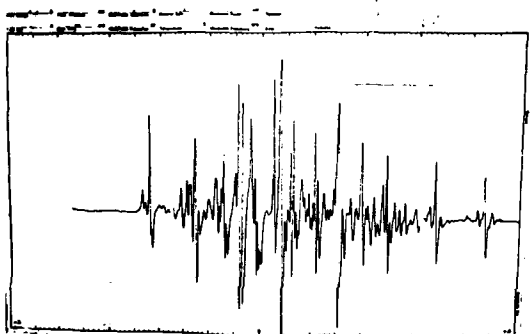


FIG. 1

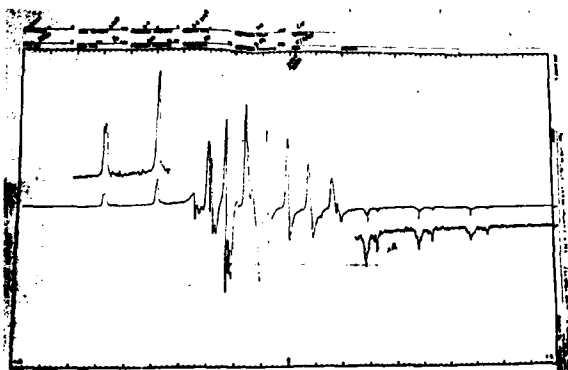


FIG. 2

#### References

1. J.E. Wertz and J.R. Bolton,  
Electron Spin Resonance, Elementary  
theory and Practical  
Applications,  
Mc Graw Hill,  
New York (1972)
2. T. Kawano and K. Furukawa, J. Phys.  
Soc. Japan, 47  
(1979) 1191
3. J. Selbin, Coord.  
Chem. Soc. Rev.,  
1 (1966) 293

F(Br<sup>-</sup>)-CENTRES IN BAFBR

F. K. Koschnick, H. Söthe, J. M. Spaeth

UNI-GH Paderborn, Fb. 6, Warburger Str. 100, D-4790 Paderborn

In alkaline earth fluoro-halides like BaFBr and BaFCl two types of F<sup>-</sup>-centres with different local symmetry can be formed. The electron is either localized in a Br<sup>-</sup> - vacancy (F(Br<sup>-</sup>)-centre) or in a F<sup>-</sup> - vacancy (F(F<sup>-</sup>)-centre). In this investigation the F(Br<sup>-</sup>)-centre in additively coloured BaFBr was measured by ENDOR. The results of these experiments were compared to the F(Cl<sup>-</sup>)-centre in BaFCl investigated earlier by Bauer [1,2] and Yuste [3].

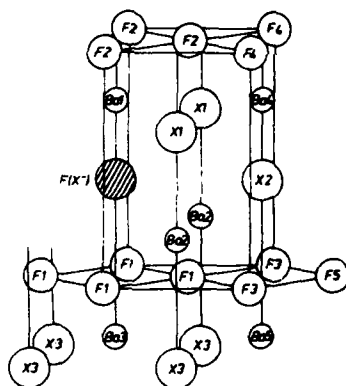


Fig. 1 structure of the F(X<sup>-</sup>)-centre in BaFX with the lattice surrounding characterized by neighbour nuclei shells as identified by ENDOR analysis ( X = Br, Cl )

The F(Br<sup>-</sup>)-centre has axial symmetry. The g-tensor can be described by the two g-values  $g_{||} = 1.98$  and  $g_{\perp} = 1.99$ . From the ENDOR analysis the values of the superhyperfine (shf) constants a, b, b' and the quadrupole constants q, q' of six neighbour shells are deduced. The z-axis of the shf-tensors of the first shells (F<sup>1</sup> and Br<sup>1</sup>/Cl<sup>1</sup>) are orientated

along the connection line between the nuclei and the F-centre, while the orientation of the tensors of the other shells differ from the connection line. In table 1 the spin densities at the nuclei of the neighbour shells calculated from the isotropic shf-constant  $a$  are listed.

Tab. 1 isotropic spin density distribution at the neighbour shells of the  $F(\text{Br}^-)$  in BaFBr and of the  $F(\text{Cl}^-)$  in BaFCl

F(Br <sup>-</sup> ) in BaFBr		F(Cl <sup>-</sup> ) in BaFCl	
shell	spin density / 10 <sup>4</sup> a.u.	shell	spin density / 10 <sup>4</sup> a.u.
F <sup>1</sup>	74.2	F <sup>1</sup>	61.0
F <sup>2</sup>	1.7	F <sup>2</sup>	4.7
F <sup>3</sup>	16.4	F <sup>3</sup>	15.9
F <sup>4</sup>	3.8	F <sup>4</sup>	2.0
F <sup>5</sup>	14.3	F <sup>5</sup>	14.5
Br <sup>1</sup>	415.2	Cl <sup>1</sup>	180.0

The spin density distribution of both centres has a large anisotropy which can be explained by a spin transfer mechanism by lattice ion overlap. The spin transfer mechanism is also responsible for the disorientation of the z-axis of the hyperfine tensors of the outer shells from the connection line to the F-centre. From the comparison of the spin densities of both centres is seen that the wave function of the  $F(\text{Br}^-)$ -centre is more diffuse than the wave function of the  $F(\text{Cl}^-)$ .

Calculations of the shf-constants  $a$  and  $b$  of the  $F(\text{Br}^-)$  in BaFBr with the model of the orthogonalized envelope function taking into account the lattice ion overlap yield the best results with the choice of a wave function with 85% part 1s type and 15% 2s type character. Bauer's calculations of the  $F(\text{Cl}^-)$  in BaFCl yields an 1s type function only. This also indicates the more diffuse character of the wave function of the  $F(\text{Br}^-)$ -centre.

- 
- 1 Bauer, Niklas, Spaeth, Phys. Stat. Sol. (b) Vol. 118, 557
  - 2 Niklas, Bauer, Spaeth, Phys. Stat. Sol. (b) Vol. 119, 171
  - 3 Yuste et al, J. Phys. Chem. Solids, Vol. 37, 961

AN ESR STUDY OF VANADIUM IMPURITY IONS IN  
SINGLE-CRYSTAL ZINC TUNGSTATE

G.J. EDWARDS, O.R. GILLIAM, R.H. BARTRAM and L.A. KAPPERS

Department of Physics and Institute of Materials Science  
University of Connecticut, Storrs, Ct. 06268, U.S.A.

A. WATTERICH and I. FÖLDVÁRI

Research Laboratory for Crystal Physics, Hungarian Academy of Sciences,  
H-1112 Budapest, Budaörsi út 45, Hungary

Recent developments in crystal growth techniques have allowed the production of single crystal  $\text{ZnWO}_4$  with very little coloration indicating significant increase in sample purity. Interest in  $\text{ZnWO}_4$  is due to the use of this material as a scintillation detector for x- and  $\gamma$ -ray spectroscopy. A discussion of the crystal structure for an isomorphic material is given by Keeling.<sup>1</sup> Some recent research on the scintillation properties of  $\text{ZnWO}_4$  has been reported by Grassmann *et al.*<sup>2</sup>, Zhu *et al.*<sup>3</sup>, and Oi *et al.*<sup>4</sup>  $\text{ZnWO}_4$  is among a class of divalent and trivalent tungstates which are reported to be potential laser materials.<sup>5</sup> The ESR spectra of  $d^1$  ions are particularly important due to their sensitivity to the crystal field.

The Research Laboratory for Crystal Physics has succeeded in growing  $\text{ZnWO}_4$  crystals with significantly reduced impurity concentrations. Crystals are grown by a balance-controlled Czochralski technique in a platinum crucible, oriented by x-ray diffraction and then cut to useful sizes for electron spin resonance work. Three types of vanadium-related defects, labeled A, B and C, can be identified in crystals doped with vanadium. In arbitrary directions, the type A defect exhibits four sets of eight hyperfine lines ( $^{51}\text{V}$ ,  $I=7/2$ , natural abundance 99.8%), and types B and C each exhibit two sets of eight lines.

Krygin *et al.*<sup>7</sup> identified a single vanadium defect with two inequivalent sites in vanadium-doped  $\text{ZnWO}_4$ . This defect was attributed to a  $\text{V}^{4+}$  ion occupying a  $\text{Zn}^{2+}$  site with a vacancy in the adjacent Zn site. This would lead to a spectrum of two sets of eight lines in arbitrary directions. In the crystals supplied to us, defect types B and C exhibit this general behavior. Preliminary calculations, however, show that the principal  $g$  and  $A$  values differ from that reported by Krygin *et al.* In addition their proposed model predicts that there should be no splitting of the Zeeman transitions for rotations of the magnetic field in the a-b plane, whereas the major transitions observed by us in this plane split into two sets of hyperfine lines. Our conclusion, then, is that we have observed three previously unreported paramagnetic vanadium defects in  $\text{ZnWO}_4$ .

Angular variations of the ESR spectra for the defects have been measured in the (010) plane and in a plane that includes the [001] direction and a vector which is  $10^\circ$  in the a-b plane from [110]. In the first plane of rotation none of the Zeeman lines split, whereas in the second each line splits into two lines. Superhyperfine interactions have been observed around defects A and B, but corresponding interactions around C are not detected presumably due to their much smaller intensity. The intensity ratio of superhyperfine line to main line is 1:4 for defect A and 1:12 for defect B.

The superhyperfine intensity ratio for defect A is consistent for interactions with  $^{195}\text{Pt}$  ( $I=1/2$ , natural abundance 33.8%). This would indicate that the  $\text{V}^{4+}$  ion occupies a  $\text{W}^{6+}$  site with an adjacent  $\text{Zn}^{2+}$  site occupied by a  $\text{Pt}^{4+}$  ion. Since there are two inequivalent tungsten sites and two inequivalent Zn sites, there would be four separate sets of lines in this model, as is seen in our measurements.

The superhyperfine splitting in defect B is most probably due to interactions with neighboring  $^{183}\text{W}$  ( $I=1/2$ , natural abundance 14.4%). This defect has two sets of Zeeman lines which split in the a-b plane, precluding vanadium substitution in a Zn site; this defect is attributed to  $\text{V}^{4+}$  in a  $\text{W}^{6+}$  site but with no local charge compensator. Defect C is likely to be a perturbed B-type defect. Resonances for defect C could only be followed in the a-c plane.

An analysis of the spin-Hamiltonian parameters including the superhyperfine interactions will be presented. A comparison of these values with those of  $d^1$  ions in similar materials will be presented.

\* Supported jointly by the U. S. National Science Foundation under grant No. INT-8617352 and the Research Foundation of the Hungarian Academy of Sciences (A.K.A.).

- 1 R.O. Keeling, Jr., *Acta Cryst.* **10**, 209-213 (1957).
- 2 H. Grassman, H.-G. Moser and E. Lorenz, *J. of Luminescence* **33**, 109-113 (1985).
- 3 Y.C. Zhu, J.G. Lu, Y.Y. Shao, H.S. Sun, J. Li, S.Y. Wang, B.Z. Dong, Z.P. Zheng and Y.D. Zhou, *Nucl. Instr. and Meth.* **A244**, 579-581 (1986).
- 4 T. Oi, K. Takagi, and T. Fukazawa, *Appl. Phys. Lett.* **36**, 278-279 (1980).
- 5 K. Petermann and G. Huber, *J. of Luminescence* **31/32**, 71-77 (1984).
- 6 F. Schmidt and R. Voszka, *Crystal Res. Technol.* **16**, K127-128 (1981).
- 7 I. M. Krygin, A. D. Prohorov, and G. A. Tsintsadze, *Phys. Stat. Sol. (b)* **55**, K107-110 (1973).

# EFFECT OF HYDROSTATIC PRESSURE ON THE $\text{Ag}^+$ OFF-CENTER MOTION IN $\text{RbCl}$

M. Fricke, O. Kanert and R. K  chler  
Institute of Physics, University of Dortmund, West Germany

Nuclear magnetic relaxation (NSR) can be successfully used to study the dynamics of off-center defects in ionic solids /1/. The resulting defect-induced NSR rate can be written as /1/

$$\frac{1}{T_1} = c_D \omega_Q^2 \left( \frac{\tau_D}{1 + (\alpha \omega \tau_D)^2} + \frac{4\tau_D}{1 + (2\alpha \omega \tau_D)^2} \right) \quad (1)$$

where  $c_D \omega_Q^2$  denotes the mean quadrupole interaction between the probe nuclei and the off-center defects of concentration  $c_D$ ,  $\omega$  is the Larmor frequency, and  $\alpha$  is a scaling factor depending on the type of the rotational motion characterized by the correlation time  $\tau_D$ . Fig 1 shows first data of the temperature dependence of the  $^{87}\text{Rb}$  NSR rate in  $\text{RbCl}:\text{80ppm Ag}^+$  for various hydrostatic pressures. As shown in a previous paper /1/ the NSR rate  $1/T_1$  is due to  $90^\circ$  rotational jumps of the  $\text{Ag}^+$  off-center defects. Obviously, below 100 MPa only a shift of the rate maximum occurs while the magnitude of the maximum remains constant. Above 100 MPa this magnitude is reduced, too. According to Eq.(1) one has to conclude that

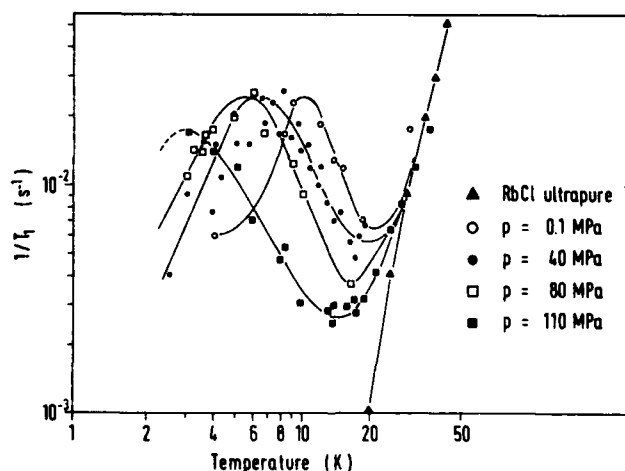


Fig.1  $^{87}\text{Rb}$  NSR rate vs temperature at various hydrostatic pressures in ultrapure and  $\text{Ag}^+$ -doped single-crystal  $\text{RbCl}$  ( $B_0 = 4.2 \text{ T}$ ).

the relative number of occupied off-center positions which is equal to  $c_D$  starts to decrease above 100 MPa. This is in agreement with the result of PER measurements in  $\text{RbCl:Ag}^+$  /2/. Using these data the pressure dependence of  $c_D$  can be expressed as /3/

$$c_D = \{ 1 + 1/12 \cdot \exp (U(p)/T) \}^{-1} \quad (2)$$

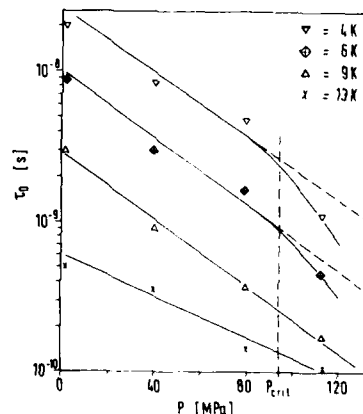
where  $U(p) = a (p - p_{\text{crit}})$  with  $a = 0.42 \text{ K/MPa}$ ,  $p_{\text{crit}} = 94 \text{ MPa}$  and  $U(p) = 0$  for  $p < p_{\text{crit}}$  /2/. By means of Eqs.(1,2) the correlation time  $\tau_D = \tau_D(p,T)$  was determined from the data in Fig.1. The result is shown in Fig.2. The findings can be interpreted with a model presented recently /3/:

i)  $T \geq 9 \text{ K}$ : The Arrhenius behavior of the temperature dependence of  $\tau_D$  /1/ leads to the experimentally observed relation  $\tau_D(p) = \tau_D(0) \cdot \exp(-p/p_2)$  with  $p_2 = T / (\partial E / \partial p)_T$ , i.e.  $p_2 \propto T$ . For the pressure dependence of the effective activation energy  $E$  of the rotational motion we found the following relation :  $(\partial E / \partial p)_T = 0.2 \text{ K/MPa}$ .

ii)  $T < 9 \text{ K}$ ;  $p < p_{\text{crit}}$ : The off-center-motion is due to phonon-assisted tunneling. Again, one finds  $\tau_D(p) = \tau_D(0) \cdot \exp(-p/p_2)$ .  $p_2 = 1/2 \cdot (\partial R / \partial p)^{-1}$ , however, which describes the effect of pressure on the polaron factor  $\exp(-R)$  of the tunneling matrix element becomes independent of  $T$ . This is confirmed by the data of Fig.2, where  $p_2 \approx 40 \text{ MPa}$ .

iii)  $T < 9 \text{ K}$ ;  $p > p_{\text{crit}}$ : Off-center to on-center jumps occur in addition to the rotational motion of  $\text{Ag}^+$  leading to the observed deviation from the Arrhenius behavior of  $\tau_D(p)$  above  $p_{\text{crit}}$ .

Fig.2 Pressure dependence of the correlation time  $\tau_D$  of the  $\text{Ag}^+$  motion at various temperatures.



#### REFERENCES

- 1 O.Kanert, Phys.Reports 91, 183 ( 1982 ).
- 2 F.Bridges & D.Chow, Phys. Rev. Lett. 54, 1532 ( 1985 ).
- 3 O.Kanert & R.Küchler, Cryst.Latt.Def. and Amorph.Mat. 16, 347 ( 1987 ).

## NUCLEAR MAGNETIC RESONANCE STUDY OF SINGLE-CRYSTAL RUTILE

O. Kanert, H. Kolem

Institute of Physics, University of Dortmund

POB 500 500, D-4600 Dortmund, West Germany

NMR measurements of  $^{47}\text{Ti}$  and  $^{49}\text{Ti}$  have been performed in single-crystalline rutile ( $\text{TiO}_{2-x}$ ) between room temperature and 1400 K at 8.5 T and 4.2 T respectively. In order to carry out the experiments a high-temperature probe head was developed including an automatically controlled oxygen partial-pressure system.

The different orientations of the EFG tensor with respect to the direction of  $\vec{B}_0$  at the two different Ti sites in the unit cell of rutile lead to a well-separated two-line NMR spectrum of  $^{47}\text{Ti}$  and  $^{49}\text{Ti}$ , respectively. While the largest eigenvalue  $V_{zz}$  is found to be only weakly dependent of temperature, the asymmetry parameter  $\eta$  reveals an uncommonly strong dependence on temperature [1].

The nuclear spin relaxation (NSR) rates  $1/T_1$  (Zeeman) and  $1/T_{1\rho}$  (rotating

frame) of  $^{49}\text{Ti}$  depicted in Fig. 1 are shown to be determined by the following mechanisms:

i) Below 400 K, the relaxation process is governed by a two-phonon quadrupole interaction.

ii) In the temperature range between 400 K and 1100 K the influence of the motion of oxygen vacancies and of interstitial Ti ions becomes important resulting in different NSR rate maxima of  $1/T_{1\rho}$  as shown in Fig. 1.

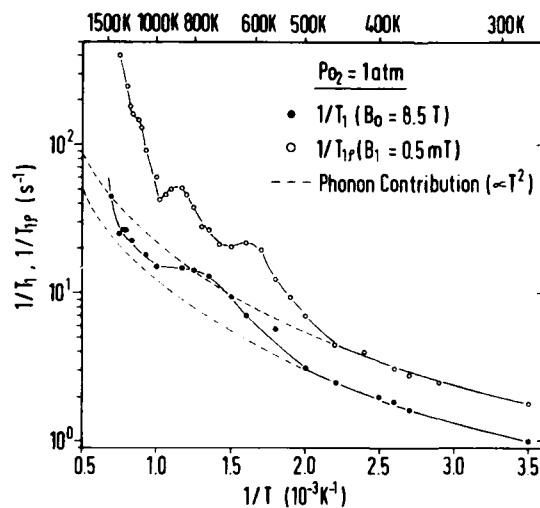


Fig. 1:  $^{49}\text{Ti}$  NSR rates vs  $1/T$  in  $\text{TiO}_{2-x}$

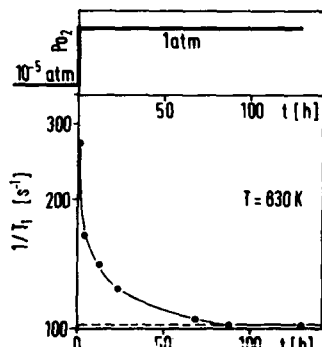


Fig.2: Time dependence of the  $^{49}\text{Ti}$  NSR rate after a sudden change of  $p_{\text{O}_2}$

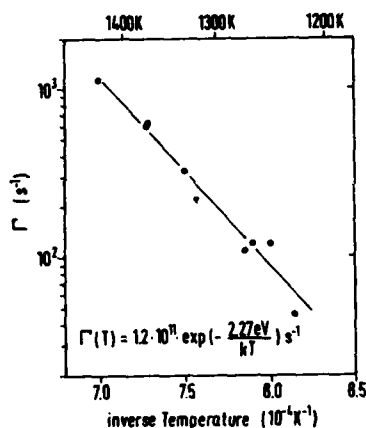


Fig.3: Jump rate of Ti between different Ti sites in  $\text{TiO}_2$  vs  $1/T$

iii) Above 1100 K, the relaxation is mainly due to Ti self-diffusion.

As demonstrated in Fig. 2 a sudden change of the magnitude of the oxygen partial pressure is followed by a time-dependent variation of the NSR rate corresponding to the actual concentration of defects determined by the nonstoichiometry parameter  $x$ . An evaluation of the data based on the solution of Fick's first law [2] leads to a chemical diffusion coefficient  $\tilde{D}$  of  $(4 \pm 1) \cdot 10^{-6} \text{ cm}^2/\text{s}$  at 830 K for the defect motion. The experiments indicate, that the recovery of the NSR rates is governed generally by different defect mechanisms.

From site-selective NSR experiments the jump rate  $\Gamma$  of Ti between nonequivalent Ti sites can be determined directly [3]. The result is shown in Fig. 3. A comparison of tracer [4] and the present NMR data confirms that interstitialcy motion is the major process of Ti mass transport. Only a very small fraction ( $\approx 1\%$ ) of the Ti diffusion occurs via jumps between different Ti lattice sites.

This work was supported by the Deutsche Forschungsgemeinschaft.

#### References:

- 1) O. Kanert, H. Kolem: J. Phys. C 1988 (in press)
- 2) J.F. Baumard: Solid State Communications, 29 859 (1976)
- 3) B. Günther, O. Kanert: Phys. Rev. B 31 20 (1985)
- 4) K. Hoshino, N.L. Peterson, C.L. Wiley: J. Phys. Chem. Solids 46 1397 (1985)

CALCULATIONS OF SOME SIMPLE DEFECTS IN PURE AND DOPED CaF<sub>2</sub>  
AND SrF<sub>2</sub> CRYSTALS WITH ALKALI IMPURITIES

A. AMARA, G. CREMER  
 F. MARTIN-BRUNETIERE, M. THUAU

*Laboratoire de Spectroscopie Atomique, ISMRA-Université de Caen  
 Boulevard Maréchal Juin  
 F-14032 CAEN CEDEX*

Computer simulation techniques (1) have been used to calculate the formation energies of some various defects by the well-known static model (2), a distorted static lattice of polarizable no-point ions (shell model) ; the large distant effects have been treated by the MOTT and LITTLETON method. The studied defects are the interstitials and vacancies ( $F^{\cdot}$ ,  $Ca^{2\cdot}$  and  $Sr^{2\cdot}$ ) and the interstitial and substitutional impurities ( $Li^+$ ,  $Na^+$  and  $K^+$ ). The reaction energies of some doping mechanisms (alkali-earth fluoride by alkali fluoride) have been deduced. The ON/OFF site feature of the impurity has been also investigated. Lastly we have calculated the capture energies linked with vacancies and impurities according to various clusters. This work is previous to the simulation of simple defects trapping electron(s).

- (1) HADES code : NORGETT J.J. (1974), UKAEA report, AERE-R 7650
- (2) CATLOW C.R.A. and MACKRODT W.C. (1982), "Computer Simulation of Solids ", Spring-Verlag, Berlin.

CALCULATION OF THE  $F_2^-$  LINEAR CENTRE IN  $\text{CaF}_2$ **A. AMARA and M. THUAU**

*Laboratoire de Spectroscopie Atomique, ISMRA-Université de Caen  
Boulevard Maréchal Juin  
F-14032 CAEN CEDEX*

The  $\text{H}_2^+$  molecular ion embedded in a dielectric continuum has provided a satisfying simulation of the  $F_2^-$  centre in many alkali halides (1) ; so, in spite of the very naïve features of this model, we similarly study the  $F_2^-$  centre in  $\text{CaF}_2$  : 2 electrons are trapped in the potential well of 3 aligned hydrogen nuclei embedded in the dielectric continuum. The 9 lowest energy levels ( $\Sigma$  and  $\Pi$ , spin-triplet and singlet states of the  $\text{H}_2^+$  linear molecular ion are) determined as a function of the nucleus distance by restricted and unrestricted Hartree-Fock calculations (2) with a gaussian basis set (24 s-like and  $3 \times 12$  p-like functions centred on the nuclei) ; then we deduced the energy-level-positions as a function of the dielectric constant  $k$ . The allowed dielectric dipolar transitions from the fundamental state ( $1\Sigma_g^+$ ) are localized in the infrared ( $1\Sigma_u^+$  excited state) and the visible range ( $1\Pi_u$ ), if  $k = 2.5$ . The oscillator strengths of these transitions are also calculated.

(1) MOLLENAUER L.F. (1979), Phys. Rev. Lett. 43, 1524.

(2) ATMOL code : SAUNDERS V.R. and GUEST M.F. (1976), Rutherford Laboratory Reports ATMOL 3.

EFFECT OF PRESSURE ON INTRA-d TRANSITIONS

M.J. Caldas, M.R. Sardela Jr. and A. Fazzio

Instituto de Física, Universidade de São Paulo,

C.P. 20.516, 01498 São Paulo, S.P., Brazil

We study, from a theoretical point of view, the effect of pressure on the lines of intra-d transitions of the ion  $Mn^{2+}$  in II-VI compounds. In particular, in this work we analyse the tetrahedral zinc-blende phase of semimagnetic compounds  $Cd_{1-x}Mn_xTe$ ,  $Zn_{1-x}Mn_xTe$  and related materials. We use a determinantal perturbative approach to multiplet splittings developed by [1] Fazzio, Caldas and Zunger (FCZ) which differs significantly from the classical BCD theory of Tanabe-Sugano [2].

In the alternative (FCZ) approach we introduce orbital deformation parameters  $\lambda_\mu = \langle \mu\mu | \frac{1}{r_{ij}} | \mu\mu \rangle S / \langle dd | \frac{1}{r_{ij}} | dd \rangle I$ , representing ration between the electron-electron  $\frac{1}{r_{ij}}$  interaction  $\frac{1}{r_{ij}}$  in the solid (S) and in the free ion (I); the label  $\mu$  refers to the crystal-field-split  $\mu = e$  or  $t_2$  orbitals. The ten independent repulsion integrals between d-electrons are then expressed in terms of  $\lambda_e$ ,  $\lambda_t$  and the Racah parameters for the free ion,  $B_0$  and  $C_0$ . Another very important difference compared to BCD theory is the renormalization of the dependence of the Racah parameter A on the occupation configuration  $e^m t^n$  (and hence on hybridization state) into an effective crystal field splitting  $\Delta_{eff}$ . This dependence is discarded in BCD theory.

The behaviour of hybridization with pressure may be analysed through the behaviour of the energy of an intra-d absorption or emission. We focus on the dependence  $dE/dP$  of the absorption line  ${}^6A_1 \rightarrow {}^4T_1$  for the compound  $Cd_{1-x}Mn_xTe$ , for which there is enough available data. We reduce the full determinantal equation for the transition energy to approximate, analytical simple equations for  $dE({}^6A_1 \rightarrow {}^4T_1)$  in terms of  $d\lambda_\mu$  and  $d\Delta_{eff}$ . These expressions are fit to experiment to yield  $d\lambda_t/dP$ ; the values are then used in similar expressions for other transition energies that can again be checked against experiment.

Our values give very good agreement with experimental results. The scheme may be extended to treat pressure effects in other systems.

- [1] A. Fazzio, M.J. Caldas and A. Zunger, Phys. Rev. B 30, 3430 (1984)
- [2] Y. Tanabe and S. Sugano, J. Phys. Soc. Japan 9, 753 (1954)

THEORETICAL STUDY ON  $\text{Ni}^+$  IN FLUORIDE LATTICES

M.T. Barriuso

Departamento de Física Moderna, Facultad de Ciencias, Universidad  
de Cantabria, 39005-Santander, Spain

J. Aramburu and M. Moreno

D.C.I.I.T.Y.M., Sección Ciencia de Materiales, Facultad de Ciencias,  
Univ. de Cantabria, 39005-Santander, Spain

In irradiated insulator materials impurities involving unusual oxidation states are sometimes stabilised. The study of such "unstable" cations offers however additional difficulties due to the lack of stable known compounds from which an important local structural information can be obtained. This fact stresses the necessity of performing theoretical calculations for different metal-ligand distances in order to gain a better understanding of the experimental results. Unfortunately an "unstable"  $3d^9$  impurity like  $\text{Ni}^+$  has received much less theoretical attention than  $\text{Cu}^{2+}$ .

The present work is devoted to the theoretical study of  $\text{Ni}^+$  impurity in fluoride lattices with  $x^2-y^2$  as ground state. The two main goals which have been pursued are:

- 1) The calculation of square-planar  $\text{NiF}_4^{3-}$  and distorted  $\text{Oh NiF}_6^{5-}$  complexes as a function of the equatorial  $\text{Ni}^+-\text{F}^-$  distance,  $R$ .
- 2) The theoretical study of the position of the electronic  $\text{Ni}^+$  levels with respect to those of the perfect host lattice.

The first aim has been accomplished through self-consistent Extended Hückel and  $X\alpha$  calculations. For the second purpose self-consistent Hückel calculations including up to 81 atoms have been carried out in the  $\text{LiF}$  lattice. With respect to the former point the calculations confirms the high ionicity of the  $\text{Ni}^+-\text{F}^-$  bond<sup>1,2</sup>,  $f_{\sigma}$  being close to 2% for  $R=2.1 \text{ \AA}$ . Moreover though  $f_{\sigma}$  increases when  $R$  decreases it is shown that  $\sqrt{f_{\sigma}}/S_{\sigma}$  is independent of the distance  $R$  in the range  $1.90-2.40 \text{ \AA}$ . This result supports the use of the experimental  $f_{\sigma}$  value in order to determine the

true equatorial  $\text{Ni}^+-\text{F}^-$  distance<sup>3</sup>.

The energy of both crystal-field and charge-transfer transitions are shown to increase upon decreasing R the latter ones being likely placed in the vacuum ultraviolet region. On the other hand the first X $\alpha$  results on  $\text{NiF}_4^{3-}$  support that the  $3d^9 \rightarrow 3d^8 4s$  and  $3d^9 \rightarrow 3d^8 4p$  transitions lie below  $45000 \text{ cm}^{-1}$  as pointed out before<sup>2</sup>.

The calculations carried out for  $\text{Ni}^+$  in LiF indicate that a)  $\text{Ni}^+$  levels are placed in the gap about 4 eV above the top of the valence band of the pure crystal, b) charge-transfer levels mainly built from the four equatorial ligands are also localized but lie just on the bottom of the valence band.

- 1 W. Hayes and J. Wilkens, Proc. Roy. Soc., A281, 340 (1964).
- 2 M. Moreno, J. Aramburu, M.T. Barriuso, J. Phys. C:Solid State Phys., 19, L315 (1986).
- 3 M.T. Barriuso, M. Moreno, Solid State Commun., 51, 335 (1984).

DEPENDENCE OF THE COVALENCY OF THE  $(\text{MnF}_6)^{4-}$  COMPLEX ION UPON  
THE  $\text{Mn}^{2+}-\text{F}^-$  DISTANCE

M.T. Barriuso

Departamento de Física Moderna, Facultad de Ciencias, Universidad  
de Cantabria, 39005-Santander, Spain

J.A. Aramburu and M. Moreno

D.C.I.T.T.Y.M., Sección Ciencia de Materiales, Universidad  
de Cantabria, 39005-Santander, Spain

and

M. Flórez, G. Fernández Rodrigo, and L. Pueyo

Departamento de Química Física y Analítica, Facultad de Química,  
Universidad de Oviedo, 33007-Oviedo, Spain

The properties of an impurity, M, in an insulator material are strongly related to the covalency of the bonding with the nearest ions X, which depends on the true M-X distance, R.

The present work explores the dependence of the covalency parameters called  $f_\sigma$ ,  $f_\pi$  and  $f_s$  upon R for the case of the  $\text{Mn}^{2+}$  impurity surrounded by six  $\text{F}^-$  ions. Such a situation is experimentally achieved for  $\text{Mn}^{2+}$  doped fluoroperovskites.

In order to investigate the present problem two complementary approaches have been used. In this way Hartree-Fock-Roothaan calculations have been performed for the  $\text{MnF}_6^{4-}$  cluster and for values of R in the range 1.90-2.3 Å. Moreover the electrostatic potential due to the rest of the lattice upon the complex has also been taken into account in the SCF process. On the other hand the covalency parameter  $f_p = f_\sigma - f_\pi$  has also been derived from a careful analysis of the experimental anisotropic superhyperfine constant  $A_p$  measured in ENDOR experiments. In it two points are shown to be specially relevant: the inclusion of lattice relaxation, which strongly affects the dipolar contribution  $A_d$ , and that of the metal-ligand term which has been

usually neglected up to date<sup>1</sup>.

The Hartree-Fock-Roothaan calculations indicate that:

- 1)  $f_s$  depends on  $R^{-8.2}$  while  $f_p$  on  $R^{-3.2}$  and then  $f_p$  varies more slowly with  $R$ .
- 2)  $f_s$  and  $f_p$  behave as local observables: changes in their observed values from crystal to crystal would be mainly determined by changes in the  $Mn^{2+}-F^-$  distance.
- 3)  $f_s$  is proportional to the square of the group overlap integral  $S_s$  and then supports the determination of the true  $R$  value from the experimental  $A_s$  constant<sup>2</sup>.

The analysis of experimental ENDOR data of  $Mn^{2+}$  doped  $KZnF_3$ <sup>3</sup>,  $CsCaF_3$ <sup>1</sup>, and  $RbCdF_3$ <sup>4</sup>, taking into account the true  $R$  values, leads to the conclusion that within the experimental errors  $f_p$  is constant in the range 2.08-2.15 Å and equal to (0.60±0.20)%. The same figure is obtained in the analysis of NMR data for the pure compound  $RbMnF_3$  when metal-ligand contributions are considered.

The present conclusions are clearly at variance with recent reported analysis<sup>1</sup> and point out the necessity of performing ENDOR experiments under hydrostatic pressure in order to detect changes of  $f_p$  due to  $R$  variations.

- (1) H. Aoki, M. Arakawa and T. Yosida, J.Phys.Soc.Jpn., 52, 2216 (1983).
- (2) M.T. Barriuso and M. Moreno, Phys.Rev., B29, 3623 (1984).
- (3) R.K. Jeck and J.J. Krebs, Phys.Rev., B5, 1677 (1972).
- (4) P. Studzinski and J.M. Spaeth, Radiat. Effects 73, 2216 (1983).

INFLUENCE OF OXYGEN OCTAHEDRON SIZE ON THE ELECTRONIC STRUCTURE  
OF CO<sup>2+</sup> DOPED PEROVSKITE

P. Moretti  
Institut des Sciences de l'Ingénierie  
et du Développement Technologique  
Université Cl. Bernard Lyon I  
43 Bd. du 11 Novembre 1918  
69622 Villeurbanne France

Detailed knowledge of the electronic structure of cobalt ions in octahedral oxygen coordination is of great interest, since this 3d metal has been incorporated and studied in various host materials<sup>(1)</sup>.

The divalent ion attracts attention particularly for two reasons. Firstly it is probably the most commonly encountered form, and secondly previous calculations<sup>(2)</sup> show that, unlike the others, it undergoes a low- high-spin conversion for a cubic lattice constant around 3.95 Å. The corresponding Co-O bond distance lies therefore in the range of the B-O ones of very numerous ABO<sub>3</sub> compounds.

In this work a series of S.C.F. X $\alpha$  spin-unrestricted calculations is carried through on cubic (CoO<sub>6</sub>)<sup>-10</sup> clusters to model the Co<sup>2+</sup> impurity located at the center of the oxygen octahedron. The unit cell parameter is allowed to vary from 3.8 to 4.2 Å, thus including most of the cubic oxides, and particularly the SrTiO<sub>3</sub> - like ones.

Besides the evolution of the energy of the crystal field transition,  ${}^2E_g \rightarrow {}^4T_{1g}$ , investigated through the transition state procedure, two main points are examined.

The energy diagrams associated to the 3d eigenvalues are reported, for both high and low spin configurations and various cell parameters, relative to the upper O2p level, which is actually the valence band edge of  $\text{ABO}_3$  compounds. In the latter consequently, the energetic evolution of the acceptor charge transfer band,  $\text{O}2\text{p} \rightarrow \text{Co}3\text{d}$ , can be inferred.

A detailed analysis of the electronic distribution within the clusters atomic spheres allows us to describe, according to the Co-O distance, the evolution of the covalent bonding strength. Indeed the latter is reflected on the variation of the "net" charges beared by the bonding and antibonding 3d levels. The behaviors of the chemical bond for the high- and low-spin configurations of the metal are found opposite to each other. Moreover, owing to the spin cross-over phenomena encountered at the critical aforesaid cell parameter, a discontinuity occurs for the 3d charges variation, and accordingly for the covalent strength.

#### References

- (1) P. Moretti, F. M. Michel-Calendini, G. Godefroy and L. Hafid, *Jpn. J. Appl. Phys.* 24 (2), 653 (1985) and references therein.
- (2) F. M. Michel-Calendini, P. Moretti and H. Chermette, *Ferroelectrics Letters* 3, 35 (1984).

CRYSTAL-FIELD MODEL OF A  $\text{Pb}^0(2)$  CENTRE IN  $\text{SrF}_2$

R. H. Bartram

Department of Physics and Institute of Materials Science,  
University of Connecticut, Storrs, CT 06268, U.S.A.

M. Fockele, F. Lohse and J.-M. Spaeth

University of Paderborn, Fachbereich 6, Warburger Strasse 100A,  
4790 Paderborn, Federal Republic of Germany

A diamagnetic centre in irradiated  $\text{SrF}_2:\text{Pb}$  which exhibits long-lived infrared luminescence with three excitation bands has been tentatively identified as a  $\text{Pb}^0(2)$  centre, consisting of a neutral Pb atom at a cation site flanked by a pair of anion vacancies along a  $\langle 111 \rangle$  direction. An off-centre displacement of the Pb atom along the line joining the two anion vacancies is postulated in order to account for weakly allowed transitions.

The computational model adopted in this work is analogous to that for  $\text{Tl}^0(1)$  centres (Mollenauer *et al.* 1983). However, the  $\text{Pb}^0(2)$  centre has two 6p electrons in the ground configuration whose electrostatic interaction is comparable with both their spin-orbit interaction and their interaction with the external crystal field. The energy-level structure can be described in terms of three parameters: a spin-orbit constant  $\zeta$ , a crystal-field parameter  $\gamma$  and a Slater integral  $F^{(2)}$  (Slater 1960). Optimized values of these parameters are listed in Table 1, together with calculated transition energies and relative intensities. The adjusted values of  $\zeta$  and  $F^{(2)}$  show a modest (21%) reduction from free-atom values. The three peaks observed in the measured excitation spectrum are ascribed to the transitions from the  $1\Sigma^-$  ground state to the  $1\Pi$ ,  $2\Pi$ ,  $3\Pi$  and  $3\Sigma^-$  excited states, with the third and fourth transitions unresolved. Both optical and non-radiative  $\Sigma^+ \rightarrow \Sigma^-$  transitions are rigorously forbidden; accordingly, the  $1\Sigma^+$  state is identified as the metastable emitting state. The observed emission energy,  $6250 \text{ cm}^{-1}$ , implies a Stokes shift  $\Delta E = 2250 \text{ cm}^{-1}$ . From this value and the full width of the emission band at half maximum, FWHM = 750

$\text{cm}^{-1}$ , we infer a Huang-Rhys factor  $S_0 = 12$  and an effective phonon energy  $\hbar\omega = 90 \text{ cm}^{-1}$ . We conclude that the crystal-field model of the  $\text{Pb}^{0(2)}$  centre provides a consistent qualitative and quantitative explanation of the observed spectra, and thus fully supports the identification of this centre.

Table 1. Comparison of calculated transition energies ( $\text{cm}^{-1}$ ) and relative transition probabilities (arbitrary units) with peak positions and relative intensities, respectively, of the excitation spectrum. Optimized parameter values ( $\text{cm}^{-1}$ ) are:  $\zeta = 5730$ ,  $\gamma = 5282$  and  $F^{(2)}/25 = 721.5$ .

transition	transition energy		relative intensity	
	theory	experiment	theory	experiment
$1\Sigma^- \rightarrow 4\Sigma^-$	37,990	---	.028	---
$1\Sigma^- \rightarrow 3\Pi, 3\Sigma^-$	28,700	28,700	.329	.41
$1\Sigma^- \rightarrow 2\Pi$	15,850	15,850	.640	.64
$1\Sigma^- \rightarrow 1\Pi$	9,830	9,825	.366	.32
$1\Sigma^- \rightarrow 1\Sigma^+$	8,500	---	.000	---
$1\Sigma^- \rightarrow 2\Sigma^-$	6,790	---	.137	---

#### Acknowledgments

This work was supported in part by the U.S. Army Research Office under Contract. No. DAAL03-86-K-0017, and in part by the North Atlantic Treaty Organization under Grant No. RG.85/0662.

#### References

- Mollenauer L F, Vieira N D and Szeto L 1983 Phys. Rev. B 27 5332  
 Slater J C 1960 Quantum Theory of Atomic Structure Vol. II (New York, McGraw-Hill)

TERM ENERGY CALCULATIONS AND OPTICAL SPECTRA  
IN  $\text{Cr}^{3+}$  - DOPED SPINEL - LIKE COMPOUNDS

F.M. Michel-Calendini, C. Linarès, W. Nie, G. Boulon

Physico-Chimie des Matériaux Luminescents  
 Université Claude Bernard de Lyon-Unité associée au CNRS  
 69622-Villeurbanne (France)

Emission and absorption spectra of  $\text{Cr}^{3+}$  - doped spinel - like compound like  $\text{ZnAl}_2\text{O}_4$  have been performed. Under  ${}^4\text{A}_2 \rightarrow {}^4\text{T}_2$  excitation, the emission spectrum exhibits at 4.2 K a complex structure : i) the  ${}^2\text{E} \rightarrow {}^4\text{A}_2$  line at 686.3 nm relevant to the regular octahedral site, associated with the vibronic spectrum, ii) another line  ${}^2\text{E} \rightarrow {}^4\text{A}_2$  at 688.5 nm due to a perturbed octahedral site, iii) the lines due to aggregates and iv) the  ${}^4\text{T}_2 \rightarrow {}^4\text{A}_2$  broad band connected either to the octahedral sites in which thermodynamical equilibrium between  ${}^2\text{E}$  and  ${}^4\text{T}_2$  occurs or to a low crystal field site. The different unequivalent sites may be related with the inversion rate of spinel-like structure whose process appears more simple in  $\text{ZnAl}_2\text{O}_4$  than in  $\text{MgAl}_2\text{O}_4$ . Such spectroscopic studies are of the highest interest to understand the nucleation mechanisms in vitreous or gel matrices where  $\text{Cr}^{3+}$  ion plays the role of the nucleating agent.

The apparition of these various structures in optical spectra is clearly related to the local geometry at the impurity site, then, the obtention of theoretical electronic structures of  $\text{Cr}^{3+}$  at the various sites in these materials is of the main importance for their interpretations. To this end, the term energy diagrams of  $\text{Cr}^{3+}$  trapped in purely or nearly cubic sites have been obtained using the electronic structures calculated with a molecular orbital model and a local spin density method, as in perovskite<sup>1</sup> and magnetoplumbite<sup>2</sup> like oxydes. The energies of the lowest

excited terms such as  $^2E$  and  $^4T_2$  allows to get the usual  $Dq$  and  $B$  parameters used to obtain the complete term energy diagram both for  $ZnAl_2O_4 : Cr^{3+}$  and  $ZnCr_2O_4$ . The crystal field strength is studied in comparison with results obtained for similar materials like  $Al_2O_3$  and  $MgAl_2O_4$ . These results are the starting point in the interpretation of the evolution of optical spectra of  $Cr^{3+}$  in the sol-gel materials.

1 - P. Moretti and F.M. Michel Calendini, Phys. Rev. B, 36, 3522 (1987)

2 - F.M. Michel Calendini,

Advances in Laser Science III - Proceedings of the 1987 International  
Laser Science Conference American Institute of Physics - Atlantic  
City (1988)

CORRECTIONS TO THE CONTINUUM APPROXIMATION FOR THE LARGE POLARON  
BOUND TO A DEFECT: THE GROUND STATE ENERGY

Y. Frongillo and Y. Lapine\*, Université de Montréal, C. P. 6128  
succursale "A", Montréal, Québec, Canada H3C 3 J7.

When considering a carrier bound to a hydrogenic charged defect in ionic or polar crystals, the defect and the carrier interaction with the longitudinal optical (LO) phonons must additionally be taken into account. In these crystals, the electron-phonon interaction is of the long range dipolar type and the lattice distortion around the bound electron extends over a large number of unit cells. This system is known as a large polaron bound to a defect.

The usual approach to the problem is to consider the crystal as a continuous and deformable medium with the electronic band structure approximated by an effective mass and the individual charges by a dielectric constant. This is the continuum approximation as introduced by Frohlich in treating the polaron problem.

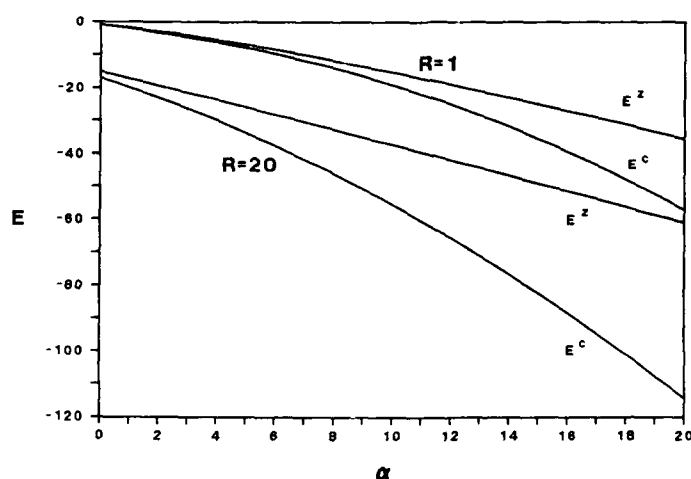
In order to go beyond this approximation we use the  $\epsilon_g$  representation of Zak<sup>1</sup>. Perturbative corrections to the continuum approximation up to second order are included in the Hamiltonian in the form of terms proportional to  $a^2$ , a parameter that measures the unit cell dimensions relative to the quantum size of the polaron. This approach takes into account a renormalization of the effective mass approximation by the electron-phonon interaction. A Debye cutoff,  $\Omega_D$ , on the wavevectors of LO phonons is also effected to eliminate wavelengths smaller than the unit cell. This approach has been previously used to treat the free polaron<sup>2</sup>.

Starting from this new Hamiltonian, an upper bound to the ground state energy,  $E_0$ , is calculated in the Fock approximation, using the Green's function formalism of Mats and Burkey<sup>3</sup>. Our treatment is valid for all electron-phonon and electron-defect coupling strengths and uses a Gaussian model as the variational trial spectrum. The resulting expression for  $E_0$  is the same as that obtained from the Feynman rigid oscillator approximation. Further this ground state energy reduces to the continuum one when  $a = 0$  and  $L \rightarrow \infty$ .

In the small coupling limit, the corrections to the continuum approximation give a renormalization of the self-energy of the polaron and of its effective mass. This renormalization was also found for the free polaron. It corresponds to a reduction of the self-energy as well as of the effective mass. In the strong coupling limit, a reduction of the self-energy is also observed in addition to a decrease in the binding energy to the defect. This is related to a decrease in the electron-phonon coupling relative to its value in the continuum case.

We present, in the figure shown, the ground state energy (obtained from numerical calculations) for  $L = 5$ , as a function of  $\alpha$ , the electron-phonon coupling constant, for two values of  $R$ , the electron-defect coupling constant. For each  $R$ ,  $E^c$  is the ground state energy calculated in the continuum approximation and  $E^z$  is the ground state energy calculated with the corrections to this approximation. Both are shown in this figure in units of LO phonon energy.

In the case of  $R = 1$ , the corrections are small when  $\alpha = 0$  and increase to 38% for  $\alpha = 20$ . For  $R = 20$ , the effect is not negligible even when  $\alpha = 0$ . These corrections increase to about 47% of the continuum result for  $\alpha = 20$ .



For real crystals, the corrections are small. They vary between 1% and 9% for GaAs, CdTe, AgBr, TiCl, KCl and RbCl. For NaCl and LiF, using the free electron mass as the effective mass, we obtain 17% and 15% for the correction, respectively. In systems with effective mass larger than the free electron mass, the corrections can become much larger.

- 1- J. Zak, Solid State Physics vol.27, ed. by Ehrenreich, Seitz and Turnbull, Academic Press (1972), p.1
- 2- Y. Lépine and Y. Frongillo, submitted for publication
- 3- D. Matz and B. C. Burkey, Phys. Rev. **B3**, 3487 (1971)

\*This research has been supported by the "Natural Sciences and Engineering Research Council of Canada" and by the "Ministère de l'Éducation du Québec (FCAR)".

A COMPUTER SIMULATION STUDY OF THE  $V_K$  CENTER  
IN ALKALI HALIDES USING HARTREE-FOCK CLUSTERS.\*

A. B. Kunz and Ravindra Pandey  
Physics Department  
Michigan Technological University  
Houghton, Michigan  
49931 USA.

The  $V_K$  center in alkali halides has long been considered as an  $X_2^-$  molecular ion resulting from the combination of a neutral halogen atom with one of its twelve neighboring halide ions inside the lattice. It is a charged molecular defect of quantum-mechanical nature and is associated with substantial local distortion around the  $X_2^-$  molecular ion in the lattice. Thus the lattice distortion and polarization need to be consistently incorporated with the electronic structure in the theoretical analysis of the  $V_K$  center in alkali halides.

In this work, we simulate the  $V_K$  center in several well-defined simple models using the program packages, UHF and ICECAP. The UHF code<sup>1</sup> treats the molecular cluster consisting of the  $X_2^-$  ion and its nearest-neighbor ions in the unrestricted Hartree-Fock self-consistent field (UHF-SCF) approximation and provides correlation correction to the UHF-SCF solution for the cluster by means of many-body perturbation theory<sup>1</sup>. On the other hand, the ICECAP code<sup>2</sup> incorporates Hartree-Fock molecular cluster in a shell-model lattice with accurate cluster-lattice consistency, and thereby includes, in a rigorous and self-consistent manner, the electronic structure with the lattice distortion and polarization, which in earlier studies were treated approximately, or were neglected<sup>3,4</sup>.

Progress will be reported for the ground state of the  $V_K$  center in alkali halides obtaining the internuclear separation of the two fluorines in  $F_2^-$  molecule, the energy stabilization of the distorted center versus the  $F_2^-$  molecule ion in a perfect-lattice configuration and the spin-density.

- <sup>1</sup>Goalwin, P.W. and Kunz, A.B., 1986, Phys.Rev. B34, 2140 and references therein.
- <sup>2</sup>Harding, J.H., Harker, A.H., Keegstra, P.B., Pandey, R., Vail, J.M. and Woodward, C.W., 1985, Physica B131, 151.
- <sup>3</sup>Cade, P., Stoneham, A.M. and Tasker, P.W., 1984, Phys.Rev. B30, 4621.
- <sup>4</sup>Williams, R.T., Song, K.S., Faust, W.L., and Leung, C.H., 1986, Phys.Rev. B33, 7232.

\* supported by U.S. Department of Energy, BES, grant DEFG02-85-ER45224.

Annihilation on percolation cluster:  
Smoluchovski theory and numerical experiment

A.G. Vitukhnovsky, B.L. Pyttel, I.M. Sokolov

P.N. Lebedev Physical Institute, Leninsky Prospekt, 53,  
117924 Moscow, USSR

The problem of triplet exciton annihilation in mixed molecular solids is extensively investigated both theoretically and experimentally. Often such systems can be adequately modeled by fractals [1,2]. In this report we present some results concerning the kinetics of  $A+A=0$  reaction on an incipient percolating cluster in two-dimensional case.

The simplest theoretical approach to describe bimolecular reactions is to deal with Smoluchovski approximation. In such an approach the concentration decay is given by equation

$$\frac{dn}{dt} = -C(t)n^2$$

where reaction rate coefficient is

$$C(t) = \frac{2\pi^{D/2}}{\Gamma(D/2)} K r_0^{D-1-\theta} \left. \frac{\partial g(r,t)}{\partial r} \right|_{r=r_0}$$

Here  $D$  is fractal dimension,  $r_0$  - recombination radius,  $K$  - fractal diffusion coefficient,  $\theta$  - anomalous diffusion exponent. The pair distribution function satisfies the fractal diffusion equation [3]:

$$\frac{\partial g}{\partial t} = K \frac{1}{r^{D-1}} \frac{\partial}{\partial r} r^{D-1-\theta} \frac{\partial}{\partial r} g \quad (1)$$

with  $g(r,0)=1$  ( $r_0 < r < \infty$ ),  $g(r_0,t)=0$ ,  $g(\infty,t)=1$ . For two-dimensional incipient infinite cluster  $D=91/48$ ,  $\theta=0.844$  and coefficient  $K$  is connected with  $\alpha = \lim_{t \rightarrow \infty} \langle l^2(t) \rangle / t^{2/(2+\theta)}$  by

$$K = 2 \left[ \frac{\Gamma(\frac{\alpha}{2})}{\Gamma(\frac{D+2}{2})} \frac{\alpha}{(2+\theta)^{4/(2+\theta)}} \right]^{1+\theta/2}$$

where  $\langle l^2(t) \rangle$  is the mean square displacement of a particle during the time  $t$  and  $\alpha = 2D/(2+\theta) \approx 4/3$ . For a percolation cluster on a square lattice  $\alpha=1.1$  and  $K=0.54$ . The numerical solution of (1) shows that for  $t \rightarrow \infty$

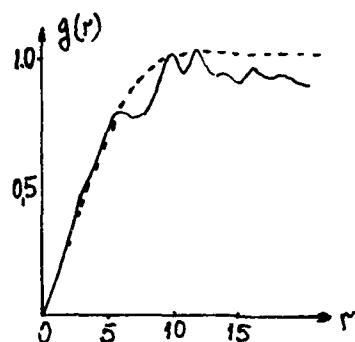
$$n(t) = 0.13 (Kt)^{-\alpha_5/2} \quad (2)$$

The asymptotical behavior of  $g(r,t)$  is

$$g(r,t) = P\left(1 - \frac{\alpha_5}{2}, \frac{r^{2+\theta}}{K(2+\theta)^2 t}\right)$$

where  $P(x,y)$  is the incomplete  $\gamma$ -function. The numerical experiment on a percolation cluster on a square lattice gives  $n(t) = 0.35 t^{-2/3}$ . This is approximately twice as given by (2) and corresponds to substitution in (2)  $K=0.2$ . The difference between the values is due to multiparticle effects.

The experimental and theoretical curves (for  $K=0.2$ ) for pair distribution function are shown on fig.1



#### Literature

1. Kopelman R. in: *Fractals in Physics*, eds. L. Petronero, A. Tosatti (North-Holland, Amsterdam, 1986) p. 359
2. Blumen A., Klafter J., Zumofen G. *ibid.*, p. 399
3. O'Shaughnessy B., Procaccia I. *Phys. Rev. B* 30 (1984) 6778

THEORETICAL SIMULATIONS OF TRIPLET SELF-TRAPPED  
EXCITONS IN  $\text{SiO}_2$  AND  $\text{KCl}$  CRYSTALS

Shluger A.L., Shidlovskaya E.K.

Latvian State University, Rainis 19, Riga, 226098 USSR

Now there exist strong experimental evidences for the self-trapped triplet excitons (TE) in alkali halides<sup>1)</sup> and both crystalline and amorphous silicon dioxide<sup>2)</sup>. However, their electronic and spatial structure is not clarified so far. The present work is aimed to perform self-consistent theoretical calculations of the electronic structure, ionic configuration and spectroscopic properties of these excitons in  $\beta$ -cristobalite and  $\text{KCl}$  making use of the many-electron model of a defective crystals. The semiempirical INDO version of the Unrestricted Hartree-Fock-Roothaan method without spin-projection was employed along with the embedded molecular cluster (MC) model<sup>3)</sup> for the localized exciton in the crystal. The corresponding energy of the singlet-triplet excitation here equals the difference of two total self-consistent energies of singlet and triplet states ( $\Delta \text{SCF}$ ) being 6,3 eV and 6,8 eV for  $\text{KCl}$  and  $\beta$ -cristobalite respectively (cf. with the experiment 7,7 and 8.5 eV). The triplet spin densities are delocalized over all cations of the MC's used ( $\text{Si}_{11}\text{O}_{22}$  and  $\text{K}_{24}\text{Cl}_{24}$ ) which means quasi-free excitonic state.

It is shown that self-trapping of the TE in  $\beta$ -cristobalite arises mainly due to the  $\approx 0,3 \text{ \AA}$  - displacement of the regular oxygen ion into the interstitial position and such breaking down of a Si-O bond that the spin density is almost equally divided between Si and O ions of this bond. The triplet-singlet emission (resulting in a perfect lattice restoration) peaks at 2,6 eV (exp. 2,8 eV). The absorption energy obtained by means of the restricted configuration interaction and arising due to an unpaired electron localized on Si ion of the broken bond is 5,6 eV which is clo-

se to that of the  $E'$  centre<sup>2)</sup>. The results obtained confirms the TSTE model in  $SiO_2$  as the nearest pair of the complementary  $E'$  centre and non-bridging oxygen<sup>2)</sup>. The experimentally observed large spin-spin interaction constant ( $D=22,6$  GHz) in our model comes from the close spins of these defects.

In its turn, the self-trapping of TE in KCl results due to the approach of two Cl-ions, nearest along the  $\langle 110 \rangle$  axis, to within the distance  $\approx 5$  a.u. and outward displacements of two nearest cations (along direction perpendicular to  $V_k$  axis) by  $\approx 0,6$  a.u. resulting in a gain of the total energy 1,2 eV. On the average the TE symmetry is  $C_{2v}$  since the cross-section of the adiabatic surface as the hole component ( $Cl_2^-$ ) vibration is very flat - its displacement by 1 a.u. the energy increases by 0,05 eV only! The electron localization in the TE depends essentially on the position of the  $Cl_2^-$  with respect to the anion site: when it is symmetrical an unpaired electron is localized in the space between the  $Cl_2^-$  nuclei, whereas for a shifted position its spin density becomes to be redistributed toward an anion vacancy left behind. This is in agreement with experimental data for ENDOR and optically detected ESR, arguing for a small asymmetry in the STE position along the  $\langle 110 \rangle$  axis and yielding the isotropic constant of the hyperfine interaction close to that of F centre<sup>1)</sup>. Our calculation of the triplet-singlet ( $\pi$ -luminescence) yields 3,4 eV (exp. 2,5 eV), whereas for an optical absorption of the TE electronic component calculated value 1,8 eV is close to the experimental ( $\approx 2$  eV<sup>1)</sup>).

1. Itoh N. Adv. in Phys. 1982, v. 31, p. 493.
2. Silin A.R., Trukhin A. Point defects and elementary excitations in crystalline and glassy  $SiO_2$ . Riga, Science (in Russian), 1985, 276 p.
3. Shluger A.L., Kotomin E.A., Kantorovich L.N. J. Phys. C.: Solid State Phys., 1986, v. 19, p. 4183.

SHORT-LIVING FRENKEL-TYPE DEFECTS IN TlCl

D.K.Millers, L.G.Grigorjeva, A.V.Nomojev

Solid State Physics Institute of the Latvian  
State University, Riga, USSR

It is a well known fact that glow peaks are observed in thallium halides /1,2/ either after X-ray or UV light irradiation at liquid nitrogen temperature, or after  $\gamma$ -irradiation at RT.  $\gamma$ -irradiation of TlCl at RT leads to the formation of colloids /3/ responsible for the broad absorption peaks at  $\sim 2,5$  eV.

This gives a clear evidence that defects are generated in thallium halides under irradiation. However, the absorption bands formed due to point defects are not observed. The present study deals with induced absorption in the TlCl. The samples were irradiated at LNT by the electron beam pulse (pulse duration - 10 ns, the acceleration voltage - 0,3 MV).

During the irradiation pulse induced absorption appeared. It was short-living and consisted of two bands (Fig.1) approximately at 1,25 and 2,4 eV with the half-widths 0,3 and 0,7 eV, respectively. The induced absorption decay can be described neither with the first nor the second order law. In the time region 50-2000 ns the decay of both absorption bands was similar (Fig.2) and followed approximately the same decay law. However, in the time region 3 - 8  $\mu$ s the decay of the band centred at 1,25 eV was unlike to the band centred at 2,4 eV.

Thus we can assume that both absorption bands were produced by the short-living Frenkel-type defects generated under irradiation. The initial stages of the absorption decay can be due to the recombination of the Frenkel-type defects. As the energy of the electron beam is not sufficient for knock-on mechanism we suggest that Frenkel-type defects

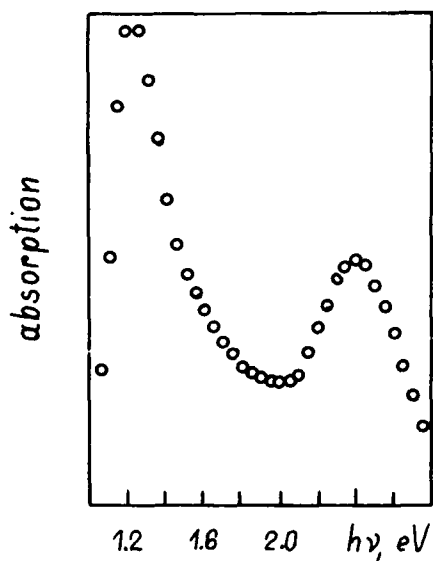


Fig. 1

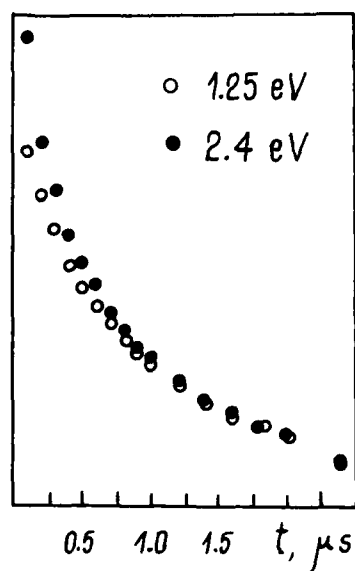


Fig. 2

are due to the nonradiative transitions from the excited electron states of the crystal.

1. V.A.Sokolov and A.N.Tolstoi, *Optika i Spektroskopiya*, 18, 97, (1965).
2. L.G.Grigorjeva, D.Ā.Millers, *Radiation Physics and Chemistry in Ionic Crystals, Abstracts, Riga*, p.264, (1983).
3. V.G.Artyushenko, V.V.Voitsekhovskii, L.S.Kornienko, I.S.Lisitskii, A.Ā.Ribaltovskii, *phys. stat. sol.*, 85, 167, (1984).

SELF-TRAPING OF HOLES AND EXCITONS IN  $\text{Al}_2\text{O}_3$  CRYSTAL

P.Kulis, Z.Rachko, M.Springis, I.Tale, J.Jansons

Institute of Solide State Physics, Latvian State University,  
8 Kengaraga Str., RIGA 226063, USSR

It is shown that both holes and excitons are self-trapped in undoped  $\text{Al}_2\text{O}_3$  crystals. The self-trapping of holes occurs below 200 K (the corresponding TSL peak at 220 K) whereas excitons reveal two configurations - A and E ones [1]. A-configuration is associated with the well-known luminescence band at 7.5 eV, but E-configuration produces an additional one discovered by us luminescence band at 3.8 eV being related to the (self-trapped hole + electron) centre whose spectroscopic parameters ( $\delta=0.35$  eV,  $\tau=280$  ns,  $I_{\parallel}/I_{\perp}=0.8$  at 80 K [1]) differ from the  $\text{F}^+$  centre luminescence.

The conclusion about hole self-trapping is proved by the facts:

- (i) the TSL peak at 220 K is the first low-temperature hole one as follows from the photostimulated hole release from V centers,
- (ii) the hole centres responsible for TSL peak at 220 K are involved in the low-temperature ( $T < 200$  K) tunneling luminescence ( $h\nu=4.3$  eV) of pure crystals,
- (iii) the TSL at 220 K observed for undoped crystals is caused by diffusion-controlled tunneling recombination of holes, which follows from very inertial increase of the luminescence intensity after step-like temperature increase (see [2] and the Abstract at the present Conference by E.Kotomin et al). The corresponding activation energy of process -  $E=0.68$  eV. The relatively small frequency factor  $10^{10}-10^{11}$   $\text{s}^{-1}$  being essentially less than that of the phonon frequencies is typical for diffusion processes,
- (iv) the spectral composition of the TSL at 220 K is identical with that of the tunneling luminescence ( $h\nu=4.3$  eV),
- (v) the spectral composition of the low-temperature electronic TSL peaks is the same as for E-band of the self-trapped exciton,
- (vi) the TSL peak at 220 K could be produced by the light with the energy exceeding the gap energy only (fig.1),
- (vii) the total concentration of impurities is so small (less than 10 ppm) that it excludes the hopping hole migration via impurities.

In its turn, the exciton self-trapping in A-configuration is proved by:

- (i) the maximum of the A-band excitation corresponds to the excitonic band at 8.85-9.05 eV at 80 K (fig.1) where mobile uncharged electronic excitations are produced (it follows from the creation spectrum of the self-trapped holes),
- (ii) the half-width of the excitation band is 0.15 eV,
- (iii) the A-band does not arise in the TSL peaks at 60, 100, 220 K and at high temperatures.

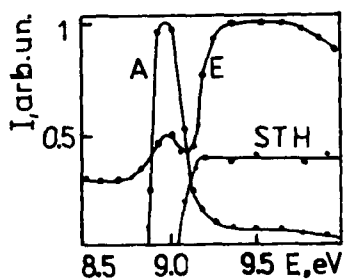


Fig.1.

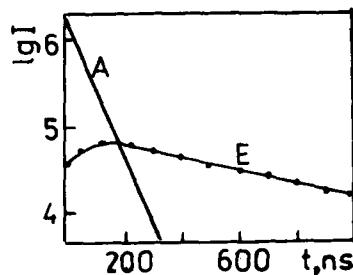


Fig.2.

Finally the exciton self-trapping in the E-configuration is proved by:

- (i) the luminescence spectrum of the electronic TSL peaks at 60 and 100 K (i.e. below the 220 K peak) coincides with the E-band (3.8 eV),
- (ii) the E-band excitation spectrum falls into excitonic band (i.e. the same as for the A-band of luminescence) and involves also band-to-band region,
- (iii) there is a rearrangement of two exciton configurations: the A-band decay is accompanied by the E-band growth (fig.2),
- (iv) the temperature quenching of the A-band produced under electron irradiation is also accompanied by the E-band increase.

1.P.Kulis, Z.Rachko, M.Springis, I.Tale, J.Jansons. Izv.AN LSSR.Ser.fiz. i tehn.nauk, 1987, V 2, p.30.  
 2.I.Tale, P.Kulis, V.Kronghauz. J.Lum.1979, V 20, p.343.

OPTICAL PROPERTIES OF TWOFOLD COORDINATED Si, Ge, AND Sn ATOMS IN  
AMORPHOUS SILICON DIOXIDE

L.N.Skuja

Institute of Solid State Physics, Latvian State University  
Kengaraga iela 8, 226063 Riga, Latvian SSR, USSR

A characteristic optical absorption band at 5.03 eV (" $B_2^*$ " - band) is present in reduced or irradiated glassy  $SiO_2$ . Photoexcitation into this band gives photoluminescence (PL) bands at 4.3 and 2.65 eV. Given the correlation of the  $B_2$  band with an oxygen deficit, it is often ascribed to oxygen vacancies. However, it was shown [1], that it is more likely due to twofold coordinated Si atoms with only 2 oxygens nearby ( $Si_2^0$  centers, 2-coordination, 0- net charge). The purpose of this paper is to show, that Ge and Sn impurity centers in  $SiO_2$  have properties, similar to  $Si_2^0$  center and form series of isoelectronic defects.

SAMPLES: neutron-irradiated ( $10^{19}$  n/cm<sup>2</sup>) high purity glassy  $SiO_2$ , 10%GeO<sub>2</sub> 90% $SiO_2$  glass, Sn-doped (0.1%) glassy  $SiO_2$ .

RESULTS AND DISCUSSION. The parameters of the Si, Sn and Ge - related PL centers are given in the table.

Dopant		Si (intrinsic)	Ge	Sn
Low energy PL peak	PL peak energy	2.65 eV	3.05 eV	3.1 eV
	Excitation peak	3.3(?), 5.03 eV	3.7, 5.2 eV	3.7, 4.7 eV
	Lifetime (300K)	10.2 ms	109 $\mu$ s	10.0 $\mu$ s
High energy PL peak	PL peak energy	4.3 eV	4.2 eV	4.0 eV
	Excitation peak	5.05 eV	5.1 eV	4.7 eV
	Lifetime (300K)	<4 ns	<20 ns	<20 ns

Certain trends, common to all three types of dopants are clearly apparent. Each dopant gives rise to two PL bands. The low energy (LE) emission is excited into two excitation bands, while the high energy (HE) PL band - only in the HE excitation band. The HE PL bands decay very fast, while the lifetimes of the LE PL bands are relatively long, temperature independent in the range 80-300 K and decrease with the atomic number of the dopant. The LE PL bands are polarized "out of plane" when excited with linearly polarized light in the HE excitation bands.

The relations between the parameters of LE and HE PL bands for each

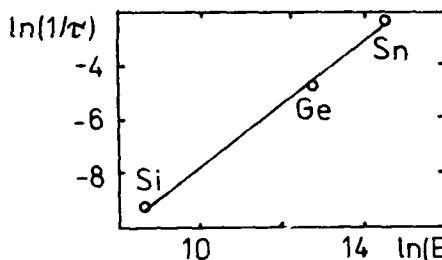
type of dopant are typical for triplet and singlet bands of a single, strongly localized PL center. The close values of the respective parameters of the Si, Ge and Sn - based centers indicate, that all these centers probably have similar structures.

The steep decrease of the lifetime of the LE PL bands with the atomic number of dopant is characteristic for the triplet-to-singlet PL. A quantitative analysis of these changes of lifetime was performed. If one assumes, that the spin-orbit coupling is determined largely by a single atom (the "central field" approximation /2/), then, using a number of other approximations, it can be demonstrated, that

$$1/\tau \sim E^3 \xi^2$$

where  $\tau$  - radiative lifetime of the triplet state,  $E$  - energy of the optical transition,  $\xi$  - spin-orbit coupling energy for the p-electron in a  $np^2$  configuration ( $n=2,3,4$ ). For Si, Ge, and Sn  $\xi=17.6$ , 109.1 and 260 meV respectively /2/.

The dependence of  $\ln(1/\tau)$  on  $\ln(E^3 \xi^2)$  is shown below. The slope of the straight line is 1.14, i.e. the observed dependence is indeed close to linear. This confirms, that the LE PL bands are triplet ones, and that Si, Ge and Sn based centers are isostructural. Hence, similarly to /1/, Ge and Sn-based centers are due to two-fold coordinated Ge and Sn atoms with only two oxygens nearby and the LE PL bands correspond to  ${}^3B_1 \rightarrow {}^1A_1$  transitions (in  $C_{2v}$  local symmetry).



The triplet PL lifetime data are inconsistent with the oxygen vacancy model, because the vacancies, neighbouring 1 or 2 impurity atoms must yield sharply different lifetimes of the triplet PL. However, in the concentration range of  $GeO_2$  from 20 ppm up to 10% LE PL decay is represented by a single exponential component with  $\tau=109 \mu s$ .

On trapping of a proton  $Si_2^0$ ,  $Ge_2^0$  and  $Sn_2^0$  centers transform into the well known ESR-active H(I), H(II) and H(III) centers, distinguished by proton hf splittings of 7.4, 11.9 and 15.0 mT. They correspond to 3-fold coordinated Si, Ge or Sn atoms, neighboring two oxygens and a proton.

1. L.N. Skuja, A.N. Streletsky, A.B. Pakovich Solid State Comm. 50, 1069 (1984)

2. S.P. McGlynn, T. Azumi, M. Kinoshita Molecular spectroscopy of the triplet state. Prentice Hall, N.J. 1969.

MAGNETIC FIELD EFFECT ON THE DECAY PROCESSES OF  
TRIPLET LOCALIZED EXCITONS IN KBr:I

Takuya Mukai, Ken-ichi Kan'no and Yoshio Nakai

Department of Physics, Kyoto University, Kyoto 606, Japan

Recently, we pointed out that the spin-lattice relaxation (SLR) in the triplet self-trapped exciton (STE) in KI is governed by the one phonon process, while that in KBr is governed by multi-phonon process.<sup>1)</sup> This difference was attributed to the difference in the zero-field splitting energy of the triplet STE, which is  $[I_2^-+e]$  for KI and  $[Br_2^-+e]$  for KBr. In this point of view, it is interesting to investigate the relaxation mechanism of the  $[IBr^-+e]$  hetero-nuclear excitons in KBr:I.

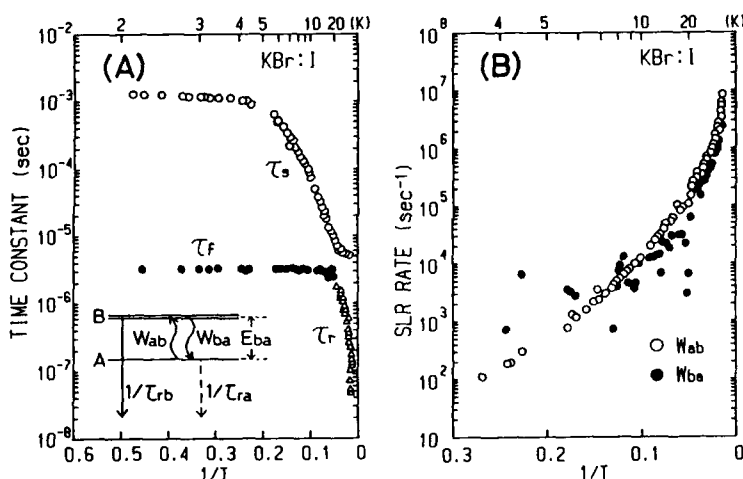


Fig. 1 Temperature dependence of (A) lifetimes and (B) SLR rates of the 3.54 eV emission in KBr:I.

Lifetimes of 3.54eV emission which arises from the  $[IBr^-+e]$  relaxed exciton in KBr:I were measured from 1.9 K up to 80 K under one-photon excitation with ArF-excimer laser. The decay curve consists of two exponential components (the slow,  $\tau_s$ , and the fast,  $\tau_f$ ) at low temperatures (Fig. 1(A)). At high temperatures, a rise component ( $\tau_r$ ) was observed. These results indicate that the initial state of the emission is a triplet which splits into nearly degenerate two B levels and a single A level (see the inset in Fig. 1(A)).<sup>2)</sup> Temperature dependence of the SLR rates between A and B lev-

els can be determined from the observed values of the lifetimes, as already reported on the triplet STE in pure alkali halides.<sup>1)</sup> As seen in Fig. 1(B), not only the upward phonon transition rate  $W_{ab}$ , but also the downward phonon transition rate  $W_{ba}$  decreases in lowering temperature. As detailed in ref. 1, if the one-phonon process is dominant,  $W_{ba}$  is expected to remain constant at low temperatures because of the spontaneous phonon emission. Therefore, instead of the one-phonon process, multi-phonon process must be assumed in the SLR mechanism of the  $[\text{IBr}^- + e]$  relaxed excitons.

In order to estimate the zero-field splitting energy  $E_{ba}$  of the  $[\text{IBr}^- + e]$  relaxed exciton, we measured lifetimes at 4.2 K under magnetic field parallel to the  $\langle 110 \rangle$  crystal axis. As shown in Fig. 2, the time constant  $\tau_f$  remains constant up to 11 kG, while the slow component ( $\tau_s$ ) separates into two components ( $\tau_{s1}$  and  $\tau_{s2}$ ). The time constant  $\tau_{s1}$  decreases monotonically with increasing magnetic field, while  $\tau_{s2}$  takes a minimum value at 9.2 kG. This behavior is quite similar to the case of CsI observed by Fowler et al.<sup>3)</sup> According to their theoretical consideration, we can conclude that the component ( $\tau_{s2}$ ) arises from the relaxed excitons whose molecular axes are parallel to the magnetic field, and the minimum point of  $\tau_{s2}$  corresponds to the crossing of A and B levels. From the magnetic field at the minimum point of  $\tau_{s2}$  (9.2 kG),  $E_{ba}$  was found to be 0.11 meV. Because of such a small  $E_{ba}$ , which corresponds to 1.3 K, the density of phonons which can resonate with  $E_{ba}$  is small. Therefore, two-phonon Raman process will exceed the one-phonon process even at 2 K in  $[\text{IBr}^- + e]$  relaxed excitons in KBr:I.

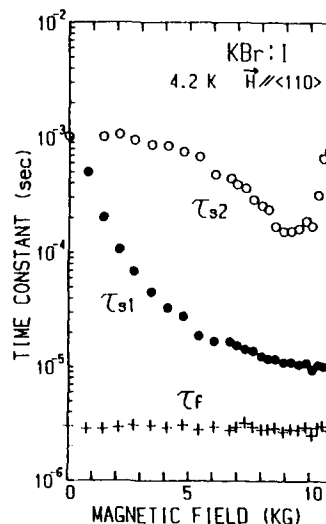


Fig. 2 Magnetic field dependence of lifetimes of the 3.54 eV emission in KBr:I.

- 1) T. Mukai, O. Arimoto, K. Kan'no and Y. Nakai: Proc. Int. Conf. Luminescence, Beijing, 1987, J. Lumin. (in press)
- 2) K. Kan'no, H. Nakatani, T. Mukai, O. Arimoto and Y. Nakai: J. Phys. Soc. Jpn. 55 (1986) 2443.
- 3) W.B. Fowler, M.J. Marrone and M.N. Kabler: Phys. Rev. B8 (1973) 5909.

**RED EMISSION AND TRAPPED-HOLE CENTERS PRODUCED BY DE-EXCITATION OF  
LOCALIZED EXCITONS IN KCl:I AND RbCl:I**

Ken-ichi KAN'NO, Koichiro TANAKA and Yoshio NAKAI  
Kyoto University, Kyoto 606, Japan

It is known that photo-excitation into the localized exciton absorption of mixed alkali halides gives rise not only to the luminescence from relaxed excitons but also to the formation of color centers.<sup>1-4)</sup> In KCl:I, two-photon excitation with an N<sub>2</sub> laser pulse ( $2h\nu=7.36$  eV) is very effective for such photo-induced defect formation.<sup>2)</sup> Interestingly, major parts of resulting color centers are intrinsic F and H centers. In addition to these intrinsic defects, it was pointed out that some other defects were also formed.<sup>2)</sup> In the present work, we report on an evidence for the formation of luminescent hole centers under the excitation of localized excitons in KCl:I and RbCl:I.

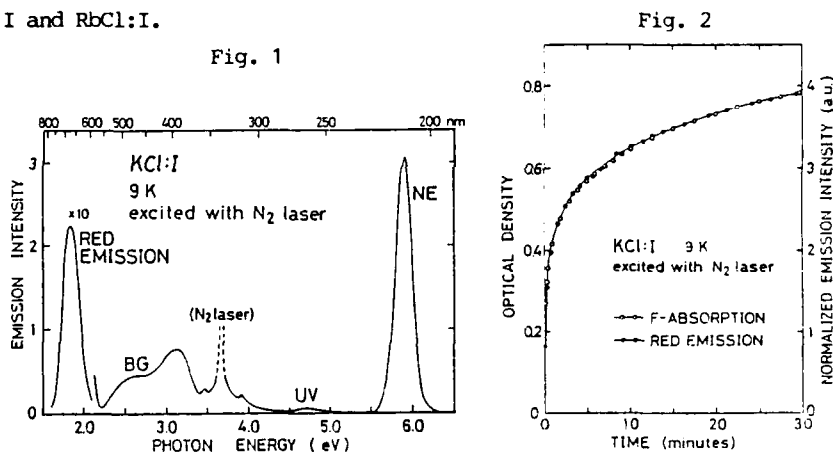


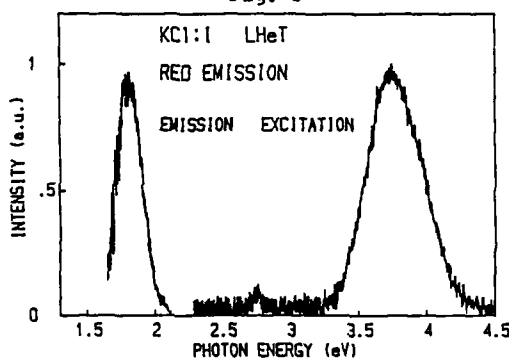
Figure 1 shows the luminescence spectrum of KCl:I stimulated by the irradiation with N<sub>2</sub> laser pulses at 9 K. A prominent luminescence band with decay time 20 ns has been induced at 1.81 eV with the half-width 0.22 eV, along with three well-known emission bands (called NE, UV, and BG) due to localized excitons.<sup>5)</sup> Its intensity grows under repeated N<sub>2</sub> laser irradiation in exactly the same way as the absorption intensity of induced F band does (Fig. 2). After a prolonged irradiation, a stationary situation is attained, saturation value of the emission intensity depending linearly upon the N<sub>2</sub> laser power. Therefore, this emission results certainly from the

one-photon absorption of the  $N_2$  laser by a new type of defect which has been produced together with F center under the two-photon excitation with preceding laser pulses. That is, the red emission results neither from the radiative recombination of short-lived defect pairs, nor from the tunneling luminescence of long-lived defect pairs. The presence of a similar emission band was confirmed also in RbCl:I (peak: 1.67 eV, half-width: 0.20 eV, decay time: 30 ns).

Absorption bands responsible for the red emission were revealed by checking with an excitation spectrum in the KCl:I crystal which had been uniformly colored by the previous  $N_2$  laser irradiation. As shown in Fig. 3, a clear excitation peak appears at 3.75 eV with the half-width of 0.53 eV. An additional small peak is seen at 2.75 eV with relatively small half-width (0.2 eV). It is to be noted that these features are very similar to those of the absorption bands due to the intrinsic H center.<sup>6)</sup>

In this measurement, the crystal was stimulated with moderate light intensity for a long period. Intensity of the red emission, however, did not decrease at all during the experiment. Therefore, photo-stimulated defect recombination will be ruled out as the origin of this emission. In other word, it is very likely that the red emission comes from the radiative decay of a relaxed excited state of the stimulated defect itself.

Fig. 3



- 1) M.Maki, N.Nagasawa and M.Hirai: Solid State Commun. 17 (1975), 1409.
- 2) M.Itoh, K.Kan'no and Y.Nakai: Solid State Commun. 26 (1978), 929.
- 3) Y.Nakai and K.Kan'no: Semicond. and Insul. 5 (1983), 505.
- 4) O.Arimoto, K.Kan'no, K.Nakamura and Y.Nakai: J. Phys. Soc. Jpn. 53 (1984), 70.
- 5) T.Higashimura, H.Nakatani, M.Itoh, K.Kan'no and Y.Nakai: J. Phys. Soc. Jpn. 53 (1984), 1878.
- 6) C.J.Delbecq, J.L.Kolopus, E.L.Yasaitis and E.L.Yuster: Phys. Rev. 154 (1967), 866; C.J.Delbecq, E.Hutchinson, D.Schoemaker, E.L.Yasaitis and P.H.Yuster: Phys. Rev. 187 (1969), 1103.

COLOR CENTERS IN SUPER IONIC CONDUCTORS  $\text{RbAg}_4\text{I}_5$  AND  $\text{KAg}_4\text{I}_5$

Teruyoshi Awano and Mikihiro Ikezawa\*

Department of Applied Physics, Tohoku Gakuin University,  
Tagajo 985, Japan

\*Department of Physics, Tohoku University, Sendai 980, Japan

Alkali silver iodide super ionic conductors  $\text{RbAg}_4\text{I}_5$  and  $\text{KAg}_4\text{I}_5$  have the high ionic conductivity above 121.8 K. We have investigated optical properties and defect formation in the two crystals. The fundamental absorption band was observed at 3.30 eV in  $\text{RbAg}_4\text{I}_5$  and at 3.31 eV in  $\text{KAg}_4\text{I}_5$  at 77 K. Small peaks were observed at 3.40 eV ( $\text{RbAg}_4\text{I}_5$ ) or 3.41 eV ( $\text{KAg}_4\text{I}_5$ ). Assuming that the peaks are  $n=1$  and  $n=2$  exciton peaks of the Wannier series, the band gap energy is estimated as 3.44 eV in the two crystals. This value is different from a previously reported one.<sup>1)</sup> X-ray and  $\gamma$ -ray irradiation at 77 K induced absorption bands at 1.35, 1.80, 2.05, 2.35 and 2.85 eV in  $\text{RbAg}_4\text{I}_5$  and at 1.75, 2.05, 2.4 and 2.9 eV in  $\text{KAg}_4\text{I}_5$ . The induced absorption spectrum in  $\text{KAg}_4\text{I}_5$  is very similar to those in  $\text{RbAg}_4\text{I}_5$  as shown in Figs. 1 and 2 and induced defects are probably the same in both crystals. Previously it had been reported that an absorption band was induced in  $\text{RbAg}_4\text{I}_5$  in  $\text{I}_2$  vapor at room temperature, and the one- $\text{Ag}^+$ -vacancy trapped hole center model had been proposed.<sup>2)</sup> The 2.85 eV peak in  $\text{RbAg}_4\text{I}_5$  seems to be caused by the same product in the case of the additive coloration. Compared with alkali halide crystals,  $\text{RbAg}_4\text{I}_5$  and  $\text{KAg}_4\text{I}_5$  are colored in the lower temperature region by the irradiation or by the vapour addition.

The 1.80 eV and 2.35 eV bands ( $\text{RbAg}_4\text{I}_5$ ) or 1.75 eV and 2.4 eV

bands ( $\text{KAg}_4\text{I}_5$ ) were bleached by irradiation of 1.80 eV ( $\text{RbAg}_4\text{I}_5$ ) or 1.75 eV ( $\text{KAg}_4\text{I}_5$ ) light. These two bands were bleached also by irradiation of 2.85 ( $\text{RbAg}_4\text{I}_5$ ) or 2.9 eV ( $\text{KAg}_4\text{I}_5$ ) light but in this case the 2.85 and 2.9 eV bands were not bleached.

Similar ESR spectra were observed in both crystals. Main structure was one peak near  $g=2.0$  and several small peaks were overlapped. This signal was not bleached by the irradiation of the sample with 1.80 eV light ( $\text{RbAg}_4\text{I}_5$ ) and seemed to belong to the center which caused 2.85 eV absorption peak. This signal may be interpreted as that from a  $\text{Ag}^+$ -vacancy trapped hole center with spin  $1/2$ . Several small structures may be super hyper fine structure by surrounding iodine ion nuclei. The detailed investigation is under way.

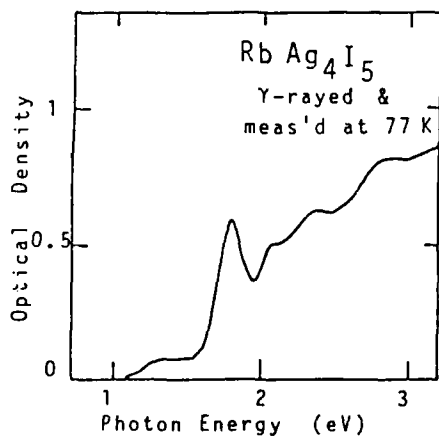


Fig. 1

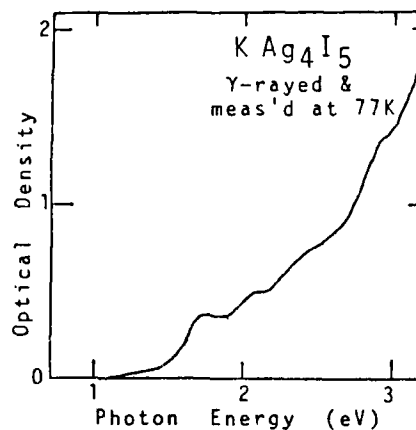


Fig. 2

#### References

- 1) R. S. Bauer and B. A. Huberman : Phys. Rev. **B13**, 3344 (1976)
- 2) V. N. Andreef and V. G. Goffman : Sov. Phys. Solid State **25**, 2004 (1983)

## OPTICAL PROPERTIES AND COLORATION OF ALKALI SILVER HALIDES

Mikihiro Ikezawa, Teruyoshi Awano\*, Keiichi Edamatsu\*\*,  
Takao Nanba, Tomochika Matsuyama\*\*\* and Hitoshi Yamaoka\*\*\*

Department of Physics, \*\* Department of Applied Physics,  
Tohoku University, Sendai 980, Japan

\* Department of Applied Physics, Tohoku Gakuin University,  
Tagajo 985, Japan

\*\*\* Research Reactor Institute, Kyoto University, Kumatori,  
Osaka 590-04, Japan

Ions of the alkali (A), silver or copper (M) and halogen (X) constitute the alkali silver halide or the alkali cuprous halide crystal of the  $A_2MX_3$  formula.<sup>1,2</sup> The symmetry of the crystals is orthorhombic and it belongs to the  $D_{2h}^{16}$  of the space group. In Fig.1 the positions of the ions projected on the  $ac$ -plane and their heights in the unit cell are shown for  $K_2AgI_3$ .<sup>2</sup> The number I, II and III in the parentheses in the figure indicate different lattice sites. We have investigated the energy band structure, optical properties of the intrinsic absorption, the luminescence and coloration.<sup>3-6</sup> In the alkali silver halide, the bottom of the conduction band is formed from the  $5s$  orbital of silver and the uppermost valence band mainly from the  $p$ -orbitals of the halogen. In the alkali cuprous halide, the conduction band and the valence band are formed from the  $4s$  and  $3d$  orbitals of the cuprous ions.<sup>6</sup>

The reflectivity spectra were measured with linearly polarized light along the three directions of the crystal axis in the energy region from 4 to 30 eV. By the Kramers-Kronig analysis, spectra of the dielectric constants were calculated. The absorption spectra were interpreted consistently with the energy band structure. The fundamental absorption bands were observed at 4.4 eV in the alkali cuprous halides and at 4.4 to 4.9 eV in the alkali silver halides. The excitation in the intrinsic absorption region induced only an intense luminescence band in alkali cuprous halides ( $K_2CuCl_3$ ,  $K_2CuBr_3$  etc.). From the life time and its temperature dependence, the luminescence is interpreted to be due to the  $^3D_3$  state of the cuprous ion placed in an approximate  $D_{2d}$  symmetry. On the other hand in the alkali silver halides of  $K_2AgI_3$  and  $Rb_2AgI_3$ , the intensity of the luminescence induced by the excitation in the intrinsic absorption region was weak even at low temperature. The emission bands and the excitation spectra in the intrinsic absorption region showed complex temperature dependence. The excitation in the intrinsic absorption region below 77 K with UV light induced coloration of the crystals. We consider that the coloration occurs in the alkali silver halide and it does not in the cuprous halide because of the properties of the valence and the conduction bands.

To get high concentration of the defects in the alkali silver halides, we have irradiated the crystals with X-ray or  $\gamma$ -ray at low temperature. Examples of the spectra induced by  $\gamma$ -ray

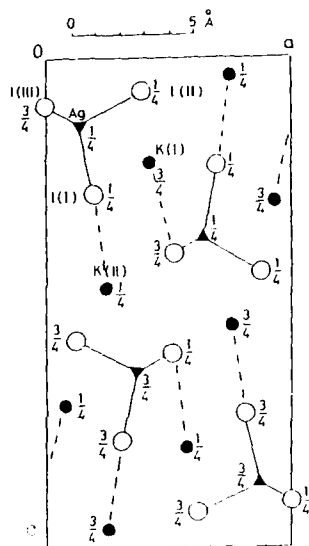


Fig. 1

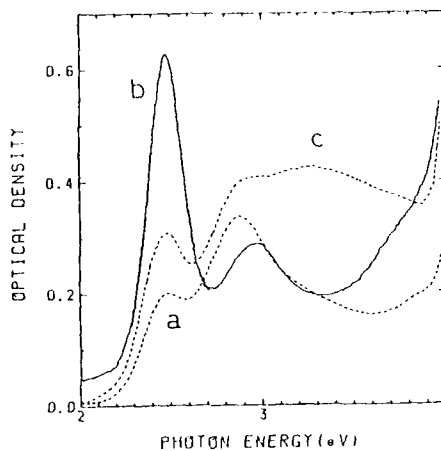


Fig. 2

at 77 K and measured with linearly polarized light along the *a*-, *b*- and *c*-axes of the crystal are shown in Fig. 2 for  $\text{Rb}_2\text{AgI}_3$ . Similar spectra were observed for  $\text{K}_2\text{AgI}_3$ . The polarization of the spectra indicates that the induced absorption bands at 2.5 eV and 3.2 eV have main transition dipoles along the *b*- and *c*-axis of the crystal. From an ESR study it is concluded that a hole center is formed at a single iodine ion which has almost the uniaxial symmetry.<sup>6)</sup> The directions of the axis of the hole center are shown by the dashed lines in Fig. 1, which are approximately along the *c*-axis.<sup>6)</sup> Therefore, the 3.2 eV band probably belongs to the hole center. A peculiar point is that the hole is trapped only by the iodine ions at the sites I and III in Fig. 1 and not at the site II. When the temperature of the irradiated sample was raised, the whole absorption bands, as well as the ESR signal, began to decrease simultaneously at about 100 K and disappeared above 140 K. This is considered to be due to the electron-hole recombination and the 2.5 eV band and another band at 2.9 eV in Fig. 2 are possibly due to trapped-electron centers.

#### References

- 1) C. Brink and C. H. MacGillivray: *Acta Cryst.* **2**, 158 (1949).
- 2) C. Brink and H. A. S. Kroese: *Acta Cryst.* **5**, 433 (1952).
- 3) S. Sasaki, M. Ikezawa, K. Sato, S. Kono and T. Sagawa: *J. Phys. Soc. Jpn.* **52**, 304 (1983).
- 4) K. Edamatsu, M. Ikezawa, K. Sato, S. Kono and T. Sagawa: *J. Phys. Soc. Jpn.* **52**, 1521 (1983).
- 5) K. Edamatsu, M. Ikezawa, H. Tokailin, T. Takahashi and T. Sagawa: *J. Phys. Soc. Jpn.* **55**, 2880 (1986).
- 6) T. Awano, T. Nanba, M. Ikezawa, T. Matsuyama and H. Yamaoka: contributed paper in this conference.

EFFECTS OF TWO-DIMENSIONAL DEFECTS ON EXCITONS IN BISMUTH IODIDE CRYSTALS

T.Komatsu, T.Karasawa, K.Watanabe,<sup>+</sup> T.Higashimura, T.Iida, I.Kaizu  
and Y.Kaifu

Department of Physics, Faculty of Science, Osaka City University,  
Sumiyoshi-ku, Osaka 558, Japan

<sup>+</sup>Department of Physics, Faculty of Liberal Arts and Education,  
Yamanashi University, Takeda, Kofu 400, Japan

We show that there exist three different types of two-dimensional defects in layered  $\text{BiI}_3$  crystals. The effects of these defects on excitonic processes are studied by precise optical measurements and by those under electric fields and high magnetic fields up to 40 tesla.

The two-dimensional defects appear often in close packed and layered structures. They take several types of stacking disorder (stacking fault) formed during crystalline growth or by deformation with shear type stress. The most characteristic features of them in contrast with point defects are: the translational symmetry of lattice is broken only along the direction normal to the defect plane, and a two-dimensional symmetry different from the bulk is newly constructed in the space containing the defect plane. The phonon states around a stacking fault have been studied theoretically by Lifshitz and Kosevich.<sup>1)</sup> However, few experimental investigations have been performed on the phonon and exciton states bound at such defects.

The exciton states localized around the two-dimensional defects are well realized in  $\text{BiI}_3$ . Three kinds of transitions to these localized states are observed in the absorption spectra depending on samples.

(1) The P-line is observed at the lower energy side of the indirect exciton transition energy but very close to it.<sup>2)</sup> From the temperature dependence of the absorption spectra, annealing effects of the deformation fault and magneto-optical measurements, the P-line can be assigned to the transition to the state associated with short range polytypic structures.

(2) Very sharp absorption lines named Q, R, S and T from the high-energy side are observed in the lower energy region close to the indirect exciton transition energy. They have been attributed to the excitonic transitions

localized at the two-dimensional defect-plane formed during crystalline growth (growth fault).<sup>3)</sup> A model based on the cationic excitons ( $6s^2 \rightarrow 6s6p$  transition in the cation) perturbed by the growth fault is proposed, which is reduced from the X-ray structural analyses<sup>3)</sup> and detailed optical measurements under electric and magnetic field<sup>4)</sup> on these sharp lines.

(3) The transitions named W-lines grow up in the lower energy region than T-line by the crystal deformation with shear type stress. They consist of a line series named  $W_1, W_2, W_3, \dots$ , and the successive energy-intervals become smaller with the lower energy side. The absorption intensity of each line depends on how strong the crystal is deformed by a shear type stress. In layered crystals, a shear type stress causes a stacking disorder called deformation fault because of the Van der Waals type interlayer weak binding. If deformation faults are formed in one layer, two layers and so on, several micro domains with different thickness are formed in the bulk crystal. In  $\text{BiI}_3$  crystals, such micro domains should be constructed planar crystals with  $D_{3d}$  symmetry<sup>5)</sup> different from the host  $C_{3i}$  symmetry. Magneto-optical measurements confirm the W-states are to be excitonic origin. The successive energy intervals among the  $W_1, W_2, \dots$  lines are well explained by a simple model of exciton confined in the micro domains.

#### References

- 1) A.A. Maradudin et al: LATTICE DYNAMICS (W.A. Benjamin, New York 1969) p53.
- 2) Y. Kaifu and T. Komatsu: J. Phys. Soc. Japan 40, 1377 (1976).
- 3) Y. Kaifu, T. Komatsu, and T. Aikami: Nuovo Cimento 38, 449 (1977).
- 4) T. Komatsu, Y. Kaifu, S. Takeyama, and N. Miura: Phys. Rev. Lett. 58, 2259 (1987).
- 5) R.W.G. Wyckoff: CRYSTAL STRUCTURES (Interscience, New York, 1964) vol.2, p46.

EPR STUDY OF HOLE TRAPPING AT CATION VACANCIES IN SILVER HALIDES\*

C.T. Kao, L.G. Rowan, and L.M. Slifkin

Dept. of Physics & Astronomy, University of North Carolina  
 CB #3255, Phillips Hall  
 University of North Carolina, Chapel Hill, NC 27599-3255, USA

The top of the valence band in AgCl and AgBr is quite unlike that of the alkali halides. It occurs at the (111) extreme of the Brillouin zone (i.e., at the L-point), and it consists of a strong mixture of silver d-states and halide p-states. One might therefore expect to find trapped hole centers in the silver halides that are very different from those in the alkali halides. For example, in AgCl the self-trapped hole is centered on a single cation, rather than on a pair of anions. It is thus of interest to search for hole trapping at cation vacancies in AgCl and AgBr, and to identify the structures and stabilities of any centers that might appear. There does exist some optical evidence<sup>(1)</sup> for deep (0.4 eV) trapping of holes at cation vacancies in AgBr, but definitive identification and structural information are lacking.

We are using electron paramagnetic resonance (EPR) techniques to explore hole centers produced in both AgCl and AgBr crystals, in which the concentrations of cation vacancies have been enhanced by doping with 45 - 100 ppm of divalent  $\text{Cd}^{2+}$  or  $\text{Zn}^{2+}$  (chosen because of the greatly different vacancy bindings). In order to preclude the electron-hole recombination that would occur if photocarriers were produced by band-gap illumination, our crystals were also provided with a second dopant, either  $\text{Fe}^{3+}$  or  $\text{Cu}^{2+}$ , which acts as a source of holes under sub-gap illumination (hence, no photoelectrons are produced). The cupric and ferric states are produced by prior annealing in halogen. We find that the behaviors of AgCl and AgBr are quite different.

In  $\text{AgCl}:\text{Cd}^{2+}$ , sub-gap irradiation produces at least two new trapped-hole centers, one of which is converted to the other at temperatures above 85K. This more stable center appears to have a [111] symmetry, and it too becomes unstable at temperatures above about 200K. One possible model which is qualitatively consistent with the spectra is an interstitial  $\text{Cd}^{3+}$  (i.e., a hole trapped at  $\text{Cd}^{2+}$ , originally

substitutional), associated with three cation vacancies. Another model involves a hole shared by 3 chlorides, adjacent to a vacancy. Quantitative fitting of the spectra has not yet been carried out.

In the doped AgBr, the anneal in halogen produces a new resonance (apart from those of the cupric and ferric ions) even before irradiation; the intensity is proportional to the concentration of Zn or Cd. The spectrum is best resolved with the magnetic field along [100], in which case 7 lines can be resolved; the g-tensor appears to be isotropic. Irradiation with sub-gap light reduces the intensity of this spectrum, and no new lines appear. Qualitatively, these results are consistent with the presence of interstitial  $\text{Zn}^{3+}$  or  $\text{Cd}^{3+}$ , associated with 4 cation vacancies, and with the trapped hole only loosely bound, so that it shows a strong super-hyperfine with the neighboring 4 bromide ions. Quantitatively, however, the number and intensities of the lines are not well described by such a model without some distortion.

Clearly, one needs to look at AgX in which the cation vacancies are provided by other, non-transition divalent ions, such as  $\text{Ca}^{2+}$ . These experiments are in progress.

-----  
Reference

(1) H. Kanzaki, *Photogr. Sci. & Engr.* 24, 219 (1980).

\*Supported by NSF Grant No. DMR-8501059.

**NONRADIATIVE DECAY OF EXCITATIONS IN DEFECTS**  
**(A PHONON TRANSPORT APPROACH)**

M. Wagner and Jorge Vázquez-Márquez  
Institut für Theoretische Physik, Universität Stuttgart,  
Pfaffenwaldring 57, 7000 Stuttgart 80, West Germany

Although the theoretical literature on the nonradiative decay problem is rather extended, there still is a number of basic questions which have not been answered in a satisfactory manner. More specifically, it has not been understood in detail, in which way the phonon transport properties, by means of which the released energy is spatially dispersed, affect the transition process. Likewise, it has not been fully clarified, in which manner the spatial extension of the respective coupling to the promoting and accepting modes modifies the decay constant. Our approach aims at elucidating these questions and emphasizes the role of phonon transport.

We treat the problem by means of a Green function technique, and formulate the decay as a generalized Bixon-Jortner<sup>1)</sup> model. The result then can be written down in the form of a single decay integral, which may be calculated numerically to any desired degree of accuracy. The self-energy part of this integral determines the decay constants and is discussed analytically. It turns out that there exist at least two decay channels, one of which may be interpreted as the "golden rule" channel, since it comprises the golden rule result as a limiting case. The decay constants of the other channels are determined by the spectral breadth of substructures in the coupling strength function. The relative weight and decay constants of the different channels depend sensibly on the interplay of 3 parameter sets, one of which characterizes the transport properties of the phonons, the other one the

spatial coupling arrangement to accepting modes in cartesian space and the final one pictures the spatial extension of the promoting mode coupling. The interplay of these influences is analysed for those cases which are of highest practical utility.

We also investigate the alterations in the decay constants which are due to disturbances of the lattice dynamics itself. These effects arise from the changes in the transport properties of the phonons, which come from the very existence of the defect center and may result in a strong suppression of spatial energy dissipation.

Our calculations are done with the *static base* approach. For the background of this approach as well as for its contrasting to the *adiabatic base* approach and to the recent discussion about the two approaches we refer to a recent paper<sup>2)</sup>.

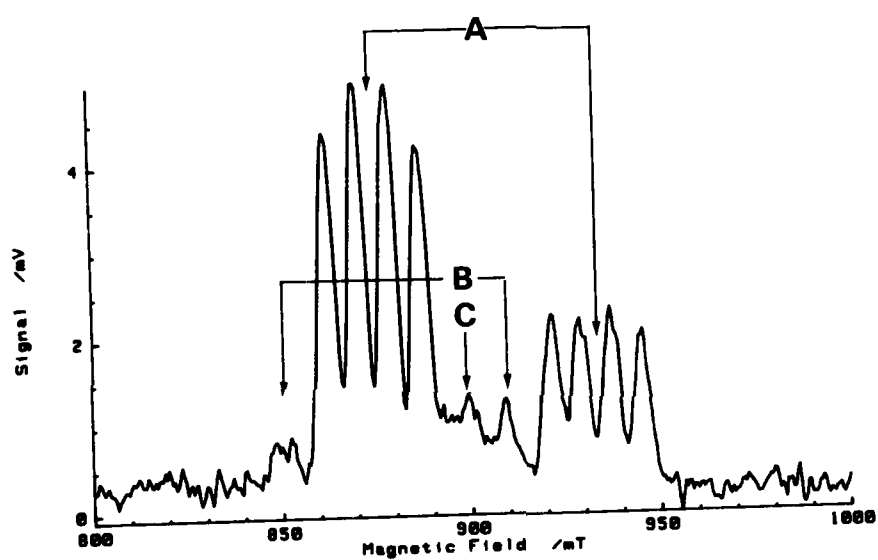
- 1) M. Bixon a. J. Jortner, J. Chem. Phys. 48, 715 (1968),  
ibid. 50, 4061 (1969)
- 2) V. Denner a. M. Wagner, J. Phys. C: Solid State Phys.,  
17, 153 (1984)

SPECTRAL DEPENDENCE OF THE ODMR TRANSITIONS  
OF THE BROMINE-BOUND STE IN AgCl

J. P. Spoonhower and F. J. Ahlers  
Research Laboratories  
Eastman Kodak Company  
Rochester, NY 14650 USA

The modulation frequency and spectral dependence (emission and excitation) of the ODMR transitions of the bromine-bound self-trapped exciton in AgCl have been measured at 24 GHz. All the measurements indicate that the lines marked A, B, and C in the figure arise from the same defect in the lattice. Thus, the assignment of Yamaga and Hayes (1) of the lines B and C to the exciton configurations perpendicular to the Ag-Br axis is confirmed.

(1) Yamaga, M., and Hayes, W., J. Phys. C: Solid State Phys., 15, L75-9 (1982); J. Phys. C: Solid State Phys., 15, L1215-9 (1982).



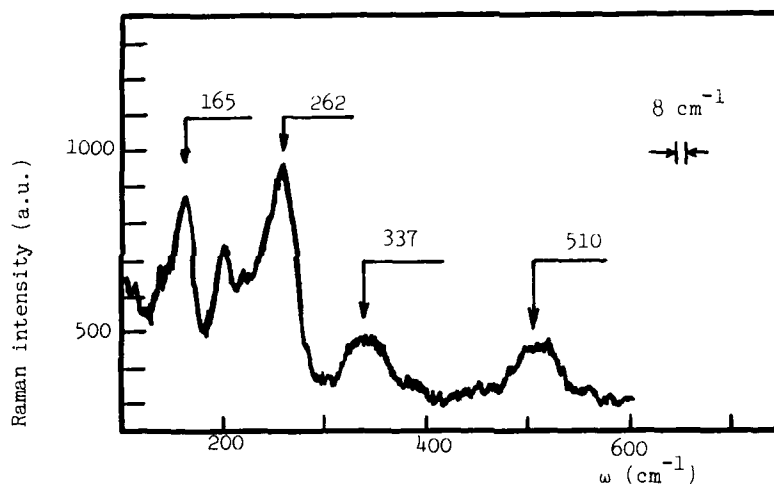
ROLE OF THE CATION ON THE FORMATION OF HALOGEN  
AGGREGATES IN X-IRRADIATED ALKALI HALIDE CRYSTALS

M. BERNARD, E. RZEPKA and S. LEFRANT  
Laboratoire de Physique Cristalline (UA CNRS n° 802),  
Université de Nantes, 2, rue de la Houssinière,  
44072 NANTES CEDEX 03, France.

Most of the positive hole centers created in irradiated alkali halide crystals have been characterized by either u.v.-visible absorption or EPR measurements. The use of quasi-resonant Raman scattering technique has been developed these recent years and proved its usefulness to determine a more precise structure for centers which are not paramagnetic (1). Most of the studies have been devoted to iodides because quasi-resonant conditions are fulfilled with available laser lines and more recently extended to bromides with the use of u.v. laser excitations. In pure crystals such as KI, RbI and KBr X-irradiated in the temperature range 100-250K,  $X_3^-$  complex ions (X : halogen atom) are evidenced by the observation in the Raman spectra of their stretching vibration. These centers are linear and symmetric. When crystals are irradiated at room temperature, only halogen aggregate  $(I_2)_n$  are observed in KI whereas both  $Br_3^-$ ,  $Br_5^-$  and  $(Br_2)_n$  are seen in KBr. In RbI, these aggregates are not created and only  $I_3^-$  are detected in the Raman spectra, even after high doses of X or  $\gamma$  rays.

In this paper, we present optical and Raman results obtained in mixed iodide crystals KI-RbI and in RbBr X-irradiated near room temperature in order to investigate the role of the cation (or the cation vacancy) on the formation of halogen aggregates. In KI-RbI crystals, only  $I_3^-$  centers are observed, as in pure RbI. In RbBr, Raman modes are detected at 165, 262  $cm^{-1}$  together with their first harmonic (see Figure), characteristic of the stretching vibration of  $Br_3^-$  (165  $cm^{-1}$ ) and of  $Br_5^-$  (262  $cm^{-1}$ ) respectively. The main point which has to be emphasized here is the absence of  $(Br_2)_n$  aggregates which are mainly

characterized by a mode at  $297\text{ cm}^{-1}$  as observed in KBr (see ref. 1). Results are discussed in terms of vacancy formation in the cation sublattice since cations must be removed from the lattice in regions where the halogen aggregation occurs. The cationic vacancy formation is associated with energy transfer in a collision sequence during irradiation and it turns out that this transfer is strongly limited by a large cation mass. This is in agreement with our experiments carried out in crystals in which large Rb ions are part of the host lattice.



Raman spectrum of RbBr crystal X-irradiated at room temperature :  
laser line =  $351\text{ nm}$  ;  $T = 78\text{K}$ .

#### REFERENCE

- 1 E. RZEPKA, M. BERNARD, S. LEFRANT and J.D. COMINS  
Cryst. Latt. Def. and Amorph. Mat., 17, 113-117 (1987),  
and references therein.

# STUDIES OF COLOUR CENTRES IN $\text{LiYF}_4$ CRYSTAL

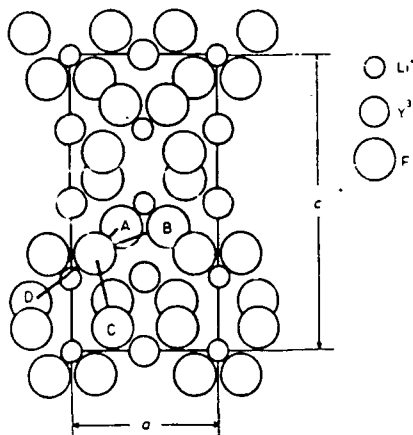
Fang Shugan, Le Zhiqiang  
Shanghai Jiao Tong University  
Department of Applied Physics  
1954 Hua San Road  
Shanghai China

In the experiments, when the samples of  $\text{LiYF}_4$  crystal are irradiated by  $\gamma$  rays at RT, five  $\sigma$  polarised optical absorption bands centred at 275nm, 335nm, 430nm, 530nm and 630nm, and five  $\pi$  polarised optical absorption bands centred at 255nm, 335nm, 410nm, 530nm and 630nm, are observed. At LNT, three broad fluorescence bands centred at 0.72 $\mu\text{m}$ , 1.16 $\mu\text{m}$ , and 1.63 $\mu\text{m}$ , which exciting peaks are at 410nm and 470nm, 630nm, and 555nm respectively, are measured for the first time.

When the coloured  $\text{LiYF}_4$  crystal is illuminated by He-Ne laser with wavelenth of 632.8nm, the 630nm band reduces remarkbly, and appeares a new absorption band centred at 555nm which is overlapped with 555nm exciting peak. But the 555nm band is unstable at RT, and it will reduce to 630nm band. Nevertheless, the 555nm band is stable below the temperature of  $-20^\circ\text{C}$ . By the methods of annealing and illuminating, it is found that the changes of 410nm, 530nm, 555nm and 630nm bands are independent of the F band centred at 335nm. After annealing at  $100^\circ\text{C}$ , the sample shows that, 410nm and 530nm bands decrease, and 630nm band increases. According to the height of 630nm and 555nm absorption peaks in  $\sigma$  and  $\pi$  polarised spectra, it is revealed that the colour centres of 630nm and 555nm bands form the angles of about  $63^\circ$  and  $61^\circ$  with the c axis respectively.

Examination of the crystal structure indicates that, in principle, four different types of  $F_2$  centre are possible, distinguished by the letters A, B, C and D in Fig.1. It is inferred that, the centre of 630nm band is the  $F_2$  centre of type B, and the centre of 555nm band is the  $F_2$  centre of type A. By experi-

ments, we conclude that, the  $F_2$  centre of type A is movable at RT, through the migration of anion, it will turn from type A to type B, in which the ground state energy is lower. In lower temperature, it is difficult that the anion migrate in the crystal, so the  $F_2$  centre of type A can exist stably below the temperature of  $-20^\circ\text{C}$ .



On the basis of continual medium model, the  $F_2$  centre is equivalent to a quasi- $H_2$  molecule. The covalent bond theorem of  $H_2$  molecule

Fig.1. Schematic projection of the unit cell of  $LiYF_4$  on to the  $ac$  plane.

is applied. The different  $F_2$  centre's ground state energy, exciting state energy and transition energy are calculated. The mean potential of all ions in crystal is introduced to correct the energy of different  $F_2$  centre approximately. The results of calculation conform to the results of experiment very well, and confirm the conclusions from the experiments.

#### References

- G.M.Renfro, L.E.Halliburton, W.A.Sibley and R.F.Belt, J. Phys. C: Solid St. Phys., 13(1980) 1941-50
- Spero Penha Morato and Tania Cristina A. Macedo, Radiation Effects, 1983, Vol.72, pp.229-235
- R.E.Thoma, C.F.Weaver, H.A.Friedman, H.Insley, L.A.Harris and H.A.Yakel, Jr., J. Phys. Chem. 65, 1096(1961)
- C.Keller, H.Schmutz, J. Inorg. Nucl. Chem. 27, 900(1965)
- W.Hayes, M.Yamaga, D.J.Robbins and B.Cockayne, J. Phys. C: Solid St. Phys., 13(1980), L1011-5
- K.H.Yang and J.A.DeLuca, Phys. Rev. B, Vol.17, 4246, 1978
- Levine Ira N. Quantum Chemistry 2d ed. Boston, Allyn and Bacon, 1974
- John C. Slater, Quantum Theory of Molecules and Solids, Vol.1, 1963

THE FORMATION OF VACANCIES DURING THERMAL DECOMPOSITION OF  
ALKALINE EARTH HYDROXIDES

Barsova L.I., Yurik T.K.

Institute of Physical Chemistry of the Academy of Sciences  
of the USSR, 117915 Moscow, Leninsky prospekt, 31

The thermal dehydration of  $\text{Mg}(\text{OH})_2$  to  $\text{MgO}$  is known to be accompanied by unusual side reactions: a release of  $\text{H}_2$ ,  $\text{O}_2$  and the arising of electron-donating and electron-deficient species on the surface (e.g. /1,2/).

In the present study surface and bulk anionic vacancies ( $V_{\text{as}}$ ,  $V_{\text{a}}$ ) and bulk cationic vacancies ( $V_{\text{c}}$ ) formed when polycrystalline  $\text{Mg}(\text{OH})_2$  and  $\text{Ca}(\text{OH})_2$  is dehydrated by heating in vacuo have been detected. Those vacancies have been identified through observation of paramagnetic  $F_{\text{s}}^+$ ,  $F^+$  and  $V_{\text{OH}}^-$  centres, which arose after  $\gamma$ -irradiation of the samples at 77K /3/. In oxides characterized by the absence of efficient generation of intrinsic radiation defects the concentration of the F- and V-type centres corresponds to the number of anionic and cationic vacancies before irradiation /4/.

The formation of anionic vacancies during dehydration of  $\text{Mg}(\text{OH})_2$  to  $\text{MgO}$  can be exemplified by direction /001/  $\text{Mg-OH-OH-Mg-OH-OH-Mg}$  of  $\text{Mg}(\text{OH})_2$  structure, which after release of water molecules is transformed to  $\text{Mg-V}_{\text{a}}-\text{O-Mg-V}_{\text{a}}-\text{O-Mg}$  followed by rearrangement of the hexagonal structure to the cubic  $\text{MgO}$  lattice. Anionic vacancies can be trapped by the surface as well as in the bulk of the novel structure. Dehydration involves the interaction between neighbouring  $\text{OH}^-$  ions as well as between those separated by several lattice parameters (as a result of the proton diffusion). According to this scheme the concentration of anionic vacancies in oxides is to increase during dehydroxylation also.

In  $\text{MgO}$  samples with large specific surfaces ( $170-200 \text{ m}^2 \text{ g}^{-1}$ ) anionic vacancies are localized preferentially on the surface while in  $\text{MgO}$  and  $\text{CaO}$  samples with specific surfaces 0.5-3.0

$m^2g^{-1}$  bulk anionic vacancies are observed. As the temperature of treatment rises the concentration of vacancies increases (to max.  $10^{18}g^{-1}$ ) but then it declines to  $10^{15}-10^{16}g^{-1}$  (CaO, 1270 K). The IR-spectra of the oxide samples demonstrated that the concentration of anionic vacancies increased in the temperature range of existence of bonded OH-groups. The drop of the concentration of anionic vacancies can be accounted for by their recombination with interstitial anions.

Cationic vacancies arose during the formation of the oxide lattice as compensators of charges of inivalent  $Me^{+3}$  cations and  $OH^-$  anions. In  $\gamma$ -irradiated samples they appeared as  $V_{Me}^{3+}$  and  $V_{OH}$  - centres. In contrast to the anionic vacancies the concentration of cationic vacancies does not change with an increase in the temperature of treatment. The hole centres of V-type have not been observed in the  $\gamma$ -irradiated samples of MgO and CaO with a low concentration of isolated OH-groups. Pairs of anionic and cationic vacancies, which are unable to trap holes but capable of trapping an electron to form P-centres possibly arose in this temperature range.

1. Martens R., Gentsch H., Freund F. J. of Cat., 1976, v.44, p.366.
2. Cordischi D., Indovina V., J.Chem.Soc., Faraday Trans., 1, 1976, v.72, p.2341.
3. Spitsyn, V.I., Barsova L.I., Popova G.Yu., Yurik T.K. Izvestiya AN SSSR ser.khim., 1976, str.963.
4. Spitsyn V.I., Yurik T.K., Izvestiya AN SSSR, Seriya khim., 1982, p.755.

# LUMINESCENCE OF NON RELAXED IODINE BOUND EXCITONS IN AgBr ?

W.Czaja et Y.Burki  
Institut de physique appliquée de l'EPFL  
CH-1015 Lausanne, Switzerland

The iodine bound exciton in AgBr has a well known absorption - and emission spectrum at low temperatures, see <sup>1)</sup> and the literature quoted therein. After prolonged low temperature illumination and repeated utilisation, weakly doped and unintentionally doped samples show a change in the spectrum from the normal form fig.1a to the fig.1b, which in its extrem form is stable. As already remarked in ref.2 after a suitable thermal treatment (24 - 48 hours at 200 °C in vacuum and slow cooling to room temperature with 7.5 to 5 degrees per hour) the original spectrum can be restored. Moreover, in time resolved luminescence at short delay times  $\tau < 100$  ns and in the limit of weak excitation, a so called Q-spectrum has been observed (fig.2)<sup>3)</sup> which is believed to be related to the presence of iodine impurities. For long delay times the normal iodine bound exciton luminescence fig.1a shows up. The Q-spectrum has been found to be identical with the stable "deformed" spectrum of fig.1.b observed with continuous excitation <sup>4)</sup> (see also fig.2).

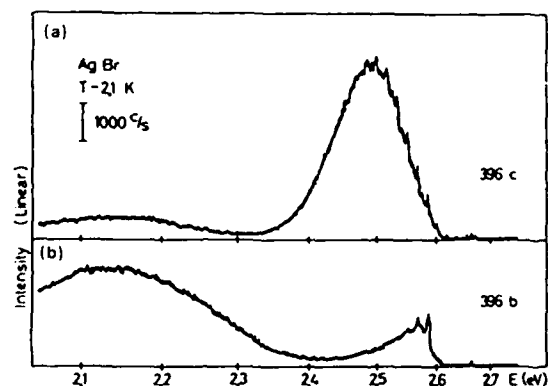


Fig.1 : a) Normal iodine bound exciton luminescence spectrum, continuous excitation.  
b) Iodine bound exciton luminescence of the same sample after prolonged use at low temperature.

We report in this contribution that the luminescence excitation spectra of the normal bound iodine luminescence fig.1a and the "Q" spectrum in fig.1b are identical in all essential features , i.e. the respective initial states are formed via the same processes .

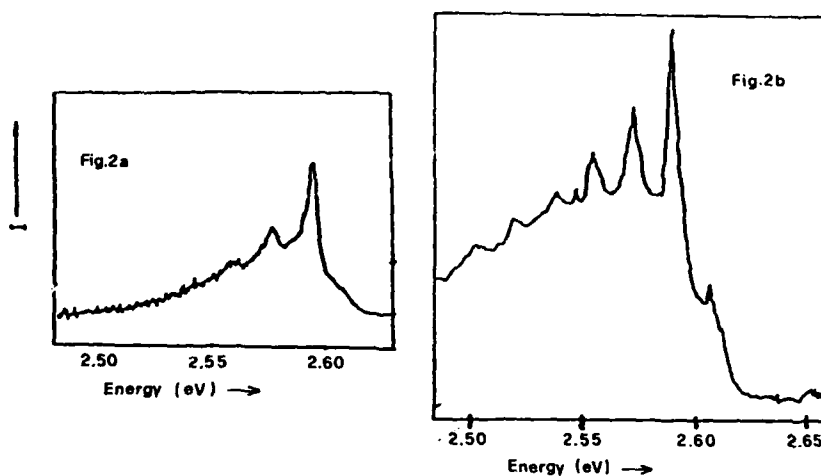


Fig.2 : a) Iodine bound exciton luminescence spectrum , time resolved with a delay  $< 100$  ns . b) Same as fig.1b with higher resolution .

As a working hypothesis we propose : since the respective initial states are identical , the Q-spectrum is the unrelaxed luminescence whereas the normal luminescence spectrum only appears after relaxation . We discuss further evidence and consequences of this working hypothesis .

Finally we mention that the broad spectrum at low energies in Fig.1a has an excitation spectrum different from that of the Q-spectrum .

- 1) A.Testa , W.Czaja , A.Quattropani and P.Schwendimann ; J. Phys. C **20** , 1253 ( 1987 )  
A.Testa , W.Czaja , A.Quattropani and P.Schwendimann ; J. of Phys. C : to be published ( 1988 ) .
- 2) W.Czaja and D.Baeriswyl , RCA Review , **36** , 5 (1975) .
- 3) Th.Kleinfeld , H.Stoltz and W.von der Osten ; Sol. Stat. Comm. **31** , 59 , ( 1979 ) .
- 4) W.von der Osten : private communication .

PHOTOLUMINESCENCE, PHOTOCONDUCTIVITY AND THERMOLUMINESCENCE  
IN  $\text{Eu}^{2+}$  DOPED ALKALI HALIDES

I. Aguirre de Cárcer, F. Cussó and F. Jaque

Departamento de Física Aplicada, C-IV, Universidad Autónoma de Madrid  
Cantoblanco, 28049 Madrid (Spain)

It has been reported that a slow non-exponential luminescence after-glow appears in  $\text{Eu}^{2+}$  doped alkali halides after Xenon flash-lamp,  $\text{N}_2$  laser or X-ray excitation. The nature of this luminescence, that only appears in annealed samples, is not well understood yet. In the present work, the after-glow processes have been investigated by means of photoluminescence (PL), photoconductivity (PC) and thermoluminescence (TL) techniques in  $\text{Eu}^{2+}$  doped NaCl, KCl, KBr and KI single crystals.

**LUMINESCENCE.** The excitation spectrum of the after-glow (AG) luminescence for  $\text{Eu}^{2+}$  doped NaCl is presented in Figure 1, where the  $\text{Eu}^{2+}$  absorption is also given for comparative purposes. As can be seen, the AG

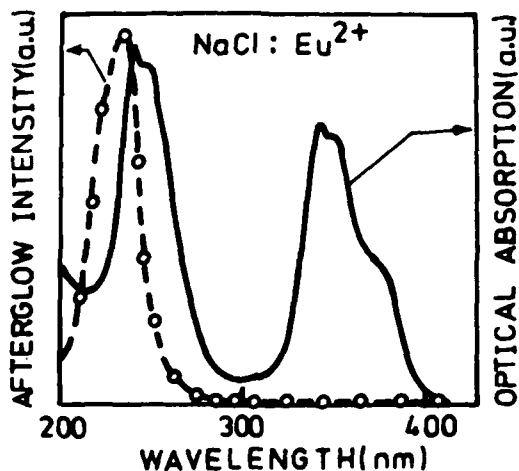


Figure 1.- Excitation spectra of the after-glow for  $\text{NaCl:Eu}^{2+}$  (O). Continuous line corresponds to the  $\text{Eu}^{2+}$  absorption.

luminescence is only excited in the high energy region of the  $\text{Eu}^{2+}$  doped KCl, KBr and KI. In relation with the AG emission spectrum, it agrees in all cases with the emission bands associated with  $\text{Eu}^{2+}$ .

**PHOTOCONDUCTIVITY.** Photoconductivity signal has been detected under UV excitation. Figure 2 shows the PC response as a function of the excitation wavelength for KCl:  $\text{Eu}^{2+}$ . It is observed that the PC spectrum agrees with the AG one and corresponds essentially to the high energy

absorption band of the  $\text{Eu}^{2+}$ . A similar result is obtained in NaCl, KBr and KI.

#### THERMOLUMINESCENCE.

TL emissions have been found after UV excitation at LNT. Several glow peaks, in the temperature range LNT to RT, appear. Figure 3 shows the TL spectrum of KI after 250 nm excitation. The emission spectra of the TL peaks are again coincident with that of the  $\text{Eu}^{2+}$  ions. After these results, it can be concluded that under UV excitation  $\text{Eu}^{2+}$  photoionization occurs. The free electrons migrate through the conduction band and are trapped in several electron traps from where they are thermally released. The presence of a variety of traps can account for the kinetics and the temperature dependence of the AG process.

Figure 3.- Thermoluminescence spectrum of KI: $\text{Eu}^{2+}$  after excitation at 250 nm at LNT.

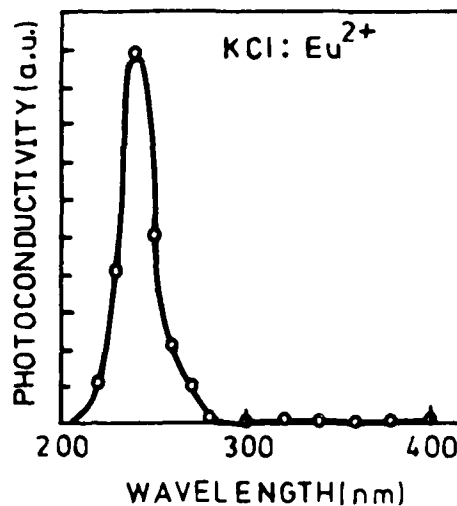
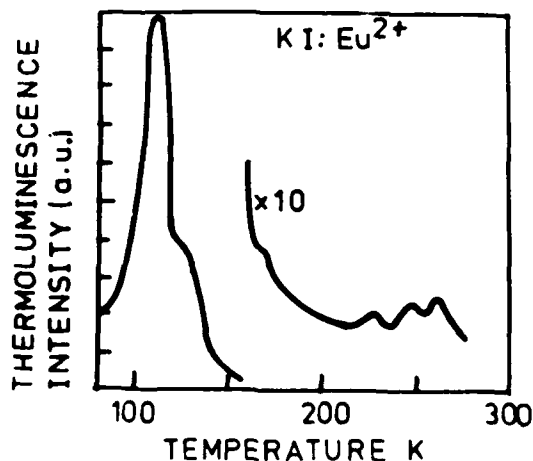


Figure 2.- Photoconductivity response as a function of the excitation wavelength for KCl: $\text{Eu}^{2+}$ .

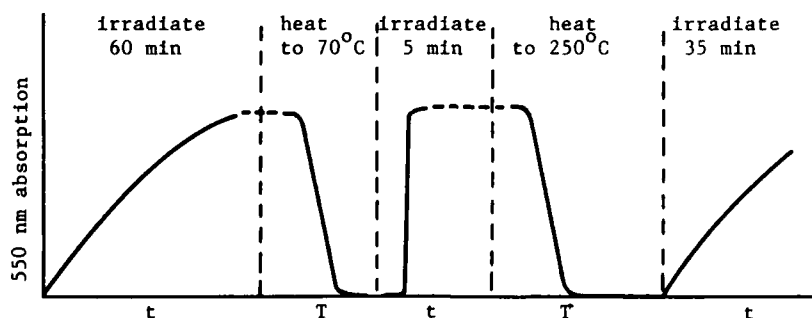


ON THE NATURE OF THE BROAD OPTICAL ABSORPTION BAND IN  $\text{LiNbO}_3$ 

F. Agulló López  
 Universidad Autónoma de Madrid, Spain  
 Canto Blanco, 28034 Madrid

E.R. Hodgson  
 C.I.E.M.A.T.  
 Avda. Complutense, 22. 28040 Madrid, Spain

Experiments have been performed irradiating stoichiometric  $\text{LiNbO}_3$  at 20 °C with up to 1.8 MeV electrons in a Van de Graaff accelerator. For electrons of energies above 1.0 MeV one observes the growth of a broad absorption band at about 550 nm. This threshold energy is in agreement with previous work on congruent  $\text{LiNbO}_3$ , and has been associated with oxygen displacement damage (1). The induced optical absorption band, undistinguishable from that produced by thermochemical reduction, is apparently identical in both the stoichiometric and congruent samples. However, whereas in the congruent case the radiation induced band is stable to above about 450°C, in the stoichiometric case the band is highly unstable and anneals out by about 70°C. The behaviour is complex (see figure). On irradiating a sample at 20 °C above the energy threshold, the band grows with irradiation time. On heating to 70 °C the band completely anneals out, but on re-irradiation immediately recovers the intensity previous to annealing. However, on heating to above 250 °C full annealing is achieved, and on reirradiation the band again grows slowly from zero with irradiation time.



The fact that the observed optical damage, although annealing out by 70 °C, may be restored by a very short reirradiation, is indicative of the existence of an unobserved residual damage. It is also clear from the observed threshold that the optical damage and the residual effect are associated with oxygen displacement damage. The short time scale involved in the restoration of the optical absorption band following annealing to only 70 °C is consistent with a purely electronic effect. This has been confirmed by performing the reirradiation below the threshold energy. One may therefore conclude that the residual damage is directly connected with the oxygen displacement, which only anneals out above 250 °C. It is reasonable to suggest that the residual damage is due to oxygen interstitials trapped within the lattice. The observed reversibility is more consistent with a situation involving oxygen vacancies and interstitials, rather than large lattice rearrangement during irradiation.

Further work is in progress to ascertain the possible role of impurities such as Fe, in the trapping of oxygen interstitials.

- 1) E.R. Hodgson and F. Agulló López, Solid State Comm. 64, 965 (1987)

EFFECTS OF VARIABLE TL SPECTRA ON TL DOSIMETRY

H M Rendell and P D Townsend

School of Mathematical and Physical Sciences,

University of Sussex

Falmer, Brighton BN1 9QH

East Sussex

UK

A very wide range of materials are being used for radiation dosimetry in thermoluminescence measurements. For personnel applications one has control over the preparation of the samples (for example LiF:Mg:Ti) and the dose range is small. One therefore expects that all samples will produce the same emission characteristics throughout the relevant dose range. In the case of archaeological and geological applications this simple situation ceases to exist, since one is dependent on the natural mineral constituents of the samples. Not only is there no control of the impurity content but one must often use a multigrain, or a polymineralic mixture which has received large radiation doses.

During the last 10 years we have been recording the details of the TL emission spectra of a variety of materials as a function of origin, dose conditions and thermal or optical stability. In many cases it has become apparent that the conventional TL readers employing a broad band blue/UV filter and blue sensitive photomultiplier can lead to a significant misinterpretation of the signals, as monitored over a wide spectral system. One such example is an assessment of 'shock' history of meteorites by the ratio of low and high temperature glow peaks. Whereas a simple 'blue' system suggests an intensity ratio of say 8:1 a wide band spectral system gives 200:1.

Widely differing TL spectra are apparent in natural crystals and in some cases such as obsidian or quartz one may

attempt to use the spectral characteristics to indicate the site of origin. Obsidian has been used in interlaboratory calibrations of radiation sources. The valuable features of the material are that for a specific source one has a reproducible and linear TL dosimeter. However with a conventional filter and photomultiplier system the number of observed glow peaks is dependent on the filter used. The reasons for this are apparent from the complete spectral analysis. For an intercalibration of similar intensity  $^{90}\text{Sr}$  sources which were packaged to provide different mixtures of the fast electron (2.27MeV and 0.54MeV) and X-rays, the source strengths determined by obsidian dosimetry were not in agreement by a factor of up to 8. In part this is interpreted as a difference in sensitivity to X-ray or electron radiation (ie LET) but the differences in ionisation rate in the crystal may also be reflected by changes in the emission spectra of the TL, with the resultant changes in detection sensitivity.

Geological dating applications use accumulated dose in 'natural dosimeters' like quartz and feldspar grains to determine age. Zeroing is assumed to have occurred by optically stimulated detrapping prior to deposition and burial. Laboratory 'bleaching experiments' to assess this base level have been undertaken and the subsequent TL monitored in various spectral regions. Once again it is apparent that the TL spectra change and are strongly modified by storage and bleaching conditions. Failure to allow for these variations produces valueless results.

In all materials studied so far it has been apparent that TL measurement taken without regard to changes in emission spectra may be misleading.

RADIATION-INDUCED DEFECT CENTRES IN  $\alpha$ -Al<sub>2</sub>O<sub>3</sub>

R A Wood

School of Mathematics and Physical Sciences

University of Sussex

Falmer, Brighton BN1 9QH

East Sussex

UK

The problems involved in measuring neutron fluxes inside nuclear reactors has led to a search for a reliable neutron dosimeter.

Certain types of optical damage in  $\alpha$ -Al<sub>2</sub>O<sub>3</sub> have been shown to exhibit a high degree of stability over the temperature range required for such a dosimeter.

Sapphire has been proposed for diagnostic windows in the JET fusion project at Culham, England. Also, large sapphire dielectric windows are being considered for use on electron-cyclotron resonance heating systems.

As part of the investigation into the defect centres in alumina, optical absorption measurements have been made, at Sussex University, of sapphire specimens which have been irradiated with neutrons over a temperature range of several hundreds of degrees. Also, the dynamics of defect growth have been observed in-situ during ion implantation, using the 3 MeV van der Graaf accelerator at Sussex.

Results and discussion of growth kinetics, and optical profiles of neutron-irradiated samples, will be given.

**RADIATION DAMAGE IN NaCl: STORED ENERGY AND MODEL CALCULATIONS\***

J.C. Groote, J.R.W. Weerkamp, J. Beersma and H.W. den Hartog.

Solid State Physics Laboratory

University of Groningen

1 Melkweg, 9718 EP Groningen, The Netherlands.

Among the problems encountered if one wants to dispose of high level radioactive waste from nuclear power plants in rocksalt formations are those associated with radiation damage and stored energy. Although many investigations have been carried out in a large number of laboratories there are several questions, which are still unanswered. In the present paper we will address some of these questions. New results will be presented on the

- dose rate effects;
- the role of impurities and
- the effect of the irradiation temperature.

We have investigated large numbers of samples, which had been irradiated by means of a van de Graaff electron accelerator. The total dose received by the samples is chosen between 2 and 25 Grad. The dose rate is varied from 12 Mrad/hr to 135 Mrad/hr, but more experiments below 12 Mrad/hr and above 135 Mrad/hr are planned for the near future. The effect of the presence of impurities has been investigated employing dopants such as Li, K, F, Br, Mn and Ba; also the effect of the concentration of the impurities has been investigated.

In our irradiation facility we irradiate simultaneously a large number of samples (as described above) at different temperatures in the range between 50 - 200°C. The irradiation runs, which have been carried out until now took 24 hours to several months.

The radiation damage has been investigated by means of DSC (differential scanning calorimetry) sometimes combined with TL

(thermoluminescence), optical absorption spectroscopy and some other methods such as EPR and Raman scattering. These methods provide us with important information such as the colloid concentration, colloid size, the presence of F and coagulated centers.

It appears that the development of Na-colloids and molecular chlorine "bubbles" is influenced drastically by the presence of impurities. Several examples will be discussed.

In an earlier paper we have treated some of the experimental data published in the literature with a modified Jain-Lidiard model<sup>1,2</sup>). Recently, we have added more modifications in order to explain both the formation and annihilation of radiation damage (during a DSC run). Results of simulations using the new model will be presented.

- 1) U. Jain and A.B. Lidiard Phil. Mag. 35A, 245 (1977).
- 2) G. van Opbroek and H.W. den Hartog J. Phys. C. (Solid State Physcis) 18, 257 (1985).

\* This research project is financed partly by the Dutch ministry of Economic Affairs.

RADIATION-INDUCED ABSORPTION BANDS DUE TO CHLORINE-RELATED  
DEFECTS IN a-SiO<sub>2</sub>

H.Takada, Y.Suzuki, H.Kimura and M.Hirai

Department of Applied Physics, Faculty of Engineering  
Tohoku University, Aramaki-Aoba, Sendai 980, Japan

As recently reviewed in references 1 and 2, radiation-induced "intrinsic" defects such as oxygen vacancies (E') and oxygen hole centers (OHC) in amorphous silicon dioxide (a-SiO<sub>2</sub>) were intensively investigated with optical and spin resonance methods. However, impurity-related radiation defects are not understood satisfactorily. Especially, with respect to defects associated with chlorine (Cl), few experimental data are available.<sup>3)</sup> It is important to clarify the radiation effect due to Cl impurities, for various applications such as radiation resistivity of optical fibers and MOS devices. In this paper, we report optical absorption bands originating from Cl-related defect centers in a-SiO<sub>2</sub> induced by  $\gamma$ -ray irradiation, and discuss the structure and the generation mechanism of the Cl centers.

The a-SiO<sub>2</sub> samples were commercially synthesized by an Ar plasma method. The OH contents were lower than 1 ppm. The dose rate of the  $\gamma$ -ray from <sup>60</sup>Co source was of  $9.4 \times 10^4$  R/h.

The curve A in Fig.1 shows the induced absorption spectrum of a-SiO<sub>2</sub> containing 3900ppm Cl after the  $\gamma$ -ray exposure for 9 hours, while the curve B shows that of Cl free (<5 ppm) a-SiO<sub>2</sub>. The samples were held at 77K during the irradiation and the optical measurements. The difference between curves A and B is apparent around 3.0eV and above 5.5eV as seen in the difference spectrum shown by the curve C. This difference spectrum is attributed to the induced defects associated directly or indirectly to Cl impurities.

The crystal showing the curve A was fractionally and successively bleached by light illuminations with different photon energies, i.e. 1.8eV, 3.0eV and 4.0eV. Consequently, the curve A was decomposed to the three Gaussian bands peaking at 2.24eV, 2.98eV and 3.95eV as shown in Fig.2, respectively. The peak energy and the half width (0.86eV) of the 2.24eV band suggest that the band is the OHC band.<sup>4)</sup> Since the absorption around 3eV on curve C in Fig.1 seems to consist of the 2.98eV and 3.95eV bands, these bands can be attributed to the Cl-related defects. Since the dichroic behavior of the 2.98eV band implies a molecule defect as its origin, we tentatively assign it to a diatomic chlorine ion (Cl<sub>2</sub><sup>-</sup>) as established in alkali halide crystals.<sup>5)</sup> On the other hand, we attributed the 3.95eV band to an interstitial halogen atom (Cl<sup>0</sup>) as confirmed by the ESR spectra by Griscom and Eriehle.<sup>6)</sup> The similar temperature dependence of the isochronal bleaching of the 3.95eV band to that of the Cl<sup>0</sup> ESR signal intensity supports the above assignment.

The fact that the absorption above 5.5eV in the curve C in Fig.1 is photo-bleached simultaneously with the 3.95eV band and that the peak energy is close to that of the E' center (5.8eV) suggest that this band is caused by an E' center neighboring to  $\text{Cl}^\circ$  according to the following reaction:  $\text{Si} - \text{Cl} \rightleftharpoons \text{Si} \cdot (\text{E}') + \text{Cl}^\circ$ .

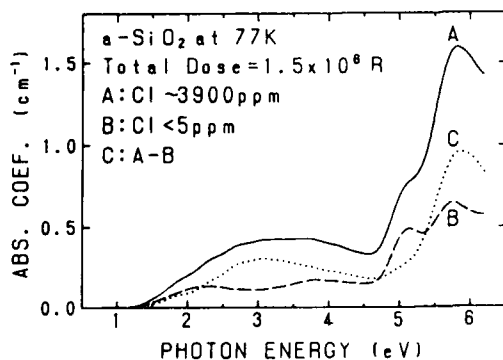


Fig.1  $\gamma$ -ray induced absorption of a-SiO<sub>2</sub> with 3900ppm (curve A) and less than 5ppm (curve B) of chlorine. Curve C is the difference between curves A and B.

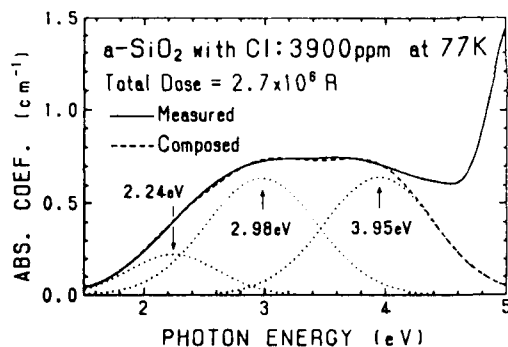


Fig.2 Absorption bands (dotted curves) in  $\gamma$ -ray induced absorption in a-SiO<sub>2</sub> with 3900ppm of chlorine (solid curve). Dashed curve is composed with dotted curves.

**Acknowledgments:** We express appreciation to Doctors H.Tanaka and T.Suzuki of Mitsubishi cable, Ltd. for providing the a-SiO<sub>2</sub> samples. We also thank Prof. M.Takebe and Mr. K.Furukawa, Department of Nuclear Engineering, Tohoku University for supporting the  $^{60}\text{Co}$   $\gamma$ -ray irradiation.

#### References

- 1) W.B.Fowler, *Semicond. Insul.* **5** (1983) 583.
- 2) D.L.Griscom, *J. Non-Cryst. Solids* **13** (1985) 51.
- 3) D.L.Griscom and E.J.Friebele, *Phys. Rev. B* **34** (1986) 7524.
- 4) E.J.Friebele and D.L.Griscom, *Mat. Res. Soc. Symp. Proc.* **61** (1986) 319.
- 5) C.J.Delbecq, W.Hayes and P.H.Yuster, *Phys. Rev.* **121** (1961) 1043.

# AN EPR STUDY OF X-RADIATION DAMAGE IN $\text{Eu}^{2+}$ -DOPED $\text{BaFBr}$

R. S. Eachus and R. H. D. Nuttall  
Research Laboratories  
Eastman Kodak Company  
Rochester, NY 14650 USA

This is a preliminary report of a spectroscopic study to determine the role of europium in the radiation damage of barium fluorohalides. Takahashi et al. (1,2) have studied the stable products of X-radiation damage in  $\text{Eu}^{2+}$ -doped  $\text{BaFBr}$  by optical, electrical and EPR methods. While their assignment of the trapped electron states as F-centres is not currently in doubt, their reported observation of the oxidation of  $\text{Eu}^{2+}$  to  $\text{Eu}^{3+}$  is surprising. EPR studies by Nicollin and Bill have shown  $\text{Eu}^{2+}$  is substitutional for  $\text{Ba}^{2+}$  in this material (3). Since the impurity is divalent, charge compensation by lattice defects is unnecessary and it should have a low coulombic cross section for hole trapping. At low dopant levels, direct ionisation of the dopant during X-irradiation is unlikely, so that a valence state change necessitates a secondary reaction with mobile intrinsic radiation damage products. Atomistic defect calculations by Baetzold suggest that an exciton collapse mechanism to produce F- and H-centres is energetically favourable in  $\text{BaFBr}$  (4). Thus, if hole trapping by  $\text{Eu}^{2+}$  does indeed occur, it probably involves a reaction with mobile H- or  $\text{V}_\text{K}$ -centres.

The present study was undertaken to identify the secondary hole centres produced by bandgap irradiation ( $E > 8.7$  eV) and to monitor their interaction with dispersed  $\text{Eu}^{2+}$  centres in  $\text{BaFBr}$ . This material crystallises with the  $\text{PbFCl}$  matlockite structure in the tetragonal space group  $\text{P4/nmm}$  (5). EPR spectra were obtained from oriented single crystals of nominally pure materials after their exposure to X-rays at 77 K. The spectra were obtained at 25 K using 50 mW of microwave power. Under these conditions, EPR signals from the F-centres were broadened, generally preventing their resolution. From rotation studies in selected crystal planes, the spectra were assigned to a  $\text{Br}_2^- \text{V}_\text{K}$ -centre oriented with the internuclear axis about  $35^\circ$  out of the  $ab$  plane. This assignment is consistent with the predictions of atomistic defect calculations (6) and with the results of similar EPR studies on  $\text{BaFCl}$  by Yuste and coworkers (7). At 120 K, the  $\text{V}_\text{K}$  centre began to decay as the result of thermally induced diffusion. At 150 K annihilation was complete.

The irradiation experiment was repeated on a series of samples containing between 1 and 100 mppm  $\text{Eu}^{2+}$ . Even at concentrations less than 10 mppm, the yield of  $\text{V}_\text{K}$ -centres was significantly reduced by the europium dopant.  $\text{Eu}^{2+}$  is paramagnetic and was easily detected by EPR in the crystals prior to and following X-irradiation. In all cases, the concentration of  $\text{Eu}^{2+}$  did not decrease as a result of X-ray exposure at 77 K, nor did it change when the irradiated samples were annealed above 120 K. These EPR studies indicate there is no propensity for  $\text{Eu}^{2+}$  to react with  $\text{V}_\text{K}$ - or H-centres in  $\text{BaFBr}$ .

Our results are consistent with recently published luminescence studies by Sun and Su (8). These authors have presented clear evidence for electron trapping by  $\text{Eu}^{3+}$  in powders of BaFBr exposed to X-rays, but have shown that the resultant  $\text{Eu}^{2+}$  has a low recombination cross section.

1. K. Takahashi, J. Miyahara, and Y. Shibahara, J. Electrochem. Soc. 132, 1492 (1985).
2. K. Takahashi, K. Kohda, and J. Miyahara. J. Lumin. 31 and 32, 266 (1984).
3. D. Nicollin and H. Bill, J. Phys. C: Solid State Phys. 11, 4803 (1978).
4. R.C. Baetzold, this conference.
5. B.W. Liebich and D. Nicollin, Acta Cryst. B33, 2790 (1977).
6. R.C. Baetzold, Phys. Rev. B 36, 9182 (1987).
7. M. Yuste, L. Taurel, M. Rahmani, and D. Lemoyne, J. Phys. Chem. Solids 37, 961 (1976).
8. X. Sun and M. Su, paper AF09, International Conference on Luminescence, Beijing, August 17-21, 1987.

# NONLINEAR POLARIZATION SPECTROSCOPY OF F<sub>2</sub>-CENTERS IN KCl

Boiko S.A., Brodin A.M., Dykman M.I., Lisitsa M.P.,  
Tarasov G.G., Voska R.<sup>\*</sup>, Feldvari I.<sup>\*</sup>

Institute of Semiconductors of AS UKR.SSR, Kiev, USSR

<sup>\*</sup>Research Laboratory for Crystal Physics of the Hungarian  
Academy of Sciences, Budapest, Hungary

The spectroscopy of self-induced change of light polarization (SCLP) is seemed to be the effective technique for study of the dynamical properties of reorienting centers in alkali halides<sup>[1,2]</sup>. We report on the investigation by means of this technique the F<sub>2</sub> centers in KCl. F<sub>2</sub> centers have D<sub>2h</sub> symmetry and reorient in field of radiation resonant with M<sub>F</sub> transitions. The latter process results in SCLP effect in cubic crystal.

For theoretical consideration of SCLP we suppose that reorientation is absent in the ground electronic state while the excited F<sub>2</sub>-center reorients in such way that F-electron and the nearest anion interchange only. In this approximation the self-induced change for light, propagating along the [001] axis is described by nonlinear differential equation

$$\frac{dV}{dz} = iF(V) \left[ -\frac{x_1}{x_1} (V + V^*) (1 - V^{*2})^{-1} + f^{-1} (2x_2 - x_1) (2x_2'' - x_1'') V (1 - |V|^2) \right],$$

$$F(V) = \frac{x_1'' |1 - V^2|^2 f}{(1 + |V|^2) [4f + x_1'' (x_1'' + 2x_2'') |1 - V^2|^2]}, \quad (I)$$

$$f \equiv f(V) = (x_1'' |V|^2 + 2x_2'') (x_1'' + 2x_2'' |V|^2).$$

Here x, y directions are parallel to <100> axes; z-coordinate is taken in units  $\frac{2\pi\omega}{cVE} N$ , where N is the concentration of defects;  $x_{1,2}$  is resonant polarizability of F<sub>2</sub> centers for the light polarized perpendicularly to the center axis.

The orientation of polarization ellipse and the degree of ellipticity are defined by parameter V. The direction of

turn of polarization at small crystal thickness depends on the orientation  $\alpha_0$  of linear polarization for incident light within the interval  $0^\circ < \alpha_0 < 45^\circ$ . Such dependence is typical for the  $\langle \text{IIO} \rangle$  centers and does not appear for the  $\langle \text{IOO} \rangle$  or the  $\langle \text{III} \rangle$  centers in cubic crystal.

The experimental dependence of angle between the major semi-axis of polarization ellipse for radiation passed through the crystal and the  $[\text{IOO}]$  crystalline axis on corresponding

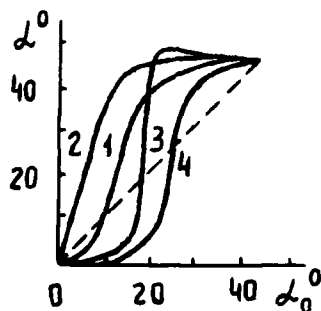


Fig.1 The dependence  $\alpha$  on  $\alpha_0$  for different wavelengths: 1 - 510.7 nm, 2 - 534 nm, 3 - 573 nm, 4 - 590 nm.

angle  $\alpha_0$  for incident light is shown in Fig.1. The turn of polarization ellipse equals to  $\alpha - \alpha_0$ . As can be seen from Fig.1 the angular dependence of SCLP is complex, nonmonotonous. All qualitative features of curves 1-4 are well described by Eq.1, if one uses simple gaussian approximation. The sharp dependence  $\alpha(\alpha_0)$  may be obtained from Eq.1 and is observed experimentally in some spectral range. Note, that the theoretical dependences are very

sensitive both to the energy positions of  $M_{F1}$ ,  $M_{F2}$  transitions and to the parameters of  $F_2$ -center on the whole.

1. Boiko S.A., Valakh M.Ya., Dykman M.I. et al. Fizika tverd. tela, 1986, 28, 2769.
2. Boiko S.A., Brodin A.M., Valakh M.Ya. et al. Fizika tverd. tela, 1987, 29, 2212.

INVESTIGATION OF IMPURITIES IN CUBIC CRYSTALS BY MEANS OF  
NONLINEAR POLARIZATION SPECTROSCOPY

Boiko S.A., Brodin A.M., Valakh M.Ya., Dykman M.I.,  
Lisitsa M.P., Tarasov G.G., Shpak A.M.

Institute of Semiconductors of AS Ukr.SSR, Kiev, USSR

In defect crystals there appear the significant nonlinear optical effects in the range of resonant absorption already at comparatively weak optical fields. The investigation of these ones allows to obtain the important data on the properties of defects. The effect of self-induced change of light polarization (SCLP) in impure cubic crystals is the matter of particular interest. The study of SCLP effect and its spectral dependence provides both the fine information on relaxation mechanism for weak-bound impurities and on the dynamical characteristics of the impurities with several equivalent orientations within the unit cell<sup>[1]</sup>. In the latter case SCLP may manifests itself even in the nonlaser fields<sup>[2]</sup>.

Here we present the results of  $F_A(\text{Li})$ -centers in KCl crystal investigation by means of SCLP spectroscopy. The question of physical SCLP mechanism in this system is bound tightly with the question about the selection rules violation in the  $F_{AI}$  absorption band which is open to argument. This violation may be caused by revealed in<sup>[3]</sup> and used for interpretation of experimental data in<sup>[4,5]</sup> off-center position of  $\text{Li}^+$  ion in  $F_A$ -configuration. In fact, however, recent evidence suggests that alternative mechanism is actual for the violation and we give here arguments for its dynamical nature.

The experimental (points) and the theoretical (solid curves) spectral dependences of SCLP in KCl with  $F_A(\text{Li})$ -centers are plotted in Fig.1. The SCLP effect is due to the optical orientation of centers which results in optical anisotropy of cubic crystal. In  $F_{AI}$  and  $F_{A2}$  bands the center absorb predominantly the light polarized along and perpendicular to its axis respectively. If the selection rules are hold the SCLP

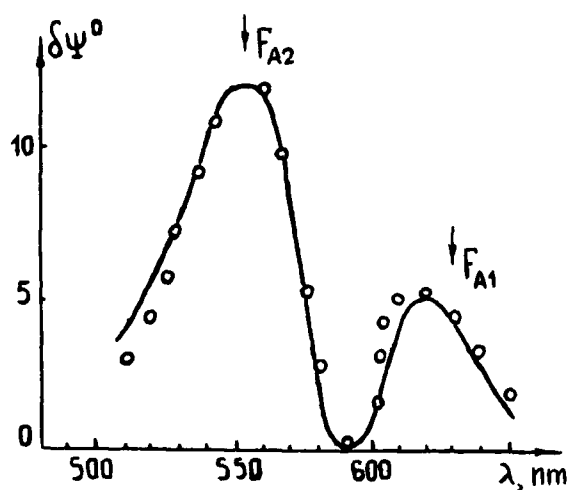


Fig.1 Spectral dependence of maximum SCLP angle in KCl with  $F_A$ (Li)-centers. Arrows point out the absorption peak positions. Radiation propagates along the  $[001]$  axis.

effect will not appear in  $F_{AI}$ -band because all centers will be oriented in  $[001]$  direction for used experimental geometry. In case of selection rules violation caused by off-center  $Li^+$  the SCLP spectrum should coincide with the absorption one. However, as can be seen from Fig.1, the spectral peak of SCLP is somewhat shifted versus the corresponding absorption one

towards short wavelengths. The nonadiabatic mechanism of selection rules violation may be responsible for observed shift. It consists in mixing of wavefunctions of nondegenerate and degenerate excited electronic states caused by the local vibration near  $F_A$ -center. The shift of peak shown in Fig.1 just corresponds to frequency of the local vibration. The consistent theory taking into account the mechanism under consideration makes it possible to describe quantitatively the spectral dependence of self-induced turn of polarization ellipse and change of the degree of polarization in crystal with different optical density, where the maximum angles of turn vary from  $2-3^\circ$  up to  $40^\circ$ .

1. Dykman M.I., Tarasov G.G. ZhETP, 1977, 72, 1081
2. Boiko S.A., Valakh M.Ya., Dykman M.I. et al. Fizika tverd. tela, 1984, 26, 2212
3. Rosenberg F., Lüty F. Sol.State Commun., 1969, 7, 983.
4. Baldacchini Y., Lallerano Y.P., Grassano V.M. et al. Phys. Rev. B, 1986, 33, 4273.
5. May M., Rzepka E., Debrus S., Hong J.P. Opt. Commun, 1987, 61, 325

MAGNETO-OPTICAL EFFECTS BY NONEQUILIBRIUM SPIN POLARIZATION  
INDUCED IN THE F-CENTER BY MODULATED AND SATURATED PUMPING

NORIO AKIYAMA, YUZO MORI,<sup>\*</sup> and HIROSHI OHKURA<sup>\*</sup>

Department of Electronic Engineering, Okayama University of Science,  
Okayama, Japan 700, and <sup>\*</sup>) Department of Applied Physics, Osaka  
City University, Sumiyoshi-ku, Osaka Japan 558.

Since the first observation of magnetic circular polarization (MCP) of the F center emission by Fontana and Fitchen,<sup>1)</sup> the magneto-optical processes in the optical pumping cycle (OPC) of F center have been extensively studied by Mollenauer and Pan,<sup>2)</sup> Winnacker et al.,<sup>3)</sup> Baldacchini et al.,<sup>4)</sup> and Ohkura.<sup>5)</sup> In the present work, we will discuss the magneto-optical effects on the absorption and emission which are caused by the nonequilibrium spin polarization (NESP) in the relaxed excited state (RES) within the same theoretical scheme of OPC. The NESP is created in the RES under the saturated and modulated pumping conditions, when the circular polarization of pumping laser light is periodically alternated between right and left ( $\sigma_+$  and  $\sigma_-$ ) with angular frequency of  $\omega$ . The NESP induces the magnetic circular dichroism (MCD) in the optical absorption and MCP in the emission: They are denoted by  $\Delta^{\text{MCD}}(\omega)$  and  $\Delta_{\eta}(\omega)$ , where  $\eta$  represents the polarizations of the analyzer ( $\sigma_+$ ,  $\sigma_-$ , and linear  $\pi$ ). So far, the  $\Delta_{\pi}(\omega)$  has been called the anomalous effect by Baldacchini et al.<sup>4)</sup> who mentioned that it is of fundamental non interest. We have measured  $\Delta_{\eta}(\omega)$  as a function of magnetic field,  $H$ , as well as photon energy excited. The form in Ref.4 did not interpret our data. In order to explain these dependences as well as  $\Delta^{\text{MCD}}(\omega)$ , which have been observed by Baldacchini et al.<sup>6)</sup>, we derived theoretical expressions of  $\Delta_{\eta}(\omega)$  and  $\Delta^{\text{MCD}}(\omega)$ , using the first order approximation of successive solutions of rate equations which govern the OPC. In these expression, the spin-lattice relaxation time in the RES,  $T_1^*(H)$ , which is dependent on  $H$ .<sup>5,7)</sup>

From fitting analysis of experimental data of  $\Delta_{\eta}(\omega)$  and  $\Delta^{\text{MCD}}(\omega)$  with theoretical expressions derived, the  $H$ -dependence of  $T_1^*$  was determined as follows,

$$\{T_1^*(H)\}^{-1} = C H^{\alpha} + (A H^3 + B H^5) \coth(g \mu H / 2kT). \quad (1)$$

where A, B, and C are constants,  $\mu$  is the Bohr magneton,  $g^*$  is the g-factor,  $\alpha$  is negative constant. Solid lines in Fig.1 are the fit curves of Eq. (1) with data for KBr and KI. Previously,  $T_1^*(H)$  was determined only in higher magnetic field range corresponding to second term in Eq.(1).<sup>6,8)</sup> The  $T_1^*(H)$  in the range below about 40 kOe is the first finding. Moreover, the  $T_1^*(H)$  determined from the present analysis of  $\Delta^{MCD}(\omega)$  are found to be the same form as Eq.(1). The fact that the first term in Eq.(1) is proportional to  $H^\alpha$  below about 40 kOe implies that the relaxation mechanism is plausibly due to the exchange effect between neighboring two RES, whose spreading radius was estimated to be about 70 Å.

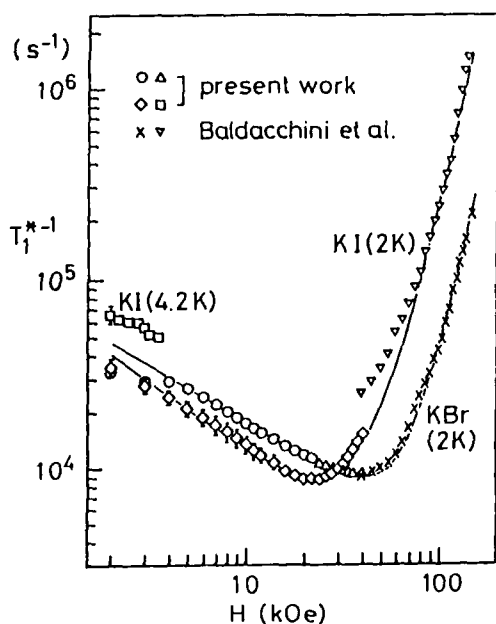


Fig.1.

Experimentally determined values of  $T_1^*$  is plotted as a function of H for KBr and KI. Solid lines are eq.(1).  $\nabla$  and  $\times$  are taken from Ref. 8.

#### References:

- 1) M.P.Fontana and D.B.Fitchen, Phys.Rev.Lett. 23, 1497 (1969).
- 2) L.F.Mollenauer and S.Pan, Phys.Rev. B6, 772 (1972).
- 3) A.Winnacker, K.E.Mauser, and B.Niesert, Z.Phys. B26, 97 (1977).
- 4) G.Baldacchini, U.M.Grassano, and A.Tanga, Phys.Rev. B16, 5570 (1977).
- 5) H.Ohkura, Cryst.Latt.Def. & Amor.Mat. 12, 401 (1985).
- 6) G.Baldacchini, U.M.Grassano, and A.Tanga, Phys.Rev. B19, 1283 (1979).
- 7) N.Akiyama, K.Kawano, Y.Mori, and H.Ohkura, J.Phys.Soc.Jpn. 53, 1927 (1984).
- 8) G.Baldacchini and U.M.Grassano, Phys.Rev. B28, 4855 (1983).

LASER EMISSION AND CONCENTRATION QUENCHING OF THE  
 $F_A(II)$  CENTERS IN KCL:LI

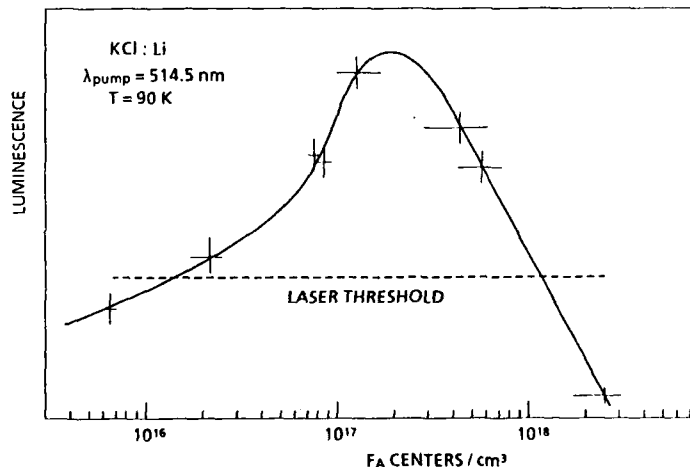
G. Baldacchini, E. Giovenale\*, U.M. Grassano†, M. Meucci<sup>o</sup>,  
 A. Scacco\*\* and M. Tonelli<sup>o</sup>  
 ENEA, Dip. TIB, U.S. Fisica Applicata, P.O. Box 65,  
 00044 Frascati (RM), Italy

The  $F_A$  center is one of the simplest perturbed F centers and, besides its importance as a model case in the physics of defects, it has been also studied in relation with the development of an important class of color center lasers, which have unique characteristics in the near infrared region.

In order to improve the efficiency of the laser, many efforts have been devoted to the optical cavity design, to the pumping geometry and to the sample preparation (1). Using the  $F_A(II)$  centers, the pumping geometry is important because of the photo stimulated reorientation of the centers.

A correct orientation of the crystal axes with respect to the cavity axis and to the pumping laser polarization is required to avoid or to minimize the bleaching of the centers (2).

To compensate for the reorientation phenomena one can increase the  $F_A$  center concentration at least up to the onset of the  $F_A$  concentration quenching of the  $F_A(II)$  emission. The 2.6  $\mu$ m luminescence of 2.0 mm thick crystals containing  $F_A(II)$  centers as a function of the concentration, is plotted in the Figure.



The dashed line shows the laser threshold for our folded astigmatically compensated cavity. It is evident the onset of the emission decrease at  $N(F_A) = 3 \cdot 10^{-17} / \text{cm}^3$ .

The mechanism of the emission quenching in a crystal containing only F centers is well known and it consists at low temperatures in a tunnelling of the excited electron towards a nearby F center, thus forming an unstable F' center (3). For the  $F_A(\text{II})$  centers, although the concentration quenching has a trend similar to that of the F centers, the mechanism must be different because we did not discover any emission change under application of a magnetic field up to 85 kGauss. The alignment of the electron spin due to the magnetic field does not increase the luminescence as found for the F center.

This fact implies, provided the spin mixing parameter is not much bigger than that of the F center, either that the quenching is not due to the  $F_A \rightarrow F'_A$  tunnelling or that the  $F'_A$  center can be formed with parallel electron spin, i.e. in a bound triplet state.

On the other hand in the heavily colored samples we have found the presence of  $M_A$  centers and of their luminescence at 1.2  $\mu\text{m}$ . However, their density more than one order of magnitude smaller than that of the F centers seems to be too low for supposing a concentration quenching due to a non radiative energy transfer towards  $F_A$  and  $M_A$  centers. New experiments are under way to check the existence of a bound triplet state of the  $F'_A$  center and clarify the nature of a new luminescence in the near infrared.

#### References and footnotes

- 1) L.F. Mollenauer in Laser Handbook, eds M.L. Stitch and M. Bass, North-Holland Amsterdam 1985, chap. 2, pag. 143
- 2) M. Meucci et al.: Opt.Comm. 51, 33 (1984)
- 3) F. Porret and F. Luty: Phys.Rev.Lett. 26, 843 (1971)
- (\*) ENEA student
- (+) Dipartimento di Fisica, II Università di Tor Vergata, Roma, Italy
- (<sup>o</sup>) Dipartimento di Fisica, Università di Pisa, Italy
- (\*\*) Dipartimento di Fisica, Università La Sapienza, Roma, Italy.

# OPTICAL PROPERTIES OF LASING COLOR CENTERS IN FLUORIDES

G. Hörsch and H. J. Paus

2. Physikalisches Institut, Universität Stuttgart  
D-7000 Stuttgart 80, Pfaffenwaldring 57, W-Germany

Color centers, suitable for tunable laser action, have been found in the perovskite crystal  $\text{KMgF}_3$  when doped with lead and irradiated with x-rays at room temperature [1,2]. Even at low temperatures, these systems show an undesirable fading effect under high power excitation. The electronic and configurational structures of the color centers are being investigated to determine the cause of their limited stability.

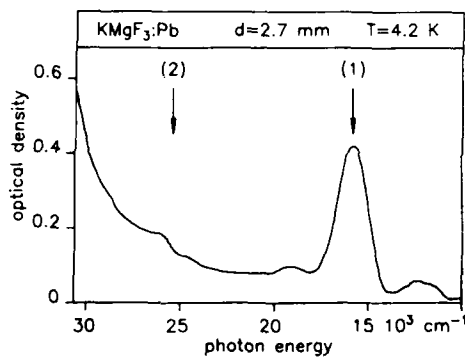


Fig.1: Absorption spectrum of  $\text{F}_Z(\text{Pb})$  centers in  $\text{KMgF}_3$  obtained by x-ray irradiation and subsequent bleaching in the F and  $\text{F}_3$  bands at room temperature.

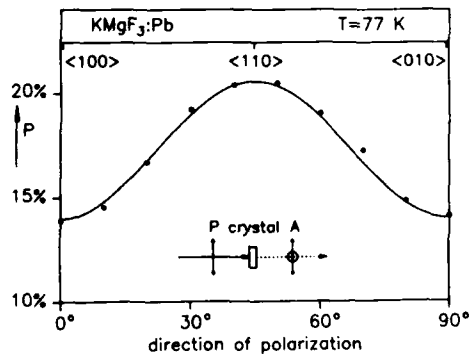


Fig.2: Angular dependence of the degree of polarization of the emission of  $\text{F}_Z(\text{Pb})$  centers.

The absorption spectrum of the center has similar features as that of the isoelectronic  $Tl^0(1)$  or  $F_A(Tl)$  center in alkali halides: three absorption bands located at (1) 15.8, (2) 25.8 and (3)  $\sim 37 \cdot 10^3 \text{ cm}^{-1}$ . Only bands (1) and (2) are shown in Fig.1; band (3) is hidden under the F band, but is unambiguously detected by excitation spectroscopy. At low temperatures, band (2) shows an interesting resolved phonon structure with a characteristic frequency of  $3.4 \cdot 10^{12} \text{ s}^{-1}$ . As proved by the degree of polarization of the emission (Fig.2) and by a linear dichroism of the absorption, the center has - at least approximately -  $\langle 110 \rangle$  axial symmetry. The thermal reorientation of the centers is characterized by an activation energy of  $0.9 \pm 0.1 \text{ eV}$  and an attempt frequency of  $1 \cdot 10^{12} \text{ s}^{-1}$ . Magneto-optical experiments reveal further similarities to the above mentioned  $F_A(Tl)$  centers. The center has therefore been called  $F_Z(Pb)$ : an F center in the immediate neighborhood of the  $Pb^{++}$  impurity built-in on a monovalent  $K^+$  site, but not on a  $Mg^{++}$  site. This position requires a charge compensating cation vacancy.

The reorientation is identified as a jump of the F center between equivalent sites around the  $Pb^{++}$  ion. The limited optical stability is probably due to an "evaporation" of the anion-cation vacancy pair into the lattice after a transfer of the electron onto the impurity.

More stable center configurations are expected in lattices where no charge compensating vacancies are necessary. First experiments have therefore been performed on alkaline earth fluorides like  $BaF_2$ . The structure of the absorption spectrum is similar to that described for  $KMgF_3$  except for the location of the F band relative to the Pb bands. Following the literature /4/ the F band should be located between the two low-energy Pb bands at  $12.9$  and  $20.6 \cdot 10^3 \text{ cm}^{-1}$ , but is not found after x-ray irradiation.

/1/ G. Hörsch and H.J. Paus Opt. Comm. **60(1,2)**, 69 (1986)

/2/ W. Flassak, A. Göth, G. Hörsch and H.J. Paus  
IEEE J. Quantum Electronics in press.

/3/ L.F. Mollenauer, N.D. Vieira and L. Szeto  
Phys. Rev. **B27**, 5332 (1983)

/4/ W. Hayes, Crystals with the fluorite structure,  
Clarendon Press, Oxford 1974

ON THE TEMPERATURE DEPENDENCE OF THE REFRACTIVE INDEX OF A LASER  
ACTIVE KCl:Li CRYSTAL

K.-E. Peiponen, P.Silfsten and K.Karttunen

Väisälä laboratory, Department of Physics, University of Joensuu,  
SF-80100, Finland

Colour centre lasers are nowadays widely used for spectroscopic studies as well as for soliton generation in optical fibers. There are several alkali halides, containing various types of defects suitable to act as a lasing material.

When pumping the colour centre crystal with a laser there will exist instabilities due to thermal changes of the lasing crystal. One reason for the frequency instability of the colour centre laser is the changing of the refractive index as a function of temperature.

We have studied the optical properties of laser active KCl:Li crystal, which possess a relatively high output power compared to other alkali halides containing  $F_A(II)$  or  $F_B(II)$  centres. We have calculated the change of the refractive index as a function of the frequency of the incident light and the temperature of the crystal, with the aid of the measured optical density data, by making use of Kramers-Kronig relations. We have been able to optimize the change of the refractive index near to zero as a function of temperature for specific wave lengths of the pumping laser. This result allows us to minimize the above mentioned instabilities. The results seem to have similar nature as those reported in refs. /1,2/.

One of us (K.-E.P ) wishes to thank the Academy of Sciences, Finland, for a grant.

References

- /1/ K.-E. Peiponen and A.Vahtinen, Phys.Lett., 103A, 209 (1984)
- /2/ K.-E. Peiponen, P. Ketolainen, A. Vahtinen and J. Riissanen, Opt. Laser Techn., 16, 203 (1984)

OPTICAL STUDIES OF ELASTIC ORDER-DISORDER TRANSFORMATIONS  
IN DOUBLE-MIXED ALKALI-HALIDE-CYANIDE CRYSTALS

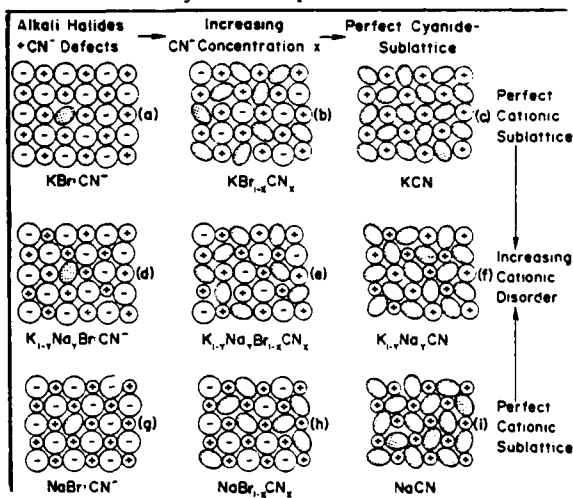
Jaime Ortiz-Lopez \*\*

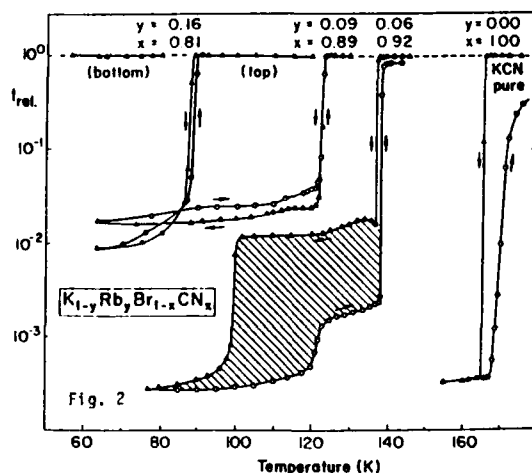
Escuela Superior de Fisica y Matematicas-IPN, UPALM, 07738 Mexico DF Mexico

Fritz Luty

Physics Dept., University of Utah, Salt Lake City, Utah 84112, USA

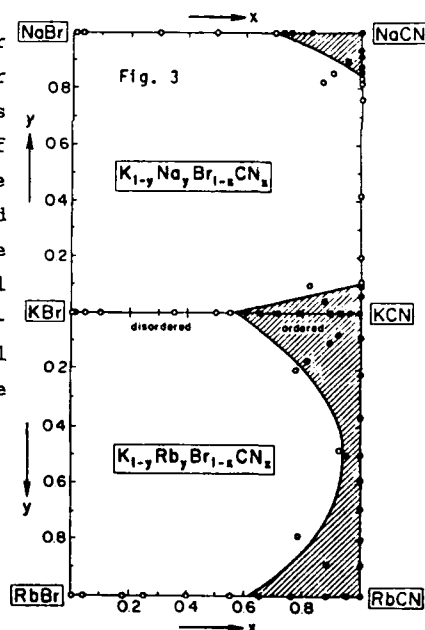
Based on the elastic and electric order-disorder transition of pure alkali-cyanides, a lot of scientific interest has focused recently on mixed cyanide crystals which serve as important model systems for the competition between long-range-order crystalline and orientational glass structure<sup>1</sup>. All crystals studied so far were produced either by variation of only the  $\text{CN}^-$  concentration  $x$  (e.g.  $\text{KBr}_{1-x}\text{KCN}_x$ ), or by mixture of the alkali-ions (e.g.  $\text{K}_{1-y}\text{Na}_y\text{CN}$ )---i.e. systems illustrated in Fig. 1 by variations of either  $x$  or  $y$  along the edges of the schematic structure-survey-diagram. For the first time we extend these studies to systems in which both the cyanide- and cationic-sublattice is disordered: proceeding gradually from the edges into the  $xy$  plane of the structures illustrated in Fig. 1. As a powerful and simple technique we use laser-light-transmission experiments, detecting accurately the presence of order/disorder changes at a critical temperature  $T_c$  by the abrupt appearance of light scattering due to the formation of multi-domain structure. Monitoring the relative optical transmission  $t_{\text{rel}}$  as a function of  $T$  and crystal composition allows us the detection of various phases as well as hysteresis and thermal cycling effects<sup>2</sup>. Fig. 2 shows as one example a measurement of  $t_{\text{rel}}(T)$  for a mixed  $(\text{K}_{1-y}\text{Rb}_y\text{Br}_{1-x}\text{CN}_x)$  system with indication of the  $x$  and  $y$  concentrations used. Starting from the pure KCN ( $x=0, y=1$ ) crystal with sharp transition at  $T_c = 163\text{K}$ , small  $x$  and  $y$  variations cause pronounced shifts of  $T_c$ , appearance of secondary





xy concentration plane in which either long range elastic order (shaded area) or glass-like disorder (white area) is obtained under cooling. Construction of detailed three-dimensional  $(x,y,T)$ -phase diagrams is at this stage still hindered by the scarcity of data, which however we are working on to overcome. Several important features and trends in the 2-dimensional  $(x,y)$  and 3-dimensional  $(x,y,T)$  order disorder behavior are already apparent and will be discussed.

intermediate phases with large hysteresis--until finally at a critical concentration  $(x_c, y_c)$  the non-appearance of light scattering under cooling is reached: the latter effect indicates the concentration-borderline between ordered and glass-like disordered behavior of the material. From numerous measurements of this type we can map out in Fig. 3 for two double-mixed systems the regions of the



\*Supported by NSF grant DMR 87-06416,

\*\*CDFAA-IPN Fellow.

- 1) F. Luty in "Defects in Insulating Crystals," Springer Verlag 1981.
- 2) J. Ortiz-Lopez and F. Luty, Phys. Rev. B 37 (part I and II) April 1988.

SPECTRAL HOLE-BURNING IN THE SECOND HARMONIC ABSORPTION  
OF ROTATIONALLY LOCALIZED CN DEFECTS IN ALKALI HALIDES

M. Schrempel, W. Gellermann, and F. Luty  
Physics Department, University of Utah  
Salt Lake City, Utah 84112

We report initial results of our investigation into the spectral hole-burning properties of  $CN^-$  defects in cesium halides which are rotationally aligned by neighboring  $K^+$  or  $Rb^+$  impurities.

The  $\text{CN}^-$ -alkali ion impurities produce two sharp vibrational absorption lines  $\nu_1$  and  $\nu_2$  corresponding to two possible orientations of the  $\text{CN}^-$  electric dipole moment with respect to the neighboring alkali-ion impurity<sup>1</sup>. The relative populations of these two dipole orientations--following a Boltzmann equilibrium at  $T \geq 100$  K--become frozen in at lower temperatures. The  $\text{CN}^-:\text{K}^+$  and  $\text{CN}^-:\text{Rb}^+$  IR absorption transitions are shifted to slightly lower energies compared to those of isolated  $\text{CN}^-$  molecules. In their second harmonic transitions near  $2.4 \mu\text{m}$ --although ~100 times weaker than the fundamental ones--they can be detected nearly free of isolated  $\text{CN}^-$  background transitions.

We used a single-mode tunable  $\text{KCl}:\text{Li}^+$  laser system (Fig. 1) to burn and probe spectral holes in these transitions at low temperatures ( $T \approx 10$  K).

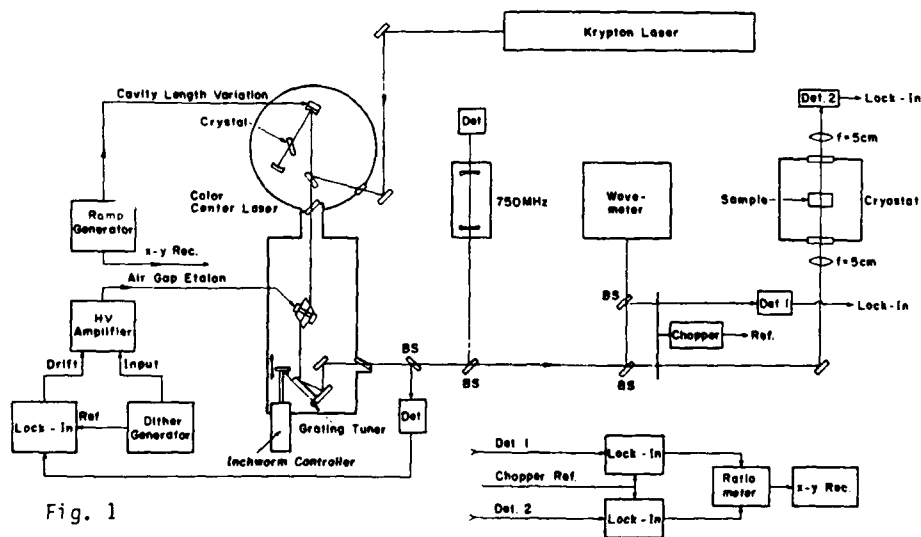


Fig. 1

Spectral holes were obtained in the  $\nu_1$  and  $\nu_2$  modes of  $\text{CN}^-:\text{K}^+$  and  $\text{CN}^-:\text{Rb}^+$  defects in CsCl, CsBr and CsI hosts. The holes appear to be persistent in CsCl and CsBr hosts while slowly decaying in CsI. The hole-burning efficiencies decrease in the sequence  $\text{CsCl} \rightarrow \text{CsBr} \rightarrow \text{CsI}$ . Comparing the hole-burning efficiencies for  $\text{CN}^-:\text{K}^+$  and  $\text{CN}^-:\text{Rb}^+$  in the same host lattice, we measure a factor  $\sim 2$  higher burning efficiency for  $\text{CN}^-:\text{K}^+$ .

In Fig. 2 a typical spectral hole is shown as an example for the  $\nu_2$  mode of  $\text{CN}^-:\text{K}^+$  defects in CsBr. After hole-

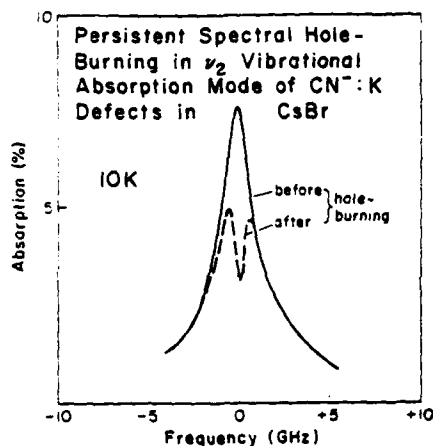


Fig. 2

burning in the  $\nu_2$  mode a spectral absorption spike (anti-hole) with equal oscillator strength was measured for this system in the  $\nu_1$  mode. Similarly, burning holes in the  $\nu_1$  mode produced anti-holes in the  $\nu_2$  mode. This reversible effect strongly suggests that 180 degree  $\text{CN}^-$  reorientations can be optically induced at low temperatures.

The burnt hole-widths measured in all defect modes were in the order of several hundred MHz to 1 GHz. Compared to the spectral hole-widths obtained recently for similar  $\text{CN}^-:\text{Na}^+$  defect modes in KBr hosts under excitation of

the fundamental transition<sup>2</sup>, these widths are about one order of magnitude larger. The nature of this broadening effect (strong homogeneous broadening contribution to the vibrational linewidth?, broadening effects due to vibrational energy transfer at the used high defect concentrations?), as well as a microscopic kinetic model for the center reorientation effect, are under current study.

This work was supported by NSF grant DMR-87-06416 and ONR contract N0014-86-K-0258.

#### References:

1. W.v.d. Osten and F. Luty, Phys. Rev. **35**, 7684 (1987).
2. R.C. Spitzer, W.B. Ambrose, and A.J. Sievers, Phys. Rev. B **36**, 7307 (1986).

## TUNABLE COLOUR CENTRE LASERS IN THE RANGE 150-800 nm

P. Fabeni, G.P. Pazzi, R. Linari, A. Ranfagni, and L. Salvini

Istituto di Ricerca sulle Onde Elettromagnetiche del C.N.R.

Via Panciatichi 64, 50127 Firenze, Italy

Laser tunability, presently offered by a lot of laser types, is very useful for linear and non linear spectroscopy. Wideband tunable lasers in the visible region, such as dye lasers, show photochemical degradation (bleaching) which reduces to some extent their applications, while the ultraviolet is covered essentially by second-harmonic generation with a large expense of intensity or by not tunable lasers, as the excimer ones. These considerations justify for a search of other types of laser materials capable of wideband optical gain in the visible and uv regions not suffering the overmentioned limitations. A number of attempts have been made to obtain lasing action in color centres, whose well known luminescent properties make them candidates for realizing new tunable lasers.

The possibility of obtaining laser action in the ir region using colour centres in alkali-halides was well established and at present the range  $0.8-4 \mu$  is almost entirely covered by solid state tunable lasers.

In the range 150-800 nm a number of impurity centres have been investigated. Table I summarizes the main features of the active media, working at room temperature, which demonstrated lasing action. In Table II other impurity centres, which exhibit optical amplification, are reported.

In these systems there is a coupling between the electronic configuration and the lattice so that the relaxed excited states suffer a distortion in order to destroy the symmetry of their configuration: the electronic degeneracy is removed and substituted by a vibronic one ( Jahn - Teller effect ).

Table I : Crystals for vibronic lasers

Doped Crystal	Acronym or common name	Tunability range (nm)	Operating modes	Reference
Cr:BeAl <sub>2</sub> O <sub>4</sub>	alexandrite	701-818	CW,pulsed	Walling(1980)
Cr:Be <sub>3</sub> Al <sub>2</sub> (SiO <sub>3</sub> ) <sub>6</sub>	emerald	729-809	pulsed	Shand(1984)
Cr:Y <sub>3</sub> Ga <sub>5</sub> O <sub>12</sub>	YGG	730-780	CW	Struve(1985)
Cr:Gd <sub>3</sub> Ga <sub>5</sub> O <sub>12</sub>	GGG	740-800	CW	idem
Cr:Y <sub>3</sub> Sc <sub>2</sub> Ga <sub>3</sub> O <sub>12</sub>	YSGG	740-800	CW	idem
Cr:Gd <sub>3</sub> Sc <sub>2</sub> Ga <sub>3</sub> O <sub>12</sub>	GSGG	745-820	CW,pulsed	idem
Cr:Gd <sub>2</sub> Sc <sub>2</sub> Al <sub>3</sub> O <sub>12</sub>	GSAG	778-790	CW	Drube(1984)
Cr:KZnF <sub>3</sub>		780-865	CW	Brauch(1984)
Ti:Al <sub>2</sub> O <sub>3</sub>	sapphire	666-1040	CW,pulsed	Moulton(1985)
Li:MgF <sub>2</sub>	} with M <sub>A</sub> centres	620-750	pulsed	Shkadarevich(85)
Na:CaF <sub>2</sub>		720-840	pulsed	Archangelskaya(79)
Ce:LiYF <sub>4</sub>	YLF	305-335	pulsed	Ehrlich(1979)
Ce:LaF <sub>3</sub>		275-315	pulsed	idem
Nd:LaF <sub>3</sub>		168-175	pulsed	Waynant(1982)

Table II : Crystals with optical amplification

Doped Crystal	Peak emission(nm)	Operating temperature	Reference
F <sup>+</sup> :CaO	360	LNT	Duran(1978)
Ag <sup>-</sup> :KI	337	LHeT	Schmitt(1985)
Ag <sup>-</sup> :RbBr	324	LHeT	idem
Tl <sup>+</sup> :CsI	430	RT-LNT	Pazzi(1983)

The trends of the research in this field concern with further investigation on the above phosphors and a search for new colour centres. For the evaluation of their optical gain an useful technique is the Amplified Spontaneous Emission (ASE). We developed a modified ASE method which permits optical gain evaluation through measurements of emission intensity as a continuous function of the pumped region length.

**FAR INFRARED REFLECTIVITY SPECTRA AND LATTICE DYNAMIC  
OF LOW-TEMPERATURE PHASES OF NaCN.**

G. Gorczyca, P. Bourson and D. Durand  
Centre Lorrain d'Optique et Electronique du Solide  
Université de Metz- Supélec - 2, rue E. Belin  
57078 Metz Cedex 03 - (France)

NaCN crystal undergoes order-disorder phase transitions. At high temperature NaCN is pseudo-cubic with NaCl structure. As the temperature is lowered a first order phase transition occurs at 288 K when  $\text{CN}^-$  dumbbells align along a  $[110]$  direction of the cubic phase. This ferroelastically ordered phase has a body centered orthorhombic structure with a space group  $D_{2h}^{21}$  (1). This order-disorder transition is accompanied by a strong light scattering due to the multidomain structure of the sample.

A second order phase transition takes place at 173 K when  $\text{CN}^-$  electric dipoles align in an antiferroelectric order of orthorhombic symmetry with a  $D_{2h}^{17}$  space group (2).

The aim of this work is to understand the ordering process of these transitions and the partially polarized Raman Spectra already measured at low temperatures (3).

IR unpolarized reflectivity spectra have been measured both in the ferroelastically ordered orthorhombic phase at 190 K and in the antiferroelectric orthorhombic phase at 10 K.

A four parameters semi quantum model (4) is used to determine LO and TO frequencies of vibration for a given polarisation of light. Since no polarized spectra can be achieved in either phase, due to the multidomain structure of the samples, this model has been adjusted in order to take into account contributions of each polarisation in the unpolarized recorded IR spectrum.

The lattice dynamic of the two ordered phases is also calculated using a rigid ion model which take into account coulombian long range interactions. From Raman and IR experimental results the phonon frequencies and their dispersion in the Brillouin zone are determined and rotational-translational mode couplings are deduced from the analysis of the phonon eigen vector. Amplitude of vibration, in relation with the polarizability of the  $\text{Na}^+$  and  $\text{CN}^-$  ions can explain the experimental Raman intensities.

From these calculations, agreement with IR experimental results appears also satisfactory and will be discussed.

- 1) J.M. Rowe, J.J. Rush and E. Prince. J. Chem. Phys. 66 n° 11, 5147 (1977)
- 2) D. Fontaine, C.R. Acad. Sci. Ser. B281, 443 (1975)
- 3) D. Durand, L.C. Scarvado Do Carmo, A. Anderson and F. Lúty. Phys. Rev. B22 4005 (1980)
- 4) D.W. Berreman and F.C. Unerwald. Phys. Rev. 174, 791 (1968)

Double bridging impurity structures and hypervalent  
state of molecular chlorine in vitreous silicon dioxide

by E.M.Dianov, V.O.Sokolov, V.B.Sulimov

Institute of general physics,  
Academy of Science of the USSR, Moscow

Hydrogen, chlorine and fluorine are known to be most characteristic technological impurities in silica glass used for optical fibers. Therefore we have performed computer simulation of defects formed by these impurities interacting with atomic net of the glass. Double bridging structures are found to exist for atomic impurities F and Cl and for molecular impurities  $H_2$ ,  $F_2$  and  $Cl_2$ . We have performed also simulation of a defect arising as a result of interaction of a  $Cl_2$  molecule with regular Si-O-Si linkage - the  $(OCl_2)$  defect.

The calculation was carried out by means of the MINDO/3 method using molecular cluster  $O_3Si_2-O-Si_2O_3$ , the dangling bonds of oxygen atoms being saturated with  $SiH_3$  groups. While calculating the  $(OX)$  defect an impurity atom  $X_C$  was placed near the bridging oxygen atom O. When dealing with the  $(X_2)$  defect the O atom was substituted by the second impurity atom X. The  $Cl_2$  molecule was placed initially near bridging oxygen atom in the  $(OCl_2)$  defect. Equilibrium configuration was obtained for each by means of minimization of the cluster formation energy relatively to positions of the defect's atoms.

For hydrogen impurity the double bridging structure was found to take place only in the  $(H_2)^0$  defect. Covalent bonds  $Si_A-H_C$ ,  $Si_B-H_C$  and  $Si_A-H_{C'}$ ,  $Si_B-H_{C'}$  turned out to form in the defect, the former two bonds being twice as intensive as the latter ones. The  $(H_2)$  defect was energetically unfavoured in comparison with neutral oxygen vacancy. It was found to form two pairs of local states near the edges of forbidden gap. Dipole transitions of an electron turned out to be allowed from the upper level of the lower twofold occupied pair to both levels of the upper (unoccupied) one.

For fluorine and chlorine impurities the double bridging structures proved to exist in defects  $(OX)^-$ ,  $(OX)^0$ , and  $(X_2)^0$ ,  $(X_2)^+$ , an extreme analogy taking place between  $(OX)$  and  $(X_2)$  defects. One can trace this analogy with the following correspondance of charge states taken into account:  $(OX)^- \sim (X_2)^0$ ,  $(OX)^0 \sim (X_2)^+$ , which is due to a superfluous electron on F or Cl atom in comparison with O atom.

$(OX)$  defects characterized by formation of  $Si_A-X_C$  and  $Si_B-X_C$  bonds the  $Si_A-O_C$  and  $Si_B-O_C$  bonds remaining practically unchanged in comparison with regular ones. In  $(X_2)$  defects one of the impurity atoms formed true bridging linkage analogous to the  $O_C$  atom in  $(OX)$  defects, the second impurity atom interacting more slightly with Si atoms. One ought to emphasize ionic part of those bonds being approximately 30% and 70% for F and Cl, respectively. The  $(OF)$ ,  $(F_2)$  and  $(OCl)$  defects were proved to be energetically favoured over both the regular linkage Si-O-Si and the neutral oxygen vacancy (the  $(Cl_2)$  defect - only over the vacancy). Hence the concentration of the defects under consideration must be significant in silica doped with fluorine or chlorine.

Electronic structure of the  $(OX)$  and  $(X_2)$  defects was found to be similar. Both defects formed four (for F) and five (for Cl) levels in forbidden gap of silicon dioxide, the two for F (three for Cl) lowest

levels being twofold occupied in (OX) and ( $X_2$ ). Electron transitions turned out to be dipole allowed from upper level of occupied ones to both unoccupied levels situated near upper edge of the gap. Wave functions of corresponding levels in (OX) and ( $X_2$ ) defects practically coincided while the atomic orbitals of  $O_C$  atom being substituted by the orbitals of  $X_C$  atom.

In the neutral defect ( $OCl_2$ ) the  $O_C, Cl_C$  and  $Cl_C'$  atoms were found to lie in a plane orthogonal to Si-Si axis forming a system with fourfold coordinated oxygen atom O: the latter in general conformed the conception of hypervalent threecenter bond between two chlorine and bridging oxygen atoms. Covalent bonds  $Si_A-O_C$ ,  $Si_B-O_C$  (twice relaxed in comparison with the regular ones) and  $O_C-Cl_C$ ,  $O_C-Cl_C'$  proved to exist in the defect. There are also Si-Cl bonds in the defect, but all of them being 60% ionic.

Electrons in many-center orbitals were found to contribute principally to the  $O_C-Cl_C$  and  $O_C-Cl_C'$  bonds, the orbitals being formed with various combinations of atomic orbitals centered on  $O_C$ ,  $Cl_C$ ,  $Cl_C'$  and also on  $Si_A$  and  $Si_B$  atoms. There were two main types of the many-center orbitals. Principal contribution to the  $O_C-Cl_C$  and  $O_C-Cl_C'$  was found to arise from 2p-orbitals of the  $O_C$  atom and 3s-orbitals of the  $Cl_C$ ,  $Cl_C'$  atoms overlapping in the first case and from p-orbitals of both  $O_C$  and  $Cl_C$ ,  $Cl_C'$  atoms in the second case. Energy levels of the many-center orbitals lie in the depth of valence band (in the region of -12...-10 eV and -8...-6 eV respectively). Besides that, electrons in the last occupied gap level of the defect (see below) were proved to contribute appreciably to the  $O_C-Cl_C$  and  $O_C-Cl_C'$  bonds causing the defect to be stabilized in the configuration with fourfold coordinated oxygen atom. It should be noted that the ( $OCl_2$ ) defect formation was accompanied by electron density transferring from the  $O_C$  atom and the  $Si_A-O_C, Si_B-O_C$  bonds to the  $Cl_C$ ,  $Cl_C'$  atoms and the  $O_C-Cl_C$ ,  $O_C-Cl_C'$  bonds. As a result, the negative charge of the  $O_C$  atom decreased almost 2.5 times compared with the regular glass net, while the  $Cl_C$  and  $Cl_C'$  atoms turned out to be negatively charged (-0.35|e|). It was the charge redistribution which caused the  $Si_A-O_C$  and  $Si_B-O_C$  bonds to be weakened and the  $O_C-Cl_C$  and  $O_C-Cl_C'$  bonds to arise. The relaxation of the silicon-oxygen bonds in comparison with regular Si-O-Si linkage proved to be practically completely compensated due to the silicon-chlorine bonds. This resulted in the values of the cluster formation energy being practically equal in both cases (-17 eV) and hence the regular linkage Si-O-Si and hypervalent one turned out to be equivalent in energetical sense.

The ( $OCl_2$ ) was found to form seven levels being localized mainly on  $Si_A$ ,  $Si_B$ ,  $O_C, Cl_C$  and  $Cl_C'$  atoms. The lowest five levels turned out to be twofold occupied with electrons in the ground state of the defect. There were no allowed dipole transitions between the defect levels. Hence the ( $OCl_2$ ) defect proved to be observable only in local phonon modes of the glass.

( $OCl_2$ )<sup>+</sup> and ( $OCl_2$ )<sup>2+</sup> charge states of the defect were also calculated. One (or, what is more, two) electron removal from the ( $OCl_2$ ) defect was proved to result in the defect destruction. Hence the ( $OCl_2$ ) defects may be regarded as sources of atomic (or even molecular) chlorine interstitials in some radiation and thermal induced processes of defect formation.

OH<sup>-</sup> Displacement in CsCl at Low Temperatures Calculated from the Frequency  
Shift Associated with the F<sub>H</sub>(OH<sup>-</sup>) Center.

by

Philip W. Gash

Physics Department, California State University

Chico, CA 95929-0202

Recently, Krantz and Luty<sup>1</sup> measured the vibrational mode IR absorption of OH<sup>-</sup> in CsCl for the isolated case, where the OH<sup>-</sup> is a substitutional impurity. They found a narrow band below 30K which broadened above 45K due to quasirotational behavior. In a separate work dealing with the perturbed case where the OH<sup>-</sup> is the n.n.n. to an F Center, thereby forming an F<sub>H</sub>(OH<sup>-</sup>) Center, they found a 58 cm<sup>-1</sup> decrease in the vibrational mode energy compared to the isolated case.<sup>2</sup> The purpose of this paper is to discuss a simplified model to account for the energy decrease.

At low temperatures prior to quasirotational behavior, the OH<sup>-</sup> dipole is modeled as two point charges with the c.m. displaced from the lattice site along either <100>, <110> or <111>. The dipole moment is allowed two orientations, either along or opposite to the c.m. displacement. The model is motivated by a recent calculation where good agreement with the F<sub>H</sub>(OH<sup>-</sup>) Center absorption bands is obtained for an OH<sup>-</sup> c.m. displacement of 0.15 Å along <100>.<sup>3</sup>

The vibrational energy decrease is attributed to the difference between the effective spring constants for the OH<sup>-</sup> dipole in the two cases. The k value is determined by calculating the total potential energy of the OH<sup>-</sup> dipole as a function of the O - H internuclear separation; it is then fitted to a polynomial in the displacements and the coefficient of the quadratic term is set equal to k/2. This method is similar to that used by Field and Sherman in their study of CN<sup>-</sup> in the alkali halides.<sup>4</sup>

The potential energy terms include the free  $\text{OH}^-$  energy, the Born-Mayer repulsive interactions with the other ions,<sup>5</sup> the interaction with the  $\text{F}_\text{H}^-$  Center electron, and the interactions with the point positive charges necessary to create the  $\text{F}_\text{H}$ -Center vacancy and the off-center  $\text{OH}^-$  displacement from the perfect lattice.

In the model, the  $k$  value difference is dependent upon the  $\text{F}_\text{H}$ -Center electron ground state wave function and the  $\text{OH}^-$  configurations for the two cases. In the perturbed case, the wave function and the corresponding dipole orientation and c.m. displacement have been calculated. The  $k$  value difference is known from the two measured vibrational mode energies; consequently, the unknowns in the model are the c.m. displacement and the dipole orientation for the isolated case. Calculation of the repulsive interaction with the n.n.  $\text{Cs}^+$  ions indicates a preferred orientation along  $\langle 100 \rangle$ , however the contribution to the energy shift is quite small because the  $\text{OH}^-$  is not in contact with the  $\text{Cs}^+$  ions. Hence, a c.m. displacement of  $0.10 \text{ \AA}$  in either  $\langle 100 \rangle$ ,  $\langle 110 \rangle$  or  $\langle 111 \rangle$  with the dipole moment pointing away from the lattice site produces agreement with the  $58 \text{ cm}^{-1}$  decrease in the vibrational energy. There is a  $10 \text{ cm}^{-1}$  decrease due to the interaction with the F Center and a  $48 \text{ cm}^{-1}$  decrease due to the c.m. shift. In contrast to the results of Field and Sherman, the Born-Mayer repulsive interaction contributes less than  $+1 \text{ cm}^{-1}$  to the shift.

The author thanks Professor Fritz Luty for two preprints and several informative discussions dealing with  $\text{OH}^-$  behavior in the alkali halides.

- 
1. M.Krantz and F.Luty, Phys. Rev. B37, April 15 (1988)
  2. M.Krantz and F.Luty, Phys. Rev. B37 May 15 (1988)
  3. P.W. Gash, Phys. Rev. B35, 774 (1987)
  4. G.Field and W.Sherman, J. Chem. Phys. 47, 2378 (1967)
  5. C.Coulson, Valence (Oxford University Press, Oxford England 1960) p.315

DEFECT STRUCTURES AND IONIC TRANSPORT IN LITHIUM OXIDE

A.V. Chadwick, K.W. Flack, J.H. Strange,  
Faculty of Natural Sciences, University of Kent,  
Canterbury, Kent, CT2 7NH, U.K.

and

J.H. Harding, Theoretical Physics Division,  
UKAEA Harwell Laboratory, Didcot, OXON, OX11 0RA, U.K.

Lithium oxide,  $\text{Li}_2\text{O}$ , has been proposed as a "blanket" material for deuterium-tritium fusion reactors and there is considerable interest in its defect and transport properties. The material adopts the anti-fluorite structure with the  $\text{Li}^+$  ions forming a simple cubic array with alternate cubes occupied by  $\text{O}^{2-}$  ions. It is usually assumed that many of the properties can be predicted by a direct analogy with the closely-related fluorite-structured crystals, e.g. alkaline earth fluorides,  $\text{PbF}_2$  and  $\text{SrCl}_2$ . Thus the dominant defects are expected to be cation-Frenkel pairs and the cation vacancies should be the more mobile defect species. If this analogy is correct then a high temperature thermal anomaly, which is common in fluorite-structures [1], might also be expected and the ionic conductivity above the temperature of the anomaly should be very high, in the "superionic" or "fast-ion" conductor range, with a low activation energy.

Recently [2], we have measured the ionic conductivity of pure and  $\text{Mg}^{2+}$  doped  $\text{Li}_2\text{O}$  in the range 300 to 1300K. The results were computer least-squares fitted on the basis of cation-Frenkel pairs being the dominant defects and cation vacancies as the mobile species. This yielded a defect formation enthalpy,  $h_F$ , of 2.53 eV and a  $\text{Li}^+$  vacancy migration enthalpy,  $h_{m+}$ , of 0.49 eV. On the basis of conductivity measurements alone it is not possible to identify unambiguously the nature of the dominant defects and therefore additional computer simulations using the HADES [3] and SHEOL [4] codes were performed for  $\text{Li}_2\text{O}$  [1]. These yielded results in excellent agreement with the conductivity, i.e.  $h_F = 2.12$  eV and  $h_{m+} = 0.21$  eV and confirmed that

Schottky defects were energetically unfavourable, the calculated formation enthalpy,  $h_s$ , being 5.15 eV. The defect entropies were also calculated and the simulated conductivity was in good agreement with experiment.

In the above work there were indications in the conductivity of the doped samples of a transition to a superionic region; however, the temperature range was not extensive. In this contribution we will report new conductivity results which extend the temperature range to 1600K. In addition, we will present calculations for  $\text{Li}_2\text{O}$  from a molecular dynamics simulation, a technique which has proved extremely powerful for fluorite-structured materials [5].

#### References

- [1] Chadwick, A.V., 1983, Solid State Ionics, 8, 209.
- [2] Chadwick, A.V., Flack, K.W., Strange, J.H., and Harding, J.H., 1988, Solid State Ionics, in press.
- [3] Catlow, C.R.A. and Mackrodt, W.C., 1983, in "Computer Simulation in Solids, Lecture Notes in Physics, Volume 166", eds. C.R.A. Catlow and W.C. Mackrodt (Springer, New York), p. 3.
- [4] Harding, J.H., 1985, Phys. Rev., B, 32, 6861
- [5] Dixon, M. and Gillan, M.J., 1980, J. Phys. C. 13, 1901 and 1919.

MOLECULAR DYNAMICS SIMULATIONS OF ALKALI BORATE GLASSES

W. Soppe and H.W. den Hartog

Solid State Physics Laboratory,  
1 Melkweg, 9718 EP Groningen, the Netherlands

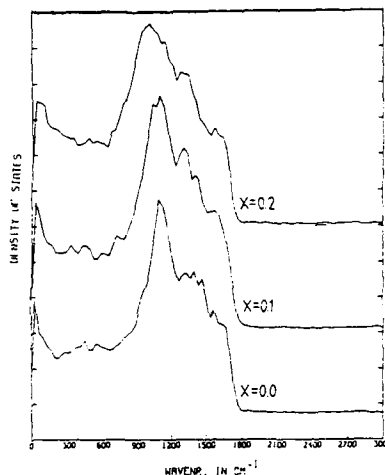
Alkali borate glasses are of great interest because of their large ionic conductivity. In order to understand these super-ionic properties, many structural investigations (e.g. X-ray, NMR, Raman and IR spectroscopy) have been performed. As a result of these studies, a model of the structure of borate glasses has been constructed; the so called Krogh-Moe model [1]. In this model it is stated that  $v\text{-B}_2\text{O}_3$  almost completely consists of randomly connected boroxol rings (six membered planar hexagonal rings). Addition of alkali oxide, according to this model would increase the coordination number of a part of the B atoms in the rings from 3 to 4. Latter structural groupings are also found in crystalline alkali borates. It should be noted however that the structure of crystalline  $\text{B}_2\text{O}_3$  does not contain boroxol rings [2]. During the last decade the doubt about the existence of these rings in the network of borate glasses has grown. X-ray, NMR and IR spectroscopy results appear to be well understandable assuming a glass structure consisting of randomly connected planar  $\text{BO}_3$  triangles and trigonal  $\text{BO}_4$  units.

In this paper we present the results of Molecular Dynamics (MD) simulations of borate glasses. The calculations were performed on the Amsterdam CYBER 205 vector processor, using the computer program library GROMOS [3]. A Born-Mayer-Huggins potential was used to calculate the atomic interactions [4,5]. We have simulated borate glasses with various lithium oxide and lithium chloride concentrations.

Analysis of the radial distribution functions yields that the network of the MD simulated glasses consists of randomly connected  $\text{BO}_3$  and  $\text{BO}_4$  units. Addition of  $\text{Li}_2\text{O}$  leads to an increase of the glass density, accompanied by an increase of the nearest neighbour (NN) distances. Addition of  $\text{LiCl}$  gives rise to a glass network with lower density and smaller NN distances. These results are confirmed by earlier experimental work [6].

Evaluation of the time-dependent self-correlation function  $G_S(r,t)$  shows that below the congelation temperature of the simulated glasses (about 1500 K) the motion of lithium atoms changes from random walk diffusion into jump diffusion. At low temperatures the lithium ions probably travel through the glass by means of a hopping mechanism, with the atoms jumping from one interstitial position to another. The vibrational properties of the glasses can well be investigated by an analysis of NN oscillations. The density of states spectrum of B-O pairs appears to agree qualitatively well with IR spectra (see Fig. )

Fourier spectrum of vibrations  
of B-O pairs at 300 K  
for  $(B_2O_3)_{1-x}(Li_2O)_x$ .



This work forms part of the research program of the "Stichting Fundamenteel Onderzoek der Materie - FOM". The MD simulations were made possible by financial support from the "Werkgroep Gebruik Supercomputers".

#### References:

1. L.D. Pye, V.D. Frechette and N.J. Kreidl, eds., Borate glasses, structure, properties, applications (Plenum, New York, 1978). / 2. G.E. Gurr, P.W. Montgomery, C.D. Knutsen and B.T. Gorres, Acta Cryst. **B26** (1970) 906. / 3. H.J.C. Berendsen et al., J. Chem. Phys. **81** (1984) 3684. / 4. T.F. Soules, J. Chem. Phys. **73** (1980) 4032. / 5. W. Soppe, C van der Marel and H.W. den Hartog, J. Non-Cryst. Solids, in the press. / 6. W. Soppe, F. Aldenkamp and H.W. den Hartog, J. Non-Cryst. Solids **91** (1987) 351.

DEFECT STRUCTURE AND ENERGETICS IN CALCIA STABILIZED ZIRCONIA

A. Dwivedi and A.N. Cormack  
NYS College of Ceramics  
Alfred University  
Alfred, NY 14802 USA

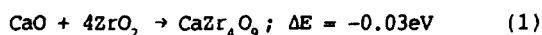
The defect structure of doped zirconia with the fluorite structure has been under investigation for some time owing to the technological importance of the material. These studies have been aimed at elucidating the role that the defect structure has in both optimising its technological performance and in controlling the long term aging or performance degradation.

Of central importance here is the question of whether the compensating oxygen vacancy occupies a nearest neighbor site with respect to the substitutional dopant (in this present case  $\text{Ca}_{2r}$ ) as suggested by Morinaga and Cohen<sup>1</sup>, on the basis of their diffuse x-ray scattering data, or whether it occupies a next nearest neighbor position as proposed by Rossell and colleagues<sup>2</sup>, based on their observations of the formation of microdomains which they identified as being  $\text{CaZr}_4\text{O}_9$  in structure.

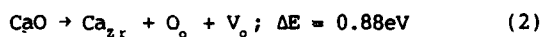
In order to provide additional insight into this problem, we have undertaken a computer simulation study of the defect structure and related energetics in calcia doped cubic zirconia. We have used an improved interatomic potential model for zirconia that takes into account the small size of the zirconium ion. Our model predicts, for example, the correct sequence of stability: cubic, tetragonal and monoclinic structures as the temperature is lowered; the large volume change in going from tetragonal to monoclinic is also reproduced and calculated static dielectric constants also follow the experimental trend. In fact, data for the tetragonal phase was not available in the literature, so we measured it and found it to be in good agreement with our previously calculated value.

In addition to calculating the stability of the  $[\text{Ca}_{2r} \cdot \text{V}_o]$  pair in both nearest neighbor and next nearest neighbor, we set up a model for  $\text{CaZr}_4\text{O}_9$

using the available structural data for the related  $\text{CaHf}_4\text{O}_9$  phase and calculated the lattice energy for this structure. By examining the energies of the following reactions:



and



We find that, firstly,  $\text{CaZr}_4\text{O}_9$  will be expected to form, but the energy of reaction (1) is small enough to suggest that this will be a long timescale process, although microdomains might form locally; secondly, the energy of reaction (2) is positive, indicating a limited solubility limit for CaO. The third conclusion is that the  $[\text{Ca}_{\text{Zr}}.\text{V}_\text{o}]$  pairs will be expected to order into superlattices or microdomains, given thermodynamic control. These results are quite consistent with our finding that the oxygen vacancy prefers to occupy the next nearest site in the case of a single  $[\text{Ca}_{\text{Zr}}.\text{V}_\text{o}]$  defect pair. Our results suggest, however, that at low dopant concentrations a number of configurations may co-exist, depending on the sample preparation history.

1. M. Morinaga, J.B. Cohen and J. Faber, *Acta Crystallogr.* A35, 789 (1979).
2. J.G. Allpress and J.H. Rossell, *J. Solid State Chem.* 15, 68 (1975).

STATIC SIMULATION STUDIES OF HIGH  $T_c$  SUPERCONDUCTORSS. M. Tomlinson<sup>(1)</sup>, C. R. A. Catlow<sup>(1)</sup>, M. S. Islam<sup>(2)</sup> and M. Leslie<sup>(3)</sup>

(1) Department of Chemistry, University of Keele, Keele, Staffs. ST5 5BG, U.K.

(2) University College London, Gordon Street, London WC1H 0AJ, U.K.

(3) Daresbury Laboratory, Daresbury, Warrington WA4 4AD, U.K.

We have used the technique of static lattice simulation to study the structural, lattice dynamical and defect properties of high  $T_c$  superconductors. Such techniques have enjoyed considerable success in previous studies of polar solids. We will briefly review the methodology of static simulation, paying particular attention to the need for a model for the lattice potential. We will show how the parameters for the potential model were derived empirically from the relevant binary oxides, including three-body terms to model the copper-oxygen interactions.

We present results for the systems  $\text{La}_2\text{CuO}_4$ <sup>(1)</sup> and  $\text{Ba}_2\text{YCu}_3\text{O}_7$ . For the former we show how the potential model correctly reproduces the structure of the orthorhombic phase. We have calculated the phonon dispersion relations for the material, which show a soft mode in the  $b$ -direction. Defect calculations have been used to investigate the energetics of oxidation and doping of the material. These reveal a large energy barrier to copper disproportionation, but find that doping with Ba and Sr are energetically favoured. The latter is shown to take place with the formation of  $\text{Cu}^{3+}$  ions, oxygen vacancies being readily annihilated. Bipolaron formation is investigated using a model which does not include a treatment of screening effects; these show that such entities are not bound.

We show how the potential model may be extended to treat screening effects in  $\text{Ba}_2\text{YCu}_3\text{O}_7$ . Using this method we are able to accurately reproduce the structure of this material. Finally we present results of defect studies of this topical material.

References

(1) M. S. Islam, M. Leslie, S. M. Tomlinson and C. R. A. Catlow, J.Phys C:Solid State Phys 21 (1988) 109.

EXTENDED X-RAY ABSORPTION AND COMPUTER SIMULATION STUDIES OF  
ELECTRO-OPTIC MATERIALS

S. M. Tomlinson<sup>(1)</sup>, C. R. A. Catlow<sup>(1)</sup>, A. V. Chadwick<sup>(2)</sup>, J. Jones<sup>(2)</sup>,  
and H. Donnerburg<sup>(3)</sup>

(1) Department of Chemistry, University of Keele, Keele, Staffs. ST5 5BG, U.K.

(2) Department of Chemistry, University of Kent, Canterbury, Kent. CT2 7NH. U.K.

(3) Department of Physics, University of Osnabruck, 4500 Osnabruck, W.Germany.

The structures of  $\text{LiNbO}_3$  and  $\text{LiTaO}_3$  were determined some years ago by X-ray diffraction techniques<sup>(1,2)</sup>. However, despite the technological importance of these materials, the nature of the intrinsic defect structure is still uncertain. Moreover, these materials are frequently used in device manufacture after doping with transition metal ions such as titanium and iron, which has a very marked effect on the refractive properties of these materials. The site preference of the dopant ions and the atomistic basis of their effect on the refractive properties are also unclear.

We have used X-ray absorption spectroscopy (EXAFS) to investigate the site preference of dopant transition metal ions (titanium, iron, cobalt and manganese) in  $\text{LiNbO}_3$  and  $\text{LiTaO}_3$ . EXAFS is a powerful technique for elucidating the local environment of dopant ions, and hence their site preference.

Our results are compared with the results of our static simulation studies. Here we also discuss the problems associated with developing models for the lattice potential of electro-optic materials. We will also discuss our results concerning the intrinsic atomistic and electronic defects in these materials.

References

- (1) S.C.Abrahams, J. M. Reddy and J. L. Bernstein, J.Phys. Chem. Solids (1966) 27, 997.
- (2) S. C. Abrahams and J. L. Bernstein, J.Phys.Chem.Solids (1967) 28, 1685.

SUBSTRUCTURES IN IONIC CRYSTALS ACCORDING TO THE SELF-CONSISTENT  
LIDIARD-DEBYE-HUECKEL THEORY

D. OUROUSHEV

FACULTY OF PHYSICS, SOFIA UNIVERSITY  
5, "A.IVANOV" Blvd., 1126 SOFIA, BULGARIA

The self-consistent electrostatic Debye-Hueckel theory was successfully applied in the theory of the point defects in ionic crystals for the first time by Lidiard (1). His approach is based on the linearized Poisson-Boltzmann equation, which is obtained by the assumption  $e\psi \ll kT$ . (Here  $\psi$  is the self-consistent electrostatic potential). The importance of solving the complete non-linear Poisson-Boltzmann equation (NPBE) was pointed out by Koehler, Langreth and Turkovich (2). Kliever and Koehler applied a solution of the NPBE to describe the subsurface space-charge layer in ionic crystals. Wide class of spatially-periodic solution of the NPBE was derived by us (4). Using these solutions an attempt have been made to explain the formation and some properties of the "Suzuki phases" (5).

In this paper all possible periodic solutions of the NPBE in the one- and two-dimensional cases will be presented (6). Using these periodic solutions it will be shown that another type of aggregates may occur in the system consisting from charged point defects. All periodic solutions of the NPBE possess divergent singularities, which makes the physical interpretation of these solutions complicated.

It will be presented an original method for the integration of these singularities and it will be shown that they are associated with localized charge with determined value. These localized charges are distributed periodically in the space and can be interpreted as a point defects substructure in the main crystal. The proposed method of

integration allows to exclude from the theory any external parameter.

According to this all characteristics of the predicted periodic substructures - period, free energy, value of the localized charge, can be expressed by the parameters of the main crystal. Consequently the presented theory describes the inherent self-organisation of the investigated defect's system.

#### REFERENCES

1. A.B. LIDIARD, Phys.Rev., 94, 29 (1954)
2. J.S. KOEHLER, D. LANGRETH and B. von TURKOVICH, Phys.Rev., 128, 573 (1962)
3. K.L. KLIEWER and J.R. KOEHLER, Phys.Rev., 140, A1226 (1965)
4. M. GEORGIEV, D. OUROUSHEV, N. MARTINOV, Crystal Latt. Defects, 9, 1 (1980)
5. N. MARTINOV, D. OUROUSHEV, M. GEORGIEV, J.Phys. C 17, 5175 (1984)
6. D. OUROUSHEV, J.Phys. A 18, L845 (1985)
7. D. OUROUSHEV, Localization of the charges according to the non-linear self-consistent theory, J.Phys. A (1988) (in press)

ATOMISTIC CALCULATIONS AND EXAFS OF HALIDE IMPURITIES IN AgBr

Y. T. Tan, R. C. Baetzold, and K. J. Lushington

Photographic and Corporate Research Laboratories,  
Eastman Kodak Company, Rochester, NY 14650 USA

The presence of halide impurities in silver bromide has been examined with atomistic simulation methods. Pair potentials are used within the framework of a central-force model for a crystal with zero lattice strain. Potentials, employed before for pure AgCl and AgBr (1), were used as the starting point for defining the Ag-Ag, Ag-Br, Br-Br, Ag-Cl, and Cl-Cl interactions. The I-I interaction was taken from potentials for the KI crystal and the Cl-Br and I-Br potentials were determined by fit to the lattice constants for solid solutions with Ag(Br,50%Cl) and Ag(Br,25%I) using a super-cell model (2,3).

Silver halide solid solutions, such as Ag(Br,I) and Ag(Br,Cl), have been simulated using these potentials together with the HADES codes. When iodide ions are substituted for bromide ions in the AgBr lattice, there is a tendency for the iodide ions to aggregate. The energy of substitution, per iodide ion, is seen to decrease upon stepwise replacement around a central silver ion. This effect is more pronounced when the central silver ion is removed, leaving a silver vacancy, as shown in Table I. When the iodide ions surround an interstitial silver ion, this energy change is smaller. Thus, when present in sufficiently high concentrations, iodide ions will exhibit a tendency for cluster formation, especially around a silver ion vacancy.

Computations of silver chloro-bromide solid solutions do not indicate any tendency towards cluster formation. The energy for substitution, per chloride ion, into the AgBr lattice remains

constant, with the 0.02 eV precision of the computations. There is no change in the substitutional energy whether the central ion is a silver ion, silver ion vacancy or interstitial silver ion. These computational results will be discussed in conjunction with EXAFS data which show the nearest neighbor positions around the substitutional halide ion in these solid solutions.

Table 1

DEFECT ENERGIES OF IODIDE AND IODIDE CLUSTERS IN AgBr

Energy (eV per iodide ion)

Defect	I - Ag	I - Ag-vac	I - Ag-int
1-I	0.885	0.805	0.93
2-I	0.885	0.77	0.78
3-I	0.625	0.44	0.69
6-I	0.40	0.04	

Acknowledgement

Discussions with C.R.A. Catlow, S. Corish, F. Healy, P.W.M. Jacobs, A. M. Stoneham, and P. W. Tasker are gratefully acknowledged.

References

1. C.R.A. Catlow, J. Corish, and P.W.M. Jacobs, J. Phys. C 12, 3433 (1979), and 13, 1977 (1980).
2. Y. T. Tan and R. C. Baetzold, submitted to J. Phys. C.
3. R. C. Baetzold, Y. T. Tan and P. W. Tasker, to be published in Surface Sci.

Deformation and Charge Transfer Effects on  
Defect Properties of Ionic Solids.

Sankar P. Sanyal and R.K.Singh

Materials Research Laboratory, Physics Department  
University of Bhopal, Bhopal-462026; INDIA.

In recent years the structure and properties of point defects in ionic crystals have been studied extensively. Because of the inherent difficulties associated with experimental investigations several theoretical methods have recently emerged [1] to explore the nature of point defects and their influence in crystalline materials. Most of these theoretical approaches use a two-body potential to represent the interactions between the ions in defect lattice. However, such a simple two-body interaction potential fails to describe the perfect crystal properties, as well as several features of defect properties, such small values of volume of formation. In an otherwise defect lattice the ions displaced appreciably from their equilibrium positions which leads to deformation of the electron shells. Recently it has been shown by Singh [2] that these deformation effects lead to many body interactions.

We have calculated the schottky defect formation energies in alkali halides, metal oxides and halides with CsCl structure using a many body interaction (MBI) potential for the first time. These MBI modify the ionic charge of the vacancy and the displaced ions and also consequent polarization mechanism in the defect lattice [3,4]. The calculated energies of formation of Schottky defects ( $E_d$ ) agree well with measured values and the contribution of MBI to  $E_d$  is about 5 to 10%. Influence of the MBI on volume of formation of Schottky defect has been investigated in details using the method suggested by Gillan [5]. The most striking feature of the present results is that it explains the low values of volume formation in four alkali halides for which data are available. The results on calculated values of F-band energies from this model are also encouraging.

1. C.R.A. Catlow and W.C. Mackrodt, 'Computer Simulation of Solids'  
Springer Verlag, Berlin (1982).
2. R.K. Singh, Physics Reports 85, 259 (1982).
3. N. Agnihotri, S.P. Sanyal and R.K. Singh, Physica B 142, 233 (1986);  
S.P. Sanyal, N. Agnihotri and R.K. Singh, Phil. Mag. 57A  
(1987); ibid Phil. Mag. Lett. 58A (1988).
4. V. Mishra, S.P. Sanyal, R.K. Singh, Phil. Mag. 55A, 583 (1987); ibid,  
Pramana 28, 217 (1987), Physica B (1988) (in press).
5. M.J. Gillan, Phil. Mag. A43, 301 (1981).

**EFFECT OF PLASTIC DEFORMATION AND  
THERMAL TREATMENTS ON THE ITC SPECTRA OF  $\text{Ba}_{1-x}\text{La}_x\text{F}_{2+x}$**

N. Suarez, M. Puma and F. Lorenzo

Physics Department, Universidad Simón Bolívar, Apartado 89.000, Caracas, Venezuela

The origin of the intense relaxation peak observed at high temperature, HT peak, in the ITC spectrum of all the solid solutions of the type  $\text{Ba}_{1-x}\text{RE}_x\text{F}_{2+x}$  where RE represents a trivalent rare-earth cation has been attributed either to the effect of the dislocations similar to a Maxwell-Wagner interfacial polarization<sup>(1)</sup> or to a space-charge relaxation due to the accumulation of charges near the electrodes<sup>(2)</sup>. The behavior of this HT peak is anomalous when compared to the well-behaved simple dipole relaxation which occurs at much lower temperatures. We present here the results of an ITC study on the  $\text{Ba}_{1-x}\text{La}_x\text{F}_{2+x}$  system for  $0.0001 \leq x \leq 0.15$  after plastic deformations or thermal treatments as compared to the non-treated crystals. The position of the maximum of the HT peak,  $T_M$ , is always a decreasing function of the doping level,  $x$ , while the height of the peak,  $H_C$ , increases for the non-treated samples as can be seen in fig. 1. After a plastic deformation consisting of a sample compression the low-temperature located dipole relaxations remain unchanged while the HT peak presents a drastic reduction in its intensity and a displacement of its maximum towards lower temperatures, as shown in fig. 2 for the crystal with  $x=0.002$  and with a deformation degree equal to 1.2%. This reduction in the  $T_M$  value was also observed for crystals quenched to room temperature from 1200K. If instead of rapidly quenching the crystals, an annealing with a low cooling rate of 10K/hr was performed the inverse behavior occurred, that is, the  $T_M$  increased again to higher temperatures. The dislocation density,  $\rho$ , was also estimated on the treated crystals and it was found that as  $x$  increases,  $\rho$  decreases for crystals with the same kind of thermal treatment. Also the polarizing conditions (applied electric field, polarization time and temperature) were varied without finding any unexpected change in the ITC spectrum of all the crystals studied here. The various results reported here can be understood in terms of the Maxwell-Wagner interfacial polarization proposed to explain polarization effects in heterogeneous dielectrics. The occlusions formed by higher conductivity regions coincident with the mobile defects cloud surrounding the charged dislocation line are characterized in this model by two geometrical factors,  $\lambda$

and  $q$  which are related to the size and fraction of the volume occupied by the occlusions. The decrease of the HT peak after the plastic deformation is interpreted following Suszyńska et al<sup>(3)</sup> by the creation of fresh dislocations together with the sweeping away of the existing dislocation lines from the charge compensating cloud that surrounded them. This effect will decrease  $\lambda$  and/or  $q$  and thus the intensity of the peak which is proportional to  $q\lambda^2$ . Also the behavior of  $T_M$  with  $x$  and the treatments of the samples is coherent with this model. The space-charge relaxation model even if it can account for some of the facts reported here does not give a complete explanation for all the experimental evidence gathered here.

- 1) E. Laredo, M. Puma and D. Figueroa, Phys. Rev. **B19**, 2224 (1979).
- 2) P. Müller, phys. stat. sol.(a). **23**, 165 (1974).
- 3) M. Suszyńska and R. Capelletti, Crystal Res. & Technol. **19**, 1385 (1984).

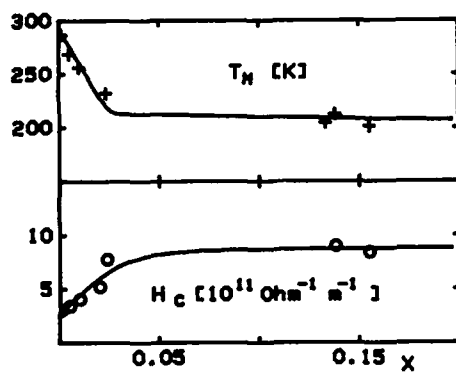


fig. 1

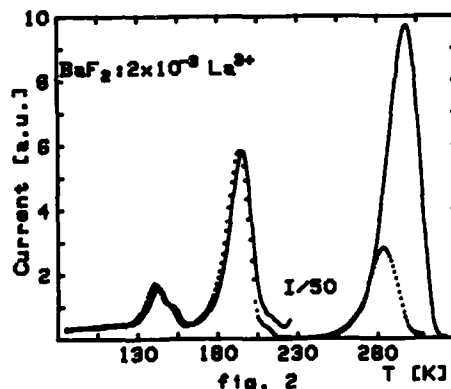


fig. 2

DIELECTRIC LOSS IN BERLINITE\*

John J. Fontanella and Mary C. Wintersgill  
Physics Department  
U. S. Naval Academy  
Annapolis, MD 210402-5026

R. D. Shannon  
Central Research and Development Department  
Experimental Station  
E. I. Du Pont de Nemours and Company  
Wilmington, DE 19898

George R. Rossman  
California Institute of Technology  
Division of Geological and Planetary Sciences  
Pasadena, CA 94025

B. H. T. Chai  
Allied Corporation  
Morristown, NJ 07960

Audio frequency complex impedance measurements have been carried out over the temperature range 5.5-380K on samples of berlinite (aluminum phosphate) both parallel and perpendicular to the optic axis. The berlinite samples contain varying amounts of water.

All berlinite samples exhibit a well-defined electrical relaxation in the vicinity of 40K. The peak is analyzed using various models such as Cole-Cole, Havriliak-Negami, and Williams-Watts and activation parameters are reported. It is found that the relaxation is about twice as strong perpendicular to the optic axis as it is parallel to the optic axis. The peak is tentatively assigned to hydroxyl ions which are incorporated into the lattice. The reason is that the strength of the peak tends to increase as the water content of the samples increases though not as fast. For example, perpendicular to the optic axis the maximum values of  $\tan(\delta)$  at 40.4K and 1000 Hz are 0.00135, 0.00168, 0.00210, and 0.00250 for nominal water concentrations of 20, 200, 250, and 1000 ppm. However, the trend is not so clear parallel to the optic axis as the 200 ppm sample fails to follow the behavior of the other samples. No direct correlation with auxiliary measurements such as IR or NMR has as yet been obtained.

With the exception of the 200 ppm sample, the materials also exhibit a relaxation above 200K. This relaxation is much stronger, with  $\tan(\delta)$  values on the order of 0.08. No trend with nominal water concentration is apparent. Also, the temperature dependence of the relaxation is not "normal" being significantly different from that observed for rare earth doped alkaline earth fluorides, for example.

Finally, the two 1000 ppm samples exhibit large conductivity losses above room temperature. This is attributed to water in the samples.

\*This work was supported in part by the Office of Naval Research.

DIELECTRIC LOSS OF OH<sup>-</sup> IONS IN ALKALI HALIDES

Laércio Gomes

Instituto de Pesquisas Energéticas e Nucleares - Caixa Postal 11049  
São Paulo - Brasil

Fritz Luty

Physics Department, University of Utah - Salt Lake City, Utah - 84112

The presence of substitutional OH<sup>-</sup> ions in crystalline matrices of KCl, KBr and RbBr at high concentrations, 10<sup>-4</sup> to 10<sup>-3</sup> mol parts, introduce low frequency dielectric loss peaks in the range of 10 to 10<sup>5</sup> Hz at LNT, measured by ac technique. The observed loss peaks are attributed to an Arrhenius type mechanism of OH<sup>-</sup> isolated dipole reorientation over the potential barrier. Each activation energy measured for reorientation is in the magnitude range of a rotational barrier height estimated for an OH<sup>-</sup> ion placed in the octahedral field of the respective host lattice. The verified linear dependence of the integrated imaginary dielectric constant  $A(\epsilon'')$  with the OH<sup>-</sup> concentration and with  $T^{-1}$ , suggested these effects were produced by isolated OH<sup>-</sup> dipoles. By correlating the loss peaks areas,  $A_2(\epsilon'')$  for the classical reorientation at LNT and  $A_1(\epsilon'')$  for quantum tunneling at LHeT, it was verified the ratio  $\frac{N_2}{N_1} = \frac{A_2 T_2}{A_1 T_1}$  between the number of OH<sup>-</sup> dipoles which effectively contribute to both processes. The ratio  $\frac{N_2}{N_1}$  was verified to be equal to  $\frac{1}{3}$  for the most dilute OH<sup>-</sup> dipole system (3.4 x 10<sup>-4</sup> mol parts of OH<sup>-</sup>) we were able to measure (by LNT loss peaks).

Our interpretation for that observation is that the classical reorientation strength is decreased by factor of 3 due to the OH<sup>-</sup> dipole quantum tunneling between the six (100) directions of equilibrium at the site. This fast tunneling decreases the effective time spent by an OH<sup>-</sup> dipole in a particular direction of the applied ac electric field during the classical jump.

THERMOLUMINESCENCE AND IONIC THERMOCURRENT IN CALCITE

J.F. de Lima

Depto. de Física, Universidade Federal de Sergipe, Brasil

E.M. Yoshimura and E. Okuno

Depto. de Física Nuclear, Instituto de Física, Universidade de  
S.Paulo, Caixa Postal 20516, CEP 01498, Brasil

In this work, samples of natural  $\text{CaCO}_3$  (crystal of trigonal symmetry) collected near Miranda, Mato Grosso do Sul, Brasil, were used. Chemical analysis of this calcite performed by X-ray fluorescent spectroscopy and atomic absorption showed the presence of the following impurities: Si, Al, Fe, Ti, Mg, Na and K. On the other hand, EPR spectrum revealed a strong characteristic signal due to Mn.

The thermoluminescence(TL) glow curves of calcite annealed at 673 K for 1h and exposed to gamma rays of  $^{137}\text{Cs}$  were obtained using a heating rate of 2.7 K/s. Figure 1 shows one typical glow curve with three peaks at 423, 523 and 623 K. Analysis using different models shows that these TL peaks obey a second order kinetics and their thermal activation energies are respectively  $(1.3 \pm 0.1)$ ,  $(1.5 \pm 0.1)$  and  $(1.7 \pm 0.1)\text{eV}$ .

Ultraviolet light strongly affects the TL induced by gamma rays, decreasing the peak heights corresponding to traps filled during the gamma irradiation. Charge transfer from deeper to shallower traps is also observed when the UV irradiation is performed after thermal annealings that eliminate the first and/or the second peaks of the TL glow curve.

The ionic thermoconductivity (ITC) spectrum of a virgin sample of calcite, shown in Figure 2, reveals four bands. The temperatures corresponding to the maxima of these bands are: 197, 212, 257 and 304 K. The amplitude of the 197 K peak is a linear function of the polarization field up to 18 kV/cm, suggesting a dipole relaxation mechanism. The activation energy corresponding to this band, obtained using the initial rise method, is 0.34 eV. Different thermal treatments could be done in order to study the nature of the bands.

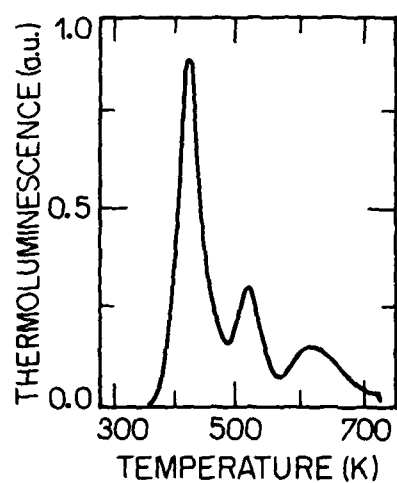


Figure 1. TL glow curve of natural  $\text{CaCO}_3$  annealed at 673 K for 1h and exposed to gamma rays of  $^{137}\text{Cs}$

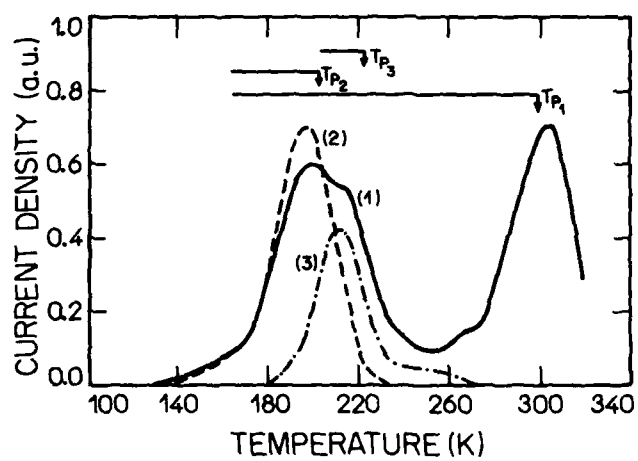


Figure 2. ITC spectrum of natural  $\text{CaCO}_3$  as received (virgin). Polarization temperatures are indicated by the arrows

IONIC THERMOCURRENTS IN NATURAL CaF<sub>2</sub>

M.E.G.Valerio, E.Okuno and A.R.Blak  
 Instituto de Física - Universidade de São Paulo  
 C.P. 20516 , CEP 01498 , São Paulo , SP , BRASIL

The present work deals with natural calcium fluoride from Criciúma , Santa Catarina. Thermally Stimulated Depolarization Currents (TSDC) can be used to determine the properties of dipole defects present in this crystal. The TSDC spectrum of this material shows three bands in the temperature range of 80 to 450 K (figure 1). The first one, at 130 K, is due to the dipoles formed by a trivalent impurity and an interstitial fluorine ion in the next nearest position of an impurity ion ( $nn R_S^{3+} - F_i^-$ )<sup>(1,2)</sup>. The second one, at 202 K, is due to the presence of small aggregates of dipoles (like a dimer)<sup>(2,3)</sup>. The last band, at 360 K is due to the formation of large clusters. The continuous distribution model gave the best fit for these bands with mean activation energies of 0.41, 0.60 and 1.02 eV for the first, second and third band respectively.

Thermal treatments can modify the number of dipoles, dimers and clusters present in the crystal. In this work we used thermal treatments between 15 minutes and 10 hours and temperatures between 473 K and 773 K. For thermal treatments at 573 K, the dipoles and dimers are created and the clusters are destroyed as the time of thermal treatment increases (figure 2a). At 673 K the clusters are created and the dipoles and dimers are destroyed (figure 2b). At 773 K the three kinds of defects are destroyed (figure 2c). An equilibrium concentration is observed after 2 to 3 hours of thermal treatment. This equilibrium concentration is a function of the thermal treatment temperature and shows a maximum, in the temperature range used around 573 K, for the dipoles and dimers, and 623 K for the clusters (figure 3).

## References:

- (1) Kitts, E.L.; Ikeya, M. and Crawford Jr., J.H.; Phys. Rev. B 8, 5840 (1973)
- (2) Capelletti, R.; Okuno, E.; Mathews, G.E. and Crawford Jr., J.H.; Phys. stat. sol. (a) 47, 617 (1978)
- (3) Laredo, E.; Puma, M.; Suarez, N. and Figueroa, D.; Sol. Stat. Ion. 9&10, 497 (1983)

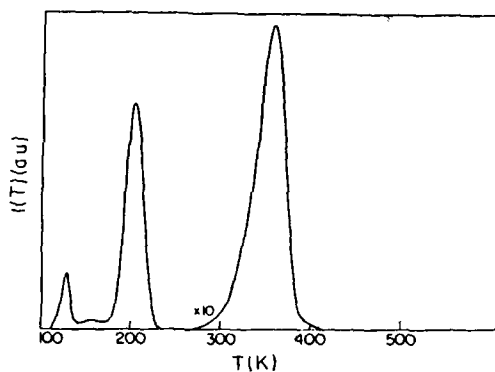


Fig. 1: ITC spectrum of a virgin green sample.

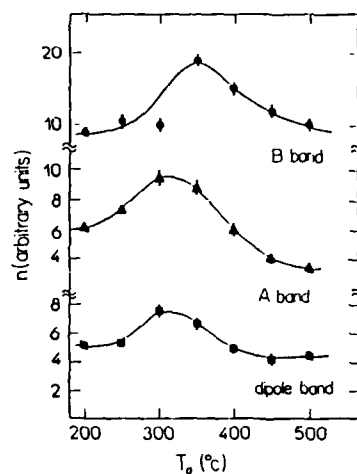


Fig. 3: Bands equilibrium area vs. thermal treatment temperatures.

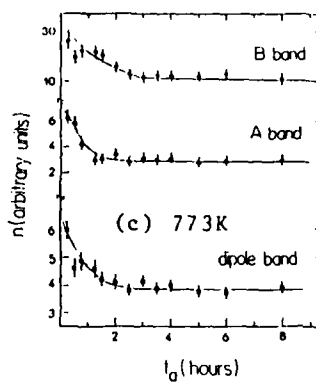
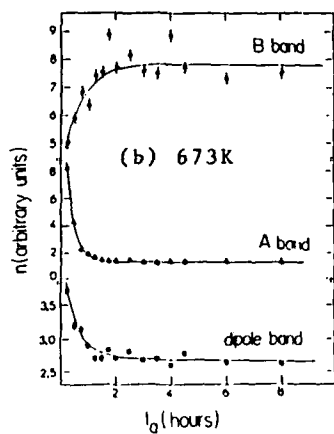
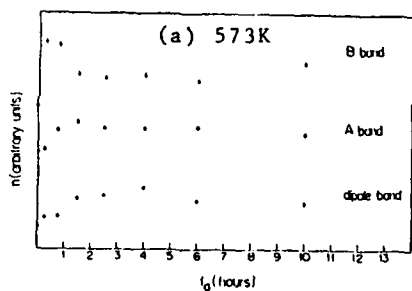


Fig. 2a, 2b, 2c: Bands area vs. time of thermal treatment at (a) 573K, (b) 673K and (c) 773K.

DIELECTRIC RELAXATIONS ASSOCIATED WITH RADIATION INDUCED  
POINT DEFECT DIPOLES IN ELECTRICALLY INSULATING CERAMICS

S.N. Buckley and P. Agnew

Materials Development Division, Harwell Laboratory, UKAEA,  
Didcot, Oxfordshire, UK

Auxiliary heating of thermonuclear plasmas by ion cyclotron resonance coupling requires prodigious quantities of radio frequency power to be transmitted into the reactor vessel via dielectric windows. The technological upper limit is defined by thermomechanical stresses induced in the window material by dielectric losses associated with point defect-impurity atom electric dipoles. Low loss compositions are essential but it is conceivable that, even then, there could be progressive deterioration in service due to high energy neutrons and  $\gamma$ -rays emanating from the plasma creating additional point defects and impurities (transmutation products) or altering their charge states.

The magnitude of such deterioration is assessed by measuring dielectric losses at MHz frequencies in refractory low loss ceramics before, during and after irradiating by 3 MeV protons, generating  $10^{-7}$  displacements per atom  $s^{-1}$ , or by 60 kV X-rays at 8 Gy  $s^{-1}$ .

Pronounced increases in dielectric loss are observed in all the materials after proton irradiation, values recorded during irradiation being marginally higher than immediately afterwards. Unlike virgin material, where low loss tends to be synonymous with purity, high grade single crystals develop much higher losses during irradiation than relatively impure polycrystalline commercial ceramics. Radiation induced defect concentrations of  $10^{-2}$  increase dielectric losses by up to three orders of magnitude.

The nature of the point defects responsible for radiation induced increases in dielectric loss is discussed.

THERMALLY STIMULATED DEPOLARIZATION CURRENTS IN  $\text{MgAl}_2\text{O}_4$ 

A. Ibarra, R. Vila and M. Jiménez de Castro

Asociación EURATOM/CIEMAT (Fusión)  
Avda. Complutense, 22.- 28040 Madrid (Spain)

Measurements of dielectric losses in a wide frequency range are of most importance for fusion applications. Besides other processes, radio frequency induced dipole oscillations might lead to energy losses at the working temperatures of fusion devices.

The thermally stimulated depolarization/polarization currents (TSD/TSP) experimental technique has been so far very useful to detect dipolar orientation (1) as well as spatial charge (2) processes. It can provide a very useful information about the dielectric constant at low frequencies.

This paper presents a study on TSD processes between 10 and 300K in polycrystalline  $\text{MgAl}_2\text{O}_4$ , which is a candidate insulator material for fusion applications. Figure 1 shows a TSD spectrum of this material at a heating rate of  $0.13 \text{ K s}^{-1}$ . Peaks at about 65 (I), 120 (II), 155 (III) and 275 (IV) K are clearly observed.

A linear dependence of peak intensities on the applied electric field ( $E_p$ ) up to  $30000 \text{ V cm}^{-1}$  has been found to occur for peaks I to III. The temperature at the maximum does not vary with the polarization temperature ( $T_p$ ). Besides this, it is unlikely to have spatial charge processes at those low temperatures; so these TSD peaks might be ascribed to dipolar relaxation processes. The peak shapes have been fitted by a recently proposed method (3) and values for activation energies and relaxation times have been obtained.

The behaviour of peak IV is different from the others. It is very wide and the temperature and the current intensity at the maximum strongly depend on the polarization temperature. These features, together with the fact that appreciable ionic conductivity values have been obtained in the temperature range in which this TSD peak appears (4) seems to indicate that it might be due to a spatial charge process.

TSP measurements are now under the way in order to confirm the proposed models.

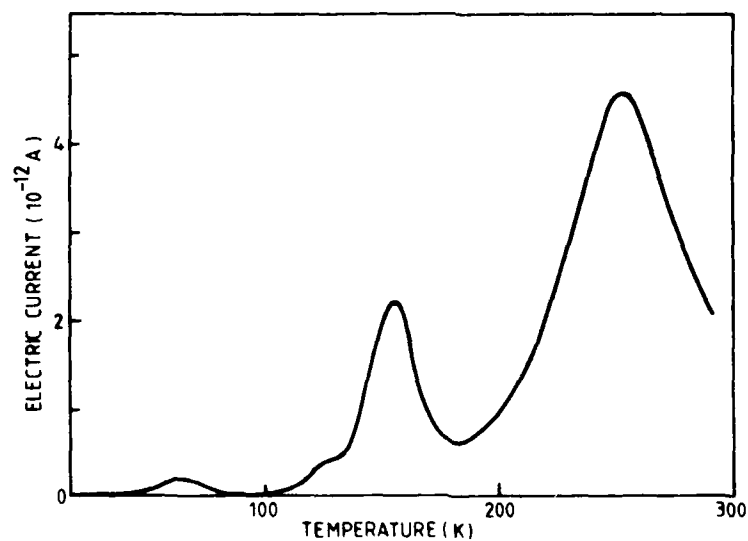


Fig. 1-TSD spectrum of  $\text{MgAl}_2\text{O}_4$  for  $E_p=6800 \text{ Vcm}^{-1}$  and  $T_p=240 \text{ K}$ .

#### REFERENCES:

1. C. Bucci, R. Fieschi and G. Guidi. Phys. Rev. 148, 816 (1966).
2. P. Müller. Phys. Stat. Solidi (a) 23, 165 (1974).
3. R. Vila, A. Ibarra and M. Jiménez de Castro. Phys. Stat. Solidi (a) (to be published).
4. A. Lorincz, M. Puma, F.J. James and J.H. Crawford Jr. J. Appl. Phys. 53, 927 (1982).

THE EVOLUTION OF DIELECTRIC PROPERTIES INDUCED BY ANNEALING OF  
NEUTRON DAMAGE IN  $\text{Al}_2\text{O}_3$

R. Heidinger<sup>a)</sup>, F. Königer<sup>b)</sup>

a) Kernforschungszentrum Karlsruhe  
Institut für Material- und Festkörperforschung  
Postfach 3640, 7500 Karlsruhe 1, FRG

b) Universität Karlsruhe  
Institut für Höchstfrequenztechnik und Elektronik  
Postfach 6980, 7500 Karlsruhe 1, FRG

Insulating ceramics form a central part for radiofrequency heating concepts in nuclear fusion technology being used as transmission windows. They combine low absorption of electromagnetic power with good mechanical behaviour, compared to insulating polymers under fast neutron irradiation originating from the D-T fusion reaction. Alumina ( $\alpha\text{-Al}_2\text{O}_3$ ), which constitutes a primary material for this application, was selected for the determination and interpretation of the changes in dielectric parameters caused by neutron induced defects.

Single crystals (sapphire) as well as dense polycrystalline material (AL23, purity: 99.5 %) were irradiated with fast neutrons to a fluence of  $2.6 \times 10^{20} \text{ n/cm}^2$  ( $E > 0.1 \text{ MeV}$ ). Model calculations for the irradiation rig revealed a maximum temperature of  $215^\circ\text{C}$ . The dielectric properties were measured at 52 MHz - within the frequency range of Ion Cyclotron Resonance Heating - and at 30 - 40 GHz - near the frequency range of Electron Cyclotron Resonance Heating (ECRH). Generally the dielectric parameters, the permittivity ( $\text{Re } \epsilon_r'$ ) and the dielectric loss tangent ( $\text{Im } \epsilon_r' / \text{Re } \epsilon_r'$ ), are increased by the stable defects set at this irradiation level. At 30 - 40 GHz for sapphire, however, an increase in dielectric loss was not resolved. Further data will be given for 145 GHz, a frequency within the range of ECRH.

The correlation of the increase in the dielectric parameters and the radiation induced defects was monitored by thermal annealing studies. Heating specimens of both materials to  $1000^\circ\text{C}$  in air for 15 h restored the dielectric parameters of the unirradiated specimens. Also the volume swelling  $\Delta V/V$ ,  $0.6 (\pm 0.1) \%$  for sapphire and  $0.5 (\pm 0.1) \%$  for AL23, in the as-irradiated samples, was no longer observed then. Series of heat treatments and dielectric measurements have been performed up to  $1100^\circ\text{C}$ , at each step increasing the annealing temperature by  $100^\circ\text{C}$ . Whereas the

curve for sapphire at 30 - 40 GHz shows only a constant small decrease in permittivity, AL23 exhibits at the same frequency strong diminuation of the dielectric parameters between 300 °C and 500 °C. For higher temperatures the behaviour approaches that of sapphire. At 52 MHz, the dielectric parameters stay at a constant elevated level up to 700 °C in sapphire. Then a rapid decrease sets in, and the values of the un-irradiated samples are reached at about 1100 °C. The annealing behaviour will be compared with heat treatments in vacuum.

Obviously the most effective sources for polarization at 30 - 40 GHz are affected by heat treatments between 300 °C - 500 °C. This type of defect is much more frequent in our polycrystalline material than in the single crystal. On the other hand, the sources for dielectric dissipation at 52 MHz are not diminished but above 700 °C. These findings will be put into relation to the investigation of Atobe et al<sup>1</sup> on aggregate centres in reactor irradiated single crystal Al<sub>2</sub>O<sub>3</sub> by thermochemical and photochemical methods, in which mono- and divacancies are seen to cluster between 350 - 450 °C and larger aggregates to anneal out between 600 °C and 900 °C.

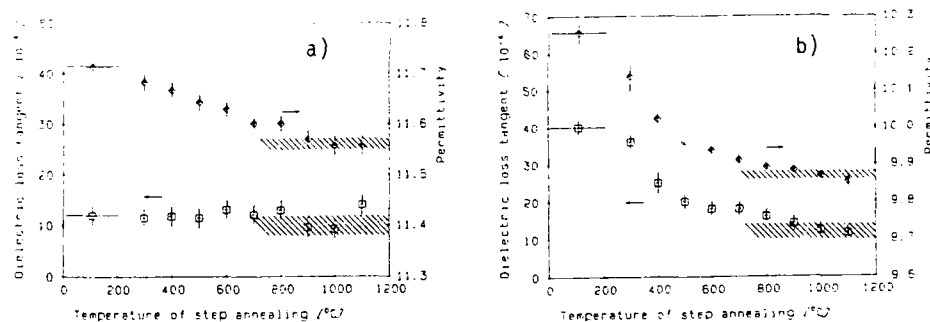


**Fig. 1:** Annealing behaviour of dielectric parameters in a) sapphire and b) AL23 irradiated to  $2.6 \times 10^{20} \text{ n/cm}^2$  ( $E > 0.1 \text{ MeV}$ ) measured at 30 - 40 GHz. Hatched areas indicate values of unirradiated material.

#### References:

- 1 K. Atobe, N. Nishimoto, M. Nagakawa, Phys. Status Solidi A 89 (1985) 155.

DIELECTRIC MEASUREMENTS OF IMPURITY INDUCED DYNAMICS IN  
Fe DOPED BaTiO<sub>3</sub>

M. Maglione, R. Böhmer, A. Loidl  
 Institut für Physik, Universität Mainz, D-6500 Mainz  
 and  
 G. Godefroy  
 Laboratoire de Physique des Solides,  
 Université de Bourgogne, F-21000 Dijon

Pure BaTiO<sub>3</sub> is an extensively studied perovskite-type crystal which undergoes a first order ferroelectric phase transition at  $T_c=403\text{K}$ . The transition is induced by the softening of an transverse optical phonon, which describes the oscillations of Ti<sup>4+</sup> ions against the surrounding oxygen cages. When the transition temperature is reached, the coherence length of these oscillations diverges giving rise to the low temperature ferroelectric phase. There is still a continuing debate whether this transition is displacive or order-disorder like. In addition, Raman scattering (1) and Electron Paramagnetic Resonance experiments (2) pointed towards a critical low frequency ( $\nu < 10^{10}\text{Hz}$ ) dynamics in BaTiO<sub>3</sub> near  $T_c$ . To elucidate some of these questions it seems essential to study the dynamics of the phase transition at frequencies from MHz to GHz and to study the influence of impurities on the behaviour at the phase transition temperature.

Here we report the first observation of the dielectric dynamics in the radio frequency range ( $1\text{MHz} < \nu < 1\text{GHz}$ ). The experimental setup was based on a Hewlett Packard 4191A Impedance Analyzer. Temperatures from 10K to 460K can be reached using a closed cycle refrigerator or an oven. The sample and the measuring port of the impedance analyzer are connected by an air line. Real and imaginary part of the dielectric constant were measured in pure Barium-Titanate and in Fe doped samples. The dielectric dispersion was measured as a function of frequency, temperature ( $T > 300\text{K}$ ) and Fe-concentration  $x$  with  $x = 0, 0.045\%, 0.075\%, 0.5\%$  and  $0.9\%$ . Special care has been taken to avoid the effects of domains on the dielectric response. Our preliminary results are consistent with low temperature ( $T < 300\text{K}$ ) data published previously (3).

Fig. 1 shows the dielectric loss  $\epsilon''$  versus frequency in BaTiO<sub>3</sub> doped with 0.075% Fe at T=414.4K. These data clearly demonstrate, that the main absorption processes occur in the MHz to GHz range. The experimental results are indicative for a single relaxation-time process. The solid line in Fig. 1 is the result of a fit using a Debye model:

$$\epsilon'' = \Delta\epsilon \Omega \tau / (1 + \Omega^2 \tau^2)$$

where the measuring frequency  $\nu = \Omega/2\pi$ ,  $\tau$  is the relaxation time and  $\Delta\epsilon$  is the dispersion step ( $\Delta\epsilon = \epsilon_s - \epsilon_\infty$ ).

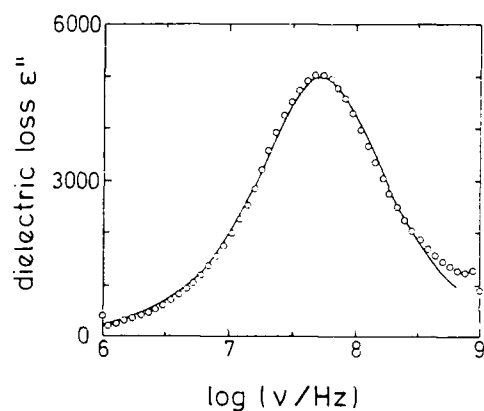


Fig. 1:  
Dielectric loss of BaTiO<sub>3</sub>  
doped with 0.075% Fe at  
T=414.4K as a function of  
frequency. The solid line  
is a result of a fit as  
described in the text.

The Debye model gives a good description of the observed dielectric dispersion and the parameters of the best fit were found to be:

$$\Delta\epsilon = 10650.$$

$$\tau = 2.94\text{ns}$$

The observed relaxational behaviour is compatible with the assumptions made from EPR experiments which were performed at 10GHz (2).

#### References:

- 1 H. Vogt, J. A. Sanjurjo and G. Rossbroich  
Phys. Rev. **B26**, 5904 (1982)
- 2 K. A. Müller and W. Berlinger  
Phys. Rev. **B34**, 6130, (1986)
- 3 M. Maglione, E. Grymaszewski and G. Godefroy  
to appear in Ferroelectrics 1988

DIELECTRIC PROPERTIES OF CONDENSED FLUOROCARBON MIXTURES

R. Böhmer and A. Loidl

Institut für Physik, Universität Mainz, D-6500 Mainz

The substitution of isotropic molecules by anisotropic species yields well defined defects states in crystals. This allows to study the molecular relaxational dynamics due to crystal field effects and due to interactions between the molecules. If the interactions are strong and dominate over single ion relaxational phenomena a glasslike freezing-in may be observed yielding a low temperature orientational glass state (1). Well studied examples of orientational glasses are alkali cyanide-alkali halide mixtures (2).

In this communication we present experimental results on mixed molecular systems. The aim was to find new candidates of orientational glasses and to investigate in detail the transition from single particle behaviour to glassy relaxation. To study the slow dynamics which is essential for an understanding of the glass state simple tetrahedrally coordinated molecules were chosen.

Attempts were made to solve the trifluorinated methanes  $\text{CHF}_3$ ,  $\text{CClF}_3$  and  $\text{CBrF}_3$  in condensed  $\text{CF}_4$ . The miscibility of liquid  $\text{CF}_4$  with various defects has been investigated in great detail (3). However, information about solubility in the solid state has so far only been achieved for the system  $\text{CF}_4:\text{Ar}$  (4). While  $\text{CF}_4$  forms a plastic crystal,  $\text{CHF}_3$  and  $\text{CBrF}_3$  freeze into dipolar rigid configurations at the melting point. Dipolar reorientations around the carbon-substituent axis could not be detected. However, in solid  $\text{CClF}_3$  (99.999% purity) dielectric relaxations were observed.

Complete solid state immiscibility of  $\text{CHF}_3$  and  $\text{CBrF}_3$  in  $\text{CF}_4$  was found, while in the mixtures with  $\text{CClF}_3$  limited solubility is observed. Here the dipolar reorientations of the  $\text{CClF}_3$  molecules in the  $\text{CF}_4$  matrix could be investigated. The miscibility behaviour is explained using arguments of solubility theories (3).

## References:

- 1 A. Loidl, J. Chim. Phys. 82, 305, 1985
- 2 F. Lüty in Defects in Insulating Crystals pp 69-99 ed. by V. M. Turkevich and K. K. Shvarts, Springer, Berlin 1981
- 3 N. Thorp and R. L. Scott, J. Phys. Chem. 60, 670, 1956
- 4 S. C. Greer and L. Meyer, J. Chem. Phys. 51, 4583, 1969

ITC - SPECTRA OF NaCl - CRYSTAL CONTAINING  $\text{Cr}^{3+}$ -IONS

M. Suszyńska\* and R. Capelletti\*\*

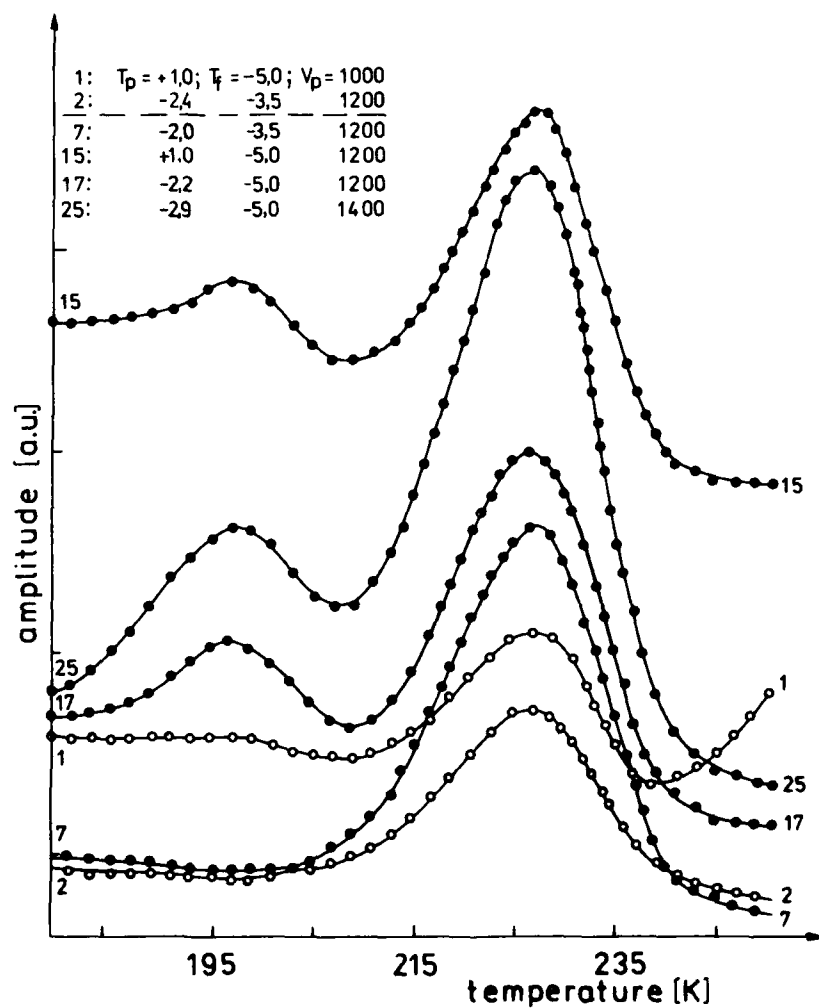
\*Institute of Low Temperature and Structure Research,  
Polish Academy of Sciences, 50-950 WROCLAW, Poland\*\*Physics Department of Parma University,  
43-100 PARMA, Italy

The purpose of the ITC-experiments described was to obtain informations concerning the properties of dipolar defects in NaCl crystals doped with  $\text{Cr}^{3+}$  ions. These studies have been complemented by spectroscopic (AAS,EPR)-, mechanical (yield stress)- and electrical (conductivity) -measurements.

Fig. 1 presents typical ITC-spectra of NaCl crystals nominally doped with 500 mppm of  $\text{Cr}^{3+}$ . Within the low -T-range the effects of polarization conditions ( $T_p, T_f, V_p$ ) are shown for as received (curves 1, 2) and, solution-treated (quenched to RT after 30 min at 873) samples (remaining curves). It is supposed that the low-T-band in as received crystals is related with I.V.V. dipoles (1  $\text{Me}^{3+}$  ion bounded with 2 cation vacancies), whereas the high-T-relaxation is of the Maxwell-Wagner type.

The analysis of these bands revealed that:

1. For the concentration range studied no simple relation between  $\text{Cr}^{3+}$ -content and band-intensities was found, indicating that the processes registered are not directly related to the dopant level. Possible reasons: not all chromium is present in the trivalent (paramagnetic) state; the small  $\text{Cr}^{3+}$  ions are partly at off-center positions with small value of dipole moments;
2. The I.V.V. ( $\text{Me}^{3+}$ ) dipole band is distinctly broader than the I.V. ( $\text{Me}^{2+}$ ) band, its amplitude is linearly dependent upon polarisation voltage, suggesting the presence of dipoles in nn- and nnn-configurations. The reaction of this peak to the choice of polarisation conditions confirms this suggestion;
3. Thermal- and mechanical-treatments are, among others related with the appearance of a new low-T-band (at the expense of the high-T-band), positioned below the dipole band. The effect of both treatments is probably related with re-distribution of the impurities segregated near fixed dislocations and with formation of complexes of much simpler nature.



Although the ITC-studies are of preliminary character, the results obtained are in qualitative (at least) agreement with the magnetical-, electrical- and mechanical-characteristics of these crystals.

# CHARACTERISTIC FEATURES OF THE BISMUTH CENTRES IN ALKALI HALIDE CRYSTALS

M. Suszyńska\* and R. Capelletti\*\*

\*Institute of Low Temperature and Structure Research,  
Polish Academy of Sciences, 50-950 WROCLAW, Poland

\*\*Physics Department of Parma University,  
43-100 PARMA, Italy

A correlated set of experiments have been performed with a view to study the defects in  $\text{Bi}^{3+}$  doped NaCl, KCl and RbCl crystals; for NaCl the effect of  $\text{BiO}^+$  centers was studied, too.

From among the data obtained the following facts merit the attention:

1. The ionic radius of the dopant ( $r_{3+}$ ) is smaller than the radius of the host cation ( $r_{1+}$ ), and for the majority of systems  $r = (r_{3+}/r_{1+}) < 0.7$  predicted as upper limit of nnn- $\text{M}^{2+}$ -I.V.-dipoles [1];
2. Hydrolytic properties of the  $\text{Bi}^{3+}$  ion are responsible for the formation of  $\text{BiO}^+$ -ions also in crystals doped with  $\text{Bi}^{3+}$  e.g. during high-T-annealing performed in air; this has been evidenced by the optical absorption- and tg  $\delta$ -measurements performed for crystals of the same origin [2];
3. Trivalent Bismuth is not paramagnetic; during all experiments performed the dopant remained in the trivalent state;
4. Optical absorption spectra of Bismuth are similar to those characteristic of other heavy metal ions with  $\text{S}^2$ -outer electronic configuration; the so called A-band was used as the concentration-band;
5. Comparison of conductivity plots ( $\sigma$  vs  $1/T$ ) with the data characteristic of nominally pure NaCl crystals proves the low solubility of  $\text{Bi}^{3+}$  in these crystals. Comparison with the data for  $\text{AH:Me}^{3+}$  systems suggests the introduction of 2 cation vacancies per each  $\text{Me}^{3+}$  ion;
6. Because of (2) and (5) some of the ITC-data are not accessible for an exact analysis, cp. the overlapping of the I.V.V.- $\text{Me}^{3+}$ -dipole band with the relaxation related to the presence of  $\text{H}_2\text{O}$ ;
7. The most characteristic features of the ITC-spectra:
  - a)  $\text{NaCl:Bi}^{3+}$ ,  $\text{BiO}^+$ : nothing in the low-T-region for as received  $\text{Bi}^{3+}$ -doped crystals; compared band for  $\text{NaCl:BiO}^+$  with relatively low activation energy; quenching from 873 K introduces a strong  $\text{H}_2\text{O}$ -relaxation; plastic

deformation introduces a second low-T-band in  $\text{BiO}^+$ -doped crystals, which strongly decreases with RT-storage;

b)  $\text{KCl:Bi}^{3+}$ : nice low-T-band (204 K) with a distinct branch at 306 K; the amplitude (H) and position (T) of the band are reacting to the choice of polarisation conditions in a similar way as was observed for  $\text{LiF:Ti}$  [3]; moreover, H is proportional to the dopant level; prolonged annealing yields a shift of T towards low T's;

c)  $\text{RbCl:Bi}^{3+}$ : distinct low-T-band (219 K), the intensity of which is practically insensitive to the choice of  $T_p$  and  $T_f$ ; prolonged annealing at 873 K introduces a second low-T-band, and causes a shift of both towards lower-T's as well as an increase of H of the high-T-band.

For all systems: H of the high-T-band is small and decreases with high-T-annealing; this treatment yields also a shift of the peak-position. The effect of plastic deformation resembles that observed for  $\text{AH:Me}^{2+}$  systems [4].

#### REFERENCES

1. R.W. Dryfus, Phys. Rev. 121 (1961) 1675
2. M. Hartmanova, M. Lébl, E. Mariani, Cryst. Lattice Def. 4 (1973) 347.
3. R. Capelletti, M.G. Bridelli, M. Frigerri, G. Ruani, I. Földvari, L. Kovacs, A. Watterich, Proc. 5th Intern. Symp. Electrets, Heidelberg (1985), New York, p. 594.
4. M. Suszyńska, R. Capelletti, Cryst. Res. Techn., 19 (1986) 1385, 1489.

KINETICS OF AGGREGATION AND PRECIPITATION  
IN NaCl CRYSTALS DOPED WITH  $\text{Eu}^{2+}$

A. Gubański\*, M. Suszyńska\*\*, D. Nowak-Woźny\*\*

\*Institute of Fundamentals of Electrotechnics and Electrotechnology,  
Technical University, 50-370 WROCLAW, Poland

\*\*Institute of Low Temperature and Structure Research,  
Polish Academy of Sciences, 50-950 WROCLAW, Poland

The kinetics of  $\text{Eu}^{2+}$ -clustering process in NaCl crystals was studied by means of the ITC technique. Two kinds of solution-treated (ST) crystals, containing 120 and 290 m ppm of  $\text{Eu}^{2+}$ , were annealed at temperatures ( $T_a$ ) between room temperature (RT) and 333 K. In order to determine the nucleation mechanism some of the ST samples were deformed. The results obtained are discussed in frames of a model elaborated previously on the basis of some optical data [1].

For an initial concentration of 97 m ppm of I.V. dipoles and  $T_a > \text{RT}$  the precipitation phenomena occur in two more or less distinct stages:

1. clustering governed by a preferential segregation near dislocations, and
2. dislocation-aided co-alescence. The former process yields clusters of unknown chemical composition, and the latter one-particles of the  $\text{Na}_2\text{EuCl}_4$ -phase [1]. The entire process is governed by the growth of loosely-bound, linear dimers already present in the ST-state.

For slightly-doped crystals (100 % of I.V. dipoles in ST-samples) the incubation-period, detected at RT, shows that this two-stage decomposition process is limited by the nucleation of dimers.

The lack - for both crystals - of a truly horizontal plateau-region suggests that the precipitation starts before the nucleation is complete.

Because the plastic deformation (1 % compression) does not change the rate of the solid solution decomposition, it has been concluded that dislocations are easy diffusion paths (promoting the growth process) rather than nucleation sites. In favour of this explanation is the activation energy characteristic of the process studied. The estimated value ( $0.7 \div 0.9$  eV) is too large for simple aggregation but distinctly smaller than

the heat of activation for a process limited by the bulk-diffusion.  
The homogeneous character of the nucleation process agrees with the coherent character of the  $\text{Na}_2\text{EuCl}_4$  particles.

#### REFERENCES

1. M. Suszyńska, A. Gubański, H. Opyrchal, Fifth Europhys. Topical Conf. "Lattice Defects in Ionic Crystals", Marid (1986), Proc. P. II 16, p. 225.

**Electron trapping in  $H^{2-}$  defects during the photoconversion of anion vacancies in thermochemically reduced CaO crystals.**

V.M.Orera

*Instituto de Ciencia de los Materiales de Aragón, Universidad de Zaragoza, Zaragoza, 50009, Spain.*

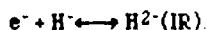
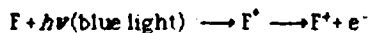
Y. Chen

*Solid State Division, Oak Ridge National Laboratory, Oak Ridge, Tennessee 37831*

The origin of the F-center phosphorescence at temperatures around 295 K in thermochemically reduced (TCR) MgO and CaO crystals has been recently elucidated [1,2]. It has been shown that the long-lived luminescence, is related to the presence of  $H^-$  ions (protons in anion sites each with two electrons) detected through their vibrational bands in the IR absorption spectra. The presence of several IR bands related to  $H^-$  ions, whose relative intensities change when samples are treated in different ways (electron irradiation, thermal annealings, doping with alkali impurities, etc) indicates that  $H^-$  ions are incorporated in the lattice during the TCR process in the form of different complexes, presumably perturbed by other defects or impurities.

Optical pumping on the F-center absorption band, which is the predominant defect in TCR crystals, produces their photoconversion to  $F^+$ -centers by a photoionization mechanism. In strongly reduced samples, the process is active even at temperatures as low as 4 K. Upon warming up, the system returns to its original state giving rise to several thermoluminescence glow peaks. Obviously, different metastable electron traps are produced during the photoconversion process. Two different electron traps involving  $H^-$  ions have been found recently in TCR MgO crystals [3]. In the present communication we show that a similar situation occurs in TCR CaO samples.

Optical pumping of the F band at temperatures above 100 K destroys one of the  $H^-$  bands ( $880\text{ cm}^{-1}$ ) and creates two new infrared bands ( $1048$  and  $1474\text{ cm}^{-1}$ ). We explain the process as follows [2]:



The reverse of this mechanism is the responsible for the F phosphorescence and thermoluminescence near 300K. The  $H^{2-}(\text{IR})$  defect is stable in the dark at lower

temperatures. The process can be efficiently reversed by exposing the samples to visible light at any temperature. In particular the  $H^{2-}(IR)$  defects are readily bleached by the F fluorescence (600nm).

Pumping with F-light at 77 K produces photoionization of F-centers and a decrease in the  $880\text{ cm}^{-1}$  local mode, but this decrease is not completely compensated by the increase of the  $H^{2-}(IR)$  bands. In contrast to F-center bleaching at higher temperatures, the  $H^-$  absorption band recovers in seconds in the dark at 77 K. The complementary evolution is observed in the EPR  $F^+$  signal. The electrons released at 77 K results in  $H^-$  complexes other than the  $H^{2-}(IR)$ . This is related with the decay of the F-center fluorescence above LNT [4].

Below 77K bleaching of F-centers does not produce any detectable change in the IR spectra. The lack of long range electronic transport is consistent with the absence of photoconductivity [4]. Near 10 K F-center bleaching is attended by the production of a different  $H^{2-}$  related defect observed by EPR [5]. The signal corresponds to a defect with low symmetry (less than axial) and can be assigned to perturbed  $H^{2-}$  ions. They are thermally unstable and accounts for the small and almost temperature independent F-center phosphorescence observed at temperatures below 30 K. The existence of close F- $H^-$  pairs in crystals having a high concentration of both F and  $H^-$  defects ( $1 \times 10^{18}\text{ cm}^{-3}$ ) is proposed. Photoionization of F-centers at low temperatures can take place via a tunnelling transfer from the F-center excited state to the  $H^-$  ions.

We conclude that at least two hydrogen related defects are active as electron metastable traps in highly coloured CaO during the  $F \longleftrightarrow F^+$  photoconversion at temperatures below RT.

- [1] V.M. Orera and Y. Chen, Phys. Rev. B 36, 6120 (1987).
- [2] V.M. Orera and Y. Chen, Phys. Rev. B 36, 1244 (1987).
- [3] Y. Chen and V.M. Orera, J. of Lumin. (in press).
- [4] L.S. Welch, A.E. Hughes and G.P. Summers, J. of Phys. C 13, 1791 (1980).
- [5] H.T. Tohver, J. Tombrello and Y. Chen, Phys. Rev. B (in press).

\* This research was sponsored by DARPA under Interagency Agreement 40-1611-85 and with Martin Marietta Energy Systems, Inc. Contract No. DE-AC05-84OR21400 with the USDOE.

AGGREGATION KINETICS OF I.V. DIPOLES IN NaCl:Eu<sup>2+</sup> CRYSTALS

B. Macalik and J. Poźniak

Institute for Low Temperature and Structure  
Research, Polish Academy of Sciences  
50950 Wrocław, P.O. Box 937 ( Poland )

The influence of thermal annealing of NaCl samples containing about 120 ppm Eu<sup>2+</sup> on the aggregation of pertinent I.V. dipoles was examined by ITC method. Additionally, the aggregation was controlled by the measurements of optical absorption spectra.

In the temperature range 30-70°C the I.V. dipole decay curves consists of three stages: initial rapid decay followed by a plateau and a renewed but much slower decay. Using the kinetic model presented in ( 1 ), it is possible to describe the decay kinetics within first two stages in terms of reversible processes of dimer and trimer formation and to calculate the activation energies of formation and decomposition of both aggregation forms ( 2 ). According to optical absorption spectra the first aggregation stage is accompanied mainly by a small and continuous absorbance drop of 238 nm band. In the second stage (plateau) there is observed a small shift of this band towards lower energies what can be explained in terms of formation of europium rich foreign phase nuclei. In the third stage a distinct growth of a band peaking at 263 nm, and possibly due to the growth of foreign phase precipitates, is observed.

The decay curves obtained annealing at 80°C and 100°C bear a complex character (transient partial recovery of impurity-vacancy dipoles following the initial rapid drop).

The changes in absorption spectra are in general similar to those observed in samples annealed at lower temperatures.

The I.V. dipole decay curves obtained for the samples annealed at 225°C, 235°C and 250°C are most probably characteristic of a process in which the major part plays foreign phase growth. The activation energy of this process amounts to 1.12 eV and is significantly higher from that characteristic of the dimer (0.64 eV) and trimer (0.35 eV) formation. The absorption spectra of the sample annealed at these temperatures reveal, from the very beginning of this treatment, a continuous growth a band with distinct structure and localized at low energy side of the original 238 nm band.

#### References

- (1) J. Poźniak, Acta Phys. Pol., A71, 969 (1987).
- (2) B. Macalik, and J. Poźniak, Acta Phys. Pol., A71, 977, (1987).

## ABOUT THE ORIGIN OF TL PEAK 2 IN THE LiF:Mg,Ti SYSTEM

Ákos Pető

Institute of Isotopes

H-1525 Budapest, P. O. Box 77

This paper reports on the thermoluminescence measurements performed on LiF:Mg,Ti(OH) crystals. The crystals were doped with 10 ppm Mg and 10 ppm Ti, and grown in free air.

The TL measurements were carried out in the dose range 50-5000 rad and for preirradiation heat treatments in the 100-400 C temperature range. A typical glow curve is shown on Fig.1. It shows only two peaks, denoted with a and b. Peak a could be perfectly fitted with first order kinetics using the parameters  $E = 1.09$  eV and  $s = 1.1 \times 10^{13}$  1/s. These are in very good agreement with the parameters published by other authors for peak 2 in TLD-100 (1). The effect of different preirradiation heat treatments on the intensities of peaks a and b can be seen in Fig.2. To establish the relation between peak a and peak 2, the glow curves of a TLD-100 single crystal and a Mg free LiF:Ti crystal were also recorded after a preirradiation annealing at 400 C for 1 h. The low temperature region of the glow curves are shown on Fig. 3.

In the generally accepted model, the charge traps responsible for peak 2 in LiF TLD-100 are I-V pairs (2). During low temperature annealing, the pairs agglomerate, decreasing peak 2 and increasing peak 5. At high annealing temperatures the agglomerates dissociate, resulting in a large peak 2 and a small peak 5. The experimental results described above do not agree with this model. Based on the following arguments, the behaviour of peak a can be understood if we assume that the charge traps responsible for this peak are Ti-OH defects.

1. Grown in free air, the crystals should contain a lot of OH.
2. In spite of the low Mg content, the intensity of peak a is higher than that of peak 2 in a typical TLD-100 sample.

3. Peak a is quite insensitive to heat treatment, which is characteristic of Ti related defects.
4. Pure first order kinetics suggest a locally related untrapping - recombination process.

If we assume peak 2 in TLD-100 and peak a to be of the same origin, then the shift in peak temperature /Fig.3/ can be interpreted as the perturbing effect of I-V pairs on Ti-OH defects, which increases with increasing Mg concentration.

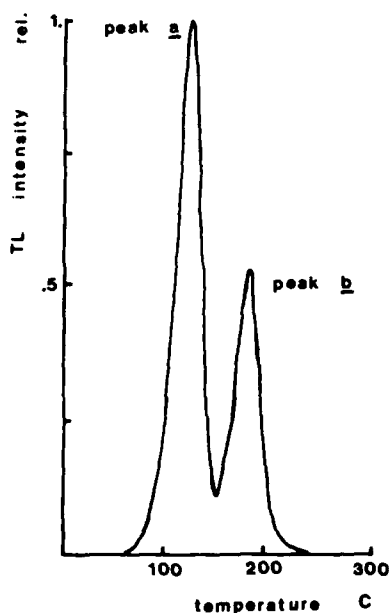


Fig. 1

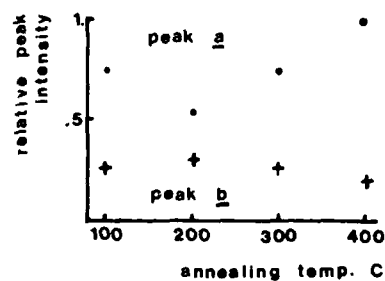


Fig. 2

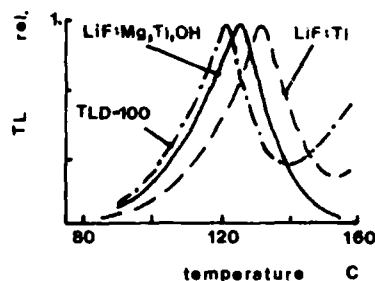


Fig. 3

#### REFERENCES

- (1) R.G. Fairchild, P.L. Mattern, K. Lengweiler, P.W. Levy  
J.Appl. Phys. 49 (8) 4523 (1978)
- (2) S.W.S. McKeever Rad. Prot. Dosimetry 8 (1-2) 3 (1984).

AGGREGATION PROCESSES IN  $\text{NaCl:Eu}^{2+}$  SYSTEM .

R.Capelletti<sup>°</sup> , R.Cywinski<sup>°°</sup> , M.Manfredi<sup>°</sup> and  
H.Opyrchal<sup>°°</sup>

<sup>°</sup>Dipartimento di Fisica , Università di Parma ,Parma  
Italy ,

<sup>°°</sup>Institute of Low Temperature and Structure Research ,  
Polish Academy of Sciences , Wroclaw , Poland .

Early optical measurements on  $\text{Eu}^{2+}$  aggregates in the  $\text{NaCl:Eu}^{2+}$  system were performed by Lopez et al. (1). The emission band of this system is peaking at 427 nm when  $\text{Eu}^{2+}$  ions are chiefly contained in the form of impurity-vacancy dipoles . When the dipoles start to aggregate , the emission spectrum becomes broader and broader and it can be decomposed in bands of assumed gaussian shape . We report the results of a set of measurements - emission and time decay spectra - that have been performed on  $\text{NaCl:Eu}^{2+}$  samples annealed at temperatures up to about 100 °C . The purpose of this work is the investigation of aggregation processes by means of optical measurements . One example of the decay signals measured at different wavelengths along the emission spectrum is shown in fig. 1 .

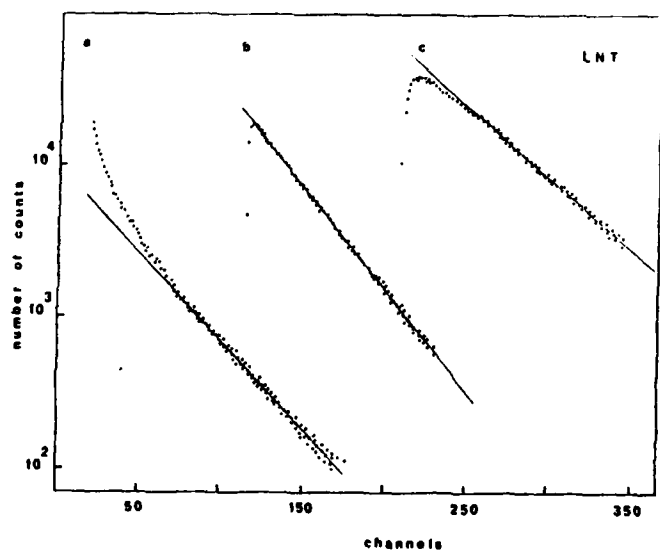


Fig. 1

$\lambda_{\text{excitation}} = 350 \text{ nm}$  ;  $\lambda_{\text{emission}} = 425 \text{ nm}$  (curve a)  
 $\approx 440 \text{ nm}$  (curve b)  
 $\approx 480 \text{ nm}$  (curve c) .

- 1) F.J.Lopez , H.Murrieta S. , J.Hernandez A. and J.Rubio O. -  
 Phys. Rev. B 22 , 6428 (1980) .

# THE ROLES OF DEFECTS IN STRUCTURAL PHASE TRANSITIONS OF COMPLEX OXIDE CRYSTALS

Feng Duan  
Institute of Solid State Physics, Nanjing University  
Nanjing, People's Republic of China

To elucidate the roles played by defects in structural phase transitions is still an important problem in solid state physics. Our approach is the direct observation of defects and phase transitions using transmission electron microscopy(TEM) as a main tool. Here we present some case studies from work done by our research group in Solid State Physics in Nanjing University.

1. Extended antiphase boundaries(APBs) in  $\text{KNbW}_2\text{O}_9$  <sup>[1]</sup> In-situ TEM observations showed that  $\beta$  -  $\alpha$  phase transition in  $\text{KNbW}_2\text{O}_9$  at  $570^\circ\text{C}$  takes place by thickening and spreading out of APBs already present in the parent phase. Analogous result is obtained in the reverse transition  $\alpha$ - $\beta$ . In this case, the extended APBs in the parent phase play the roles of prefabricated nuclei for the new phase.
2. "Ordered" domains in perovskites <sup>[2]</sup> In-situ TEM observations showed that within the temperature range of several degrees centigrade below the Curie points of  $\text{KNbO}_3$  and  $\text{BaTiO}_3$ , the specimen are filled with quasi-regular microdomains, which are not normal ferroelectric domains, but "ordered" domains. In each "ordered" domains, the distribution of Nb or Ti ions along different  $\langle 111 \rangle$  directions in tetragonal phase are ordered. So the dispute between the displacive type and order-disorder one of ferroelectric phase transitions in perovskites may be resolved by a mixed model involving ordered domains.
3. The effect of dislocations on  $\alpha$ - $\beta$  transitions in quartz <sup>[3]</sup> Work reported by van Tendeloo et al <sup>[4]</sup> showed that  $\alpha$ - $\beta$  transition in quartz takes place by gradually refining the scale of the

array of microdomains consisted of alternating dauphine twins. Our in-situ TEM observations showed that the transition temperature is raised on one side and lowered on the other side of a dislocation. This phenomenon may be explained by the pressure effect of soft mode phase transitions, so it is expected that the dilation part and contraction part of the strain field of a dislocation should produce opposite effect.

4. Discommensurations in incommensurate-commensurate phase transitions [56] In commensurate-incommensurate phase transition the discommensurations play the decisive role. Our in-situ observations showed that this phase transition in  $\text{Ba}_2\text{NaNb}_5\text{O}_{15}$  takes place by the nucleation and multiplication of discommensurations. The situation is quite analogous to dislocation-mediated melting of solids envisaged by some theorists, however, discommensuration-mediated phase transition stands on firm experimental foundation.

#### Reference:

1. Feng Duan, Hu Meisheng and Tao Ye, Proc. XI th Int. Cong. Electron Microscopy, Kyoto, 1986, p1225.
2. Chen Jun, Ph D. thesis, Nanjing University, 1987.
3. Pu Anle, M A. thesis, Nanjing University, 1986.
4. G. van Tendeloo et al, Phys. Stat.Sol.,a18(1973),85.
5. Pan Xiao-qing, Hu Meisheng, Yao Ming-hui and Feng Duan, Phys. Stat. Sol. a91(1985), 57.
6. Feng Duan and Pan Xiaoqing, Proc. Int. Cong. on Electron Microscopy, Kyoto, 1986, p1239.

## THERMAL AND DYNAMICAL PROPERTIES OF MIXED LEAD HALIDES



M. Lumbreras and C. Carabatos-Nédelec

C.L.O.E.S. - Université de Metz - Supélec Technopôle de  
Metz -

2, rue Edouard Belin, 57078 Metz Cedex 3, France

Lead chloride and lead bromide show complete mutual solid solubility. The solid solutions  $\text{PbCl}_{2x}\text{Br}_{2(1-x)}$  have been grown using the Bridgman technique ; all single crystals exhibit the  $\text{PbCl}_2$ - type orthorhombic symmetry. Two non-equivalent anion sites characterize this structure.

X-rays scattering experiments reveal preferential site occupancy for Cl and Br, while the anion array of  $\text{PbClBr}$  is completely ordered . The variations of the shortest interatomic distances vs. composition are in complete accordance with this observation. The ionic conductivity of mixed lead halides is assumed to be due to the movement of the anions .

Raman spectra of  $\text{PbCl}_2$  were published by several authors: a rapid decrease of the intensity of all Raman peaks with increasing temperature has been observed. An increasing disorder in one anion sublattice, until melting of this sublattice has been claimed as an explanation .

Nevertheless, all specific heat of ten different compositions show the same narrow peak, proving that there is no such partial melting of one anion sublattice.

For the equimolecular composition, we can note a change of behaviour of the variation of the melting enthalpy, mainly due to the disappearance of the shortest interatomic bond concerning Cl occupied sites (1), while the maximum of the melting entropy seems due to the more complete order of this composition.

A group theory study shows that all Raman peaks are due, in principle, to the movement of the three sorts of ions (lead, anion site (1), anion site (2)). The Raman spectra of mixed lead halides show a complex "one-mode" and "two-mode" type. The variation vs. composition of the wavelength of most Raman peaks reveal the same behaviour as the shortest interatomic distances measured by X- Rays scattering. A comparison between X- Rays and Raman results allows to identify the ions mainly responsible of each lattice vibration. The variation of the Raman linewidths vs. temperature reveals that the maximum of disorder occurs for  $x = 0,25$  and  $x = 0,75$ , i.e. when one of the anion sublattices is occupied half by each sort of ions (Br, Cl). This increasing disorder involves local deformations and relaxations, affecting the atomic binding and the electronic clouds, inducing perturbations of the dielectric properties of these compounds .

The equimolecular composition  $\text{PbClBr}$  Raman spectrum exhibits the narrowest peaks, indicating that this composition is the more completely ordered.

In conclusion, our results prove that the substitution of mobile ions by other chemically different ions but on the same equivalent site induces lattice disorder and can explain the variation of conductivity along with the composition.

INVESTIGATION OF THERMALLY INDUCED  $\text{Li}^+$  ION DISORDER IN  $\text{Li}_2\text{O}$   
USING NEUTRON DIFFRACTION

T.W.D.Farley<sup>a</sup>, W.Hayes<sup>a</sup>, S.Hull<sup>a</sup>, M.T.Hutchings<sup>b</sup>, M.Vrtis<sup>c</sup>

- a. Clarendon Laboratory, Parks Road, Oxford OX1 3PU, U.K.
- b. Materials Physics & Metallurgy Division, A.E.R.E. Harwell Laboratory, Didcot, Oxon. OX11 0RA, U.K.
- c. Institut Laue-Langevin, 156X Grenoble Cedex, 38042 France.

In this paper we report the results of a neutron diffraction investigation aimed at understanding the defect properties of lithium oxide,  $\text{Li}_2\text{O}$ , at temperatures up to close to its melting temperature,  $T_m=1705\text{K}$ .  $\text{Li}_2\text{O}$  possesses the antifluorite crystal structure which can be viewed as a simple cubic array of  $\text{Li}^+$  ions with alternate cube centres occupied by  $\text{O}^{2-}$  ions.  $\text{Li}_2\text{O}$  is expected to exhibit fast-ion conduction at elevated temperatures by analogy with the ionic fluorites such as  $\text{CaF}_2$  and  $\text{SrCl}_2$  in which dynamic Frenkel disorder has been shown to occur<sup>[1]</sup>. Indeed, high  $\text{Li}^+$  ion self-diffusion coefficients at  $T>1250\text{K}$  have been observed using a tracer diffusion technique<sup>[2]</sup>.  $\text{Li}_2\text{O}$  is of technological importance as a possible tritium breeding blanket material for future nuclear fusion reactors on account of the high values of its lithium density, thermal conductivity and melting point.

The measurements were made using single crystal samples of isotopic  $^7\text{Li}_2\text{O}$  grown from the melt by Dr.R.Ward at the Clarendon Laboratory which were encapsulated under vacuum in sealed platinum tubes.

Extensive neutron diffraction measurements have been made at temperatures between 293K and 1605K using the single crystal diffractometer, D15, at I.L.L., Grenoble. These measurements, after correction for thermal diffuse scattering and extinction, have been used to determine the time-averaged defect structure of  $\text{Li}_2\text{O}$  as a function of temperature. The Li sublattice becomes significantly disordered at temperatures above 1000K and at 1605K about 13% of the  $\text{Li}^+$  ions leave their regular lattice sites to form dynamic Frenkel interstitials (see fig 1). The mean position of these interstitial ions in the regular lattice is shown not to be in the empty cube centres that exist in the fluorite structure, but close to the cube edges (see fig 2). There is also some evidence for slight relaxation of the nearest neighbour  $\text{Li}^+$  ions in  $\langle 111 \rangle$  directions away from the interstitial and towards the empty cube centres. This disorder is analogous to that observed in the fluorite compounds in their fast-ion phase<sup>[1]</sup> and is consistent with the geometry of  $\text{Li}^+$  ion diffusion determined by incoherent quasi-elastic neutron scattering measurements at 1623K<sup>[3]</sup>.

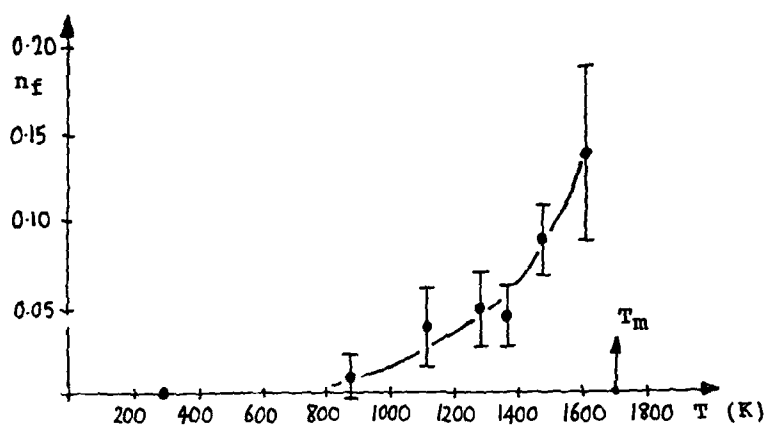


Figure 1. Fraction,  $n_f$ , of  $\text{Li}^+$  ions occupying Frenkel interstitial sites

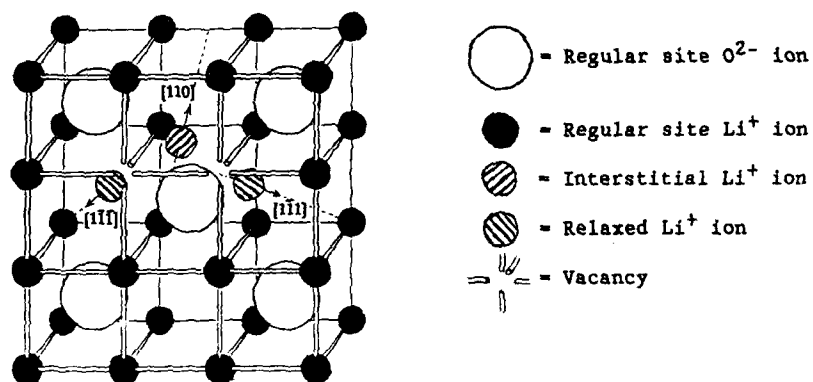


Figure 2. Defect cluster model comprising of a  $\text{Li}^+$  Frenkel interstitial and associated relaxed nearest neighbour  $\text{Li}^+$  ions which best fits the neutron diffraction data at 1605K.

#### References

1. M.T. Hutchings, K. Clausen, M.H. Dickens, W. Hayes, J.K. Kjems, P.G. Schnabel and C. Smith, *J.Phys.C*, **17**, 3903 (1984).
2. Y. Oishi, Y. Kamei, M. Akiyama and T. Yanagi, *J.Nucl.Mater.*, **87**, 341 (1979).
3. T.W.D. Farley, M.A. Hackett, W. Hayes, S. Hull, M.T. Hutchings, R. Ward and M. Alba, *Solid State Ionics* (to be published).

XES CHARACTERIZATION AND DEFECT STRUCTURE OF  
 $\text{TmBa}_2\text{Cu}_3\text{O}_x$  SINGLE CRYSTALS

Gabriel JASIOLEK and Anna PAJACZKOWSKA  
 Institute of Physics, Polish Academy of Sciences  
 02-668 Warsaw, Al.Lotnikow 32/46, Poland

The present paper aims to present the results of the X-ray emission spectroscopy (XES) of the  $\text{TmBa}_2\text{Cu}_3\text{O}_x$  (TBCO) superconducting single crystals. It focuses on determination of the mean valence of copper in relation to the density of twin boundaries and the second phase precipitates as well as on the role of barium in the crystals studied.

Single crystals of TBCO were grown from the nonstoichiometric melt of composition with molar ratio  $\text{Tm}:\text{Ba}:\text{Cu} = 1:4:10$ . Crystals grew from melt heated up to  $1050^\circ\text{C}$  and then slowly cooled to room temperature in air [1]. Their transition temperature was close to 81 K.

The crystals have been exposed on electron beam in the JXA-50A electron probe microanalyser (EPMA). An accelerating voltage of 25 kV and a beam current of  $0.3\ \mu\text{A}$  have been used. The defocusing of electron beam allow to limit the influence of incident electrons on the sample composition. Measurements have been made on the  $\text{K}\alpha_1$  line of Cu and  $\text{L}\alpha_1$  lines of Ba and Tm for the quantitative analysis of the chemical composition. Investigations for the XES characterization have been performed on the  $\text{CuL}\alpha$  line of Cu and  $\text{L}\gamma_4$  line of Ba [2]. Single crystal spectrometers of the Johann type with a RAP and a LiF analysing crystal have been used, respectively. Energetic resolution for the analysis of copper spectrum was equal to 0.06 eV and 0.4 eV for barium one.

The morphology of the crystals revealed the characteristic

features similar as reported in ref.[3]. Growth ledges on the (001) face were observed. However, they appeared only close to the large precipitates consisting mainly with  $\text{BaCuO}_2$  compound. Twin boundaries occurred in the ledge areas.

EPMA analysis showed that the ration between cations forming the crystals corresponds to the following 0.94:2.03:2.97. This analysis revealed also presence of 1 at.% of Al (0.06 in the scale used above). The precipitates contained 0.2 wt.% of Tm but their were free of aluminum.

The mean valence of Cu in the ledge areas of the crystals was estimated to be +2.04 and +2.02 in the regions free of the ledges.

The XES pattern of the crystals suggests that barium valence orbitals interact stronger with oxygen orbitals in the matrix of the TBCO crystals than in the  $\text{BaCuO}_4$  precipitates and in the reference samples such as  $\text{BaF}_2$ .

Mean valence of copper ions estimated for TBCO is lower than in other superconducting crystal basing on yttrium and gadolinium [2]. It can be caused by the large precipitates and the small amount of twins in TBCO. Twins seem to be one of the main cause of the increasing of superconducting properties basing on the Cu (3+) contribution [3].

One can expect aluminum ions entering the copper as well as thulium positions in the crystallographic lattice leading to lowered transition temperatures. In our opinion in TBCO crystal the first type of the interaction have a dominant role.

[1] H. Niculescu, A. Pajaczowska, A. Wisniewski and M. Baran preprint, Int. Discussion Meeting on HTSC, Mautendorf, 07.02.1988.

[2] G. Jasiolek, H. Niculescu and A. Pajaczowska, preprint, Int. Conf. HTSC-M2S, Interlaken, 28.02.1988.

[3] D.L. Kaiser, F. Holtzberg, M.F. Chisholm and T.K. Worthington, J. Cryst. Growth 85 (1987) 593.

# OPTICAL AND THERMODYNAMIC PROPERTIES OF FERROELECTRICS WITH HYDROGEN BONDS IN THE PRESENCE OF DEFECTS

I.V. Stasyuk, R.Y. Stetsiv, A.L. Ivankiv

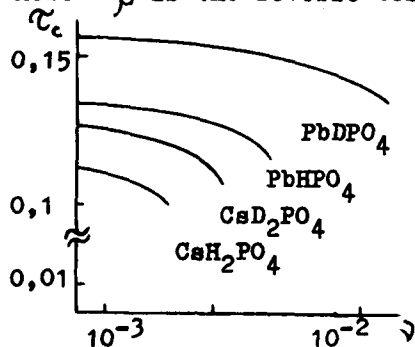
Lvov Division of Inst. for Theoret. Phys. Ukr. Ac. Sci.,  
Dragomanov str., 14/16, 290 005 Lvov, U.S.S.R.

The influence of defects caused by radiation on the optical and thermodynamic properties of ferroelectrics with hydrogen bonds is investigated.

1. The quasionedimensional  $\text{CsH}_2\text{PO}_4$  - type crystals with the defects of destroyed hydrogen bonds type are considered. It is shown, that these damages lead, in particular, to the appearance of the internal field acting at the damaged site, which stimulate the redistribution of protons within a chain. The Hamiltonian of the crystal consisting of one-dimensional chains of ionic groups bounded by the hydrogen bonds includes the short-range interaction between protons in the chain. The partition sum for the chain segment cut out from the endless chain by using the transfer matrix method is calculated. The analytical expressions for the free energy and the static susceptibility of the both averaged over defect distribution for the chain containing  $N$  hydrogen bonds with  $m$  defects are obtained,

$$\chi_{N(m)} = \frac{\beta}{4(m+1)} \exp\left(\frac{\beta J}{2}\right) \left[ \left(\frac{C_N^m}{N}\right)^{-1} \sum_{j=m-1}^{N-1} C_j^{m-1} (N-j) \frac{1 + (\tanh \frac{\beta J}{4})^{N-j}}{1 - (\tanh \frac{\beta J}{4})^{N-j}} - \exp\left(\frac{\beta J}{2}\right) \right].$$

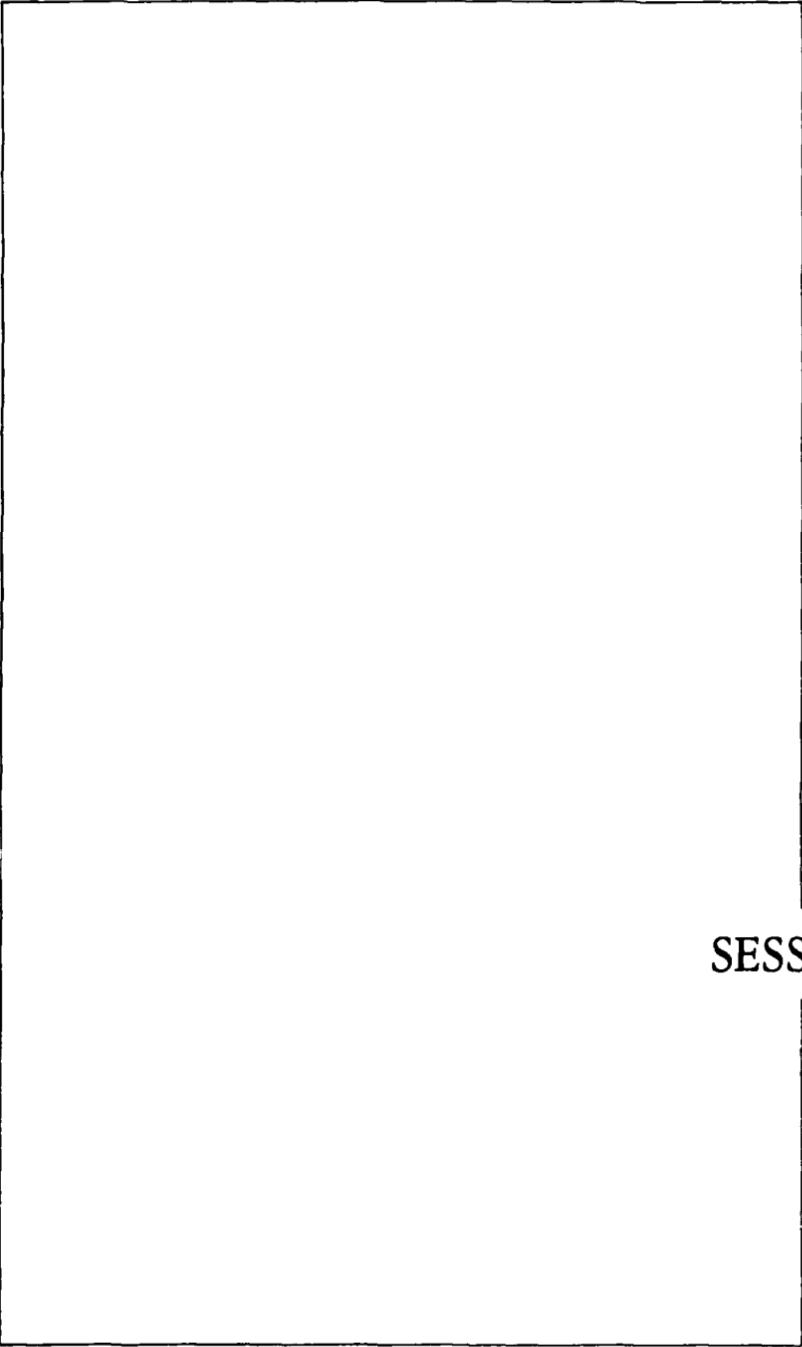
Here  $\beta$  is the reverse temperature and  $J$  is the parameter of



short-range interaction of protons in the chain. The equation defining the second order phase transition temperature with account of the long-range interaction between the chains in the mean field approximation is given. The phase diagrams "critical temperature ( $T_c = T_c/J$ ) -

concentration of defects ( $\gamma = m/N$ )" for  $\text{CsH}_2\text{PO}_4$ ,  $\text{CsD}_2\text{PO}_4$ ,  $\text{PbHPO}_4$  and  $\text{PbDPO}_4$  crystals are given in the region of small  $\gamma$  and the temperatures near  $T_c$  at  $\gamma = 0$ . The increase of  $\gamma$  leads to the weakening of ferroelectric properties of crystals, in particular, for  $\text{CsH}_2\text{PO}_4$  one the fall of  $T_c$  by 1 K is caused by  $\gamma = 3,78 \cdot 10^{-4}$ .

2. The theory of natural optical activity is developed for the KDP type crystals with nonequilibrium distribution of  $\text{H}_n\text{PO}_4$  configurations and  $\text{H}_2\text{PO}_4^{2-}$  defects which are the Slater's configurations with one additional electron. Proceeding from the microscopic expression for the dielectric permeability tensor in terms of two-time retarded Green functions (constructed of the operators of dipole, quadrupole and magnetic dipole momenta) the gyration tensor is calculated; the ionic and crystalline components of the tensor are separated. The molecular orbital calculation within the extended Huckel method of the electron energy spectrum, the wave functions, the matrix elements of electric and magnetic dipole electron momenta of the  $\text{H}_n\text{PO}_4$  ( $n=0, \dots, 4$ ) groups is performed. We have calculated the contributions of  $\text{H}_n\text{PO}_4$  groups and  $\text{H}_2\text{PO}_4^{2-}$  defects into the effect of gyration. The presence of the  $\text{H}_2\text{PO}_4^{2-}$  defects leads to the increase of  $g_{xx}$  component of the gyration tensor both at the short wave part of transparency region and near the infrared absorption edge of a crystal. It is shown that this component is anomal large both near  $\lambda = 269$  nm that agrees with experimentally observed new absorption peaks and near  $\lambda = 2021$  nm, providing interest for experimental investigations of  $g_{xx}$  component at these frequencies.



SESSION 5

### X-Ray Storage Phosphors: Physical Mechanisms and Applications

Heinz von Seggern, Siemens AG, Central Research and Development, 8520 Erlangen, West Germany

Defect centers in ionic crystals play a major role in determining the properties of scintillator materials in various high energy and medical applications. In these applications the spontaneous luminescence in the visible or near-visible as a result of X- or  $\gamma$ -irradiation is detected as a measure for the impinging radiation dose. In some materials the information on the received radiation dose is stored and can be recovered by thermal [1] or optical excitation [2]. The best known application is the thermoluminescence dosimetry used in long term radiation monitoring.

Recently, a new medical application has been suggested utilizing the energy storage in the alkali-earth halide BaFBr:Eu [3] to produce a new kind of imaging plate for X-ray diagnostics replacing the conventional film/screen system. The stored information in the BaFBr:Eu plate can be recovered by optical excitation which is accompanied by a dose-proportional emission (PSL: photostimulated luminescence) [4,5]. A schematic setup of such an X-ray diagnostic system is shown in Fig.1.

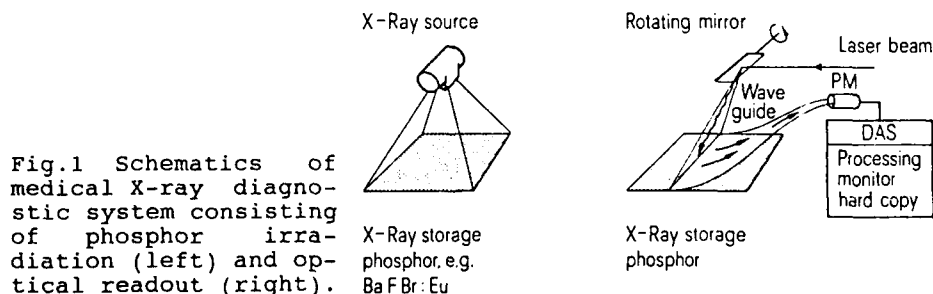


Fig.1 Schematics of medical X-ray diagnostic system consisting of phosphor irradiation (left) and optical readout (right).

In this talk I will describe the concept of the new X-ray diagnostic system. The principle of this imaging technique is discussed. The advantages, like,

- X-ray dose linearity,
- lower dose consumption,
- easy digitizing,
- reusability, etc.,

and disadvantages are compared to the established film-screen systems. Furthermore, the physics of the photostimulable X-ray storage phosphors BaFBr:Eu and RbBr:Tl are addressed which are presently the only materials of commercial interest [3,5,6]. The nature of the excitation, storage, and recovery mechanisms will be discussed supported by experimental results obtained partially in our laboratories. The main features of the storage and the recovery can be traced back to the properties of the color centers participating in the process. Based on these results, criteria for new and improved X-ray storage phosphors will be outlined from the physical, imaging and the commercial standpoint.

#### References

- [1] Chen R., Kirsh Y.: Analysis of thermally Stimulated Processes Pergamon Press, Oxford 1981
- [2] Pringsheim, P.: Fluorescence and Phosphorescence Interscience Publishers, New York 1949
- [3] Sonoda, M., Takano M., Miyahara J., Kato H., Radiology 148, 833(1983)
- [4] Takahashi K., Kohda K., Miyahara J., J. Luminescence 31&32, 266(1984)
- [5] von Seggern H., Voigt T., Knüpfer W., Lange G., J. Appl. Phys., accepted for publication
- [6] Amitani K., Kano A., Tsuchino H., Shimada F., SPIE's Conf. and Exhib.: Electr. Imaging, 26th Fall Symp., Printing and Paper Summaries, p.180 (1986)

ION IMPLANTATION IN ELECTRO-OPTIC MATERIALS  
P D TOWNSEND  
MAPS, UNIVERSITY OF SUSSEX, BRIGHTON, BN1 9QH, UK

Many electro-optic devices are designed to process optical signals carried by optical waveguides in surface layers. Such guides have dimensions of the wavelength used and so are of micron size cross section. This depth scale can therefore be readily influenced by ion implantation. The mechanism by which implantation changes the electro-optic properties depends on the host material as well as the ion species. For semiconducting material impurity doping alters the optical properties via free carrier effects and/or optical absorption. In the case of wider energy gap insulators the impurity effects may be less important and the major changes are a consequence of point defects or amorphisation. In addition to optical changes many other properties such as chemical stability are significantly modified.

In order to retain the electro-optic properties it is essential to retain the crystallinity of the host. This can be achieved by using the implantation to define the boundaries of the waveguides. A clear example of this is shown by the ion beam bombardment of quartz with helium ions. Energy is transferred to the lattice by a mixture of ionisation and nuclear collision processes. The quartz lattice is stable against ionisation but in the region of nuclear collision damage it is amorphised into silica. This transformation reduces the refractive index from 1.54 to 1.48 and so provides a region of low index which acts as the boundary to the waveguide. Alternatively one may use the change in chemical stability to etch ridge or strip waveguide features on the surface of the crystal. The process is effective as there is an enhancement of chemical etch rate in HF by a factor of 200 in the damaged material.

A side effect of ion implantation is the production of optical absorption from colour centres, however the stability of these electronic features is generally much less than the structural modifications and so the absorption can be removed by annealing. Quartz is an extreme example as annealing to 1200°C does not cause reconversion of the silica to crystalline quartz. The process outlined for quartz is very simple and the general approach is effective in a wide range of materials.

Obvious advantages of ion implantation are that it can be performed at low temperature and so utilise crystals with several phases or a low temperature Curie point. Control of ion energy and dose allows one to form structures with well specified refractive index profiles or to extend the method to multilayer waveguides.

One may combine the ion implantation effects with materials formed by diffusion or layer deposition.

Effects which have so far received less attention are control of the birefringence and temperature dependence of the index. Such features are of interest for waveguide laser structures and for second harmonic generation. These possibilities will be mentioned.

SURFACE DEFECTS EXPLOITED FOR GAS SENSING

Wolfgang Göpel  
Institute of Physical and Theoretical Chemistry  
University of Tübingen, Auf der Morgenstelle 8  
D-7400 Tübingen 1, FRG

Single crystals, thin-film and thick-film structures of inorganic and organic materials with electron-, defect-electron and ion- conducting properties may be optimized for their use as chemical sensors to detect selectively molecules in the gas phase /1/.

Examples will be discussed of prototype materials for systematic research, i.e., doped and undoped tin oxide, titanium dioxide, different oxides of perovskite structure, zirconia and phthalocyanines.

Thermodynamically and kinetically controlled conditions are discussed first for reproducible sensor/gas interactions by characterizing the sensor performances with respect to sensitivity, cross contamination, selectively, response time and longterm stability. Structures have to be optimized of prototype AC- and DC- conductivity as well as potentiometric sensors.

Comparative spectroscopic studies must utilize ultrahighvacuum (UHV) transfer vessels. This makes possible to characterize sensors before and after their use under practical application conditions with respect to their elemental composition (by using X-ray

photoemission, secondary-ion-mass, and ion backscattering spectroscopy), with respect to their electronic structure (by using UV-photoemission spectroscopy), with respect to their dynamical structure (by applying high resolution electron energy loss and Fourier transform infrared spectroscopy), with respect to their work function changes (by using the Kelvin vibrating method), with respect to their microscopic geometric structure (by applying scanning electron microscopy and scanning Auger spectroscopy) and with respect to their geometric structure on the atomic scale (by using low energy electron diffraction techniques for single crystal structures) /2/.

The results make possible an atomistic interpretation of the sensing mechanisms of optimized sensor structures. In this context, the importance will be demonstrated of thermodynamically controlled preparation steps.

It will be shown, that most sensors may in principle be operated as high temperature (bulk-defect) sensors, medium temperature (surface defect) sensors, or low temperature (chemisorption or physisorption) sensors.

Careful control of intrinsic and/or extrinsic surface defects will be demonstrated to play the key role in controlling the sensing mechanisms based upon changes in the conductivity and/or electrical potentials at the

interfaces. Surface defect equilibria in particular may be controlled from the gas phase and/or from the bulk.

/1/ W. Göpel, "Chemisorption and Charge Transfer at Ionic Semiconductor Surfaces: Implications in Designing Gas Sensors", Prog. in Surf.Sci. 20,1(1985)9.

/2/ W. Göpel, "Solid State Chemical Sensors: Atomistic Models and Research Trends", Conf.Proc. of Eurosensors I, Cambridge (1987) and "Sensors and Act." in press.

THE ROLE OF IONIC DEFECTS IN THE RADIATION PHYSICS OF THE  
SILVER HALIDES, AND THEIR EXPLOITATION IN PHOTOGRAPHY.

R. S. Eachus and Myra T. Olm  
Corporate Research Laboratory  
Eastman Kodak Company, Rochester, New York 14650

One hundred and fifty years after their initial use in imaging, the silver halides have yet to yield to the onslaught of electronic recording systems, nor have they been displaced by less expensive compounds as light recording media. For many imaging applications, the silver halides remain unmatched in resolution and sensitivity. This unusual technological tenacity is the result of a unique combination of fundamental solid state properties. This paper reviews the relationship between ionic defect properties and photographic response, with particular emphasis on the role of aliovalent dopants in practical systems.

The primary photographic process is a complex mechanism involving the alternate trapping of electrons and interstitial silver ions at "sensitivity centers" to form a developable "latent image". It owes its efficiency in part to the cationic Frenkel defect structures of silver bromide and silver chloride and to the high mobility of the interstitial silver ion in these materials. Studies of Frenkel disorder have related the ionic properties of silver halide microcrystals to their size, morphology, halide composition, and aliovalent impurity content. In practical systems these characteristics can be manipulated to control "speed", resolution, image stability, and the development process.

Silver bromide and silver chloride are indirect band gap solids having high dielectric constants. These properties also contribute to the high quantum efficiency of the photographic process, since they result in a propensity for shallow electron trapping. Representative studies of intrinsic and extrinsic shallow trapping centres will be reviewed in this talk. The nature and concentration of the intrinsic centres depend on the morphology and halide composition of the grains. The extrinsic traps are generally divalent cationic impurities with closed shell electronic configurations. These centres affect image dispersity and, thereby, photographic speed. While optical, magnetic resonance and photoconductivity studies have been useful in their detection and for probing their role in photography, detailed structural knowledge about shallow traps remains elusive. This is in part the result of the small central cell correction to the effective mass description of these trapping sites.

Aliovalent cations with incomplete valence shells are also used in practical emulsions where they are generally added at part per million or part per billion levels. They can indirectly modify latent image formation by changing the Frenkel equilibrium, or they can directly affect the process by serving as recombination centres or as deep traps for photocarriers. The vast majority of transition metal cations used in practical systems act as electron traps. These addenda are used for a wide variety of purposes including the control of image dispersity and contrast, to enhance speed, to reduce reciprocity effects, and to achieve image reversal. The effects of doping are a function of the impurity's cross-section and trap depth, as well as the lifetime of the resultant trapped carrier state and the exact sequence of chemical reactions that follow trapping. These in turn are governed by the location of the dopant in the photographic grain, its dispersity, and the degree and nature of charge compensation by Frenkel defects. In many respects the impurity can be viewed as a molecular complex whose trapping behaviour is not only governed by the electronic structure of the metal ion, but also by the composition of the ligand shell. Trapping behaviour is also affected by lattice composition. In mixed silver halide grains, the dopant may segregate to sites of preferred lattice composition in the random binary or ternary mixture. Representative optical and magnetic resonance studies with parallel studies of photographic effects will be presented.

The difficulties encountered in extrapolating results from some studies of model single crystals to emulsion microcrystals grown in an aqueous gelatin environment will be described. These comments are particularly pertinent to transition metal ions with low valence states which often function as deep hole traps in single crystals of AgBr and AgCl. As yet, all attempts to mimic this behaviour in practical grains have failed. Similar problems have been experienced with aliovalent anion doping, where evidence for hole trapping in single crystals has not been duplicated in emulsion grains.

HIGH TEMPERATURE ELECTRON IRRADIATION OF FUSION MATERIALS

E.R. Hodgson

EURATOM/CIEMAT Fusion Association  
Avda. Complutense, 22.- 28040 Madrid, Spain

It is becoming increasingly clear that the problem of choosing suitable electrically insulating materials for future fusion reactors is far more serious than initially anticipated. Undoubtedly in the long term, the general materials problem will prove to be the most difficult aspect of the whole project. Although data for metals, in particular stainless steels, under extreme radiation conditions have been available for many years, data for insulating materials were until very recently almost non-existent. However the urgent necessity for such information is beginning to produce results.

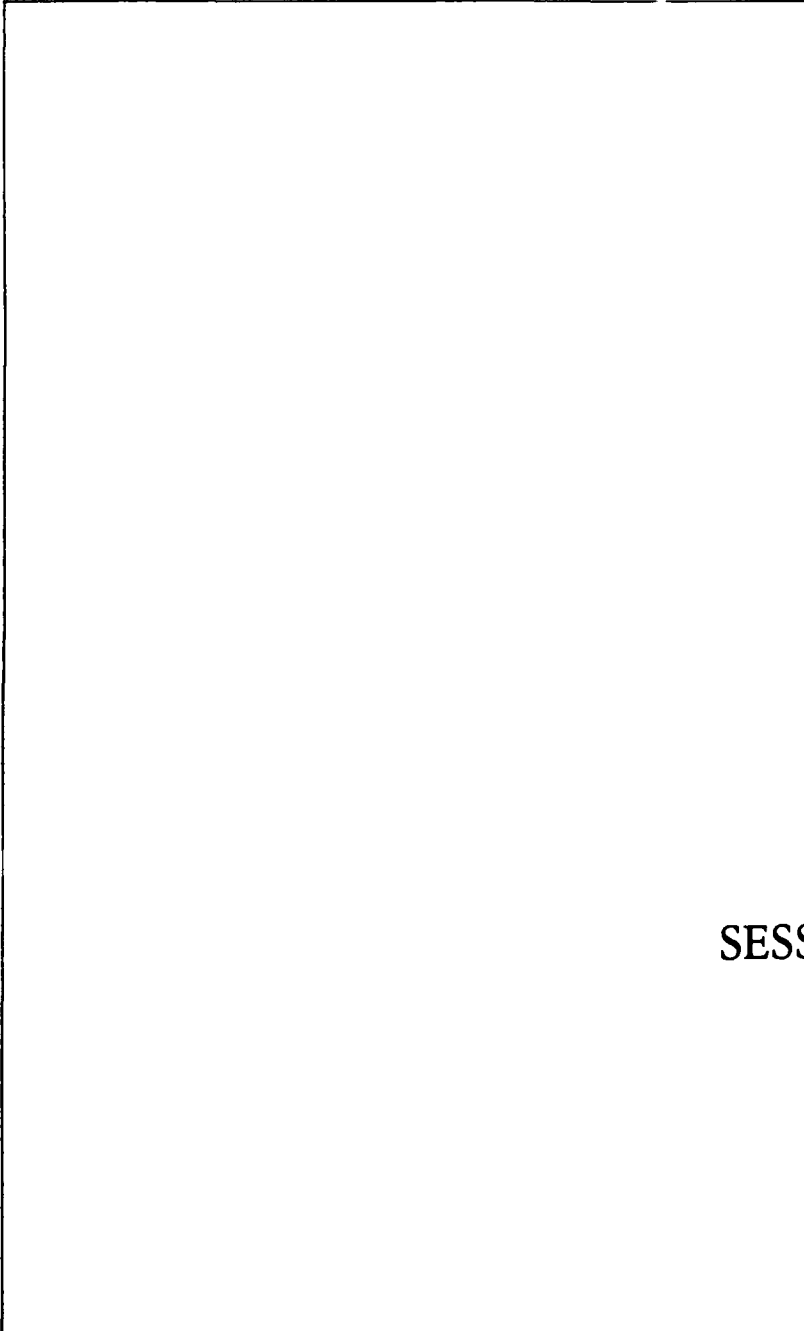
The chosen materials, most probably refractory oxides or ceramics, will have to maintain their high electrical resistivity, thermal conductivity, mechanical strength, and dielectric properties during prolonged irradiation. As at present no perfect radiation source is available, the conditions are being simulated using nuclear fission reactors and particle accelerators. Ideally, measurements should be made where possible during irradiation, and such experiments are now being performed on both electron and proton accelerators which produce localized high radiation conditions. Although these experiments can only simulate some of the actual operating conditions, they are producing useful data which help to highlight problem areas.

One of the immediate problems which has been addressed, is that of radiation enhanced electrical conductivity, for which a rather complex

dependence on both dose rate and temperature has emerged, however agreement between experiment and theory is encouraging. Initial results suggested that this increase in electrical conductivity would not lead to a serious Joule heating problem, and further results pointing to a saturation effect at high dose rates were viewed with satisfaction. But more recent results have revealed a hitherto unsuspected problem-radiation enhanced electrical breakdown. This effect is most probably related to the radiation enhanced impurity diffusion, which in these materials has been observed to occur at relatively low temperatures. The problem of the ever present impurities and those which will be produced by nuclear reactions within the materials has so far received little attention, however the important rôle that impurities are known to play in material properties means that this problem needs careful consideration.

The effects of purely ionising radiation and displacement damage are at present being studied by comparing results obtained from electron and proton irradiations. These two aspects of the radiation field will vary at different positions around the fusion reactor and it is necessary to understand their relative importance.

The size and importance of the materials problem for the fusion reactor project will require that an ever increasing effort be made. Clearly at the present time only a few of the necessary questions have been addressed. Thermal conductivity, mechanical strength, and to a lesser extent dielectric loss, have hardly been looked at under anything approaching a fusion reactor environment.



## SESSION 6

DEFECTS AND STRUCTURAL CHANGES IN PEROVSKITE SYSTEMS:  
FROM INSULATORS TO SUPERCONDUCTORS

D. M. Smyth  
 Materials Research Center, Bldg. 32  
 Lehigh University  
 Bethlehem, PA 18015, U. S. A.

For materials having the composition  $ABO_3$ , when A is substantially larger than B, the perovskite structure is invariably favored. The tenacity of this structure is demonstrated by the persistence with which the basic pattern is maintained even when the composition deviates significantly from the ideal formula. For compositional deviations at the percent level that can be achieved by reduction or by the substitution of aliovalent cations, the accommodation is usually by the formation of point defects or electronic defects in random solid solution, and the systems can be successfully treated by classical defect chemistry and dilute solution thermodynamics. For larger deviations, a superlattice is frequently developed that corresponds to an ordering of the defects in a way that retains blocks or layers having the basic perovskite symmetry. In this review, we will describe the way in which the perovskite structure adjusts in response to various compositional variations, and will introduce the concept of "perovskite space", a diagrammatic way of showing the interrelationships of the different patterns.

Reduction of a typical perovskite such as  $SrTiO_3$ , or the substitution of acceptor impurities, e.g.  $Al^{+3}$  for  $Ti^{+4}$ , leads to the formation of randomly distributed oxygen vacancies up to the percent level. For very large substitutions in some systems, notably  $CaTiO_3$ , the vacancies effectively order into layers that separate two-dimensional slabs of the perovskite structure. This leads to a homologous series of ordered compositions that can be described as  $Ca_nFe_{2n-2}Ti_{n-2}O_{3n-1}$ . The perovskite layers are  $n-1$  unit cells thick, and the B ions in the intervening layers that contain strings of aligned vacancies are reduced to four coordination. The series terminates with  $Ca_2Fe_2O_5$ ,  $n = 2$ , in what is commonly called the brownmillerite structure.

The substitution of donor impurities, e.g.  $Nb^{+5}$  for  $Ti^{+4}$ , leads to

the formation of cation vacancies in random solid solution. At large concentrations, however, the system may separate into two dimensional perovskite layers separated by oxygen-rich layers. Once again, a homologous series of structures may develop, such as  $\text{Sr}_n\text{Nb}_4\text{Ti}_{n-4}\text{O}_{3n+2}$ , with perovskite layers  $n$  unit cells thick. This series terminates at  $\text{Sr}_2\text{Nb}_2\text{O}_7$  with  $n = 4$ , and two-dimensional perovskite layers four unit cells thick.

Thirty years ago, Ruddlesden and Popper described a perovskite-related structural series based on the general formula  $\text{SrO} \cdot n\text{SrTiO}_3$  or  $\text{Sr}_{n+1}\text{Ti}_n\text{O}_{3n+1}$ . These structures consist, once again, of two-dimensional layers of the perovskite structure,  $n$  unit cells thick, separated by an extra layer of  $\text{SrO}$  in the  $\text{NaCl}$  structure. One end of this series,  $n = 1$ , corresponds to  $\text{Sr}_2\text{TiO}_4$ , the orthotitanate in what is commonly called the  $\text{K}_2\text{NiF}_4$  structure, and contains perovskite layers that are one unit cell thick. The other end of the series is, of course, ordinary perovskite.

Given this demonstrated tendency for materials to retain layers of various thicknesses that have the perovskite structure, it is not too surprising to find that the very complex compositions that have been found to be high temperature superconductors can be described in similar terms. It is suggested that they can be characterized by a generalized Ruddlesden-Popper formula of the type  $m\text{AO} \cdot n\text{ABO}_3$ , that allows for a variable number of  $\text{NaCl}$ -like layers separating layers of various thicknesses having perovskite-like structures. Thus when described in terms of the  $m:n$  ratio,  $\text{Bi}_2\text{Sr}_2\text{CaCu}_2\text{O}_8$  ( $T_c = 85 \text{ K}$ ) corresponds to 3:2, and has triple  $\text{NaCl}$ -like layers separating double perovskite-like layers, and  $\text{Bi}_2\text{Sr}_2\text{Ca}_2\text{Cu}_3\text{O}_{10}$  ( $T_c = 110 \text{ K}$ ) corresponds to 3:3. All of the high  $T_c$  superconductors discovered to date can be described in this way, and this suggests a structural pattern that may serve as a basis for designing new compositions.

In summary, the perovskite structural pattern shows a remarkable ability to survive gross deviations from the ideal composition. It thus appears in many unexpected places. After all, more than half of the volume of our planet Earth has the perovskite structure!

## IMPURITIES AND DEFECTS IN FLUORIDE GLASSES

Marcel POULAIN  
 Centre d'Etude des Matériaux Avancés  
 UNIVERSITE de RENNES

Heavy metal fluoride glasses are now extensively studied for a set of applications in telecommunications and infrared technologies. Most of their development problems are related to various physical and chemical defects. Some of them are under control while others remain under investigation. In practice, the correct identification of these defects is the more difficult step as exemplified by various examples.

A first group of physical defects includes heterogeneities and bubbles inside bulk glass. Their origin will be discussed as a function of starting materials and processing. Residual free volume and thermally induced stresses are often observed as glass melt must usually be quenched.

Devitrification, either homogenous or heterogenous may appear as the major problem in fluoride glass technology. Heterogenous nucleation is controlled by extrinsic contamination while homogenous nucleation depends on glass composition. At the present stage of sample size and optical quality, devitrification problems have been largely solved.

Chemical impurities make the most serious source of optical defects. At the first place, transition metals - eg Cr, Fe, Co, Ni, Cu - and rare earth cations take a major part in absorption losses. Therefore high purity reagents are required for low loss optical components. On the other hand, anionic impurities do not only increase absorption losses but they may also induce scattering losses as they are not homogeneously distributed in bulk glass. Hydroxyle radicals are not stable in fluoride glass melts and consequently are easily removed. Anionic oxygen is more difficult to control and is likely to induce various defects, especially when oxydo reduction processes occur. When Zirconium IV is reduced, it results in significant scattering losses. The influence of gamma ray irradiation will be shortly described in relation with corresponding chemical defects.

Finally, consequences of physical and chemical defects on fluoride glass fibres appear to be critical both for optical and mechanical properties. Current state of art and technological trends will be reviewed. In this respect, new synthesis processes must be investigated and the limits of conventionnal technology has to be evaluated.

SESSION 6A

OPTICAL PROPERTIES OF COLOR CENTERS IN GADOLINIUM GALLIUM GARNET  
CRYSTALS\*

L. S. Cain  
Physics Department, Davidson College  
Davidson, NC 28036 USA  
G. J. Pogatshnik and Y. Chen  
Solid State Division, Oak Ridge National Laboratory  
Oak Ridge, TN 37831 USA

The addition of small amounts of calcium during the crystal growth of large diameter, gadolinium gallium garnet crystals produces color centers which absorb in the near uv region of the spectrum.<sup>1</sup> Optical excitation of these color centers produces luminescence from several defects in the crystals. Two relatively broad emission bands are observed in the visible region at 420 and 550 nm, along with other luminescence bands in the infrared. We attribute the broad emission band at 420 nm to the presence of trace amounts of  $\text{Eu}^{2+}$  ions. Reduction of the samples at high temperatures enhanced the intensity of the 420 nm emission band at the expense of the narrow emission bands near 620 nm identified as  $\text{Eu}^{3+}$  emission. Oxidation of the samples produced a large decrease in the intensity of the 420 nm emission. The 550 nm band is unidentified, but is likely due to several types of defect centers in the crystal. The peak position of the 550 nm emission band was found to shift to lower energy as the excitation wavelength was scanned from lower to higher energy through the color center absorption band. The infrared emission bands are identified as  $\text{Fe}^{3+}$  emission near 800 nm and  $\text{Cr}^{3+}$  emission at 710 nm. The  $\text{Fe}^{3+}$  luminescence is primarily excited through the  $\text{Fe}^{3+}$  charge transfer bands near 260 nm. The  $\text{Cr}^{3+}$  emission is produced by Gd to Cr energy transfer. The excitation spectrum of the chromium emission line at 695 nm exhibited resonances at all of the transition energies of the constituent  $\text{Gd}^{3+}$  ions.

Ultraviolet and gamma irradiation of the crystals produced changes in the intensities of the uv color center bands along

with a broad absorption throughout the visible. Optical bleaching at 350 nm produced a brown coloration in the visible, and a slight decrease in the 350 nm absorption band. The results indicate that the color center which produces the 350 nm absorption band serves as a photoionizable donor center. Electrons released by the optical excitation are trapped at other sites in the crystal, possibly as  $Gd^{2+}$  ions, to produce the visible coloration. Gamma irradiation produced similar effects. We have also examined the effects of oxidation and reduction treatments on the radiation response of the material. Oxidation at temperatures above 700°C produced an enhancement of the 350 nm absorption band. Gamma irradiation following oxidation resulted in a much stronger coloration than that observed in untreated GGG crystals. Reduction of the samples for temperatures above 600°C decreased the 350 nm absorption band and led to an improved radiation response of the material. Reduction treatments at temperatures above 1100°C produced changes in the structure of the material. X-ray diffraction showed that the crystal turned amorphous following 30 minutes reduction at 1200°C. Reduction at higher temperatures led to the extraction of metal ions from the sample.

The coloration effects that result from the presence of the uv color center absorption bands may be significant during flashlamp pumping of laser rods which utilize large diameter GGG crystals as the laser host. The changes in the optical properties of the material under uv excitation indicate that the addition of small amounts of calcium to assist in the growth of large diameter crystals is likely to result in the degradation of laser performance.

I.M. Pardavi-Horv'ath, I. Foldv'ari, I. Fellegv'ari,  
L. Gosztonya, and J. Paitz, Phys. Stat. Sol. (a), 84, 547  
(1984).

\* Supported by DARPA under interagency agreement 40-1611-85 with Martin Marietta Energy Systems Inc., contract DE-AC05-84OR21400 with US DOE.

COMPUTER MODELING OF PRESSURE-DEPENDENT  
CHROMIUM PHOTOLUMINESCENCE

R. H. Bartram, J. C. Charpie, A. M. Woods and R. S. Sinkovits  
Department of Physics and Institute of Materials Science  
University of Connecticut, Storrs, CT 06268, U.S.A.

Photoluminescence spectra and lifetimes of chromium-doped ordered perovskites have been measured as functions of pressure and temperature with laser excitation in a diamond-anvil cell as part of a coordinated experimental and theoretical investigation of potential tunable solid-state laser materials. Computer modeling of pressure and temperature effects was initiated with the object of achieving a quantitative understanding of thermal quenching mechanisms.

The materials investigated,  $K_2NaGaF_6:Cr^{3+}$ ,  $K_2NaScF_6:Cr^{3+}$  and  $Cs_2NaYCl_6:Cr^{3+}$ , provide examples of low-crystal-field chromium complexes characterized by broad-band, spin-allowed  ${}^4T_{2g} \rightarrow {}^4A_{2g}$  fluorescence, of interest in tunable laser applications. A pressure-induced enhancement of the crystal field leads to a blue shift of the fluorescence band and, in the fluoride compounds, culminates in a re-ordering of the excited states (Dolan *et al.* 1986). The resolved vibronic structure of the resulting spin-forbidden  ${}^2E_g \rightarrow {}^4A_{2g}$  phosphorescence reveals a pressure-induced enhancement of vibration frequencies, as well. Finally, a large positive pressure-induced shift of thermal quenching temperature is inferred from lifetime measurements (Bartram *et al.* 1987).

Ab-initio molecular cluster calculations (MELD) yield equilibrium chromium-fluorine separations and frequencies of  $a_{1g}$ ,  $e_g$  and  $t_{2g}$  vibrations as a function of lattice parameter. Lattice-statics calculations (HADES) provide hydrostatic pressure as a function of lattice parameter. In combination, these calculations yield a pressure-dependent local compressibility of the chromium complex in reasonable agreement with that inferred from the pressure-induced blue-shift of fluorescence. The pressure dependence of the  $a_{1g}$  and  $e_g$

vibration frequencies in the gallium compound is predicted correctly. The model also predicts the  $t_{2g}$  frequency at ambient pressure, but not its observed pressure dependence. A model incorporating simultaneous linear coupling to an  $a_{1g}$  mode and quadratic coupling to a  $t_{2g}$  mode, developed to explain thermal quenching at ambient pressure (Bartram et al. 1986), provides a qualitative explanation of the positive pressure dependence of the thermal quenching temperature.

#### Acknowledgment

This work was supported by the U.S. Army Research Office under Contract No. DAAL03-86-K-0017.

#### References

Bartram R H, Charpie J C, Andrews L J and Lempicki A 1986 Phys. Rev. B 34, 2741

Bartram R H, Dolan J F, Charpie J C, Rinzler A G and Kappers L A 1987 Cryst. Latt. Def. and Amorph. Mat. 15, 165

Dolan J F, Kappers L A and Bartram R H 1986 Phys. Rev. B 10, 7339

**THEORETICAL IMPURITY LEVELS OF Ni AND V IONS IN THE BaTiO<sub>3</sub>**  
**PEROVSKITE HOST**

P. Moretti\* and F.M. Michel-Calendini\*\*

\*Institut des Sciences de l'Ingénierie  
et du Développement Technologique

\*\*Physico-Chimie des Matériaux Luminescents UA 442  
Université Cl. Bernard Lyon I  
43 Bd. du 11 Novembre 1918  
69622 Villeurbanne France

Over the past few years, 3d cations trapped in oxides, particularly in BaTiO<sub>3</sub>, have been extensively investigated. Various attractive potential applications, in solar energy conversion or in coherent optic technology for instance, are widely correlated to the optical properties of the associated defects. In order to understand the latter, it seems then to be of the utmost importance to know the energy-level diagrams of the referred elements.

The spin-unrestricted X $\alpha$  method has been successfully used to obtain molecular-orbital diagrams relevant to Fe<sup>(1)</sup>, Co<sup>(2)</sup>, Cr and Mn<sup>(3)</sup> embedded in BaTiO<sub>3</sub>. This paper is devoted to Ni and V ions in the same host.

In order to determine the electronic structure of these cations, small size clusters of MO<sub>6</sub><sup>-12·n</sup> type are studied, where M stands for the impurity with a nominal ionicity n varying from 2 to 5, thus including a great number of electronic configurations.

Through the transition state concept, we particularly address to the determination of the ground state of some species, since the value of the corresponding D<sub>q</sub>/B parameter, the ratio between the crystal field strength and the electronic interaction, could be situated close to cross over points in the so called Tanabe-Sugano diagrams.

The energy levels of the ground term of the  $V^{2+}$  and  $Ni^{2+}$  ions are provided. For the sake of comparison and in order to discuss on the stability of the species in  $BaTiO_3$ , all the eigenvalues are referred to the same state ( $t_{1g}$ ), identified as the top of the valence band edge of the crystal. These results are compared with those recently obtained<sup>(4)</sup> by a tight-binding model describing the same impurities in  $SrTiO_3$ .

Moreover some charge transfer- and crystal field- transitions are calculated and discussed, comparatively to available experimental data.

#### **References**

- (1) F. M. Michel-Calendini, Solid State Commun. 52, 167 (1984)
- (2) F. M. Michel-Calendini and P. Moretti, Phys. Rev. B27, 763 (1983)
- (3) P. Moretti and F. M. Michel-Calendini, Phys. Rev. B36 (1987)
- (4) Selme M.O., Pecheur P. and Toussaint G., J. Phys. C Solid State Phys. 19, 5995 (1986)

SELF-TRAPPED ELECTRON CENTERS IN ELECTRON-IRRADIATED  
ZINC TUNGSTATE SINGLE CRYSTALS\*

A. WATTERICH<sup>†</sup>, G.J. EDWARDS, O.R. GILLIAM, and R.H. BARTRAM

Department of Physics and Institute of Materials Science  
University of Connecticut, Storrs, Ct. 06268, U.S.A.

Á. PÉTER and R. VOSZKA

Research Laboratory for Crystal Physics, Hungarian Academy of Sciences  
H-1112 Budapest, Budaörsi út 45, Hungary

Single crystals of zinc tungstate have been of considerable interest recently because of their potential application for x-,  $\gamma$ - and particle-ray scintillation detectors.<sup>1-3</sup> The study of radiation-induced point defects can facilitate further improvement in crystal growth and detector performance. We are not aware of any previous radiation-damage investigations in this material. By contrast, extensive studies of that kind have been reported in materials of other tungstates, e.g.  $\text{CaWO}_4$ .

$\text{ZnWO}_4$  belongs to an isostructural series of divalent monoclinic tungstates<sup>4</sup> with small cations (Mg, Mn, Fe, Co and Ni) and has the space group  $C_{2h}^4$  ( $P2_1/c$ ) with two formula units per unit cell. Single crystals of  $\text{ZnWO}_4$  were grown in air using a balance-controlled Czochralski technique with a platinum crucible.<sup>5</sup>

In the present investigation, single crystals of  $\text{ZnWO}_4$  were subjected to 1.65-MeV electron irradiations at 6  $\mu\text{A}$  for two hours at room temperature. The resulting defects were characterized by electron spin resonance (ESR) spectroscopy.

The ESR spectrum of the  $\text{ZnWO}_4$  crystal, measured at 90 K, reveals a single spin-1/2 defect in two inequivalent sites, with an anisotropic  $\vec{g}$  tensor similar to those of  $\text{W}^{5+}$  in other materials. The principal  $g$  values, based on preliminary evaluation, are as follows: 1.91, 1.80 and 1.69. Around the two main lines, two pairs of smaller lines having equal intensities are observable. The satellite lines are paired symmetrically around the main lines, with intensity ratio 1:12. These facts suggest that the satellite lines are due to hyperfine interactions with two inequivalent  $^{183}\text{W}$  nuclei having nuclear spins  $I = 1/2$  and an isotopic abundance of 14.4%. The larger splitting, which varies between 7.5 and 13.5 mT, is characteristic of  $\text{W}^{5+}$  in other materials. The smaller splitting (with a maximum value of  $\approx 1.5$  mT) is due to superhyperfine (SHF) interaction with a neighboring  $\text{W}^{6+}$  ion.

From the angular variations of the Zeeman and SHF lines, the principal axes of the self-trapped electron at a W ion and the relative orientation of the neighboring interacting W ion are determined, respectively. The SHF interaction is not due to the nearest tungsten sites, but those which are bound through two  $\text{ZnO}_6$  octahedra. The present

center differs from several defects published in  $\text{CaWO}_4$ , one attributed to a  $\text{WO}_4^{3-}$  ion adjacent to a defect<sup>6</sup>, and others attributed to different charge states of oxygen divacancy centers located on adjacent  $\text{WO}_4^{2-}$  complexes.<sup>7</sup>

<sup>†</sup>Permanent affiliation: Research Laboratory for Crystal Physics, Budapest, Hungary.

<sup>\*</sup>Supported jointly by the U. S. National Science Foundation under grant No. INT-8617352 and the Research Foundation of the Hungarian Academy of Sciences (A.K.A.).

- <sup>1</sup> T. Oi, K. Takagi, and T. Fukazawa, *Appl. Phys. Lett.* **36**, 278-279 (1980).
- <sup>2</sup> B.C. Grabmaier, *IEEE Trans. on Nucl. Sci.* **NS-31**, 372-376 (1984).
- <sup>3</sup> H. Grassman, H.-G. Moser and E. Lorenz, *J. of Luminescence*, **33**, 109-113 (1985).
- <sup>4</sup> R.O. Keeling, Jr., *Acta Cryst.* **10**, 209-213 (1957).
- <sup>5</sup> F. Schmidt and R. Voszka, *Crystal Res. Technol.* **16**, K127-128 (1981).
- <sup>6</sup> H. Zeldes and R. Livingston, *J. Chem. Phys.* **34**, 247-252 (1961).
- <sup>7</sup> P. Weightman, B. Henderson and D.E. Dugdale, *Phys. Stat. Sol.(b)* **58**, 321-330 (1973).

PHOTOIONIZATION, TRAPPED EXCITONS AND LUMINESCENCES OF  $\text{Eu}^{2+}$  AND  $\text{Yb}^{2+}$  RARE EARTH IONS IN CRYSTALS OF ALKALINE EARTH FLUORIDES

B. MOINE, B. COURTOIS, C. PEDRINI  
 Unite Associee au CNRS n° 442, Universite Lyon I  
 69622 VILLEURBANNE (FRANCE)

D.S. MCCLURE  
 Department of Chemistry, Princeton University, Princeton  
 NEW JERSEY 08544 USA

We have found that the photoionization energies of the divalent rare earth ions in  $\text{CaF}_2$ ,  $\text{SrF}_2$  and  $\text{BaF}_2$  are on the order of a few eV [1-3]. The values of the photoionization energies are estimated as the threshold energies of the photocurrent obtained from photoconductivity measurements. These values have been reviewed and compared to a simple electrostatic model which works quite well.

We have observed several cases in which all the localized excited states of the impurity ion lie in the conduction band of the host crystal. Examples are  $\text{Yb}^{2+}$  in  $\text{MF}_2$  ( $M=\text{Ca}, \text{Sr}, \text{Ba}$ ) [4,5],  $\text{Cu}^+$  in  $\text{CdCl}_2$  and  $\text{CdBr}_2$  [6] and  $\text{Eu}^{2+}$  in  $\text{BaF}_2$  [7,8]. In these cases, the impurity ions can emit an "anomalous luminescence" which was not correctly assigned in the past, and that we have interpreted in terms of the impurity trapped exciton [5,8].

In this paper, we present recent results obtained more especially from  $\text{Eu}^{2+}$  and  $\text{Yb}^{2+}$  doped  $\text{SrF}_2$  and  $\text{BaF}_2$  single crystals. Spectroscopic and photoconductivity data are reported and analyzed in detail. Among these four systems,  $\text{SrF}_2:\text{Eu}^{2+}$  is the only one which has its lowest excited state below the bottom of the conduction band. It gives a normal blue luminescence of  $\text{Eu}^{2+}$  while the other compounds have all their excited states degenerated in the conduction band and show yellow or red emissions considered "anomalous" since they are Stokes shifted

by 2 eV from their lowest excited states. In this case, recombination of the electron with the ion left behind, now a trivalent impurity ion, do not lead to a localized excited state but instead to an exciton-like state with an electron delocalized over the 12 next-neighbor metal-ion sites in the Coulomb field of the trivalent rare earth ion. The luminescence is therefore interpreted as the decay of this exciton into the ground state of the divalent impurity. The collapse of the  $F_{\text{cube}}^-$  around the  $RE^{3+}$  could displace the  $F^-$  ion by about 0.2 Å and would account for the large Stokes shift. In order to explain the photo-conductive and luminescence behavior of the systems, a model is proposed, constructed in terms of configuration coordinate diagrams.

#### REFERENCES

1. C. PEDRINI, D.S. McCLURE and C.H. ANDERSON  
J. Chem. Phys. 70, 4959 (1979).
2. C. PEDRINI, P.O. PAGOST, C. MADEJ and D.S. McCLURE  
J. Phys. Paris 42, 323 (1981).
3. C. PEDRINI, F. ROGEMOND and D.S. McCLURE  
J. Appl. Phys. 59, 1196 (1986).
4. D.S. McCLURE and C. PEDRINI  
J. Phys. Paris C7, 46, 459 (1985).
5. D.S. McCLURE and C. PEDRINI  
Phys. Rev. B 32, 8465 (1985).
6. B. SOLLER, M. VODA and D.S. McCLURE  
J. Lumin., 24/25, 201 (1981).
7. D.S. McCLURE, B. MOINE and C. PEDRINI  
J. Less-Common Metals 126, 297 (1986).
8. D.S. McCLURE, B. MOINE and C. PEDRINI  
To be published.

THERMOCHEMICAL REDUCTION AND RADIATION EFFECTS IN  
LANTHANUM MAGNESIUM ALUMINATE CRYSTALS\*

Y. Chen,<sup>a</sup> M. M. Abraham,<sup>a</sup> M. R. Kokta,<sup>b</sup> G. J. Pogatschnik,<sup>a,c</sup>  
 L. S. Cain,<sup>a,d</sup> J. L. Park,<sup>a,c</sup> and C. Y. Chen.<sup>a,c</sup>

<sup>a</sup> Solid State Division, Oak Ridge National Laboratory,  
 Oak Ridge, TN 37831 USA

<sup>b</sup> Union Carbide Corporation, Washougal, WA 98671 USA

<sup>c</sup> Dept. of Materials Science and Engineering,  
 North Carolina State University, Raleigh NC 27695 USA

<sup>d</sup> Department of Physics, Davidson College, Davidson, NC 28036  
 USA

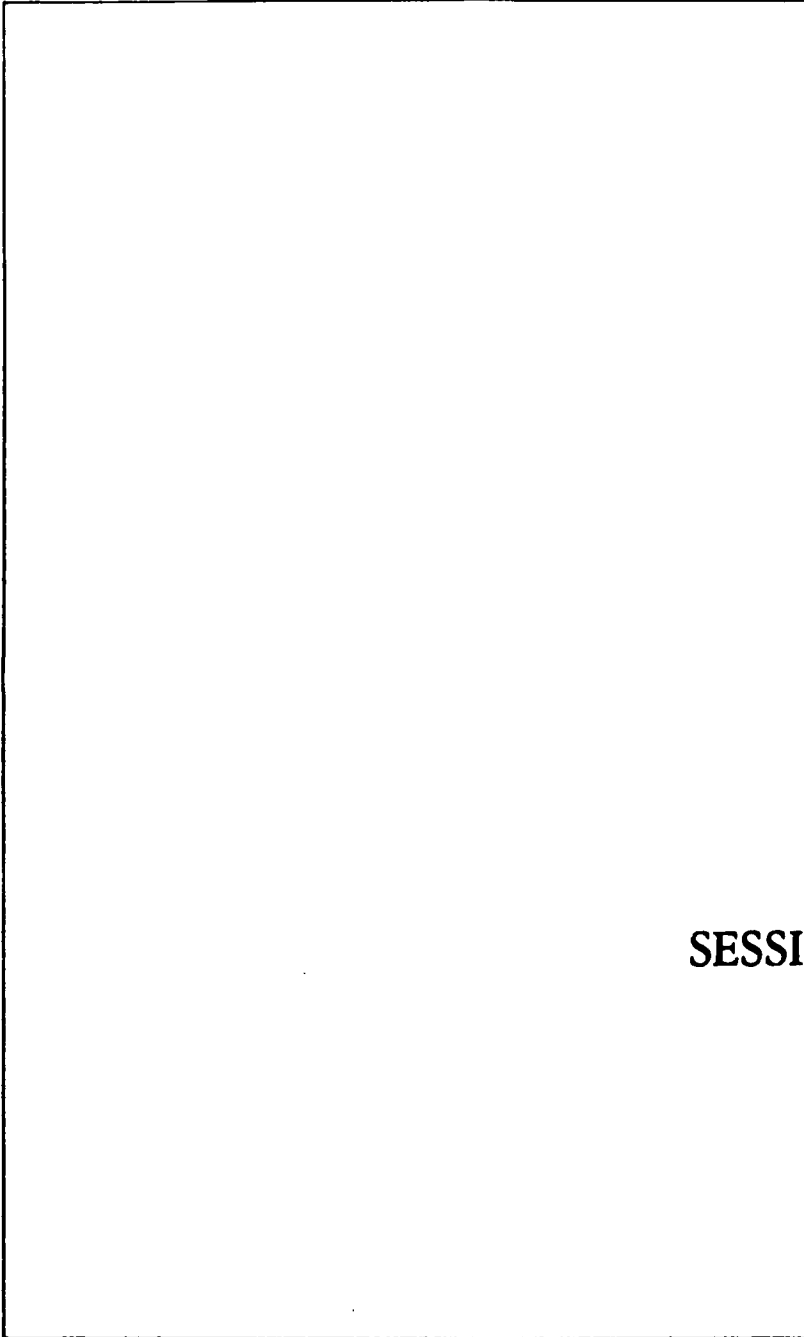
Lanthanum magnesium aluminate ( $\text{LaMgAl}_{11}\text{O}_{19}$ , or simply LMA) has recently attracted attention as a viable laser host.<sup>1</sup> Neodymium doped LMA has been shown to be a new laser material accommodating an enhanced Nd concentration which is optically superior to YAG:Nd. We report on (1) the effects of thermochemical reduction of LMA, and (2) the solarization of LMA, which is the tendency for the crystals to color during optical excitation or exposure to ionizing radiation. Thermochemical reduction results in the creation of several optical absorption bands, at least one of which yields efficient luminescence in the visible region. The solarization effects are examined because they can hamper the ability of a material to lase.

Thermochemical reduction was performed on undoped LMA crystals at temperatures up to 1800 K. Several prominent optical absorption bands were observed. The absorption coefficient of these bands increased with the temperature of reduction; there was no saturation, suggesting that vacancies were involved. These bands were highly anisotropic. The two most prominent bands peaked at 320 and 270 nm, with a FWHM of  $\sim 0.4$  eV. They gave rise to efficient luminescence at 565 nm and 410 nm, respectively. The quantum efficiency of the former is approximately unity.

Optical and electron paramagnetic resonance (EPR) techniques were used to study the effects of gamma irradiation on undoped LMA crystals. A broad optical absorption band at 400 nm, with a strong polarization anisotropy, was intensity correlated with an EPR signal (X-band) attributed to trapped hole centers.<sup>2</sup> When the samples were irradiated at 77 K, the EPR spectrum showed additional lines at higher magnetic field. These high field lines exhibited superhyperfine structure, presumably due to the interaction of other centers with aluminum neighbors. K-band EPR measurements at 4 K, following gamma irradiation at 77 K, showed that the single line observed at X-band resolved into two lines which nearly coalesced when the magnetic field was either parallel or perpendicular to the c-axis of the crystal. One of the lines disappeared after warming to room temperature, indicating the existence of at least two different centers. The growth of the 400 nm optical absorption band and the growth of the magnetic resonance signal of the hole center as a function of gamma dose were well correlated. However, the decay rate of the optical band was slower than that of the EPR signal. The difference is primarily attributed to absorption bands of more stable centers which contribute to the absorption at 400 nm. The oscillator strength was found to be  $0.07 \pm 0.02$ . The optical absorption band can be bleached at 295 and 77 K, indicating that the excited states of the holes are close to the valence band. Polarized bleaching experiments failed to show any linear dichroism, so that the holes do not appear to be strongly localized on a single oxygen site.

1. Kh. S. Bagdasarov, L. M. Dorozhkin, A. M. Keverkov, Yu. I. Krasilov, A.V. Potemkin, A. V. Shestakov, and I. I. Kuratev, Sov. J. Quantum Electron. 13, (5) (1983).
2. D. Gourier, F. Laville, D. Vivien, and C. Valladas, J. Solid State Chem. 61, 67 (1986).

\* Supported by DARPA under interagency agreement 40-1611-85 with Martin Marietta Energy Systems Inc., contract DE-AC05-84OR21400 with US DOE.



SESSION 6B

CALCULATED LATTICE AND DEFECT PROPERTIES OF  $M_2CuO_4$   
(M = La, Y, Nd, Pr, Al) RELATED TO HIGH  $T_c$  SUPERCONDUCTIVITY

N.L. Allan and W.C. Mackrodt  
ICI Chemicals & Polymers Ltd., P.O. Box 8,  
The Heath, Runcorn, Cheshire WA7 4QD, England

Since the discovery in 1987 of high temperature superconductivity in rare-earth cuprates, there has been extensive experimental investigation of the physical, chemical and materials properties of these materials to the point where there is now a consensus view as to most of the important features. Theoretical interest has focussed principally on coupling mechanisms, but here a divergence of views still exists. Rather less attention has been devoted to understanding the defect structure and properties of these materials despite their evident importance in controlling  $T_c$  [1]. This paper is concerned with the calculated lattice (static and dynamic) and defect properties of  $M_2CuO_4$  (M = La, Y, Nd, Pr, Al) with the principal aim of trying to understand why only M = La leads to high  $T_c$  materials and not the remainder. Among the properties considered in detail are the phonon density of states, the fundamental defect structure, the nature of the electronic defects, oxidative and reductive non-stoichiometry and the defect structure associated with divalent impurities, notably Mg, Ca, Sr and Ba.

- 1 N.L. Allan and W.C. Mackrodt, Proc. Mat. Res. Soc. Symp. (1987) - In press.

EXTENDED DEFECTS IN  $\text{YBa}_2\text{Cu}_3\text{O}_{7-x}$  AND RELATED PEROVSKITES

T. E. Mitchell and T. Roy  
Center for Materials Science  
Los Alamos National Laboratory  
Los Alamos, New Mexico 87545, USA

The discovery of high  $T_c$  superconductivity in  $\text{La}_{2-x}\text{Sr}_x\text{CuO}_{4-\delta}$  and  $\text{MBa}_2\text{Cu}_3\text{O}_{7-y}$  ( $M = \text{Y}$  or rare earth element) has stimulated interest in the crystal chemistry and defect structure of these and related perovskites. In the present investigation, transmission electron microscopy has been used to study the nature of the extended defects in (a)  $\text{YBa}_2\text{Cu}_3\text{O}_{7-y}$ , (b)  $\text{La}_2\text{CuO}_4$  and  $\text{La}_{2-x}\text{Sr}_x\text{CuO}_{4-\delta}$  and (c)  $\text{Eu}_2\text{CuO}_4$ . All have a triple perovskite unit cell but all have distinctly different structure and microstructure and, of course, electrical conductivity behavior.

$\text{YBa}_2\text{Cu}_3\text{O}_{7-y}$  is orthorhombic  $\text{Pmmm}$  with  $c/b \approx 3$  and  $b/a \approx 1.017$ . The most characteristic feature of the microstructure is the high density of  $\{110\}$  twins (Fig. 1) which are formed during the transformation from the high temperature tetragonal phase at  $\sim 700^\circ\text{C}$ . The twins help to accommodate the small (1.7%) shear distortion. The twin density is observed to increase by in situ cooling and the twins can be removed by heating or by electron irradiation. Both treatments have the effect of disordering the oxygen atoms in the Cu-O chains in the structure so that there is a transformation to the tetragonal phase. The orthorhombic structure is not always restored by cooling due to loss of oxygen; instead, the diffraction pattern shows a variety of extra spots (Fig. 2) due to different ordering schemes of the oxygen vacancies.

$\text{La}_2\text{CuO}_4$  is also orthorhombic with a space group variously reported as  $\text{Fmmm}$  and  $\text{Abma}$ ; we find extra diffraction spots consistent with  $\text{Pccn}$ . The structure transforms from the tetragonal phase ( $\text{F4/mmm}$ ) at  $\sim 200^\circ\text{C}$  and again the microstructure consists of sets of twins on the  $\{110\}$  planes (Fig. 3). The spot splitting corresponds to  $b/a \approx 1.008$  at ambient temperatures but increases to  $\sim 1.024$  at liquid nitrogen temperatures. The basic twin structure is observed to remain unchanged

during cooling but more secondary twins are seen. In addition extra spots are seen at  $(110)$  positions in the  $[001]$  pattern which are streaked along  $\langle 110 \rangle$ , indicating the possibility of another phase change. Superconducting  $\text{La}_{2-x}\text{Sr}_x\text{CuO}_{4-\delta}$  has also been studied. It is tetragonal at room temperature but transforms to orthorhombic at  $\sim 200\text{K}$ . Lenticular twins are observed to form and, as the temperature is lowered, the twins become clearer and more regular.

$\text{Eu}_2\text{CuO}_4$  and  $\text{Gd}_2\text{CuO}_4$ , both with the same tetragonal  $I4/mmm$  structure, have also been investigated. Whether specimens were prepared by ion milling or grinding, they almost always contained extra reflections at  $(\frac{1}{4} \frac{1}{4} 0)$ ,  $(\frac{1}{2} \frac{1}{2} 0)$ ,  $(\frac{3}{4} \frac{3}{4} 0)$  positions in the  $[001]$  zone (Fig. 4). Different regions gave this quadrupling along the two  $\langle 110 \rangle$  directions indicating that the base of the unit cell is probably  $2\sqrt{2} \times \sqrt{2}$  of the tetragonal  $a$  axis. It is likely that the oxides are slightly reduced and the oxygen vacancies are ordered in the Cu-O planes, much as in the 123 material. Possible schemes will be discussed.



Fig. 1  $\{110\}$  twins in  $\text{YBa}_2\text{Cu}_3\text{O}_{7-y}$



Fig. 3  $\{110\}$  twins in  $\text{La}_2\text{CuO}_4$

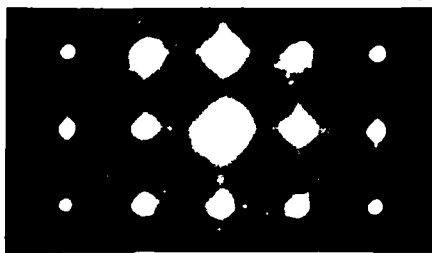


Fig. 2  $[001]$  pattern of  $\text{YBa}_2\text{Cu}_3\text{O}_{7-y}$  after pulse heating.



Fig. 4  $[001]$  pattern of  $\text{Eu}_2\text{CuO}_4$

The influence of local electric field and of correlation in the  
electronic transport: the case of CdF<sub>2</sub>

V.Dallacasa, C.Paracchini

Dipartimento di Fisica, Università di Parma - Parma -Italy

The electronic transport process in a compound is usually dominated by the temperature. At high temperatures thermally activated processes are favoured and the field assisted thermal ionization is a common mechanism. The original theory of the effect, as formulated by Frenkel, leads to two main discrepancies when compared with the experimental results: a) the value of the Poole-Frenkel constant is smaller than that expected, b) the ohmic behaviour is not explained. Subsequent developments of the theory obtain substantial agreement with the experiments but, though important for the identification of the effect, they are mainly based on ad-hoc hypotheses [1].

A new model which considers the contribution of the internal electric fields is proposed [2] and the results of previous single centre theories are now reobtained as a consequence of averaging over the internal field distributions. Two possible emission cases are examined: one where the electron emission takes place mainly in the direction of the applied field, the other for isotropic emission.

At low temperatures the thermal ionization becomes improbable and other mechanisms like hopping prevail. Then the transport takes place by jumps of fixed or variable range between centres in a narrow impurity band energetically localized around the Fermi level [3]. A comprehensive theory of the effect including low and high applied field conditions is given by Apsley and Hughes [4].

However when the carrier concentration is so low to avoid screening, collective states may be produced by the electron-electron interactions. Then hops occur involving many carriers simultaneously, leading to a correlated electron motion. At softer interactions the correlation results in a splitting of impurity band into two parts separated by a gap (Coulomb gap) [5]. At stronger Coulomb repulsions charge ordering may occur with the formation of an electron lattice (Wigner glass) [6].

Such correlations give rise to a reduction of the carrier mobility leading to deviations from the current-voltage-temperature characteristics obtained in non-correlated conditions. The analysis of the deviations give informations about the kind of correlation.

The study of the experimental data from semiconducting CdF<sub>2</sub> crystals over a wide range of temperature (10-300 K) and applied field (up to 50 KV/cm) evidence the forementioned effects and give an evaluation of the local electric field, the transport activation energy, the density of states at the Fermi level and the localization radius.

The results altogether point out the importance of the electric local field and of the electronic correlations in the electrical transport mechanisms.

[1] D.M.Pai, J.Appl.Phys. 46 , 5122-5126 (1975)

[2] V.Dallacasa, C.Paracchini, Phys.Rev. B 34 , 10 (1986)

V.Dallacasa, C.Paracchini, IEEE Trans. Electr. Insul. EI-22 , 467 (1987)

[3] N.F.Mott, Phil.Mag. 19 , 835-852 (1969)

[4] N.Apsley and H.P.Hughes, Phil.Mag. 31 , 1327 (1975)

[5] M.Pollak, Phil.Mag.B 42 , 781 (1980)

[6] M.Pepper, J.Phys.C 12 , L610 (1979)

V.Dallacasa, J.Phys.C 19 , L485-L489 (1986)

**Molecular Dynamics of the Fast-Ion Conductor  $\delta$ -Bismuth Oxide:  
Effect of Crystal Potential and Number of Particles**

D.A. Mac Dónaill, Department of Chemistry, Trinity College, Dublin  
2, Ireland.

and

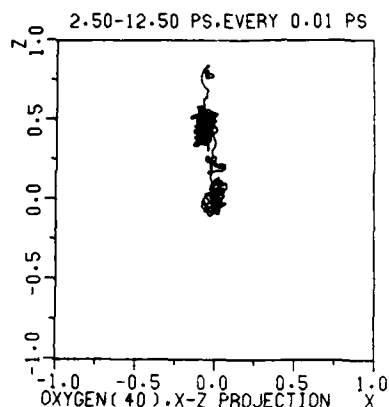
P.W.M. Jacobs and Z.A. Rycerz, Department of Chemistry, The  
University of Western Ontario, London, Ontario, Canada N6A 5B7.

In the fluorite phase of  $\text{Bi}_2\text{O}_3$  only three quarters of the anion sites are occupied by oxide ions. Consequently the  $\delta$ -phase has the highest known conductivity among the oxides. This high conductivity is related to the highly disordered oxygen sub-lattice. Static-lattice simulations of  $\delta\text{-Bi}_2\text{O}_3$  [1,2] have shown that: (i) a disordered oxygen sub-lattice is favoured over regular ordering of the vacant sites; (ii) that oxygen migration proceeds predominately via  $\langle\langle 100 \rangle\rangle$  jumps; (iii) that cube-centre interstitials are unlikely to form, but instead relaxed cube-edge interstitials are favoured, in agreement with neutron scattering studies on the stabilized  $\delta$ -phase and (iv) that the  $\delta$ -phase is prone to orthorhombic distortions and has a tendency to adopt closely related structures of lower symmetry. To obtain greater insight into the remarkable properties of  $\delta\text{-Bi}_2\text{O}_3$  we have begun an extensive series of dynamic simulations. Some preliminary results have been published elsewhere [3,4]. Here we present new results on the effect of crystal potential, lattice constant and the size of the simulation sample on the two sub-lattices and on oxygen diffusivity.

Various potentials were derived for the static-lattice single-defect and periodic boundary simulations and two of these, called R and D1 respectively were used in initial MD simulations. With Harwig's experimental lattice constant of  $a = 5.644\text{\AA}$  at 1029 K, potential R predicts only limited mobility in the oxygen sub-lattice, but potential D1 (with the short-range hardness parameter adjusted to fit the static dielectric constant) gives somewhat greater mobility in the oxygen sub-lattice, as shown by histograms of total ion displacements and projections of ion positions. Radial distribution functions show a less - ordered oxygen sub-lattice, for D1, but this is still far from liquid-like. A reassessment of all available published data on the  $\delta$ -phase lattice parameter of  $\text{Bi}_2\text{O}_3$  solid solutions led to a new value for  $a$  of  $5.531\text{\AA}$  at 0 K, and potentials D2 and D3 were derived by refitting to the density at 0 K, assuming  $\langle 111 \rangle$  and  $\langle 100 \rangle$  vacancy ordering respectively. These potentials are softer than D1, and D3 yields a very disordered oxygen sub-lattice with suggestions of a lower-symmetry structure. This feature, and also the strong tendency to superlattice formation shown by periodic-boundary static-lattice simulations has promoted a series of MD simulations that use a primary domain of  $4 \times 4 \times 4$  unit cells instead of  $3 \times 3 \times 3$  unit cells employed in the simulations described above. Results derived

from all these simulations: radial distribution functions, the velocity autocorrelation function and its integral and Fourier Transform, histograms, projections of ion-positions and ion-trajectories (figure) will be contrasted. The conductivity calculated from the oxygen diffusion coefficient will be compared with experiment.

Financial support from the Natural Sciences and Engineering Research Council of Canada is gratefully acknowledged.



Projection in the ZX plane of the trajectory of a single oxide ion in  $\delta\text{-Bi}_2\text{O}_3$  during a 10 ps simulation.

1. P.W.M. Jacobs and D.A. MacDónaill, Solid State Ionics, 25, 279 (1987); *ibid.*, 25, 295 (1987). *ibid.*, 25, 307 1987;
2. P.W.M. Jacobs, D.A. MacDónaill and A.N. Cormack, Adv. Ceram., 23, 307 (1987),
3. P.W.M. Jacobs and D.A. MacDónaill, Cryst. Latt. Def. Amorph. Mat., 15, 325 (1987).
4. D.A. MacDónaill, P.W.M. Jacobs and Z.A. Rycerz submitted for publication.

DEFECT STRUCTURE AND TRANSPORT PROPERTIES OF MIXED IRON-MANGANESE-OXIDES

Rüdiger Dieckmann and Peter Franke

Cornell University, Department of Materials Science and Engineering  
Bard Hall, Ithaca, NY 14853-1501, U.S.A.

In general, transport of matter in crystalline solids is determined by defects. At sufficiently high temperatures, the influence of one- or higher-dimensional defects is often negligibly small. Then the transport properties are determined by the different point defects being present in the solid. In the case of oxides containing transition metal ions, the presence of point defects causes a deviation from stoichiometry. The extent of this deviation from stoichiometry as well as the transport properties are unequivocally determined by the values of the independent thermodynamic variables of the system. Consequently, the results of systematic investigations of nonstoichiometry and transport properties as a function of the thermodynamic variables allow conclusions with regard to the kind of the point defects present and with regard to the mechanisms of migration of ions and point defects.

The present investigation deals with the relationships between point defect concentrations and transport properties in ternary oxides at absence of potential gradients. The ternary oxides investigated are  $(\text{Fe,Mn})\text{O}$  and  $(\text{Fe,Mn})_3\text{O}_4$  mixed oxides.

The deviation from stoichiometry, the diffusion coefficients of the radioactive isotopes Fe-59 and Mn-54, and the DC-conductivity have been measured as a function of oxygen activity and cationic composition across the entire stability range of the  $(\text{Fe,Mn})\text{O}$ -phase at 1000 °C. The samples used consisted of dense, polycrystalline materials. A microbalance was used for the nonstoichiometry measurements. Tracer diffusion coefficients were measured by a residual activity method. Electrical conductivity was studied by a 4-probe-technique. Oxygen activities were established by  $\text{CO}/\text{CO}_2$ -mixtures and monitored electrochemically.

It was found that the tracer diffusion coefficients of both cations behave very similar with respect to the thermodynamic variables. The absolute values of both diffusion coefficients do not differ significantly at given oxygen activity and cationic composition. The diffusivities increase with increasing iron contents.

At constant cationic composition, the DC conductivities of mixed oxides with large manganese contents show minima as a function of oxygen activity and deviation from stoichiometry, respectively. At lower MnO contents no minima occur and the conductivity increases with increasing oxygen activity. The deviation from stoichiometry and the DC-conductivity are almost proportional at high oxygen activity.

For the  $(\text{Fe,Mn})_3\text{O}_4$ -phase, tracer diffusion coefficients of Fe-59 and Mn-54 were determined at 1200 °C as a function of oxygen activity and cationic composition. For all cationic compositions it was found that the diffusion coefficients of both cations show minima as a function of oxygen activity. This indicates a change of the diffusion process and of the kind of defects being dominant for cation diffusion. It is concluded that at low oxygen activities interstitial cations and at high oxygen activities cation vacancies are the predominant defect species for cation tracer diffusion. At constant cationic composition, the minima of both cation diffusivities occur approximately at the same oxygen activity. This suggests that an interstitialcy diffusion process predominates at low oxygen activity.

STRUCTURAL AND DYNAMIC PROPERTIES OF MIXED CATION FLUORIDE  
CONDUCTORS

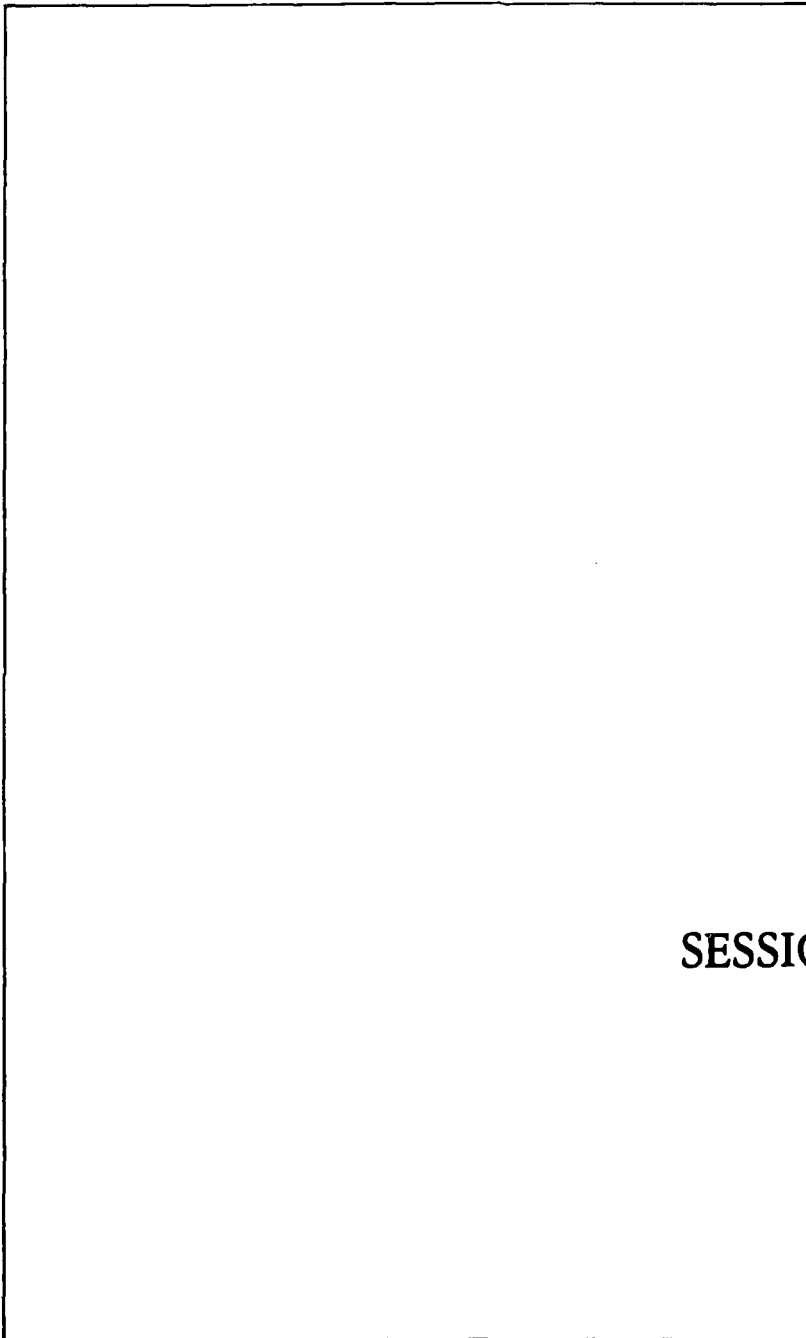
P. A. Cox and C. R. A. Catlow

Department of Chemistry, University of Keele, Keele, Staffs. ST5 5BG, U.K.

The fluorite-structured mixed metal fluorides  $\text{Rb}_{1-x}\text{Bi}_x\text{F}_{1+2x}$  are exceptionally good  $\text{F}^-$  ion conductors: a property which is clearly related to the nature of the cation distribution in the materials. We have recently studied these materials using two techniques:-

EXAFS has been used to study the local structure of the two types of cation. Data was collected both as a function of temperature and  $x$  (in the range  $0.5 < x < 0.75$ ). The results reveal considerable differences between the two types of cation. In particular for an Rb/Bi ratio of one, it is clear that defects are preferentially generated in the vicinity of Rb rather than Bi - a feature which is essential for the superionic behaviour of the materials. Moreover, we find that considerable short-range order develops as  $x$  deviates from 0.5, and in the limit of Bi/Rb=3, a fully ordered structure develops.

Molecular dynamics has been used to yield valuable information on atomic migration within  $\text{RbBiF}_4$ . Data was obtained for a series of temperatures between 80K and 750K. Excellent agreement between the structural prediction of EXAFS and MD is obtained. A non-colinear interstitialcy mechanism is proposed for anion diffusion within  $\text{RbBiF}_4$ ; and more complex correlated lattice-interstitial migration mechanisms are revealed by the MD studies.



SESSION 7A

## LOCAL STRUCTURE AROUND IMPURITIES INFERRED FROM OPTICAL AND E.P.R. SPECTROSCOPY

M. Moreno

D.C.I.T.T.Y.M., Sección Ciencia de Materiales. Facultad de Ciencias.  
Universidad de Cantabria. 39005 Santander. (Spain)

The new properties due to an impurity M in an insulator material can be understood to a great extent in terms of the  $MX_n$  unit formed by M and the n ions X in nearest neighbour position. Because of this fact the knowledge of the true M-X distance, termed R, between impurity and ligands and its variation under applied pressures or temperature changes plays a key role for a right microscopic understanding of the properties associated with the impurity. This task is however not easy to be achieved.

Though the EXAFS technique can be applied to any type of impurities it offers however some drawbacks. In particular changes in R,  $\Delta R$  less than 2 pm can hardly be detected which means that EXAFS technique is not suitable for measuring  $\Delta R$  induced by applied pressures less than about 1 GPa or by thermal expansion effects or even by structural phase transitions undergone by the host lattice. On the other hand that technique is not likely to be good for the case of "unstable" impurities (like  $Ni^{2+}$  for instance) due to the simultaneous presence of the stable impurity (like  $Ni^{2+}$ ) in the sample as well as the absence of reference compounds.

The present work emphasizes the usefulness of traditional optical and magnetic resonance measurements for obtaining reasonable information on the true M-X distance and its variations induced by applied pressures, phase transitions, etc... A particular attention is paid to the methods founded on reliable self consistent calculations of the complex as a function of R rather than to those involving empirical not proved assumptions.

A first part will be devoted to the information derived from spin-hamiltonian parameters and particularly from the isotropic superhyperfine constant  $A_s$  for the case of paramagnetic impurities containing unpaired  $\sigma$ -electrons. Calculations for different 3d complexes establish that  $A_s$  depends upon the square of the group overlap integral  $S_g$ . The application of this law will be illustrated with different examples going from  $Mn^{2+}$  in fluorides to unstable impurities like  $Ni^{2+}$ ,  $Cr^{3+}$  or  $Ag^{2+}$  in several host lattices. For the latter case strong outward lattice relaxations of up to 25% are obtained. It is also pointed out that by measuring  $A_s$  through ENDOR  $\Delta R$  changes well below 0.1 pm can be detected.

A second part devoted to optical properties will be mainly focused on crystal-field spectra of  $Mn^{2+}$  and  $V^{2+}$  in fluorides. Reliable calculations for  $MnF_6^{4-}$  and  $VF_6^{4-}$  point out that the effective Racah parameters, B and C, are nearly independent of R while  $10 Dq$  is proportional to  $R^{-m}$  m being close to five. Using this idea the R values obtained for  $Mn^{2+}$  in fluorides concur with those obtained from  $A_s$  data as well as with those derived from EXAFS. The

dependence upon R of other optical excitations (such as charge transfer,  $3d \rightarrow 4s$ , etc...) will also be discussed. A particular attention will be paid to charge transfer transitions of  $Cu^{2+}$  complexes. Finally the implications of local relaxation on other physical aspects such as the position of the impurity levels within the band scheme of the host lattice or the determination of covalency from E.P.R. data will also be analysed.

APPLICATION OF MAGNETIC MULTIPLE RESONANCES  
TO STUDY DEFECTS IN III-V COMPOUNDS

J.-M. Spaeth

Fachbereich Physik, University of Paderborn  
Warburger Str. 100A, D-4790 Paderborn, FRG

Optical detection of electron spin resonance by measuring the microwave induced changes of the magnetic circular dichroism (MCD) of the absorption band was first used to study both the ground and excited states of F centres in alkali halides (1). The method was somewhat *forgotten* for a long time until rather recently it proved to be a very useful tool for the study of defects in III-V semiconductors like GaAs and GaP. This paper reviews recent results of the application of the "MCD-method" to the investigation of extrinsic and intrinsic defects in GaAs.

In s.i. as-grown GaAs the most important deep donor is the EL2 defect, which is paramagnetic in its singly ionised form ( $EL2^+$ ). Although its optical absorption band is very weak and not observed in a straight absorption experiment, the MCD is of the order  $10^{-3}$  and easily observable. The ESR effect is about 20% of the MCD as measured in each of the 4 resolved  $^{75}As$  hyperfine lines. It was possible to measure also electron nuclear double resonance (ENDOR) by monitoring the rf and microwave induced changes of the MCD. The superhyperfine and quadrupole interactions with  $^{17}As$ -neighbours could be resolved and determined accurately. The ODENDOR effect is several orders of magnitude higher than expected from simple spin occupation statistics, which is not yet understood. It is of the same order as the ODESR effect. The  $EL2^+$  defect model could be derived from the superhyperfine interactions to be an As-antisite/As-interstitial pair defect (2).

In semiconductors it is very important not only to determine the structure, but also to determine the energy levels of a defect. This can be done in materials where the level under investigation is empty. Then by photo-ODESR and photo-ENDOR experiments, in which the level is occupied by raising electrons from the valence band, the level position can be determined.

The MCD method was also used to investigate transition metals in GaAs and InP. It turned out that the ODESr effect cannot only be observed in intracenter absorption transitions but also in ionisation transitions to both the valence and conduction band. This observation makes the applicability of the method rather general. Examples are given for  $V^{3+}$  and  $V^{2+}$  in GaAs and  $Fe^{3+}$  in InP. A novel method was derived recently to determine the spin and thus charge state of a defect based on measurements of the temperature and field dependence of the MCD and its comparison to the Brillouin function once the g-factor is known. It could be shown that  $V^{2+}$  on a Ga-site in GaAs, a  $3d^3$  configuration, has  $S=1/2$ , i.e. is in a low spin state. This was the first such observation in III-V compounds and in accordance with recent theoretical predictions (3). In recent MCD experiments of s.i. GaAs also a diamagnetic MCD was discovered, which was assigned to ionised shallow C and Zn acceptors. The MCD method allows thus also to observe spin paired states.

The MCD's of defects can be more characteristic than their ESR spectra. It could be demonstrated that the same ODESr spectrum for several As antisite-like defects was measured within experimental error, which belongs, however, to very different MCD spectra, which were measured as a sort of excitation spectrum of the ODESr lines ("MCD tagged by ESR") (4).

It will also be shown that the optical detection of ESR and ENDOR lends itself to spatially resolved ESR and ENDOR experiments. An example for such a mapping investigation in s.i. GaAs will be given.

ODESR experiments via donor-acceptor recombination luminescence are a long established method in semiconductors. They have, however, definite disadvantages compared to the MCD method, which will be briefly discussed.

- (1) Mollenauer and S. Pan, Phys. Rev. B6, 772 (1972)
- (2) B.K. Meyer, D.M. Hofmann, J.R. Niklas and J.-M. Spaeth, Phys.Rev. B36, 1332 (1987)
- (3) A. Görger, B.K. Meyer, J.-M. Spaeth and A. Hennel, J Phys. C, in press (1988)
- (4) F.J. Ahlers, F. Lohse, J.-M. Spaeth and L.F. Mollenauer Phys. Rev. B 28, 1249 (1983)



SESSION 7B

THE PHYSICS OF LATTICE DEFECTS IN THE SILVER HALIDES\*

L. M. Slifkin

Department of Physics and Astronomy, University of North Carolina  
Chapel Hill, NC 27599-3255, USA

In silver bromide and silver chloride, the crystal defects -- both electronic and ionic -- exhibit unusual and interesting physical properties. These properties are not only essential to the efficient functioning of the photographic process, but they also provide significant research opportunities. This paper will deal only with the ionic point defects -- the Frenkel defects and impurity ions -- and will consider a variety of recent developments that have enhanced our understanding. These include:

- (a) An appreciation of the role and near-uniqueness of the easy quadrupolar deformability of the silver ion, giving rise to an extraordinarily high jump frequency of the interstitial, even at quite low temperatures.
- (b) Progress in computer simulation studies of the defect formation and migration enthalpies and entropies, along with a revival of the question of the direct migration of the interstitial, vis-a-vis the interstitialcy replacement mechanisms.
- (c) Experimental resolution of the Frenkel pair formation enthalpy and entropy into the separate contributions associated with the interstitial and the vacancy, leading to an appreciation of the large effect of the entropy change due to shifts in phonon frequencies.
- (d) An investigation of the possible Hall effect due to the migration of independent interstitials in the crystal lattice, as contrasted with the liquid-like behavior of superionic conductors.
- (e) Experimental observations of surprisingly enhanced conductivities of composites of silver halides with fine particles of oxides, and the development of several (possibly competing) theoretical models.

(f) The demonstration and determination of the non-linearity of the temperature-dependence of the Frenkel formation free energy.

(g) Experimental elucidation of the roles of ion size, charge, and electronic configuration in the diffusion of impurity tracers in AgBr and AgCl.

(h) Evidence for the creation of Frenkel defects as a result of the trapping of photocarriers at impurities, and evidence for the trapping of photocarriers at or near to vacancies and interstitials.

A number of questions do, however, remain unanswered. For example:

(a) Why does the activation energy for vacancy migration decrease rapidly upon heavy doping with divalent cations?

(b) How are we to understand the anomalously high values of activation energy and pre-exponential factor in the high-temperature diffusion of halides and some other ions in silver bromide?

(c) What are the sources and sinks for point defects inside the bulk crystals?

\*Supported by the National Science Foundation under Grant DMR-8722476.

## IMPURITY AGGREGATION IN IONIC CRYSTALS

M. Manfredi

Department of Physics - University of Parma and G.N.S.M. - C.I.S.M.  
Viale delle Scienze - 43100 Parma - ITALY

The aggregation process of impurities in ionic crystals can be monitored by means of techniques such as ionic thermocurrents (ITC) [1] or electron paramagnetic resonance (EPR) and, at the late stages of the process where large aggregates are produced, by means of electron microscopy or X-ray diffraction.

Measurements of optical absorption, emission and luminescence time decay spectra have been widely used in the last years in order to get complementary information about the above process.

Recently two kinds of measurements have been utilized, that look promising in order to increase the knowledge about the aggregation processes, particularly in certain stages where the above mentioned techniques could be less sensitive.

The idea, which these measurements are based, is as follows: to the impurities whose behaviour is being studied (referred as "aggregating impurities") a small percentage of a second impurity is added, that acts as a "probe" of the aggregation process. These last impurities (the "probe impurities") are optically active.

If the aggregation impurities are not optically active [2], the changes on the optical properties of the probe impurities are assumed as a tool for monitoring the aggregation processes. If both impurities are optically active [3, 4], the aggregating and probe impurities can act as donors and acceptors respectively, so it is possible in principle that energy transfer between them takes place.

The energy transfer is very sensitive to the distance between donors and acceptors as shown by the transfer probability, that in the case of a dipole-dipole mechanism is:

$$P(DD) \propto Q_A R^{-6} \tau_D^{-1} E^{-4} \int f_D(E) F_A(E) dE$$

where  $Q_A$  is related to the oscillator strength of the transition,  $R$  is the distance between donors and acceptors,  $\tau_D$  is the decay time of donors,  $f_D(E)$  and  $F_A(E)$  represent in the overlapping integral, the normalized shape of the donor emission band and the acceptor absorption band, respectively and  $E$  is the average value of the energy involved in the transition.

When the distance between donor-acceptor pairs becomes shorter than the interaction distance  $R^*$  the transfer is detected experimentally.

Furthermore the time decay signals change their shape depending on the kind of aggregates that are formed and it is possible to distinguish between mechanisms as single

pair transfer or energy migration along donor chains before the transfer takes place. Systems such as NaCl: Eu, Mn, KCl: Eu, Mn, NaCl: Pb, Mn etc. have been examined from an experimental point of view. Starting from a quenched situation, in which the distance between the impurities is larger than the interaction distance aggregation processes have been induced, and step by step the energy transfer mechanisms have been analysed.

- [1] R. Capelletti, Radiation Effects **74**, 119 (1983).
- [2] J. Garcia Solà, C. Zaldo, and F. Agulló-Lopez, Phys. Review **B 25**, 3050 (1981).
- [3] P. Aceituno, C. Zaldo, F. Cussó, and F. Jaque, J. Phys. Chem. Solids **45**, 637 (1984).
- [4] J. Rubio O., H. Murrieta S., R. C. Powell, and W. A. Sibley, Phys. Review **B 31** (1985).

POSTER SESSION II  
THURSDAY

OPTICAL PROPERTIES OF IMPURITY PERTURBED COLOR CENTERS IN  
INSULATING OXIDE CRYSTALS\*

G. J. Pogatshnik and Y. Chen  
Solid State Division, Oak Ridge National Laboratory  
Oak Ridge, TN 37831 USA

The optical properties of impurity perturbed color centers in alkali-halide crystals have been studied extensively and have found important applications in color center lasers. However, much less is known about the analogous centers in oxide crystals. We examine three different systems whose optical properties depend on the perturbing ion and the host:  $\text{Cr}^{3+}$  ions perturbed by F centers in neutron irradiated  $\text{MgAl}_2\text{O}_4$  spinel,  $\text{Ce}^{3+}$  perturbed color centers in  $\text{Ce}:\text{CaO}$ , and color centers perturbed by rare earth ions in YAG.

Chromium ions are present in trace amounts in most spinel crystals. These impurities can be detected by the characteristic  $\text{Cr}^{3+}$  emission in the near infrared. Neutron irradiation produces F centers with broad absorption bands in the ultraviolet. While no luminescence is observed from the F centers themselves, their presence alters the observed characteristics of the  $\text{Cr}^{3+}$  emission.<sup>1</sup> Excitation spectra of the 695 nm  $\text{Cr}^{3+}$  emission following neutron irradiation showed that the Cr excitation bands increase in intensity and shift to higher energy with increased exposure to neutron irradiation. F centers created by neutron irradiation can be located at random next to  $\text{Cr}^{3+}$  impurities, and the perturbation produces the increased strength of the chromium excitation bands. This effect has previously been observed in some fluoride crystals and was attributed to exchange coupling between the F center and the Cr impurity which increases the oscillator strength of the Cr transitions.<sup>2</sup>

Calcium oxide crystals doped with cerium present a contrasting case to the chromium in spinel. Crystals of  $\text{CaO}$  doped with ~0.1% Ce exhibited broad color center absorption bands at 470, 400, and 300 nm. The 400 nm absorption band is similar to that of the F center in  $\text{CaO}$ , and the 470 nm band is attributed to cerium perturbed color centers. Excitation near 470 nm produced a broad band emission which peaked at 580 nm. The fluorescence lifetime at room temperature and 77 K is approximately 80 ns. While the cerium perturbed color center is an efficient emitter, we have observed no fluorescence which we can attribute to the 5d to 4f luminescence of the  $\text{Ce}^{3+}$  ion, even though EPR measurements show an abundance of  $\text{Ce}^{3+}$  ions at cubic symmetry sites.<sup>3</sup>

Finally, we examine the optical properties of a color center in YAG which is perturbed by a rare earth ion. These crystals were grown by the Institute of Optics and Fine Mechanics, Shanghai, P.R.C. and were provided by Wu Guangzhao. Some of the crystals have a color center absorption band at 370 nm and an efficient emission at 400 nm.<sup>4</sup> Excitation near 240 nm also produces narrow emission lines which we believe are due to Tb<sup>3+</sup> ions. We presume that the color center is associated with Tb ions since we have not observed this color center in crystals where the narrow emission lines of the Tb were absent. The presence of the color center produces changes in the expected optical properties of the perturbing ion. While the emission lines from the Tb <sup>5</sup>D<sub>4</sub> level are similar to those in uncolored Tb:YAG, the emission lines from the <sup>5</sup>D<sub>3</sub> state are shifted to lower energy than those normally observed in Tb:YAG. The shift is approximately 1000 cm<sup>-1</sup>, which is extremely large for a rare earth ion. The fluorescence lifetimes of the narrow emission bands are less than 5 μs, which again is very uncharacteristic of 4f transitions in the rare earths.

The optical properties of the impurity perturbed color centers examined above exhibit a wide variety of properties which are not well understood. It is hoped that further investigation of these centers may lead to useful applications in optical devices.

1. L. S. Cain, G. J. Pogatshnik, and Y. Chen, Phys. Rev. B (in press)
2. K. H. Lee and W. A. Sibley, Phys. Rev. B12, 3392 (1975).
3. G. J. Pogatshnik, M. M. Abraham, and Y. Chen, (to be published).
4. W. Guangzhao and Z. Xiurong, Chin. J. Lasers 14, 318 (1987).

\* Supported by DARPA under interagency agreement 40-1611-85 with Martin Marietta Energy Systems Inc., contract DE-AC05-84OR21400 with US DOE.

OPTICAL AND E.P.R. INVESTIGATION ON AS GROWN  $\text{NaBr:Mn}^{2+}$  AND  
 $\text{LiCl:Mn}^{2+}$  SINGLE CRYSTALS

C. Marco de Lucas, F. Rodríguez, M. Moreno

D.C.I.T.T.Y.M., Sección Física de Materiales, Universidad de  
 Cantabria, 39005-Santander, Spain.

Excitation and emission spectra in the range 14-300 K as well as EPR spectra in the range 7-300 K have been recorded for as grown  $\text{NaBr:Mn}^{2+}$  and  $\text{LiCl:Mn}^{2+}$  single crystals containing about 500 and 1500 ppm of  $\text{Mn}^{2+}$  respectively. In the case of  $\text{NaBr:Mn}^{2+}$  the EPR spectrum consists only of an isotropic band with  $\Delta H_{pp} = 133$  G and displaying a truncated Lorentzian shape similar to that found for  $\text{Mn}^{2+}$  and other 3d ions compounds. The value of  $\Delta H_{pp}$  remains essentially unchanged from 300 to 7 K.

This result indicates that the EPR signal is due to a precipitated phase of  $\text{Mn}^{2+}$  whose magnetic phase transition is placed well below 7 K. No traces of isolated  $\text{Mn}^{2+}$  have been detected.

The excitation spectrum displayed in Figure 1 reveals the presence of a double excitation peak at 214 nm reflecting the existence of exchange interaction. Moreover the crystal-field bands suggest a local  $O_h$  symmetry for  $\text{Mn}^{2+}$ . The inspection of the excitation spectrum in the 7-300 K range does not show indications of either structural or magnetic phase transitions. The emission peak is placed at 622 nm at 14 K and at 601 nm at room temperature. No signs of transfer processes and trap luminescence have been detected.

The comparison of these results with those found for  $\text{NaCl:Mn}^{2+}$  strongly support the formation of Suzuki phase precipitates, as it was previously indicated<sup>1,2</sup>. Moreover a careful analysis of the  ${}^4T_1(G)$  band (Figure 2) shows the presence of vibronic progressions associated to a phonon frequency  $\Omega = 130 \text{ cm}^{-1}$ , which is close to that associated<sup>2</sup> to the  $A_{1g}$  mode by Raman spectroscopy. This result also supports that  $\text{Mn}^{2+}$  is surrounded by 6  $\text{Br}^-$  ions in spite of the position of the  ${}^4A, {}^4E$  peak at 420 nm, usually found at 430 nm for  $\text{MnBr}_6^{4-}$ .

The results on  $\text{LiCl:Mn}^{2+}$  are rather similar to those obtained for  $\text{NaBr:Mn}^{2+}$ . They discard the formation of the  $\text{Li}_2\text{MnCl}_4$  compound having the inverse spinel structure while they support the presence of the Suzuki phase. The large value  $\Delta H_{\text{pp}} = 600 \text{ G}$  found for the EPR band-width points out that in this case the exchange constant  $J$  is about half that found for the Suzuki phase in  $\text{NaCl:Mn}^{2+}$ .

- 1 F. Rodríguez, M. Moreno, Solid St. Commun. 58, 701 (1986).
- 2 A. de Andrés, J.M. Calleja, J. Mol. Structure, 143, 71 (1986).

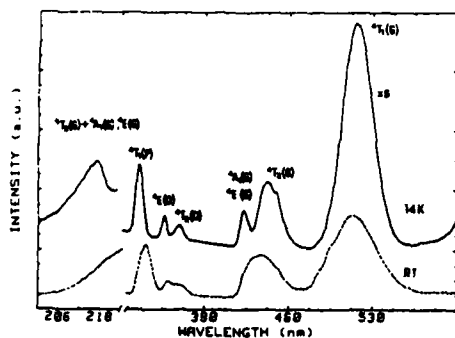


Figure 1

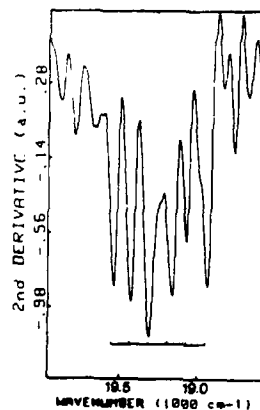


Figure 2

OPTICAL INVESTIGATIONS ON  $\text{NH}_4\text{Br}:\text{Cu}^{2+}$  AND  $\text{NH}_4\text{Cl}:\text{Cu}^{2+}$ 

A.G. Breñosa, F. Rodriguez, M. Moreno

D.C.I.T.T.Y.M., Sección Ciencia de Materiales, Universidad de Cantabria, 39005-Santander, Spain

Ammonium halides are interesting basic materials because they display simple crystal structures and at the same time exhibit phase transitions related to the ordering of  $\text{NH}_4^+$  tetrahedra.

In such materials particular efforts have been devoted in order to found sensitive probes for detecting the phase transitions. In this way E.P.R. experiments have been carried out using well characterized  $\text{Cu}^{2+}$  centers as a probe. Nevertheless much less attention has been focused on the optical properties of such centers. In particular no studies have been reported up to date on the sensitivity of charge-transfer (C.T.) bands of  $\text{Cu}^{2+}$  centers in spite of the low  $\text{Cu}^{2+}$  concentration ( $\sim 5$  ppm) needed to detect them. A main goal of the present work is just

to emphasize the good sensitivity of CT bands of center II in  $\text{NH}_4\text{Br}$  and  $\text{NH}_4\text{Cl}$  as probes for revealing the phase transitions due to ordering of  $\text{NH}_4^+$  ions in both materials.

Figure 1 depicts the Optical Absorption spectrum of a  $\text{NH}_4\text{Br}$  sample containing about 100 ppm of center II. At 83 K the spectrum is composed of two bands peaking at  $26200\text{ cm}^{-1}$  and  $29700\text{ cm}^{-1}$  respectively. The first band lies about  $7000\text{ cm}^{-1}$  lower than the corresponding for  $\text{NH}_4\text{Cl}:\text{Cu}^{2+}$ . This figure supports that such bands arise from halogen to  $\text{Cu}^{2+}$  one-electron jumps.

When upon cooling the sluggish

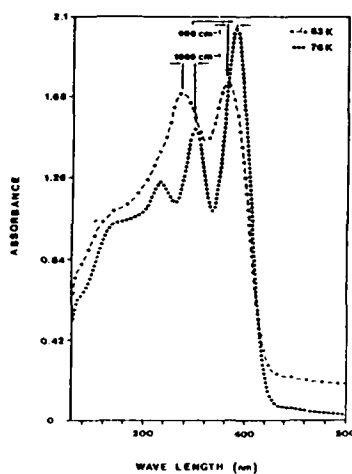


Fig. 1

transition<sup>1</sup> at 78 K occurs (involving "ferromagnetic" ordering of  $\text{NH}_4^+$ ) the peak position of the  $e_u(\sigma + \pi) \rightarrow a_{1g}^*$  band experiences a drastic red shift of  $1200 \text{ cm}^{-1}$  (Figures 1 and 2).

Upon warming

however the jump

occurs at 108 K in agreement with the large hysteresis involved in this phase transition<sup>1</sup>. These facts stress the greater sensitivity of CT bands of  $\text{NH}_4\text{Br}:\text{Cu}^{2+}$  for detecting this transition when compared to that of the  $\{g\}$  tensor<sup>2</sup>. Figure 2 also reveals the existence of the phase transition at 234 K (involving an antiferromagnetic ordering of  $\text{NH}_4^+$ ) and supports that this transition has a dominant second order character at variance with what is found for the transition at 78 K.

In  $\text{NH}_4\text{Cl}:\text{Cu}^{2+}$  the appearance of "ferromagnetic order" at 243 K gives also rise to a red-shift of the first CT band decreasing by  $900 \text{ cm}^{-1}$  in the 243-190 K range. The influence of variations of  $\text{Cu}^{2+}$  ligand distances upon the red shifts of CT bands will be discussed.

Finally the crystal-field spectra at 14 K of both  $\text{NH}_4\text{Cl}:\text{Cu}^{2+}$  and  $\text{NH}_4\text{Br}:\text{Cu}^{2+}$  show the presence of well resolved progressions assigned to the  $\text{NH}_3-\text{Cu}^{2+}$  stretching mode.

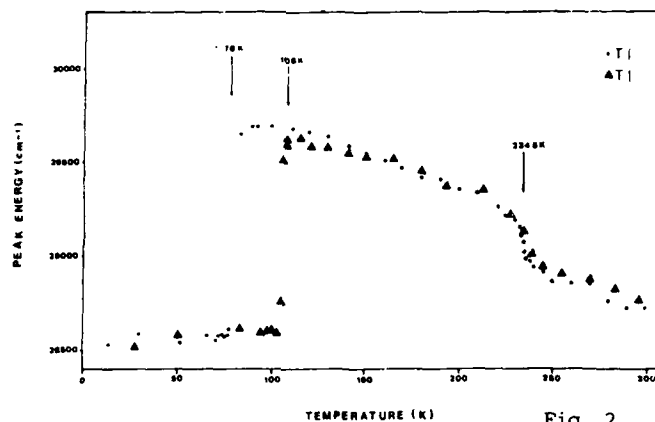


Fig. 2

1 A. Bonilla, C.W. Garland and N.E. Schumaker, Acta Cryst. A26, 156 (1970).

2 A. Kawamori and J.L. Rao, Bull. Mag. Res. 5, 203 (1983).

DEPENDENCE OF CRYSTAL-FIELD SPECTRUM OF  
 $\text{RbMnF}_3$  AND  $\text{KMnF}_3$  WITH TEMPERATURE  
 IN THE 14-600 K RANGE

F. Rodríguez, M. Moreno

D.C.I.T.Y.Y.M., Sección Ciencia de Materiales, Facultad de Ciencias,  
 Universidad de Cantabria, 39005-Santander, Spain.

J.M. Dance, A. Tressaud

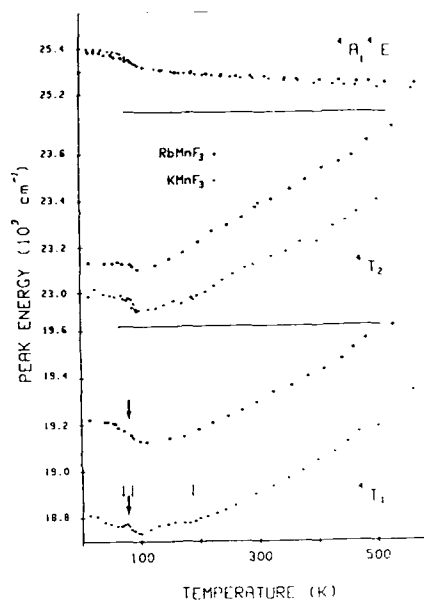
Laboratoire de Chimie du Solide du C.N.R.S., Université de Bordeaux, I,  
 33405 Talence Cedex, France.

The Optical Absorption peaks due to an impurity in insulator materials depend on both the temperature of the sample and the pressure. Microscopically the observed variations in the peak positions reflect the structural changes around the impurity, induced by temperature or pressure variations.

In the case of  $\text{Mn}^{2+}$  doped fluoroperovskites the variations undergone by the crystal field spectrum have been well explained as being due to different  $\text{Mn}^{2+}-\text{F}^-$  distances in the  $\text{MnF}_6^{4-}$  unit induced by a different "chemical pressure" of the rest of the lattice upon it. With regard to this problem theoretical Hartree-Fock-Roothaan calculations as well as experimental measurements on  $\text{Mn}^{2+}$  doped fluoroperovskites point out that the Racah parameters B and C for  $\text{MnF}_6^{4-}$  are practically independent of the  $\text{Mn}^{2+}-\text{F}^-$  distance, R, while  $10 Dq$  depends on  $R^{-n}$  with  $n=4.65^{1,2}$ .

The understanding of the changes experienced by the peak positions due to temperature variations is however a more complicated task. In fact if E denotes the energy of a peak, the experimentally measured quantity  $(\partial E / \partial T)_p$  is given by  $(\partial E / \partial T)_p = (\partial E / \partial V)_T (\partial V / \partial T)_p + (\partial E / \partial T)_V$  so it is governed not only by thermal expansion effects but also by the so called explicit term  $(\partial E / \partial T)_V$ , which is not easy to calculate a priori. In order to determine what is the importance of each contribution it is necessary to study a pure compound whose optical properties are

however well described in terms of complexes such as it happens for  $\text{RbMnF}_3$  and  $\text{KMnF}_3$ . In such cases the local thermal expansion is known<sup>3,4</sup> and then the explicit term can be obtained a posteriori from the experimental  $(\partial E / \partial T)_P$  values. In the present work we have studied the changes undergone by the Optical Absorption peaks of  $\text{RbMnF}_3$  and  $\text{KMnF}_3$  single crystals in the 14-600 K temperature range. The results for the  ${}^4T_1(G)$ ,  ${}^4T_2(G)$  and  ${}^4A_1(G)$ ,  ${}^4E(G)$  peaks of  $\text{RbMnF}_3$  and  $\text{KMnF}_3$  are shown on the Figure. Aside from the existence of known phase transitions in such materials (indicated by arrows) it reveals that above 150 K the



peaks depending upon  $10 Dq$  experience in fact a much more pronounced variation with temperature than the  ${}^4A_1(G)$ ,  ${}^4E(G)$  peak. The analysis of these data using the known thermal expansion coefficients for  $\text{KMnF}_3$  and  $\text{RbMnF}_3$  as well as the dependence of the peak energies with  $R$  leads to the conclusion that for both crystals the thermal expansion contributions to  $(\partial E / \partial T)_P$  is 40% while the explicit contribution amounts to 60%. This conclusion is at variance with that recently reached by Darwish et al. pointing out that the explicit term is dominant<sup>5</sup>. The present results are not encouraging in order to obtain information about the local thermal expansion around an impurity from optical data.

- 1 F. Rodríguez, M. Moreno, A. Tressaud and J.P. Chaminade, Crys.Latt.Def. 16, 221 (1987)
- 2 M. Flórez, L. Seijo and L. Pueyo, Phys.Rev.B34, 1200 (1986).
- 3 E. Dormann, J.R.D. Copley and V. Jaccarino, J.Phys.C:Solid State Phys., 10, 2767 (1977)
- 4 L.J. de Jongh and D.J. Breed, Solid State Comm., 15, 1061 (1974)
- 5 S. Darwish, S. Abumansor and M.S. Seehra, Phys.Rev. B34, 3198 (1986)

# EVOLUTION OF THE F AGGREGATE CENTERS UNDER F LIGHT BLEACHING: A SIMPLE MODEL

V. D. Rodríguez<sup>1</sup> & E. Pérez<sup>2</sup>

<sup>1</sup> Dpto. Física, Univ. La Laguna, Tenerife (Spain)

<sup>2</sup> Inst. Astrofísica de Canarias. La Laguna, Tenerife (Spain)

## INTRODUCTION

The optical excitation of  $F$  centers in alkali halides induces the bleaching of these centers and also modifies the concentration of  $F$  aggregate centers (1).

It has been observed that the decay of  $F$  centers in  $\text{NaCl}$  and  $\text{KCl}$  obeys to a 1<sup>st</sup> order kinetic (2,3). In this communication we present a simple model to describe the evolution shown by  $F$  aggregate centers under  $F$  light illumination. The model is contrasted with experimental results corresponding to  $\text{NaF}$  with color centers produced via X irradiation.

## THE MODEL

We consider that the concentration of each kind of aggregate grows from lower aggregates and decreases by the formation of larger aggregates. This can be expressed by the following differential equations:

$$\frac{dM}{dt} = \beta F^2 - \beta' FM$$

$$\frac{dR}{dt} = \beta' FM - \beta'' FR$$

$$\frac{dN}{dt} = \beta'' FR - \beta''' FN$$

where  $M$ ,  $R$  and  $N$  represent aggregates of 2, 3 and 4  $F$  centers respectively. Considering that the decay of  $F$  centers is governed by a 1<sup>st</sup> order kinetic, this is:

$$F = F_0 e^{-\alpha t}$$

it is possible to integrate the above equations obtaining:

$$M = \frac{\beta}{\beta'} F + C e^{\frac{\beta'}{\alpha} F} + \frac{\alpha \beta}{\beta'^2}$$

$$R = \frac{\beta}{\beta''} F - \frac{C \beta'}{\beta' - \beta''} e^{\frac{\beta'}{\alpha} F} + C' e^{\frac{\beta''}{\alpha} F} + \frac{\alpha \beta}{\beta''} \left( \frac{1}{\beta'} + \frac{1}{\beta''} \right)$$

$$N = \frac{\beta}{\beta'''} F + \frac{C \beta' \beta''}{(\beta' - \beta'')(\beta' - \beta''')} e^{\frac{\beta'}{\alpha} F} - \frac{C' \beta''}{\beta'' - \beta'''} e^{\frac{\beta''}{\alpha} F} + C'' e^{\frac{\beta'''}{\alpha} F} + \frac{\alpha \beta}{\beta'''} \left( \frac{1}{\beta'} + \frac{1}{\beta''} + \frac{1}{\beta'''} \right)$$

where  $C$ ,  $C'$  and  $C''$  are constants.

## RESULTS FOR NaF

In figures 1 and 2 we present the experimental data for the evolution of the different centers under  $F$  light bleaching at room temperature (RT) and at 145°C respectively. The continuous lines show our model fit to the data points.

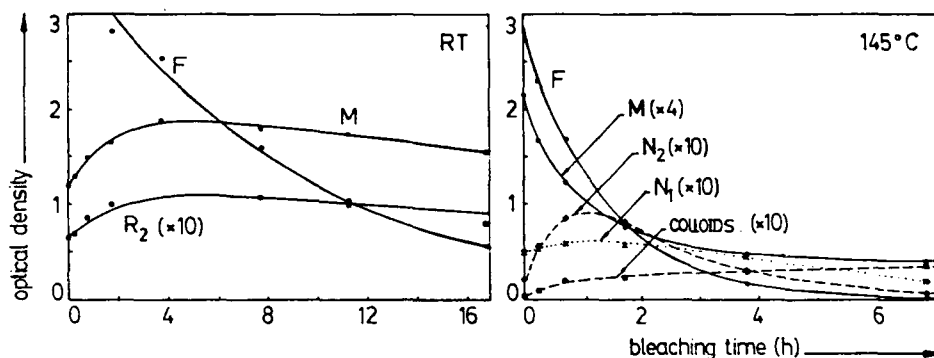
In both figures we observed that the decay of  $F$  centers is exponential and quicker at 145°C. The thermal activation energy obtained is 0.25 eV.

The  $M$  centers adopt a very different behaviour with the two temperatures considered. It can be outlined that our model is able to reproduce both of them. Parameters  $\beta$  and  $\beta'$ , which account for the formation and destruction of  $M$  centers, have similar values at RT, 0.046 and 0.043 respectively. When measured at  $145^\circ\text{C}$ ,  $\beta$  increases by a factor of 2 while  $\beta'$  increases by a factor 18. On the other hand,  $\beta'$  is the parameter associated to the formation of  $R$  centers.

At RT the concentration of  $R$  centers only changes slightly under  $F$  light illumination. Larger  $F$  aggregate centers are not formed in an appreciable quantity.

When the sample is heated at  $145^\circ\text{C}$  most of the  $R$  centers disappear and  $N$  centers are formed. The most interesting behaviour at this temperature is that under  $F$  light illumination  $N$  centers and even colloids are formed. This is shown in figure 2.

To conclude, we report that when  $F$  light bleaching is made above RT the formation of large aggregate centers is enhanced. This is accounted for in our model by the increment of the corresponding parameters.



- (1) Dale Compton, W. & Rabin, H., 1964, *Sol. State Phys.* **16**, 121.
- (2) Jaque, F. & Agulló López, 1974, *Cryst. Latt. Defects*, **5**, 65.
- (3) Deshpande, A.V., Chandratillake, M.R., Hamblett, I.H., Newton, G.W.A., Patil, S.F. & Robinson, V.J., 1981, *J. Chem. Soc., Faraday Trans.*, **77**, 135.

THERMAL AND OPTICAL BLEACHING OF ABSORPTION SPECTRA IN REDUCED  $\text{LiNbO}_3$ 

A.García-Cabañes, E.Diéguez, J.M.Cabrera and F.Agulló-López

Departamento de Física Aplicada C-IV, Universidad Autónoma de Madrid  
Cantoblanco, 28049 Madrid (Spain)

Thermal reduction of  $\text{LiNbO}_3$  introduces a complex absorption band, very likely made up of several components, some of them associated with oxygen vacancy centres (1). The study of the thermal and optical stability of the spectra may provide some clues on the various components and reactions among them.  $\text{LiNbO}_3$  crystals with different Li/Nb ratios (0.83, 1.1 and 1.2 in the melt) have been reduced in vacuum at 800-900°C as to develop the typical absorption band extending up to the near IR. Then, the evolution of the band with heating above RT (up to 250°C) has been measured. As previously reported for congruent reduced (2) and e-irradiated samples (3), the band decreases for all Li-deficient compositions in the VIS-UV region to the benefit of a clear band growing at 1.6 eV (associated with small polarons  $\text{Nb}^{+4}$ ). The effect is clearly reversible in the range RT-250°C.

Parallel experiments have been carried out by subjecting the reduced samples to monochromatic illumination at LNT ( $\lambda_1 = 405 \text{ nm}$ ,  $\lambda_2 = 480 \text{ nm}$ ). As previously reported for congruent reduced samples (4), it is again found that the absorption above 2 eV decreases to the benefit of a well-defined band peaked at 1.5-1.6 eV. As for thermal excitation, the magnitude of the effect is highest for the most Li-deficient samples, although the spectral changes are qualitatively similar for all Li/Nb. A typical spectrum showing the spectral changes brought about by a) illumination, and b) heating, is shown in Figure 1.

Thermal and optical bleaching experiments have been also performed on Fe, as well as Fe- and Mg- doped  $\text{LiNbO}_3$ . Some differences with regard to the undoped samples are to be noted:

a) The magnitude of the induced changes is much smaller for the doped samples.

b) The IR band growing at the expenses of the UV-VIS band peaks at 1.6-1.7 eV ( $\text{Fe:LiNbO}_3$ ) and 1.8-1.9 eV ( $\text{Fe:Mg:LiNbO}_3$ ).

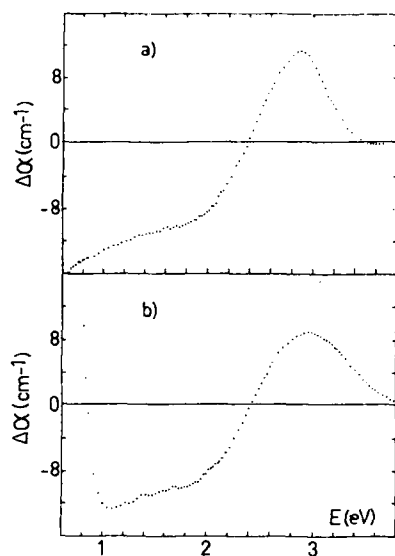


**Figure 1**

Incremental absorption coefficient of a reduced  $\text{LiNbO}_3$  sample,  $\text{Li} / \text{Nb} = 0.908$ , after: a) illumination at  $\lambda = 480 \text{ nm}$  ( $T=77 \text{ K}$ ), b) heating and measuring at  $573 \text{ K}$ .

#### REFERENCES

- (1) L.Arizmendi, J.M.Cabrera and F.Agulló-López, J.Phys.C: Solid State Phys., 17, 515 (1984)
- (2) O.F.Schirmer, S.Juppe and J.Koppitz, Cryst.Latt.Def.and Amorph.Mat., 16, 353 (1987)
- (3) E.Hodgson and F.Agulló-López, Solid State Commun., 64, 965 (1987)
- (4) K.L.Sweeney and L.E.Halliburton, Appl.Phys.Lett., 43, 336 (1983)

THE RELAXATION DYNAMICS OF OPTICALLY EXCITED  
F CENTERS IN ALKALI HALIDES

Yuzo MORI and Hiroshi OHKURA

Department of Applied Physics, Osaka City University,

Sumiyoshi-ku, Osaka, JAPAN 558

When the F center is optically excited, the strong electron-lattice interaction of F center yields a simultaneous dynamics of electrons, radiation field and surrounding lattice associated with its large relaxation. This process can appear in the resonant secondary emission (RSE) which occurs subsequently as the resonant Raman scattering (RRS), the hot luminescence (HL) and the ordinary F luminescence (OL). [1,2] Although the RSE has been studied theoretically and experimentally, it was treated within a limited spectral region and/or within a lowest order approximation. [3-8] We have measured the RSE over the whole spectral region [9], and tried to understand the whole optical process in a unified framework. [10,11] We described the whole optical process in terms of a semi-classical model based on the Franck-Condon principle. We demonstrated that (1) the Franck-Condon principle is applicable to describe the optical process from unthermalized dynamical state (2) the large lattice relaxation can basically be expressed by an exponential type unharmonic adiabatic potential which is taken from the Born-Mayer potential, (3) a transition between 2s and 2p state occurs during the dynamical relaxation. From these results, we suggested that the higher order effect such as quadratic electron-lattice interaction and unharmonic lattice

force should be included in the explanation of the optically excited F center.

In the present work, in order to check the validity of the model discussed above, we measured the dependence of RSE on the resonant light frequency of  $\Omega_1$ . The results are summarized as  $\Omega_1$  dependence of (a) the line shape of the HL and OL, (b) relative intensity of the HL to the OL, (c) the linear polarization of both RRS and HL, (d) the effective lattice temperature which is obtained from the intensity ratio between the anti-Stokes and Stokes components and (e) the averaged frequency of coupled lattice vibration. We analyzed these results by adopting the model mentioned above within a lowest order approximation in which a linear electron-lattice interaction in a harmonic potential is solely taken into account. The result calculated is not sufficient to fit whole data. This may be related to the neglect of higher order terms in the analysis. In the conference, we will show more details on this topics.

#### References:

- [1] V. Hizhnyakov and I. Tehver: Phys. Stat. Sol. 21 (1967) 755. [2] Y. Toyozawa: J. Phys. Soc. Jpn. 41 (1976) 400. [3] D. B. Fitchen, D. S. Pan and F. Luty: Abstract of Int. Conf. Color Centers, Sendai, 1974, E89. [4] J. P. Buisson, S. Lefrant, A. Sadoc, L. Taurel and M. Bilardon: Phys. Stat. Sol. (b) 78 (1976) 779. [5] Y. Kondo, T. Noto, S. Sato and M. Hirai: J. Lum. 38 (1987) 164. [6] S. Muramatsu, M. Aihara and K. Nasu: J. Phys. C Sol. St. Phys. 19 (1986) 2585. [7] V. Hizhnyakov: Phys. Rev. B 30 (1984) 3490. [8] Y. Kayanuma, Y. Mori and H. Ohkura: J. Lum. 38 (1987) 139. [9] Y. Mori, R. Hattori and H. Ohkura: J. Phys. Soc. Jpn. 51 (1982) 2713. [10] H. Ohkura, Y. Mori, H. Kobayashi, and Y. Kimura: Proc. of the IXth int. conf. Raman Spec. [11] Y. Mori, H. Hanzawa and H. Ohkura: J. Lum. 38 (1987) 159.

EFFECT OF IONIZING RADIATIONS ON  $\text{CsCdBr}_3$  CRYSTALS.

C. Andraud, F. Pellé, O. Pilla (+), J.P. Denis  
and B. Blanzat

C.N.R.S - ER211, Place A. Briland 92190 Meudon  
Bellevue FRANCE

(+) permanent address : dipartimento di Fisica,  
Universita di Trento, 38050 POVO (TRENTO) ITALY.

Recently optical properties of pure  $\text{CsCdBr}_3$  crystals have been studied (1,2,3). These consist in three emission bands A, B and C ; at low temperature, the A and B emission peak at 3.3 and 1.9 eV respectively and the C emission is structured in two bands at 1.8 and 1.6 eV. A and B have the same excitation spectrum, which is constituted of two sharp components at 3.91 and 3.97 eV ; the excitation spectrum of C is a large band at 5 eV. These features have been tentatively attributed to the presence of  $\text{Br}_2^{1-}$  molecules located on stacking faults of the uniaxial structure of  $\text{CsCdBr}_3$  crystals. These have an hexagonal structure (space group  $P_6_3 / mmc$ ), where  $(\text{CdBr}_6)^{4-}$  octahedra are connected by faces forming infinite chains parallel to the C axis;  $\text{Cs}^+$  ions occupy positions between these chains (4). As regards the effect of doping by  $\text{Pb}^{2+}$  or  $\text{Sn}^{2+}$  ions which increases the concentration of  $\text{Br}_2^{1-}$  centers due to the formation of cubic microdomains of  $\text{CsPbBr}_3$  or  $\text{CsSnBr}_3$ , these centers have been supposed to be located in shifted chains (1).

This paper concerns the confirmation of the origin of these bands using ionizing radiation by analogy with the study of the luminescence of self-trapped excitons in alkali halides crystals.

Two types of experiments are performed. Firstly, the intrinsic luminescence of crystals which is the recombination luminescence of electrons with  $V_K$  centers is studied under X rays or electron beam excitation. This is mainly constituted of a band at 1.9 eV, which corresponds exactly to the energy of the B emission, confirming the attribution of the latter to  $Br_2^{2-}$  centers.

Secondly, the behaviour of the intensity of the A emission and of its excitation doublet is discussed after X rays irradiation and then after thermal annealing of crystals at 300 K. The intensity of these bands decreases after X rays irradiation and then recovers its initial value after annealing of crystals. Assuming the presence of  $Br_2^{2-}$  pseudomolecules, this is ascribed to the substitution of these centers by  $V_K$  and then to the recombination of electrons with them.

#### References :

- 1 - C. ANDRAUD, F. PELLE and O. PILLA, J .de phys. C.7, 489 (1985)
- 2- C. ANDRAUD, F. PELLE, O. PILLA, J.P. DENIS and B. BLANZAT, Cryst. Latt. Def. and Amorphous Mat. 16, 395 (1987)
- 3- C. ANDRAUD, F. PELLE, O. PILLA, J.P. DENIS and B. BLANZAT, to be published.
- 4- D. VISSER, G.C. VERSHOOR and D.J.W. IJDO, Acta Crystallogr. B. 36,28 (1980)

SPECTROSCOPIC PROPERTIES OF EXCHANGE COUPLED PAIRS  
OF  $\text{Cr}^{3+}$  IN THE UNIDIMENSIONAL CRYSTAL  $\text{CsCdBr}_3$

F. PELLÉ, J.P. DENIS O. PILLA (\*) and B. BLANZAT

CNRS ER 211 1 place A. Briand

92190 Meudon Bellevue FRANCE

(\*) dipartimento di fisica, Università di Trento  
38050 POVO, (TRENTO) ITALY

$\text{CsCdBr}_3$  belongs to the large family of the  $\text{AMX}_3$  compounds which adopt the hexagonal  $\text{CsNiCl}_3$  structure (space group  $D_{6h}^4\text{-P6}_3/\text{mmc}$ ). This consists in infinite linear chains of  $(\text{MX}_6^{4-})$  octahedra sharing opposite faces where the  $\text{M}^{2+}$  ions occupy a nearly cubic site, and the Cs ions are in positions between the chains assuring the electric charge compensation.

These systems, when doped with trivalent impurities, show a very peculiar characteristic. In fact, even at very low concentrations the impurities enter almost exclusively in pairs to form coupled pair-vacancy systems ( $\text{M}^{3+}\text{-vacancy-M}^{3+}$ ) as shown by EPR measurements (1). These pairs are not interacting, at least in the low concentration limit, and it is possible to study their spectroscopic properties without a superposition of the isolated ions contribution (as in the case of ruby f.i.) and of other effects arising from interactions with neighboring pairs like in  $\text{Cs}_2\text{Cr}_2\text{Cl}_9$  (2).

In this paper we report the study of the optical properties (absorption, emission, lifetimes) of the exchange coupled pair  $\text{Cr}^{3+}\text{-Vac-Cr}^{3+}$  in the diamagnetic host crystal  $\text{CsCdBr}_3$ .

The low temperature ground state absorption spectrum of the pairs consists mainly in two broad featureless bands centered at 12150 and 16700  $\text{cm}^{-1}$ . Much weaker sharp structures are observed in the energy ranges 13900-14925  $\text{cm}^{-1}$  and 18500-20000  $\text{cm}^{-1}$ . These features have been assigned in order of increasing energy to the transitions from the  ${}^4\text{A}_2 \times {}^4\text{A}_2$  ground state to the  ${}^4\text{A}_2 \times {}^4\text{T}_2$ ,  ${}^4\text{A}_2 \times {}^2\text{E} + {}^4\text{A}_2 \times {}^2\text{T}_1$ ,  ${}^4\text{A}_2 \times {}^4\text{T}_1$ , and  ${}^4\text{A}_2 \times {}^2\text{T}_2$  excited states of the pair respectively. Since the pair axis coincides with the crystallographic c axis, polarized absorption spectra have been taken and the splitting of the two broad spin-allowed bands has been related to a slight trigonal distortion of the  $(\text{CrBr}_6^{3-})$

octahedra. The study of the sharp features allows an estimate of the exchange parameters both in the ground and in the excited states.

In the low crystalline field systems, such as  $\text{CsCdBr}_2:\text{Cr}^{3+}$ , the luminescence arises from the  ${}^4\text{A}_2\text{x}{}^4\text{T}_2 \rightarrow {}^4\text{A}_2\text{x}{}^4\text{A}_2$  transition. Usually it consists in a broad band with a lifetime in the microseconds range, and, depending on the strength of the electron-phonon coupling, zero-phonon lines and vibronic replicas could be detected. The emission spectrum of this compound consists in a broad and unstructured band peaked at  $10000\text{ cm}^{-1}$  which could be due to the  ${}^4\text{A}_2\text{x}{}^4\text{T}_2 \rightarrow {}^4\text{A}_2\text{x}{}^4\text{A}_2$  transition; lifetime and intensity of this band have been recorded from 10K up to room temperature; the decay which is in the microseconds range, is non exponential, and the emission, not detectable at room temperature, has a maximum at about 140K and decreases to 2/3 of the maximum intensity at 10K. A definite assignment of this emission to the  ${}^4\text{A}_2\text{x}{}^4\text{T}_2 \rightarrow {}^4\text{A}_2\text{x}{}^4\text{A}_2$  transition is not possible on the light of existing experimental data, nevertheless it seems to be related to the chromium pairs. Experiments are in progress to understand the origin of this luminescence.

#### References

- 1 - G.L. Mc PHERSON and L.M. HENLING, Phys. Rev. B16, 1889, (1977)
- 2 - B. BRIAT, M.F. RUSSEL, J.C. RIVOAL, J.P. CHAPELLE and O. KAHN, Mol. Phys. 34,5, 1357-1389, (1977)

HIGH PRESSURE AND LOW TEMPERATURE PHOTOLUMINESCENCE  
OF  $\text{Cr}^{3+}$  IN  $\text{Na}_3\text{In}_2\text{Li}_3\text{F}_{12}$ .

D. de Viry, F. Pellé, N. Tercier,  
J.P. Denis and B. Blanzat.  
L.P.C.M. (C.N.R.S., E.R.211)  
1 place A. Briand 92190 Meudon.

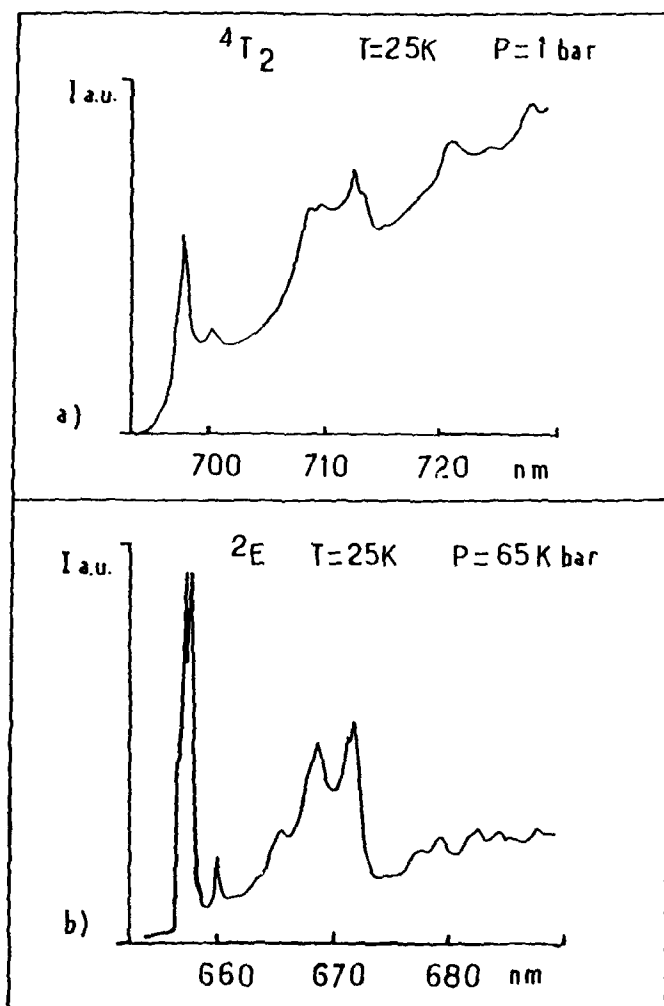
The fluorescence behaviour of  $\text{Cr}^{3+}$  in the fluoride garnet  $\text{Na}_3\text{In}_2\text{Li}_3\text{F}_{12}$  under high pressure (0-65 kbar) and low temperature (25 K) will be presented.

In this study the crystal field could be varied applying high pressure, from the low field case where the emission is purely  ${}^4\text{T}_2$ , to the intermediate field case where the  ${}^4\text{T}_2$  and  ${}^2\text{E}$  levels are close together, leading to the observation of the crossing. The knowledge of the fine structure of both levels will allow the determination of spin orbit coupling and distortion of the Chromium sites. Relative population of the two levels will be discussed, altogether with the emission lifetime variation. Contrarily to the previous measurements at ambient temperature (1), the lifetime decreases under pressure when the emission is purely  ${}^4\text{T}_2$ , and begins to increase exponentially before the crossing with the  ${}^2\text{E}$  level. Comparisons with similar compounds will be made (2).

(1) D. de Viry, J.P. Denis, N. Tercier  
and B. Blanzat, Sol. State Com., 63, 1183-88, (1987)

(2) J.F. Dolan, L.A. Kappers, and R.H. Bartram,  
Phys. Rev. B, 33, 7339-41, (1986).

Figure 1: Photoluminescence spectrum of  $\text{Cr}^{3+}$  in  $\text{Na}_3\text{In}_2\text{Li}_3\text{F}_{12}$  at 25 K: a)  ${}^4\text{T}_2 - {}^4\text{A}_2$  emission at ambient pressure, b)  ${}^2\text{E} - {}^4\text{A}_2$  emission at 65 Kbar.



ZERO-PHONON LINE AND PHONON-SIDEBAND OF  $\text{Sm}^{2+}$ -DOPED  $\text{CaF}_2$  :  
MIXING EFFECT OF THE  $f^6$  AND  $f^5d$  ELECTRON CONFIGURATIONS

T. Tsuboi

Physics Department, Kyoto Sangyo University, Kamigamo, Kyoto 603,  
Japan.

The electronic-vibrational bands appearing in the absorption or luminescence spectra due to impurity centers give a rich information about the dynamical properties of crystal lattice. The phonon-sideband appears at the high energy side (6900-6600 Å region) of a sharp line at 6901 Å in the absorption spectrum of  $\text{CaF}_2:\text{Sm}^{2+}$  [1]. Although the optical properties of  $\text{Sm}^{2+}$  center in various alkali-earth halide crystals, which exhibit a sharp line accompanied by a broad and structured sideband, have been investigated by many workers, the origin of the structure has not been clarified yet. We have measured the absorption, magnetic circular dichroism, luminescence and Raman spectra of  $\text{CaF}_2:\text{Sm}^{2+}$  crystal to establish the structure assignment.

The peak-position, half-width and intensity of the 6901 Å sharp line show the same temperature dependence as the zero-phonon line [2] observed in  $\text{Sm}^{2+}$ -doped alkali halide crystals. Therefore, taking into account the energy level calculation of the  $4f^55d$  state of  $\text{Sm}^{2+}$  in  $\text{CaF}_2$ , the sharp line is attributable to the zero-phonon line associated with the electric dipole allowed transition from the  $^7F_0(4f^6)$  state to the  $J=2$  state of the  $4f^5(^6H)5d(e_g)$  configuration.

From the vibrational spectrum, density of phonon state and Raman spectrum, the fine structure accompanied by the 6901 Å zero-phonon line appears to be associated with the vibrational modes of bulk crystal lattice.

A prominent interval of about  $377\text{ cm}^{-1}$  is observed in the phonon-sideband. It is assigned that the low energy vibrational structure is accompanied by the zero-phonon line due to the  $f^6 \rightarrow f^5d$  electric dipole allowed inter-

configurational transition, whereas the high-energy vibrational structure is accompanied by the  ${}^7F_0(f^6) \rightarrow {}^5D_1(f^6)$  magnetic dipole allowed intra-configurational transition. Unlike the cases of other  $\text{Sm}^{2+}$ -doped alkali halide crystals, the mixing effect between the  $f^6$  and  $f^5d$  configurations is observed in the sideband structure since the  ${}^5D_1$  energy level of  $f^6$  configuration is located near and above the  $J=2$  level of  $f^5d$  configuration.

[1] T. Tsuboi, J. Phys. C 14(1981)4727.

[2] G. Baldini and M. Guzzi, phys. stat. sol. 30(1968)601.

LUMINESCENCE OF F AND F<sup>+</sup> CENTERS IN MAGNESIUM OXIDE

G. P. Williams, Jr., G. H. Rosenblatt, and R. T. Williams  
Department of Physics, Wake Forest University  
Winston-Salem, NC 27109 USA

Y. Chen  
Solid State Division, Oak Ridge National Laboratory  
Oak Ridge, TN 37831 USA

We have studied F and F<sup>+</sup> luminescence in MgO excited at 248 nm by KrF excimer laser pulses and cw excitation. Figure 1 shows the evolution of F (530 nm) and F<sup>+</sup> (390 nm) emission bands in a thermochemically-reduced crystal recorded over 8 decades of time and intensity. From analysis of these and other data, we conclude that both F and F<sup>+</sup> centers ionize by electron release following 248-nm excitation at room temperature and above. While this is expected for F centers, it makes the rather surprising statement that the F<sup>+</sup> excited state is also near the conduction band edge. We discuss the probable role of the F<sup>++</sup> charge state in the luminescence of F<sup>+</sup> centers and in apparent hole release upon excitation in the F/F<sup>+</sup> absorption bands.

The dependence of luminescence spectra and efficiency upon excitation power density has been measured from 1.18 milliwatts/cm<sup>2</sup> up to 38 megawatts/cm<sup>2</sup>. Results are shown in Fig. 2 for the same thermochemically reduced crystal whose time dependence is shown in Fig. 1. Higher pumping power shifts the luminescence toward F luminescence rather than F<sup>+</sup>. This is true in all thermochemically reduced crystals studied. The simplest expectation would have been that harder pumping should ionize more F centers to the F<sup>+</sup> charge state. We will show that the observed behavior is consistent with our hypothesis of the complete F/F<sup>+</sup>/F<sup>++</sup> pumping cycle. Results for different H<sup>-</sup> concentrations and for neutron-irradiated crystals are compared. We believe a rather detailed description of F and F<sup>+</sup> luminescence can now be constructed.

Acknowledgment: This work was supported by DARPA under Inter Agency Agreement 40-1611-85 with Martin Marietta Energy Systems, Inc., contract DE-AC05-804R-21400 with the U.S. Department of Energy.

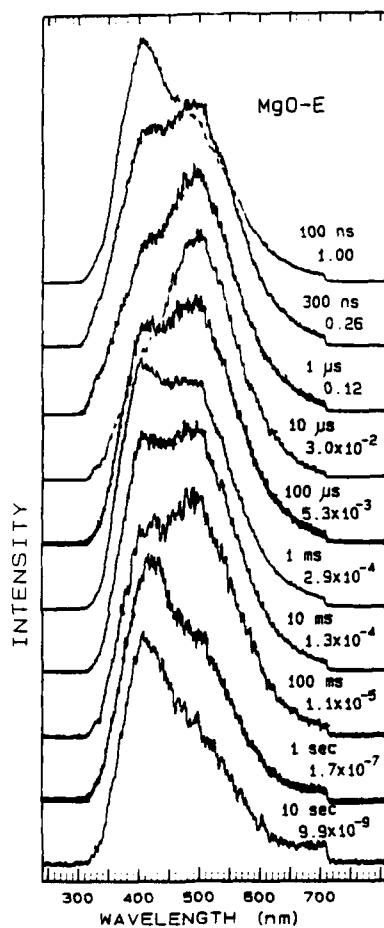


Fig. 1. Luminescence spectra in thermochemically reduced MgO at various delays after 248-nm excitation at 293 K. Delay times and peak intensities (normalized to the 100 ns spectrum) are shown at the lower right of each spectrum.

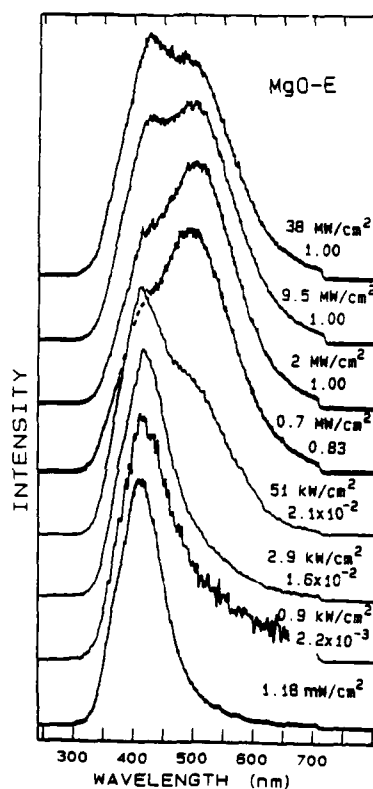


Fig. 2. Luminescence spectra for various pump power densities, as labeled at lower right. Also labeled is the peak luminescence intensity normalized to that for the highest pump power density.

STOKES AND ANTI-STOKES RESONANT RAMAN SCATTERING  
OF  $F_H(CN^-)$  DEFECTS IN CsBr

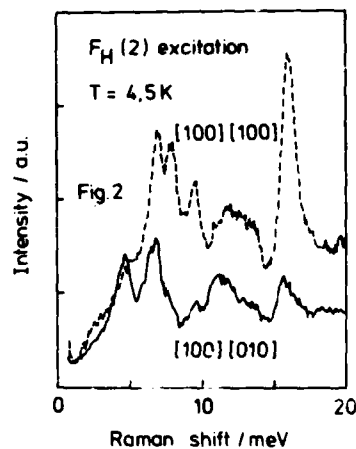
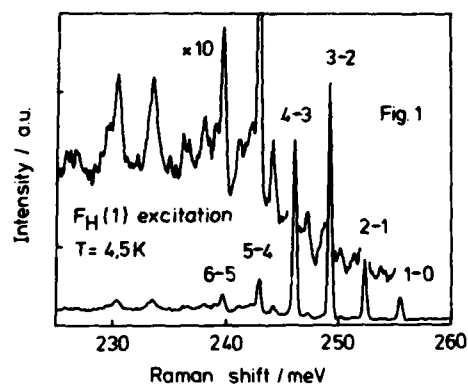
G. Cachei, H. Stolz, W. von der Osten and F. Lüty\*

Fachbereich Physik, Universität-GH, 4790 Paderborn, FRG

\*Physics Department, University of Utah, Salt Lake City, UT 84112, USA

The  $F_H(CN^-)$  defect in the body-centered cubic cesium halides consists of an F center- $CN^-$  molecule pair along a  $\langle 100 \rangle$  crystal axis. Due to the interaction with the F center, the attached  $CN^-$  splits the F absorption into two separate transitions,  $F_H(1)$  and  $F_H(2)$ , polarized predominantly parallel and perpendicular to the pair axis. Besides this interaction in the electronic absorption, strong coupling of the excited F center to the molecule has been observed [1]. It leads to efficient electron-vibrational energy transfer that so far was investigated by infrared vibrational emission [2] and pulsed anti-Stokes resonant Raman scattering [3].

To study this highly interesting phenomena in greater detail, we have performed high resolution cw resonant Raman measurements of this defect in CsBr. Excitation in either absorption band at low temperature gives rise to a series of up to seven narrow and strongly polarized Raman lines that occur in both the anti-Stokes (Fig. 1) and Stokes spectrum. The nearly equally spaced lines correspond



to  $\Delta v = \pm 1$  transitions between the vibrational states of the  $\text{CN}^-$  stretching mode slightly shifted by anharmonicity. The spectra dramatically demonstrate that excited vibrational states participate in the energy transfer process. Due to the long lifetime of the order of milliseconds of these states substantial population is accumulated during the much more rapid electronic relaxation.

We have measured the spectra for various excitation photon energies as function of sample temperature and laser power. Lifetime reduction at higher temperatures causes the observed relative increase in population of lower vibrational states. Low excitation powers in the milliwatt range reveal a quadratic dependence of scattered intensity as expected from the two-step nature of the process involving population of states and scattering from these. Deviations from this dependence at high powers (up to 300 mW) are attributed to sample heating and concomitant reduction in vibrational lifetime. Under all excitation conditions the population of excited vibrational states is only a small fraction of the ground state population. Opposite to the infrared vibrational emission, isolated  $\text{CN}^-$  give only negligible signals in the Raman spectra, since in comparison to the F center- $\text{CN}^-$  pair any resonance mechanism is lacking.

In addition to the prominent Raman series due to  $^{12}\text{C}^{14}\text{N}^-$ , two weaker sequences are observed associated with the isotopes  $^{13}\text{C}^{14}\text{N}^-$  and  $^{12}\text{C}^{15}\text{N}^-$ . We also find coupling of several other modes to the  $\text{F}_\text{H}(\text{CN}^-)$  center. One of these appears in all anti-Stokes spectra as broader replicas to the strongest  $\text{CN}^-$  Raman transitions shifted by about 16 meV to smaller Raman energies (Fig. 1). A strong peak of this energy due to  $\text{CN}^-$  emerges in the low energetic Stokes Raman spectrum of the  $\text{F}_\text{H}(\text{CN}^-)$  center (Fig. 2) and most probably corresponds to the  $\text{CN}^-$  local mode. We suggest the replicas are due to a two-phonon difference process in which the  $\text{CN}^-$  molecular vibration couples to the local mode via the excited electronic state of the defect. Further experiments with this defect center are under way.

- [1] Y. Yang, W. von der Osten and F. Lüty, Phys. Rev. 32, 2724 (1985)
- [2] Y. Yang and F. Lüty (this conference)
- [3] K.T. Tsen, G. Halama, and F. Lüty, Phys. Rev. B 36, 9247 (1987)

MECHANISM FOR THE PHOTOREFRACTIVE  
EFFECT IN PLZT 9/65/35

J. P. Spoonhower, R. S. Eachus, and J. A. Agostinelli  
Research Laboratories  
Eastman Kodak Company  
Rochester, NY 14650 USA

Photorefractivity has been observed in lead lanthanum zirconium titanate (PLZT) 9/65/35 by the observation of photo- and field-induced optical transmission. We have found that, in the presence of electric fields on the order of 1 V/micron, the photorefractive regions are displaced from the irradiated regions by approximately one micron. We have identified the mobile charge carriers as positive holes; the carrier drift range was found to be independent of the applied field.

Electron paramagnetic resonance studies of dark-adapted PLZT samples have identified iron as an impurity in these materials. The iron impurity does not appear to trap electrons or holes as a result of exposure to UV radiation between 10 and 300K. Ionization of  $Pb^{2+}$  is an important photochemical process in a range of PLZT compositions. Under the same conditions, three structurally inequivalent  $Pb^{3+}$  sites have been detected by EPR in irradiated PLZT samples. In the two compositions 10/40/60 and 9/65/35, two of the EPR-detected sites were dominant. The role of these impurity states in the photorefractive mechanism will be discussed.

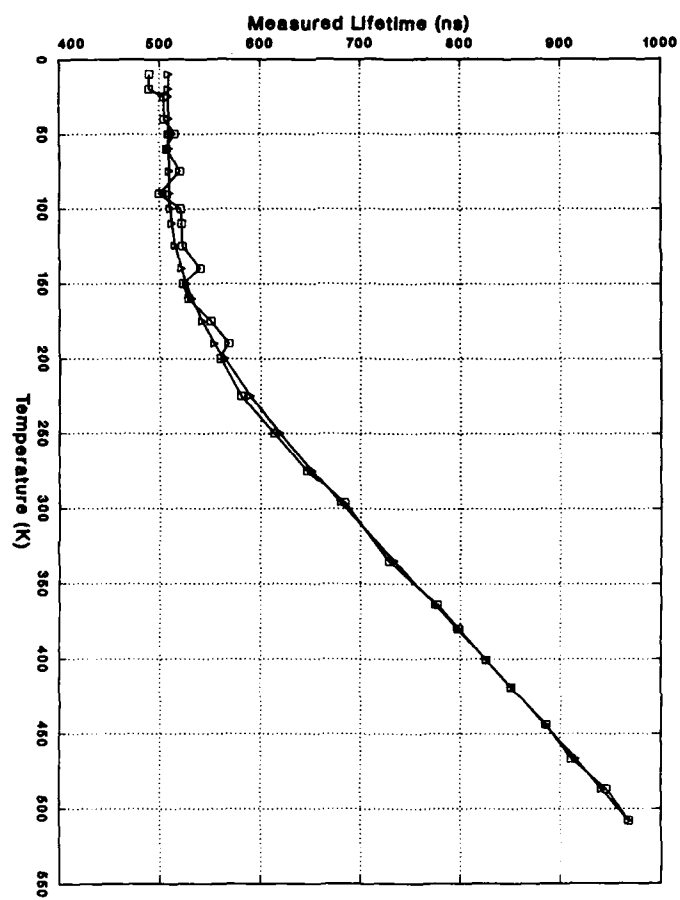
TIME-RESOLVED SPECTROSCOPY OF BaFBr/Eu(2+)

J. P. Spoonhower and M. S. Burberry  
 Research Laboratories  
 Eastman Kodak Company  
 Rochester, NY 14650 USA

The time and wavelength dependence of the Eu(2+) 5d-4f emission in BaFBr was measured over the extended temperature range 10-506 K. The excitation wavelength was 355 nm. Analysis of the emission lineshape over the same temperature range was also performed. At 10 K the measured emission lifetime is  $500 \pm 5$  nsec; at 506 K the lifetime increases to  $968 \pm 5$  nsec. In our kinetic analysis (1), three parameters are required to fit the data (see figure): we determine the low-temperature lifetime limit, the difference in energy for two relatively close-spaced excited state levels, and the degeneracy ratio for the two levels. Our best fit to the data yields  $508 \pm 7$  nsec,  $476 \pm 8$  cm<sup>-1</sup>, and  $3.5 \pm 1 = g_2/g_1$  respectively, for these parameters. Two parameter fits to the data, of the type already described in the literature (2), were quite unsuccessful in reproducing the experimental temperature dependence, especially in the high temperature limit. These differences will be discussed.

Corrected cw emission spectra show that the 5d-4f lineshape is asymmetric at low temperatures. The spectral dependence of the emission lifetime, however, shows no such asymmetry. These results must be reconciled with other studies (3) which show the Eu(2+) ion substitutions for Ba(2+) in the lattice and the expected lack of charge compensation for the Eu(2+) in this host. These effects are discussed within the context of the dual excited state model cited above.

- (1) P.P. Feofilov and N.M. Tolstoi, Opt. Spectry. 13, 164 (1962).
- (2) J.L. Sommerdijk, J.M.P.J. Verstegen, and A. Bril, J. Lumines., 8, 502 (1974).
- (3) (a) L.H. Brixner, J.D. Bierlein, and V. Johnson, Current Topics in Materials Science 4, 47 (1980); (b) R.S. Eachus, private communication; (c) D. Nicollin and H. Bill, J. Phys. C: Solid State Phys. 11, 4803 (1978).



# RESONANT RAMAN SCATTERING OF THE $F_A(Li^+)$ CENTER IN KBr

M. Leblans, W. Joosen, E. Goovaerts, and D. Schoemaker  
Physics Department, University of Antwerp (UIA)  
Universiteitsplein 1, B-2610 Wilrijk (Antwerp), Belgium

A polarized Raman study was performed of the  $F_A(Li^+)$  center in KBr under resonant excitation of its  $F_{A1}$  and  $F_{A2}$  absorption bands. A continuum of defect induced lattice modes is observed in the Raman spectrum. The spectral positions of the peaks at  $97\text{ cm}^{-1}$ ,  $107\text{ cm}^{-1}$ , and  $119\text{ cm}^{-1}$  (see Fig.1) are very near to those of the sharp features in the F-center induced first order phonon spectrum. Additional modes are observed at  $28\text{ cm}^{-1}$  and  $225\text{ cm}^{-1}$ . The former is an  $F_A(Li^+)$ -induced breathing mode of the surrounding ions and does not exhibit an isotope effect upon  $^7Li^+$  to  $^6Li^+$  substitution.<sup>1</sup> The latter exhibits a normal isotope shift and reflects the motion of the  $Li^+$  ion along the  $\langle 100 \rangle$  defect axis.<sup>1</sup>

The frequency dependence of the polarized Raman intensities is illustrated in Fig.1. Apart from the continuum of  $F_A(Li^+)$ -induced phonon modes, the depolarized Raman scattering ( $I_{yz,x}$ ) is negligibly small. The  $F_A(Li^+)$  modes predominantly show up in the two other polarized Raman spectra. According to the Behavior Type (BT) method, the observed  $F_A(Li^+)$  modes all transform according to the  $A_1$  representation of  $C_{4v}$ . There is no indication for an off-center position of the  $Li^+$  ion.<sup>2</sup> This is in agreement with previous experimental work on the naked  $Li^+$  center in KBr.<sup>3</sup>

Because of *selective* resonant enhancement (SRE) of particular components of the Raman tensor, it is possible that the *observed* form of the Raman tensor corresponds to a higher symmetry than the actual defect symmetry. This phenomenon was observed for the  $F_A(Li^+)$  center in KCl under  $F_{A1}$  excitation.<sup>2</sup> For  $F_A(Li^+)$  in KBr, it is reflected in the  $r/q$  ratio, which is nearer to zero for excitation at  $676\text{ nm}$ , i.e., for frequencies tuned in the  $F_{A1}$  transition. The non-zero  $r/q$  ratio illustrates the larger overlap of the  $F_{A1}$  and  $F_{A2}$  transitions and the smaller effect of SRE of  $F_A(Li^+)$  in KBr in comparison with  $F_A(Li^+)$  in KCl. The negative sign of  $r/q$  shows that the derived polarizabilities parallel and perpendicular to the  $\langle 100 \rangle$  defect axis are modulated the opposite way by the  $A_1$  modes of  $F_A(Li^+)$ , and, in particular, by the motion of the  $Li^+$  ion along  $\langle 100 \rangle$ .<sup>4</sup> A more profound analysis of the polarized Raman data can be performed by calculating the population numbers of the  $F_A(Li^+)$  centers among its six possible orientations

for a particular excitation frequency: This allows one to further characterize the  $F_A(\text{Li}^+)$  modes according to their anisotropy, i.e., the ratio  $a/a_3$  of the  $C_{4v}:A_1$  Raman tensor.

1. A. Mabud and F. Lüty, in Abstract Book of the International Conference on Defects in Insulating Crystals, Salt Lake City 1984, p.301, (unpublished).
2. See, e.g., M. Leblans, W. Joosen, E. Goovaerts, and D. Schoemaker, Phys. Rev.B **35**, 2405 (1987).
3. R.J. Russell and F. Bridges, Phys. Rev.B **26**, 3386 (1982); L.H. Greene and A.J. Sievers, Phys. Rev.B **31**, 3948 (1985).
4. M. Leblans, W. Joosen, E. Goovaerts, D. Schoemaker, A. Mabud, and F. Lüty, to be submitted to Phys. Rev.B.

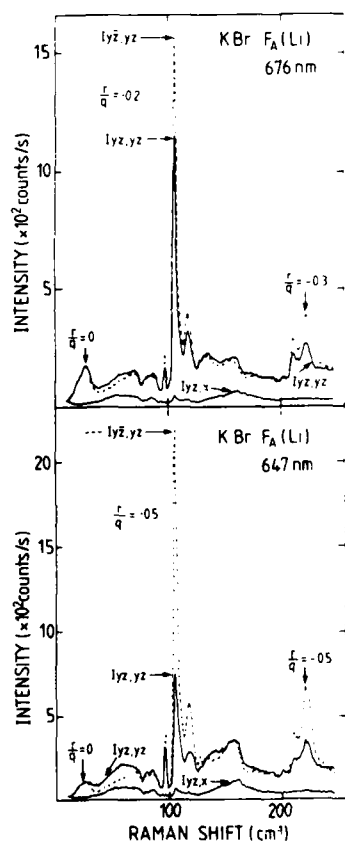
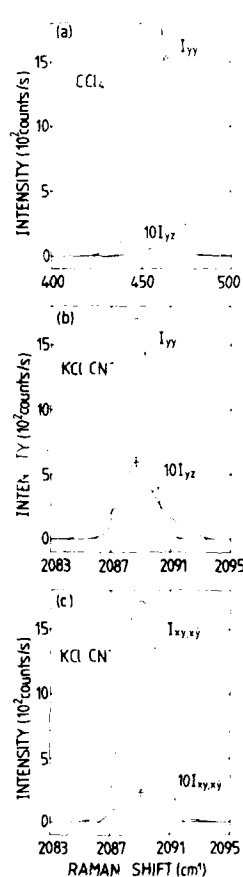


Fig.1 Polarized Raman spectra of the  $F_A(^{6.7}\text{Li}^+)$  center in KBr under 647-nm and 676-nm excitation. The subscripts  $\alpha$  and  $\beta$  in  $I_{\alpha,\beta}$  indicate the polarization directions of the incident and the scattered light, respectively, and are expressed in the reference frame of the crystal  $\langle 100 \rangle$  directions.

# EQUILIBRIUM ORIENTATIONS OF DIATOMIC MOLECULAR IMPURITIES IN CUBIC CRYSTALS DETERMINED BY A POLARIZED RAMAN STUDY OF THE STRETCHING MODE

H. Fleurent, W. Joosen, and D. Schoemaker

Physics Department, University of Antwerp (U.I.A.), B-2610 Wilrijk (Belgium)



Polarized Raman measurements were performed on the  $\Lambda_1$  stretching mode of static or reorienting diatomic molecular impurities in cubic crystals. A Behavior Type (BT) analysis<sup>1</sup> of the spectra yields the orientation(s) of the molecular axes, most commonly lying along either the  $\langle 110 \rangle$ ,  $\langle 111 \rangle$ , or  $\langle 100 \rangle$  directions. The symmetry is thus established without applying any secondary fields and without studying the experimentally less accessible tunneling sidebands.<sup>2</sup> This approach applies both to static *and* reorienting impurities, as the non-resonant Raman process probes the instantaneous configuration of the orientational potential wells, in which the high frequency stretching motion takes place, and not the averaged cubic symmetry resulting from the low frequency reorientational motion.

The correspondence between the polarized Raman intensities and the actual defect symmetry can be obscured, when the stretching vibration is strongly coupled to the reorientational degrees of freedom, or, when the anisotropy of the derived polarizability is relatively small. In this case very accurate measurements are necessary to perform the BT analysis.

This new method was tested on the stretching mode of  $\text{CN}^-$  in KCl, yielding a  $C_{3v}$  symmetry in agreement with the  $T_{2g}$  character of the tunneling sidebands found

Fig. 1 Polarized Raman spectra of the stretching vibration of  $\text{CN}^-$  in KCl.

in earlier Raman studies.<sup>2</sup> For the first time the  $C_{3v}$  symmetry of  $SH^-$  in KCl was established. The polarized Raman data of  $NaCl:OH^-$  probably reflect a small tilting of the  $OH^-$  axis with the  $\langle 100 \rangle$  direction.<sup>3</sup>

In Fig. 1 the polarized Raman spectra for  $KCl:CN^-$  are shown, including a set of calibration measurements on the  $460\text{-cm}^{-1}$  mode in liquid  $CCl_4$  as a reference for the accuracy. The spectra are indicated by the conventional notation  $I_{\alpha\beta}$ . In Table I data are presented for  $CN^-$  and  $SH^-$  in KCl, and for  $OH^-$  in NaCl. The intensity parameters (IP)  $s$ ,  $r$ , and  $q$  employed there are defined according to Ref. 1 :

$$\begin{aligned} s &= 8kNI_0 (T_{12}^2 + T_{13}^2 + T_{23}^2) \quad , \\ r &= 8kNI_0 (T_{11}T_{22} + T_{11}T_{33} + T_{22}T_{33}) \quad , \\ q &= 8kNI_0 (T_{11}^2 + T_{22}^2 + T_{33}^2) \quad . \end{aligned}$$

in which  $k$  is an instrumental efficiency factor,  $N$  is proportional to the defect concentration and  $I_0$  is the intensity of the exciting light beam.  $T$  is the Raman tensor of the studied vibrational mode. For a totally symmetric  $A_1$  mode four different sets of IP relations (BT) can be observed, allowing one to identify the defect symmetry (see Table I).

Table I : Results of the Behavior Type (BT) analysis of the stretching mode for  $CN^-$  and  $SH^-$  in KCl, and  $OH^-$  in NaCl. The experimentally determined  $s/q$  and  $r/q$  ratios yield the observed BT (numbered according to Ref. 1), and the observed BT symmetry (BTS). The latter is compared to the actual symmetry (AS), as determined by other experimental techniques.

	$s/q$	$r/q$	BT	BTS	AS
KCl: $CN^-$	$0.04 \pm 0.01$	$0.98 \pm 0.03$	39	$C_{3v}$	$C_{3v}$
KCl: $SH^-$	$0.38 \pm 0.03$	$0.97 \pm 0.07$	39	$C_{3v}$	
NaCl: $OH^-$	$0.06 \pm 0.01$	$0.85 \pm 0.04$	60	$C_{1h}$	$C_{4v}, C_{1h}$

1. J.F. Zhou, E. Goovaerts, and D. Schoemaker, Phys. Rev. B **29**, 5509 (1984); E. Goovaerts, J.F. Zhou, W. Joosen, and D. Schoemaker, Cryst. Latt. Def. and Amorph. Mat. **12**, 317 (1985).
2. D. Durand and F. Lüty, Phys. Stat. Sol. B **81**, 443 (1977).
3. M.E. Baur and W.R. Salzman, Phys. Rev. Lett. **18**, 590 (1967).

PHOTOINDUCED REORIENTATION OF  $F_A$  CENTRES IN ALKALI HALIDES

G. Baldacchini and E. Giovenale  
 ENEA, Dipartimento TIB, Divisione Fisica Applicata  
 Centro Ricerche Energia Frascati, C.P. 65, 00044 Frascati, Italy

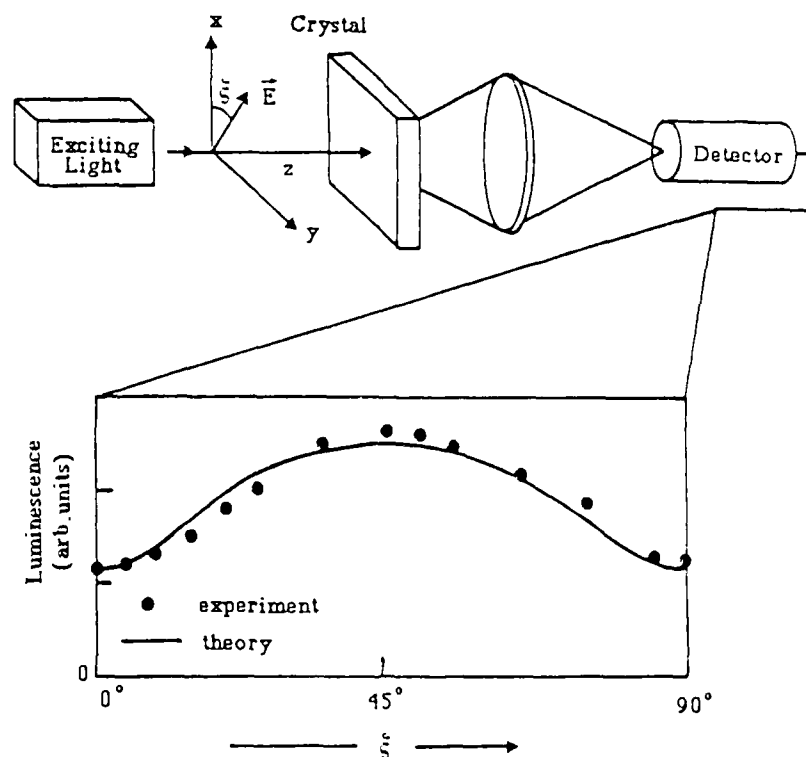
F. De Matteis, A. Scacco, and F. Somma  
 Dipartimento di Fisica, Università "La Sapienza", P.le A. Moro 2, 00185 Roma, Italy

U.M. Grassano  
 Dipartimento di Fisica, Università di Roma - Tor Vergata  
 V. Orazio Raimondo, 00173 Roma, Italy

The  $F_A$  centre in alkali halides is formed by an anion vacancy, trapping an electron, nearest neighbour to an impurity alkali ion, replacing a cation in the host crystal lattice. Such axial center can lie, in the cubic symmetry, along three different directions coincident with the crystallographic axes. The isotropic distribution of the  $F_A$  centres in a crystal can be modified by the absorption of monochromatic polarized light: optical pumping into one of the two  $F_A$  absorption bands induces electronic transitions to excited states, and during the subsequent relaxation the centres can change their orientation because of the vacancy mobility around the impurity ion. Such a reorientation, causing anisotropy in the optical properties of the crystal, depends upon the wavelength of the irradiating light and on the configuration of the dipoles in the lattice. In case of monovalent small impurity ions in crystals with sufficiently large lattice parameter, the usual substitutional position is not the equilibrium position and an off-centre configuration is energetically favoured [1]. As a consequence, the  $F_A$  dipole in the above crystals is not lying along the crystal axis, but it forms with it an off-axis angle [2]. For this reason, a detailed investigation on the reorientation process of the  $F_A$  centres can supply information on their configuration. Moreover, the dependence of the reorientation on the wavelength of the exciting light can be used to determine the overlap of the  $F_A$  absorption bands and consequently their lineshapes.

We have studied the photoinduced reorientation of the  $F_A(I)$  centres in  $KCl:Na^+$  and of the  $F_A(II)$  centres in  $KCl:Li^+$  and in  $RbCl:Li^+$ . In the Figure below we report a typical measurements of  $F_A(II)$  centres in  $RbCl:Li^+$  along with the experimental set-up. The emission intensity is measured versus the angle,  $\xi$ , between one of the [100] crystal axes and the polarization of the exciting light ( $\lambda = 6328 \text{ \AA}$ ) at 2 K.

The comparison of the experimental results with a theoretical model, taking into account the overlap of the absorption bands for both  $F_A(I)$  and  $F_A(II)$  centres, and the



off-axis configuration for  $F_A(\text{II})$  centres, leads to a quantitative determination of the off-axis angle of the  $F_A$  dipoles in  $\text{KCl}:\text{Li}^+$  and  $\text{RbCl}:\text{Li}^+$ , and to a calculation of the lineshape of the  $F_A$  bands. As far as the off-axis angle  $\theta$  is concerned, we have obtained  $\theta \cong 5^\circ$  for  $\text{KCl}:\text{Li}^+$  and  $\theta \cong 7^\circ$  for  $\text{RbCl}:\text{Li}^+$ . This study demonstrates that a larger off-centre ionic configuration induces a larger off-axis deviation of the dipoles, and besides that the lineshape of  $F_A$  absorption bands is much more close to a Lorentzian curve in the tails than to a Gaussian one or a Poissonian one, as it is in the case of F centres [3].

#### References

1. A.M. Stoneham, *Theory of Defects in Solids* (Clarendon, Oxford, 1975) Chap. 21.
2. F. Rosenberger and F. Lüty, *Solid State Commun.* **7**, 983 (1969).
3. J.J. Markham, *F-centers in Alkali Halides* (Academic, N.Y., 1966) Chap. IX-X.

SUBBAND GAP EXCITATION SPECTRA OF SILVER HALIDES

Alfred Marchetti & Mitchell Burberry  
 Eastman Kodak Company,  
 Rochester, NY 14650

Investigations of AgCl, AgBr and  $\text{AgBr}_{1-x}\text{I}_x$  ( $x = 0.01$  to  $0.25$ ) have shown that the optical emission bands that peak at 500, 580 and 540 nm, respectively, can be characterized as donor-acceptor pair recombination.<sup>1-3</sup> The emission from  $\text{AgBr}_{.97}\text{I}_{.03}$  exhibits the characteristic hyperbolic time decay of donor-acceptor systems as well as a red shift of the emission peak with delay after pulsed excitation.<sup>2</sup> AgCl and AgBr exhibit the characteristic donor-acceptor emission decay.<sup>1</sup>

The optically detected magnetic resonance (ODMR) spectra of all three materials have spin  $1/2$  resonances which have been interpreted as shallowly (donor) trapped electrons and (acceptor) trapped holes.<sup>2,4-6</sup> The ODMR spectrum of AgCl also contained resonances due to self-trapped excitons.<sup>5</sup>

The optical emission data, the bandgap energy ( $E_g$ ), and other data have been used to estimate the upper limits for the donor and acceptor trap depth.<sup>1-3,6,7</sup> The existence of these levels within the bandgap suggests that there should be weak subband gap transitions between the donor and acceptor levels and with these levels and the valence and conduction band as observed in other semiconductors.<sup>8,9</sup> Three possible transitions might be observed: valence band to donor, acceptor to conduction band and acceptor to donor. These transitions would be band to trap, trap to band, and trap to trap respectively. These transitions may be broadened from a distribution of trap depths and from interactions (i.e., Coulomb).

Subband gap excitation spectra have been obtained on AgCl, AgBr and divalent cation doped AgCl and AgBr. Doped AgBr has absorptions near the band edge which are dependent on the monitoring wavelength. These transitions are tentatively interpreted as valence band to donor and acceptor to conduction band transitions. AgBr also has a weak transition in the 530 nm region which is dependent on monitoring wavelength. This may be an acceptor to donor transition. Some  $\text{AgBr}_{1-x}\text{I}_x$  samples have a very broad absorption extending from the band edge which is also dependent on monitoring wavelength. This broad transition is thought to reflect local variations in the valence band or acceptor energies due to the inhomogeneous distribution of iodide.

1. M. S. Burberry and A. P. Marchetti, Phys. Rev. B, 32 1192 (1985).
2. A. P. Marchetti and M. S. Burberry, Phys. Rev. B, 28 2130 (1983).
3. A. P. Marchetti and M. S. Burberry, Phys. Rev. B, accepted for publication (1988)
4. A. P. Marchetti, J. Phys. C: Solid State Phys., 14 961 (1981).
5. A. P. Marchetti and D. S. Tinti, Phys. Rev. B, 24 7361 (1981).
6. A. P. Marchetti and M. S. Burberry, Cryst. Lattice Defects Amorph. Mat., 12 329 (1985).
7. R. C. Brandt and F. C. Brown, Phys. Rev., 181 1241 (1969).
8. H. Venghaus, J. Phys. C: Solid State Phys., 17 6229 (1984).
9. S. Nakashima, T. Hattori, and Y. Yamaguchi, Solid State Comm., 25 137 (1978).

OFF-CENTER DIRECTION OF  $\text{Cu}^+$  ION IN NaBr

Shuichi EMURA, Takatoshi MURATA\*, Hironobu MAEDA\*\*, Hiroyuki ITO  
and Masakazu ISHIGURO\*\*\*

The Institute of Scientific and Industrial Research,  
Osaka University, Ibaraki, Osaka 567, JAPAN

\*Department of Physics, Kyoto University of Education,  
Fushimiku, Kyoto 612, JAPAN

\*\*Department of Chemistry, Faculty of Science,  
Okayama University, Tsushimanaka, Okayama 700, JAPAN

\*\*\*Department of Electronics, Kanazawa Institute of Technology,  
Nonoichi, Kanazawa 921, JAPAN

At the last conference on defects in insulating crystals held at Salt Lake City, U.S.A., we presented the off-center distance of  $\text{NaBr}:\text{Cu}^+$  system.[1] The off-center distance is one of the important three parameters identifying the off-center circumstances. The rest parameters, i.e. the off-center direction and the energy depth of the off-center potential, have not developed yet. Then, we will discuss the off-center direction with the assistance of the recent experimental technique, EXAFS (Extended X-ray Absorption Fine Structure).

EXAFS measurements on Cu K-edge in a fluorescence mode were made at EXAFS station installed at a Blanch BL-7C at Photon Factory in KEK, using a fluorescence detector developed by Lytle et al..[2] The spectra were observed at 50 K and room temperature.

The off-center distance was evaluated to be 0.55 Å in Ref. [1]. The value of 0.55 Å shows the good agreement with the theoretical predict of 0.53 Å by Nagasaka.[3] Figures 1(a) and 1(b) show the cross-sectional view around  $\text{Cu}^+$  defect ion in (100) plane and (110) plane, respectively, where  $\text{Cu}^+$  ion is illustrated with the off-center displacement of 0.55 Å along  $\langle 100 \rangle$  axis and  $\langle 110 \rangle$  axis in 1(a) and  $\langle 111 \rangle$  axis in 1(b). The framework built with  $\text{Br}^-$  and  $\text{Na}^+$  ions is illustrated to be rigid.

In the cases of three off-center directions with the off-center displacement of 0.55 Å apart from lattice site, the nearest neighbor distances are summarized in Table 1.

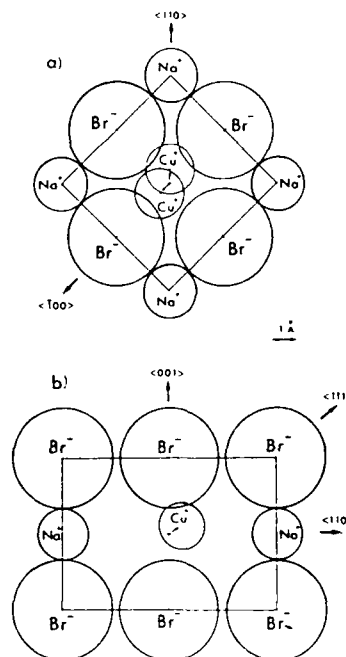


Figure 1

EXAFS experiment [4] gives for the dilute limit in zinc blend structure that the bond length deviation in the solute is only quarter of the difference between that of the compounds constituting the solid solution and in rock salt structure it is only half. The difference of the bond length between Cu-Br (2.464 Å) in CuBr and Na-Br (2.99 Å) in NaBr is 0.53 Å. If one follows above criterion, the Cu-Br distance in NaBr in the dilute solution will take 2.60 Å or 2.73 Å which is close to Cu-Br distance on the off-center displacement of 0.55 Å along  $\langle 110 \rangle$  axis or  $\langle 111 \rangle$  axis.

Table I The nearest neighbor distances and coordinate numbers.

	Cu-Br (Å)	C.N.
$\langle 100 \rangle$	2.44	1
	3.04	4
	3.54	1
$\langle 110 \rangle$	2.63	2
	3.04	2
	3.40	2
$\langle 111 \rangle$	2.71	3
	3.33	3

In Fig. 2 is shown the spectra of magnitude of Fourier transform of the EXAFS at 50 K for NaBr:Cu<sup>+</sup> sample. The correction for a phase shift is not made. The best fit values of the first and the second shell distances obtained from inverse Fourier transformed EXAFS spectra are 2.54 ± 0.02 Å and 3.51 ± 0.02 Å, respectively. The distance of 2.54 Å is compared to the case of the off-center direction along  $\langle 110 \rangle$  axis. However, the simulation fitting is favorable to the off-center direction along  $\langle 111 \rangle$  axis. The  $\langle 100 \rangle$  axis for the off-center direction is surely rejected.

Non-negligible discrepancy between the value obtained from the change of the oscillator strength by hydrostatic pressure [1] and that from EXAFS is attributed to the deformation of Br<sup>-</sup> ligands. The deformation of even symmetry of Br<sup>-</sup> ligands does not reflect the change of the oscillator strength.

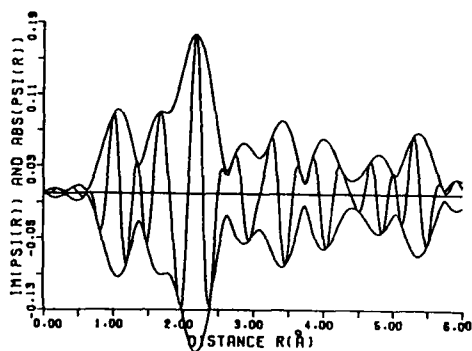


Figure 2

#### References

- [1] S.Emura and M.Ishiguro; International Conference on Defects in Insulating Crystals, Salt Lake City, U.S.A. (1984) pl42.
- [2] F.W.Lytle, R.B.Geogor, D.R. Sandstorm, E.C.Marques, J.Wong, C.L.Spiro, G.P.Huffman, and F.E.Huggis; Nucl. Instr. Meth. 226 (1984) 542.
- [3] S.Nagasaka; J.Phys.Soc.Jpn., 52 (1982) 898.
- [4] T.Murata, S.Emura, H.Ito, and H.Maeda; Photon Factory activity Report #5 (1987).

# **Ni<sup>+</sup> CENTERS IN RbCaF<sub>3</sub>: A PARAMAGNETIC PROBE FOR STUDYING THE 195 K STRUCTURAL PHASE TRANSITION**

R. Alcalá, E. Zorita and P.J. Alonso

Instituto de Ciencia de Materiales de Aragón (U. Zaragoza-C.S.I.C.)  
Fac. Ciencias. Pza. S. Francisco s/n. 50009 Zaragoza. SPAIN

Ni<sup>+</sup> centers can be easily produced in nickel doped ionic fluoride crystals by X-irradiation. So, several Ni<sup>+</sup> centers with tetragonal or near tetragonal symmetry have been recently reported in the literature and both,  $|z^2\rangle$  and  $|x^2-y^2\rangle$  orbitals have been found as the ground state. Recently we have reported an EPR study on tetragonal Ni<sup>+</sup> centers found in KMgF<sub>3</sub> <sup>(1)</sup> and K<sub>2</sub>MgF<sub>4</sub> <sup>(2)</sup> crystals. In both cases three different tetragonal Ni<sup>+</sup> centers have been found, all of them with the  $|x^2-y^2\rangle$  ground state. The models proposed for these defects are the same for both compounds. In one of them, the Ni<sup>+</sup> ion is in the center of one elongated octahedron of fluorines (Ni<sup>+</sup>-I), while in the other two the monovalent nickel has one (Ni<sup>+</sup>-II) and two (Ni<sup>+</sup>-III) fluorine vacancies placed along the four-fold axis of the crystal.

In this communication we present an extension of these EPR studies to X-irradiated RbCaF<sub>3</sub>:Ni. The samples have been kindly provided by Prof. Dr. J.M. Spaeth (Gesamthochschule Paderborn, FRG). RbCaF<sub>3</sub> undergoes two phase structural phase transitions at about 195 K and 50 K <sup>(3)</sup>. The high temperature structure is the cubic perovskite (space group O<sub>h</sub><sup>1</sup>). The 195 K transition consists of a tilting of the fluorine octahedra around one cubic  $\langle 100 \rangle$  axis and an elongation of the unit cell along the rotation axis (space group D<sub>4h</sub><sup>18</sup>). In the 50 K transition the rotation takes place around the  $\langle 110 \rangle$  cubic axis (space group D<sub>2h</sub><sup>16</sup>).

Three types of Ni<sup>+</sup> centers similar to those found in KMgF<sub>3</sub> and K<sub>2</sub>MgF<sub>4</sub> have been created in RbCaF<sub>3</sub> by X-irradiation. The EPR spectra of an irradiated sample have been measured at different temperatures between 30 K and 230 K. At 230 K the EPR spectrum only shows Ni<sup>+</sup>-II and Ni<sup>+</sup>-III signals. Both correspond to Ni<sup>+</sup> ions in an tetragonal environment. The spin-Hamiltonian parameters for these centers are given in table I. Unfortunately the Ni<sup>+</sup>-III signal is too weak and we can not make a full analysis of it. When the sample is cold down to 77 K the Ni<sup>+</sup>-II spectra changes and splits in a tetragonal and an orthorhombic signal, corresponding to defects whose z-axis is parallel or perpendicular to the c-axis of the tetragonal crystal. A study of these EPR signals in a monodomain sample let us obtain the spin-Hamiltonian parameters for both types of Ni<sup>+</sup>-II defects (see

table I). Below 65 K another  $\text{Ni}^{2+}$  signal is observed ( $\text{Ni}^{2+}$ -I). This is the only one that appears in 77 K X-irradiated samples.  $\text{Ni}^{2+}$ -I center signal shows a superhyperfine structure that corresponds to an interaction with six fluorines in an elongated octahedron, resulting that the four-fold axis of this distorted octahedron is along the c-axis of the tetragonal  $\text{RbCaF}_3$  crystal. The superhyperfine constants for the basal fluorines ( $A_{\parallel}$  and  $A_{\perp}$ ) and for the apical ones ( $A'_{\parallel}$  and  $A'_{\perp}$ ) are also given in table I.

TABLE I. Values of the spin-Hamiltonian parameters of the different  $\text{Ni}^{2+}$  centers in  $\text{RbCaF}_3$ . SHF values in MHz.

Center	T(K)	$g_x$	$g_y$	$g_z$	$A_{\parallel}$	$A_{\perp}$	$A'_{\parallel}$	$A'_{\perp}$
I	30	2.133		2.778	203	88	25	37
II	230	2.115		2.688	221	90	--	--
II (tetra)	77	2.114		2.663	233	94	--	--
II (orth)	77	2.111	2.121	2.672	232	93	--	--
III	77	--	--	2.651	--	98	--	--

The  $\text{Ni}^{2+}$ -II signal has been used to monitor the 195 K phase transition. The tilt of the g-tensor ( $\phi$ ) has been measured at temperatures near the phase transition and it has been found that the evolution of  $\phi$  can be fitted to the power law  $\phi = \phi_0 (T - T_0)^{\beta}$  with  $T_0 = 202$  K and  $\beta = .26$ . A discontinuity of 0.72 is obtained at  $T_0$  corresponding to the first order component of the phase transition. Although the absolute values of the rotation angle  $\phi$  are smaller than the intrinsic one the critical exponent  $\beta$  we have obtained agrees quite well with the one measured by other techniques, for instance, neutron diffraction  $\beta = .25$  (4) and X-ray diffraction  $\beta = .27$  (5).

#### REFERENCES

- (1) E. Zorita, P.J. Alonso and R. Alcalá. Phys.Rev. **B35**, 3116 (1987)
- (2) R. Alcalá, E. Zorita and P.J. Alonso. J.Phys. **C21**, 461 (1988)
- (3) C. Ridou, M. Rousseau and J. Bouilliot. Ferroelectric **36**, 463 (1981)
- (4) J. Jex, J. Maetz and M. Muellner. Phys.Rev. **B21**, 1209 (1980)
- (5) J. Maetz, M. Muellner and J. Jex. phys.stat.sol. (a) **50**, K117 (1978)

## INFLUENCE OF $Mn^{2+}$ IMPURITIES ON HYDROLYSIS PROCESSES INDUCED IN $SrF_2$ BY HIGH TEMPERATURE ANNEALING

P. J. Alonso, J.I. Peña and R. Alcalá

Instituto de Ciencia de Materiales de Aragón (U. Zaragoza-C.S.I.C.)  
Fac. Ciencias. Pza. S. Francisco s/n. 50009 Zaragoza. SPAIN

It is known that hydroxyl and oxygen impurities are incorporated into fluorite type fluoride crystals by annealing above 700°C in a moist atmosphere<sup>(1)</sup>.  $OH^-$  ions occupy an anion site and substitutional  $O^{2-}$  ions are compensated by fluorine vacancies ( $F^+$  centers). Both,  $OH^-$  and  $O^{2-}$ , are incorporated as a consequence of an hydrolysis process. The hydroxyl ions, formed in the surface after reaction with the surrounding water, migrate into the crystal and can decompose giving out  $O^{2-}$ - $F^+$  pairs and HF molecules. The equilibrium of this reaction explain the presence of both types of species<sup>(2)</sup>.

Doping with rare earth (RE) modify this behaviour, and then, only oxygen impurities are incorporated into the lattice. RE enter as trivalent and charge compensation is provided by interstitial fluorine ions ( $F_i^-$ ). The reaction of bulk  $OH^-$  with these  $F_i^-$  gives out HF molecules and  $O^{2-}$  substitutional ions. This explains the lack of hydroxyl ions in doped crystals<sup>(2)</sup>.

To our knowledge there is little information about the role of 3d impurities in these hydrolysis processes in fluorite type fluorides. 3d impurities usually enter these lattices in a divalent charge state and occupy a substitutional site without any charge compensator.

Keeping in mind these ideas we have undertaken a study on the modification of some spectroscopic properties (EPR and optical absorption) of  $Mn^{2+}$  doped  $SrF_2$  single crystals after annealing above 700°C in several moist atmospheres. Manganese enters  $SrF_2$  lattice as  $Mn^{2+}$  in a  $Sr^{2+}$  site ( $Mn^{2+}-I$ ). This center is responsible for an EPR signal but it does not give any optical absorption between 50,000  $cm^{-1}$  and 1,000  $cm^{-1}$ . Annealing doped sample above 700°C in a dry atmosphere does not induce neither new EPR lines nor any new absorptions but a small decrease (~10-30 %) of  $Mn^{2+}-I$  signal is observed when the annealings are done above 800°C.

Annealings in a moist atmosphere at temperatures between 700°C and 900°C induce changes in the EPR as well as in the optical absorption spectra. A strong decrease (at least by a factor 100) of

the  $\text{Mn}^{2+}$ -I signal is observed and four different  $\text{Mn}^{2+}$  paramagnetic defects have been detected which relative intensities depend on the annealing temperature. One of them can not be isolated and another one coincides with that reported by Alonso and Alcalá<sup>(3)</sup>.

The third signal that appears after treatment at 900°C results to be isotropic. A comparison with that found in powdered SrO doped with  $\text{Mn}^{2+}$  <sup>(4)</sup> indicates that it correspond to  $\text{Mn}^{2+}$  impurities in SrO clusters diluted in the  $\text{SrF}_2$  lattice.

The last center (hereafter  $\text{Mn}^{2+}$ -V) is mainly formed by annealing at 800°C and results to be tetragonal. Its EPR spectrum can be described using the corresponding spin-Hamiltonian with the following values for its parameters:  $g = 2.000 \pm 0.005$ ,  $b_0^0 = 10.990 \pm 20$  MHz,  $b_4^0 = 24 \pm 2$  MHz,  $b_4^4 = -309 \pm 2$  MHz, and with an axial hyperfine interaction giving by  $A_{||} = -193 \pm 3$  MHz and  $A_{\perp} = -163 \pm 3$  MHz. No superhyperfine structure is observed in any of its lines.

Besides that an strong increase (stronger than that observed in pure  $\text{SrF}_2$  crystals) of the optical absorption at wavelengths shorter than 500 nm is observed. This is associated with the presence of oxygen impurities<sup>(5)</sup>. On the other hand the free  $\text{OH}^-$  stretching mode band ( $3635 \text{ cm}^{-1}$ ) together with a broad band at lower energies (peaked at about  $3450 \text{ cm}^{-1}$ ) grow. This broad band is associated with perturbed hydroxyl ions and can be correlated with the  $\text{Mn}^{2+}$ -V EPR signal. This, together with an analysis of the spin-Hamiltonian parameters within the frame of the Newmann superposition model let us propose as a model for this defect ( $\text{Mn}^{2+}$ -V) a  $\text{Mn}^{2+}$  ion in the center of a oxygen tetrahedron distorted by two neighbour  $\text{OH}^-$  ions.

## REFERENCES

- (1) J.I. Peña, P.J. Alonso and R. Alcalá. J. Phys. Chem. Sol. (in press)
- (2) C.R.A. Catlow. J. Phys. Chem. Sol. **38**, 1131 (1977)
- (3) P.J. Alonso and R. Alcalá. phys. stat. sol. (b) **128**, K153 (1985)
- (4) J. Rubio, E. Muñoz, J. Boldú, Y. Chen and H. M. Abraham. J. Chem. Phys. **70**, 633 (1979)
- (5) R. Nakata, K. Kawano, M. Sumita and E. Higuchi. J. Phys. Chem. Sol. **40**, 995 (1979)

ZEEMAN EFFECT AND MAGNETIC CIRCULAR DICHROISM OF ANISOTROPIC  
CENTRES IN CUBIC CRYSTALS

W.A. Runciman and N.B. Manson

Laser Physics Centre, Research School of Physical Sciences,  
The Australian National University, G.P.O. Box 4, Canberra, A.C.T. 2601, Australia

Although there have been extensive reviews of the Zeeman effect in cubic crystals<sup>1,2</sup> the emphasis has been on presenting results for linear polarization<sup>3</sup>. Treatments of magneto-optics including magnetic circular dichroism (MCD)<sup>4,5</sup> do not consider the cases of anisotropic centres in cubic crystals in detail. Calculations have been made of the Zeeman effect for circular polarization for  $A \rightarrow E$  transitions in trigonal ( $C_{3v}$ ) and tetragonal ( $C_{4v}$ ) centres in crystals of cubic symmetry following the procedures used<sup>6</sup> in a study of the fluorescence of  $U^{6+}$  in calcium fluoride. These are the symmetries which occur when a trivalent rare earth ion incorporated into calcium fluoride at a calcium site is charge compensated by an  $O^{2-}$  ion at a fluorine site and by an interstitial  $F^-$  ion respectively. In both cases  $g_{\perp} = 0$ . The consequences of  $g_{\perp}$  being zero are that it is only the component of the field along the centre axis which splits the levels and the eigenstates are not changed by the field direction.

The MCD can be readily calculated from the Zeeman pattern for circular polarization.

For an  $A \rightarrow T_1$  electric dipole transition at a centre of cubic symmetry<sup>7</sup>, the MCD is expressed by

$$\frac{\langle \Delta A \rangle_1}{\langle A \rangle_0} = 2g\beta H. \quad (1)$$

$\Delta A$  is the difference in optical absorption coefficients of left- and right-circular polarization,  $\langle \Delta A \rangle_1$  is the first moment of the MCD spectrum and  $\langle A \rangle_0$  is the zeroth moment of the absorption. Formula (1) also applies for an  $A \rightarrow E$  transition in a trigonal or tetragonal centre with the magnetic field along the centre axis. However for a distribution of trigonal or tetragonal centres equally divided between the different possible orientations in a cubic crystal the result is

$$\frac{\langle \Delta A \rangle_1}{\langle A \rangle_0} = g\beta H. \quad (2)$$

This simple result is obtained for the three orientations of both centres in agreement with the expected isotropy of the MCD<sup>8</sup>. The principal fluorescent centres formed by hexavalent

uranium incorporated into lithium fluoride and sodium fluoride consist of a  $U^{6+}$  ion surrounded by five  $O^{2-}$  ions and an  $F^-$  ion in centres of  $C_{4v}$  symmetry. Previously reported g-values<sup>9</sup> need to be multiplied by 2 as g-values were derived using (1) rather than (2).

Calculations have also been made for  $E \rightarrow E$  transitions. Review articles<sup>1,2</sup> have claimed that transitions between E states are doublets for an even number of electrons. This is not true for trigonal  $E \rightarrow E$  transitions where similarly circularly polarized components are found as for  $A \rightarrow E$  transitions in addition to linearly polarized transitions. This can be seen since in  $C_{3v}$  symmetry  $E \times E = A_1 + A_2 + E$  which contains the representations corresponding to electric dipole transitions of  $\pi$  symmetry  $A_1$  and  $\sigma$  symmetry E. The circularly polarized components lead to MCD but it is not possible to determine the g-values from (2) as the measured absorption will include components from the linearly polarized transitions. In contrast for  $C_{4v}$  centres  $E \times E = A_1 + A_2 + B_1 + B_2$  so that only linearly polarized transitions of  $A_1$  symmetry result and no MCD is expected. Information on the g-values for  $E \rightarrow E$  transitions for centres of trigonal or tetragonal symmetry can be obtained from resolved Zeeman spectra.

#### REFERENCES

1. Arkhangel'skaya V A and Feofilov P P 1958 *Optika i Spektroskopiya* **4** 602-19
2. Feofilov P P and Kaplyanskii A A 1962 *Usp. Fiz. Nauk.* **76** 201-38
3. Runciman W A 1969 *Physics of Solids in Intense Magnetic Fields* ed. E D Haidemenakis (New York: Plenum Press) pp. 344-58
4. Starostin N V and Feofilov P P 1969 *Soviet Physics Uspekhi* **12**, 252-70
5. Zapasskii V S and Feofilov P P 1975 *Soviet Physics Uspekhi* **18**, 323-42
6. Manson N B, Shah G A and Runciman W A 1975 *Solid State Comm.* **16** 645-9
7. Modine F A 1973 *Phys. Rev.* **B7**, 1574-7
8. Manson N B, Newman D J and Wong K Y 1977 *J. Phys.C: Solid State Phys.* **10** 4619-29
9. Srinivasan B, Hasan Z, Manson N B and Runciman W A 1985 *J.Phys.C:Solid State Phys.* **18** 2381-91

**ON THE DEFECT EQUILIBRIUM IN THE  $\text{Ba}_{1-x}\text{Gd}_x\text{F}_{2+x}$**   
**SOLID SOLUTIONS: A STUDY BY EPR AND ITC**

E. Laredo, A. Bello and M.E. Galavis

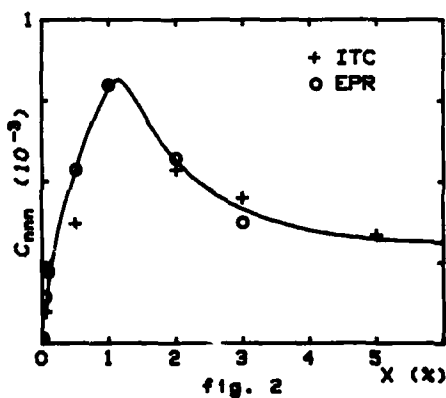
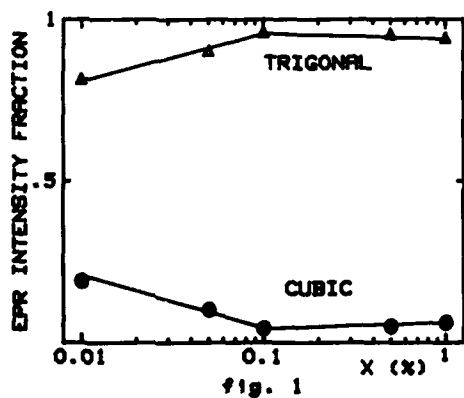
Physics Department, Universidad Simón Bolívar, Apartado 89000, Caracas, Venezuela.

Recently, the solid solutions of alkaline earth fluorides highly doped with trivalent rare-earth ions have been the object of several studies oriented to the search of the existence of higher clusters formed by the gettering or aggregation of the well accepted simple dipoles created by the binding of the  $\text{RE}^{3+}$  cation with its charge compensating defect, the interstitial fluorine. In  $\text{BaF}_2^{(1)}$  where the nnn (next nearest neighbor) dipole is the predominant defect the existence of clusters is not as well established as in the case of  $\text{CaF}_2^{(2)}$ . Electron Paramagnetic Resonance and ITC techniques have been used here to study the co-existence of the different types of defects in the  $\text{Ba}_{1-x}\text{Gd}_x\text{F}_{2+x}$  system for  $0.0001 \leq x \leq 0.05$ .

The EPR spectrum for all concentrations shows the existence of a trigonal center which is predominant and whose concentration increases until  $x=0.01$ . At higher concentrations the EPR lines broaden but their intensities decrease until the higher concentration studied by EPR is reached. The effective spin Hamiltonian parameters for  $J=7/2$  and trigonal symmetry were determined by fitting the experimental spectrum obtained for  $x=0.001$  and following a new approach for this kind of calculus based on the simulated annealing of the system using a Monte Carlo method. The parameters obtained are in excellent agreement with those first reported by Boatner et al.<sup>(3)</sup>, however our uncertainties are much lower. Besides this weak trigonal center, which is due to the nnn dipole, there is also a cubic spectrum present in all our EPR runs. The relative concentration of these two centers was estimated by computer fitting each of the experimental spectrum varying the relative abundance of the cubic and trigonal sites and the results are plotted on fig. 1. These same crystals were studied by ITC technique where the low-temperature spectrum shows an intense relaxation peak which is assigned to the relaxation of the nnn dipoles. From the intensity of this predominant ITC peak the absolute molar concentration of  $\text{Gd}^{3+}$  in nnn dipoles,  $c_{nnn}$ , was calculated and its variation with  $x$  is presented in fig. 2 together with the variation of the abundance of the trigonal center calculated after the intensity of carefully chosen EPR lines. The com-

parison of this two behaviors obtained from two completely different techniques shows an excellent agreement. The existence of a maximum molar concentration of dipoles equal to  $8 \times 10^{-4}$  for the crystal with  $x=.01$  found for both EPR and ITC experiments indicates that there is a high number of  $Gd^{3+}$  which is not under the nnn dipolar form and that this number increases rapidly for the most highly doped crystals forming higher clusters of lower symmetry which are not clearly seen due to the broadening of the EPR spectrum at these high concentrations. Also, from the information gathered in figures 1 and 2 for the less doped crystal where clustering should be unimportant, the association energy of the nnn dipoles could be estimated from the equilibrium between the associated species and the free defects and found to be equal to 0.41 eV to be compared to the value of .44 eV found by ionic conductivity techniques.

- 1) H.W. den Hartog, P. Dorenbos and W.J. Postma, Phys. Rev. **B34**, 7496 (1986).
- 2) R.H. Petit, P. Evesque and J. Duran, J. Phys. C **14**, 5081 (1981).
- 3) L.A. Boatner, R.W. Reynolds and M.M. Abraham, J. Chem. Phys. **52**, 1248 (1970).



$Mn^{2+}$  ON Li-SITE IN  $LiNbO_3$ : AN ENDOR INVESTIGATIONG. Corradi<sup>a,b</sup>, H. Söthe<sup>b</sup>, J.-M. Spaeth<sup>b</sup> and K. Polgár<sup>b</sup><sup>a</sup>University of Paderborn, Fachbereich Physik,  
Warburger Str. 100A, D-4790 Paderborn, FRG<sup>b</sup>Research Laboratory for Crystal Physics of the  
Hungarian Academy of Sciences, P.O.B. 132,  
H-1502 Budapest, Hungary

The geometry and electronic structure of defect centers due to the presence of transition metal ions in lithium niobate is of basic interest for the understanding of the photo-refractive effect in  $LiNbO_3$  devices.

Earlier arguments on the positions of these ions in the  $LiNbO_3$  lattice and in particular the arguments about  $Mn^{2+}$  substituting for Li are rather qualitative /1/. A somewhat clearer indication for Li-substitution of  $Mn^{2+}$  is coming from the value of the electric field gradient acting on the  $Mn^{2+}$  nucleus as determined from the splittings of the forbidden transitions in EPR /2/.

In the present ENDOR investigations congruent single domain high quality  $LiNbO_3$  crystals doped with 0.01 molar%  $Mn^{2+}$  in the melt prepared from Merck suprapure and Johnson-Matthey materials have been used. The spectra have been measured at  $T \sim 12$  K for magnetic field orientations  $B \parallel c$  and  $B \perp c$ . Due to the EPR line broadening a detailed angular dependence of the ENDOR spectra could be taken only by rotation of the crystal around the threefold c-axis, thus maintaining  $B \perp c$ .

For the five nearest Li-shells (see Fig. 1) the hyperfine (HF) parameters are shown in Table 1. Additional experimental results can be summarized as follows:

- a) The I. Li-shell consists of two partly resolved subshells.
- b) The II. Li-shell shows no splitting effect whatsoever.
- c) No close Li-neighbour along the c-axis (z-direction) within  $\sim 6 \text{ \AA}$  can be detected.

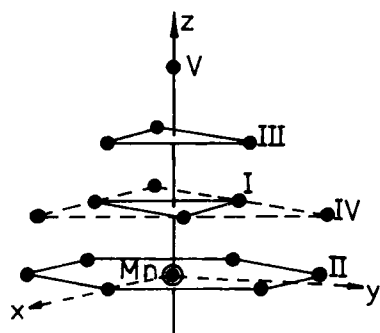


Fig. 1. Li-shells around  $Mn_{Li}$  in  $LiNbO_3$

The results can be explained by assuming that the  $Mn^{2+}$  ion is located at or very close to an empty Li-site in  $LiNbO_3$  lattice. No agreement can be obtained for Nb-substitution nor for any intermediary position of the  $Mn^{2+}$  ion. Arguments against an alternative model, where  $Mn^{2+}$  substitutes for a Li pair in an assumed local ilmenite stacking sequence [3] are also discussed.

A point dipole calculation for the case of Li-substitution in  $LiNbO_3$  structure gives quantitative agreement for the anisotropic HF interaction parameters of shells II-V, i.e. for Mn-Li distances  $> 5 \text{ \AA}$ .

Further experiments on stoichiometric  $LiNbO_3:Mn$  crystals are under way.

Table 1.

Fitted values of the isotropic (a) and anisotropic (b, b') ligand HF parameters (MHz) and of Euler angles for the tensor axes ( $\psi=0^\circ$  can be assumed) for Li-shells.

Li-shell	$I_a$	$I_b$	II	III	IV	V
a	-.05	-.02	.003	~.10	~-.03	
b-b'	.48	.45	.224	~.21	~.09	~.08
b'			<.01			
$\theta$	$47^\circ$	$47^\circ$	$90^\circ \pm 15^\circ$	$\sim 43^\circ$	$\sim 63^\circ$	$0^\circ$
$\phi$	$180^\circ$	$180^\circ$	$30^\circ$	$0^\circ$	$0^\circ$	-

/1/ A. R  uber, Current Topics in Material Science, Vol.1, ed. by E. Kaldis, 1978, North Holland Publ. Comp., p. 481

/2/ G.I. Malovichko and V.G. Grachev, Fiz. Tv. Tela 27, 2789 (1985), Sov. Phys. Sol. St. 27, 1678 (1985)

/3/ D.M. Smyth, Ferroelectrics, 50, 93 (1983)

$\text{Ag}^{++}$  AND  $\text{Ag}^{++}\text{-Ag}^+$  CENTRES IN  $\text{Na}_x\text{Ag}_{1-x}\text{Cl}$   
AN ENDOR INVESTIGATION

J.R. Niklas, U. Leonhardt and J.-M. Spaeth

*University of Paderborn, Fachbereich Physik, Warburger Str. 100, D 4790 Paderborn, F.R.G.*

The centres were produced by x- irradiation of NaCl crystals doped with 0.2 mol % AgCl at temperatures of about 10 K. V centres generated simultaneously were destroyed by in-situ annealing of the samples at 220 K [1]. The g- values for the  $\text{Ag}^{++}$  as obtained from the ESR- spectra are consistent with data in the literature [1,2].

ENDOR spectra were measured in the frequency range from .5 to about 80 MHz. They reflect the interactions of the  $S=1/2$  electron spin with 3  $\text{Cl}^-$ , 3  $\text{Na}^+$ , and 1  $\text{Ag}^+$  shell. The data for the ligand hyperfine interactions and the quadrupole interactions give a precise picture of the Jahn-Teller distortion [3,1] of the  $\text{Ag}^{++}$ . This is discussed in detail. The values are given in Table 1 in terms of the isotropic hyperfine constant, a, the anisotropic constant, b, and the quadrupole interaction constant, q.

Additional  $\text{Ag}^+$  and  $\text{Na}^+$  ENDOR- lines were analyzed to correspond to  $\text{Ag}^{++}\text{-Ag}^+$  compound centres. As for the  $\text{Ag}^0\text{-Ag}^+$  centre [4], the  $\text{Ag}^+$  was again found in a [100] position rather than in [110].

Table 1

symmetry	isotope	a/MHz	b/Mhz	q/MHz
(100)	$^{109}\text{Ag}$	92.2	13.6	-
(100)	$^{35}\text{Cl}$	36	29	2.1
(100)	$^{35}\text{Cl}$	7.5	.2	.08
(110)	Na	.54	.03	.05
(111)	$^{35}\text{Cl}$	.41	.07	.05
(100)	Na	5.54	.39	.15
(100)	Na	.76	.31	.03

- [1] J. Sierro, *J. Phys. Chem. Solids* **28** 417 (1967)
- [2] T. Müssig, *Thesis, Frankfurt/M.* (1986)
- [3] C.J. Delbecq, W. Hayes, M.C.M. O'Brien, P.H. Yuster, *Proc. R. Soc. Lond.* **A271**, 243 (1963)
- [4] Th. Müssig, J.R. Niklas, F. Granzer and J.-M. Spaeth, *Proc. 5<sup>th</sup> Europhysical Topical Conf.*, Madrid (1986)

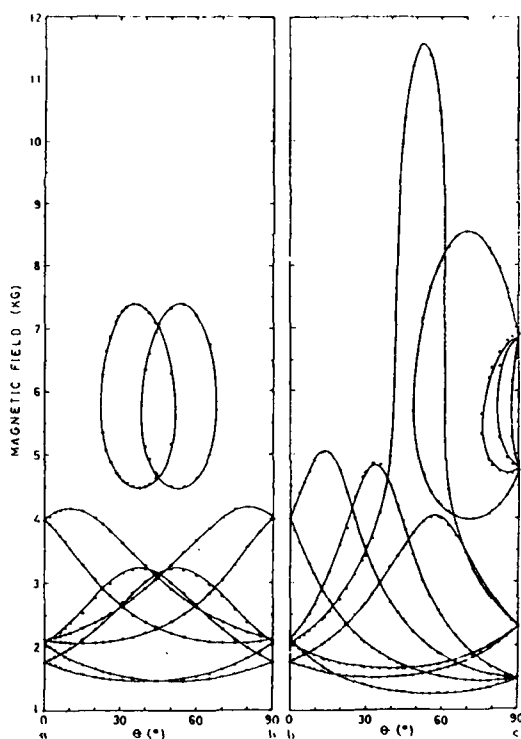
EPR SPECTROSCOPY OF  $\text{KDP:Cr}^{3+}$ 

D. Bravo, F. J. López, E. Diéguez and J. M. Cabrera

Dpto. Física Aplicada C-IV, Facultad de Ciencias,  
Universidad Autónoma de Madrid, Cantoblanco, 28049 MADRID

KDP is a crystal utilized for electrooptic devices such as modulators or second harmonic generation devices. The E.P.R. studies of impurities in this material usually present the difficulty of a low concentration level due to the low distribution coefficients they have at the temperature ( $\sim$ RT) KDP crystals are normally grown from aqueous solutions. However, it is known [1], that the so called "growth bands" at the external part of the block exhibit a higher impurity concentration than the rest of the crystal. In this work, an E.P.R. study of the growth bands of  $\text{Cr}^{3+}$  doped KDP has been performed at RT.

The figure shows the angular variation of the E.P.R. spectrum (dots) in the ab and bc planes for the more intense lines. From the symmetry of the angular variations of the resonance field it has been determined that the defect has orthorhombic symmetry. Thus the spectra were



fitted to the spin Hamiltonian

$$\mathcal{H} = \beta H \cdot \vec{g} \cdot \vec{S} + D [ S_z^2 - 1/3 S(S+1) ] + E [ S_x^2 - S_y^2 ]$$

where  $S = 3/2$ . The direction of maximum splitting has been chosen as the Z-axis of the defect and the defect principal axes X, Y, Z are related to the crystallographic ones a, b, c by the Eulerian angles. The best values for the fitting are:

$g_z = 1.972$	$ D  = 0.4372 \text{ cm}^{-1}$	$\Theta = 145.9^\circ$
$g_x = 1.967$	$ E  = 0.1285 \text{ cm}^{-1}$	$\Phi = 73.2^\circ$
$g_y = 1.972$		$\Psi = 119.3^\circ$

the continuous lines in the figure showing the computed values.

In a previous work by Kobayashi [2], a defect with similar principal axes has been reported and attributed to  $\text{Cr}^{3+}$  substituting for  $\text{K}^+$  with two proton vacancies as local charge compensators. The defect here presented has slightly lower values of D, E and the ratio  $3E/D$ , which indicates the orthorhombic distortion strength. Moreover, the Z-axis in the growth band sample, defined as the one exhibiting maximum splitting is exchanged ( within a few degrees ) with the Y-axis in Kobayashi's paper.

These results can be interpreted in the sense that the defect for the growth band sample consists also in  $\text{Cr}^{3+}$  in the  $\text{K}^+$  site with two proton vacancies. However, the growth method should affect the local distortion of the lattice.

#### References

- [1] E. Diéguez, A. Cintas, P. Hernández and J.M. Cabrera, J. Cryst. Growth 73, 193 (1985)
- [2] T. Kobayashi, J. of the Phys. Soc. of Japan 35, 558-572 (1973).

EPR AND ITC OF THE SUPERIONIC CONDUCTOR SYSTEM  $\text{PbF}_2\text{-GdF}_3$ 

I.V. MURIN, S.V. CHERNOV

Department of Chemistry, Leningrad State University  
Leningrad, USSR

W. Gunsser, J. Henning

Institut für Physikalische Chemie der Universität  
Hamburg, FRG

The renewal of interest in the physical properties of superionic conductors is part of the general development of the physics and chemistry of noncrystalline phases, abetted in this case by technological applications of these materials as solid electrolytes in batteries and other electrochemical devices.

The system  $\text{PbF}_2\text{-GdF}_3$  is a fluoride-type material suitable as a model of superionic conductors due to its relative structural simplicity.  $\text{PbF}_2$  has the largest conductivity of the fluorite group and the disordering of the anion sublattice occurs at the lowest temperature (1). Substitution of Pb with RE-elements has a great influence on the electrical and thermodynamical properties of the material (2).

Several experimental investigations involving optical, infrared and Raman spectroscopy as well as electrical conductivity, dielectric and inelastic neutron diffraction (3) are used for studying static and dynamic properties of these compounds.

We prepared solid solutions of  $\text{Pb}_{1-x}\text{Gd}_x\text{F}_{2+x}$  ( $x = 0.02 \dots 0.4$ ) by direct solid state synthesis. High purity  $\alpha\text{-PbF}_2$  and  $\text{GdF}_3$  were used as starting materials. Well ground mixtures of compounds were placed into Ni-ampules and then in an evacuated Ni-container with hydrofluorinating agent ( $\text{BaF}_2 \cdot \text{HF}$ ). Syntheses were carried out at  $800^\circ\text{C}$  during 7 hours. Solid solutions were quenched in water (room temperature). X-ray powder diffraction patterns showed no unidentified phases and were indexed in a  $\text{Fm}\bar{3}\text{m}$  space group ( $\text{CaF}_2$ -type). Maximal solubility of  $\text{GdF}_3$  in  $\beta\text{-PbF}_2$  was estimated to be  $38 \pm 3$  mole/%.

Our results of concentration dependence of electrical conductivity and activation energy of the solid solution are shown in figs. 1 and 2. We also performed ITC (thermal depolarization) measurements (2).

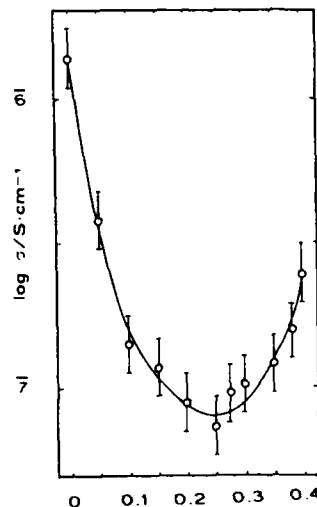


Fig. 1. Electrical conductivity of  $\text{Pb}_{1-x}\text{Gd}_x\text{F}_{2+x}$  as a function of Gd-mole-concentration at 293 K.

In the temperature range of 150 to 350 K, we studied EPR spectroscopic behaviour (X-band) of the fluorite-type solid solutions. EPR is not only a good monitor for local site symmetry of the trivalent paramagnetic ion  $Gd^{3+}$  ( $S = 7/2$ ), which is not mobile in the  $PbF_2$  lattice, but the mobile ions in the superionic conduct can also influence the EPR spectrum through the modulation of crystal field splittings and hyperfine interactions at very low Gd-concentrations.

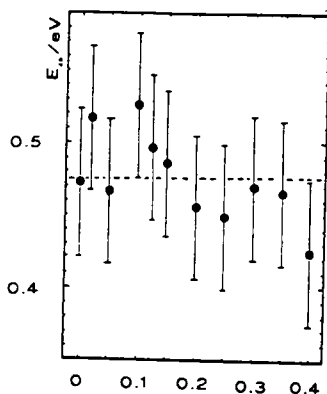


Fig. 2. Activation energy as a function of mole concentration  $x$  for  $Pb_{1-x}Gd_xF_{2+x}$ .

At intermediate and higher dopand levels, no hyperfine structure is seen in the EPR spectra. Here an association of the impurity atoms and interstitial fluorine ion vacancies into clusters of different kind and extension occurs (4). The simplest cluster is a 2:2:2 association, which can be described as a dimer of  $C_{4v}(NNN)$  dipoles stabilized by the formation of vacancies and relaxed fluorines. The EPR parameters  $g$ -value, relative intensity and line width as a function of Gd-content and temperature (an example is shown in fig. 3) give information about interactions of cations and interstitials in the clusters. More details regarding the coupling process are concluded from EPR line form analysis.

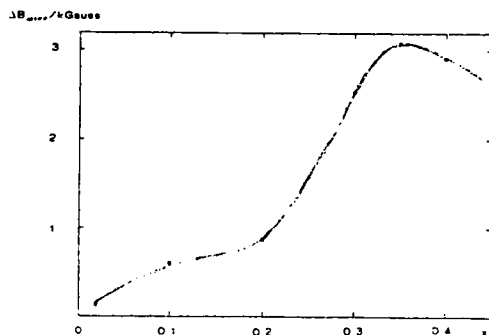


Fig. 3. Differential line width as a function of Gd-concentration in  $Pb_{1-x}Gd_xF_{2+x}$  at 350 K.

#### References:

- (1) K. Funke, Progr. Solid State Chem. **11**, 345 (1976).
- (2) I.V. Murin, S.V. Chernov, Solid State Ionics (to be published).
- (3) M.H. Dickens, M.T. Hutchins, J. Phys. C **11**, 461 (1978).
- (4) C.R.A. Catlow, M.J. Norgett, J.A. Ross, J. Phys. C **10**, 1627 (1977).

THE ROLE OF IMPURITY METAL-VACANCY COMPLEXES IN THE  
PHOTOCHEMISTRY OF THE SILVER HALIDES.

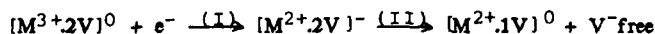
M. T. Olm, R. S. Eachus and R. C. Baetzold  
Research Laboratories  
Eastman Kodak Company  
Rochester, NY 14650 USA

During exposure to actinic radiation, the silver halides decompose to silver metal and free halogen at rates that are affected by impurities, particularly aliovalent cations of the Group VIII elements (1). These impurities generally introduce states in the forbidden energy gap of the host crystal, functioning as deep traps for photocarriers or as recombination centres. They are, therefore, of potential value as addenda for photographic materials; there is particular interest in how to exploit the electron trapping propensities of many of the Group VIII ions.

The precise photochemical effect of a transition metal impurity on the silver halides is determined by a number of factors, one of which is its association with other point defects. AgCl and AgBr are cubic solids with cationic Frenkel defect structures. Charge compensation for aliovalent impurity cations is generally provided by silver ion vacancies. The number and geometrical distribution of vacancies about an impurity ion can be particularly important for electron traps. An incomplete complement of vacancies adjacent to the impurity increases its trapping cross section and the lifetime of the trapped-carrier state.

More subtle effects on trapping characteristics result from variations in the relative lattice positions of the impurity and vacancies. For example, both  $\text{Ru}^{3+}$  and  $\text{Os}^{3+}$  substitute for silver when doped into AgBr and AgCl. They have low-spin  $d^5$  electronic configurations, are paramagnetic, and detectable by EPR before photolysis. In  $\text{Ru}^{3+}$ -doped AgBr single crystals, four structurally inequivalent sites were observed, each of which is believed to be a geometrical variant of the fully charge-compensated centre  $[\text{M}^{3+}2\text{V}]^0$ . (Here the two associated silver ion vacancies, V, render the site neutral with respect to the host lattice, as indicated by the superscript.) Similar results have been obtained for  $\text{AgCl}:\text{Ru}^{3+}$ ,  $\text{AgBr}:\text{Os}^{3+}$ , and  $\text{AgCl}:\text{Os}^{3+}$ . Rotations performed in orthogonal planes led to the derivation of a g-matrix for each site. It was possible to deduce reasonable structural models for these sites from the EPR data if they were combined with the results of atomistic calculations. By employing the computer programme CASCADE (2) and using only two body central forces with standard AgBr or AgCl potentials, energies were computed for the nine possible impurity-vacancy configurations involving nn and nnn positions. The most reasonable configurations for the observed four sites were then selected from the energetically favourable structures using symmetry arguments based on the observed g-matrices. These structures will be discussed in detail. During exposure to bandgap radiation, both  $\text{Ru}^{3+}$  and  $\text{Os}^{3+}$  trapped photoelectrons, and EPR signals from these ions were quenched at rates which were dependent upon the geometry of the  $[\text{M}^{3+}2\text{V}]^0$  site.

When the  $\text{Os}^{3+}$ - or  $\text{Ru}^{3+}$ -doped materials were photolysed at room temperature, the following sequence of reactions was expected to occur:



The ionic relaxation step (II), thought to be necessary to stabilize the trapped electron state, is facile only above about 150-170 K in the silver halides (1). To determine the effectiveness of this reaction, crystals exposed above 170 K were subsequently cooled to about 10 K and given a second irradiation with red light to ionise the trapped electron centres. At this temperature, vacancy motion is frozen so that EPR spectra from  $[M^{3+}.1V]^+$  centres should be observed. Surprisingly, the four original  $[M^{3+}.2V]^0$  centres were regenerated in their original concentration ratios. Apparently, ionic relaxation of the  $[M^{2+}.2V]^-$  trapped electron states did not occur at room temperature, implying a relatively strong binding energy for the second vacancy to the divalent  $M^{2+}$  ion. Atomistic defect calculations indicated that this second binding energy can be as large as 0.23 eV. The significance of this result for  $Ru^{3+}$ - and  $Os^{3+}$ -doped photographic systems is that the  $[M^{2+}.2V]^-$  centres are not rapidly stabilised by ionic relaxation at room temperature. Because of this, they tend to act as recombination centres, leading to a lower rate of photodecomposition in both AgBr and AgCl.

(1) R. S. Eachus and J. P. Spoonhower, "Progress in Basic Principles of Imaging Systems", edited by F. Granzer and E. Moisar, (Vieweg, Braunschweig, 1987), p. 175.

(2) M. Leslie, SERC Daresbury Laboratories, UK.

# LUMINESCENT PROPERTIES OF ALKALI-EARTH ZIRCONATES DOPED BY Ti and Eu

A.N. Belskiy, I.A. Kamenskikh, V.V. Mikhailin, A.N. Vasil'ev  
Moscow State University, USSR

I. Davoli, S. Stizza  
Camerino University, Italy

For phosphors  $AZrO_3$  doped by Ti or Eu ( $A=Ca, Sr, Ba$ ) photoluminescence spectra (LS) in the range 300-600 nm, diffuse reflection spectra (DR) in the range 150-500 nm luminescence quantum yield (LE) excited by photons with energies from 4 to 35 eV have been measured. LE was measured using monochromatized synchrotron radiation of the storage ring "Siberia-1" of Kurchatov Institute. These data enabled us to evaluate energy band gaps for these compounds (1).

Temperature and energy dependence of emission is characteristic for Ti in oxygen-containing compounds, where luminescent centers are formed by titanate groups  $TiO_x$ . The shift of DR edge of titanium-doped zirconates to lower energies is due to the absorption by titanate groups.

Emission of  $AZrO_3$ -Eu shows sharp lines in the red region characteristic for  $Eu^{3+}$ . LS prove that Eu creates not a unique type of luminescent centers.

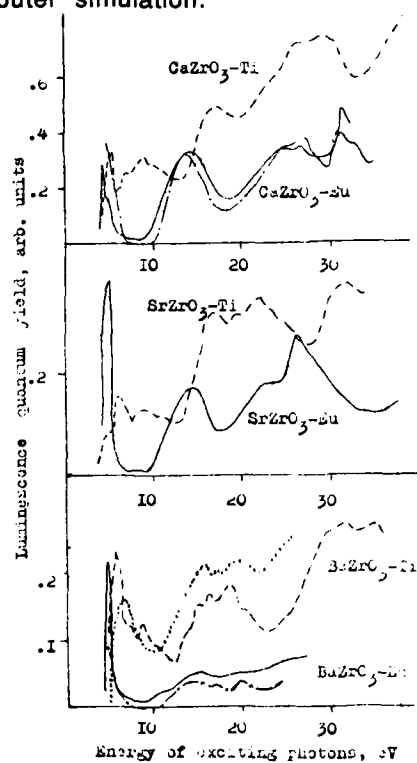
Spectra of LE in the range 4-35 eV provide information on the inelastic scattering of electronic excitations leading to a step-wise increase of  $\eta(h\nu)$ , as well as on transitions from the core levels. Utterly different view of LE spectra for two activators can be explained supposing different mechanisms of energy transfer to luminescent centers: predominantly electron-hole one in the case of Ti and excitonic one in the case of Eu. This hypothesis is confirmed by computer simulation  $\eta(h\nu)$  according to ref. (2).

## REFERENCES

1. A.N.Belskiy et. al.: Proceedings of International Conference on Solid State Chemistry, Karlovy Vary, Czechoslovakia, 1986, p.180-182.
2. A.N.Vasil'ev et.al.: Izv.AN SSSR, ser.Phys., 49, (1985) 2044

## FIGURE CAPTIONS

Fig.1-Luminescence yield versus exciting photon energies, RT: solid curve -  $\text{AZrO}_3\text{-Eu}$ , dashed -  $\text{AZrO}_3\text{-Ti}$ , dashed-dotted and dotted - computer simulation.



QUANTUM EFFICIENCY OF  $\text{Eu}^{2+}$  PHOTOLUMINESCENCE IN  $\text{NaCl}$  CRYSTALS

I. Mugańska, R. Cywiński

Institute of Low Temperature and Structure Research  
Polish Academy of Sciences, Wrocław, Poland

$\text{NaCl}:\text{Eu}(2+)$  crystals used in this work (about 100 ppm mol  $\text{Eu}(2+)$  in the host) were grown by the Bridgman method in vacuum-sealed quartz ampoules (1).

Absolute quantum yield of photoluminescence excited by 366 nm Hg line was measured at 300 K by the Vavilov method using rodamine B quantum counter and magnesium oxide standard. Temperature dependence of quantum yield within 15 - 300 K was determined by the integration of corrected emission spectra.

The photoluminescence quantum yield of  $\text{NaCl}:\text{Eu}(2+)$  sample quenched from 500°C or quenched from 500°C and annealed at room temperature was equal to unity independently of the temperature. For samples annealed within 100 - 250°C the photoluminescence quantum yield was equal to unity at 15 K and decreased down to about 0.2 - 0.8 at 300 K respectively.

Apart from the dipole six different  $\text{Eu}(2+)$  luminescent centers ("i"- "vi") in  $\text{NaCl}$  crystals are formed (2). The photoluminescence quantum yield of the dipole and their aggregates "i" formed at room temperature (probably dimers or trimers) is practically equal to unity and the contribution of radiationless processes can be neglected.

The photoluminescence quantum yield of the foreign phase precipitates "ii" - "vi" can be described by the equation  $\eta = [1 + (I_0 - I_T)/I_0]^{-1}$  where  $I_0, I_T$  are the integral intensities of the emission bands. Activation energies calculated from the pertinent Arrhenius plots suggest existence of two luminescence quenching mechanisms. The first mechanism with activation energy values characteristic of the dipole resonance oscillation energy (about 50  $\text{cm}^{-1}$  and 200  $\text{cm}^{-1}$ ) is responsible for the luminescence quenching of "ii" and "iii" precipitates below 100 K. The second mechanism is related with the configuration curve crossing with activation energies above 600  $\text{cm}^{-1}$ . The latter mechanism dominates in quenching of luminescence at higher temperatures (within 100 - 300 K) and seems to be valid only for "v" and "vi" precipitates.

- 1) R. Voszka, I. Garjan, L. Burkes, J. Radsovszky, Kristall und Technik 1, 423 (1966).
- 2) I. Mugańska, R. Cywiński, phys. stat. sol. (b) 128, 475 (1985).

EFFECT OF AGGREGATION AND ENERGY TRANSFER ON OPTICAL  
PROPERTIES OF  $Mn^{2+}$  IONS IN  $NaCl:Eu,Mn$  AND  $KCl:Eu,Mn$  SYSTEMS

R.Cywiński and E.Muġeński

Institute for Low Temperature and Structure Research,  
Polish Academy of Sciences  
50-950 Wrocław, P.O.Box 937, Poland

The excitation energy transfer from europium to manganese ions in doubly doped  $NaCl:Eu,Mn$  and  $KCl:Eu,Mn$  crystals aged at room temperature or annealed at higher temperatures is examined. As shown earlier [1,2] this energy transfer proceeds in simple aggregates or foreign phase precipitates containing both dopant ions.

It is ascertained that the temperature function of the manganese luminescence decay time ( $\tau$ ) can be described by the dependence  $\tau^{-1} = \tau_0^{-1} + s_1 \exp(-E_1/kT) + s_2 \exp(-E_2/kT)$ , in which two temperature ranges are considered (up to 100 K and above 100 K) with appropriate activation energy values  $E_1$  and  $E_2$ . In freshly quenched  $NaCl:Eu,Mn$  and  $KCl:Eu,Mn$  crystals as well as in  $KCl:Eu,Mn$  ones aged at room temperature (presence of the aggregates of loosely bound dipoles), the  $E_1$  values are comprised between 20 and 40  $cm^{-1}$  and  $E_2$  values between 200 and 250  $cm^{-1}$ , being characteristic of the resonance vibrations of the dopant ions. In  $NaCl:Eu,Mn$  crystals aged at room temperature and in  $KCl:Eu,Mn$  ones annealed at about 250 °C  $E_2$  values are equal to 300  $cm^{-1}$  and 550  $cm^{-1}$ , respectively. The above values distinctly exceed the phonon range of the crystal lattice (local vibrations) and are possibly characteristic of the foreign phase precipitates containing both dopant ions.

- [1] R.Capelletti, M.Manfredi, R.Cywiński, J.Z.Damm, E.Muġeński and M.Solzi, Phys.Rev.B 36, 5124 (1987).
- [2] R.Cywiński, R.Fava, M.Manfredi and E.Muġeński, phys.stat.sol.(b) 143, 433 (1987).

A NEW TYPE OF COLOR CENTER IN CESIUM HALIDES:  
F CENTER ASSOCIATED TO A PAIR OF OH<sup>-</sup> DEFECTS

Mathias Krantz and Fritz Luty

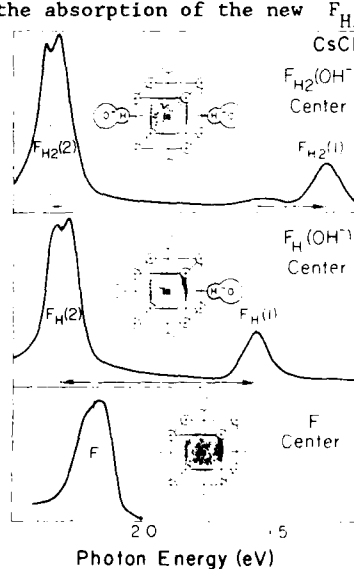
Physics Department, University of Utah, Salt Lake City, Utah 84112, USA

V. Dierolf and H.J. Paus

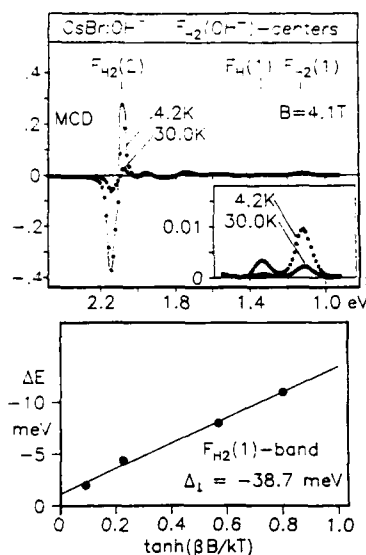
Physikalisches Institut, Universität Stuttgart, D-7000 Stuttgart W.-Germany

F centers in crystals of NaCl structure cannot only be attached to isolated cationic defects ( $F_A$  centers) but also--in highly doped crystals--to impurity-pairs ( $F_B$  centers). The full analogy in  $C_{4v}$  symmetry of F centers associated to single anionic defects in Cs-halides ( $F_H$  centers) raises the question if F-association to anionic impurity-pairs is possible also.

We found indeed a first complex of this type which we call " $F_{H2}$  center". Optical bleaching at 180 K of the "primary"  $F_H(OH^-)$  center in highly  $OH^-$  doped CsCl and CsBr crystals leads--besides  $F_H \rightarrow F$  back-conversion--to the gradual appearances of this "secondary" center. Multiple repetition of the optical  $F \rightarrow F_H$  formation and  $F_H \rightarrow F$  destruction produces accumulation of this new center, until its predominance (~100% in CsCl and ~80% in CsBr) compared to the primary  $F_H$  center is reached. Fig. 1 shows--besides the single F band and the widely split  $F_H$  bands--the absorption of the new  $F_{H2}$  center. It remains similar in spectral structure and indication of SO splitting to the  $F_H$  absorption, the main change being a strong increase of the two-band-separation  $\Delta E$  from 0.75 eV ( $F_H$ ) to 1.0 eV ( $F_{H2}$ ). The symmetry of the new defect was determined by using polarized light in the  $F_H \rightarrow F_{H2}$  conversion cycle:  $\langle 110 \rangle$  light produces no dichroism, while  $\langle 100 \rangle$  light creates  $\langle 100 \rangle$  dichroism of opposite sign for the two bands. This clearly shows  $\langle 100 \rangle$  orientation of this complex with a two-fold (spin-orbit-split)  $F_{H2}(2)$  transition  $\perp$  and a single  $F_{H2}(1)$  transition  $\parallel$  to the center axis. All these features and the fact that it is formed only in high  $OH^-$  doped crystals suggests the



following structural model: An F center and two  $\text{OH}^-$  defects on three adjacent lattice sites in  $\langle 100 \rangle$  direction--mostly likely arranged with the F center in the middle between the two  $\text{OH}^-$  ions, as sketched in Fig. 1. This is exactly analogous to the tetragonal  $D_{4h}$  ("configuration I") of the  $F_B(\text{Na})$  center in  $\text{KCl}$ <sup>1</sup>. While in the latter the two opposite  $\text{Na}^+$  neighbors increase the F band splitting compared to the single  $\text{Na}^+$  neighbor in the  $F_A$  defect, the same is achieved by the two  $\text{OH}^-$  ions ( $F_{H2}$  center) compared to the single  $\text{OH}^-$  neighbor in the  $F_H(\text{OH}^-)$  center. Oppositely oriented molecular and displacement dipoles from the two  $\text{OH}^-$  neighbors (see Fig. 1) obviously produce the enormous  $\Delta E \approx 1$  eV splitting of the 2p state for transitions  $\parallel$  and  $\perp$  to the center axis--totally unique in size among all known one-electron F-aggregate centers.



This model has been confirmed by measurements of the MCD spectra in  $\text{CsBr}$  (Fig. 2) which in spite of the enormous splitting are typical for tetragonal centers. Due to the incomplete  $F_H \rightarrow F_{H2}$  conversion, their close-lying high-energy spectral bands overlap partially and make analysis difficult. Their well-separated low-energy bands, however, allow reliable measurement of T-dependent MCD spectra and their accurate moment analysis. The measured B/T dependence (Fig. 2) yields  $\Delta_1 = -38.7 \text{ meV}$  confirming the one-electron F center type defect structure of tetragonal symmetry. The further reduction of the  $|\Delta_1|$  value compared to the  $F_H(\text{OH}^-)$  center indicates the strong perturbation effect due to the added second  $\text{OH}^-$  neighbor. Qualitatively the same behavior has been observed for  $\text{CsCl}$  crystals.

\*Supported by NSF grant DMR 87-06416.

1. N. Nishimaki, Y. Matsusaka, Y. Doi, J. Phys. Soc. Japan **33**, 424 (1971).

NATURE OF ENERGY TRANSFER IN F CENTER/OH<sup>-</sup> DEFECT PAIRS IN KCl.  
TESTED WITH ANTI-STOKES RESONANCE RAMAN SCATTERING

G. Halama and K.T. Tsen

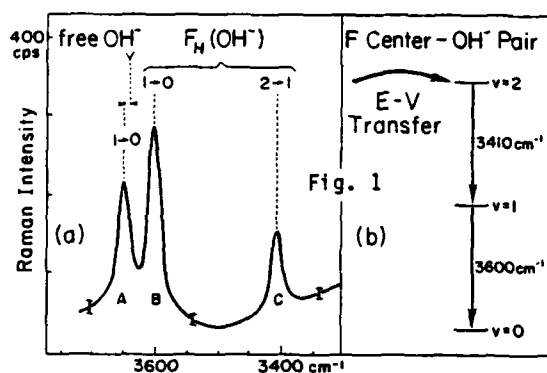
Physics Department, Arizona State University, Tempe, Arizona 85287

Fritz Luty

Physics Department, University of Utah, Salt Lake City, Utah 84112

Optical aggregation of F centers in highly OH<sup>-</sup> doped KCl crystals at 240 K leads to the formation of F center/OH<sup>-</sup> ion pairs. In contrast to normal F centers these "F<sub>H</sub>(OH<sup>-</sup>)" defects are characterized by a broadened and red-shifted single absorption band and total quenching of the normal Stokes-shifted electronic emission<sup>1</sup>. Measurements of the F<sub>H</sub> center ground-state-bleach recovery kinetics under pulsed laser excitation shows that the nonradiative de-excitation of the F<sub>H</sub> electron occurs extremely rapidly in the pico-second regime<sup>2</sup>. Opposite to the case of F center/CN<sup>-</sup> ion pairs no trace of OH<sup>-</sup> stretching vibration emission has been observed<sup>1</sup>. The most basic question therefore remained unanswered so far: what is the coupling or energy transfer process by which the F<sub>H</sub> electron loses its excitation energy so efficiently to the OH<sup>-</sup> ion neighbor?

We tested this open question for F<sub>H</sub>(OH<sup>-</sup>) defects in KCl using 60 psec-pulsed frequency-doubled YAG laser radiation of 532 nm both to pump the F<sub>H</sub> absorption and to probe its resonance Raman response. Based on the time-averaged laser power (~1 W), pulse repetition rate and pumping volume, the delay-time between pump and probe of the same F<sub>H</sub> center is  $\tau \approx 10^{-6}$  sec. Due to the rapid (pico-second) return of the excited electron, any molecular excitation preserved after pumping over this time-period  $\tau$  will be accessible for detection by anti-Stokes resonance Raman scattering. Fig. 1a shows the result obtained for F<sub>H</sub>(OH<sup>-</sup>) defects in KCl at 10 K: three Raman lines (A,B,C) appear at 3650, 3600 and 3410 cm<sup>-1</sup>, extremely weak but remaining well observable up to ~80 K. The highest energy line A lies very close to the stretching mode  $\nu_1 = 3643$  cm<sup>-1</sup> of the isolated OH<sup>-</sup> defect. The two lower energy lines B and C we attribute, as sketched in Fig. 1b, to the  $v = 1 \rightarrow 0$  and  $v = 2 \rightarrow 1$  vibrational OH<sup>-</sup> transitions in the F<sub>H</sub>(OH<sup>-</sup>) complex: The presence of a "soft" F center neighbor lowers slightly the OH<sup>-</sup> stretching-frequency relative to that of the isolated defect, while our observed anharmonicity shift  $\nu(B) - \nu(C) \approx 190$  cm<sup>-1</sup> coincides closely with the one (~170 cm<sup>-1</sup>) observed for isolated OH<sup>-</sup> defects.



Within these assignments the interpretation is sketched in Fig. 1b. A good part of the electronic excitation energy ( $-0.87\text{eV}$ ) of the close  $F_H(OH^-)$  center is transferred into the  $v = 2$  state of the attached  $OH^-$ . The cascading relaxation  $v = 2 \rightarrow 1 \rightarrow 0$  of the excited  $OH^-$  ion is obviously a very rapid nonradiative process

(no vibrational emission observed!), so that after the pump-probe delay-time  $\tau$  only very small remaining populations in the  $v=2$  and  $v=1$  excited states can be detected by anti-Stokes Raman scattering. The presence of an additional line A indicates that besides the "close  $F/OH^-$  pair" a more distant  $F/OH^-$  pair-configuration exists, characterized by an  $OH^-$  frequency nearly equal to that of the isolated  $OH^-$  ion and by a weaker  $e - v$  transfer process populating only the  $v = 1$  state.

Under  $\langle 100 \rangle$  polarized excitation light, all 3 bands A, B and C show about 6-10 times stronger Raman signal for  $\perp \langle 010 \rangle$  compared to  $\parallel \langle 100 \rangle$  polarization. Consequences of this amazing result will be discussed, particularly in terms of the [200] neighboring-site pair model, derived for the  $F_H(OH^-)$  center in KCl from ENDOR measurements<sup>3</sup>.

Most interesting is extension of this work to F centers paired with  $OD^-$  defects (having a stretching frequency  $\sqrt{2}$  smaller than  $OH^-$ ). Preliminary experiments with  $F_H(OD^-)$  centers show only two weak anti-Stokes Raman lines A and B at  $2680$  and  $2660\text{ cm}^{-1}$ , line A (like in the  $OH^-$  case) located close to the frequency of the isolated defect. These results indicate weak  $e - v$  energy transfer only into the  $v=1$  state of two  $F_H(OD^-)$  pair configurations. Improved experiments are under way and will be discussed and interpreted, in comparison to the  $F_H(OH^-)$  results and to the (orders of magnitude stronger) anti-Stokes Raman results obtained for  $F_H(CN^-)$  defects<sup>4</sup>.

\*Supported by NSF grants DMR 87-18228 and DMR 87-06416

1. L. Gomez and F. Luty, Phys. Rev. B **30**, 7194 (1984).
2. D.J. Jang, M.A. El-Sayed, L. Gomez and F. Luty, Ultrafast Phenomena V, Springer Verlag, Berlin, 1986.
3. M. Jordan, H. Söthe, J.M. Spaeth and F. Luty (paper in this meeting).
4. K.T. Tsen, G. Halama and F. Luty, Phys. Rev. B **36**, 9247 (1987).

Q-SWITCHING OF A Nd:YLF PULSED LASER USING  $F_2^-$  COLOR CENTER IN LiF<sup>+</sup>

N.D. Vieira Jr., F.E. da Costa, W. de Rossi, S.L. Baldochi and S.P. Morato  
 Instituto de Pesquisas Energéticas e Nucleares - Caixa Postal 11049  
 01000 - São Paulo - Brasil

We report pulsed Q-switched operation of a Nd:YLF laser using  $F_2^-$  color centers in LiF crystals.  $F_2^-$  color centers are produced in heavily irradiated ultra pure LiF crystals. These crystals are first zone refined in a HF atmosphere and then pulled by a Czochralsky technique. The same technique is used to prepare and pull Nd:YLF crystals. Color centers are then created in LiF by irradiation with a  $\gamma$ -cell ( $^{60}\text{Co}$  in with 20MRad) producing an absorption band of  $0.31 \text{ cm}^{-1}$  peaking at 960 nm with almost negligible formation of adjacent higher aggregates of F centers. These  $F_2^-$  centers have an emission band peaking at  $1.15 \mu\text{m}$  with a reported decay time of 54 ns at room temperature. We used a plane-parallel laser cavity with a closed coupled configuration pumping cavity. The gain medium is a 3 inches long, 1/4 inch diameter Nd:YLF crystal pumped by a xenon lamp.

Without Q-switching the laser delivers 300 mJ of pulse energy in 120  $\mu\text{s}$ . Introducing in this cavity a  $F_2^-$ :LiF crystal (initial absorption of 46% at  $1.047 \mu\text{m}$ ) of dimensions  $63 \times 15 \times 15 \text{ mm}^3$ , we obtained a train of pulses (3 to 4) with 15 ns of pulse duration and minimal loss of output energy. This lack of loss in energy is due to an stimulated emission mechanism by the  $F_2^-$  color centers.

+ Financed by FINEP.

SENSITIZED LUMINESCENCE OF DOPED  $\text{NaNO}_2$  SINGLE CRYSTALS

T.Schmidt, J.Köhler and D.Schmid

Institut für Physik der kondensierten Materie

Lehrstuhl für Festkörperspektroskopie

Universität Düsseldorf; Universitätsstr.1; D-4000 Düsseldorf 1; FRG

For many years sensitized luminescence has been a valuable tool in the investigation of excitonic energy transfer in organic molecular crystals /1/. Some years ago we have found the system  $\text{NaNO}_2:\text{KNO}_2$  to be an interesting model of excitonic energy transfer in ionic crystals /2/. The fluorescence and absorption spectra of the pure crystal are investigated in detail /3...5/.

By doping a  $\text{NaNO}_2$  single crystal with only 0.1%  $\text{KNO}_2$  the absorption and fluorescence spectra changes drastically. Fig.1 shows the fluorescence spectrum of a  $\text{NaNO}_2$  crystal which was doped by 0.1%  $\text{KNO}_2$  at 5K near the (0-2) vibronic transition of the pure crystal /2/. The lines A to G are assigned to  $\text{NO}_2^-$  molecule-ions which are perturbed by neighboring  $\text{K}^+$  impurities and act as traps for the excitation energy. In the absorption spectra of  $\text{NaNO}_2:\text{KNO}_2$  we could establish new lines on the low energy side of the 0-0 transition of the pure crystal ( $25980\text{cm}^{-1}$ ) due to the absorption of disturbed  $\text{NO}_2^-$  molecules (fig.2) /7/. The absorption lines have been assigned to the respective fluorescence lines using fluorescence-excitation spectroscopy /7/.

We could show by time-resolved measurements /6,7/ that the traps are arranged in so called "trap-systems" with a deep trap ( $\Delta \approx 1000\text{cm}^{-1}$ ) and a shallow trap ( $\delta \approx 100\text{cm}^{-1}$ ) each, and where the energy transfer between the shallow and the deep trap is very effective. At least the results are interpreted in terms of a generalized master equation approach /8/. From this approach it is seen that the process of energy transfer to the traps in  $\text{NaNO}_2:\text{KNO}_2$  is controlled by the motion of the singlet-exciton.

# References

- /1/ H.C.Wolf, Adv.Atom.Mol.Phys. 3,119 (1967)
- /2/ F.Lisse,J.Köhler,H.Pufahl,D.Schmid, phys.stat.sol.(b) 140,605 (1987)
- /3/ J.W.Sidman, J.Amer.Chem.Soc. 79,2669 (1957)
- /4/ M.Kamada,M.Yoshikawa,R.Kato, J.Phys.Soc.Jap. 39,1004 (1975)
- /5/ M.Kamada,T.Yoshimura,R.Kato, J.Phys.Soc.Jap. 42,1660 (1977)
- /6/ H.Pufahl,J.Köhler,T.Schmidt,D.Schmid,V.M.Kenkre  
phys.stat.sol.(b) 141,303 (1987)
- /7/ T.Schmidt,J.Köhler,C.Krysch,D.Schmid, phys.stat.sol.(b) (1988) -  
in print
- /8/ V.M.Kenkre, Excitation Dynamics in Molecular Crystals, Springer (1982)

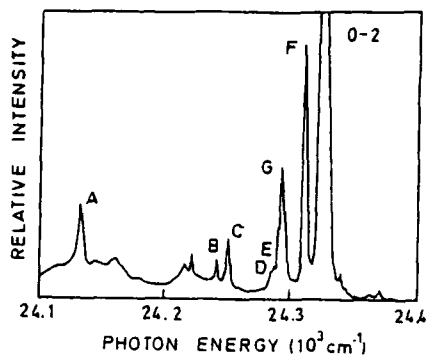


fig.1 : Fluorescence of  $\text{NaNO}_2:\text{KNO}_2$  near the (0-2)-transition of the pure crystal.

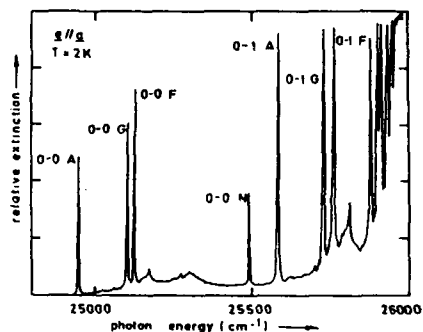


fig.2 : Extinction of  $\text{NaNO}_2:\text{KNO}_2$  on the low energy side of the pure crystal (0-0) transition at  $25980\text{cm}^{-1}$ .

# KINETICS OF NON-STEADY-STATE DIFFUSION-CONTROLLED TUNNELLING RECOMBINATION OF DEFECTS IN KCl, $\alpha$ -Al<sub>2</sub>O<sub>3</sub>, DNA

E. Kotomin, I. Tale, V. Tale, P. Butlers, P. Kulis

Institute of Solid State Physics, Latvian State University, RIGA, USSR

In interpreting the results of the steady-state experiments on diffusion-controlled recombination kinetics of radiation defects in solids, often the following difficulty is encountered: the reaction rate  $K=4\pi DR^*$  is a product of two temperature dependent factors - the relative diffusion coefficient  $D$  and the effective recombination radius  $R^*$ . For contact recombination mechanism (approach of defects to within a distance  $r \leq R_0$ ),  $R^*=R_0=\text{const}$ . In the case of the long-range interaction (e.g. tunnelling recombination whose probability (per second) is  $W(R)=W_0 \exp(-r/a)$ ,  $W_0, a$  are constants)  $R^*$  and the joint distribution function of the dissimilar defects,  $Y$ , appear to be temperature ( $D$ ) dependent /1/. It can be used as a method to estimate independently both co-factors:  $D$  and  $R^*$ . The idea of the method /2/ is to make use of the step-like increase (decrease) of the temperature, which in its turn changes instantly the diffusion coefficient  $D=D_0 \exp(-E/kT)$ . The second co-factor,  $R^*$  changes inertially which results in delayed increase (decrease) of both  $K$  and the recombinational luminescence intensity  $J \sim K$ . Indeed, after the increment of  $T$  by  $\Delta T = T_2 - T_1$  and of  $D$  by  $D_2/D_1 = \exp(-E\Delta T/T_1^2)$  the initial steady-state recombination profile and radius,  $Y_1(r, T_1)$  and  $R^*(T_1)$ , transform into  $Y_2(r, T_2)$ ,  $R^*(T_2)$ , which are calculated in /1/.

We have made theoretical and experimental studies of the non-steady-state kinetics of the diffusion-controlled tunnelling recombination of radiation defects in quite different insulating crystals: KCl,  $\alpha$ -Al<sub>2</sub>O<sub>3</sub>, Na-salt of DNA. We used such experimental conditions, that the relative change of the defect concentration were negligibly small, and thus the behaviour of the  $J(\tau)$  was entirely due to the change of the reaction rate  $K$ .

Two models of the delayed kinetics are compared. (i) Assuming that  $Y(r, t)$  changes as due to a very slow heating and that the delay time in  $Y$  and  $R^*$  change results entirely from the diffusive passage between  $R^*(T_1)$  and  $R^*(T_2)$ , one gets  $\Delta J \sim K = 4\pi D \Delta R^* \sim D^{1/2} \sqrt{\tau}$ . Indeed, such a behaviour fits well the experimental kinetics for self-trapped holes ( $V_K$  centers) in KCl and KBr. However, the activation energies obtained are essentially underestimate. (ii) A more correct model is based on a direct solution of the diffusion equation (in the dimensionless units  $x=r/a$ ,  $\tau=Dt/a^2$ )

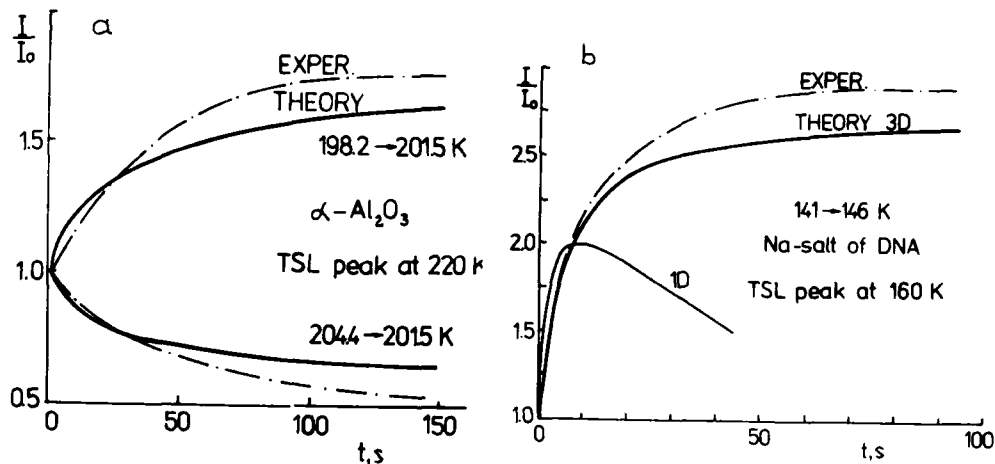
$$\frac{\partial Y}{\partial \tau} = 2^* \left\{ Y'' + \frac{2}{x} Y' \right\} - \frac{W_0 a^2}{2} e^{-x}, \quad Y \sim \int_{R_0}^{\infty} e^{-x} Y(x, \tau) x^2 dx.$$

Therefore the delayed kinetics is governed by the parameters

$W_0$ ,  $a^2/D$ ,  $D^* = D_2/D_1$ , describing defect motion and recombination. These parameters can be obtained by a fitting of theoretical kinetics  $J(t)$  to the experimental one. The latter can be characterized qualitatively by an increment of  $J$  (y scale) and transition time (x scale) which yield the parameters  $E$  and  $a^2/D$ , respectively. Making use of an estimate for the electronic partner of the  $V_K$  center in KCl:Tl (0.1 mol%)  $a(Tl^0) = 1 \text{ \AA}$ , we have arrived at the pre-exponent  $D_0(V_K) = (12 \pm 5) \cdot 10^{-3} \text{ cm}^2 \text{ s}^{-1}$  which agrees qualitatively with the result of the optical dichroism studies  $D = 4 \cdot 10^{-3} \text{ cm}^2 \text{ s}^{-1}$  [3]. The corresponding  $R^*(T) = a/kT$  [1] being about  $20 \text{ \AA}$  at  $180 \text{ K}$ . In its turn, for hypothetical self-trapped holes in  $\alpha\text{-Al}_2\text{O}_3$  (fig 1,a) and Na-salt of DNA (fig 1,b) we arrive at  $a^2/D = (30 \pm 10) \text{ s}$  and  $(7 \pm 3) \text{ s}$ , respectively. The relevant models of these centers are proposed.

To sum up, we have demonstrated that:

- i) the fact of delayed (hundreds of seconds) increment of the luminescence intensity  $J$  observed in a number of insulating crystals serves as a qualitative criterium of the elementary excitation self-trapping and electron tunnelling,
- (ii) the non-steady-state recombination regime permits to get independently the parameters determining both defect motion and tunnelling recombination,
- (iii) the discrepancy between theory and experiment seems to be due to the continuous description of defect motion (eq. (1))
- (iv) the delayed kinetics in DNA does not result due to 1D motion and recombination process.



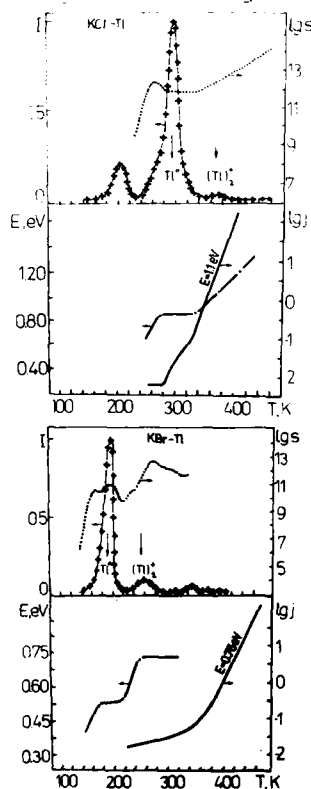
- 1) Kotomin E.A., Doktorov A.B. Phys Stat Sol. 1982, v.114, 287.
- 2) Tale I.A., Kulis P., Krønghaus V. J. Lumin. 1979 v.20 343.
- 3) Kabler M.N. In: "Point Defects in Solids", v.1, Plenum, 1972.

# THE EFFECT OF DYNAMICAL DISORDERING UPON THERMOSTIMULATED PROCESSES IN IONIC CRYSTALS

I.A.Tale, V.G.Tale

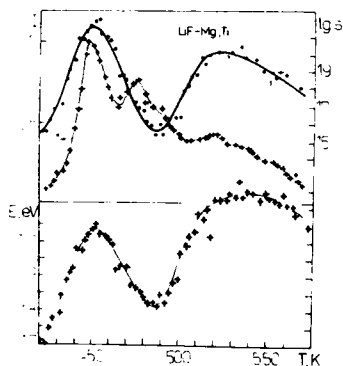
Institute of Solid State Physics, Latvian State University  
Kengaraga,8, RIGA 226063, USSR

Annealing of both electronic and hole centres (e.g.  $F_2^+$ ,  $V_2^+$ , ..centres in KCl[1]) at high temperatures is usually due to association of centres with mobile vacancies. The relevant activation energy is determined by the enthalpies of both a release and the migration of vacancies, the frequency factor being of the order of optical phonon frequency ( $\sim 10^{12} \text{ s}^{-1}$ ). The results of trap spectroscopy by fractional glow technique (FGT) in doped KCl, KBr, LiF,  $\text{CaF}_2$ , which contradict to the traditional idea of reactions limited by capture of mobile vacancies, are discussed. The concept of dynamical disordering of defects is developed and accordingly an alternative mechanism of high temperature defect annealing proposed.



Experimental. KCl;KBr (100ppm Tl). The mean activation energy,  $E$  and frequency factor,  $s$  as functions of stimulation temperature for ionization of the single ( $\text{Tl}^0$ ) and dimer ( $\text{Tl}_2^+$ ) electronic centres differ qualitatively in KCl and KBr crystals: (i) Only in KBr exchange and Coloumb interactions result in a significant change of the ionization energy of  $\text{Tl}^0$  thus broadening the activation energy spectrum with respect to an unperturbed one (0.5eV [2]). (ii) Because of their lower concentration  $\text{Tl}_2^+$ -centres in KBr are monoenergetic ( $E=0.72\text{eV}$ ). (iii) Unlike KBr, in KCl the  $E$  for the  $\text{Tl}_2^+$ -centres increases with the stimulation temperature.  $\text{Tl}_2^+$ -centres become ionized at temperatures at which cation vacancies begin to be mobile[2]. The plastic deformation of a sample reduces the temperature at which both the  $E$  and the ionic conductivity  $j$  begin to increase. (iv) In KCl the frequency factor of the ionization of the  $\text{Tl}_2^+$ -centres significantly exceeds the limiting optical phonon frequency thus indicating that the standard explanation of the reaction is no more valid. The similar effect of the extremally high measured values of  $E$  and  $s$  was also observed in dosymetric TSL peaks of

LiF-Ti,Mg crystals[3], as well as high temperature TSL peaks of  $\text{CaF}_2$ . In the case of LiF the dosymetric TSL peaks



correspond to the temperature range where dissociation of  $[\text{Mg}-\text{V}_\text{c}]$  complexes takes place. Therefore an sharp increase of mobile cation vacancy concentration with temperature perturbs the thermoactivated electronic process.

The model proposed. Defrozen of an ionic system causes a dynamical disordering of the defect and/or its surrounding. Due to some ionic process the structure of a defect can be changed (perturbed) for a short time. It is assumed that perturbed configurations occur as fluctuations of the perfect ones[4]. Perfect and all perturbed configurations are characterized by its own ionization (dissociation) energy. The effective ionization energy,  $\bar{E}$ , is the statistical average over all states of defect. In the case of only two - perfect (u) and perturbed (p) configurations

$$\bar{E} = \frac{E_u W_u + E_p W_p}{W_u + W_p}$$

where  $E_u, W_u, E_p, W_p$  - the ionization energy and the probabilities (per unit time) of the realization of perfect and perturbed configurations. Assuming that the perturbation requires the activation energy  $Q$ , we obtain

$\bar{E} = E_p + \Delta E (1 + W_0 \exp(-Q/kT))^{-1}$ ;  $\Delta E = E_u - E_p$ ;  $W_p = W_{p0} \exp(-Q/kT)$ , where  $W_0 = W_{p0}/W_u$ . The dynamical disordering manifests itself as the reversible changes with the temperature of the effective  $\bar{E}$ . If the perturbation produced due to approach of mobile cation vacancy to the defect ( $\text{Ti}_2^+$ ) reduces its ionization energy, the relevant ionization process will be additionally stimulated when temperature increase with respect to the case of  $\bar{E} = \text{const}$ . It will result in anomalously high mean values of  $\bar{E}$  and  $s$  get by FGT. The dynamical disordering can, in principle, be caused by the following mechanisms: vacancy (defect) migration, phase transition (in particular, local one in the vicinity of a defect[4]), conformation of the complex defect. Mobile negatively charged defects act to reduce the ionization energies of electronic centres but to increase those of hole centres. Thus a reduction of the ionization energy of traps in LiF-Ti,Mg due to cation vacancies [3] confirms their electronic nature.

1. Зирап В.Э. Изв.АН СССР.Сер.физ.,1986,т.50,с.563.
2. Тале В.Г. Изв.АН Латв.ССР.Сер.ф.-т.н.,1987,с.37.
3. Тале И.А. Изв.АН СССР.Сер.физ.,1986,т.50,с.536.
4. Tale I. et.al. Solid St.Comm.,1983,v.48,p.135.

CATHODOLUMINESCENCE AND THERMOLUMINESCENCE SPECTRA OF QUARTZ

B J Luff, A C Cox and P D Townsend

School of Mathematical and Physical Sciences

University of Sussex

Falmer, Brighton BN1 9QH

East Sussex

UK

Despite an extensive literature on CL and TL of quartz the interpretation of signals is difficult because of trace impurities. The present measurements were considered as samples of ultra pure quartz and Ge doped ultra pure material became available for comparison with normal purity crystals. Spectra have been recorded over the range 260 to 810nm. For CL the data were taken from 50 to 300K and for TL from 300 to 700K. The two techniques gave similar spectra for a particular sample.

The spectra from different crystals varied quite widely and a variety of emission bands were detected ranging from blue to red, even in the purest material. Samples of normal commercial purity were 'improved' by electric field sweeping to remove alkali ions, with a consequent reduction in the number of emission bands.

Ultra pure material prepared by GEC contains less than 1% of the normal OH or Al concentrations of "pure" quartz. The ultra pure samples produce greatly reduced TL signals compared with normal "pure" quartz but were of similar luminescence efficiency during radioluminescence.

During the CL measurements attempts to resolve the emission bands by lifetime resolution were made. In normal purity crystals this was difficult due to long lifetime luminescence ( $\tau \sim 1$  sec), but in some superpure material the lifetimes dropped to msec.

In Ge doped superpure crystals a series of closely spaced narrow band emission features were detected. From the line spacing these are tentatively ascribed to states of molecular oxygen trapped in the lattice.

GENERATION-RECOMBINATION AGGREGATION OF RADIATION  
DEFECTS: VOLUME AND SURFACE EFFECTS IN SOLIDS

F. Pirogov

Institute of Physics, Latvian SSR Academy of Sciences  
 229021 Riga, Salaspils 1, USSR

Radiation induced spatial redistribution and aggregation of point defects affects greatly the physics of radiation stimulated processes: impurity diffusion, phase transitions et al. In strongly nonequilibrium systems with reactions (when defects generation, recombination and capture rates exceed those for the spatial distribution relaxation processes), spontaneous clusterization of single-type defects (even when long-range interaction potentials are absent) occurs. This effect is known as generation-recombination aggregation (GRA), and was studied by means of computer simulation [1-3].

The present work is devoted to discussion of the basic insights into GRA of radiation defects and its role in various processes in solids under irradiation. The effects of irradiation dose rate upon GRA at low temperatures are studied for a simple model: random generation of vacancy-interstitial pairs (rate  $\lambda$ ), mobile interstitials (diffusion coefficient  $-D_I$ ); instantaneous vacancy - interstitial recombination, when  $r \leq r_R$  (recombination radii  $r_R$ , vacancy interstitial separation  $r$ ); formation of immobile complexes via interstitial collisions (aggregation radii  $r_a$ ).

It is shown that the efficiency of aggregation increases with the increase of parameters  $p_1 = 2\lambda r_R^2 / D_I n_I$ ,  
 $p_2 = r_a / r_R$  ( $n_I$  - defect concentration).  
 For  $p_1, p_2 \gg 1$  aggregates of interstitials (containing

$10^{-10} - 10^{-2}$  defects) are formed in the lattice with high probability and large generation-recombination induced time and space fluctuations of local defect and cluster concentrations are present .

At higher temperatures, when both types of defects are mobile it is shown that due to the presence of various sinks, internal and external boundaries, the local GRA efficiency is increased and local phase transitions occur. If  $D_I \gg D_V \gg D_{2V}$  (  $D_{2V}$  - diffusion coefficient for bivacancy), two temperature ranges exist:  $T < T_c$  and  $T > T_c$  (where  $T_c$  becomes smaller with the increase of  $\lambda$  ). For  $T < T_c$  , radiation-induced nucleation takes place via conventional diffusion - controlled mechanism, but for  $T > T_c$  via coalescence of small clusters.

Many-particle analytical theory for defect accumulation and aggregation (valid for large vacancy, interstitial, sink concentrations and pair interaction between them) is given. It is found that in the case when GRA is present, the defect recombination and capture rates depend nonlinearly upon  $\lambda$  .

1. Pirogov F., Palagashvili E. Izv. AN Latv.SSR, ser.fiz. teh.nauk, 1985, No 6, p. 113-116.
2. Pirogov F., Shvarts K. The influence of radiation and light on heterogeneous systems. Abstr., Kemerovo, 1986, p. 61-63.
3. Pirogov F. Rad. Phys. and Chem. of Ionic Crystals. Abstr. Riga, 1986, p. 44-47.

LASER DAMAGE MECHANISM REVEALED BY THE MORPHOLOGY OF DAMAGED  
REGIONS

L.C. Nistor, V. Teodorescu, S.V. Nistor  
Central Institute of Physics, P.O. Box MG-6 Magurele  
Bucuresti, ROMANIA 76900

The damage mechanism induced by high power lasers in transparent materials, as well as the absorption of the laser beam depends on the presence of defects such as impurities or inclusions [1]. We are presenting a comparative study of the laser damage mechanism reflected in the morphology of the damaged regions, for KCl and ZnSe crystals of low and high purities. The irradiations have been performed in standard experimental setups for the determination of damage threshold using TEA-CO<sub>2</sub> lasers ( $\lambda = 10.6 \mu\text{m}$ , energy per pulse up to 0.1 J, pulse duration  $\approx 100$  nsec.). Standard calorimetric method was used for absorption coefficients determinations, while the damaged regions were studied by optical microscopy.

Low purity single crystals of usual optical quality with absorption coefficients of:  $\beta_{\text{KCl}} = 1.8 \times 10^{-2} \text{ cm}^{-1}$  and  $\beta_{\text{ZnSe}} = 2 \times 10^{-3} \text{ cm}^{-1}$ , have been irradiated in a single laser pulse with power densities close to the respective damage thresholds ( $P_{\text{KCl}} = 4 \times 10^7 \text{ W.cm}^{-2}$ ;  $P_{\text{ZnSe}} = 10^8 \text{ W.cm}^{-2}$ ). The microscopic investigations show the appearance of filamentary damaged regions (fig. 1 - KCl; fig. 2 - ZnSe) inside the crystal, along the direction of the laser beam. These filaments consist of a sequence of small damaged zones, having dimensions of  $10\text{-}40 \mu\text{m}$ , between them the crystal remaining undisturbed. Some of these damaged zones contain microcleavages in the main crystallographic directions. These elementary damaged zones reveal the sites in the crystals where absorbing centers for the laser radiation exist. Such centers could be formed by impurity agglomerates or inclusions. Indeed, further spectro-

photometric investigations revealed anionic impurities ( $\text{NO}_3^-$ ,  $\text{NO}_2^-$ ,  $\text{SO}_4^{2-}$ ) in KCl crystals, while transmission electron microscopy studies show graphite inclusions of micron size in ZnSe crystals. The laser damage is due in this case to local heating at these specific sites.

On the contrary, the morphology of laser damages in specially grown high purity crystals for high power lasers ( $\beta_{\text{KCl}} = 2 \times 10^{-4} \text{ cm}^{-2}$ ;  $P_{\text{KCl}} = 4 \times 10^9 \text{ W.cm}^{-2}$ ) is very different. The damage has the aspect of a cross (fig. 3-KCl) formed of microcleavages, following the principal crystallographic directions, and appearing only in one site. The morphology resembles the electrical breakdown in insulating materials, suggesting an avalanche ionisation mechanism for laser damage. Similar morphological aspects have been observed in windows made from CVD ZnSe, but the sample being polycrystalline, the damaged zone are not related to any crystallographic direction.

/1/ R.M. WOOD, "Laser Damage in Optical Materials, Adam Hilger Series on Optics and Optoelectronics, IOP Publishing Ltd, Bristol (1986)

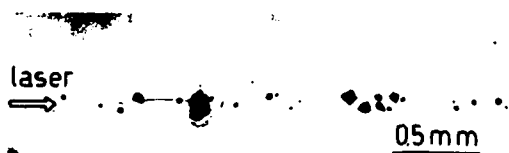


Fig. 1



Fig. 2

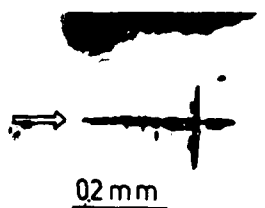


Fig. 3

RADIATION-INDUCED DEFECTS IN QUARTZ: RELEVANCE TO THE PRE-DOSE  
EFFECT IN THERMOLUMINESCENCE DOSIMETRY

S.W.S. McKeever, X.H. Yang and R. Chen, Department of Physics, Oklahoma  
State University, Stillwater, OK 74078-0444, USA.

We have used Electron Spin Resonance (ESR), Thermoluminescence (TL) and Infra-Red Absorption Spectroscopy to monitor a variety of radiation-induced defects in synthetic quartz, as functions of various annealing and sweeping treatments. Our purpose has been to establish correlations between the behavior of certain defect-types and the so-called 'Pre-Dose Effect' in this material. This effect is used in both radiation dosimetry and archaeological dating applications to calculate the dose of radiation absorbed in quartz samples of different origins. In addition, the data obtained are relevant to an understanding of the behavior of quartz oscillator crystals in radiation environments.

The 110 °C TL peak of as-received, synthetic quartz (Electronic Grade and Premium Q, x- and z-cut crystals; Sawyer Research Products) has been found to be strongly supralinear with the dose of excitation. Quadratic and nearly cubic dependencies have been observed with both  $\gamma$ - and  $\beta$  irradiation. Annealing the samples at 300 °C or higher substantially increases the sensitivity and removes the supralinearity. Increases in the sensitivity by factors of 30 - 1000 have been observed, depending on annealing temperature and sample type. Furthermore, shifts in the TL peak position are clearly observed, depending on the dose used and the temperature to which the samples were annealed.

Measurements of the post-irradiation thermal stability of several radiation-induced ESR signals establish a clear correlation between the 110 °C TL peak and  $(\text{AlO}_4)^{\cdot 0}$  centers. The thermal stability data indicate that these trapped-hole centers are acting as recombination sites in the TL production process. The identity of the trapped-electron site is less certain, but  $(\text{GeO}_4)^{\cdot -}$  centers appear to be involved. The thermal stability measurements also reveal that the hydrogen-related defects,  $(\text{H}_3\text{O}_4)^{\cdot 0}$ , may also be playing a part in the production of the TL in this temperature range. The involvement of hydrogen in the TL mechanism is also suggested by high-temperature annealing effects on the infra-red absorption data, and by the effects on the TL curves of hydrogen sweeping.

Based on our observations we forward a suggestion to explain the supralinear growth of the TL with absorbed dose in as-received samples and its subsequent removal following high-temperature annealing. A model based on competition during the heating phase of TL production can be satisfactorily used to account for the observed shifts of the TL peak temperature, the sensitivity increase following annealing, and the transition from a supralinear to a linear dose response. From the ESR data we are able to suggest the identity of the defects involved in the competition process. The relevance of our findings to the Pre-Dose Effect will be discussed.

THERMALLY STIMULATED CONDUCTIVITY AND LUMINESCENCE IN FLUOROPEROVSKITES

N. Kristianpoller\*, B. Trieman\*, R. Chen\* and Y. Kirsh\*

\*School of Physics and Astronomy, Tel Aviv University

\*Everyman's University, Tel Aviv, Israel

The formation of point defects in various perovskite-type fluoride crystals was studied by methods of thermally stimulated conductivity (TSC) and luminescence (TSL). Optical absorption was measured as well. The defects were induced in nominally pure and in variously doped specimens by X-rays or by monochromatic UV radiation. The experimental techniques were essentially the same as previously described <sup>(1)</sup>.

The kinetic parameters of the main TSL and TSC peaks were evaluated by the initial-rise method and by Chen's <sup>(2)</sup> half-width method. Emission and excitation spectra of the main TSL peaks were also measured.

The comparison of our results with those previously obtained in these crystals by gamma or fast electron irradiations (e.g. 3) showed that the same  $V_k$  and F-type centres were induced by X-rays as by the gamma or fast electron irradiations. The  $V_k$  centres in these crystals become generally mobile between 100 and 300K and the thermally released holes recombine with the electron centres. Our finding that most of the X-induced TSL peaks were accompanied by TSC peaks, indicates that these recombination processes are due to charge transport over several unit cells rather than to local transitions.

Some of the X-induced TSL peaks also appeared after UV irradiation at 80K, indicating that the same defects are involved in both cases. The excitation spectra of the UV induced TSL peaks showed generally maxima at the low energy tail of the first exciton absorption bands of the crystals. It appears that radiolysis processes are responsible for the formation of the defects induced in these crystals by the various types of irradiation.

However, no measurable TSC could be detected after UV irradiation of these crystals. This might be due to the relatively low concentration of defects induced by the low-intensity monochromatic UV radiation. Alternatively, this could indicate that the UV light mainly causes the formation of hole and electron centres in close proximity. In this event the recombination might be through a local transition, or might be due to a process in which the free carriers remain in the bands for a very short time only. It might be noted that a different behaviour has been reported for UV irradiated alkali halides. In these crystals mainly Frenkel pairs are formed by low temperature irradiations and it was found that mainly separated Frenkel pairs are produced in case of VUV irradiation <sup>(4)</sup>. In some of the here examined fluoroperovskite crystals, thermally stimulated polarization (TSP) and depolarization (TSD) currents were also recorded, indicating that these unirradiated crystals contain dipoles, which are probably due to impurities in the vicinity of their charge compensators.

#### REFERENCES

- (1) B. Trieman and N. Kristianpoller, Phys. Stat. Sol. (b) 105, 739 (1981).
- (2) R. Chen and Y. Kirsh, *Analysis of Thermally Stimulated Processes*, Pergamon, 1981.
- (3) A. Podinsh and W.A. Sibley, Phys. Rev. B18, 5921 (1978).
- (4) N. Kristianpoller and Z. Davidson, Digest Int. Conf. on Luminescence, Beijing 1987, p.36.

RADIATION DEFECTS IN A  $\text{KTiOPO}_4$  SINGLE CRYSTAL

L.G.Karaseva, B.V.Andreev, V.V.Gromov

Institute of Physical Chemistry of the Academy of Sciences  
of the USSR, 117915 Leninsky prospekt, 31, Moscow, USSR

The method of ESR-spectroscopy, spectrophotometry, thermoluminescence (TL) and thermally stimulated currents (TSC) were used for the study of radiation defects formed upon

$\gamma$ -irradiation of  $\text{KTiOPO}_4$  single crystals, which is a new nonlinear optical material [1]. The generation of defects was performed at a temperature of 77 K and 300 K by means of the  $^{60}\text{Co}$   $\gamma$ -source over the dose range  $10^3$ - $10^6$  Gy (dose rate 13 Gy/s.)

Main radiation defects of the given matrix over the studied dose range were determined. They are: two structurally nonequivalent titanium centres  $\text{Ti}^{3+}-\text{V}_\text{O}-\text{Ti}^{4+}$ , which appear during the capture of the electron on the 3d-orbital of titanium, lying next to the oxygen vacancy  $\text{V}_\text{O}$ ; and two hole  $\text{PO}_4^{2-}$ -centres.

The ESR spectra of electron centres possess a super-hyperfine structure due to the interaction of an unpaired  $\text{Ti}^{3+}$  electron with the two nearest  $^{39}\text{K}$  atoms. Radiospectroscopic parameters of the electron centres are as follows:

$$g_{\text{Ix}} \approx g_{\text{Iy}} = 1.965 \pm 0.001; \quad g_{\text{Iz}} = 1.961 \pm 0.001;$$

$$g_{2x} \approx g_{2y} = 1.957 \pm 0.001; \quad g_{2z} = 1.951 \pm 0.001$$

$$A_x = A_y = 1.5 \pm 0.5 \text{ E}$$

$$A_z = 6 \pm 0.5 \text{ E}$$

A wide anisotropic band in the spectrum of additional optical absorption with weakly resolved maxima in the region of 490 and 550 nm makes a superposition of absorption bands, one being caused by  $\text{Ti}^{3+}$  ions in an octahedral crystalline field with considerable tetragonal distortions and the other

by  $\text{PO}_4^{2-}$  -centres. Radiospectroscopic parameters of the hole centre are as follows:

$$g_x = 2.012 \pm 0.001;$$

$$g_y = 2.005 \pm 0.001;$$

$$g_z = 2.032 \pm 0.001;$$

$$A_{x\text{p}}^{31} < 1.5 \text{ E};$$

$$A_{y\text{p}}^{31} = 3 \pm 0.5 \text{ E};$$

$$A_{z\text{p}}^{31} = 9 \pm 0.5 \text{ E}.$$

The thermal annealing of  $\text{PO}_4^{2-}$  centres is accompanied by TL with the maximum at 330 K and by a partial decrease in the concentration of electron titanium centres. The peak of the TSC curve at 360 K (the current was measured along the x-axis of the sample) corresponded to a complete disappearance of titanium centres.

#### References.

1. L.G.Karaseva et al. Dokl.Akad.Nauk SSSR, t.289, s. 1152, 1986.

THERMOLUMINESCENCE OF  $\text{Eu}^{3+}$  AGGREGATES IN  $\text{CdF}_2$  CRYSTALSS.Benci<sup>+++</sup>, F.Fermi<sup>++</sup> and A.Nagorny<sup>+++</sup><sup>+</sup> Dipartimento di Fisica - Università di Parma - Italy<sup>++</sup> Istituto di Scienze Fisiche - Università di Parma - Italy<sup>\*</sup> and Unità di Parma, Centro Interuniversitario di Struttura della Materia del Ministero della Pubblica Istruzione - 43100 Parma, Italy and Gruppo Nazionale di Struttura della Materia del C.N.R. - 43100 Parma - Italy<sup>+++</sup> Institute of Solid State Physics, Latvian State University, Riga USSR.

The thermostimulated luminescence glow curve of  $\text{CdF}_2:\text{Eu}^{3+}$  crystal irradiated by u.v. light or X-rays shows a complex structure due to the presence of  $\text{Eu}^{3+}\text{-Fi}^-$  dipoles and dipoles aggregates of different symmetries and complexities. As a consequence the correlation between glow peaks and well defined impurity recombination centers is a not resolved problem. Interesting informations can be supplied comparing thermostimulated luminescence and high resolution emission spectroscopy measurements.

Thermostimulated luminescence (TSL) and fractional thermoluminescence (FTSL) measurements of  $\text{CdF}_2$  crystals doped with  $\text{Eu}^{3+}$  (0.1% mol.) irradiated at 77 K have been performed in the temperature range 77-300 K. The TSL glow curves of as received samples irradiated UV light and X-rays are shown in fig.1. The glow curves after X-rays or UV irradiation show a very different behaviour. For quenched samples, X irradiated, the TSL main peak shifts to 160 K and a second peak increases at low temperature. The TSL curve for quenched samples UV light irradiated changes with respect to that obtained for as-received crystal: the main TSL peak is at 170 K, another weaker peak is at 185 K and a peak at low temperature increases as for the X-ray irradiated samples. The FTSL spectra for as-received samples X-rays and UV light irradiated are shown in fig.2. In fig.3 the FTSL spectra for quenched samples, if UV or X-rays irradiated, point out electron traps with the same depth, characterized by activation energies of about 0.33 eV and 0.44 eV. According to the attribution of the lines observed in photoluminescence by Kingsley et al (1), Jouart et al (2) and de Murcia et al (3)

the photoluminescence experimental measurements have pointed out that in the as-received crystal few  $\text{Eu}^{3+}$  cubic centers are present, prevailing dimer centers, that decrease after the quenching, increasing cubic  $\text{Eu}^{3+}$  and dipole centers. Considering these results, an attribution of the peak at 160 K to  $\text{Eu}^{3+}$  cubic centers, of the peak at 175 K to dipole centers and of the peak at 240 K to dimer centers can be discussed.

- 1) J.D.Kingsley, J.S.Prenner, Phys.Rev. 126, 458 (1962).
- 2) J.P.Jouart, C.Bissiaux, M.Egec, G.Mary and M.de Murcia, J.Phys.C:Solid State Phys. 14, 4923 (1981).
- 3) M.de Murcia, Jin Yixin, P.Bräunlich, J.P.Jonartand, H.J.von Bardeleben, J.Phys.C:Solid State Phys. 15, 2069 (1982).

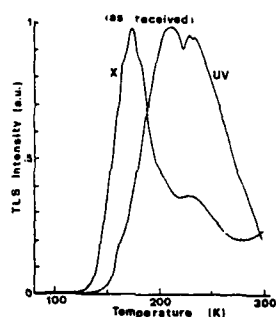


Fig. 1

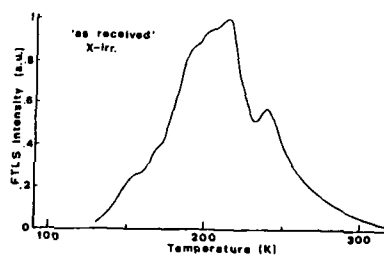


Fig. 2

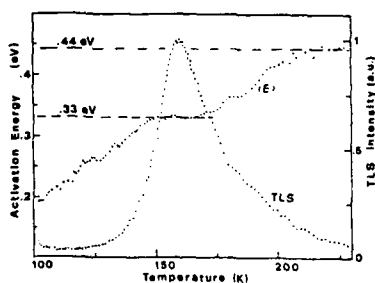


Fig. 3

DEFECT LUMINESCENCE IN UNDOPED YAG

G. Wu\*, A. Wu, R. P. Shafer, G. P. Williams, Jr.,  
and R. T. Williams  
Department of Physics, Wake Forest University  
Winston-Salem, NC 27109 USA

C. Y. Chen<sup>+</sup>  
Dept. of Materials Engineering, North Carolina State University  
Raleigh, NC 27695 USA

Y. Chen  
Solid State Division, Oak Ridge National Laboratory  
Oak Ridge, TN 37831 USA

Crystals of YAG (yttrium aluminum garnet,  $\text{Y}_3\text{Al}_5\text{O}_{12}$ ) which have not been intentionally doped with luminescent ions have been subjected to particular growth conditions, thermochemical reduction, and neutron irradiation. Luminescence from the resulting defects has been studied under pulsed laser and cw excitation. Crystals used were grown at the Shanghai Institute of Optics and Fine Mechanics (SIOFM), at Allied Signal Corp., and at Union Carbide. Photobleaching and annealing properties which affect the luminescence have been studied. The most prominent band not directly attributable to a trace impurity is found in luminescence at 400 nm and in absorption at 370 nm. It is enhanced by both thermochemical reduction and by neutron irradiation. It is most prominent in undoped crystals grown in reducing CO atmosphere and Mo crucibles at SIOFM.

Acknowledgment: This work was supported by DARPA under Inter Agency Agreement 40-1611-85 with Martin Marietta Energy Systems, Inc., contract DE-AC05-84OR-21400 with the U. S. Department of Energy.

\*Shanghai Institute of Optics and Fine Mechanics, Shanghai, People's Republic of China.

<sup>+</sup>Present address: Department of Physics, Oklahoma State University, Stillwater, OK 74074 USA.

Study of Threshold Effect in Mg-doped Lithium Niobate Crystal

Fengxiqi, Ying jifong, Liu Jingchen  
 Shanghai Institute of Ceramics, Academia Sinica  
 865 Chang-ning Road, Shanghai, China  
 Zhang Qiren  
 Suzhou Railway Normal College

Laser-induced refractive index changes, which have been labeled "Optical damage", often seriously impede the application of the crystal as modulators, waveguide devices or frequency doublers because light beams are decollimated and scattered. It was reported by Zhong et al. (1) that resistance to optical damage in LiNbO<sub>3</sub> was improved if more than 4.5% MgO was added to the congruent melt. Then Bryan et al. demonstrated the existence of a threshold effect with regard to MgO doping levels (2). In the last few years, a series of publications dealt with the anomalous properties of heavy Mg-doped LiNbO<sub>3</sub> crystals. These publications showed that the defect structure of the Mg-doped LiNbO<sub>3</sub> has significant influence on the optical damage resistance in LiNbO<sub>3</sub> crystal.

In this paper, measurements of OH<sup>-</sup> absorption bands, fundamental optical absorption edge, lattice constant, density, color center absorption spectra, and Fe<sup>3+</sup> ESR spectra under room temperature in a series of magnesium doped, iron doped lithium Niobate crystal and their dependence on magnesium concentration are made. It is observed that there exist the threshold effect of magnesium dopant concentration in the measurements. The influence of magnesium ion on defect structure of LiNbO<sub>3</sub> crystal is studied by use of the defect chemistry in magnesium doped LiNbO<sub>3</sub> crystal. Therefore the formation of various defect lattices in the crystal with different magnesium dopant concentration and their growth and decay rules are proposed. It is shown by the calculation that the defect lattice with Nb-site Mg<sup>4+</sup> will be formed in a congruent LiNbO<sub>3</sub> crystal when the MgO doping level approaches 5.3%, and it should be the main mark of the "threshold". It is satisfactory to demonstrate the previous experimental results by use of the change of the ionic environment in the LiNbO<sub>3</sub> crystal caused by the "threshold", and the calculation of the threshold concentration coincides with the experiments. It seems that the model proposed

is reasonable. The conclusion in this paper can be used to explain the origin of the highly increasing anti-optical damage capability in a highly magnesium doped  $\text{LiNbO}_3$ . This is significant so as to the research work of the modification in other  $\text{ABO}_3$  type electro-optic crystals.

- (1) Gi-Guo Zhong, Jin Jian and Zhong-Kang Wu, 11th Inter. Quan. Elect. Conf., IEEE Cat. No. 80 CH1561-0, June 1980, p. 631.
- (2) D. A. Bryan, Robert Gerson and H. E. Tomaschke, Appl. Phys. Lett., 44(1984)847.

EFFECT OF TEMPERATURE ON  $\gamma$ -RADIATION INDUCED I.V. DIPOLESAGGREGATION IN  $\text{KCl:Eu}^{2+}$  CRYSTALS

H. Opyrchał, K.D. Nierzewski, B. Macalik and M. Manfredi<sup>\*)</sup>

Institute of Low Temperature and Structure Research,  
Polish Academy of Sciences, Wrocław, P.O.Box 937, Poland

<sup>\*)</sup> Institute of Physics, University of Parma, Italy

The state of  $\text{Eu}^{2+}$  ions, originally present in the form of isolated I.V. dipoles, in KCl crystals  $\gamma$ -irradiated at 80K, 200K, 295K, 373K and 423K was studied by the ITC, EPR and optical method.

The significant decrease of the concentration of  $\text{Eu}^{2+}$ - cation vacancy dipoles found in the whole temperature range on the basis of ITC measurements, is interpreted in terms of radiation stimulated diffusion resulting in the formation of some aggregates. By employing the EPR, optical absorption and emission measurements, it is shown that structure of aggregation products depends on the radiation temperature.

Low temperature irradiation (80K and 200K) induces the formation of small dipole aggregates possible like dimers and trimers. Irradiation at 295K, 373K and 423K induces formation of the  $\text{Eu}^{2+}$ - rich foreign phase precipitates. The comparison of the results obtained by the same methods in nonirradiated  $\text{KCl:Eu}^{2+}$  crystals annealed at various temperatures with those obtained in this work, permits to conclude that:

a) during 295K irradiation the precipitates of  $\text{Eu}^{2+}$ - rich phase similar to that found in  $\text{KCl:Eu}^{2+}$  stored for several years at RT [1,2] are formed;

b) the precipitates of the phase appearing in  $\text{Eu}^{2+}$ - doped crystals annealed at 473K  $\pm$  523K [3] can be produced during relatively short irradiation (about 10h) at 373K or 423K.

The F center growth curves obtained for pure and  $\text{Eu}^{2+}$ -doped crystals resemble in the whole temperature range the growth curves found for the other  $\text{KCl:Me}^{2+}$  systems [1]. On the other hand, the V band behavior

displays essential differences resulting from radiation induced changes in  $\text{Eu}^{2+}$  dipoles state.

At low temperatures (80K and 200K) the V-type band increases proportionally to F band, independently of the dopant concentration. For 295K the relation between F and V-type bands depends on the dopant concentration:

- a) for low concentration (up to 15ppm) V band increases proportionally to F band;
- b) for medium range (15-100ppm) V band increases slower than F band;
- c) no V-type band could be detected at samples containing more than 100ppm  $\text{Eu}^{2+}$ .

After irradiation at 373K and 423K no V-type band has been found in absorption spectra independently of dopant concentration.

The results obtained cannot be explained in terms of the coloration models based on the assumption of the interstitial trapping by isolated dipoles.

The present work supports the mechanism of interstitial stabilization by the aggregation products formed during the irradiation. The temperature and concentration dependence of V-type band formation can be understood by assuming that trapping cross-section of the vacancies introduced by impurity is much larger than that of isolated dipoles and their small aggregates (80K and 200K; formation of distinct V-band) and much smaller than that of large particles of precipitates (high  $\text{Eu}^{2+}$  concentration at 295K, or 373K and 423K irradiation) yielding the centers with very low oscillator strength.

#### References

- [1] D.Cassi, M.Manfredi, and M.Solzi, *phys.stat.sol.(b)* **135** (1986) K143.
- [2] H.Opyrchał, K.D.Nierzewski, and H.Drulis, *phys.stat.sol. (b)* **118** (1983) K125.
- [3] J.Rubio O., H.Murrieta S., J. Hernández A., and F.J.López, *Phys. Rev. B* **24** (1981) 4847.
- [4] E.Sonder and W.A.Sibley in: *Point Defects in Solids*, Ed.: J.H.Crawford, Jr. and L.M.Slifkin, Vol.1 (Plenum Press, New York-London, 1972), p.257.

THERMOLUMINESCENCE AND OPTICAL ABSORPTION IN  
CALCIUM ALUMINATE GLASSES

R. Verzini and A.R. Blak

Instituto de Física da Universidade de São Paulo  
 C.P. 20516, CEP 01498, São Paulo, SP, BRASIL

Interest in calcium aluminate glass is stimulated by the optical transmittance property which it possesses in the infrared spectral range. Considerable work to improve the infrared transmission of this kind of glass has been done.

The base glass used in this study is a calcium aluminate type with mol% composition 40.8Al<sub>2</sub>O<sub>3</sub>, 49.0CaO, 6.1SiO<sub>2</sub> and 4.1MgO. It is well known that calcium aluminate, when UV-irradiated, changes colour from blue to green. In the present work, a detailed investigation of the thermoluminescence (TL) emission by such glass is investigated and a search for the colour centers using Optical Absorption (OA) spectra is pursued. In addition, samples with impurities of MgF<sub>2</sub> (0.5, 1.0, 2.0 and 5.0 wt%), CaF<sub>2</sub> (1.0, 1.5 and 2.0 wt%) and Nd<sub>2</sub>O<sub>3</sub> (4.0 wt%) are included.

In the UV-irradiated calcium aluminate OA spectra a 420nm band is observed. For the samples containing MgF<sub>2</sub> the spectra are similar to the results for the base samples and in the case of CaF<sub>2</sub> impurity, the cutoff UV limit is extended by 30nm. Thermal decay kinetics of the 420nm band was studied for temperatures between room temperature and 100°C.

TL measurements show that the peak temperature of the glow curve varies from sample to sample, in the range 110°C up to 170°C. The thermal decay of the peak is also different for different samples.

It has not been possible to describe the TL thermal process in terms of first or second order kinetics. The initial rise method showed that the TL curve is a superposition of several peaks, resulting in a continuous distribution of energy levels of the traps.

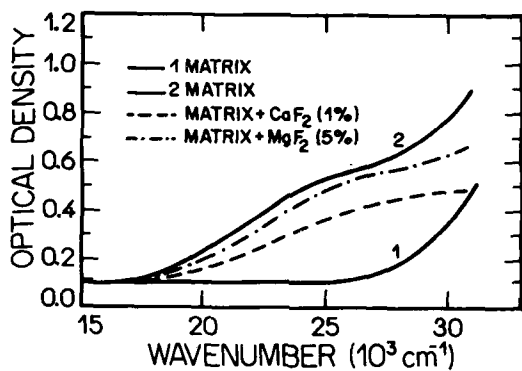


Figure 1: Absorption bands induced in calcium aluminate glass after 10 minutes UV irradiation.

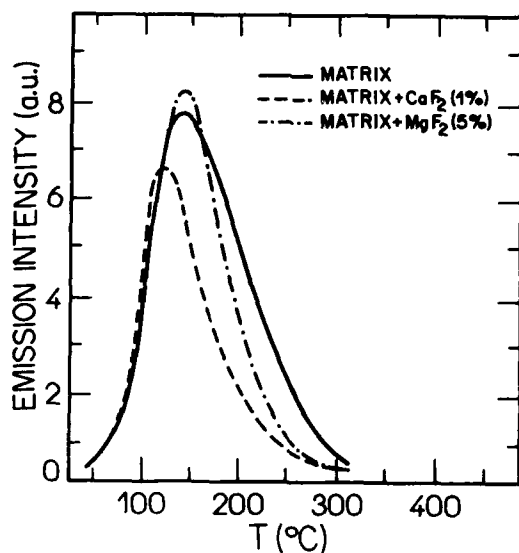


Figure 2: TL glow curves in calcium aluminate glass after 10 minutes UV irradiation.

#### REFERENCES:

- Z.P. Argüello, S.A. Bilac, J.I. Cisneros, M. Tomyiama, P. Donoso and L.C.M. Miranda  
Glass Tech., 22, 186 (1981).
- A.A. Ahmed, A.F. Abbas and F.M. Ezz EL-Din,  
Phys. and Chem. of Glasses 25, 22 (1984)
- S.W.S. McKeever  
Phys. Stat. Sol. (a) 62, 331 (1980)

NUMERICAL INTEGRATION METHOD APPLIED TO THE STUDY OF ATOMIC  
HYDROGEN IN a-Si:(H,O,N) AND NATURAL BERYL DECAY KINETICS

W.W. Furtado, S. Isotani, R. Antonini, A.R. Blak  
and W.M. Pontuschka

Instituto de Física da Universidade de São Paulo  
C.P. 20516, 01498 - São Paulo, SP, BRASIL

A method of data processing has been developed and applied in the study of decay kinetics of interstitial atomic hydrogen  $H_i^0$  in X-irradiated a-Si:(H,O,N) and in UV-irradiated natural beryl.

A system of differential kinetic equations was constructed, which included several possible reactions. The solutions were evaluated by Runge-Kutta's method of numerical integration.

Pontuschka et al. observed that the X-irradiated hydrogenated amorphous silicon containing oxygen and nitrogen impurities a-Si:(H,O,N) shows the characteristic  $H_i^0$  doublet in the EPR spectrum. The absence of this center in X-irradiated nominally pure a-Si:H led to the conclusion that the presence of oxygen is needed to stabilize this center. For the description of the decay of the  $H_i^0$  center, they assumed a second order thermal decay kinetics, yielding an activation energy of about 0.5eV. Samples were irradiated till saturation at room temperature.

In the case of the isothermal decay measurements for the  $H_i^0$  centers in beryl, UV-irradiated at room temperature, Blak et al. verified that it was not possible to describe the process in terms of first or second order kinetics. This suggests the need of considering the superposition of several kinetic processes occurring simultaneously.

It was assumed here that the  $H_i^0$  was produced by radiolytic irradiation of R-H type molecules and trapped at interstitial sites of both materials. In beryl, R is attributed to  $OH^-$  from dissociation of  $H_2O$  and in a-Si:(H,O,N), R is a portion of the disordered chain of its amorphous structure during irradiation. Heating the samples then releases the  $H_i^0$  which is quickly either retrapped, recombined with a R-radical left in the matrix, or combined with other H atoms forming  $H_2$  molecules.

The parameters related to untrapping and recombination processes were found to obey Arrhenius law. The retrapping and  $H_2$  formation parameters were fit to a function proportional to  $(T_1^{1/2} - T_0^{1/2})$ , where  $T_0$  is the temperature at which these parameters vanish. To explain this dependence it may be assumed that upon release from its trap,  $H^0$  behaves like a free atom, forming a gas-like system described by elementary gas kinetics theory.

#### REFERENCES:

- A.R. BLAK, S. ISOTANI and S. WATANABE  
Rev. Bras. Fís. 12, 285 (1982)
- A.R. BLAK, W.M. PONTUSCHKA and S. ISOTANI  
An. da Acad. Bras. de Ciências - to be published (1988)
- W.E. MILNE  
"Numerical Solution of Differential Equations"  
Dover Publications, Inc., New York (1970)
- W.M. PONTUSCHKA, W.W. CARLOS, P.C. TAYLOR and R.W. GRIFFITH  
Phys. Rev. B25, 4362 (1982)

CHARACTERISATION OF PLANAR OPTICAL WAVEGUIDES IN ION-IMPLANTED QUARTZ

L Zhang, P J Chandler, P D Townsend, F L Lama  
 School of Mathematical and Physical Sciences  
 University of Sussex  
 Falmer, Brighton BN1 9QH  
 East Sussex, UK

Introduction

Optical waveguides may be fabricated in many crystalline materials by ion implantation with energetic light ions. The radiation damage near the end of the ion track (nuclear stopping) destroys the material's crystallinity, and the resulting physical reduction in density produces a low index optical isolation layer or barrier. Very little permanent change occurs along the major part of the ion track (electronic stopping), leaving the surface guiding region intact. In quartz the barrier eventually reaches a saturation height due to amorphisation, and with increasing ion dose a flat-topped barrier is produced.

The purpose of the present work is to characterise planar waveguides produced by He ions in quartz. A detailed analysis has been made of the refractive index profiles as a function of ion energy and dose, and implant temperature; their stability at high temperatures; and optimisation for attenuation and scattering losses.

Profiles

Planar waveguides have been fabricated in Y-cut quartz (Roditi) using He<sup>+</sup> ions of energy 0.7 to 2.2 MeV with doses from  $5 \times 10^{15}$  to  $1.6 \times 10^{17}$  cm<sup>-2</sup> at 300K and 77K. The *complete* index profiles of these guides (including barrier shape) have been determined for both indices ( $n_o$  and  $n_e$ ) from their experimentally measured dark mode spacings (at 0.6328 and 0.488 $\mu$ m). This was achieved by means of our recently-developed technique <sup>[1]</sup> involving a reflectivity calculation which assesses the positions of all real and apparent dark modes.

For low doses the barrier can be represented by a narrow skewed Gaussian (~0.3 $\mu$ m half width) consistent with the nuclear-stopping power profile. Its depth beneath the surface varies almost linearly with energy, and the confined layer has a negligible index change. The barrier height increases with dose and reaches a saturation value of  $-\Delta n \sim 5\%$  for  $\sim 10^{16}$  ions cm<sup>-2</sup>. At higher doses the barrier is flat-topped and progressively broadens asymmetrically maintaining the skew of the

original Gaussian, initially showing a linear dose dependence. At doses  $>10^{17}$   $\text{cm}^{-2}$  the width increases super-linearly suggesting an enhancement due to defect diffusion, or the sensitisation of nuclear-damaged regions to subsequent electronic damage. Implants at 77K produce broader barriers consistent with a reduced self-annealing mechanism. The profiles are stable to above  $1000^\circ\text{C}$  — and in fact at  $300^\circ\text{C}$  slight barrier broadening has been observed.

#### Attenuation

Planar waveguides have been fabricated with 1.5 MeV  $\text{He}^+$  on 30mm long Y-cut crystals at doses from 1 to  $6 \times 10^{16}$   $\text{cm}^{-2}$ , giving barrier widths from 0.4 to  $1.5\mu\text{m}$ . These guides exhibit from 2 to 4 guiding modes, and their losses have been determined at  $0.6328\mu\text{m}$  with X propagation for  $\text{TE}(n_0)$  and  $\text{TM}(n_0)$  polarisations. A method similar to the three prism technique was used, replacing the third prism by a direct end-spot monitor.

The as-implanted guides show losses  $\sim 3$  dB/cm for the broad barrier (dose 6) but as high as 10 dB/cm for the low dose narrow barriers due to tunneling. These values have been considerably improved by annealing out the colour centres in the guiding region, eventually reaching  $\sim 1$  dB/cm for the broad barriers after annealing at  $500^\circ\text{C}$ . The residual loss is attributed mainly to surface scatter and tests have been performed to reduce this by post-implant polishing, and also by the use of low energy implants ( $\sim 0.1$  MeV  $\text{O}^+$ ) to confine the guide away from the surface. In the latter case an end-coupling insertion-loss method has been applied to estimate the attenuation.

#### Conclusion

The refractive index profiles of ion-implanted quartz waveguides have been characterised as a function of energy, dose and temperature. Their stability has been ascertained up to  $1000^\circ\text{C}$  and losses achieved of better than 1 dB/cm. More complex overlaid structures using this method are discussed [2].

#### References

1. Chandler, P.J. and Lama, F.L., Optica Acta, 33, 127-143, 1986.
2. Chandler, P.J., Lama, F.L., Townsend, P.D. and Zhang, L., submitted to Appl. Phys. Lett., 1988.

LUMINESCENCE OF  $\text{Al}_2\text{O}_3$  DURING ION IMPLANTATION

A A AlGhamdi and P D Townsend

School of Mathematical and Physical Sciences

University of Sussex

Falmer, Brighton BN1 9QH

East Sussex

UK

Ion implantation of sapphire produces luminescence characteristic of the F and  $\text{F}^+$  centres, together with development of their optical absorption bands. The peak wavelengths of the emission features are not identical for the ion bombarded case and more conventional excitation methods. The F and  $\text{F}^+$  luminescence are seen at 414 and 336nm or 414 and 342nm respectively, depending on the polarisation of the light with respect to the crystal axes. For the  $\text{F}^+$  band this is 6 or 12nm displaced from the UV or electron excited emission.

The relative strengths of the F and  $\text{F}^+$  bands are strongly dependent on the ion dose, the temperature of implantation (77 or 300K), and the relative magnitude of the rates of energy deposition via electronic excitation or nuclear collisions. Consequently the relative concentration of F and  $\text{F}^+$  features are dependent on ion species and ion energy. In addition to the standard F and  $\text{F}^+$  centres additional bands are produced in emission and absorption by heavy ion bombardment. This is most apparent in emission at 390nm.

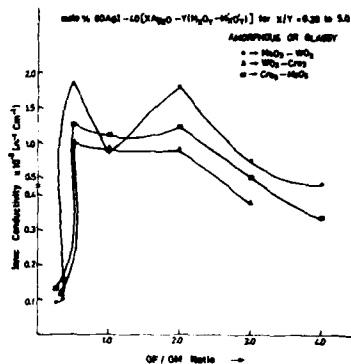
Although one expects to produce the defects primarily by nuclear collisions at the end of the ion range one may also excite luminescence from pre-existing defects by the electronic loss mechanisms. In principle one might separate the contributions of light production within the damage volume and the surrounding lattice by analysing data taken with a

range of ion energies. Such data are sensitive to the sequence in which one varies the energy, and ion dose, in a particular crystal. The present experiments show that the signal growth and subsequent luminescence quenching with increasing dose at a fixed energy are different for the F and  $F^+$  centre. Conversion between these centres further results in differences in 77 and 300K behaviour. Although energy is deposited in the region of nuclear collision damage the light associated with this occurs both in the damage volume and in regions of the crystal adjacent to it. The results suggests that energy transport to the undamaged regions is a major source of the luminescence and luminescence efficiency falls as defects are produced. An estimate of the diffusion range for the energy transport, by electrons or excitons, is in excess of 0.1microns.

CHARACTERISATION OF SILVER IODO - SILVER OXYSALT METAL OXIDES  
AND A MODEL OF STRUCTURAL DEFECTS

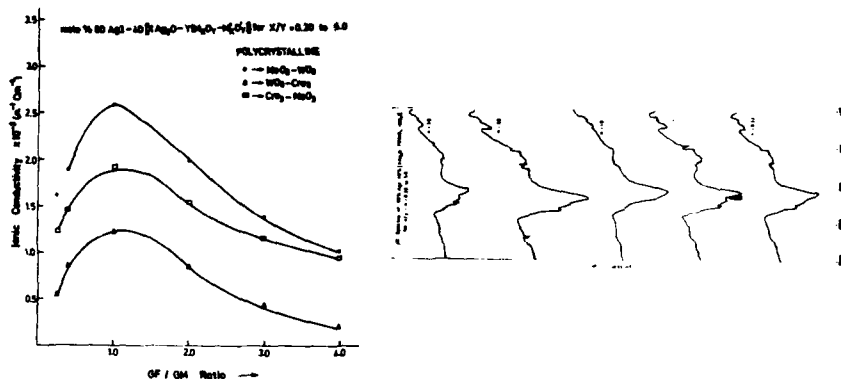
A.N.DURGA RANI, P.SATHYA SAINATH PRASAD AND S.RADHAKRISHNA  
 DEPARTMENT OF PHYSICS, INDIAN INSTITUTE OF TECHNOLOGY  
 MADRAS - 600 036 - INDIA

Silver iodo - Silver oxysalt metal oxides of the general formula  $\text{AgI-Ag}_2\text{O-M}_x\text{O}_y\text{-M}'_x\text{O}'_y$  ( $\text{M, M}' = \text{Mo, Cr \& W}$ ) as solid electrolytes for various device applications like solid state batteries, analog memory devices, electrochemical capacitors and electrochromic devices have been studied over a wide range of compositions to establish the highest conducting composition. Both polycrystalline and amorphous materials with a general composition, mole%  $60\text{AgI-40}(x\text{Ag}_2\text{O-y}(\text{M}_x\text{O}_y\text{-M}'_x\text{O}'_y))$  for  $x/y=0.2$  to  $5.0$  were prepared by the rapid quenching technique and slow cooling method from the same melt, so as to compare the transport and structural properties. The vitreous and polycrystalline nature of the samples were confirmed by recording x-ray diffractogram. The ionic conductivity studies on the three systems as shown in Fig.1 revealed that the general variation of ionic conductivity with glass former to glass modifier ratio (GF/GM) is the same but the order of magnitude differs. Also the nature of variation is different for polycrystalline samples. From this it can be assumed that different mechanisms exist which govern the transport properties.



On variation of the GF/GM ratio, different values were observed for amorphous and polycrystalline samples corresponding to the same composition. The highest conducting compositions were different for amorphous and polycrystalline samples belonging to the same system. The variation of  $\log \sigma T$  for polycrystalline samples for all the three systems follow a general pattern. Hence it can be concluded that the hexavalent cation glass forming oxides form the same type of glassy networks. On the analysis of the transport properties and relating them with the ionic radii, the glass forming tendency and the covalent nature of the individual cations, it was concluded that the  $\text{MoO}_3\text{-WO}_3$  system has a higher value of ionic conductivity than  $\text{WO}_3\text{-CrO}_3$  and  $\text{CrO}_3\text{-MoO}_3$ .

On investigation of the spectroscopic properties of glasses and polycrystalline materials of all the compositions in all the three systems, IR and Raman spectra corresponding to the highest conducting compositions show clear bands, from which it can be concluded that ionic structural units of the type  $(\text{MoO}_6/2)$ ,  $(\text{WO}_6/2)$  and  $(\text{CrO}_6/2)$  octahedral and  $(\text{MoO}_3/2)$ ,  $(\text{WO}_3/2)$  and  $(\text{CrO}_3/2)$  tetrahedral structures do exist in the highest conducting composition. The effect of glass modifier to glass former ratio on ionic conductivity is due to different glass forming networks which create different skeletons for  $\text{Ag}^+$  ion mobility. The effect of added  $\text{Ag}_2\text{O}$  which degrades such a network and creates unshared corners has been considered in detail by comparing the properties of the corresponding polycrystalline samples and proposing a model structural defects. The nature and concentration of various defects depend upon the glass composition and relative energies of covalent linkages leading to different activation energies of migration, ultimately determining the ionic mobility.



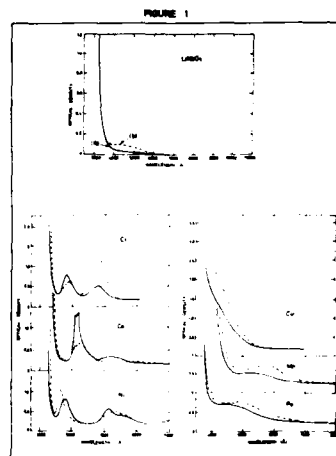
The contribution of defects in polycrystalline materials other than grain boundaries is generally analysed in terms of Matthessen rule. The electron paramagnetic resonance spectra of all the compositions were studied to determine the reduced metal ion ratio  $\text{M}^{5+}/\text{M}^{6+}$  and relate the structural properties with the observed electronic conductivities where small polaron hopping between the  $\text{M}^{5+}-\text{O}-\text{M}^{6+}$  states is believed to be responsible for the electronic conductivity. Thus a weak electrolyte type of theory was used to explain the transport mechanism in glasses and defect type mechanism to explain the transport phenomena in polycrystalline materials. The structural properties are utilised to supplement the theories proposed to explain the conduction mechanism in both polycrystalline and amorphous silveriodo-silveroxysalt metal oxides.

IR, RAMAN AND OPTICAL PROPERTIES OF  $R_2MX_4$  FERROELECTRIC  
CRYSTALS FOR APPLICATION IN HOLOGRAPHIC RECORDERS AS OPTICAL  
STORAGE ELEMENTS

P. SATHYA SAINATH PRASAD AND S. RADHAKRISHNA  
DEPARTMENT OF PHYSICS , INDIAN INSTITUTE OF TECHNOLOGY  
MADRAS - 600 036 - INDIA

Application of ferroelectric materials to the development of optical and electrical devices is not a new concept. The classical ferroelectric crystals like  $BaTiO_3$ ,  $LiNbO_3$ , KDP and ADP have been used as materials in holographic recorder photoconductor memories and optical modulators. But due to the non availability of good optically transparent ferroelectric materials with phase transition temperature ( $T_c$ ) above the room temperature ( $25^\circ C$ ) and high spontaneous polarisation, much progress has not been achieved in the last five years. After the discovery of ferroelectricity in  $R_2MX_4$  type single crystals (7-10), where high spontaneous polarisation of values  $200 \mu C/cm^2$ , are observed, it is proposed in this paper that these materials have a high potential for device applications in holographic recorders as optical storage elements.

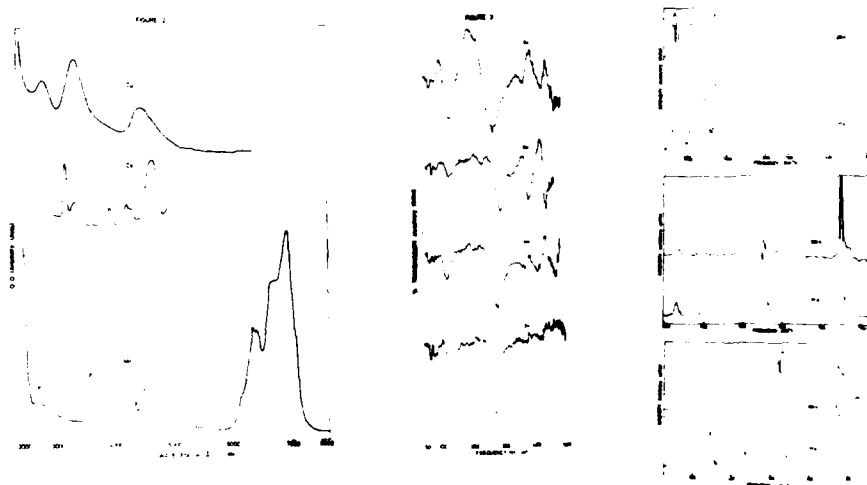
Preliminary studies of crystal structure analysis, D.T.A., conductivity and dielectric phenomena in a few  $R_2MX_4$  crystals with tetramethyl ammonium as cation and chlorine as anion with Zinc and Cadmium as metals revealed that they are transparent and have ferroelectric phase transition near the room temperature with high spontaneous polarisation. In a systematic investigation of the optical properties of  $R_2MX_4$  type crystals doped with first row transition metal ions, it was found that the  $T_c$  increases and approaches the room temperature. The optical absorption, IR, FIR, and Raman spectra of the above crystals showed the same nature of those of the classical ferroelectrics. Fig.1 shows the optical absorption of pure and transition metal ion doped  $LiNbO_3$  which was widely used in applications and the observed spectra of  $R_2MX_4$  crystals which have a close resemblance to that of  $LiNbO_3$  doped with  $Mn^{2+}$ ,  $Co^{2+}$ ,



$\text{Ni}^{2+}$  &  $\text{Cu}^{2+}$  is shown in Fig.2.

From the optical absorption spectra in the region 2000 Å - 15000 Å, the crystal field parameters are calculated which provided us with additional information on the ionic nature of the crystal. The infrared spectra in the region  $4000\text{ cm}^{-1}$  -  $200\text{ cm}^{-1}$  provided the information on the vibrational frequencies of tetrahedral structures,  $(\text{MX}_4)^{2-}$  molecules and the effect of transition metal ion doping on the distortion produced in the  $T_d$  symmetry. The stretching frequencies of the metal halide molecules in the  $T_d$  symmetry are supported from the FIR spectra as shown in Fig. 3. The structural breakdown of the  $T_d$  symmetry and the influence of cation on the lattice dynamics are studied by recording Raman spectra (Fig.4), at room temperature and below the phase transition temperature.

The effect of doping, on the phase transition temperature and the spectroscopic properties are reported in the paper. On introducing impurity ions, the observed differences in  $T_d$  are related to the defect property and their influence on ferroelectric phenomena. The host ions are substituted by impurity ions in the tetrahedral structures of metal halides which create more Schottky and Frenkel defects. The observed properties are explained in analogy with the results published on the transition metal ion doped KDP and ADP (11). The above mentioned studies indicate that the anion is not involved in the phase transition mechanism and only the cation in coordination with the metal ion plays an important role in the phenomena of ferroelectricity and hence on the optical properties of the material as an optical storage element.



PHOTOTHERMAL IMAGING BY F-Z<sub>2</sub> CONVERSION IN KCl:Gd<sup>2+</sup>C. Vijayan<sup>1</sup> and Y.V.G.S. Murti<sup>2</sup>

1. Dept. of Physics, Central University of Pondicherry  
JIPMER Campus, Pondicherry, India-605 006.
2. Dept. of Physics, Indian Institute of Technology,  
Madras, India-600 036.

This paper presents a new scheme of information storage using the photothermal conversion of F centers into Z<sub>2</sub> centers in additively colored crystals of KCl:Gd<sup>2+</sup>. Figure.1 shows the optical absorption spectra recorded at 80 K of additively colored KCl: Gd<sup>2+</sup> before and after the photothermal transformation, brought about by bleaching the crystals at 375 K for 10 minutes with F-band light at 550 nm (2.25 eV). The emergence of the Z<sub>2</sub> band can be seen clearly on the lower-energy side of the F band. Fig.2 depicts the decay of the optical density at 550 nm on F-band bleaching in the temperature range 300 K to 400 K. The optical density at 550 nm is plotted against logarithm of exposure to obtain the Hurter-Driffeld curves used to characterize optical memories. The initial fog region probably represents some precursory steps

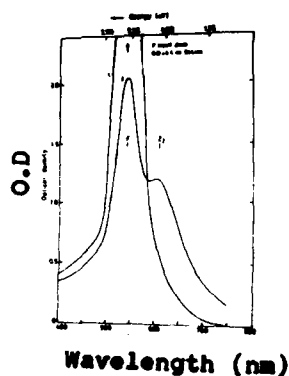


Fig.1 Optical absorption

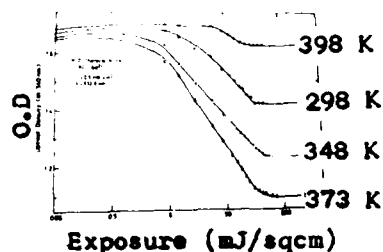


Fig.2 H-D Curves

prior to Z center formation. This region is followed by a linear fall, the slope of which gives the writing sensitivity of the medium, defined as the energy required per unit area to bring about a change of 10% in the optical density. At room temperature, the decay in the F band is due mainly to  $F-Z_1$  conversion. At higher temperatures,  $Z_2$  centers also are produced. At 375 K, the conversion is mainly  $F-Z_2$ . Above 398 K, the back conversion of  $Z_2-F$  dominates and the net change in optical density is little. The sensitivity at 375K is found to be 14 mJ/sqcm. in the present case.

'Writing' of the information is done by illuminating a two-dimensional mask by F-band light and imaging it onto the crystal kept at 375 K. The image gets fixed in the crystal as it cools down to room temperature. Readout is non-destructive since the transformation occurs at a higher temperature, as opposed to other photochromic processes(1). The image can be seen as a modulation of contrast in the color of the crystal and continues to be preserved even after about a year. A few cycles of Write-Read-Erase-Write cycles have been tried out in the same crystal. Further studies aimed at understanding the structure of  $Z_2$  centers (2,3) and the physics behind  $F-Z_2$  conversion are necessary to get a clear insight into the mechanism of the storage process.

#### References:

1. S.V. Pappu  
Contemp. Phys. 26 479 (1985)
2. H.J. Paus and K.M. Strohm  
J.Phys.C 13 57 (1980)
3. C.Vijayan and Y.V.G.S. Murti  
Phys. Stat. Solidi (b) (1988)  
(In press).



Photograph of a crystal  
with stored information

POINT DEFECTS IN SILICA-BASED OPTICAL FIBERS :  
EFFECTS ON OPTICAL PROPERTIES

B. Poumellec\*, H. Février, J.M. Gabriagues,  
G. Lavanant and P. Ledoux

LABORATOIRES DE MARCOUSSIS (Compagnie Générale d'Electricité)  
Route de Nozay 91460 MARCOUSSIS F

\* CNRS.UA 446 Laboratoire des Composés non-stoechiométriques  
Bât. 415 UPS 91405 ORSAY Cédex F

Though glasses have no periodic structure, there are point defects and they are inferred either in degradation of some technological properties of fibers or in recent observations of optical non-linear effect which can be used in laser applications.

In the context of disordered media, defects are primarily defined from features appearing either in absorption spectra or in the EPR spectra or in Raman spectra. In the case of silica, E'i centers (with  $i = \alpha, \beta, \gamma$ ) were so defined [1]. Later on, when one was able to draw fibers for the optical telecommunications, absorption losses in the I.R., visible range were prejudicial and so largely studied. The most common feature encountered was the drawing induced band at about 630 nm [2] related to a hole center in EPR [3].

After theoretical analysis, the following structures have been proposed for the above defects : the E' centers are non-bonding orbitals on silicon which is also called oxygen vacancies (because they originate from the breaking of a Si-Si bond). The 630 nm absorbing defect is a non-bonding orbital on an oxygen (NBOHC) [4], the structure proposed is partially confirmed by other observations such as a fluorescence at around 630 nm.

The above description is an example of our way of studying the defects in optical fibers in order to improve the fabrication process to lower the absorption losses and on the other hand to use the optical properties of some defects.

Therefore, we will show the absorption losses and the fluorescence bands in the IR, visible, U.V. range arising from intrinsic defects and from dopants, from analysis of the literature.

We will propose a synthetic scheme of the localized states in the silica gap in order to explain the dependence of the 850 and 630 nm absorption with the oxygen partial pressure in the chemical vapor deposition process and their disappearance when the core is Ge-doped (the fermi level raise). A variation of the formal charge on the defects will be investigated.

On the other hand, the structure of the optical fiber as a waveguide allows to obtain high power densities in the core and so non-linear optical properties.

One of them is the stimulated fluorescence (or super-radiance). We have obtained generations at 618 nm and about 900 nm by pumping fibers at 1,064  $\mu\text{m}$  (Nd : YAG laser). These light generations at higher energy than the pump light arise either by multiphotonic absorption or U.V. absorption (third-order process) followed by a radiative relaxation of intrinsic defects.

Lastly, we will mention that second harmonic generation is obtained in fiber with Ge- or P- doped core although it is forbidden in glasses (because of the existence of an inversion center). This phenomenon is obviously related to defects created and/or oriented by laser irradiation and having a high hyper-polarisability like resonant  $\Pi$  bonds but they are not yet known.

#### REFERENCES

- [1] D.L. Griscom  
Mat.Res.Soc.Symp.Proc., 61 (1986), p. 213.
- [2] P. Kaiser  
J. of the Optical Society of America, 64, n° 4 (1974), p. 475.
- [3] Y. Hibino and H. Hanafusa  
J.Appl.Phys., 60 (5), 1986, p. 1797.
- [4] A.R. Silin, L.N. Skuja, A.N. Trukhin  
J. of Non-Crystalline Solids, 38 and 39 (1980), p. 195.

## LIGHT SCATTERING AND ABSORPTION IN POLYCRYSTALLINE FIBERS

L.N. Butvina, E.M. Dianov

General Physics Institute, Academy of Sciences of the USSR  
38 Vavilov Street, Moscow 117942, USSR

Recently there has been a considerable growth of interest in the materials whose high transparency region lies within the middle infrared. There is the possibility of obtaining the materials with ultimate low losses ( $10^{-1} - 10^{-3}$  dB/km) that determines this interest. Besides, infrared fibers with moderate losses are promising for the technological and medical purposes. Such fibers are fabricated from monocrystals by extrusion as well as by growing them from the melt, e.g. from monocrystals of silver and thallium halides [1,2]. The necessity to take into consideration the absorption by free carriers (polaron conductivity  $\sigma_e(\omega)$  and ionic conductivity  $\sigma_i(\omega)$ ) in silver and thallium halides for the evaluation of minimal optical losses in these materials and fibers in the range  $2-25\mu\text{m}$  is pointed out for the first time. It is shown that the absorption coefficient  $\beta(\omega)$  by free carriers exceeds for 1-2 orders the previous minimal loss evaluations:

$$\beta(\omega) = \frac{120\pi}{n} \sigma_{e,i}(\Omega^{-1} \text{cm}^{-1})$$

( $n$  is the refractive index) and its value is found to be  $10^{-1} - 10^{-2}$  dB/km for AgCl, AgBr and  $10 - 1$  dB/km for AgBrI (Fig.1). The mechanism of light scattering losses  $\alpha_S$  in fibers fabricated by plastic deformation of silver and thallium halide crystals have been analyzed. It was found that the power index  $\eta$  in the loss dependence on wavelength  $\lambda(\alpha_S \propto \lambda^{-\eta})$  continuously changes in the range  $-0.5 < \eta(\lambda) < 3$  depending on the crystal material and its history, manufacturing conditions and evolution of fibers. On the basis of this and on the consideration of the plastic deformation we suggested that vacancy micropores or voids are the fundamental physical reason which determines the scattering losses in polycrystalline fibers. The cross-section of scattering and  $\eta(\lambda)$  is calculated for inclusions and voids with the relative refractive index  $0.2 < m < 1.2$ . By the numerical methods we calculated the cross-section of scattering  $K(\rho, m) = \alpha_S / \pi R^2$ , the power index  $\eta(\rho, m)$  in a wide range of parameters variation  $m = n_0/n$  ( $n_0$  is the inclusion refractive index, for a micropore  $n_0 = 1$ ) and  $\rho = 2\pi Rn/\lambda$  ( $R$  is the micropore radius). Then using logarithmic differentiation we obtained

$$\eta(\rho, m) = \frac{\partial \ln(K(\rho, m))}{\partial \ln \rho}$$

values for the power index (Fig.2). The remarkable characteristic of  $\eta(\rho, m)$  is the following: scattering centres with low  $m$  (pores in a material with  $n > 1.5$ ) cause the quick and nearly linear decrease of the power  $\eta(\rho)$  on  $\rho < 6$  in the region  $-1 < \eta < 4$ . We explain the behaviour of  $\alpha_S$  and  $\eta$  by the evolution of micropores distribution and by the existence of vacancy excess in fibers. The average diameter  $D$  of effective micropores and their concentration  $N$  are determined from the spectra. We observed these micropores

in KRS-5 and KRS-13 polycrystalline fibers [3]. Linear absorption in infrared region by surface plasmons in silver colloids and nonlinear scattering (optical second-harmonic generation) are discussed. The effect of UV-irradiation on optical losses in IR region for silver halide fibers has been examined. AgBrI fibers proved to be the most resistant to UV irradiation among them, which depends on spectra of UV induced absorption  $\alpha \propto \lambda^{-\eta}$  ( $\eta = 3.7$  for AgBrI, AgClBrI fibers) [4].

#### References

1. Pinnow D.A., Gentile A.L., Standlee A.G. and Timper A. - Appl.Phys.Lett. 1978, v.33, p.28-29
2. Butvina L.N. and Dianov E.M. - Proc.SPIE 1984, v.484, p.21-29.
3. Butvina L.N., Vojsekhovskiy V.V., Dianov E.M., Prokhorov A.M. - Sov. Journ. "Pis'ma Zh.Tech.Fiz." 1987, v.13, p.543-549.
4. Artjushenko V.G., Butvina L.N., Vojtsekhovskiy V.V., Dianov E.M. - Sov.Journ. "Pis'ma Zh.Eksp.Teor.Fiz." (to be publ.) 1988.

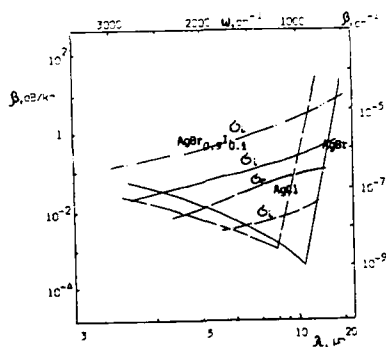


Fig. 1

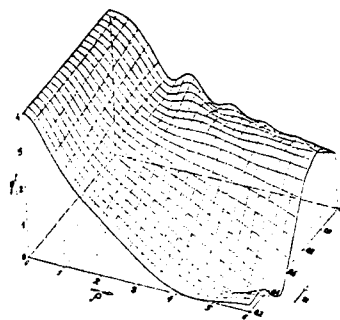


Fig. 2

THEORY OF FLUORESCENCE AND AMPLIFICATION OF LIGHT BY LOCALIZED  
VIBRATIONS

M.I.Dykman and V.N.Smelyanski

Institute of Semiconductors, Academy of Sciences of the UkrSSR,  
Kiev, USSR

The nonequilibrium localized vibrations (LV) can emit spontaneously and, under certain conditions, amplify radiation near their eigenfrequency  $\Omega$ . The feature of the LV optical spectra is due to them being formed by several radiative transitions with close frequencies. The shape of the spectra is determined by a ratio between the difference  $V$  in the transition frequencies (which is due to LV anharmonicity,  $V \ll \Omega$ ) and the relaxation broadening  $\Gamma_0$ . For  $V \gg \Gamma_0$  the partial spectra corresponding to different transitions do not overlap practically and the spectrum as a whole has a pronounced fine structure. For  $V \ll \Gamma_0$  all transitions "interfere" and the spectrum presents a single peak which is slightly asymmetric. In the general case the shape of the LV optical spectrum is rather complicated [1].

In the present paper the explicit expressions are given for the emission and amplification spectra and their evolution in time. These expressions are valid for arbitrary  $V/\Gamma_0$  and arbitrary initial distribution over the LV states. The excitation of high-frequency LV in course of a radiationless electron transition is investigated, and the distribution over the LV states for the case of stationary photoexcitation of a localized electron subsystem coupled to LV is found. The results are compared with beautiful experimental results [2] on multiple-state emission by LV coupled to an electron transition.

From the viewpoint of investigation of fluorescence the most interesting are the high-frequency LV,  $\Omega \gg \omega_{ph}$  ( $\omega_{ph}$  is the

characteristic phonon frequency), since the probability of their radiative decay is relatively large. The electron energy transfer to such LV turns out to be very efficient even for small values of the electron-LV coupling parameter  $\mathcal{V}$  (we suppose that the "bare" electron transition frequency  $\omega_e \gg \Omega$ ). The distribution  $\Lambda(n)$  over the transferred energy ( $\Delta E = n\hbar\Omega$ ) at  $\Omega \ll \tilde{\gamma}^2/\omega_{ph}$  and  $\nu^2 \ll \Omega^2$  is of the form [3]:

$$\Lambda(n) \approx \Lambda_0 \exp[-\alpha(n-n_0)^2], \quad n_0 = \Omega^{-1}(\omega_e - \tilde{P}), \quad \alpha = \frac{1}{2}[(\Omega/\tilde{\gamma})^2 + n_0^{-1}],$$

$$\tilde{P} = P + (\gamma^2/\Omega) \ln(\Omega^2/\nu^2), \quad \tilde{\gamma} = \gamma + (\omega_{ph}^2 P/\gamma\Omega) \ln(\Omega^2/\nu^2),$$

where  $\gamma\sqrt{\ln 4}$  and  $2P$  are the halfwidth and the Stokes shift of the electron optical-absorption spectrum. For  $\alpha \gg 1$  the excitation of LV is highly selective in  $n$ , while at  $\alpha \ll 1$  it is smooth. The difference between optical parameters  $\gamma$ ,  $P$  and  $\tilde{\gamma}$ ,  $\tilde{P}$  depends on the electron-LV coupling.

The feature of the LV distribution at stationary optical pumping of the electron transition is the population inversion for several LV levels simultaneously. It arises when  $G|\vec{E}|^2 > \Gamma$  ( $G|\vec{E}|^2$  and  $\Gamma$  are the probability density of the electron excitation and the reciprocal LV lifetime respectively).

The present theory explains high efficiency of LV excitation and the distribution  $\Lambda(n)$  observed in Ref.2. The theory explains as well the interesting fact of a nonmonotonic dependence of the intensities of fine structure lines in the fluorescence spectrum on their numbers. It is related to the resonant time-dependent light reabsorption by relaxing LV.

1. M.I.Dykman. Zh. Eksp. Teor. Fiz. 68, 2082 (1975).
2. Y.Yang, W. von der Osten, F.Lüty. Phys. Rev. B 32, 2724 (1985).
3. M.I.Dykman, V.N.Smelyanski. Preprint IF AS UkrSSR N 87/9, Kiev, 1987.

# HOLE NARROWING IN INHOMOGENEOUS SPECTRA OF DEFECTS ON BURNING BY TWO TIME-DELAYED PULSES

I. Rebane

Institute of Physics, ESSR Academy of Sciences,  
202400 Tartu, Riia 142, USSR

Photochemical hole burning (PHB) is widely used as the method of eliminating the inhomogeneous broadening of spectra [1]. PHB by pulses of picosecond duration allows a simultaneous burning of a number of spectral holes (SH), which forms the basis for the time-and-space-domain holographic information storage in an inhomogeneously broadened absorption band of a two-level system (2 LS) [2]. Thereby the width of each SH  $\sigma_0 = \gamma + \Gamma + \Delta$ , where  $\gamma$  and  $\Gamma$  are the constants of energetic and phase relaxation of the 1st excited level,  $\Delta$  is the spectral width of the pulses. The optical information recorded on a 2 LS is inevitably impaired on playback. This can be avoided by using three-level systems (3 LS) with a two-step PHB, where the selective excitation of the first step is "fixed" by photochemical transformation through the second excitation step [3]. In this paper, a theoretical possibility of a further narrowing of SH on 3 LS is shown, which is based on the introduction of a time delay  $T$  between the selective and fixing pulses.

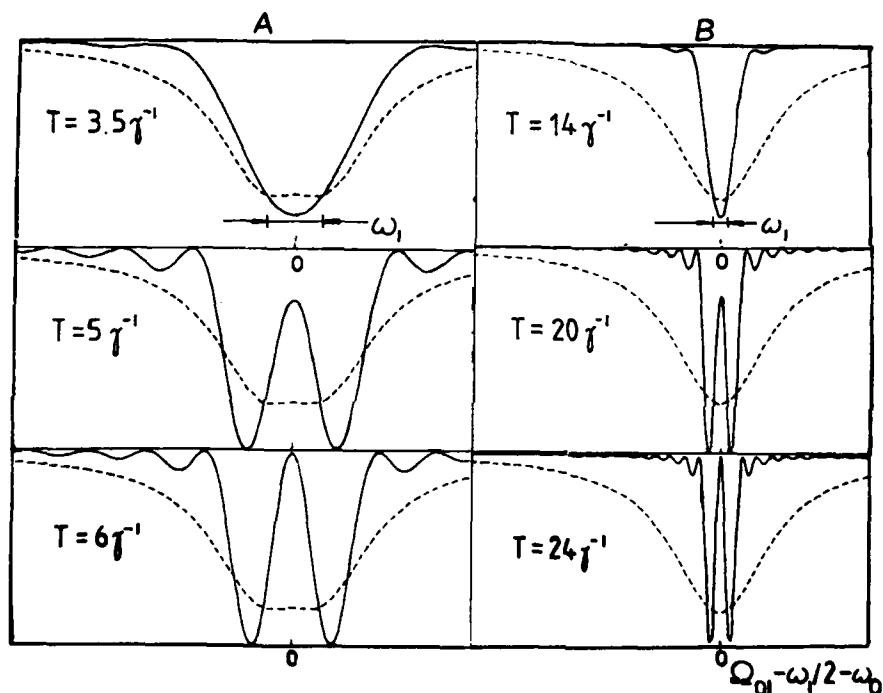
1. In a 3 LS excited by two consecutive pulses, the kinetics of the forming SH differs essentially from that on a stationary burning [4,5].

2. If the selective pulses is coherent and single-sided exponential, then in case of an extremely short pulse ( $\delta$ -pulse) on the increase of the delay  $T$ , a monotonous narrowing of the SH takes place up to the limit width  $\sigma = \Gamma + |\gamma - \Delta|$ . If  $\Gamma, T^{-1}$  and  $|\gamma - \Delta| \ll \gamma$  and  $\Delta$ , then  $\sigma \ll \sigma_0$  [5].

3. It is shown that the SH can further be narrowed up to  $|\gamma - \Gamma - \Delta|$ , if the interference of the selective pulse with an additional  $\delta$ -pulse at the first burning step is used [6].

4. The improvement of the spectral resolution of the PHB

method in case of two-step pulse PHB is depicted in the figure. The contour of a SH obtained on a simultaneous burning by two selective pulses with frequencies  $\omega_0$  and  $\omega_0 + \omega_1$  in 2 LS ( $0 \rightarrow 1$ ) is shown (dashed line). In 3 LS, these two selective pulses lead to the appearance of two SH (solid line) with the increase of the delay  $T$  [7].



Parameters:  $\Delta = 0.99\gamma$ ,  $\Gamma = 0$ ; A -  $\omega_1 = \gamma$ , B -  $\omega_1 = 0.25\gamma$  ( $\Omega_{01}$  is the frequency of the transition  $0 \rightarrow 1$ ).

1. L.A.Rebane, A.A.Gorokhovskii, J.V.Kikas, Appl. Phys. B, 29, 235 (1982).
2. P.Saari, R.Kaarli, A.Rebane, J.Opt. Soc. Am.B, 3, 527 (1986).
3. H.W.Lee, M.Gehrtz, E.E.Marinero, W.E.Moerner, Chem. Phys. Lett., 118, 611 (1985).
4. I.Rebane, Izv. Akad. Nauk, ESSR, fiz. mat., 35, 296, 400 (1986).
5. I.Rebane, phys. stat. sol. 145, (1988).
6. I.Rebane, Izv. Akad. Nauk, ESSR, fiz.mat., 36, 204 (1987).
7. I.Rebane, Izv. Akad. Nauk, ESSR, fiz. mat., 37, (1988).

## SUM RULES OF NONLINEAR SUSCEPTIBILITIES OF MATERIAL CONTAINING DEFECTS

K.-E. Peiponen

Väisälä laboratory, Department of Physics, University of Joensuu,  
SF-80100, Finland.

Recently the author has given a set of sum rules for nonlinear susceptibilities of material /1/. The derivation of these sum rules is based on the results of the theory of several complex variables. The sum rules for nonlinear optical constants resemble those of the linear ones given by Altarelli et al /2/. Sum rules can be given in the case of sum and difference frequency generation respectively /3,4/. Even in the case when only the intensity  $| \chi^{(n)} |^2$ , usually the measureable quantity, is known, one can calculate  $\text{Re}(\chi^{(n)})$  and  $\text{Im}(\chi^{(n)})$  and test them with the aid of the sum rules /5/.

Nowadays we know that for instance colour centres of alkali halides possess nonlinear optical properties which can be exploited e.g. in four-wave mixing /6,7/. As in the linear case the nonlinear optical data of defects can be separated from that of the host crystal by making use of sum rules. This property allows us to test the consistency between theory and experimental data as well as to predict some properties of the defects.

## References

- /1/ K.-E. Peiponen, Phys. Rev., B35, 4116 (1987)
- /2/ M. Altarelli, D.L.Dexter, H.M.Nussenzveig and D.Y.Smith, Phys.Rev., 86, 4502 (1972)
- /3/ K.-E. Peiponen, J.Phys.C., 20, L285 (1987)
- /4/ K.-E. Peiponen, J.Phys.C., 20, 2785 (1987)
- /5/ K.-E. Peiponen, Phys.Rev.B. (in press)
- /6/ T. Zhang, L. Wan and Y. Run, Chinese Phys. Lett, 2, 369 (1985)
- /7/ T. Zhang, J. Yao and Y. Run, Optics Communications, 60, 314 (1986)

DEFECT STRUCTURE AND ELECTRICAL CONDUCTIVITY IN  $\text{LiNbO}_3$ 

A. Mehta, E. K. Chang, and D. M. Smyth  
 Materials Research Center, Coxe Lab. #32  
 Lehigh University, Bethlehem, PA 18015 U.S.A.

The  $\text{LiNbO}_3$  phase exists from the stoichiometric composition to compositions that are deficient in  $\text{Li}_2\text{O}$  and/or O to the level of several percent. The congruently melting composition that is most commonly used in electrooptic devices contains 48.6%  $\text{Li}_2\text{O}$  and 51.4%  $\text{Nb}_2\text{O}_5$ . Detailed structural studies by x-ray diffraction indicate that the resulting defects are a combination of Nb vacancies and Nb misplaced on Li sites (1). It has been shown that this can be viewed as local regions with the cation stacking sequence of the ilmerite structure containing Li vacancies, and embedded in the  $\text{LiNbO}_3$  matrix (2).

Equilibration of  $\text{LiNbO}_3$  with reducing atmospheres leads to n-type conductivity that varies with the oxygen partial pressure,  $P(\text{O}_2)$ , as  $P(\text{O}_2)^{-1/4}$ , superimposed on a pressure-independent ionic contribution related to the nonstoichiometric disorder (3). In this work, the electronic conductivity has been correlated with the reduction reaction, carrier concentrations and mobilities, and their temperature dependences to obtain a self-consistent description of the conduction process.

The temperature dependence of the equilibrium conductivity at constant  $P(\text{O}_2)$  at 900-1100 C corresponds to an activation energy of 2.50 eV per electron. This should correspond to the enthalpy of the reduction reaction plus the enthalpy of mobility of the electrons. The temperature dependence of the equilibrium oxygen pressure at constant composition was measured in a sealed cell with a zirconia sensor and corresponds to 1.96 eV. This should be the enthalpy of the reduction reaction. By means of coulometric titration in a similar sealed cell, known amounts of oxygen can be transported into or out of the cell electrochemically, and the resulting change in equilibrium  $P(\text{O}_2)$  measured. Evaluation of the results gives the electron concentration at  $P(\text{O}_2) = 1$  atm, and hence at any value of  $P(\text{O}_2)$ , since the pressure dependence is known. The temperature dependence gives a value of 2.05 eV for the enthalpy of formation of a carrier, in good agreement

with the value obtained at constant composition. An extrapolation of these results leads to excellent agreement with the carrier concentration obtained from a thermogravimetric measurement by Holmes (4).

The electrical conductivity was measured at constant composition over the temperature range 300-1000 C. The results are best described in terms of two slopes. The slope above 500 C corresponds to 0.55 eV, and this is proposed to be the enthalpy of electron mobility, since it has been concluded that the carrier concentration is not temperature dependent at constant composition at these high temperatures. For temperatures below 500 C, Nagels reported an activation energy of 0.66 eV, and proposed that this included both the ionization and the mobility of the carriers (5). We observed an activation energy of 0.65 eV, and the excess over the mobility term, 0.11 eV, is close to that expected from the bipolaron binding energy ( $0.27/2 = 0.14$  eV) reported by Schirmer (6).

The sum of the enthalpies of electron mobility (0.55 eV) and of the reduction reaction (1.96-2.05 eV) is in good agreement with the temperature dependence of the equilibrium conductivity at constant  $P(O_2)$  (2.50 eV).

The ionic conductivity and its temperature dependence have been deduced from the curvature of the equilibrium conductivity isotherms. The results agree well with those obtained from oxygen concentration cells and give an activation energy of 1.35 eV.

#### References

- (1) S. C. Abrahams and P. Marsh, *Acta Cryst.* **B42**, 61-8 (1986).
- (2) E. K. Chang, A. Mehta, and D. M. Smyth, to appear in *Advances in Ceramics*, NATO Adv. Res. Workshop on Nonstoichiometric Compounds.
- (3) D. M. Smyth, *Ferroelectrics* **50**, 419 (1983).
- (4) R. J. Holmes, AT&T Bell Laboratories, Allentown, PA, described in Ref. (3).
- (5) P. Nagels, in *The Hall Effect and Its Applications*, C. L. Chien and C. R. Westlake, Eds. (Plenum Press, New York, 1980).
- (6) O. F. Schirmer, Universität Osnabrück, private communication.

## CATION INTERDIFFUSION IN ALKALINE EARTH TITANATES

E. P. Butler, H. Jain, and D. M. Smyth  
 Department of Materials Science and Engineering, Whitaker Lab #5  
 Lehigh University, Bethlehem, PA 18015 U.S.A.

A systematic study has been undertaken to determine the cation interdiffusion coefficients,  $D$ , for the alkaline earth ions in calcium, strontium, and barium titanates. Diffusion couples have been prepared from pairs of these compounds that show complete solid solubility. The concentration profiles, after diffusion anneals, have been determined by quantitative microprobe analysis, as shown in Figure 1 for  $\text{SrTiO}_3/\text{CaTiO}_3$ . The interdiffusion coefficient was determined from these data using the analysis for  $D=D(C)$  by Wagner (1). Further analysis using the approach by Oishi (2) estimated that the lattice contribution to the interdiffusion coefficient was 3 to 4 orders of magnitude greater than the grain boundary contribution so, although the materials studied were polycrystalline, grain boundary diffusion was insignificant.

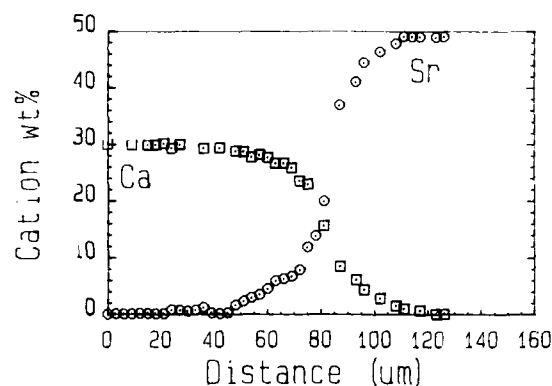


Fig. 1. Concentration profile for  $\text{CaTiO}_3$ - $\text{SrTiO}_3$  couple.

The diffusion distance was found to be proportional to the square root of the anneal time and the calculated diffusivities were found to be independent of this time. Thus there was little, if any, enhancement of the diffusion profile due to grain and densification for the samples studied. Figure 2 represents this relationship graphically.  $D$  for both the  $\text{CaTiO}_3/\text{SrTiO}_3$  couple and the  $\text{SrTiO}_3/\text{BaTiO}_3$  couple was found to be

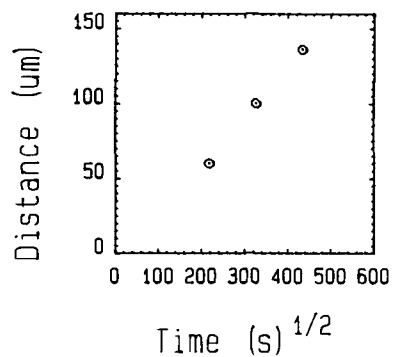


Fig. 2. Graph showing relationship between (anneal time)<sup>1/2</sup> and diffusion distance for CaTiO<sub>3</sub>/SrTiO<sub>3</sub>, T = 1350°C.

independent of relative cation concentration when the concentration of the larger radius ion was greater than the concentration of the smaller radius ion. D at the end points of the couples was found to decrease in the order:  $D_{Ca} > D_{Sr} > D_{Ba}$ . These results are shown in Figure 3 where D is plotted as a function of cation molar fraction.

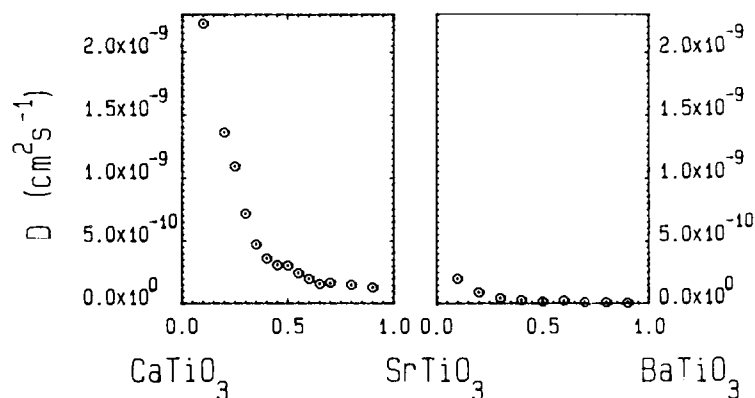


Fig. 3. Graph showing the relationship between D and cation molar fraction. Anneal temp. = 1350°C.

#### References

- (1) C. Wagner, Acta Metallurgica 17 (1969).
- (2) Y. Oishi and H. Ichimura, J. Chem. Phys. 71(12) 15 (1979).

AD-A206 030

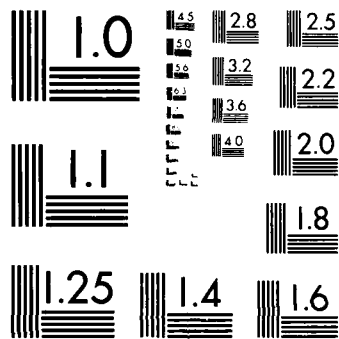
INTERNATIONAL CONFERENCE ON DEFECTS IN INSULATING  
CRYSTALS HELD AT PAVIA, ITALY ON AUGUST 29-SEPTEMBER 2  
1988(U) PAVIA UNIV (ITALY) DIPT DI FISICA SEP 81

67

UNCLASSIFIED

P/G 1/2

ML



MICROCOPY RESOLUTION TEST CHART  
NATIONAL BUREAU OF STANDARDS 1963 A

# HIGH TEMPERATURE TREATED INCLUSION COMPLEXES OF ZEOLITE A AS FAST IONIC CONDUCTORS

N. Petranović and D. Minić

Institute of Physical Chemistry, Faculty of Science,  
Belgrade University, Belgrade, Yugoslavia

Zeolite, in the classification of solid electrolytes is among solid ionic conductors in the group of non-ideal ionic crystals, the subgroup of a structure with interstitions. The charge carriers are counter ions and included cations when inclusion complexes of zeolite are formed. In inclusion complexes the number of charge carriers is increased by the number of included cations, however appearance of new cationic positions inside channels and cages, is also significant. Occupancy factor of these positions is statistical, what is very important for the increasing mobility of cations<sup>(1,2)</sup>.

We studied different inclusion complexes of zeolite A as ionic conductors started from  $\text{Na}_{22}(\text{NO}_3)_{10}\text{A}$  (A is the aluminosilicate part of the framework), sodium nitrate inclusion complex<sup>(2-4)</sup>. The exchange of  $\text{Na}^+$  with  $\text{Cd}^{2+}$  changes cationic density and increases system disorder, causing electric conductivity increase. However, it is observed that there is an optimal concentration of  $\text{Cd}^{2+}$  in zeolite unit-cell in which conductivity is the greatest. This is the cation mole fraction 0.36 for cadmium in the solid phase<sup>(3)</sup>. The heteroionic conductor based on cadmium,  $\text{Na}_{22-4x}\text{Cd}_{2x}(\text{NO}_3)_{10}\text{A}$ ,  $x=2$ , is coming closer to the group of good ionic conductors, Figure 1.a. However above 620 K the conductivity decreases because the thermal decomposition of included nitrate takes place.

In order to find a good fast ionic conductor thermally stable in wide temperature range we studied the electric conductivity of high temperature treated zeolite inclusion complexes. When exposed to a temperature of 1273 K zeolites  $\text{Na}_{22-2x}\text{Cd}_x(\text{NO}_3)_{10}\text{A}$  and  $\text{Na}_{22-4x}\text{Cd}_{2x}(\text{NO}_3)_{10}\text{A}$  the process of

denitration and structural transformation occur and new forms corresponding to the formulas:  $(11-x)\text{Na}_2\text{O}-x\text{CdO}-12\text{Al}_2\text{O}_3-12\text{SiO}_2$  and  $(11-2x)\text{Na}_2\text{O}-2x\text{CdO}-12\text{Al}_2\text{O}_3-12\text{SiO}_2$  obtain. Electric conductivity measurements of these samples are presented in Figure 1.b. The conductivity changes linearly over a wide temperature range with the activation energy of  $E=25.4 \text{ kJ mol}^{-1}$ .

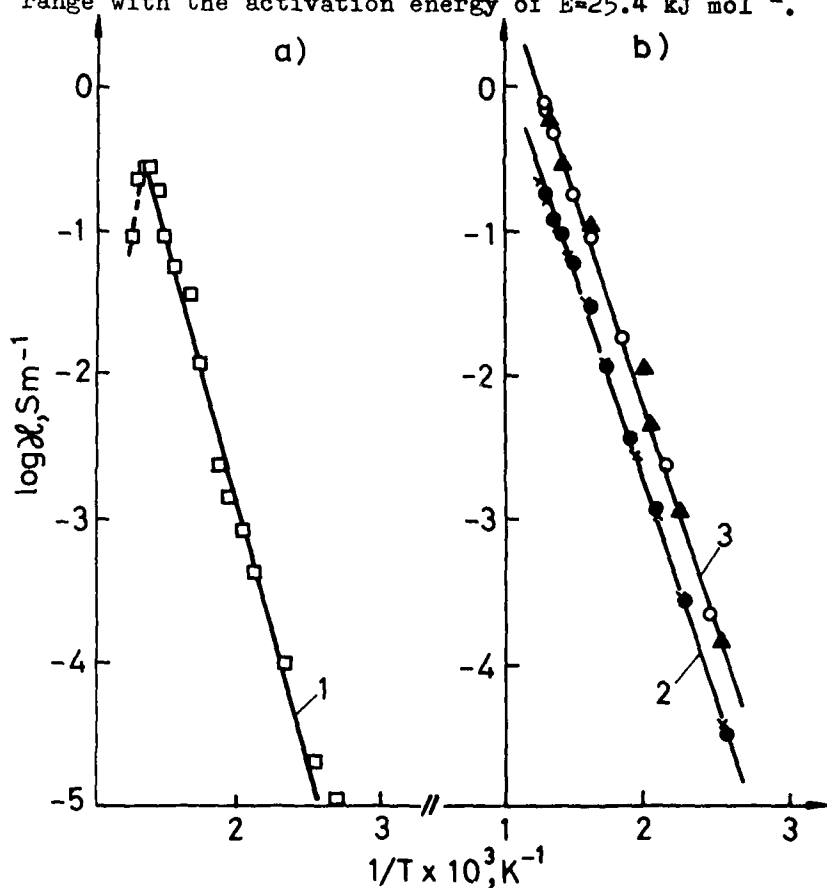


Figure 1. Electric conductivity of: a)  $\text{Na}_{22.4x}\text{Cd}_{2x}(\text{NO}_3)_{10}^{\text{A}}$  (1)  
b)  $(11-x)\text{Na}_2\text{O}-x\text{CdO}-\text{A}$  (2),  $(11-2x)\text{Na}_2\text{O}-2x\text{CdO}-\text{A}$  (3)

1. N.Petranović et al., J.Chem.Soc., Faraday Trans.1, 77(1981)379
2. N.Petranović and M.Šušić, *ibid.*, 75(1979) 2083
3. N.Petranović and M.Šušić, 33 ISE Meeting, Lyon 1982, Extended Abstracts Vol.II, p.501
4. M.Šušić and N.Petranović, Bull.Acad.Serbe Sci.Cl.Sci.Nat. LXVIII, 19(1979)21

THE INFLUENCE OF STRUCTURE DEFECTS ON THE SPECIFIC HEAT, OPTICAL AND ELECTRICAL PROPERTIES OF THE  $\text{PbF}_2$  - TYPE SUPERIONIC CRYSTALS<sup>x</sup>

I. Kosacki

Technical University of Radom, ul. Malczewskiego 29, Radom, Poland

A. P. Litvinchuk, M. Ya. Valakh

Institute of Semiconductors Academy of Sciences of the Ukr. SSR  
252028 Kiev, Prospekt Nauki 115, USSR

The superionic properties of fluorine crystals are connected with high disordering in anion sublattice. The transition of these crystals into the superionic state proceeds monotonically with increasing temperature. At temperatures significantly lower than the melting point a specific heat anomaly is observed. This anomaly is interpreted as a result of collective interactions between the anion Frenkel's defects which are formed during the "melting" process of the fluorine sublattice.

Among the fluorites,  $\text{PbF}_2$  exhibits the lowest superionic state transition temperature  $/T_c \approx 700\text{K}/$  and the lowest cation-anion interaction coefficient. This interaction is determined by the specific valence electron configurations of the Pb atoms and causes an anomalous character of the fundamental absorption edge in mixed  $\text{Cd}_{1-x}\text{Pb}_x\text{F}_2$  crystals. The high concentration of defects can be attained not only by heating but also as a result of doping or  $\gamma$ -irradiation.

The aim of this work has been to study the influence of the ion disordering of  $\text{Cd}_{1-x}\text{Pb}_x\text{F}_2$  crystals on their superionic properties. The effect of fluorine sublattice disordering is closely connected with crystal lattice dynamics and should be

<sup>x</sup>Work support by Institute of Physics of Polish Academy of Sciences 02-668 Warszawa, Al. Lotników 32/46, Poland.

reflected in ionic conductivity, specific heat and phonon spectra. In the present work the results of the measurements of Raman scattering, ionic conductivity and specific heat of  $\text{PbF}_2:\text{LiF}$  and  $\text{Cd}_{1-x}\text{Pb}_x\text{F}_2$  crystals are presented. A difference between ionic radii of  $\text{Cd}^{2+}$  and  $\text{Pb}^{2+}$  ions indicates that these crystals should be characterized by a particularly high level of disordering.

The anion disordering in these crystals is manifested by anomalies in Raman scattering and ionic transport. The  $\text{Cd}_{1-x}\text{Pb}_x\text{F}_2$  crystals are characterized by better superionic properties in comparison with  $\text{PbF}_2$ . This is manifested in a rise of the ionic conductivity, a drop in values of the activation energy of conductivity as well as in a decrease of the superionic state transition temperature. For  $\text{Cd}_{0.4}\text{Pb}_{0.6}\text{F}_2$  it is lowest and equals  $T_c = 485\text{K}$ . The correlation has been found between the ionic conductivity and the superionic state transition temperature for  $\text{Cd}_{1-x}\text{Pb}_x\text{F}_2$  crystals.

1. Physics of Superionic Conductors, Ed.M.B.Salamon, Springer Verlag, Berlin, Heidelberg, New York, 1979.
2. I.Kosacki, K.Hibner, A.P.Litvinchuk, M.Ya.Valakh, Solid State Commun.57,No8,729-733 (1986).
3. I.Kosacki, J.M.Langer, Phys.Rev.B,33,No8,5972-5973 (1986).
4. I.Kosacki, A.P.Litvinchuk, Proc.,5th Europhys.Topic.Conf. Lattice Defects in Ionic Crystals, Madrid 1986, Crystal Lattice Defects and Amorphous Materials 15,No1-4,351-356 (1987).

## THERMAL CONDUCTIVITY OF NEUTRON IRRADIATED OXYDES

B. SALCE and A.M. de GOER

Centre d'Etudes Nucléaires - Département de Recherche Fondamentale/SBT-LCP

85 X - 38041 GRENOBLE Cedex - FRANCE

Although damage induced by neutrons on dielectric crystals has been studied for small irradiation doses (1), effects resulting from large doses are not well understood yet. Depending on the material, the nature of created defects and the structural phase obtained for the highest doses are different. We report on changes induced by neutron irradiations on a very pure  $\text{Al}_2\text{O}_3$  single crystal and we compare the results to the effect of similar doses on a natural quartz. Particular care was taken to measure the neutron flux intensities, in order to get reliable quantitative estimations.

The thermal conductivity  $K(T)$  of  $\text{Al}_2\text{O}_3$  was nearly unaffected by  $\gamma$  or electron irradiations ( $\sim 3 \times 10^{19} \text{ e}^-/\text{cm}^2$ ), which indicates a very high purity of the sample. By contrast,  $K(T)$  measurements performed after 4 different neutron irradiations show strong decreases above 1K (Figure 1). Neutron irradiations create a large number of point defects (or small clusters) and also strain fields in the bulk. Then, the data have been fitted using the Callaway model, assuming the induced high temperature phonon scattering is mainly of the Rayleigh type ( $\tau^{-1} = A \omega^4$ ) and that  $K(T)$  is dominated by dislocations ( $\tau^{-1} = G \omega$ ) at low temperature. The parameters obtained from the fits are reported in the table. The variation of  $A_{\text{fit}}$  with dose (insert fig.1) displays no saturation. The number of point defects created by neutrons can be estimated using a simple model of atomic displacements (2). The values of  $N_d$  such calculated are given in the table (for details see (3)) as well as the corresponding values of  $A_{\text{calc}}$  (the defects being supposed to be vacancies or interstitials). The agreement between  $A_{\text{fit}}$  and  $A_{\text{calc}}$  is quite good for  $\text{Al}_2\text{O}_3$ , in view of the crudness of the model.

Quartz behaves differently from  $\text{Al}_2\text{O}_3$  as shown in figure 1 (and insert). This means that created defects are different in the two compounds (the very large  $G$  term in quartz was assigned to TLS(4)). The fitted values for the Rayleigh terms are 100 times higher and are too large to be physically meaningful. Variation of  $A_{\text{fit}}$  with neutron

Dose $\text{n/cm}^2$ ( $E > 0.1 \text{ Mev}$ )	$A_{\text{fit}}$ ( $\text{s}^3$ )	$N_d$ ( $\text{cm}^{-3}$ )	$A_{\text{calc.}}$ ( $\text{s}^3$ )	$G_{\text{fit}}$	Nb disl. ( $\text{cm}^{-2}$ )
$\text{Al}_2\text{O}_3$ (virgin)	$1.7 \times 10^{-46}$	-	-	$3.8 \times 10^{-7}$	$6.3 \times 10^8$
$3 \times 10^{18}$	$7 \times 10^{-44}$	$1.8 \times 10^{21}$	$3 \times 10^{-44}$	$3.8 \times 10^{-6}$	$6.3 \times 10^9$
$1.1 \times 10^{19}$	$1.9 \times 10^{-43}$	$6.5 \times 10^{21}$	$1.1 \times 10^{-43}$	$5.3 \times 10^{-6}$	$8.8 \times 10^9$
$1.8 \times 10^{19}$	$2.8 \times 10^{-43}$	$1.1 \times 10^{22}$	$1.8 \times 10^{-43}$	$5.3 \times 10^{-6}$	$8.8 \times 10^9$
$1.8 \times 10^{20}$	$2 \times 10^{-42}$	$1.1 \times 10^{23}$	$1.8 \times 10^{-42}$	$3.8 \times 10^{-5}$	$6.3 \times 10^{10}$
Quartz $2.2 \times 10^{20}$	$1.7 \times 10^{-40}$	$6 \times 10^{23}$	$9 \times 10^{-42}$	$3.8 \times 10^{-4}$	-

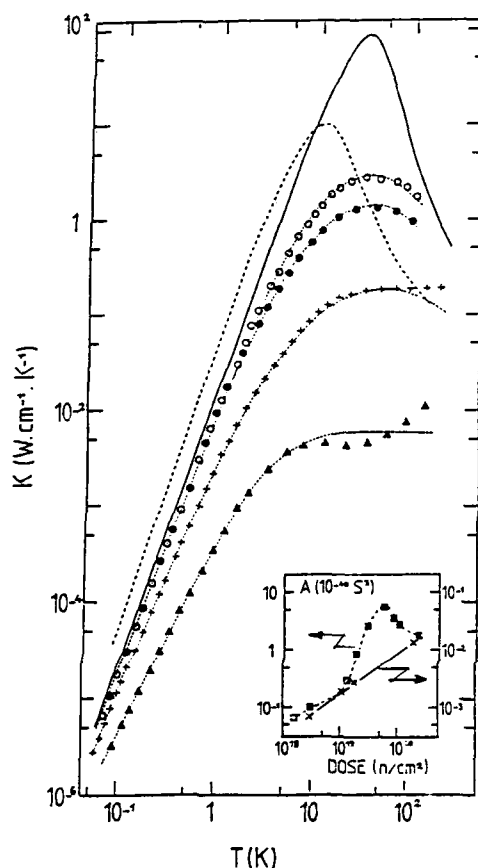


**Figure 1** - Thermal conductivity as a function of temperature from 50 mK to 150 K.

Pure Al<sub>2</sub>O<sub>3</sub> :

Before irradiation (solid line)  
 After neutron irradiations :  
 1<sup>st</sup> dose (o) - 2<sup>nd</sup> dose (•)  
 4<sup>th</sup> dose (+) (résultat for the 3<sup>rd</sup> dose are not very different from those for 2<sup>nd</sup> dose)  
 Dotted lines : calculated curves (see text).

Natural quartz :

Before irradiation (dashed line)  
 After neutron irradiation  
 2.2 × 10<sup>20</sup> n/cm<sup>2</sup> (E > 0.1 Mev) (▲)  
 Dotted line : calculated curve

Insert : Fitted Rayleigh coefficient A as a function of dose :

Al<sub>2</sub>O<sub>3</sub> (x) - right side scale  
 Quartz (□, ■) - left side scale  
 Lines are guides for the eyes.

dose (insert fig.1) does not exhibit a monotonic law and tends to saturation. In fact, the main difference comes from the possibility to obtain, for large irradiations doses, a highly disordered phase in quartz, apparently identical to neutron irradiated amorphous silica. Such a phase change does not occur in Al<sub>2</sub>O<sub>3</sub> up to 1.8 × 10<sup>20</sup> n/cm<sup>2</sup>.

- (1) R.BERMAN, E.L.FOSTER and H.M.ROSENBERG  
 "Defects in Crystalline Solids", Bristol (1954)
- (2) D.S.BILLINGTON and J.M.CRAWFORD  
 "Radiation damage in Solids", (1961), Princeton University Press, chap.2.
- (3) A.M.de GOER, Note interne DRFG/SBT/LCP (1988)
- (4) A.M.de GOER, N.DEVISMES and B.SALCE, "Phonon Scattering in Condensed Matter V", Springer Series in Solid State Sciences, 68, (1986) p.70.

IRRADIATION EFFECTS ON DIFFUSION IN GLASSES

P. CALMON, Y. SERRUYS, G. BREBEC

*Centre d'Etudes Nucléaires de Saclay*

*Section de Recherches de Métallurgie Physique*

*91191 GIF SUR YVETTE CEDEX, France*

The effects of irradiation on the atomic diffusion with ion and electron beams. Evidence is given for a large enhancement of diffusion rates, mostly related to electronic defect formation under irradiation. Different cases - high-energy heavy ions, 1 MeV protons, low-energy electrons etc... - are presented.

HIGH TEMPERATURE STUDIES OF RARE EARTH FLUORIDES  
USING BRILLOUIN SCATTERING

P.E. Ngoepe<sup>+o</sup> and J.D. Comins<sup>+</sup>

<sup>+</sup>Department of Physics, University of the Witwatersrand, Johannesburg  
P.O. Wits 2050, South Africa

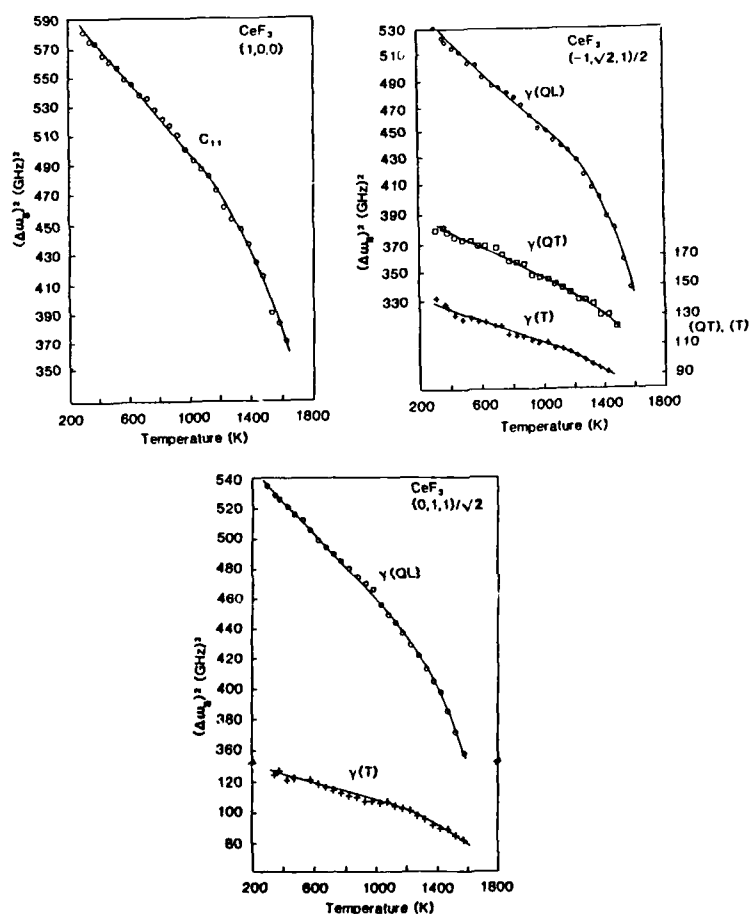
<sup>o</sup>Department of Physics, University of the North,  
Sovenga 0727, South Africa

The rare earth fluorides,  $\text{LaF}_3$ ,  $\text{CeF}_3$ ,  $\text{PrF}_3$  and  $\text{NdF}_3$  have the tysonite ( $\text{D}_{3d}^4$ ) structure. There is interest in the defect structure of these compounds regarding the nature of the dominant defects, the mechanism of the rather high ambient temperature ionic conductivity and the high temperature ( $>1100\text{K}$ ) phase in which there is evidence for a diffuse phase transition to a disordered state.(1)

Measurements of acoustic mode frequencies have provided useful information on superionic transitions and results for  $\text{LaF}_3$  and  $\text{CeF}_3$  are reported. Brillouin spectra were analysed by means of a Fabry-Perot interferometer. Birefringence effects are negligibly small and the hexagonal approximation to the trigonal structure is adequate. The temperature dependence of the elastic constants has been extracted from measurements of the square of the acoustic mode frequencies  $(\Delta\omega_B)^2$  for appropriate phonon propagation directions.

Figure 1 shows results for  $\text{CeF}_3$ ; results for  $\text{LaF}_3$  are similar. Linear decreases in  $(\Delta\omega_B)^2$  with temperature are attributed to anharmonicity associated with lattice expansion. The substantial decreases in  $(\Delta\omega_B)^2$  above about 1150K may be attributed to thermal defect generation, higher-order anharmonicity or both. The decreases correspond quite well with the substantial increase in the heat capacity of  $\text{LaF}_3$ (2) but not as convincingly with the rather smaller increase for  $\text{CeF}_3$ (3). In the light of similar studies on fluorites, we favour the generation of defects as the major contribution to the reduction in mode frequencies. The nature of the dominant defect species is as yet uncertain. Recent theoretical work by Jordan and Catlow(4) favours Frenkel disorder, whereas lattice parameter

and dilatation measurements have been interpreted in terms of Schottky defects(5).



- (1) P.E. Ngoepe, J.D. Comins and A.G. Every, Phys. Rev. B34 (1986) 8153.
- (2) W.G. Lyon, D.W. Osborne, H.E. Flotow, F. Grandjean, W.N. Hubbard and G.K. Johnson, J. Chem Phys. 69 (1978) 167.
- (3) F.H. Spedding, B.J. Beaudry, D.C. Henderson and J. Moorman, J. Chem. Phys. 60 (1974) 1578.
- (4) W.M. Jordan and C.R.A. Catlow, Cryst. Latt. Def. and Amor. Mat. 15 (1987) 81.
- (5) A. Sher, R. Solomon, K. Lee and M.W. Muller, Phys. Rev. 144 (1966) 593.

# **VISUAL OBSERVATION OF FAST CHEMICAL DIFFUSION IN STABILIZED ZIRCONIA**

Erick Fredj and D.S. Tannhauser  
 Department of Physics  
 Technion, Israel Institute of Technology, Haifa, Israel

Crystals of yttria or calcia stabilized zirconia reduced very strongly by annealing at 1000 C in hydrogen in a fairly tight zirconium wrapping are black and completely opaque. These samples can be reoxidized at T=350 C in air and the process can be observed visually. Since the process is one of ambipolar chemical diffusion and since electrons are the minority carriers in strongly reduced crystals the diffusion constant is given by  $D^{\text{chem}} = D_e$ .  $D_e$  can therefore be estimated by comparing the progress of the reoxidation front with a solution of the diffusion equation for the geometry of our samples which resemble a rod with a rectangular cross section. The values of  $D_e$  obtained are in the range  $D_e(350) = 10^{-6} \text{ cm}^2/\text{sec}$  to  $D_e(550) = 10^{-5} \text{ cm}^2/\text{sec}$ . They fit reasonably well to values extrapolated from measurements done by other method in the temperature range 700-900 C<sup>1</sup>. The reoxidation at 350 C and somewhat higher temperatures stops at a point where the sample is yellow and still has a strong ESR signal, i.e. is still fairly reduced<sup>2</sup>. This is compatible with the fact the dominant minority carriers are holes at high oxygen pressure and electrons at low pressure and that  $D_e \gg D_h$ . Therefore diffusion is fast during the initial reoxidation when  $D^{\text{chem}} = D_e$ , and stops when the oxygen potential gets high enough to make  $\sigma_h \gg \sigma_e$  and  $D^{\text{chem}} = D_h$ .

A video film of the progress of reoxidation will be shown.

- 
1. W. Weppner, Electrochemical Transient Investigations of the Diffusion and Concentration of Electrons in Yttria Stabilized Zirconia-Solid Electrolytes, Z.Naturforsch. 31a, 1336 (1976)
  2. J. Genossar and D.S. Tannhauser, The Nature of ESR Centers in Reduced Stabilized Zirconia, Proc. Conf. S.S. Ionics, Garmisch-Partenkirchen 1987, J.S.S. Ionics, to be published.

THE CHARGE SEPARATING AND RECTIFYING BEHAVIOUR OF PHASE TH - P69

BOUNDARIES IN SILVER HALIDE MIXED CRYSTALS

F. Granzer<sup>1</sup>, R. Kricsanowits<sup>1</sup>, Th. Müssig<sup>2</sup>

J. Niklas<sup>3</sup> and B. Pischel<sup>1</sup>

<sup>1</sup> Institut Angewandte Physik, Universität  
D-6000 Frankfurt/Main, Robert-Mayer-Str. 2-4

<sup>2</sup> Du Pont de Nemours (Deutschland), D-6078 Neu-Isenburg

<sup>3</sup> Fachbereich Physik, Universität D-4790 Paderborn, Warburger Str. 100 A

The extremely high speed of contemporary photographic systems based on silver halides is achieved in the following two ways:

- 1) by the use of tabular silver halide microcrystals with large projections areas as emulsion grains (T-grains)
- 2) by the incorporation of phase boundaries into these grains (core-shell-emulsions)

It is believed that phase boundaries in silver halide mixed crystals lead to a better utilization of the photoelectrons which, together with the interstitial silver ions, are forming the latent image speck consisting of a few, say 4, silver atoms. The electronic behaviour of phase boundaries in insulating crystals like alkali and silver halides may be compared with that of heterojunctions in semiconductors. In semiconducting mixed crystals, like  $\text{Al}_x\text{Ga}_{1-x}\text{As}$ , extremely long living photogenerated electrons ("persistent photo-currents") have been attributed to charge separating potentials of heterojunctions formed at phase boundaries. Similar results, obtained recently by CESR-measurements on decomposed  $\text{Na}_x\text{Ag}_{1-x}\text{Cl}$ -crystals after X-ray irradiation at 77 K [1], have stimulated corresponding investigations on  $\text{AgBr}_x\text{I}_{1-x}$ -crystals.

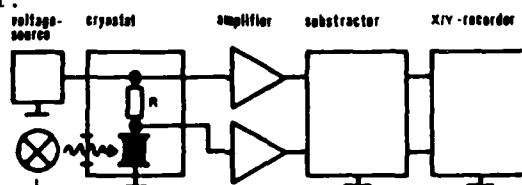
The composition and the thermal treatment of the  $\text{AgBr}_x\text{I}_{1-x}$ -crystals has been optimized in accordance with a reliable AgBr/AgI-phase diagram [2] in order to obtain well defined phase boundaries in the decomposed  $\text{AgBr}_x\text{I}_{1-x}$ -crystals.

The CESR-measurements were performed on  $\text{AgBr}_{60}\text{I}_{40}$ -crystals which decompose into a bromine rich  $\text{AgBr}_{83}\text{I}_{17}$ -phase (NaCl-structure) and an iodine rich  $\text{AgBr}_{06}\text{I}_{94}$ -phase (Wurtzit) if cooled down below 120° C. The microstructure and the chemical composition of these crystals has been controlled by light- and scanning electron-microscopical investigations and by X-ray mapping. Decomposed

AgBr<sub>60</sub>I<sub>40</sub>-crystals showing well defined phase boundaries were used as samples for the CESR-spectroscopy. After X-ray irradiation at 6 K a strong CESR-line starts to develop indicating the presence of long living conduction electrons. This line was stable up to 60 K.

The results obtained by CESR-spectroscopy will be compared with existing models of the band structure of phase boundaries in AgBr<sub>x</sub>I<sub>1-x</sub>-crystals. In a first attempt the band structure of an abrupt phase boundary between the pure phases has been calculated by using the energetic positions of the valence and conduction bands of AgBr and AgI respectively and by allowing thermal equilibration of the corresponding Fermi-levels. The best check of the validity of such a model is to measure the current-voltage-characteristic of the phase boundary in question in the dark and under actinic illumination. This was done with the experimental setup scetched in Fig. 1.

Fig. 1  
experimental  
setup



The measurements were carried out with AgI single crystals brought into mechanical contact with monocrystalline AgBr sheet crystals in an evacuated cryostat. Conductive silver is used to ensure best thermal and electrical contact between the crystal surfaces and the two silver electrodes. To avoid ionic conductivity the samples are cooled down to liquid nitrogen temperature. A variable DC field is applied to the sample in series with a  $10^8 \Omega$  load resistor (R). The voltage drop in the resistor representing the current through the crystal system (S) is measured with a high sensitive current amplifier and plotted vs. the voltage drop in the sample on a X/Y-recorder. The crystals were exposed to the light of a mercury arc lamp (L). The rectifying behaviour of the AgBr/AgI-contact in the dark and upon illumination will be compared with the band structure of the corresponding phase boundary.

- [1] Th. Müssig and F. Granzer: phys. stat. sol. (a) 87, K85 (1985)
- [2] Y. Xu, R. Kricsanowits, E. Palm and F. Granzer: Proc. ICPS Cologne, 323 (1986)

TRANSFER OF PHOTOGENERATED ELECTRONS AND HOLES THROUGH PHASE  
BOUNDARIES BETWEEN DIFFERENT SILVER HALIDES

R. Alhäuser and F. Granzer

Institut Angewandte Physik, Universität D-6000 Frankfurt/Main  
Robert-Mayer-Str. 2-4

Emulsion grains with internal phase boundaries have become a subject of great interest in the classical silver halide photography. It is presumed that the increase of the sensitivity of these grains is primarily caused by a better utilization of the photoelectrons which by combination with silver ions are forming the latent image. In the models discussed so far it is assumed that phase boundaries in silver halide crystals act like heterojunctions in semiconductors. In the electric field of a heterojunction electrons and holes which are generated pairwise by the absorption of light get separated, their recombination is impeded and as a consequence the lifetime of the electrons is augmented.

In order to get a better understanding of the electronic properties of phase boundaries in silver halide mixed crystals and in order to substantiate the existing models of the corresponding heterojunctions, the knowledge of the band structure of the phase boundary is unavoidable.

A method, delivering the relative positions of the valence and conduction bands of the two different phases brought into intimate contact has been applied by Kawasaki et al [1] to the abrupt AgBr/AgCl-phase boundary.

Their experimental set up which has been slightly modified in our experiments is sketched in Fig. 1.

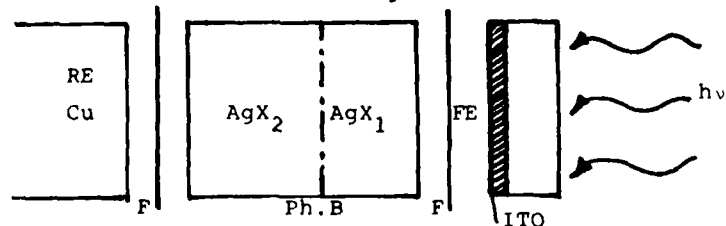


Fig. 1 Experimental arrangement

The two different silver halide crystals  $\text{AgX}_1$  and  $\text{AgX}_2$  ( $\text{X}_{1,2} = \text{Cl, Br, I}$ ) are brought into mechanical contact within a capacitor, thus forming the abrupt phase boundary (Ph.B.). The front electrode (FE), transparent for UV-light, was a quartz glass plate covered with a conducting ITO-film (thickness 200 Å). The rear electrode (RE) was a block of copper. The silver halide crystals were compressed by the two electrodes which are separated by insulating foils (F) from the crystals.

By using light flashes with an appropriate wavelength, electron-hole pairs are generated only in a thin layer near the front electrode. The charge carriers are separated by a pulsed electric field suitable synchronized with the light flashes. The resulting photomoment, increasing the capacitance of the assembly, could be measured by the rise of the voltage of a reference capacitor being in series with the assembly. From a plot of this voltage vs. the effective field strength in the crystal it is possible to get information about the influence of the phase boundary on the charge carriers (electrons and holes) passing through it.

With this information it should be possible to indicate the relative positions of the conduction- and valence band of the two crystals forming the abrupt phase boundary.

Preliminary results obtained with  $\text{AgBr/AgCl}$ - and  $\text{AgBr/AgI}$  phase boundaries will be presented.

- [1] Mitsuo Kawasaki, Hiroshi Hada and Hiroyuki Uchida:  
J. Appl. Phys., Vol. 60, No. 11 (1986)

## Shallow donor impact ionization in semiinsulating GaAs

C. Paracchini

Dipartimento di Fisica, Università di Parma, Parma, Italy

Semiinsulating (SI) GaAs crystals have gained importance as substrate of integrated circuits but the electronic conduction in this material still has some unclear aspects. In this paper the electronic transport in the superlinear part of the  $i$ - $V$  characteristic of this compound is examined.

The current - voltage characteristic obtained at R.T. exhibits at low applied fields ( $< 2.5 \cdot 10^2$  V/cm) a linear dependence followed by a region where low frequency oscillations with a nearly constant average current value are observed. Then at about  $2 \cdot 10^3$  V/cm an abrupt increase of the current takes place. In this part the current  $i$  increases with the applied field  $E$  as:

$$i = i_0 \exp(-A/E)$$

where  $A = 2-3 \cdot 10^4$  V/cm, suggesting an impact ionization process. Then:  $A = w/el$ , where  $w$  is the ionization energy and  $l$  is the path length.

Since the applied field is varied in the range where the mobility  $u$  is constant ( $E < 3.3 \cdot 10^3$  V/cm), one has:

$$u = e l / (2m^* kT)^{(1/2)}$$

where  $m^*$  is the effective mass. With the value of  $u$  given by the Hall measurements one obtains:  $l = 5.7 \cdot 10^{-6}$  cm and from a typical experimental value of  $A$  ( $2.9 \cdot 10^4$  V/cm), one deduces  $w = 0.16$  eV.

Donor centres with such activation energy do exist in semiinsulating GaAs and also if their concentration is relatively small compared with that of other deeper centres, their smaller depth makes them more easily ionizable during an impact process.

The temperature dependence of the current is determined by the path length variations. Then, if  $N$  is the centre concentration and  $Q$  the impact cross section:

$$l = 1/QN = B^*/T^2, \text{ with } B^* = (N Y/2)/(4 \pi k/e^2)^{1/2}$$

where  $\epsilon$  is the dielectric constant and  $Y$  a proportionality factor of the order of  $10^{-1/2}$ . This leads to a current - temperature dependence of the form:

$$i = i_0 \exp(-B/T^2)$$

with  $B = w B^*/e E$ . Such theoretical trend is in agreement with the experimental results which typically give  $B = 1.5 \cdot 10^5 \text{ K}^2$ . Then one can evaluate the concentration of the shallow donor centre involved in the impact process. From the experimental datum of  $B$  one has  $N = 7.7 \cdot 10^{15} \text{ cm}^{-3}$ , which is a reasonable result, considering that the concentration of more dense centres like EL 2 or EL 6 is about  $10^{15} - 10^{16} \text{ cm}^{-3}$ .

Moreover, using the previous data, one has  $Q = 2.2 \cdot 10^{-11} \text{ cm}^2$ , which is comparable with the reported values [2].

-----

1/ B.K.Ridley, Quantum processes in semiconductors, Clarendon (1982) pg.165

2/ G.M.Martin, Semiinsulating III-V materials. ed. G.J. Rees, pg. 13. Nottingham (1980)

INJECTION OF CHARGE CARRIERS IN DEFECT INDUCED ALKALIHALIDES

By

K. Goswami and A. K. Maiti

Department of Physics, Jadavpur University,  
Calcutta 700032, India.

Single crystals of KCl, KBr, and KCl : KBr have been grown by Kyropoulos method in our laboratory. Electron injection has been employed in these crystals through heterogeneous contact (1) under different temperatures and applied electric fields. The ionic zone followed by electron trapping zone is observed and during the trapping zone simultaneous current growth and optical absorption have been studied. The space charge limited current (2) operation is discontinued before the advent of the third zone (3) and the original transparency is regained when the decay of these induced defect centers has been recorded.

An equation has been derived (4) for the ionic zone as

$$J \approx A \exp (-W_0 / kT),$$

thereby yielding the activation energy ( $W_0$ ) associated with the conduction. The mobility of defect centers ( $\mu_F$ ) is measured experimentally from the observation of the

time of decay during which the crystal attains its transparency. Activation energy (U) involved for the migration of the defect centers has been obtained through

$$\mu_T = \mu_0 \exp (-U / kT),$$

The current growth pattern during trapping in KCl and KBr is found to be different from the standpoint of same scale of applied field and temperature. KCl takes indefinitely longer time to pass SCLC stage while for KBr this region is steeper and well defined. Systematic doping of KBr into KCl yields the results of the activation energy connected to ionic and trapping regions which are found to be characteristic of the alkali halides.

Reference :

- (1) A. K. Maiti and K. Goswami et.al.  
Fizika 14, 7, (1982).
- (2) M. A. Lampert and P. Mark, Current Injection  
in Solids, Academic Press Inc. New York (1970)
- (3) G. A. Andreev et.al. Sov. Phys. Solid State,  
9, 2564, (1968).
- (4) A. K. Lahiri, A. K. Maiti and K. Goswami,  
Solid State Communications, 50, 7, (1986).

## HIGH TEMPERATURE MÖSSBAUER STUDIES OF DIFFUSION IN THE IRON OXIDES

K.D. Becker and V. v.Wurmb

Institut für Physikalische Chemie und Elektrochemie

Callinstr. 3-3A, D-3000 Hannover, FRG

Little is known about details of microscopic migration mechanisms in structurally and chemically complex solids. We have started Mössbauer investigations of such processes in the three iron oxides, hematite ( $\text{Fe}_2\text{O}_{3-\epsilon}$ ), magnetite ( $\text{Fe}_{3-\delta}\text{O}_4$ ) and wustite ( $\text{Fe}_{1-\Delta}\text{O}$ ) which, each under different aspects, provide interesting examples for such a study. As a further important feature of these nonstoichiometric compounds defect concentrations at constant temperatures can be influenced and adjusted by external oxygen activities,  $a_{\text{O}_2}$ .

Magnetite with its spinel structure provides an example for a crystal with two different coordinated cation sites. Therefore, cation vacancy migration can take place on and between these two interpenetrating cation sublattices. Mössbauer transmission spectra of magnetite have been measured at temperatures up to 1400 °C under defined oxygen activities. At temperatures above 1100 °C, the lineshape of the isothermal spectra exhibits an oxygen activity dependence that is attributed to cation diffusion. An analysis of the spectra shows that cation diffusion in crystals with iron deficit,  $\delta > 0$ , is dominated by cation migration on the octahedral sublattice. Contributions from exchange jumps between the two cation sublattices as well as from diffusion on the tetrahedral sublattice can only

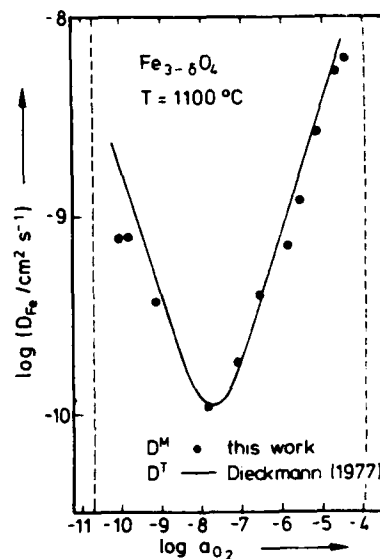


Fig. 1 Cation diffusion in magnetite

play a minor role /2/. The observed diffusion broadening of octahedrally coordinated iron ions exhibits an oxygen activity dependence which is proportional to  $a_{O_2}^{2/3}$ , which is in agreement with the existence of a vacancy mechanism /1/. Fig. 1 demonstrates that the spectroscopic data in the vacancy regime are in excellent agreement with results from tracer diffusion experiments /1/. At 1100 °C such an agreement also is observed for the interstitial regime with iron excess,  $\delta < 0$ . At higher temperatures, however, increasing discrepancies are encountered for the interstitial region. A model accounting for these observations is presented which is based on an extended interstitial migration process of cations in the interstitial space.

In hematite with its noncubic  $\alpha\text{-Al}_2\text{O}_3$  structure our measurements on polycrystalline samples are in good agreement with the data from tracer experiments /3-5/. Angular dependent measurements on high purity synthetic single crystals are expected to yield information on the anisotropy of diffusion in this structure.

Due to its large deviation from stoichiometry wustite can be considered as a model compound for fcc crystals with high defect concentrations. First results are reported of a transmission study using single crystalline absorbers.

/1/ R. Dieckmann, H. Schmalzried, Ber. Bunsenges. Phys. Chem. 81, 344 (1977)

/2/ K.D. Becker, V. v.Wurmb, Z. Phys. Chem. NF 149, 77 (1986)

/3/ K.D. Becker, V. v.Wurmb, Z. Phys. Chem. NF 149, 91 (1986)

/4/ R.H. Chang, J.B. Wagner, J. Am. Ceram. Soc. 55, 211 (1972)

/5/ K. Hoshino, N.L. Peterson, J. Phys. Chem. Solids 46 375 (1985)

## DEFECT PARAMETERS FOR SODIUM CHLORIDE FROM IONIC CONDUCTIVITY MEASUREMENTS

Irene E. Hooton and P.W.J. Jacobs  
Department of Chemistry  
University of Western Ontario  
London, Ontario N6A 5B7

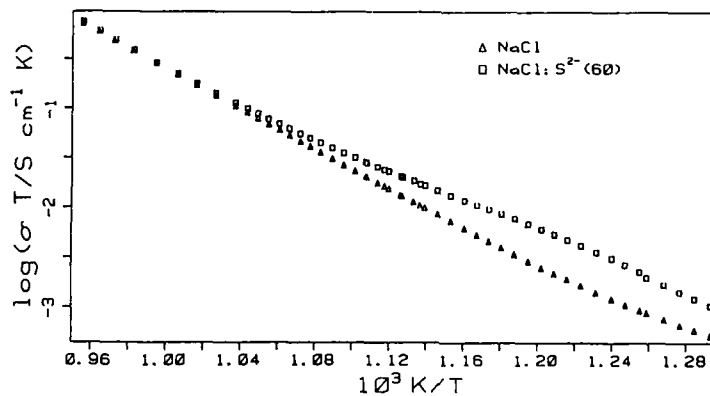
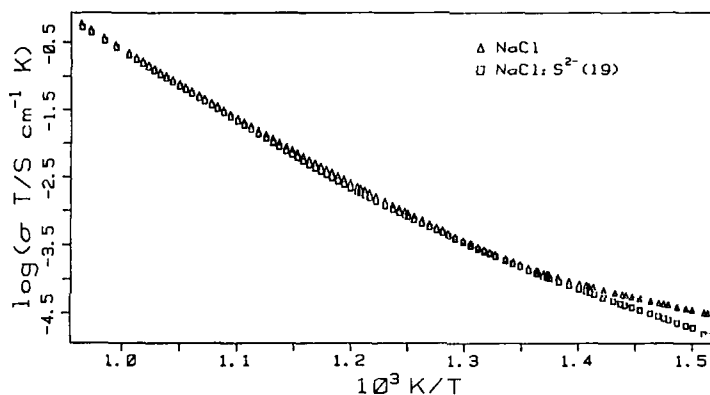
Computer fitting of the temperature dependence of the conductivity of an ionic crystal yields numerical values of the energy and entropy of formation, migration and association of the crystal defects. The traditional method assumes that these defect parameters are independent of temperature. However, computer-simulation calculations in the quasiharmonic approximation show that the defect energies at constant volume ( $u^V$ ) decrease with increasing temperature. To fit the conductivity to a set of temperature-dependent parameters involves too many unknowns in the least squares procedure, unless we utilize the calculated temperature dependence of the defect energies. New measurements of the ionic conductivity of well-annealed crystals of pure NaCl, and of NaCl crystals doped with  $Sr^{2+}$  and  $S^{2-}$  have been analyzed to yield numerical values for the defect energies and entropies, assumed to be temperature-independent. These results will be compared with a further analysis which allows for temperature dependent energies and entropies as given by the simulation results. The latter analysis allows  $u^V(T = 0 \text{ K})$  and  $s^V(T_0 = 298.15 \text{ K})$  as free parameters to be determined in the analysis, where  $s^V$  is a defect entropy at constant volume. Thus the simulation results are used to predict the temperature-dependence but not the absolute values of the parameters. Once  $u^V(T = 0 \text{ K})$  and  $s^V(T_0)$  have been determined, the corresponding energies and entropies, and also defect volume changes, at constant pressure, may be calculated using the quasiharmonic approximation.

Results of the analysis with temperature-independent parameters yield an enthalpy for anion motion of 0.74 eV in good agreement with diffusion measurements and computer simulation results<sup>2</sup>, but lower than values derived from measurements of the

temperature dependence of ionic conductivity or of the isothermal time-dependence of the permittivity of quenched crystals of NaCl containing Na<sub>2</sub>S<sup>3,4</sup>.

This research was supported by the Natural Sciences and Engineering Research Council of Canada.

1. M. Bènière, F. Bènière and M. Chemla, J. Phys. Chem. Solids, 37, 525 (1976).
2. C.R.A. Catlow, J. Corish, K.M. Diller, P.W.M. Jacobs and M.J. Norgett, J. Phys. (Paris), 37, C7-253 (1976).
3. J.S. Cook and J.S. Dryden, J. Phys. C, 12, 4207 (1979).
4. J.S. Cook and J.S. Dryden, J. Phys. (Paris), 14, C6-425 (1980).



Arrhenius plots of the ionic conductivity of pure NaCl and of NaCl containing 19 and 60 ppm of Na<sub>2</sub>S. Notice the reduction in conductivity induced at the lower doping level.

EFFECT OF FRENKEL DEFECTS ON IONIC CONDUCTION  
AND BULK MODULUS OF  $\text{SrCl}_2$  AND  $\text{PbF}_2$ .

Sujata Ghosh <sup>1)</sup> and Mohua Makur <sup>2)</sup>

1) Physics Department, B.K.C. College, Calcutta-700035, INDIA.

2) Physics Dept., Jadavpur University, Calcutta-700032, INDIA.

The superionic halides with fluorite structure ( $\text{SrCl}_2$ ,  $\text{PbF}_2$ ,  $\text{CaF}_2$  etc) show anomalies in properties such as specific heat ( $C_V$ ), thermal expansion ( $\alpha_T$ ) bulk modulus ( $\beta$ ) and have very high ionic conductivities ( $\sigma$ ) at high temperatures. These peculiarities are attributed to the presence of Frenkel defects.

A phenomenological model treating the crystal as a collection of two-level systems (TLS) can explain the  $C_V$ -T,  $\alpha_T$ -T and  $\sigma$ -T curves qualitatively. The present work shows that an extension of the model can reproduce the  $\beta$ -T curve and the pressure dependence of  $\sigma$  for  $\text{SrCl}_2$  and  $\text{PbF}_2$ .

Physically, the TLS are groups of  $N_C$  ions each which form a defect-cluster on introduction of one or more Frenkel defects. The energy gap (E) between the two levels is the difference between the energy in the perfect crystal state and the energy in the defect-cluster configuration.

$C_V$  calculated from the partition function for the crystal gives a peak at a temperature  $T_C$ .  $T_C$ ,  $N_C$  and E are obtained from a best-fit of the  $C_V$ -T curve.  $N_C$  agrees with cluster sizes suggested by neutron diffraction studies [1].

$\sigma$  is calculated assuming a percolation mechanism, considering the 'excited' TLS to be conducting regions in a non-conducting matrix of ground state TLS.  $\sigma$  is given by

$$\sigma = \sigma_0 (n_f - n_c)^{1.5} \dots (1)$$

where  $n_f$  = fraction of excited TLS and  $n_c$  = concentration threshold of conducting regions where percolation starts, here 0.33.

It is further assumed that excited TLS have a volume  $v + \Delta v$ , larger than the volume  $v$  of ground state TLS.  $\Delta v/v$  is chosen so

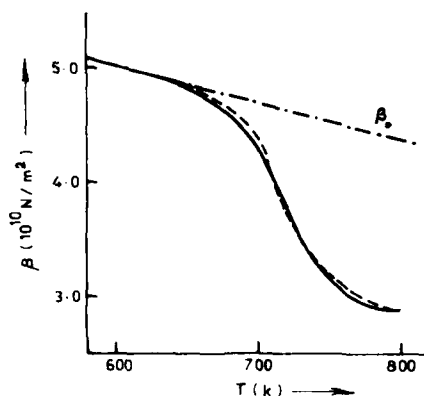


Fig.1.  $\beta$  for  $\text{PbF}_2$ .  
(— expt, ---- calculated).

From (1)

$$\gamma = \frac{1.5}{n_f - n_c} \cdot \frac{\partial n_f}{\partial P} \quad \dots \quad (3)$$

calculated from (2) shows excellent agreement with the experimental curve for  $\text{PbF}_2$  [3] as shown in fig. 1. Similar results are obtained for  $\text{SrCl}_2$ .

The value of  $\gamma$  used is -2.5 which agrees with the experimental value which is  $\sim -2$ .

The TLS model is thus capable of giving a unified picture of different anomalous properties of the superionic fluorites.

- [1] M.T. Hutchings, K. Clausen, M.H. Dickens, W. Hayes, J.K. Kjems, P.G. Schnaball and C. Smith, J. Phys C17, 3903 (1984).
- [2] G.A. Sanara, J. Phys.Chem. Solid 40, 509 (1979).
- [3] M.O. Manasreh and D.O. Pederson, Phys Rev B30, 3482 (1984).

as to fit the  $\alpha_T$ -T curve.

Pressure dependence of  $\sigma$  shows that  $n_f$  decreases with pressure [2]. From our model the bulk modulus is given by

$$\beta = \frac{\beta_0}{1 + \frac{\Delta v}{v} n_f - \beta_0 \frac{\Delta v}{v} \frac{\partial n_f}{\partial P}} \quad \dots \quad (2)$$

$\beta_0$  being the bulk modulus without the TLS contribution.

According to experimental results  $\frac{\partial \ln \sigma}{\partial P} = \gamma$  (a constant).

CALCULATED DEFECT PROPERTIES AND SUPER-IONIC TRANSITION IN  $\text{Li}_2\text{O}$ 

N.L. Allan, W.C. Mackrodt and S. Rimmington  
ICI Chemicals & Polymers Ltd., P.O. Box 8,  
The Heath, Runcorn, Cheshire WA7 4QD, England

Over the past few years, advances in atomistic simulation techniques, particularly for ionic and quasi-ionic materials, have enabled the calculation of an increasingly wide range of solid state properties. This paper is concerned with the temperature-dependent defect structure of anti-fluorite  $\text{Li}_2\text{O}$  and the prediction of a super-ionic transition involving the lithium sublattice.

As in a previous study [1], the theoretical methods comprise a combination of lattice statics and dynamics based on two sets of interatomic potentials, one empirical and the other derived from electron-gas theory [2]. The lattice expansion is calculated self-consistently within a quasi-harmonic approximation [1] and from this, the free energies of formation and migration of the fundamental lattice defects are calculated as a function of temperature. It is shown that at approximately 1250 K both the formation and migration free energies of lithium vacancies decrease to zero, thereby indicating a fast-ion transition at this temperature. Also considered in this paper are the association energies to di- and tri-valent dopants. Comparisons are made with experimental diffusion and conductivity data resulting in good agreement with both sets of interatomic potentials.

- 1 N.L. Allan, M. Leslie and W.C. Mackrodt, Adv. in Ceramics **23** (1988).
- 2 W.C. Mackrodt and R.F. Stewart, J. Phys. C**12**, 431 (1979).

CALCULATED TEMPERATURE-DEPENDENCE OF LATTICE AND IMPURITY MIGRATION IN MgOJ.C.G. Carroll<sup>(a)</sup>, J. Corish<sup>(a)</sup> and W.C. Mackrodt<sup>(b)</sup>

(a) Department of Chemistry, Trinity College,  
Dublin 2, Ireland

(b) ICI Chemicals and Polymers Ltd., P.O. Box 8,  
The Heath, Runcorn, Cheshire WA7 4QD, England

A major development in the atomistic simulation of ionic materials in recent years has concerned the self-consistent treatment of temperature effects both for the perfect and defective lattice. This has enabled detailed comparisons of calculated defect energies to be made with high temperature experimental data: these are particularly important in the case of ceramic materials. This paper is concerned with the calculated temperature-dependence of lattice and impurity migration in MgO and with such comparisons that can be made with experiment.

Two sets of interatomic potentials, one empirical the other non-empirical, are considered, as in a previous study of impurities in MgO [1]. These are then used to calculate the expansion coefficient, ie the temperature-lattice parameter relationship, of MgO within a quasi-harmonic approximation [2]. Next, the migration energies of the host ions are calculated as a function of temperature (lattice parameter), including vacancy, interstitial and neutral vacancy and interstitial pair migration. Finally, the migration of di-, tri- and quadrivalent impurities will be examined. Among the points that will be considered in detail are why migration energies calculated at absolute zero accord with activation energies derived from high-temperature experimental data and the contribution that the temperature coefficient of the migration energy makes to the pre-exponential factor.

1. J.C.G. Carroll, J. Corish, B. Henderson and W.C. Mackrodt, J. Mat. Sci. (1988) - In press
2. N.L. Allan, M. Leslie and W.C. Mackrodt, Adv. in Ceramics 23 (1988)

COHERENT NEGATIVE PHOTOVOLTAIC CURRENT AND POLAR  
DOMAIN INSTABILITY IN DOPED INSULATORS

N. Kristoffel

Institute of Physics, ESSR Academy of Sciences,  
202400 Tartu, Riia 142, USSR

Polar domain structure formation in ruby samples under laser illumination has raised the problem of negative photovoltaic conductivity in a centrosymmetric crystal [1]. In non-centrosymmetric crystals (ferroelectrics) a negative (opposite to the electric field) bulk photovoltaic current is well known. A coherent mechanism for this phenomenon was proposed originally in [2,3]. The corresponding direct current ( $j$ ) is generated by a nonlinear quantum interference process of several real and virtual transition channels. The characteristic time for this mechanism is the phase relaxation time\*. Another effect of second order in the light-matter interaction is the well-known optical rectification. The corresponding electronic polarization equals  $\mathcal{P} = \eta^{-1} j$  [4], where  $\eta$  is the inverse relaxation time. The  $\mathcal{P}$  is a nondissipative quantity;  $j \neq 0$  is assisted by energy absorption.

The negative photovoltaic conductivity may be generated in an impurity doped centrosymmetric crystal in an external electric field ( $\vec{E}$ ) by the coherent mechanism mentioned [5]. The use of impurities allows to induce this current in a spectral region where the usual photoconductivity is negligible. A general formula for the  $j$  is obtained, from which it is evident that with a suitable energy level scheme  $j < 0$  becomes possible.

We consider in more details a model consisting of two impurity levels of the same symmetry on both sides of a valence

---

\*The ballistic current component is directly connected with the momentum relaxation times.

band, which combine with the band states. A negative  $\vec{j} = -\sigma(I)\vec{E}$  of observable magnitude ( $I$  is the light intensity) is obtained at the frequency of the intra-impurity transition, which now becomes allowed.

This current is accompanied by the polarization  $\vec{P} = -\lambda(I)\vec{E}$ ,  $\lambda = \sigma\eta^{-1}$  increasing the crystal free energy by the amount  $\lambda E^2$ . As a result the crystal lowers its free energy by dividing into opposite electric domains.

1. S.A.Basun, A.A.Kaplyanskii, S.P.Feofilov, Zh. ETF, 87, 2047 (1984).
2. N.Kristoffel, A.Gulbis, Proc. Acad. Sci. ESSR, Phys. Mathem., 28, 268 (1979).
3. R. von Baltz, W.Kraut, Phys. Rev., 19B, 1548 (1979).
4. N.Kristoffel, A.Pishchev, Optics Commun., 62, 108 (1987).
5. N.Kristoffel, Solid State Commun., 55, 919 (1985).

LOW-TEMPERATURE ANOMALY OF DISLOCATION MOBILITY  
IN PURE AND DOPED ALKALI-HALIDE CRYSTALS

Yu.S.Boyarskaya, D.Z.Grabko, R.P.Zhitaru

Institute of Applied Physics, Moldavian Academy  
of Sciences, Grosul Str.5, 277028, Kishinev, USSR

The investigation of the dislocation ensemble mobility in the stress field of a concentrated load was performed in alkali-halide crystals (KCl, NaCl, NaF, LiF) and MgO. NaCl crystals, doped by different types of impurities ( $\text{Ca}^{2+}$  - a well dissolving, hole-accepting impurity, and  $\text{Pb}^{2+}$  - a poorly dissolving, electron-accepted impurity), were chosen for the study of the point defect influence on the peculiarities of the dislocation motion. The length of the dislocation ensemble track  $\ell$  or the parameter  $\gamma = \ell/d$  ( $d$  - the size of the indentation diagonal) were taken as a measure of the dislocation mobility.

An interesting phenomenon was observed for all the crystals under investigation - the significant crystal hardening (the rise of the microhardness  $H$  and critical resolved shear stress  $\sigma$ ) in the lowering of the deformation temperature from 293 to 77K was followed, as a rule, by the increase of the dislocation ensemble mobility, but not by its decrease. The

T A B L E

The change of the dislocation mobility and microhardness for the ionic crystals due to the temperature lowering

Cry-: The (001) plane: The (111) plane stal: $H_{77}/H_{293}$ : $\ell_{77}/\ell_{293}$ : $H_{77}/H_{293}$ : $\ell_{77}/\ell_{293}$				
NaCl	4,10	1,60	2,50	1,14
LiF	2,00	1,20	3,70	1,19
MgO	1,60	0,95	1,30	0,87

table lists the results for three crystals. As it is seen, the effect is somewhat more pronounced in the (001) indentation as against the (111) one. The clear de-

pendence of the effect intensity on the crystal microhardness is observed for the first plane (microhardness rises in the NaCl-LiF-MgO series). The low-temperature anomaly of the dislocation mobility was also observed for the doped crystals,

containing a different impurity concentration. It was more distinct in NaCl:Pb than in NaCl:Ca (Fig.). Such a situation

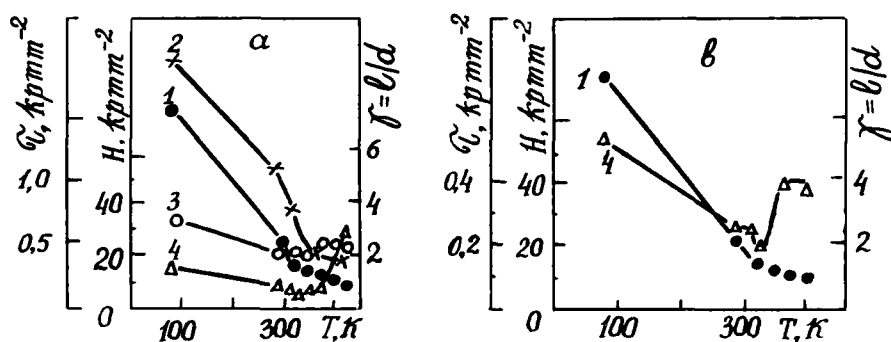


Figure. Temperature dependences of microhardness (1), critical resolved shear stress (2), mobility of edge (3) and screw (4) dislocations for NaCl:Ca (a) and NaCl:Pb (b) crystals. The impurity concentration  $C \approx 10^{-2}$  mol.%

seems to take place due to a different impurity state in crystals under investigation. Not only the dislocation mobility but also the regularities of the dislocation distribution near the indentation were affected by the impurity type. It was reflected especially clearly for the (111) plane.

It is of interest to clear up the reason of an anomalous behaviour of the dislocation in the stress field of a concentrated load because in these crystals an usual situation takes place for the individual dislocation - the dislocation mobility decreases by the temperature lowering from 293 to 77K [1,2]. At present we suggest the hypothesis about the impulse process of the dislocation structure formation for an indentation time [3]. It explains the low-temperature anomaly of the dislocation mobility in the stress field of a concentrated load.

1. Gutmanas E.L. J. Physiq., 32, Suppl. N12, C7 - 595 (1976).
2. Appel F. et al. Phys. Stat. Sol. (a), 83, 179 (1984).
3. Boyarskaya Yu.S., Grabko D.Z., Kats M.S. Physics of the microindentation processes (In Russian). Kishinev (1986).

# THE CHANGE IN THE DEFECT STRUCTURE AND MECHANICAL PROPERTIES OF LiF CRYSTALS IN THE PROCESS OF POSTRADIATION ANNEALING

M.V.Galustashvili, D.G.Driyaev, Z.K.Saralidze

Institute of Physics, Academy of Sciences of the Georgian SSR

Tbilisi 380077, USSR

The evolution of the basic mechanical characteristics of neutron-irradiated LiF crystals (yield strength, maximum plastic deformation and specific energy of the crystal destruction  $W$ ) in the process of postradiation annealing and its relation with the structural changes in the crystal at its thermal treatment are investigated.

It is shown that at any neutron fluence in the temperature range of the annealing of vacancies and their small complexes (150-400°C),

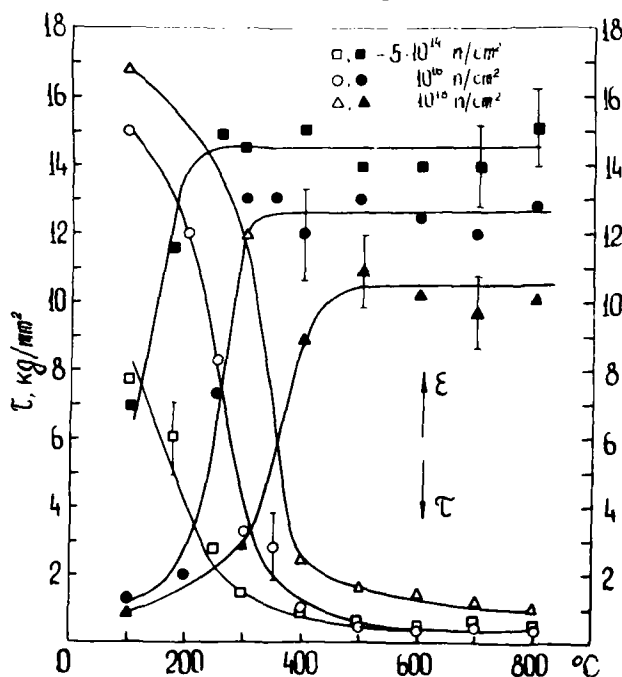


Fig.1

the recovery of the mechanical characteristics of the crystal takes place (Fig.1). Above 400°C the density of dislocation loops in the crystal volume (observed by etch pits) increases sharply, the loops being also annealed with the increasing temperature. In the crystal irradiated to a high neutron fluence

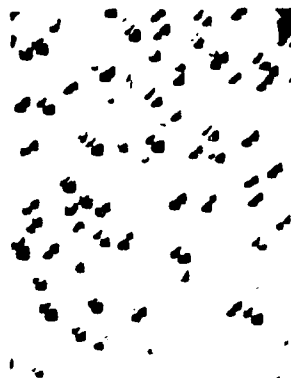


Fig. 2a



Fig. 2b

( $10^{18}$  n/cm<sup>2</sup>), gaseous pores are growing, which represent potential sources of the destruction and cause a comparatively low plasticity of the crystal.

To establish the nature of the dislocations formed in the irradiated crystals, the method of joint action of the temperature field and mechanical load (uniaxial compression along  $\langle 100 \rangle$  in the region of the crystal yield strength) upon the crystal was used.

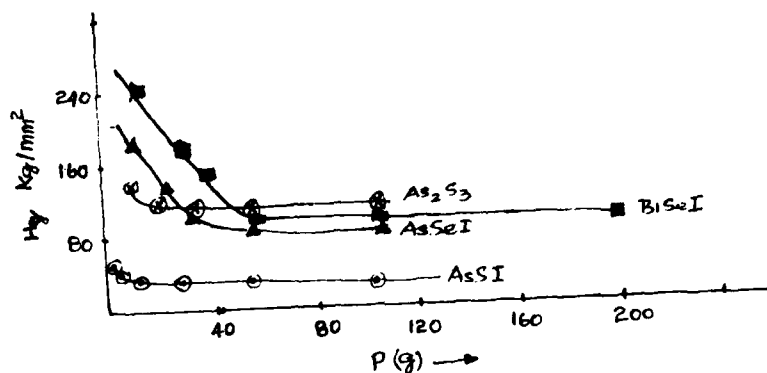
Etch patterns of the crystal surfaces treated in such a way show that paired etch pits orientated preferentially along  $\langle 110 \rangle$  appear in the planes perpendicular to the load (Fig. 2a), while those orientated along  $\langle 100 \rangle$  - in the plane parallel to the load (Fig. 2b).

The critical analysis of the etch patterns and simultaneous calculations of the orientational dependence of the interaction energy of dislocation loops with the elastic field generated by the load allow us to conclude that the observed dislocations are prismatic dislocation loops of the interstitial type formed at the expense of the condensation of the radiation point defects.

Microindentation studies of some chalcogenide glasses

D. Arivuoli, F.D. Gnanam and P. Ramasamy  
Crystal Growth Centre, Anna University, Madras-600 025, India.

Glasses of  $\text{As}_2\text{Se}_3$ ,  $\text{AsSI}$ ,  $\text{AsSeI}$  and  $\text{BiSeI}$  have been prepared by quenching method. These compounds readily form glasses and hence the difficulty in growing single crystals by any method. But there are reports regarding the crystallization of glasses like  $\text{AsTeI}$  [1]  $\text{AsSeI}$  [2] as polycrystals. Vicker's microhardness studies have been done using a specimen of size 5 mm x 5 mm x 5 mm. The loads have been varied from 2 g to 200 g, for a constant time of indentation (10 seconds). For all glasses, the microhardness is found to decrease with increases of load as shown in figure.



Using Meyer's equation  $P = kd$  (where  $P$  is the load in Kg,  $d$  is the diagonal length in mm and  $n$  is the work-hardening coefficient) the value of  $n$  is found to be less than 2. It is interesting to note that the Heys and Kendals [3] idea of resistance pressure to crystal specimen is also found to be

applicable for these glasses. A plot of band gap of these glasses and micro-hardness value is found to lie in a straight line and this empirical relation will be very much useful in determining the band gap of the other chalcogenide glasses.

References:

- [1]. R. Kniep and H.D. Reski, *Angew. Chem.* 20 (1981) 212.
- [2]. D. Arivuoli, F.D. Gnanam and P. Ramasamy, *J. Crystal Growth*, 1988, to be published.
- [3]. C. Hays and E.G. Kendal, *Metallography*, 6 (1973) 275.

FORMATION OF DERESSED MACROSPIRALS IN THE  
FLUX GROWN YAG CRYSTALS

M. THIRUMAVALAVAN, J. KUMAR\*, F.D. GNANAM\*\* and  
P. RAMASAMY

CRYSTAL GROWTH CENTRE, ANNA UNIVERSITY, MADRAS 25. INDIA.

The existence of spirals on habit faces of many crystals have been reported by several investigators. Frank(1) proposed a growth theory based on spiral growth. He suggested that the spiral growth is due to the presence of screw dislocations. But experimentally observed spirals are often not in the order of unit cell dimensions, but may be built up to the dimension of 100 to 1000 unit cells. A qualitative theory for such macrospiral formation is still lacking. Lang(2) proposed a theory stating that a "BLUFF" could be the cause for their formation. Arora et al(3) discussed the formation of macro spirals on Barium Molybdate. The YAG single crystals were grown from the typical 0.41 BaO - 0.41 B<sub>2</sub>O<sub>3</sub> - 0.18 BaF<sub>2</sub> flux composition. The stoichiometric composition of Y<sub>2</sub>O<sub>3</sub> and Al<sub>2</sub>O<sub>3</sub> is charged in a 40ml Platinum crucible with the proper amount of flux. The crystal is grown using slow cooling technique. Some of the obtained crystals are platelets. Microscopic observation reveals a few of these crystals exhibiting spirally depressed pattern. These spirals are initially in Rhombus like shape and in the process of spreading two of the edges get truncated and give rise to final closed hexagonal shape. The microscopic observation supports the theory of formation of large single step which is due to crowding or bunching of individual hundreds of steps. According to Frank(1) the spiral may be born at the sites of screw dislocation. The crystal is etched with hot phosphoric acid to clarify the origin of the spiral. After etching it was observed that the etch pits were spread all over the face, with no pit at the centre. Hence, other possible mechanism and the reasons for the generation of these macro spirals will be discussed. Possible reasons for the truncation of initial shape will also be discussed in detail. It is concluded that the observed macro spirals are growth defects which are mainly due to the fluctuations of the growth conditions.

References:

- (1) F.C. Frank, Diss. Faraday Soc., 5 (1949) 48
  - (2) A.R. Lang, J. APPL. Phys., 28 (1957) 497
  - (3) S.K. Arora and G.S. Trivikrama Rao, J. Cryst. Growth, 53 (1981) 627
- 

Present Address:

\* MASPEC-CNR, PARMA, ITALY.

\*\*INSTITUT FUR KRISTALLOGRAPHIE, KOLN, WEST GERMANY.

STRAIN - AGEING EFFECTS IN PURE AND DOPED SILVER HALIDE CRYSTALS.

J.A. BELLIS &amp; M.T. SPRACKLING

DEPARTMENT OF PHYSICS, KING'S COLLEGE LONDON, STRAND, LONDON WC2R 2LS, U.K.

Most crystalline materials deform plastically by the movement of dislocations through them. An edge dislocation has an associated strain field which enables it to interact with other dislocations and point defects such as vacancies and impurities. To reduce this interaction energy, point defects diffuse to the neighbourhood of the dislocation line thereby forming an 'atmosphere' which prevents the dislocation from moving until the energy lost is replaced. The impurity is said to have pinned the dislocation.

The mechanical properties of these materials are governed mainly by the movement of dislocations and their interaction with point defects, which may be studied through strain - ageing experiments. The technique used in this type of experiment is to determine the change in hardness ( $\Delta\sigma$ ) of the material as a function of the ageing time ( $t_a$ ) following straining (Fig 1). From a plot of  $\Delta\sigma$  vs.  $\ln t_a$ , the ageing curve, the interactions encountered over a period of time can be identified. For a single crystal of zone - refined AgCl supplied by B.D.H. Ltd., U.K., the room temperature ageing curve is shown in Fig 2, and displays four regions. The hardening in region I of the curve is attributed to weak dislocation pinning by vacancies, which changes to a softening (region II) as the vacancies are absorbed into the dislocation core. In region III, there is a steady hardening of the material which results from the pinning of the dislocations by divalent metal impurities; in this region the Cottrell - Bilby  $t^{2/3}$  law is satisfied. With prolonged ageing (region IV) a saturation of hardening is encountered when most of the available impurities are locked in dense atmospheres, requiring new dislocations to be produced for deformation.

Pure silver bromide, prepared by precipitation from recrystallised silver nitrate supplied by Kodak Ltd., U.S.A ; and hydrobromic acid (Aristar quality) supplied by B.D.H., U.K.; was used to grow single crystals by a Bridgman technique. For silver bromide crystals, the dopant was added to the melt prior to crystal growth. The crystals were sectioned to produce specimens with a height to diameter ratio of 2:1 and their plane faces were mechanically and chemically polished. To reduce internal stresses that may

have been introduced during the growth and preparation, the specimens were annealed at  $380^{\circ}\text{C}$  for 24 hours and furnace cooled at a rate of  $1\text{ Kmin}^{-1}$ . Strain - ageing experiments, in compression, were carried out at room temperature ( $21^{\circ}\text{C}$ ) on pure silver bromide for ageing times ranging from 5 seconds to 9 days, and the material was found to soften continuously with increasing ageing time.

In photographic theory, an unexplained phenomenon is the change in photographic sensitivity of an emulsion caused by mechanical deformation, which is known as kink desensitisation. It has been found empirically that the sensitivity to kink desensitisation is considerably reduced by the addition of group VIII (platinum) metals, especially iridium, in the  $10^{-8}$  to  $10^{-4}$  molar range (1) (2). Room temperature strain - ageing tests on silver bromide single crystals with small additions of iridium are reported.

**Fig.1**

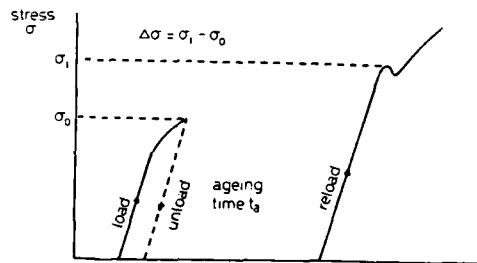
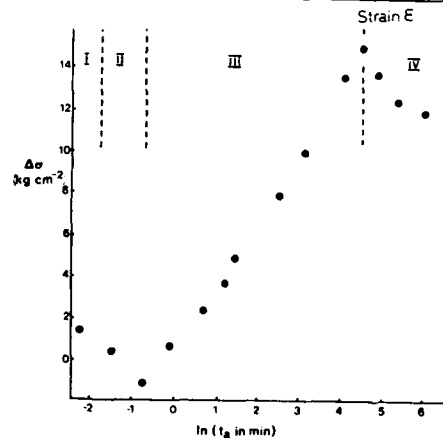


**Fig.2**



(1) British Patent 1,097,999 (1968)

(2) Carroll B.H Phot. Sci. Eng. 24 265 - 267 (1980)

CRACKS AND PLASTIC DEFORMATION IN AN INDENTATION IN  
MgO

MARIA ROSA DALMAU GARCIA  
 ESCOLA TECNICA SUPERIOR D'ARQUITECTURA DE BARCELONA  
 Av.Diagonal 649,08028 BARCELONA, SPAIN.

The aim of this paper is to attempt to find out how deformation and cracks are caused by indentation in a brittle material with a simple cristalline stucture in order to better understand the mechanism which causes the cracks under the surface to break out and chip the material when brittle material is indented several times in the same place (Vaughan, Guiu and Dalmau,1987).

EXPERIMENTAL

MgO monocrystals were indented by Vickers indentor with different loads and photographs of cracks and dislocation distribution at different depths taken. Indentator base diagonal was in  $\langle 100 \rangle$  direction. Dislocations were visualized by etching and layers of material extracted from the surface by chemically polishing the samples.

RESULTS

1- Three kinds of cracks exist:

- a) Cracks visible at surface level in a  $\langle 110 \rangle$  direction that lie in  $\{110\}$  plans and are very superficial (radial cracks)
- b) Cracks that start from areas near and under the indentator and spread upwards, without reaching the surface, and are not very deep either (lateral cracks)
- c) Cracks delimiting a more or less cylindrical area under the indentation which start very near the surface

and are deeper than a) and b) (median cracks). Their shape is not reproducible.

Lateral cracks are, without any doubt the ones that grow in repeated indentations and can lead to chipping of the material.

2- There are also different types of dislocations:

a) superficial dislocation loops lying in  $\{100\}$  planes perpendicular to the indentation surface. These are edge dislocations at the point of emergence.

b) Two assemblies of dislocation loops lying in  $\{110\}$  planes inclined at  $45^\circ$  to the indentation surface. They are helicoidal dislocations at the point of emergence. One of these loop assemblies goes three times deeper than the other.

c) Squares of dislocations with  $\langle 100 \rangle$  sides centered in the indent can clearly be seen in the surface. The most external of these has the radial crack as diagonals. Our results therefore do not disagree with the model proposed by Munawar (1986), in which lateral cracks are caused by dislocation intersection, but the large number of dislocations in the area do not permit us to affirm that the dislocations towards the surface is real.

3- The relation between indentator load (P) and crack length (c) was  $P = c^{3/2}$

#### REFERENCES

- M. Munawar Chaudhri, Phil. Mag. A 1986, 53, 4, L55-L63.  
D.A. Vaughan, F. Guiu, M.R. Dalmau, Jour. Mat. Sci. Let.  
6 (1987) 689-691

MICROSTRUCTURE AND PHYSICAL PROPERTIES OF YTTRIA-STABILIZED  
ZrO<sub>2</sub> (YSZ) DOPED WITH WO<sub>3</sub>

M. Hartmanová<sup>1)</sup>, F. Hanic<sup>2)</sup>, A.A. Urusovskaya<sup>3)</sup>, I. Travněc<sup>1)</sup>,  
 E. Morháčová<sup>1)</sup>, G.G. Knab<sup>3)</sup>

<sup>1)</sup> Institute of Physics, EPRC, Slovak Acad.Sci.,  
 84228 Bratislava, Czechoslovakia

<sup>2)</sup> Institute of Inorganic Chemistry, CChR, Slovak Acad.Sci.,  
 84236 Bratislava, Czechoslovakia

<sup>3)</sup> Institute of Crystallography, Acad.Sci.USSR,  
 117333 Moscow, USSR

Dependence of lattice parameter of YSZ on the type of solid solution and WO<sub>3</sub> concentration was analysed by X-ray diffraction method on the ceramic samples. The significant increase in lattice parameter of Zr<sub>x</sub>Y<sub>1-x</sub>O<sub>2-x/2</sub> solid solution after doping with 0.2 wt% WO<sub>3</sub> indicates the formation of interstitial solid solution. A satellite phase appeared in the X-ray record of the system with 0.5 wt% WO<sub>3</sub>. This fact is related with a decrease in the lattice parameter (Fig.1). The results of crystallo-chemical analysis were compared with the optical and mechanical characteristics of crystals. The changes of optical and mechanical properties caused by introduction of WO<sub>3</sub> were found in a good agreement with the predictions of crystallo-chemical analysis. Both intensity of absorption edge at  $\lambda = 245$  nm related to the oxygen vacancy concentration in the crystal and the absorption coefficient of absorption maximum at  $\lambda = 280 - 290$  nm due to WO<sub>3</sub> activator were used as the optical characteristics. The microhardness according to Wickers was used as mechanical characteristics of investigated material. It was found that the introduction of WO<sub>3</sub> caused plastification of YSZ due to structural changes of the doped crystals.

The ac complex impedance plots of ceramic and crystalline samples at different temperatures are discussed. The microstructure, grain size and grain distribution, is related to the chemical composition of investigated systems.

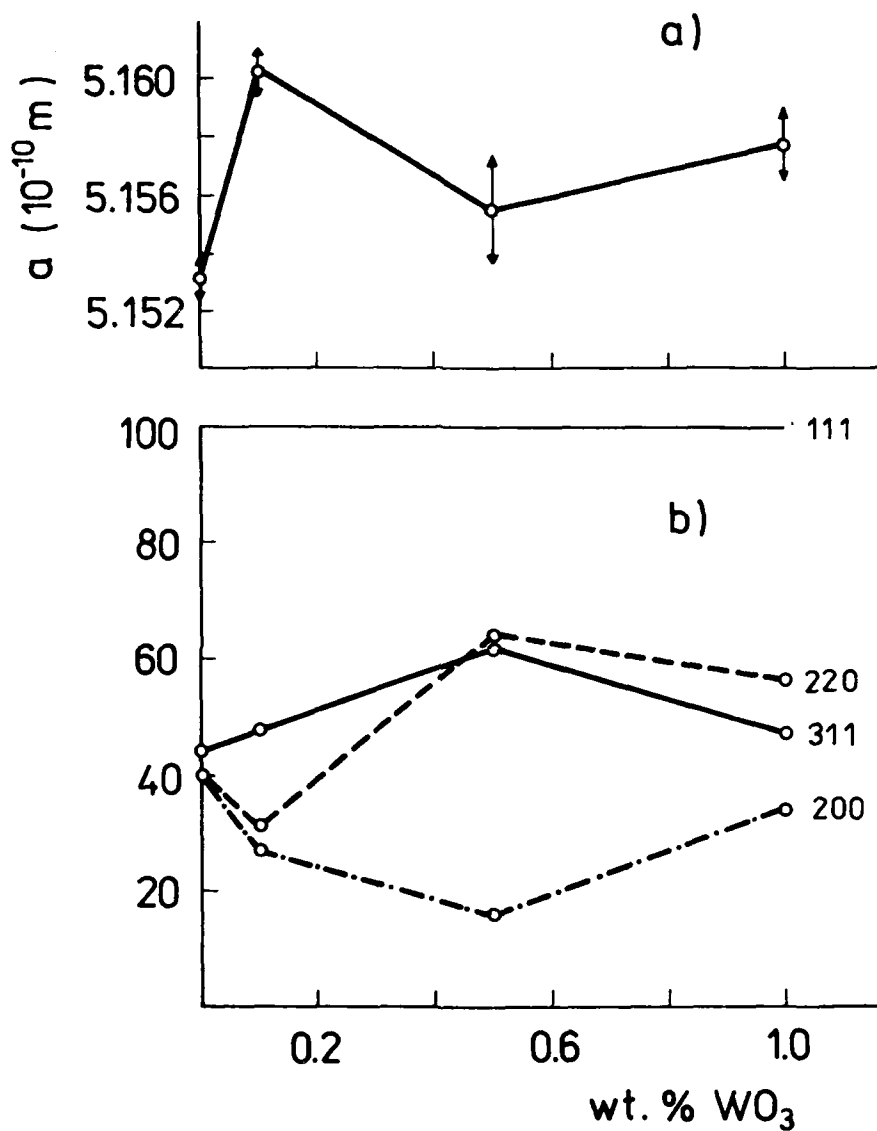


Fig.1 X-ray diffraction data on solid solutions in the system  $\text{Zr}_{0.85}\text{Y}_{0.15}\text{O}_{1.925} - \text{WO}_3$  : a) the change of the lattice parameter ; b) the change of intensities of selected X-ray diffractions

SEM , EDS & DISLOCATION ETCHING STUDIES ON FLUX  
GROWN SUBSTRATE CRYSTALS FOR LIQUID PHASE  
EPITAXIAL GROWTH OF HEXAFERRITE FILMS.

P.N.Kotru\*, F.Licci and G.Salviati  
 Istituto MASPEC - CNR , Via Chiavari 18/A ,  
 43100 Parma , Italy.

Single crystals of Ga and In doped hexaferrites of composition  $\text{Sr Ga}_x \text{In}_y \text{Fe}_{12-(x+y)}\text{O}_{19}$  (  $x = 5, 7, 9$  and  $y = 0.8, 1.3, 1$  ) were grown , using flux technique in order to obtain suitable substrates for the liquid phase epitaxial growth of hexaferrite layers. An idoneous substrate for epitaxial growth should have a high order of physical and chemical perfection , besides being isomorphous with the film to be grown and , as far as the specific case of hexaferrite is concerned, being non-magnetic at room temperature and having both a and c lattice constants matching those of the film as closely as possible <sup>1)</sup> . In order to test the physical perfection of such potential substrates , a few crystals were cleaved parallel to (0001) planes and their fractography was studied. Such an investigation gave the following results :

1. Comparison of the matched (0001) cleaved surfaces indicates that : (i) there is perfect correspondence between the cleavage lines on the two matched surfaces ; measurements on these lines demonstrate that a step-up on one corresponds to a step-down on the other, (ii) no part of the cleavage surface is normally chipped off over wide areas , (iii) the reflectivity of the cleaved surfaces is visibly quite high and (iv) the cleaved surfaces generally exhibit sharp cleavage steps, though there are areas which are reasonably flat. The observations indicate perfect (0001) cleavage in these materials.
2. (0001) surfaces were etched in hot phosphoric acid and they exhibit circular and pear-shaped pits. Results of experiments on successive etching , etching of matched cleavages and etching of grain boundaries suggest dislocations as the origin of point bottomed pits. Hot phosphoric acid was established as a dislocation etchant for these materials. In addition, it revealed other types of imperfections such as grain boundaries, cracks, twinning and superficial defects.
3. Beaked etch pits ( pear - shaped ) oriented at  $60^\circ$  and  $120^\circ$

with respect to each other were observed. They were suggesting a mis-orientation in different regions of the surface which can be attributed to some micro-twinning in the crystals ; the crystals being twinned with (0001) as the composition plane and  $[0001]$  as the axis of rotation. Etching of matched cleavages evidenced correspondence of mis-oriented regions, indicating deep penetration of such defects.

The dislocation densities were assessed and the morphological features of the dislocation etch pits studied by SEM.

Results of micromorphological investigations carried out by optical and scanning electron microscopy will be presented and compared. A classification of the revealed defects included spiral patterns , hillocks , cracks , cavities and micro-disc patterns. Presence of possible impurities and secondary phases was also investigated with the application of EDS technique .

#### Acknowledgements

One of the authors (P.N.Kotru) has carried out this work with the support of the " ICTP programme for training and research in Italian laboratories, Trieste, Italy".

#### References

1. F. Licci, S. Rinaldi and T. Besagini, Materials Letters, 1, ( 1983 ) 163.

---

\* Permanent address : Department of Physics, University of Jammu, Jammu- 180001, Jammu & Kashmir State, INDIA.

MICROHARDNESS MEASUREMENTS ON FLUX GROWN PURE, DOPED  
AND MIXED RARE EARTH ALUMINATE AND ORTHOCHROMITE  
CRYSTALS.

P.N.Kotru\*, Ashok K.Razdan  
Department of Physics, University of Jammu,  
Jammu-180001, Jammu & Kashmir State, India,

B.M.Wanklyn  
Department of Physics, Clarendon Laboratory,  
University of Oxford, Oxford, U.K.

Hardness is a complex property showing dependence on factors which control growth, structure and perfection of crystals, viz., temperature, composition and defects (such as dislocations, impurities and vacancies). The dependence of microhardness on load is an important property which needs to be thoroughly investigated in order to know about the laws governing the mechanical properties of materials. Kotru et al<sup>1-3</sup>) and Pratap and Haribabu<sup>4</sup>) showed that the microhardness follows Hays and Kendall's law<sup>5</sup>) However, their study was confined to pure crystals. It is interesting to investigate whether the law governing microhardness is applicable to doped and mixed crystals of rare earth aluminates and orthochromites. To understand this aspect of mechanical property, the indentation induced hardness testing studies were carried out on (i) pure rare earth aluminates ( $RAIO_3$ ,  $R=Eu, Gd, Dy, Er$ ) and orthochromites ( $RCrO_3$ ,  $R=Y, Gd, Yb$ ), (ii) doped rare earth aluminates and orthochromites ( $LaAlO_3$ , doped with  $Nd, Er, Yb$ ;  $EuAlO_3$  doped with  $Nd, Ho$ ;  $GdAlO_3$  doped with  $Er$  and  $YCrO_3$  doped with  $Er$ ) and (iii) mixed rare earth aluminates of the type ( $La_{1-x} : Pr_x$ )  $AlO_3$  where  $x = 0, 0.25, 0.75$  and  $1$ . The results of this investigation show the following:

1. Microhardness values of the rare earth aluminates and orthochromites range from 972 to 1809 and from 981 to 1532  $Kg\ mm^{-2}$  respectively at saturation values got from the curves of load versus vicker's hardness number.
2. The variations of microhardness with load are non-linear irrespective of whether the crystals are pure or doped rare earth aluminates or orthochromites, or mixed rare earth aluminate crystals of the composition ( $La_{1-x} : Pr_x$ )  $AlO_3$ , where  $x = 0, 0.25, 0.75$  and  $1$ .
3. Kick's law ( $P = K_1 d^n$ ) fails to explain the observed variat-

ions of microhardness value with load irrespective of whether the crystals considered are pure , doped or of mixed type . The hardness results are best explained on consideration of the idea of materials resistance pressure in the modified law proposed by Hays and Kendall (  $P - W = K_2 d^2$  ).

4. The hardness value depends on the composition of the parent material as well as the dopant entering into the crystal lattice. Doping does not increase the microhardness value in case of all the types of crystals . The addition of Nd,Er and Yb makes  $\text{LaAlO}_3$  crystals harder. Doping of  $\text{YCrO}_3$  with Er also hardens the crystal. Contrary to this , the microhardness values of the following crystals decrease : i)  $\text{ErAlO}_3$  doped with Nd or Ho and ii)  $\text{GdAlO}_3$  doped with Er.
5. The mixed crystals of the type (  $\text{La}_{1-x} : \text{Pr}_x$  )  $\text{AlO}_3$  are harder than the pure ones.

#### References

1. P.N.Kotru, K.K.Raina, S.K.Kachroo, B.M.Wanklyn, Jr. Mat. Sci. 19 (1984) 2582.
2. P.N.Kotru , B.L.Gupta, (1986) Unpublished.
3. P.N.Kotru , Anima Jain, A.K.Razdan, B.M.Wanklyn (1986) Unpublished.
4. K.J.Pratap and V.Haribabu, Bull. Mater. Sci., 2 (1980) 43.
5. C.Hays and E.G.Kendall, Metallography, 6 (1973) 275.

---

\* Present address (till Oct., 1988 ) : Istituto MASPEC -CNR, via Chiavari 18/A , 43100 Parma , Italy .

TWO-PARAMETERS DESCRIPTION OF  $\text{Eu}^{2+}$  DISTRIBUTION  
IN KCl SINGLE CRYSTAL

Marek Czapelski and Teresa Morawska - Kowal

Institute of Low Temperature and Structure  
Research, Polish Academy of Sciences  
50950 Wrocław, P.O. Box 937 (Poland)

The Pfann's theory describing one-dimensional distribution of the dopant along the crystal ingot grown from the melt anticipates, that the ratio of the dopant concentration in the liquid ( $c_L$ ) to that in the solid ( $c$ ) at the freezing is constant (expressed by the distribution coefficient,  $k = c / c_L$ ) during the whole crystallization process [1]. The comparison of experimental data with Pfann's theory (see for example [2]) shows, that this condition is not strictly fulfilled. This is particularly apparent at advanced stage of solidification, when  $c_L$  is drastically different from the initial dopant concentration in the melt ( $c_0$ ).

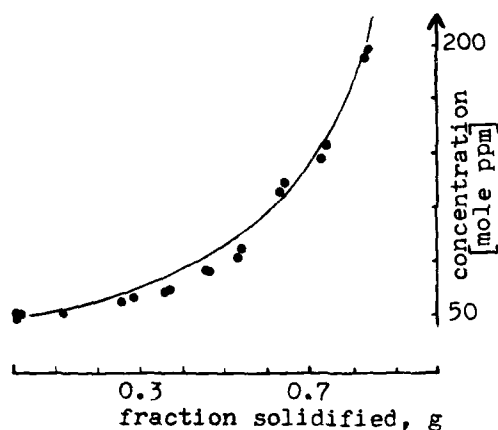
This paper presents a simple extension of Pfann's theory on the case of "variable" distribution coefficient. Its purpose is to describe the relation at the freezing interface by two constants,  $a$  and  $b$ , in the form  $c = a c_L^{1-b}$ . For  $b=0$ , this relation is the same as proposed originally by Pfann ( $a=k$ ).

In consequence, for homogeneous distribution of dopant in the molten part of the ingot, the following equation describing concentration along the crystal is derived:

$$c = \begin{cases} k c_0 (1 - g)^{k-1} & , \text{ for } b = 0 \\ a \left[ a + (c_0^b - a)(1 - g)^{-b} \right]^{b/(1-b)} & , \text{ for } b \neq 0 \end{cases} \quad (1)$$

where  $g$  is the fraction of solidified part of ingot and varies from 0, for "pure" end, until 1, for "dirty" end of crystal.

From the analysis of the set of KCl crystals grown from the melt containing the initial europium concentrations,  $c_0$ , in the range of 10 - 1000 mole ppm, the empirical values of  $a = 1.4$  and  $b = 1/3$  were obtained. An example of complying of europium distribution, derived from eq. (1) with that measured for  $c_0 = 360$  ppm is shown in figure.



#### References:

- [1] W.G. Pfann: Zone Melting. New York, London: John Wiley and Sons Inc., Chapman and Hall Ltd. 1958
- [2] J. Hernandez A., W.K. Cory, J. Rubio O.: Jap. J. Appl. Phys., 18, 533 (1979)

GROWTH DEFECTS IN BARIUM-STRONTIUM;NIORATE CRYSTALS.

Yu.S.Kuz'minov, L.I.Ivleva, N.M.Polozkov  
 Institute of General Physics  
 Academy of Sciences, USSR  
 38, Vavilov street, Moscow, 117942, USSR

Crystals based on  $\text{Ba}_x\text{Sr}_{1-x}\text{Nb}_2\text{O}_6$  (BSN) solid solutions are of growing interest as suitable objects for fabrication of electrooptical modulators and devices for wave front conversion in dynamic holography. The major shortcomings of the crystals grown are optical inhomogeneity giving rise to residual light flux increase, laser beam scattering in the crystal bulk, and modulation instability.

Optical instability of BSN manifests itself in growth striations and a seeding rod passing along the whole crystal. The growth striations occur due to the melt composition fluctuations at the crystal-melt interface, in particular, the ratio of Ba and Sr ions changes. The methods of perfection of the crystal optical quality are reduced to the improvement of the melt temperature stabilization up to the level of  $\pm 0.1^\circ\text{C}$  and to the decrease of convective fluxes in the melt.

The seeding rod passes through the whole crystal along its central part and in the cross section it assumes the shape of a seeding crystal (triangle, square, circle).

Variation of vertical and radial temperature gradients does not virtually change the formation of the defect in a growing crystal. The defect develops at different shapes of the crystallization front. In our experiments crystallization front was either plane or slightly concave.

In the defect region one could observe the crystal enrichment with Ba ions and corresponding impoverishment in Sr.

For samples with  $x=0.5$  the change of the Ba/Sr ratio amounts to 3-4% and with  $x=0.25$  - 1-2%.

The defect region of crystals with high Ba content is more localized. If to take into account a considerable difference in Ba and Sr ions' radii which are equal to  $1.34\text{\AA}$  and  $1.12\text{\AA}$ , respectively, the reasons for the stresses and microsplittings emerging along the defect boundary become clear.

The composition change in the defect region is also indicated by the lattice parameter change. The "C" parameter changes by  $0.0014-0.0018\text{\AA}$  for  $x=0.5$ , which is manifested more smoothly compared to the Ba/Sr ratio change. In the defect region one could observe the lattice parameter decreasing, instead of increasing which could be expected when substituting Ba for Sr. The X-ray topograms taken at copper radiation also indicate the lattice parameter change in the defect region of crystals. In single crystals containing considerable amounts of impurity, the presence of dispersion separations of the second phase is possible due to decomposition of saturable solid solutions with the bulk cooling from the melt temperature. In etching these crystals there is observed the formation of a specific background of plane holes whose density may considerably exceed that of the etching dislocation holes.

The tetragonal-monoclinic modification phase transition ( $1320^{\circ}\text{C}$ ) may probably lead to falling out of the second phase responsible for optical inhomogeneities in BSN crystals.

## TIN OXIDES IN THIN FILMS

D. D. Nihtianova\*, S. K. Peneva and L. L. Petrov\*

\* Institute of Applied Mineralogy, Bulgarian Academy of Sciences, Rakovski 92, Sofia 1000, Bulgaria; Department of Chemistry, University of Sofia, Anton Ivanov 1, Sofia 1126

SEM (SEM-515, Philips), TEM (TEM-420, Philips), RHEED (EF4, Karl Zeiss Jena) and a thin film Mossbauer spectroscopy method (DSMS) were used to study single crystal islands in: (i) chemically vapour grown textured (200 - 10000Å) tin oxide films deposited on (111) Si, (100) NaCl, quartz glass (TOF-CVD); (ii) rate frequency sputtered polycrystalline 1000Å TOF deposited on quartz glass, borosilicate glass (TOF-RFS) and (iii) partly oxidized (200 - 1000Å) tin films.

The DSMS data showed that TOF grown at and above 400 - 450°C consist of tetravalent tin oxides. The RHEED data of TOF-CVD showed that the tin (IV) oxides had complicated textured superlattices. The TOF-RFS consisted of polycrystalline  $\text{SnO}_2$  (cassiterite) and textured  $\text{SnO}_2$  ( $\text{CaF}_2$  structure) [1]. The RHEED and TEM single crystal diffraction data were indexed by a local computer program [2] utilizing the crystal data of all known tin oxides and the related oxides of isomorphous with tin elements.

The existence of  $\text{SnO}_2$  ( $\text{CaF}_2$ ) and so far unobserved  $\text{SnO}_2$ , probably an analogue of the monoclinic  $\text{VO}_2$ , e.g. ( $\text{SnO}_2(\text{VO}_2)$ ), was confirmed with more than six reciprocal lattice projections (RLP). There are series of  $\text{SnO}_x$  structures, defined by two RLP and considered as analogues of nonstoichiometric  $\text{Ti}_n\text{O}_{2n-1}$  ( $n = 4$  to 9) [3,4] ( $\text{Sn}_n\text{O}_{2n-1}$ ). In these series some  $\text{SnO}_x$  phases can be considered as a brookite type  $\text{SnO}_2$  [5]. Other  $\text{SnO}_x$  phases are found to belong to the hexagonal and anatase types  $\text{SnO}_2$  [6,7].

Also some lower valency tin oxides - (SnO) 16 O,  $\text{Sn}_2\text{O}_3$  and  $\text{Sn}_3\text{O}_4$  were found.

References:

1. S. K. Peneva, R. K. Rudarska, D. D. Nihtianova and I. Avramov (1984). TSF, 112, 247.
2. J. Macicek, Computer program "EMS" (unpublished).
3. S. Andersson (1960). Acta Chem. Scand. 14, 1161.
4. L. A. Bursill and B. G. Hyde (1972). Progr. Solid State Chem. 7, 177.
5. V. Krasevec, A. Prodan, M. Hudomalj and S. Sulcic (1985). Phys. Stat. Sol. (a), 87, 127.
6. N. V. Belov (1976). "Ocherki Strukturnoj Mineralogii", "Nedra", Moscow, p. 30.
7. N. A. Dubrovskaya, D. A. Hramov and K. I. Tabelko (1987). Materials of the 13th scientific conference of the young scientists in University of Moscow, Ref. Zh., Phys. Chem., 10B 2016, Moscow.

# PHASE AND CHEMICAL INHOMOGENEITY OF $\text{PbMoO}_4$ SINGLE CRYSTALS

M.P.Tarasov, D.D.Nihtianova and M.N.Maleev

Laboratory of Electron Microscopy, Institute of Applied Mineralogy, Bulg. Acad. Sci., Rakovski str., 92, Sofia-1000, Bulgaria

$\text{PbMoO}_4$  single crystals grown along the [001] orientation by the Czochralski method [1] from a stoichiometric nutrient in the Institute of Applied Mineralogy were investigated by EPMA (SEM S15 Philips-WEDAX 3A), TEM (TEM-420 Philips), and RHEED (EF4, Karl Zeiss Jena).

The EPMA data showed a significant deviation of the Pb/Mo ratio from the stoichiometric  $\text{PbMoO}_4$  one, as well as a deviation of the final sum ( $\Sigma\text{PbO} + \text{MoO}_3$ , in wt %) from 100% in some point microanalyses. The most significant deviations were observed in the crystal circumference (excess of Mo up to 0.67 at%), the registered minimal  $\Sigma\text{PbO} + \text{MoO}_3$  being 90%. In the central part of the crystal the single point analyses fixed deviation in both directions to an excess (up to 0.46 at %) and an insufficiency (up to 0.15 at %) of Mo content. Simultaneously a deviation of the  $\Sigma\text{PbO} + \text{MoO}_3$  from 100% varied from 95-96 wt% at the top of the crystal to 99-100 wt% at its end. This is probably due to the presence of microcavities and microcracks which occur more frequently in both the upper part and circumference of the crystal than in its lower part.

The comparison of our data for Pb/Mo ratio with those of V.T.Gabrielian et al. [2] showed that the deviations of Mo content along the axis of crystal exceed the region of the homogeneous  $\text{PbMoO}_4$  in both directions (between +0.14 and -0.13 at%). A stable high Mo content deviation (up to +0.40 at%) was observed in circumferent crystal parts.

A regular changes in the crystal composition in the process of a crystal growth, consisting of Mo decrease at the end of the crystal are known [2]. In our case only a tendency of increase of Pb/Mo ratio was registered.

The EPMA data of the crystal suggest an existence of phase inclusions in its matrix. It was confirmed by SEM applied to natural, split or polished surfaces in the process of their aging. An appearance of particles with needlelike, irregular or dendritic shape, thin films and extrusive formations were observed. The TEM and RHEED analyses of the front of the crystallization, external and split surfaces of the crystal boule also showed the existence of different crystal inclusions in  $\text{PbMoO}_4$  matrix, which might be interpreted as  $\text{Pb}_2\text{MoO}_5$ , nonstoichiometric Mo oxides, and nonstoichiometric Pb oxides (scarcely spread).

References:

1. G. M. Loiacono, J. F. Balascio, R. Bonner, and A. Savage (1974). J. Cryst. Growth 21, 1-11.
2. V. T. Gabrielian, L. M. Fedorova, E. B. Tkachenko, A. Y. Neiman, N. S. Nikogosian (1986). Cryst. Res. Technol. 21(4), 439-448.

OXYGEN VACANCY ORDERING IN THE  $\text{BaFeO}_{3-y}$   
AND  $\text{Ba}_x\text{La}_{1-x}\text{FeO}_{3-y}$  SYSTEMS

J-C GRENIER, M. PARRAS\*, J.M. GONZALEZ-CALBET\*,  
M. VALLET-REGI\* and M. POUCHARD

Laboratoire de Chimie du Solide du CNRS,  
Université de BORDEAUX I, 33405 TALENCE-Cédex, FRANCE.  
(\*) Facultad de Ciencias Químicas,  
Dpto. Química Inorgánica  
Universidad Complutense, 28040-MADRID, SPAIN.

The non-stoichiometry phenomena have been studied in the perovskite-related ferrites of the Ba-La-Fe-O system using various techniques ( X-ray diffraction, HRTEM, Mössbauer spectroscopy.. ).

When lanthanum is lacking, - i.e. in the  $\text{BaFe}^{2+}\text{O}_3 - \text{BaFe}^{3+}\text{O}_{3-y}$  system -, the structure and the vacancy ordering of the  $\text{BaFeO}_{3-y}$  phases depend on the oxygen vacancy content (y) and correlatively on the  $\text{Fe}^{2+}/\text{Fe}^{3+}$  ( $\tau/1-\tau$ ) ratio directly related to the synthesis conditions (  $p\text{O}_2$ , T ). For  $y < 0.37$  the stacking is hexagonal leading to 12H and 6H non-stoichiometric perovskite-related structures since for higher values (  $y > 0.40$  ) it becomes cubic. The non-stoichiometry is accommodated through the formation of intergrowths or microdomains of four ordered phases. In the hexagonal-type structures the vacancies are rather randomly distributed when in the cubic-type domain, two well ordered phases appear for  $y = 0.49 \pm 0.44$  ( orthorhombic symmetry ) and for  $y = 0.50$  ( $\text{Ba}_2\text{Fe}_2\text{O}_9$ ). The monoclinic symmetry of the latter observed in electron diffraction patterns as well as its Mössbauer spectrum reveal a vacancy ordering more complex than that previously found in the well-known  $\text{A}_2\text{M}_2\text{O}_9$  brownmillerite structure. The vacancy ordering is discussed taking account of the various coordination of iron determined from Mössbauer spectroscopy results.

In the  $\text{LaFeO}_3$  -  $\text{Ba}_x\text{Fe}_{1-x}\text{O}_3$  system, four different phases which are metrically multiple of the perovskite cubic cell, appear as a function of the Ba/La ratio ( $x/1-x$ ). Their microstructure ranges from three-dimensional multitwinning as in  $\text{LaFeO}_3$  to the stoichiometric line phase  $\text{Ba}_x\text{Fe}_{1-x}\text{O}_3$ . The results are discussed on the basis of the ordering of the bigger cations (Ba or La) and of the anionic vacancies.

INHOMOGENEITIES AND THE SPURIOUS MODES IN GaYIG

E. Beregi, L. Fetter  
Research Institute for Telecommunications  
H-1026 Gábor Áron-u 65. Hungary

G. Nagy  
Research Laboratory for Geochemistry of the  
HAS, H-1112 Budapest, Hungary

and E. Pál  
Research Institute for Technical Physics of  
the HAS, H-1325 Budapest, Hungary

In this paper we report some experimental results on the influence of chemical inhomogeneities related to the growth technology on the spurious modes in GaYIG garnets.

The GaYIG crystals were grown from  $\text{PbO-PbF}_2\text{-B}_2\text{O}_3$  flux by cooling from  $1200^\circ\text{C}$  to  $1000^\circ\text{C}$ . The temperature gradient in the crucible was  $2^\circ\text{C/cm}$ , the cooling rate  $0.5\text{-}1^\circ\text{C/h}$ . Crystals of GaYIG were sliced parallel to their (211) planes and the cross sections were studied by double-crystal X-ray topography using  $\text{CuK}_\alpha$  radiation. Striations with various shade of contrast caused by composition inhomogeneities in the main components could be seen on the topographs.

After the X-ray topography the slices were cut to cubes ground by SiC and finally polished to spheres.

After magnetic and microwave measurements spheres exciting spurious modes "m" and spheres not exciting them "n" were chosen in order to study differences in their homogeneity by microprobe analysis. On each sphere a flat face of at least half of the spherical diameter was ground and polished and then examined in 15 different points.

Comparison of the concentration distribution on the samples "m" and "n" indicated an inhomogeneous

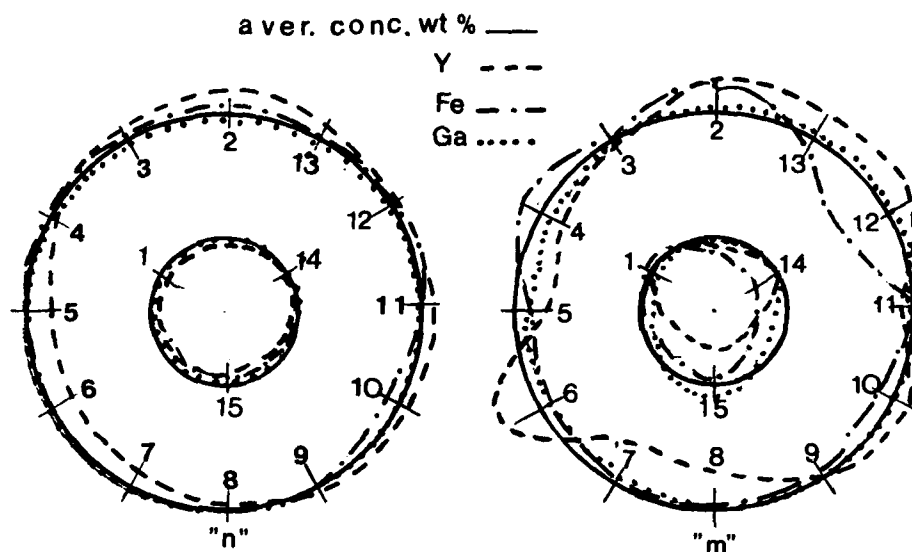


Fig.1. Deviation of the concentration in weight % from the average concentration of "m" and "n" types of GaYIG.

Distribution of  $\text{Fe}^{3+}$ ,  $\text{Ga}^{3+}$  and  $\text{Y}^{3+}$ -ions in the "m" sample in contrary to "n" (Fig.1.) and thus suggests that these inhomogeneities are responsible for the generation of spurious modes. These findings are in agreement with other results reported in [1,2]. The inhomogeneities of the crystals grown by the flux method were also compared with the inhomogeneities of crystals grown by the isothermal method.

#### Acknowledgements

We are grateful to Mr. Šrámek of Tesla, Prague, Czechoslovakia for the isotherm. grown GaYIG samples.

#### References

- [1] P. Röschmann and H. Dötach, Phys. Stat. Sol. (b) **82**, 11 (1977)
- [2] E. Beregi, L. Fetter, G. Nagy and E. Pál, Digests of the Badgastein Conference on Soft Magnetic Materials 8, 1987, Austria, p. 216.

# NONSTOICHIOMETRY DEFECTS IN $A^2B_2^3C_4^6$ COMPOUNDS

S.I.Radautsan, I.M.Tiginyanu, Yu.O.Derid

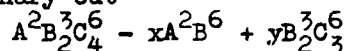
Institute of Applied Physics, Academy of

Sciences of the Moldavian SSR, 277028

Kishinev, USSR

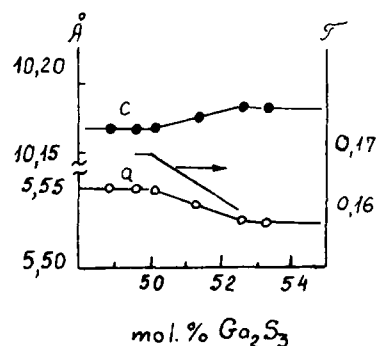
The results of the analytical studies of native defect composition in the wide band gap  $A^2B_2^3C_4^6$  compounds as well as of experimental research of the nonstoichiometry influence on their physical properties are presented. The composition of the samples has been changed when growing the single crystals by Bridgmen or chemical iodine transport techniques [1].

If one represents the ternary compounds as a composition of the quasi-binary cut



then the degree of the deviation from stoichiometry can be defined by the parameter  $\delta = \frac{x}{y} - 1$ . In this work  $B_A$  and  $A_B$  defects are shown to be the most probable ones in the crystals with stoichiometric composition. When deviating from stoichiometry  $B_A$  and  $V_A$  defects will predominate for  $\delta < 0$  whereas  $A_B$  and  $A_i$  ones - for  $\delta > 0$ .

Lattice parameters  $a, c$  and tetragonal compression degree  $\tau$  of cadmium thiogallate as a function of the crystal composition on the  $CdS-Ga_2S_3$  quasi-binary cut (close to the  $CdGa_2S_4$  homogeneity range).



The X-ray examination has shown the loosening of the crystal lattice for  $\delta < 0$  and the diminution of the tetragonal

compression degree  $\tau = 2 - \frac{c}{a}$  (c and a - elementary cell parameters). These results for  $\text{CdGa}_2\text{S}_4$  are presented in the Figure.

The luminescent properties of  $\text{A}^2\text{B}_2^3\text{C}_4^6$  compounds are found to be effectively controlled by the deviation of stoichiometry. It has been established, in particular, that the shorter wavelength luminescence is observed in the samples corresponding to  $\delta > 0$  as compared with  $\delta < 0$ . In some single crystals the narrow photoluminescence lines have been observed, that seems to be caused by stimulated radiation [2]. In the table the energy gap values  $E_g$  as well as the photoluminescence bands data at 80 K are summarised.

Compound	Space group	$E_g$ , eV	Luminescence bands, eV			
			$A_B$	$B_A$	$V_A$	
$\text{CdGa}_2\text{S}_4$	$S_4^2$	3,76	2,75	1,8	2,26	
$\text{CdIn}_2\text{S}_4$	$O_h^7$	2,62	1,77	1,3	1,45	
$\text{HgGa}_2\text{Se}_4$	$S_4^2$	2,10	1,74	1,2	1,30	

The slight dependence of the ternary compound dark resistivity upon crystal composition has been noticed. That behavior may be accounted for the self-compensation defect model. The nature of the quasi-continuously distributed electron states in  $\text{A}^2\text{B}_2^3\text{C}_4^6$  compounds is being discussed.

#### REFERENCES :

1. Radautsan S.I., Georgobiani A.N., Tiginyanu I.M. - Progr. Cryst. Growth and Charact., 1985, v.10, N 1-4, p. 403-412.
2. Derid Yu.O., Georgobiani A.N., Gruzintsev A.N., Radautsan S.I., Tiginyanu I.M. - Cryst. Res. Technol., 1985, v.20, N°6, p. 857-861.

SOME CONNECTIONS BETWEEN LUMINESCENCE PROPERTIES AND  
LATTICE POINT DEFECTS IN  $Y_2SiO_5:Tb^{3+}$

R. Morlotti, A. Viglienzoni - 3M Italia Ricerche SpA,  
I-17016-Ferrania

S. Kemmler-Sack, J. Reichardt - Institut of Inorganic  
Chemistry, Eberhard-Karl Univ., D-7400 Tübingen 1

$Y_2SiO_5:Tb^{3+}$  phosphors are known to emit in the UV-green spectral range under UV, cathodic or X ray exposure. We have prepared them by usual solid state methods, obtaining the known crystal structure monoclinic  $X_2$ -type, with space group  $I2/c$ . Samples prepared with a slight defect or excess of silica, i.e. about 3 p.c. by weight in both cases, show the same structure with no presence of other phases. Diffuse reflectance spectra (fig. 4), cathodoluminescence spectra (fig. 1), thermoluminescence curves from r.t. to 300°C (figs 2, 3; table 1) and electrical conductivity from 500 to 1100°C, oxygen partial pressure from 1 to  $10^{-5}$  Atm, were used to relate the luminescence properties to the supposed lattice defect situation. Making reference to published point defect equilibria concerning silicatic structures (1, 2, 3), the following have been assumed in the present case: I. Defect of silica;  $Si_{Si}^{x} + 2O_{O}^{x} \rightarrow V_{Si}^{m} + 2V_{O}^{x} + SiO_2$  (1)

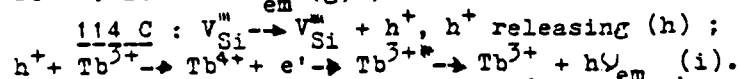
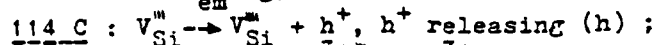
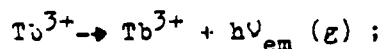
II. Excess of silica;  $SiO_2 \rightarrow Si_{Si}^{x} + 2V_{Y}^{m} + 3V_{O}^{x} + 2O_{O}^{x}$  (2), or

$SiO_2 + O_2 \rightarrow Si_{Si}^{x} + 2V_{Y}^{m} + 6h^{+} + 4O_{O}^{x}$  (3), or

$SiO_2 + Si_{Si}^{x} + O_2 \rightarrow 2V_{Si}^{m} + 6h^{+} + 2Si_{Y}^{x} + 4O_{O}^{x}$  (4), where

$Si_{Si}^{x}$ ,  $O_{O}^{x}$ ,  $V_{Si}^{m}$ ,  $V_{O}^{x}$ ,  $V_{Y}^{m}$ ,  $h^{+}$  indicate  $Si^{4+}$  and  $O^{2-}$  at normal lattice sites,  $Si_{Y}^{x}$ ,  $O_{O}^{x}$  and  $Y^{3+}$  vacancies,  $Si^{4+}$  on  $Y^{3+}$  sites, electron holes, respectively. If the electronic conductivity increases with the oxygen partial pressure - as we have verified - at a given  $SiO_2$  excess (in the solubility range) and Tb concentration, equilibria (3) or (4), rather than (2), must be supposed to control the defect situation. Considering the thermolum. curves, it appears further that eq. (1), with silica defect, and eq. (4), with silica excess are operative indeed, as they have in common the second main glow (at  $\approx 114^\circ C$ ), that could be referred to silicon vacancies. Taking into account the behaviour of  $Tb^{3+}$ , as luminescence activator in various hosts (4, 5, 6), the overall luminescence processes in  $Y_2SiO_5:Tb^{3+}$  from r.t. to those corresponding to the main glows (the related spectra show  $Tb^{3+}$  emission), can be schematized as follows:

Room temp.: cathodic (X)  $\rightarrow e' + h^{+}$  + thermal losses (a);  
 $h^{+} + Tb^{3+} \rightarrow Tb^{4+} + e'$ ,  $Tb^{4+} \rightarrow Tb^{3+} + h^{+}$  and  $e'$  capture sequence and  $Tb^{3+}$  excitation (b);  $Tb^{3+} \rightarrow Tb^{3+} + h\nu$ ,  $Tb^{3+}$  emission (c);  
 $h^{+} + V_{Si}^{m} \rightarrow V_{Si}^{m}$ ,  $h^{+}$  trapping (d);  $e' + V_{O}^{x} \rightarrow V_{O}^{x}$ ,  $e'$  trapping (e).  
 $95^\circ C$ :  $V_{O}^{x} \rightarrow V_{O}^{x} + e'$ ,  $e'$  releasing (f);  $e' + Tb^{4+} \rightarrow Tb^{3+}$



The outlined scheme evidences how the  $e', h^+$  pairs exciting the activators  $\text{Tb}^{3+}$  could be, in general, only a part of those disposable at the end of the avalanche process with which the absorbed primary energy is dissipated. A satisfying determination of the 'intrinsic conversion efficiency' (7, 8) of phosphors must take into account the stored energy, recoverable however by thermal or optical stimulation.

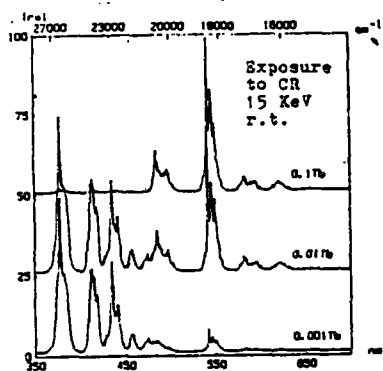


Fig. 1. Cathodoluminescence spectra

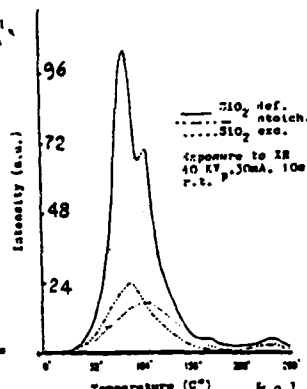


Fig. 2. Thermoluminescence vs  $\frac{[\text{Tb}^{3+}]}{[\text{SiO}_2]}$

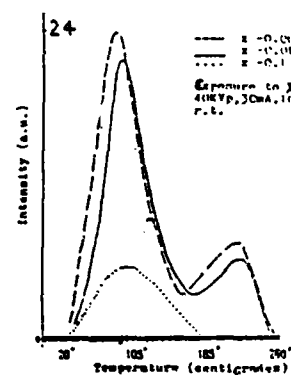


Fig. 3. Thermoluminescence vs Th conc

Y <sub>2</sub> SiO <sub>5</sub> :Tb <sup>3+</sup> <sub>x</sub>	Silica cont.		
	x	def.	sto. exc.
0.001		89 (100)	57 (40) 59 (30)
0.01		90	89 (36) 91
0.1		65	100 (11) 98

Table 1. Relative cathodolum. and thermolum. (in parenthesis) efficiencies. The two sets of values can not be directly quantitatively compared.

#### References :

1. R. Morlotti, G. Ottonello; Phys. Chem. Minerals, 8, 87 (1982)
2. R. Morlotti, G. Ottonello; Geochim. Cosm. Acta, 48, 1173 (1984)
3. P. Abelard, J. F. Baumard; J. Phys. Chem. Solids, 43, 617 (1982)
4. D. J. Robbins and others; J. Electrochem. Soc., 126, 1556 (1979)
5. D. Wolf, S. Kemmler-Sack; phys. stat. sol. (a), 98, 567 (1986)
6. L. Ozawa; J. Electrochem. Soc., 128, 140 (1981)
7. D. J. Robbins; J. Electrochem. Soc., 127, 2694 (1980)
8. G. W. Ludwig; J. Electrochem. Soc., 118, 1152 (1971)

NEAR-ELECTRODE REGIONS IN AN ELECTROCHEMICAL CELL  
OF  $\text{Ag/RbAg}_4\text{J}_5/\text{Me}$  TYPE AS STUDIED BY OPTICAL METHODS

A.V.Boris, S.I.Bredikhin, N.N.Kovaleva, N.V.Lichkova

Institute of Solid State Physics USSR Academy of  
Sciences, Chernogolovka, Moscow district, 142432,  
USSR

The photoluminescence technique was used to determine the concentration distribution of silver cations and vacancies in a  $\text{RbAg}_4\text{J}_5$  solid electrolyte being in contact with various electrode materials (Ag; Pt; C; Mo; W; etc). The photoluminescence spectra of near-electrode regions of  $\text{RbAg}_4\text{J}_5$  crystals exhibit increase in the intensity of band  $\lambda_{\text{PL}_3} = 455 \text{ nm}$  and decrease in the intensity of band  $\lambda_{\text{PL}_1} = 390 \text{ nm}$  as compared with the spectra of the central part of the sample. This evidences that the concentration of silver interstitial cations in the near-electrode regions is the higher, the larger the contact difference between the potentials of solid electrolyte and corresponding electrode. The measurements of the double layer voltage in the electrolyte-electrode boundary revealed the correlation between the voltage value and that of the electrode work function.

The applicability of the Hebb-Wagner polarization technique is discussed.

THE ELECTRICAL AND STRUCTURAL PROPERTIES OF TIN OXIDE

A.V. Chadwick, R.M. Geatches, J.M. Steele, J.D. Wright,  
University Chemical Laboratory, University of Kent,  
Kent, CT2 7NH, U.K.

S.J. Peacock, British Gas plc, London Research Station,  
Michael Road, London, SW6 2AD, U.K.

S.M. Tomlinson, Chemistry Department, University of Keele,  
Keele, Staffs, ST5 5BG, U.K.

Semiconducting metal oxides, e.g. tin oxide ( $\text{SnO}_2$ ) and zinc oxide ( $\text{ZnO}$ ) are widely used as sensors for hydrocarbons and reducing gases [1]. The basis of the operation of these sensors is effect of the gas on the surface electrical resistance of the oxide. The commercial gas detectors usually employ the oxide in the form of polycrystalline pellets, often doped with other metal oxides, and are operated at elevated temperatures, typically in the range 200 - 600°C. Two approaches have been adopted to enhance the selectivity of these detectors to particular gases. A common approach is to dope the oxide with metal cations. A more recent approach, which has proved very successful in the case of carbon monoxide sensing with  $\text{ZnO}$  [2], is to use single crystal oxides. We are currently investigating both these approaches to  $\text{SnO}_2$  sensors using well-characterized materials. In this contribution we will report the progress of this work with particular emphasis on  $\text{SnO}_2$  doped with Sb ions.

Polycrystalline samples of doped  $\text{SnO}_2$  were prepared by standard co-precipitation methods and prolonged heating in air at 1000°C [3]. Single crystals, typically 3 x 1 x 1 mm, were grown by the high temperature hydrolysis of  $\text{SnCl}_4$  [4]. It is possible to grow doped crystals by introducing volatile metal compounds into the  $\text{SnCl}_4$  stream, a technique which has proved particularly successful for Sb doped  $\text{SnO}_2$ . Structural characterization of the materials has been achieved by X-ray powder diffraction (XRPD) and extended X-ray absorption fine structure (EXAFS). The former technique was used to ascertain the solubility of the impurities in  $\text{SnO}_2$ . The EXAFS measurements allowed identification of the local environment of the

dopant ions. The electrical resistance of the samples has been determined as a function of temperature and in varying gas ambients in a computer-controlled test rig.

$\text{SnO}_2$  has been doped with Sb ions to levels of a few mole per cent and the XRPD measurements confirmed the samples were single phase. The effect of the dopant is to markedly decrease the room temperature resistance of  $\text{SnO}_2$ . The pure  $\text{SnO}_2$  crystals had resistances typically of  $10^8$  ohms which was reduced to around 1 ohm by doping with Sb at the level of 1 mole per cent. In addition, the resistance of pure  $\text{SnO}_2$  crystals was dependent on oxygen partial pressure; however, this dependence was decreased by the dopant. The dopant also altered the response of single crystal  $\text{SnO}_2$  sensors to gases. Pure  $\text{SnO}_2$  crystals were sensitive to methane,  $\text{CH}_4$ , and carbon monoxide, CO. However,  $\text{SnO}_2$  crystals lightly doped with Sb ions were selective to CO. These results will be discussed in the light of the structural information and possible mechanisms for the mode of gas detection.

#### References

- [1] Heiland, G., 1982, *Sensors and Actuators*, 2, 343.
- [2] Jones, T.A., 1982, *Sensor Review*, 4, 14; Bott, B., Jones, T.A. and Mann, B., 1984, *Sensors and Actuators*, 5, 65.
- [3] Egdell, R.G., Flavell, W.R. and Tavener, P., 1984, *J. Solid State Chem.*, 51, 345.
- [4] Nagasawa, M., Shinoya, S. and Makishima, S., 1965, *Jap. J. App. Phys.*, 1, 195.

A MODEL OF NEAR-UV-PHOTOEMISSION FROM CATION-VACANCY-  
-BONDED  $H_2O$  ON ALKALI FLUORIDE (100) FACES.

L. Ernst

Kali und Salz AG, Kaliforschungs-Institut, Hannover  
and  
Institut für Physikalische Chemie der  
Freien Universität Berlin, Berlin-West.

$LiF(100)$  (1) and  $NaF(100)$  crystal faces exposed to atmospheric air can adsorb small amounts of water at room temperature, which may give rise to photoemission upon near-uv excitation.

A model is proposed in order to explain why the threshold energy of this photoemission can be significantly lower than expected.

The sub-bandgap photoemission is ascribed to photon stimulated field ionization of  $H_2O$  molecules bonded to surface cation vacancies. The high electric field required for this process is the Coulomb field of the vacancy, enhanced by the effect of a lattice-depolarization through the  $H_2O$  dipole. It is calculated using the polarizable continuum approach with an estimation of the possible deviation from the exact value. One obtains excitation energy dependent field ionization rates, which yield photoemission thresholds in good agreement with the observed values.

The proposed model can also explain the observed exponential form of the yield function. However, it is not applicable to all types of sub-bandgap photoemission caused by extrinsic surface states on alkali halide crystals. For instance, it is thought that such states may often arise as a consequence of gas discharges occurring during crystal cleaving (2,3).

References:

- 1.) W.Pong, D.Paudyal, D.Brandt, J.Electron Spectr. 21(1980)261
- 2.) J.T.Dickinson, L.C.Jensen, A.Jahan-Latibari, J.Vac.Sci.  
Technol. A2(1984) 1112
- 3.) L.Ernst, Surface Sci. 176(1986) L825

PHOTOINDUCED PROCESSES IN ARSENIC AND  
ANTIMONY CHALCOGENIDES

V.Pashkevich, V.Gerbreder, A.Cvetkov

Daugavpils Pedagogical Institute  
228400 Daugavpils, 5 Augusta street 13,  
Latvian SSR, USSR.

Self-enhancement of holograms in  $\text{As}_2\text{S}_3$  films and photo-crystallization in  $\text{Sb}_x\text{Se}_{100-x}$  compositions were investigated. Presence of chalcogen atoms which have lone-pair electrons in arsenic and antimony chalcogenides results in forming defects accompanied by essential structural changes.

Self-enhancement was obtained in the following way. The initial holographic grating (HG) was recorded up to the small diffraction efficiency  $\eta_0 = (10^{-5} - 10^{-3})\%$ . This HG was then read by a single beam and the intensity of the diffracted beam which increases during readout up to the maximal value was measured. The self-enhancement (SE) magnitude was described by the  $k = \eta(t)/\eta_0$ , called SE factor, where  $\eta_0$  is the diffraction efficiency of HG at the beginning of readout ( $t = 0$ ), whereas  $\eta(t)$  is the same at the moment  $t$ . Recording and readout of the elementary HG were carried out at room temperature mainly by Ar laser (at light wavelength 514 nm and 488). The He-Ne laser has been used for readout in some experiments. The smaller is  $\eta_0$ , the larger is SE factor and it decreases with decreasing of recording-readout wavelength at the same  $\eta_0$ . It is possible to make recording of initial grating by  $\lambda = 514\text{nm}$  and readout by  $\lambda = 633\text{nm}$ . In this case  $k = 1600$  at  $\eta_0 = 10^{-5}\%$ . SE factor essentially depends on the period of HG. The maximum of SE factor is obtained at  $\Lambda = 1,5 \text{ mkm}$  independently on  $\eta_0$  using  $\lambda = 514\text{nm}$ . The SE phenomena have been observed only in as-evaporated  $\text{As}_2\text{S}_3$  films. It allows to assume that SE of HG is connected with non-reversible component of optical recording in As-S

films due to the forming of certain type of structural defects [1].

Experimental results of dependence of band-gap and refractive index on composition of antimony chalcogenides during crystallization under influence of light are discussed. Fig.1.

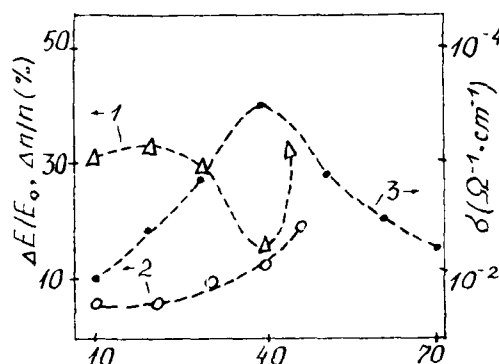


Fig.1. Relative changes of band-gap  $\Delta E/E_0$  (1) and refractive index  $\Delta n/n$  at transition from amorphous to crystalline state of  $Sb_xSe_{100-x}$  films (2) and (3) - conductivity of amorphous films versus  $x$ .

Photocrystallization of antimony sulphides begins after creation of certain concentration of electron-hole pairs  $n_0$  by light, where

$$n_0 = \frac{N\Delta E - E_k}{E_0 + 3\Delta E}$$

$N$  - number of electrons changing their energetical state due to crystallization (i.e. number of defects states);  $\Delta E$  - variation of band-gap;  $E_k$  - average value of vibrational energy of the system at definite temperature. Value for  $n_0$ ,  $\Delta E$  and  $E_g$  has been obtained from the experiment, assuming vibrational energy in the first approximation to

be  $E_k = \frac{1}{2} \sum M_i w_i^2 y_i^2$ , where  $y_i$  - normal mode of frequency  $w_i$ ,  $M_i$  - is mass factor. We obtained  $N \approx 10^{21} \text{ cm}^{-3}$ . This result is in accordance with the value obtained for As-Se compositions by other authors. There is a threshold of light intensity in  $Sb_xSe_{100-x}$  below which photo-induced changes do not occur. The mechanism of photostimulated changes in  $As_2S_3$  and  $Sb_xSe_{100-x}$  is discussed.

- 1) Yu.Ekmanis, V.Pashkevich, Ya.Teteris, Proc. conf. "Defects in Insulating Crystals", Riga, 1981, p. 362.

## LOW FREQUENCY RAMAN SCATTERING FROM METAL COLLOIDS IN NaCl

G. Mariotto, M. Montagna, G. Villani  
Dipartimento di Fisica, Università di Trento  
38050 Povo, Trento, Italy

E. Duval  
Physico-Chimie des Matériaux Luminescents  
Université Claude-Bernard, 69622 Villeurbanne, France

C. Mai  
Laboratoire GEMPPM, U.A. 341 C.N.R.S., INSA  
69621 Villeurbanne, France

Raman scattering from modes of colloids in NaCl shows a strong enhancement when the exciting light is resonant with surface plasmons of the metallic aggregates [1,2]. Completely different low-frequency spectra are observed depending on the aggregate nature. Silver aggregates give rise to well defined peaks as shown in Fig. 1, while sodium particles in the same spectral region produce an almost featureless spectrum, see Fig. 2(a).

Since the Raman effect is enhanced by resonance with surface plasmons, what we observe is the scattering from the metal-insulator interface; therefore, the difference between the spectra in the two cases must reflect a different structure of this interface.

Duval et al [3] reported Raman scattering from spherical or spheroidal vibrational modes of spherical microcrystallites in silicate glass, and showed that from the frequency of the low-energy peak it is possible to evaluate the size of the microcrystallites. The present data on Ag particles are interpreted in a similar way. Here, we consider the surface modes of spheroidal particles, whose wavefunction are spherical harmonics  $Y(l,m)$ , and calculate the relative Raman intensities in the two polarisations. The results are reported in Table I, where  $\Omega$  is the 1:2 frequency for spherical shape and  $\beta$  is the eccentricity of the particle. From the experimental frequencies of the spectra reported in Fig. 1 and by using the expressions of Table I, we find  $\Omega = 10.5 \text{ cm}^{-1}$ ,  $\beta \approx 1$ . From Ref. 3 we have  $\Omega \approx 0.85v_T/2R_c$ , where  $v_T$  is the velocity

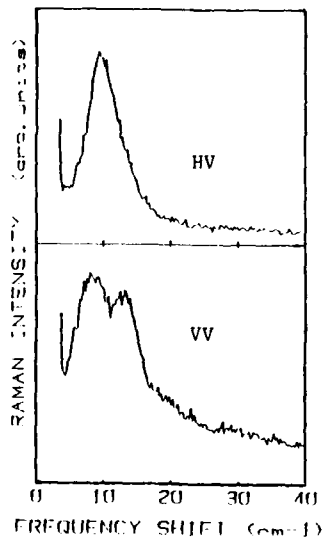


Fig. 1. Room temperature polarised Raman spectra of NaCl:Ag under 514.5 nm excitation.

mode	VV	HV	Frequency
$m = \pm 2$	2	1	$Q (1 + 4B/21)$
$m = \pm 1$	0	2	$Q (1 - 2B/21)$
$m = 0$	2	0	$Q (1 - 4B/21)$

of transverse acoustic waves in silver,  $2R$  is the mean diameter of the particle,  $c$  is the vacuum light velocity. Taking  $v_T = 1.6 \times 10^5$  cm/s, we find  $2R = 43$  Å. SAXS measurements on the same sample are in very good agreement with this value (see Ref. 2).

In the case of Na aggregates in NaCl, however, the spectra do not show evidence for metal particles of well defined shape: rather the data indicate a roughness of the surface with an extended range of curvatures. We have assumed a fractal picture of the surface [1], and this is expected to lead to a continuum spectrum which follows the law  $I(Q) \approx N(Q,T) \cdot Q^X$ , where  $N(Q,T)$  is the appropriate population factor. The value of  $X$  depends on the characteristic parameters of the system:  $X = 2dd_s/D + d - 2$ . Here,  $D$  is the fractal dimension,  $d$  the spectral dimension,  $d_s$  the superlocalisation parameter. In Fig. 2(b), which is the log-log plot of the Bose-Einstein normalised spectra of Fig. 2(a), the power-law behaviour is evidenced. The obtained value ( $X \approx 0.4$ ) is in reasonable agreement with that predicted on the basis of present knowledge of the parameters' values. Preliminary SAXS results seem to confirm the presence of fractal structure.

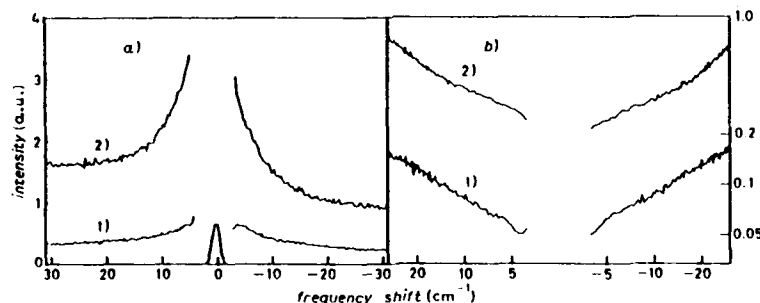


Fig. 2. (a): Polarised (HV) Raman spectra of NaCl:Na with two different excitations,  $T=100$  K. 1: 514.5 nm; 2: 647.1 nm. (b): Log-log plot of the reduced spectra of Fig. 2(a).

#### REFERENCES

- 1 E. Duval, G. Mariotto, M. Montagna, O. Pilla, G. Villiani and M. Barland, *Europhys. Lett.* **3** 333 (1987).
- 2 G. Mariotto, M. Montagna, G. Villiani, E. Duval, S. Lefrant, E. Rzepka and C. Mai, *Europhys. Lett.* (1988).
- 3 E. Duval, A. Boukenter and B. Champagnon, *Phys. Rev. Lett.* **56** 2052 (1986).



SESSION 8

SYNCHROTRON RADIATION STUDIES OF DEFECTS IN SOLIDS

A.V. Chadwick,  
University Chemical Laboratory,  
University of Kent,  
Canterbury, Kent, CT2 7NH, U.K.

In a synchrotron charged particles, electrons or protons, are confined to a fixed path by variable magnetic fields and are accelerated to high energies. The prime function of synchrotrons was initially as a tool for high-energy research as the energetic particles could be stored for use in colliding-beam experiments. In some of the earliest experiments with synchrotrons it was found that they also acted as sources of electromagnetic radiation. At the relativistic velocities achieved in a synchrotron an electron will emit radiation in the form of a very intense beam at a tangent to the curved orbit. In addition, this radiation covers a broad spectral range ("white light"), is highly polarized and by the very nature of the synchrotron source, occurs in pulses. This combination of properties makes synchrotron radiation a very powerful probe for a wide range of experiments. As a result the last decade has seen the construction in several countries of synchrotrons which are dedicated radiation sources, and a European facility is under construction at Grenoble. In the future there will be a wider access to synchrotron sources and the objective of this contribution is to outline the specific applications of synchrotron radiation to problems in defect chemistry and physics.

The lecture will be in the nature of a basic tutorial in synchrotron studies and will begin with a brief review of the special properties of synchrotron radiation and a survey of

available facilities. This will be followed by a discussion of the role of synchrotron radiation in defect research. In the last few years this has been an area of growth in terms of both range and sophistication and it will be necessary to focus the discussion. The topics covered will be mainly those involving X-rays; namely, extended X-ray absorption fine structure (EXAFS), X-ray diffraction and X-ray topography. The aim will be to outline the principles and experimental facilities and to emphasize the unique information or specific advantages of the techniques. For example, the EXAFS technique, which has come to prominence due to synchrotron sources, provides local structures around specific atoms in a solid and is not restricted, as is the case with diffraction techniques, to crystalline materials. In the case of diffraction and topography the advantages of synchrotron radiation are due to the natural collimation, tunability and high intensity resulting in high resolution and very rapid experiments.

The lecture will be illustrated with specific examples showing how defect problems, involving both point and line defects, have been resolved. In addition to the discussion of established experiments the talk will include some of the novel developments that are currently in progress.

It is hoped that this lecture will provide a good introduction to this large and growing field and encourage other workers to consider synchrotron radiation techniques in their research programmes.

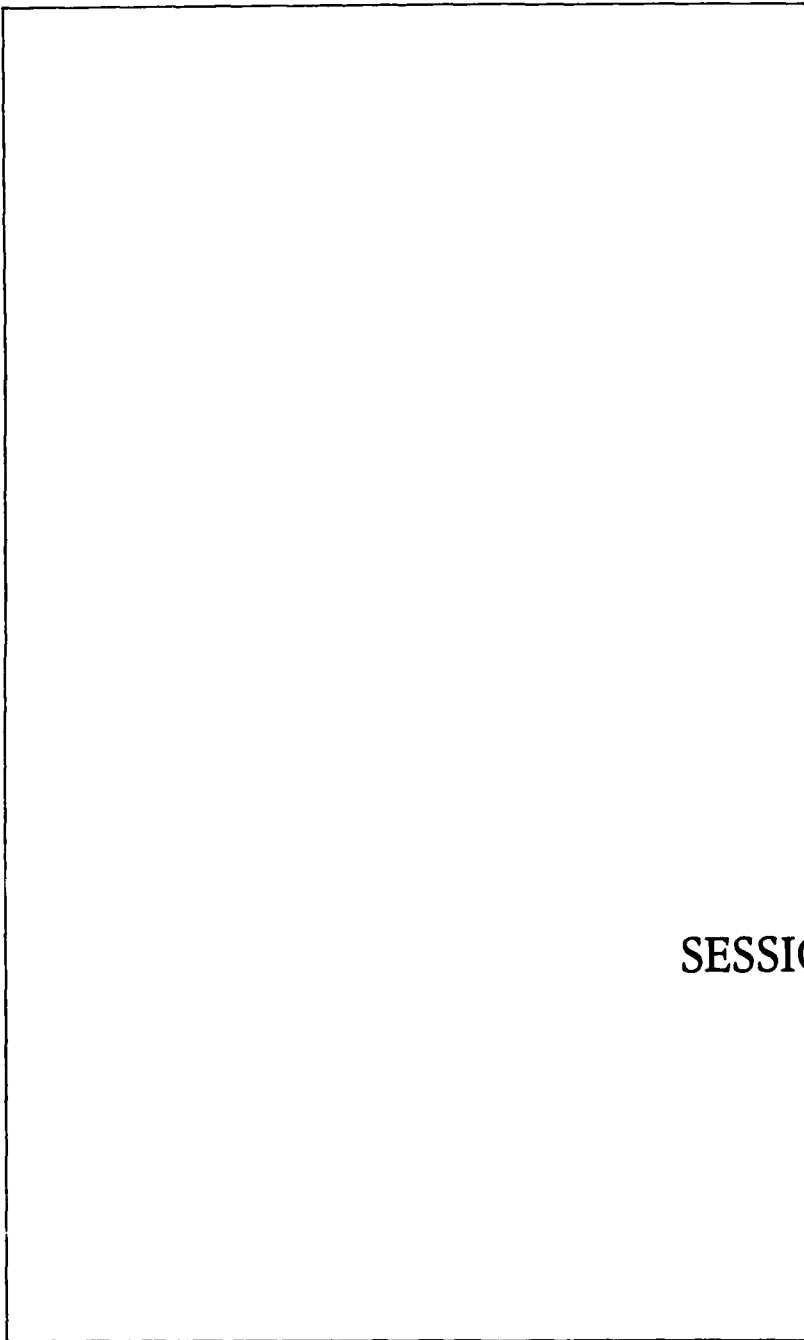
QUASIELASTIC DIFFUSE NEUTRON SCATTERING TO STUDY DEFECTS AND DISORDER  
IN IONIC MATERIALS

M T Hutchings

Materials Physics & Metallurgy Division, Harwell Laboratory, Didcot,  
Oxon. OX11 0RA

The techniques of neutron scattering which may be used to study the dynamic behaviour of defects and disorder in ionic materials will be described. Neutrons have the principal advantage over other probes of condensed matter in that they penetrate deeply into most materials and therefore measure a statistically averaged bulk property. They also readily penetrate the metal walls and heater of a furnace, allowing in-situ measurements at temperatures necessary to create mobile defects in crystals. Both the wavelength and the energy of a thermal neutron are of the same order of magnitude as the spatial variation and energy of fluctuations, respectively, of the ionic density in a crystal, allowing both structural and dynamic behaviour to be studied.

Particular emphasis will be given to the use of coherent and incoherent quasielastic diffuse scattering which give information on the correlated motion and individual motion of the diffusing ions respectively. Diffraction, giving a time-average distribution of ionic density, and inelastic scattering, giving the energy and lifetime of collective modes of the system, can also provide important ancillary information on the nature of the disorder. The investigation of thermally induced fast-ion, or superionic, behaviour in stoichiometric and doped fluorite structures will be used to illustrate the methods and the nature of the information obtained. Information which is important for understanding not only the behaviour of ionic conductors but also the thermophysical properties of nuclear fuels. Results from the study of other materials, particularly silver compounds, will be used to show the variety in behaviour observed. Often a simple model may be used to interpret the data and provide a visual picture of the complex dynamic state of a crystal. Molecular dynamics provides a more fundamental analysis, and can help to identify different contributions to the scattering.



SESSION 8A

# **INFRARED CHARACTERIZATION OF TRITIUM IN $\text{LiNbO}_3$ SINGLE CRYSTALS**

R. González and C. Ballesteros

Depto. de Física del Estado Sólido, Facultad de Ciencias Físicas  
Universidad Complutense, 28040 Madrid. Spain

Y. Chen and M.M. Abraham

Solid State Division, Oak Ridge National Laboratory,  
Oak Ridge, Tennessee 37831

Infrared absorption (IR) of  $\text{OT}^-$  and  $\text{OH}^-$  ions is used to monitor the presence of  $\text{T}^+$  and  $\text{H}^+$  in  $\text{LiNbO}_3$  single crystal irradiated with thermal neutrons. Tritium is produced via the nuclear reaction  ${}^6_3\text{Li} + {}^1_0\text{n} \rightarrow {}^3_1\text{T} + {}^4_2\text{He}$ .

After irradiation the most significant changes occurred in the IR region of the spectrum. The "as grown" crystals exhibited an  $\text{OH}^-$  vibration band at  $3480\text{ cm}^{-1}$ . After the neutron irradiation, this band vanished and two new bands at  $3500$  and  $3550\text{ cm}^{-1}$  appeared in the  $\text{OH}^-$  region. In addition, two very weak bands at  $2180$  and  $2211\text{ cm}^{-1}$  were observed (Fig.1 bottom).

Following an anneal at  $625\text{ K}$  for  $1\text{ h}$ , the band at  $3500\text{ cm}^{-1}$  was replaced

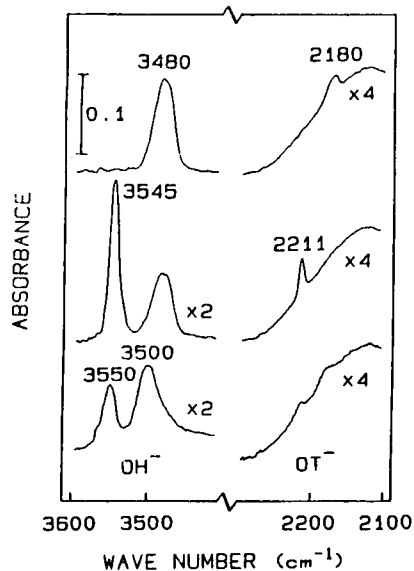


Fig. 1: Absorption spectra of a  $\text{LiNbO}_3$  crystal: (bottom) irradiated with thermal neutrons (center, after subsequent annealing for  $1\text{ h}$  at  $625\text{ K}$  in air, and (top) after additional annealing for  $1\text{ h}$  at  $775\text{ K}$  in air. The thickness of the sample was  $1\text{ mm}$ .

by one at  $3480\text{ cm}^{-1}$ . The band at  $3550\text{ cm}^{-1}$  disappeared and a new band at  $3545\text{ cm}^{-1}$  appeared. In the lower energy region, the band at  $2211\text{ cm}^{-1}$  is now well resolved and the band at  $2180\text{ cm}^{-1}$  almost disappeared (see Fig. 1, center). This overall spectrum was not noticeably modified by annealing the sample for 2 more hours at 625 K. A subsequent annealing for 1 h at a higher temperature (775 K) greatly increased the intensity of the  $3480\text{ cm}^{-1}$  band and annihilated that at  $3545\text{ cm}^{-1}$ . Correspondingly, the band at  $2211\text{ cm}^{-1}$  disappeared and the band at  $2180\text{ cm}^{-1}$  became more prominent (See Fig. 2, top). The frequency ratios between the two  $\text{OH}^-$  bands at 3545 and  $3480\text{ cm}^{-1}$  and their analogs at 2211 and  $2180\text{ cm}^{-1}$  are both 1.61, which corresponds well to the theoretical expectation of  $[\mu(\text{OT}^-)/\mu(\text{OH}^-)]^{1/2} = 1.64$ . Here  $\mu$  is the reduced mass of the radicals. Consequently, we attribute these two bands to  $\text{OT}^-$  stretching vibrations.

The tritium concentration in the neutron-irradiated crystals can be estimated by taking into account that the original  $^6\text{Li}$  concentration in the crystals was  $\sim 1.4 \times 10^{21}\text{ cm}^{-3}$  and the total neutron dose was  $\sim 7.5 \times 10^{17}\text{ n cm}^{-2}$ . Using the cross section of 910 barns, the resulting tritium concentration was  $n(\text{T}) \approx 9.5 \times 10^{17}\text{ cm}^{-3}$ .

The out diffusion rates for  $\text{H}^+$  and  $\text{T}^+$  in crystals heated in flowing oxygen has also been studied using a one-dimensional model. The diffusion equation has been previously solved by Crank (1). The diffusion coefficient can be calculated from the slope  $M$  of a semilogarithmic plot of the  $2180\text{ cm}^{-1}$  band absorbance against annealing time. The values obtained are close to those previously measured for  $\text{D}^+$  in-diffusion (2) in as-grown  $\text{LiNbO}_3$  single crystal.

#### References

- (1) J. Crank, *The Mathematics of Diffusion* (Clarendon, Oxford, 1956).
- (2) R. González, Y. Chen, K.L. Tsang, G.P. Summers, *Appl. Phys. Lett.* **41**, 739 (1982)

Acknowledgments: This research was sponsored by the C.A.I.C.Y.T. of Spain, the Defense Advanced Research Projects Agency under Interagency Agreement 40-1611-85 with U.S. Department of Energy, and the Materials Science Division, Office of Basic Energy Sciences, U.S. Department of Energy with Martin Marietta Energy Systems, Inc. contract DE-AC05-84OR21400-

Computed Properties of Charged Defects in Alkaline-Earth  
Fluorohalide Crystals

R. C. Baetzold  
Research Laboratories  
Eastman Kodak Company  
Rochester, NY 14650 USA

The Alkaline-Earth Fluorohalide Crystals possess the Matlockite Structure which is characterized by layers of like ions normal to the c axis of the tetragonal crystal. These materials, of which BaFBr is prototypical, are strongly ionic. Technological applications as storage phosphors have been identified for these materials(1). This technology involves exposure of the crystal to X-rays which generates oppositely charged carriers that can be stabilized. These defects include F centers, H centers and Vk centers. We have been computing properties of these defects in cooperation with the spectroscopic studies of R.S.Eachus of these laboratories. The purpose of this paper is to review some of the properties of these defects which we compute including structure, energy and mobility.

It is generally thought that an exciton formed upon X-ray exposure decays to a F center and a H center in these materials. We(2) have treated the energetics of F centers using the hybrid-potential method which has been discussed by Song(3). We find a conventional energy level pattern where a ground s state is separated from excited p states by the indicated transition energies shown in table 1. Note that the F- ground state is always deeper than the Cl- or Br- ground states in these materials.

Table 1. Ground State and Transition-Energies (eV.) for F Centers in BaFBr, BaFCl and SrFCl.

Material	F Center	$A_1$ (eV)	$A_1 \rightarrow B_2$	$A_1 \rightarrow E$	$A_1 \rightarrow A_1'$
BaFCl	F-	-7.24	2.53(2.33)*	2.97(2.82)	-
	Cl-	-4.62	-	2.84(2.25)	3.56(2.83)
BaFBr	F-	-7.84	2.42	2.58	-
	Br-	-6.66	-	2.11	2.15
SrFCl	F-	-6.39	3.05(3.02)	4.05(3.49)	-
	Cl-	-4.54	-	3.46(2.66)	4.22(3.26)

\*experimental values in parenthesis

The hole-trapped defects in BaFBr have been studied by atomistic simulation methods(4). An H center Br<sub>2</sub><sup>-</sup> species possesses a low energy site off-center and displaced towards the adjacent layer of Br<sup>-</sup> ions. This behavior contrasts to the F<sub>2</sub><sup>-</sup> center which occupies a site in the F<sup>-</sup> plane symmetrically along a diagonal. The low energy site for Br<sub>2</sub> and Br<sub>3</sub><sup>-</sup> are within the Br<sup>-</sup> plane and centered on a lattice site. Formation Energies computed for these species are shown in table 2. We predict that Br<sub>3</sub><sup>-</sup> (Cl<sub>3</sub><sup>-</sup>) is more stable than Br<sub>2</sub> (Cl<sub>2</sub>) as the ultimate decay products of two H centers reacting. Mobility of H centers in BaFBr is required for these reactions.

Table 2 Formation Energies(eV) of Hole Species in BaFBr, SrFCl and BaFCl. (Halogen atom reference 0 at infinity)

Material	X <sub>2</sub> <sup>-</sup>	X <sub>2</sub>	X <sub>3</sub> <sup>-</sup>
BaFBr	5.10	7.64	4.64
BaFCl	3.97	2.31	1.62
SrFCl	4.39	3.66	2.75

1. K.Takahashi and J.Miyahara, J. Electrochem. Soc. 132, 1492 (1984).
2. R.C.Baetzold, C.H.Leung and K.S.Song, to appear in Solid State Commun.
3. K.S.Song,L.Emery,G.Brunet and C.H.Leung, Nucl.Instrum. Methods B1, 456 (1984).
4. R.C.Baetzold, Phys. Rev. B 36, 9182 (1987).

**ISOTOPE AND ANHARMONICITY EFFECTS ON OH<sup>-</sup> DIPOLES  
PERTURBED BY Mg - INDUCED DEFECTS IN LiF AND NaF**

**R. Capelletti**

Department of Physics - University of Parma and G.N.S.M. - C.I.S.M.  
Viale delle Scienze - 43100 Parma - ITALY

**W. Beall Fowler**

Department of Physics - Lehigh University  
Bethlehem, PA - USA

**I. Foldvari and L. Kovacs**

Research Laboratory for Crystal Physics - Hungarian Academy of Sciences  
Budapest - HUNGARY

The double doping of LiF and NaF with OH<sup>-</sup> and Mg<sup>2+</sup> causes the appearance of a complex line spectrum in the infrared region between 3700 and 3500 cm<sup>-1</sup>. The attribution of the spectrum to the stretching mode of OH<sup>-</sup> interacting with different Mg-induced defects is supported by:

- 1) the growth of the same spectrum in OH<sup>-</sup>-free, but Mg<sup>2+</sup>-doped samples, submitted to thermal treatment at high temperature in moist atmosphere;
- 2) the observed shift of the whole spectrum, towards the low energy side, either by substituting H with D and <sup>16</sup>O with <sup>18</sup>O.

The ratio between the reduced masses of OH<sup>-</sup> and OD<sup>-</sup> dipoles, perturbed by the Mg-induced defects, as determined by the observed isotope shift, is slightly different from that expected for free OH and OD molecules and suggests that anharmonicity effects are relevant for describing the behaviour of OH oscillator in Mg doped LiF and NaF. Such effects are confirmed by the detection of weak overtones, on the high energy side of the fundamental spectrum.

The spectra (fundamental, overtone, and the one shifted as consequence of the isotopic substitution) have been analyzed in the temperature range 10 - 300K. By decreasing the temperature the lines of all the spectra sharpen, shift towards high energy and the amplitudes of the overtone lines increase in comparison with those of the fundamental ones. The results have been interpreted in the framework of the diatomic anharmonic oscillator model, by using the Morse potential <sup>(1)</sup>. In this approach the stretching mode term values  $G(n)$  are:

$$G(n) = \omega_e(n + 1/2)[1 - x_e(n + 1/2)]$$

where  $\omega_e$  is a frequency, commonly given in cm<sup>-1</sup>,  $x_e$  the anharmonicity parameter, and  $n$  the vibrational quantum number. The wavenumber for the transition from  $n = 0$  to  $n$  is:

$$\Delta G_{n0} \equiv G(n) - G(0) = n\omega_e[1 - x_e(n + 1)]$$

From the first overtone  $\Delta G_{20}$  and the fundamental  $\Delta G_{10}$  wavenumbers one obtains:

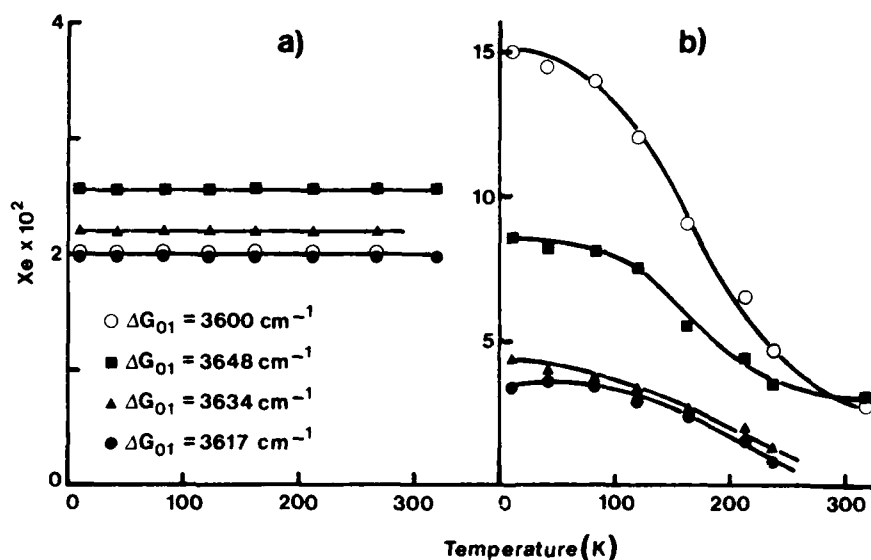
$$\Delta G_{20}/2\Delta G_{10} = (1 - 3x_e)(1 - 2x_e)^{-1}$$

Hence the measurement of fundamental and overtone gives  $x_e$ . The values of  $x_e$  for various lines of NaF: Mg are plotted in the figure a) versus temperature. They practically don't depend on the temperature. On the other hand in the same model, the ratio between the transition strengths takes the form:

$$I_{0 \rightarrow n}/I_{0 \rightarrow 1} \approx (n - 1)! x_e^{n-1}$$

So one would expect that the ratio of the first overtone to the fundamental absorption strength, which can be evaluated by the absorption spectra, would equal  $x_e$ . The experimental results for  $x_e$ , determined in this way, are shown in figure b). They are strongly temperature dependent and much larger than those displayed in figure a): this discrepancy suggests the existence of electric anharmonicity in addition to the mechanical one. The effect in NaF is much larger than that previously reported in LiF <sup>(1)</sup>. Moreover, if the ratio between the wavenumber of a given fundamental line in the hydrogenated sample and that in the deuterated sample is measured, one can obtain the ratio between the reduced masses of the perturbed OH and OD dipoles and compare the experimental results with the proposed theoretical models.

1) R. Capelletti, W.B. Fowler, P. Ruani and L. Kovacs - Cryst. Latt. Def. and Amorph. Mat. 16, 189 (1987)



MICROSCOPIC PROBING OF THE DYNAMICS OF TI IONS IN BaTiO<sub>3</sub> BY NMR

A. Hackmann, O. Kanert, H. Kolem, H. Schulz  
Institute of Physics, University of Dortmund, West Germany

K.A. Müller  
IBM Research Laboratory, Rüschlikon, Switzerland

J. Albers  
Physics Department, Universität des Saarlandes, West Germany

Measurements of the static quadrupole shift and of nuclear spin relaxation (NSR) are reported for <sup>47</sup>Ti and <sup>49</sup>Ti in BaTiO<sub>3</sub> single crystals between room temperature and about 600 K, i. e. below and above the tetragonal - to - cubic transition temperature T<sub>C</sub> (400 K). The aim of the present study is to prove the existence of reorientational motion of the Ti<sup>4+</sup> ions between equivalent <111> off-center sites as proposed by Guittet and Lambert [1]. In particular, in the tetragonal phase the reorientation is assumed to occur between four <111> displacements leading to a <100> polarisation, and in the cubic phase between all eight <111> off-center sites.

The Ti NMR spectrum of a single-domain BaTiO<sub>3</sub> crystal is due to second-order-quadrupole perturbed central transitions ( $m = 1/2 \rightarrow -1/2$ ) and consists of a sharp single line for each of the isotopes over the entire temperature range. Fig. 1 (upper part) shows the temperature dependence of both the resonance frequencies  $\nu = \nu_0 + \nu_c(T)$  where  $\nu_c$  is proportional to the square of the largest eigenvalue  $V_{zz}$  of the EFG tensor at the Ti site. As expected  $\nu_c(T)$  is zero in the cubic phase. In the tetragonal phase we found  $V_{zz}(T) \propto (T/T_C - 1)^\beta$  with  $\beta = 0.25$  indicating a displacive contribution to the phase transition. Supposing that the EFG tensor at the Ti sites is mainly due to the off-center shift of Ti while the contribution of the surrounding slightly distorted oxygen octahedron to  $V_{zz}$  is negligible one has to conclude that the Ti displacement from the octahedral center which was found to be 0.14 Å by Müller [2] is remarkably reduced near T<sub>C</sub>. However, the temperature dependence of the <sup>49</sup>Ti-NSR rate, depicted in Fig. 1 (lower part), demonstrates clearly that the Ti ions also remain off-center in the cubic phase. While the sharp peak of the NSR rate at  $T = T_{CF}$  is obviously caused by a cross-relaxation process between <sup>47</sup>Ti and <sup>49</sup>Ti we attribute the BPP like part of the NSR rate near T<sub>C</sub> to

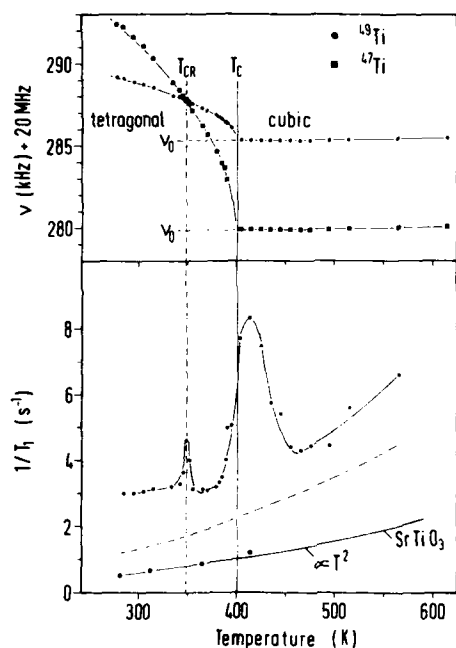


Fig.1 Resonance frequencies of  $^{47}\text{Ti}$  and  $^{49}\text{Ti}$  (upper part) and  $^{49}\text{Ti}$  NSR rates (lower part) vs. temperature in single-domain  $\text{BaTiO}_3$ . Dashed line: Phonon contribution estimated from  $^{49}\text{Ti}$  NMR in  $\text{SrTiO}_3$ .

reorientational jumps of the Ti ions among the off-center positions very similar to NSR due to the rotational motion of dilute off-center defects in alkali halides /3/. A preliminary analysis of the data leads to an activation energy of about 0.8 eV for the Ti jump rate while the magnitude of the jump rate was found to be  $2 \cdot 10^8 \text{ s}^{-1}$  at  $T = 420 \text{ K}$ .

In order to estimate the phonon-quadrupole contribution to the  $^{49}\text{Ti}$  NSR rate in  $\text{BaTiO}_3$  we have carried out additional  $^{49}\text{Ti}$  NSR measurements in  $\text{SrTiO}_3$  where the Ti ion is known to be on-center. The result is also depicted in Fig. 1 confirming a  $T^2$ -law as expected for phonon-quadrupole relaxation /4/. The dashed line in Fig. 1 shows an attempt to scale these data to  $\text{BaTiO}_3$ . Although the uncertainties of the scaling procedure are quite large the observed NSR rates in  $\text{BaTiO}_3$  exceed considerably the proposed phonon contribution.

This indicates that the off-center reorientational motion of Ti also occurs in the tetragonal phase far below  $T_C$ .

This work was supported by the Deutsche Forschungsgemeinschaft.

#### References

- 1.) A.M. Guittet, M. Lambert: *Com. Sol. St. Phys.* **12** 1053 (1973)
- 2.) K.A. Müller et al.: *Sol. State Com.* **61** 21 (1987)
- 3.) O. Kanert: *Phys. Reports* **91** 185 (1982)
- 4.) J. van Kranendonk: *Physica* **20** 781 (1954)

COLOR CENTERS WAVEGUIDES ON ALKALI HALIDES:  
FIRST MEASUREMENTS OF THE INSERTION LOSS

H.J. Kalinowski, L.C. Scavarda do Carmo,  
 Departamento de Engenharia de Telecomunicações,  
 Universidade Federal Fluminense, 24210 Niterói (Brazil)

R.A. Nunes and S. Paciornik  
 Departamento de Ciência dos Materiais e Metalurgia,  
 Pontifícia Universidade Católica, Rio de Janeiro (Brazil).

#### INTRODUCTION

The physical properties of color centers in alkali halides are extensively studied from several approaches, including optical techniques[1], but they have little technological applications. The best use of them are the color center lasers, tunable in the near infrared, with high peak power and short pulses. However, these lasers still require moderately high pump powers, like the obtainable with Ar<sup>+</sup> or Nd:Yag lasers. This constraint makes color center lasers useless in some aspects of present optical technology like optical communications, laser printers or integrated optics development. If color centers lasers might be miniaturized, they would find an important role in these branches of today's science.

The use of electron beam lithography to produce color center waveguides in alkali halides, specifically on LiF substrates, has been recently proposed[2]. The change in the refractive index, linked to the color center absorption, has been calculated to be enough to warrant optical guiding in the produced waveguides for wavelengths smaller than 1.2  $\mu\text{m}$ . This work presents the first evidences for optical guiding in these waveguides.

#### EXPERIMENTAL

The used waveguides have dimensions about 8  $\mu\text{m}$  depth, 150  $\mu\text{m}$  wide and 1 to 2 cm long. They were produced on polished LiF slabs by electron beam lithography, with a beam of 30 kV and 0.01 to 0.1  $\mu\text{A}$  current, while moving the substrate through a precision driver[3]. After the exposition the samples were characterized by their optical absorption band and handled like described in reference [2]. The insertion loss measurements were done using a 1 mW HeNe laser at 0.633  $\mu\text{m}$ . The light from the laser was focused on a single mode fiber (9  $\mu\text{m}$  core diameter) and butt coupled to the waveguides. The emerging light was focused through a 20X microscope objective on an Integrated Silicon Photodiode (UDT 450) and then lock-in detected. The reference measurements were done focusing directly the emerging light from the fiber on the detector. The present results are still preliminary,

showing the average value of measurements done in different moments, to prevent effects of the laser oscillations in the measured optical power. They reflect a high insertion loss, as discussed below.

#### RESULT AND DISCUSSION

The optical guiding of the laser light was observed through a microscope mounted perpendicular to the crystal surface. As the injection spot was moved in the lateral direction, light was observed to be guided in the color center strip. The amount of scattered light was, however, quite high. The obtained value for the insertion loss in these waveguides were:

$$41 \pm 4 \text{ dB}$$

This is a high value and cannot be associated only to the optical absorption at the selected wavelength, estimated to be an order of magnitude smaller. Inspection of the waveguide surface under higher gain in the optical microscope revealed an extensive pattern caused by microcracks on the waveguide surface. These cracks were the origin of the strong scattering of light observed visually and certainly the main source of the high insertion loss. The pattern consists of small rectangles with edges along  $\langle 110 \rangle$  crystalline directions. It is proposed that it results from local recrystallization of the substrate, after melting by the electron beam. To the moment we were unable to remove this effect lowering the electron beam current until the microprobe limit. When we vaporized a thin metallic film on the substrate prior to the application of the electronic beam the effect was reduced, probably due to the better heat transfer condition.

Although these results are still very preliminary, we think they open the study of color center waveguides and the production of better guides probably will lead to optical lasing. We expect they would require a low power yield for laser action, suitable to their miniaturization.

This work was supported by Research Grants from FAPERJ and CNPq (Brazilian Agencies) and from TWAS (Trieste, Italy).

[1] W.B. Fowler, Physics of Colour Centers, Academic Press, New York (1968).

[2] R.A. Nunes, H.J. Kalinowski, S. Paciornik, A.M. de Souza and L.C. Scavarda do Carmo, accepted for publication in Nucl. Instrum. Methods B (1988).

[3] R.A. Nunes, S. Paciornik, L.E. Sutter, E.G. Galucio, A.M. de Souza and L.C. Scavarda do Carmo, to appear in Rev. Bras. Fis. Apl. Instrum.

INTRINSIC DEFECT IN  $\text{SiO}_2$  GLASSES AND CRYSTALS

A.R.Silin

Institute of Solid State Physics  
Latvian State University,  
8 Kengaraga str., 226063 Riga,  
Latvian SSR, USSR

Intrinsic defects in a glass are created due to violations of the short range order in the glassy structure. For the fused silica they could arise in two ways: 1) by a change of a coordination number (CN), 2) by the appearance of atom in the nearest coordination sphere not corresponding to the chemical composition not altering right coordination number. The simultaneous reduction of the CN by one for nearest silicon and oxygen atoms must be considered a breaking of the Si-O bond and the creation of the pair of elementary structure defects nonbridging O atom and three fold coordinated Si atom with well known spectroscopic characteristics [1/].

An appearance of the not corresponding atom in the nearest vicinity of regular atom could be interpreted as a formation of "wrong" chemical bonds in the fused silica network. In such a way there could be created Si-Si and O-O direct chemical bonds, which are absent in a "perfect" structure of the silica glass. These defects could be considered as simplest aggregates of the elementary defects: two nonbridging O atoms could create the O-O bond whereas two three fold coordinated Si atoms - the Si-Si bond. Since these defects are charge and chemically neutral ones, they could exist in the silica glass network at any relative concentrations.

It should be mentioned, that the real structure of fused silica often is characterized by oxygen deficit, caused by the technological reasons. As it follows from the experimental results, in such glasses the oxygen deficit gives rise to another silicon - rich intrinsic defects - two-fold coordinated Si atoms [2/]. These defects belong to the class of atoms

with reduced CN that for Si is reduced by two, but such a rearrangement does not need essential activation energy, since the type of chemical bonds there is changed /3/.

All mentioned above intrinsic defects are typical only for a glassy state of  $\text{SiO}_2$ . In the  $\text{SiO}_2$  crystalline structures such defects could not exist in a stable form because of the long-range order restrictions. The elementary intrinsic defects in the irradiated  $\alpha$  quartz produce transient absorption bands only with the some short life time close to for the self-trapped exciton. It means that the exciton self-trapping in crystalline  $\text{SiO}_2$  is connected with the Si-O bond breaking /1/.

A more stable intrinsic defect of both crystalline and glassy  $\text{SiO}_2$  is the E'-center. Its model in a crystal is an O vacancy trapped a hole, whereas in a glass the same spectroscopic properties reveals a neutral three fold coordinated Si atom. The conclusion suggests itself, that in a crystal the spectroscopic characteristics of E'-center are determined also mainly by a neutral three fold coordinated Si atom near close to the O vacancy. It means that an unpaired electron occupying the  $\text{sp}^3$ -orbital of the three fold coordinated Si atom has a strongly localized wave function.

#### References

1. Silin A.R., Trukhin A.N. Point defects and elementary excitations in crystalline and glassy  $\text{SiO}_2$ . Riga: Zinātne (in Russian), 1985, 244 p.
2. Skuja L.N., Streletsky A.N., Pakovich A.R. A New Intrinsic Defect in Amorphous  $\text{SiO}_2$ : Two fold Coordinated Silicon. - Solid State Comm., 1984, vol.50, N 12, p.1069-1072.
3. Silin A.R., Skuja L.N. Intrinsic Defects in Fused Silica.- J.Non.Crystall.Solids, 1985, v.71, p.443-445.



SESSION 8B

# RADIATION DEFECT BEHAVIOR IN $\text{UO}_2$ - A CHANNELING STUDY

A. Turos<sup>1\*)</sup>, Hj. Matzke<sup>2)</sup> and S. Fritz<sup>2)</sup>

1) Kernforschungszentrum Karlsruhe, INFP, Postfach 3640, D-7500 Karlsruhe, FRG

2) European Institute for Transuranium Elements, CEC, JRC, Postfach 2340, D- 7500 Karlsruhe, FRG

The purpose of this study was to investigate the formation of radiation damage and its recovery in  $\text{UO}_2$ .  $\text{UO}_2$  single crystals of  $\langle 100 \rangle$  and  $\langle 111 \rangle$  orientation were implanted with different doses of Te-ions (heavy fission product,  $M = 128$ ) and Kr-ions (light fission product,  $M = 84$ ). In order to study the recovery of radiation damage, the implanted samples were subjected to furnace annealings at different temperatures ranging from 300 °C to 1500 °C. The as-implanted and the annealed samples were analyzed by means of the Rutherford backscattering-channeling technique [1].

Ion implantation of  $\text{UO}_2$  crystals resulted in the appearance in the aligned spectra of large damage peaks due to the displacement of U-atoms. Because of the great mass difference between U and O, the radiation damage in the U-sublattice can easily be analyzed, whereas the damage in the O-sublattice cannot be analyzed due to the low mass number of O. The number of displaced atoms  $N_d$  increased with the implantation fluence. The displacement efficiency (DE), i.e. the number of displaced atoms per incident ion, however, decreased with increasing implantation fluence ( $n$ ).  $DE = 14$  for  $n = 0.5 \times 10^{15} \text{ at/cm}^2$  and  $DE = 0.6$  for  $n = 50 \times 10^{15} \text{ at/cm}^2$ . The displacement efficiency estimated according to the Kinchin-Pease model [2] amounts to about 250. This indicates that important defect recombination takes place during implantation. Another interesting and new feature of the radiation damage in  $\text{UO}_2$  is its strong orientation dependence. The number of displaced atoms for  $\langle 111 \rangle$  oriented crystals is substantially higher than that for the  $\langle 100 \rangle$  direction. This indicates that rearrangement of defects in the  $\langle 111 \rangle$  direction is much less pronounced than in the  $\langle 100 \rangle$  direction.

The analysis of radiation damage recovery upon thermal annealing by means of the channeling-backscattering technique is based on measurements of the dechanneling yield  $\chi_{\min}$ . The results of annealing experiments for Te-ion implantation are shown in Fig. 1. For  $\langle 100 \rangle$  oriented samples, the dechanneling level  $\chi_{\min}$  did not exceed 10% even for the highest dose, i.e.  $8 \times 10^{16} \text{ at/cm}^2$ . No changes were observed up to 400 °C. With increasing annealing temperature,  $\chi_{\min}$  decreases and attains the value typical for unimplanted samples after annealing at 1300 °C for higher dose and at 1200 °C for low dose implantation. As can be expected, thermal recovery of  $\langle 111 \rangle$  cut crystals is much slower. The recovery begins again above 400 °C, however, the value characteristic for unimplanted samples can be attained only after annealing at about 1500 °C.

\* on leave from the Institute for Nuclear Studies, Warsaw, Poland

The detailed analysis of the dependence of  $\chi_{\min}$  vs. annealing temperature shows that two annealing stages exist. A first recovery stage occurs above about 400 °C. The  $\chi_{\min}$  varies rapidly in the temperature interval 400-800 °C. The slope of the curve changes at 800 °C. For temperatures above 800 °C, the recovery proceeds much slower.

The variation of  $\chi_{\min}$  as a function of annealing temperature for Kr-ion implantation is shown in Fig. 2. The most characteristic feature of the annealing curves is the presence of a critical temperature above which the damage recovery begins. This temperature is dose-dependent and amounts to 400 °C, 550 °C and 700 °C for the doses of  $1 \times 10^{15}$ ,  $5 \times 10^{15}$  and  $1 \times 10^{16}$  Kr-ions/cm<sup>2</sup>, respectively. Above this critical temperature, the  $\chi_{\min}$ -value decreases approximately linearly (or else in 3 stages) with annealing temperature until the value characteristic for an unimplanted sample is reached. One notes that for the sample implanted with the highest dose, this occurs at about 1500 °C. The fact that for the sample implanted with  $1 \times 10^{15}$  at/cm<sup>2</sup>  $\chi_{\min}$  does not decrease as much as for the other samples can be attributed to the inferior quality of the crystal and has nothing to do with the annealing behavior.

#### References

1. L.C. Feldmann, J.W. Mayer, and S.T. Picraux, Materials Analysis by Ion Channeling, Academic Press, N.Y. 1982.
2. G. Kinchin and R.S. Pease, Rep. Progr. Phys. 18 (1955) 1.

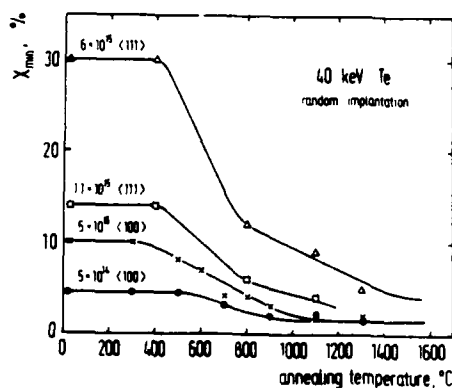


Fig. 1

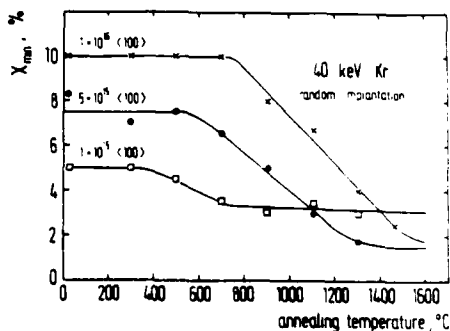


Fig. 2

Recovery of the dechanneling yield,  $\chi_{\min}$  upon annealing of UO<sub>2</sub> single crystals implanted with Te (Fig. 1) or Kr (Fig. 2)

$V_K$  CENTERS IN TETRAHALIDES

A. Martín and F. J. López

Dpto. Física Aplicada, C-IV, Facultad de Ciencias,  
Universidad Autónoma de Madrid, Cantoblanco, 28049 MADRID (Spain)

The processes and defects induced by ionizing radiation in simple halide crystals (AX) are well known at present. Progressively less is known in dihalide ( $BX_2$ ) and trihalide ( $ABX_3$ ) crystals, although it appears that photolitic damage takes place in all these materials. The situation is much worse for tetrahalide ( $A_2BX_4$ ) crystals. Martín et al. [1,2] have studied the X-ray induced luminescence and the thermoluminescence [1], as well as the optical absorption bands induced by low temperature X-irradiation [2] in tetrahalide crystals, mainly  $Rb_2ZnCl_4$  and  $K_2ZnCl_4$ . The authors have pointed out that a broad absorption band at  $\sim 370$  nm has features of a  $V_K$ -type center, although a confirmation is needed.

This work presents the EPR spectrum associated to self-trapped holes produced by X-irradiation at 77 K in tetrahalides. Also, the dichroic optical absorption of these  $V_K$ -centers has been identified.

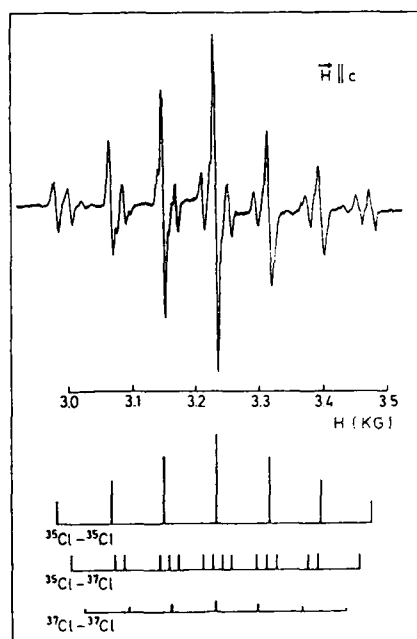


Figure 1

Figure 1 shows the EPR spectrum measured at 85 K of a  $Rb_2ZnCl_4$  sample with the magnetic field  $\vec{H}$  parallel to the crystallographic c-axis.

This center consists in a  $\text{Cl}_2^-$  molecular ion. The lines due to the three types of pairs  $^{35}\text{Cl}-^{35}\text{Cl}$ ,  $^{35}\text{Cl}-^{37}\text{Cl}$ ,  $^{37}\text{Cl}-^{37}\text{Cl}$ , are schematized in the figure 1. The orientation of the molecular axis has been inferred from the angular variation of the hyperfine structure. The axis is  $9.5^\circ$  out of the bc plane from a line at  $35^\circ$  from the c-axis of the lattice. This gives rise to four different spectra of the  $V_K$ -center for a general orientation of  $\vec{H}$ , which reduce to one for  $\vec{H}$  parallel to the a, b or c axes.

The spin Hamiltonian parameters are similar to those for the  $V_K$ -center in alkali chlorides and dichlorides.

On the other hand, the  $V_K$ -centers in tetrachlorides present a dichroic absorption band which is  $\sigma$ -polarized (see figure 2). The position (385 nm) and width ( $\sim 0.8$  eV) are also similar to the data for self-trapped holes in other materials.

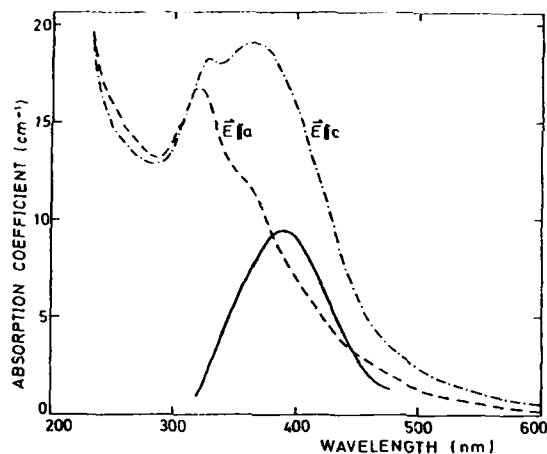


Figure 2

#### References

- [1] A. Martín, F. J. López, E. Diéguez, F. Agulló-López and H. Arend, Phys. Stat. Sol. (b) **138**, 245 (1986).
- [2] A. Martín, F. J. López, E. Diéguez, F. Agulló-López and H. Arend, Cryst. Latt. Def. and amorph. cryst. **17**, 69 (1987).

ANNEALING BEHAVIOUR OF THE LOW TEMPERATURE PROPERTIES  
OF NEUTRON-IRRADIATED QUARTZ CRYSTALS

L. Michiels, N. Vanreyten and I. Mangelschots  
Katholieke Universiteit Leuven  
Dept. Natuurkunde  
Celestijnenlaan 200 D,  
B-3030 Leuven-Belgium.

Through measurements of the thermal<sup>1</sup> and acoustical<sup>2</sup> properties of neutron-irradiated crystalline quartz it is well established that neutron-irradiated quartz possesses a broad spectrum of two-level tunneling systems (TLS) similar as those found in amorphous SiO<sub>2</sub>. These TLS are strongly coupled to phonons and the resonant interaction leads to a logarithmic temperature dependence of the sound velocity. A question which is still of interest is, whether or not the TLS are associated with the amorphous regions created by the neutron irradiation. Since evidence was found that the amorphous regions completely anneal out<sup>3</sup> at 700°C, while the concentration of TLS only decreases by a factor of two by annealing up to 790°C,<sup>4</sup> we performed a further study of the annealing behaviour of the low temperature properties of neutron-irradiated quartz.

A quartz crystal is irradiated with fast neutrons (dose  $8.7 \times 10^{19} \text{ cm}^{-2}$ ,  $E > 0.1 \text{ MeV}$ ) at SCK, Mol Belgium. After this irradiation the measured relative density change is -4%. From the measurements of the variation of sound velocity at 9.3 GHz with temperature we can determine the parameter  $C_L$ , which is equal to  $\bar{P} \gamma_L^2 / \rho v_L^2$ , with  $\bar{P}$  the spectral density of the TLS.  $\gamma_L$  is the longitudinal coupling parameter between the TLS and the phonons,  $\rho$  is the mass density,  $v_L$  is the sound velocity. Figure 1 shows the change of the parameter  $C_L$  with annealing temperature, together with the change in optical activity of a crystal irradiated with approximately the same dose<sup>5</sup>. As we can see, the concentration of the TLS (proportional to  $C_L$ ) after annealing up to 970°C is still 8% of the original value. Also the annealing behaviour of the optical activity in the studied temperature region is the same as the behaviour of the TLS in this region.

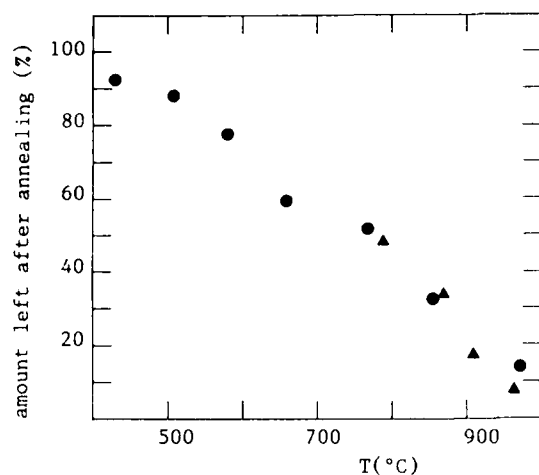


Figure 1 :

The annealing behaviour of the parameter  $C_L$  and the optical activity.

▲ :  $C_L$  ( the parameter  $C_L$  is set to 100% before annealing).

● the optical activity ( the change in optical activity is set 100% before annealing).

Since the amorphous regions already disappear on heating up to 700°C, as was found from X-ray measurements<sup>3</sup>, it seems unlikely that the TLS are located in these disordered regions which are created by the thermal spike mechanisms.

The model which we propose to explain these annealing experiments is based on the theoretical prediction<sup>6</sup> of the occurrence of TLS at grain boundaries and is supported by the behaviour of the optical activity.

#### References

1. G.W. Gardner and A.C. Anderson, Phys. Rev. **B23**, 474 (1981).
2. N. Vanreyten and L. Michiels, Solid State Comm. **66**, 63 (1986).
3. D. Grasse, O. Docar, J. Peisl and S.C. Moss, Rad. Effects **66**, 61 (1982).
4. N. Vanreyten and L. Michiels, Phys. Rev. **B** in press.
5. W. Primak, Phys. Rev. **110**, 1240 (1958).
6. T. Gszti, Phys. Rev. **B30**, 1811 (1984).

LOW TEMPERATURE THERMOLUMINESCENCE AND PHOSPHORESCENCE OF  
X-IRRADIATED GE-DOPED QUARTZ

A. Halperin

Racah Institute of Physics, The Hebrew University, Jerusalem 91904, Israel

Germanium in quartz is a well known electron trap and defects related with electron excess Ge-centers with  $\text{Na}^+$  or  $\text{Li}^+$  ions as charge compensators have been established long ago<sup>1</sup>. Recently, germanium impurities were also found to affect adversely the irradiation frequency offset of quartz resonators and to induce a strong elasticity loss peak at 246K in crystals containing  $\text{Li}^+$  as charge compensators<sup>2</sup>. Most of the earlier investigations on Ge-doped quartz were limited to temperatures above 77K. Hayes and Jenkin<sup>3</sup> have examined x-irradiated Ge-doped quartz down to 4K. Using EPR they have observed several Ge-associated spectra assigned by them as H(I), H(II) and H(III). H(I) was found to decay on warming to 35K, and the intensity of H(III) decayed at 58K.

In the present work we have examined the low temperature phosphorescence (at about 20K) and the thermoluminescence (TSL) of x-irradiated Ge-doped quartz. The measurements were carried out separately on samples cut from the Z- and X-growth zones of a Y-plate, cut from a high purity crystal described in Ref. 2. The z-growth zone of this crystal contained 0.5 ppm of Al compensated by Li and the concentration of Al in the x-growth zone was higher by about one order of magnitude. Both growth zones contained about 30 ppm of germanium.

The glow curves of both the Z- and X-samples revealed an extremely intense TSL peak at 53K (at a warming rate of  $10^0/\text{min}$ ) which is associated with germanium and may be related with the H(III) center decaying at 58K<sup>3</sup>. A weaker TSL peak appeared as a low temperature shoulder at about 37K fitting the temperature at which the H(I) center was observed to decay (35K). Some measurements carried out on samples which contained about 600 ppm of Ge exhibited the above TSL peaks at still higher intensities. Thermal activation energies measured by the method of initial rise gave values of about 0.08 eV below 40K and 0.09 eV for the main peak at 53K. The emission of the TSL at 53K peaked at 2.60eV (477 nm). Heavy irradiation at room temperature is known to affect strongly the TSL peaks in quartz appearing in the temperature range 110-230K<sup>4</sup>. This effect was attributed to the migration of the  $\text{Li}^+$  ions

AD-A206 030

INTERNATIONAL CONFERENCE ON DEFECTS IN INSULATING  
CRYSTALS HELD AT PAVIA ITALY ON AUGUST 29-SEPTEMBER 2  
1988 (U) PAVIA UNIV (ITALY) DIPT DI FISICA SEP 88

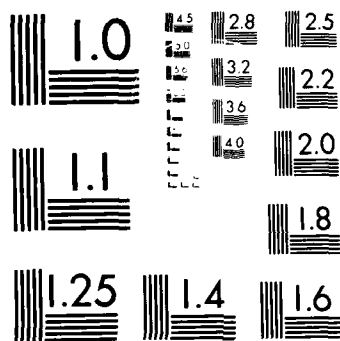
7/7

UNCLASSIFIED

P/G 7/2

ML

END  
DATE  
FILMED  
5 89



MICROCOPY RESOLUTION TEST CHART  
NATIONAL BUREAU OF STANDARDS-1963-A

from the Al defects, and their eventual trapping various defect sites in the crystal. They then are no more available for the less stable defects responsible for the TSL below 230K. The 53K TSL was found not to be affected by prolonged irradiation at room temperature which seems to indicate that the involved defects are not associated with lithium.

The phosphorescence at 20K also emitted the 260 eV band, and it is very likely that it is related to the release of carriers from the center associated with the 53K TSL. It decayed with time. On warming it showed two steps of fast decay, at about 110 and 175 K. The same steps reappeared on cooling when the phosphorescence was recovered (partly) back.

Other effects observed in the TSL of the Ge-doped quartz samples will be described and discussed. It should be noted that TSL peaks in the temperature range 30-60K are usually observed in crystals not deliberately doped with Ge. The intensities of the TSL peak above 50K is in these cases lower by about four orders of magnitude compared to that in our sample containing 30 ppm of Ge. They may thus indicate the presence of Ge at concentrations of the order of  $10^{-9}$ - $10^{-8}$ . Our measurements indicate that under controlled conditions of excitation, the TSL at 53K may serve as a method for the determination of concentrations of Ge in quartz.

#### References

1. J.A. Weil, Phys. Chem. Miner. **10**, 149 (1984).
2. F.K. Euler and A. Kahan, Phys. Rev. **B35**, 4351 (1987).
3. W.Hayes and T.J.L.Jenkin, J.Phys.C:Solid State Phys. **18**, L84 (1985).
4. A. Halperin and S. Katz, J. Phys. Chem. Solids, in press.

#### Acknowledgement

The author thanks Drs.F.K. Euler and A. Kahan of the Department of the Air Force, HQ. Rome Air Development Center, Hanscom, Mass. for supplying some of the crystals used in the present work.

# A SELF TRAPPED HOLE IN ALKALI SILVER HALIDE CRYSTALS

Teruyoshi Awano, Takao Nanba\*, Mikihiro Ikezawa\*,  
Tomochika Matsuyama\*\*, and Hitoshi Yamaoka\*\*  
Department of Applied Physics, Tohoku Gakuin University,  
Tagajo 985, Japan

\* Department of Physics, Tohoku University,  
Sendai 980, Japan

\*\* Research Reactor Institute, Kyoto University, Kumatori,  
Osaka 590-04, Japan

The alkali silver halide belongs to the orthorhombic crystal structure.<sup>1)</sup>  $\gamma$ -ray irradiation at 77 K induced defects in  $\text{Rb}_2\text{AgI}_3$  and  $\text{K}_2\text{AgI}_3$ . The structure of defects was investigated by optical and ESR studies.

Single crystals were prepared from aqueous solutions.<sup>2)</sup> Absorption bands were observed to grow at 2.9, 2.5 and 3.2 eV with polarized light in the  $\{100\}$ ,  $\{010\}$  and  $\{001\}$  directions in the two crystals after  $\gamma$ -ray irradiation at 77 K. As described below, a trapped hole center has uniaxial symmetry with the axis approximately along the  $\{001\}$  direction. So the 3.2 eV band in the  $\{001\}$  direction is probably due to the hole center.

ESR spectra were observed at 77 K after  $\gamma$ -ray irradiation at the same temperature. Figs. 1 and 2 show examples. Magnetic field is parallel to  $\{100\}$  in Figs. 1-a and 2-a and it is parallel to  $\{001\}$  in Figs. 1-d and 2-d. The magnetic field is in intermediate directions in Figs. 1-b,c and 2-b,c. The spectra have been analyzed to be composed of four sets of components and each set has six hyperfine structure of an equal intensity. Each of the six hyperfine components has super-hyperfine structure in it. The position of the components in each of the four sets were expressed by the following uniaxial spin Hamiltonian parameters:

$$g_{\parallel} = 1.98, g_{\perp} = 2.14, A_{\parallel} = 530 \text{ G}, A_{\perp} = 215 \text{ G (hyperfine term)}, \\ A(\text{Rb}^{85}) = 10 \text{ G}, A(\text{Rb}^{87}) = 30 \text{ G in } \text{Rb}_2\text{AgI}_3$$

$$g_{\parallel} = 1.98, g_{\perp} = 2.14, A_{\parallel} = 650 \text{ G}, A_{\perp} = 260 \text{ G (hyperfine term)}, \\ A_{\parallel}(\text{K}^{39}) = 25 \text{ G}, A_{\perp}(\text{K}^{39}) = 40 \text{ G in } \text{K}_2\text{AgI}_3$$

The angle between the axes of the four sets of defects and the c-axis of the crystals were determined to be  $\pm 7$  and  $\pm 9$  degrees ( $\text{Rb}_2\text{AgI}_3$ ) or  $\pm 10$  and  $\pm 15$  degrees ( $\text{K}_2\text{AgI}_3$ ). The directions of the four axes almost coincide with the directions of the iodines to the alkali metal. The lower spectra in the Figs. 1 and 2 are calculated by using the above parameters and giving a half width of 12 gauss ( $\text{Rb}_2\text{AgI}_3$ ) or 18 gauss ( $\text{K}_2\text{AgI}_3$ ) to each

component line. From a good agreement between the observed and calculated spectra, we conclude that the formed defect in both crystals is a pair of iodine ion and an alkali ion which traps a hole mainly around the iodine ion, i.e.  $KI^+$  or  $RI^+$ .

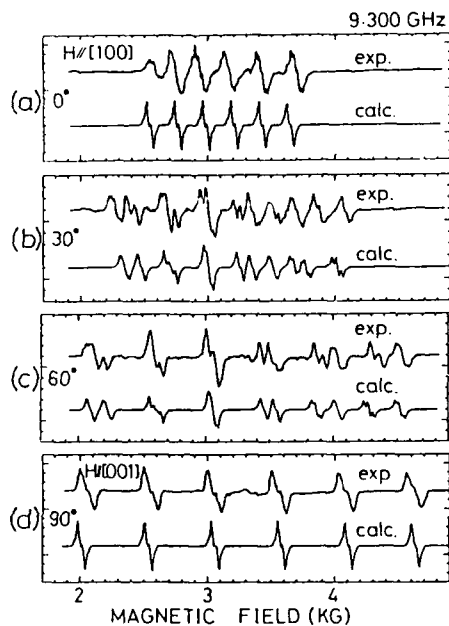


Fig. 1  $Rb_2AgI_6$

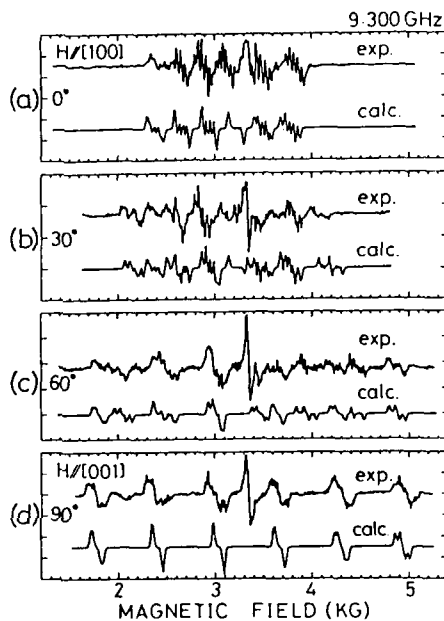


Fig. 2  $K_2AgI_6$

#### References

- 1) C. Blink and H. A. S. Kroese: *Acta Cryst.* 5, 433 (1952)
- 2) K. Edamatsu, M. Ikezawa, K. Sato, S. Kono and T. Sagawa: *J. Phys. Soc. Jpn.* 52, 1521 (1983)

Nd:YAG LASER STIMULATED LUMINESCENCE AT ROOM  
TEMPERATURE IN THERMOCHEMICALLY REDUCED AND IN  
NEUTRON IRRADIATED MgO

K. CHAKRABARTI\* AND V. K. MATHUR  
NAVAL SURFACE WARFARE CENTER  
WHITE OAK, SILVER SPRING, MD 20903-5000 USA  
G. P. SUMMERS  
NAVAL RESEARCH LABORATORY  
WASHINGTON, DC 20375 USA

Both thermochemical reduction and neutron irradiation in MgO produce F type defects which absorb in UV region ( $\sim 5.0\text{eV}$ ). In reduced MgO, it has been observed<sup>1</sup> that the life-time of F center luminescence at room temperature is controlled by the concentration of  $\text{H}^+$  ions, which act as electron traps. At room temperature, these traps are unstable and the electrons are released from the  $\text{H}^+$  ions. These electrons can be retrapped many times at  $\text{H}^+$  ions before finally being captured at  $\text{F}^+$  centers, leading to long lived F center luminescence. On lowering the temperature to 77K,  $\text{H}^+$  ions become stable and the luminescence is quenched. However, the luminescence can be reactivated<sup>2,3</sup> by a short pulse of long wavelength light.

There is, however, at least one deeper trap in these materials, which plays a key role in our present investigation of infrared-to-visible conversion in MgO at room temperature. Thermal release of electrons from these traps is associated with a thermoluminescence (TL) glow curve (Fig. 1) which peaks at  $-175^\circ\text{C}$  in reduced MgO and at  $-125^\circ\text{C}$  in neutron irradiated MgO. It is this high temperature TL peak which makes these materials ideal for storage device. These traps can be filled by exciting the sample with UV light at room temperature. On subsequent stimulation with light from a  $1.06\mu\text{m}$  Nd:YAG laser, an intense blue luminescence is observed (Fig. 2) which peaks at  $\sim 370\text{nm}$  in reduced MgO, and at  $\sim 420\text{nm}$  in neutron irradiated MgO. This optically stimulated luminescence (OSL) is not observed, if subsequent to UV irradiation, the samples are heated through high temperature peaks. In neutron irradiated sample, three TL peaks are observed (Fig. 1). On annealing the sample over the  $90^\circ\text{C}$  peak, the OSL continued to be observed, suggesting that the  $125^\circ\text{C}$  trap is responsible for the OSL. The TL emissions from the glow peaks in both reduced and in neutron irradiated MgO are predominantly in the green region  $\sim 550\text{nm}$  and are different from the OSL emissions. A similar spectral shift with visibly distinct color changes from TL to OSL emissions has been observed<sup>4</sup> in other phosphors. However, the most striking result in MgO is that the laser stimulated luminescence is extremely long lived and the intensity decays only by 50% after half an hour of continuous irradiation by a  $1.06\mu\text{m}$  Nd:YAG laser. One possible explanation for this long lived laser stimulated luminescence is the reexcitation of the F centers by the

stimulated luminescence. By exciting these samples by a ~300nm light, which is the tail end of the stimulated luminescence spectra, we could generate the laser stimulated luminescence. These properties suggest a potential use of MgO as an infrared sensor and as a laser detector

\*On leave from Southwestern Oklahoma State University, Weatherford, OK 73096 USA

1. B. T. Jeffries, R. Gonzalez, Y. Chen and G. P. Summers, Phys. Rev B25, 2077 (1982).
2. G. P. Summers, T. M. Wilson, B. T. Jeffries, H. T. Tohver, Y. Chen and M. M. Abraham, Phys. Rev. B27, 122283 (1983).
3. K. Chakrabarti and G. P. Summers, Phys. Lett. A120, 466 (1987).
4. K. Chakrabarti, V. K. Mathur, J. F. Rhodes and R. J. Abbundi, Bull. Am. Phys. Soc. 33, 693 (1988).

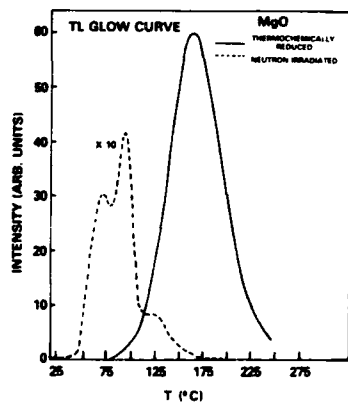


FIG.1

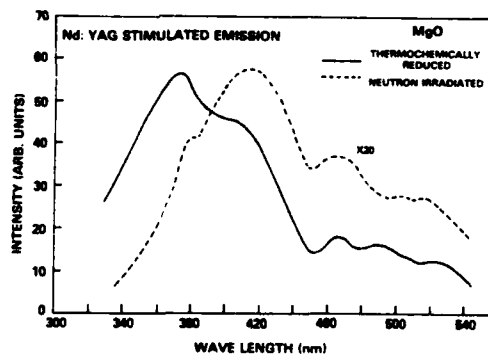


FIG.2

SESSION 9A

THEORY OF DEFECTS IN SILICON DIOXIDE: E' CENTERS NEAR THE  
SiO<sub>2</sub> - Si INTERFACE\*

Andrew X. Chu and W. Beall Fowler  
 Physics Department and Sherman Fairchild Laboratory  
 Lehigh University  
 Bethlehem, PA 18015 U. S. A.

We report the results of calculations of oxygen-vacancy defects in silicon dioxide near the (100) SiO<sub>2</sub> - Si interface, based on the tridymite-layer model recently proposed by Ourmazd *et al.*<sup>1</sup> We first refined and tested the Ourmazd model by doing quasi-classical calculations of the atomic structure near the interface, utilizing the force-field "molecular mechanics" technique developed by Allinger<sup>2</sup>. Using clusters of more than 200 atoms with suitable termination, we have investigated the nature of the atomic relaxations and the residual stresses for several different detailed atomic arrangements.

These calculations were followed by semiempirical molecular-orbital studies of smaller clusters using the routines MINDO/3 and MOPN, developed by Dewar and co-workers<sup>3</sup>. These techniques have been successfully applied<sup>4</sup> to study a variety of defects in silicon dioxide, including several oxygen-vacancy (E') centers in alpha-quartz. They are used here to further test the Ourmazd model of the interfacial region, to investigate the presence or absence of oxygen bonded to two interface silicon atoms, and to assess the extent of atomic relaxation associated with the formation of the oxide.

Of particular interest is the question whether oxygen-vacancy defects near the SiO<sub>2</sub> - Si interface will differ substantially from those in the bulk silicon dioxide, which may or may not include atomic hydrogen as a constituent.<sup>5</sup> Given the extensive experimental evidence

supporting the existence of such defects, it is important to understand them fully. Thus the calculations reported here will focus on the properties of O vacancies near the interface, in different charge states and both with and without hydrogen.

\*Research supported by the Electronic and Solid State Science Program of the U. S. Office of Naval Research.

1. A. Ourmazd, D. W. Taylor, J. A. Rentschler, and J. Bevk, Phys. Rev. Lett. 59, 213 (1987).
2. N. L. Allinger, Adv. Phys. Org. Chem. 13, 1 (1976).
3. R. C. Bingham, M. J. S. Dewar, and D. H. Lo, J. Am. Chem. Soc. 97, 1285 (1975); P. Bischof, *ibid.* 98, 6844 (1976).
4. A. H. Edwards and W. B. Fowler, J. Phys. Chem. Solids 46, 841 (1985); J. K. Rudra, W. Beall Fowler, and F. J. Feigl, Phys. Rev. Lett. 55, 2614 (1985); J. K. Rudra and W. Beall Fowler, Phys. Rev. B35, 8223 (1987).
5. P. M. Lenahan and P. V. Dressendorfer, J. Appl. Phys. 55, 3495 (1984); H. S. Witham and P. M. Lenahan, Appl. Phys. Lett. 51, 1007 (1987); M. E. Zvanut, F. J. Feigl, W. B. Fowler, and J. K. Rudra (to be published).

# EVIDENCE FOR A TEMPERATURE DEPENDENT TUNNELING PARAMETER

Frank Bridges and Michael Jost  
Physics Board of Study  
University of California, Santa Cruz CA 95064

$RbCl : Ag^+$  is a model off-center system and has been extensively studied<sup>1-3</sup>. Although the  $Ag^+$  ion substitutionally replaces the  $Rb^+$  ion, it occupies off-center positions which are located along the 12 -  $\langle 110 \rangle$  directions in the crystal, as a result of its smaller ionic radius. Reorientation from one off-center position to another takes place via a tunneling process at low temperatures. As a result of the off-center displacement, the defect carries an electric dipole moment,  $p$ , ( $p = 0.78eA$ )<sup>2,3</sup> and the 12 off-center states are split when an electric field  $\vec{E}$  is applied. At  $\vec{E} = 0$ , tunneling lifts the 12-fold degeneracy. Measurements clearly show that the dominant tunneling parameter, is the second neighbor tunneling parameter<sup>2</sup>,  $\mu$ , which corresponds to a rotation of the off-center dipole by  $90^\circ$ . When hydrostatic pressure,  $P$ , is applied,  $\mu$  increases and reaches 31 GHz at  $P = 1.85$  kbar. Over this range  $p$  decreases by roughly 60%.

A more striking effect under pressure is the discovery of a new resonance that is very strongly pressure dependent<sup>4</sup> (only observed over the range  $1.0 < P < 1.3$  kbar). We have interpreted our results in terms of a two configuration model for  $Ag^+$  in  $RbCl$ : over a limited range in hydrostatic pressure both on-center and off-center configurations for the  $Ag^+$  ion can exist. Some of the  $Ag^+$  ions are off-center as observed at low pressures and some are on-center. As the pressure is increased, the lowest state of the on-center configuration decreases rapidly in energy and lies below the off-center tunneling state for  $P > 940$  bar. The new resonance line has been identified as a transition between an on-center ground state and the lowest energy of the (excited) tunneling states.

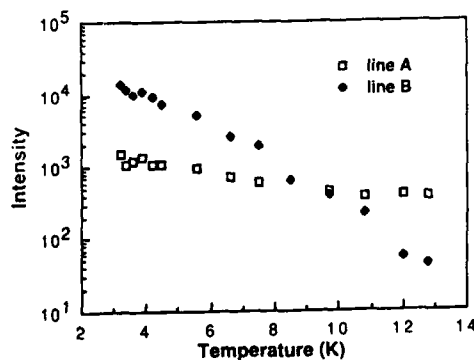


Fig-1 A comparison of the temperature dependence of the A and B lines at  $\nu = 68.05$  GHz and  $P = 1.105$  kbar.  $I_A$  (left) and  $I_B$  (right) are in arbitrary units.

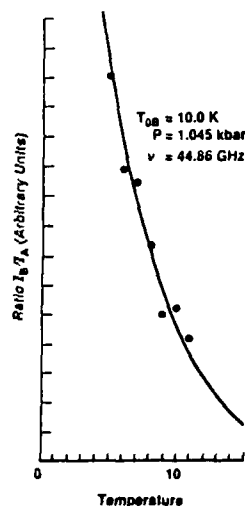


Fig-2 A fit of the ratio  $R$  assuming a temperature dependent tunneling element. The best fit of  $T_{0B}$  is indicated.

Recently we have found that the intensity of the on-center to off-center transition is extremely temperature dependent. Over the range 4 to 15K the signal intensity of this line decreases by nearly two orders of magnitude, an effect that is inconsistent with simple population changes. This paper is a report on these new results.

Fig. 1 compares the temperature dependence of the intensities ( $I_A$  and  $I_B$ ) of the A and B lines (line A is the usual paraelectric transition and line B is the transition between on- and off-center states) at  $\nu = 68.05$  GHz and  $P = 1.105$  kbar. Above 4K,  $I_A$  decreases with temperature, somewhat more rapidly than expected from simple population effects.  $I_B$ , on the other hand decreases catastrophically, in contrast to simple population considerations which only predict a decrease of order 4. Since the behavior of the tunneling levels is quite well understood, we use the intensity of line A as our reference for studying line B. We then plot the ratio of intensities  $I_B / I_A$  as a function of T as shown in Figure 2.

The intensity of a resonance line depends on the populations of the levels and the transition matrix elements. To explain the rapid intensity change, one of these factors must be strongly temperature dependent. Note however, that a strong population effect, caused for example by a low lying, highly degenerate state that becomes populated for  $T > 6K$ , would decrease both ( $I_A$  and  $I_B$ ). Thus we propose that the strong T dependence arises primarily in the matrix element for line B. Since  $p$  is constant the only remaining factor is the tunneling parameter  $\Delta$ . Several theoretical treatments of the polaron dressing of these matrix elements<sup>5</sup> yield a Debye-Waller-like factor

$$\Delta^2 = \Delta_0^2 e^{-W_0} e^{-(T/T_0)^2} \\ = \Delta_1^2 e^{-(T/T_0)^2}$$

where  $\Delta_0$  is the bare tunneling parameter,  $W_0$  is a temperature independent constant,  $\Delta_1$  is the value of  $\Delta$  at low temperatures and  $T_0$  is a parameter that depends on the potential well parameters and the coupling of the defect to the lattice vibrations. For our case, two parameters are needed ( $T_{0A}$  and  $T_{0B}$ ).

To have a very strong T dependence for line B, but not line A, requires  $T_{0B} < T_{0A}$ . We obtain a good fit to the ratio data if we let  $T_{0B} \approx 10K$ , as shown by the solid line in Fig. 2. We can also describe the  $I_A$  data by assuming that  $T_{0A} \approx 22K$ . We believe this is clear evidence that the effective tunneling parameters are indeed temperature dependent as predicted. To our knowledge this is the first time that such a temperature dependence has been observed directly.

The effects of a T-dependent tunneling matrix element have been previously observed indirectly in the T dependence of the relaxation. The present measurements indicate that it can be observed spectroscopically and that it will change the matrix elements of transitions induced by phonons and oscillating electric fields at elevated temperatures. For glasses this may have a very important consequence if the value of  $T_0$  for such systems is low for the rapidly tunneling atoms. Then tunneling splittings and matrix elements can no longer be treated as constants, independent of temperature.

This work is supported by NSF Grant DMR 85-05549.

#### References

1. R.D. Kirby, A.E. Hughes, and A.J. Sievers, Phys. Rev. **B2**, 481 (1970).
2. S. Kapphan and F. Luty, Phys. Rev. **B6**, 1537 (1972).
3. F. Bridges, Phys. Rev. **B5**, 3321 (1972).
4. F. Bridges and D. Chow, Phys. Rev. Lett. **54**, 1532 (1985).
5. L.M. Sander and H.B. Shore, Phys. Rev. **B3**, 1472 (1971); Phys. Rev. **B6**, 1551 (1972); R. Pirc and P. Gosar, Phys. Rev. Kondens Materie **9**, 377 (1969).

TWO-PHOTON SPECTROSCOPY IN  $\text{Ag}^-$  DOPED ALKALI HALIDES

M.Casalboni, R.Francini, U.M.Grassano and F.J.Lohmeier \*

Dipartimento di Fisica, Universita' di Roma "Tor Vergata"

Via Orazio Raimondo, 00173 Roma, Italia

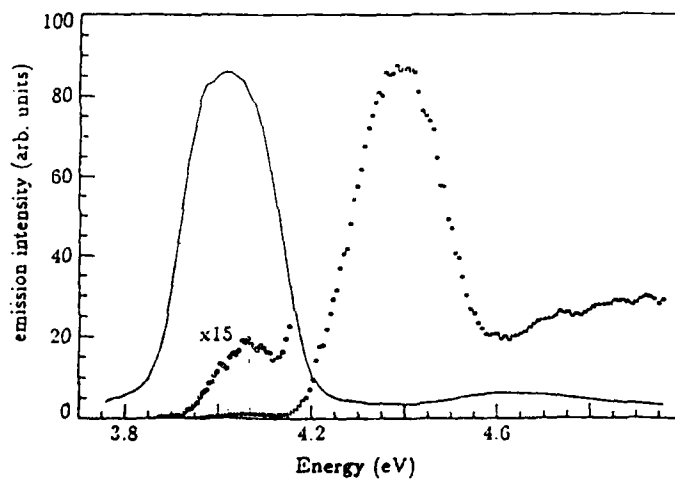
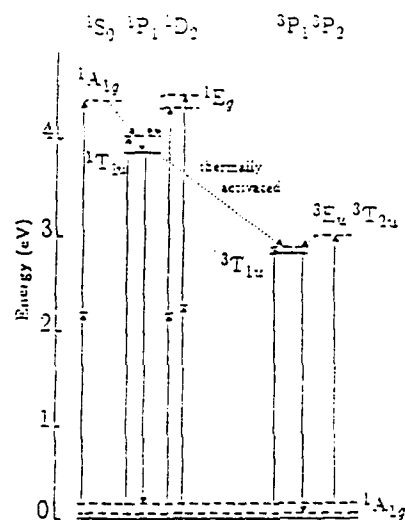
One-photon spectroscopy of impurity ions of the  $(ns)^2$  family (like  $\text{Tl}^+$ ) in alkali halides has been the most important research tool for the physical interpretation of the properties of these phosphors. Because of lack of suitable laser sources not many studies have been made with two-photon spectroscopical techniques in order to measure the even parity levels forbidden in the one-photon observation.

Using one or two dye lasers with  $h\nu_1 + h\nu_2$  tunable from 250 to 330 nm and the favorable position of the absorption and emission band of the  $\text{Ag}^-$  impurity in alkali halides we have investigated the properties of the higher even parity states of s and d symmetry. The results, so far complete only for  $\text{Ag}^-$  in Rbr, have confirmed some earlier data /1/ and in particular we have found

- i - the position of the transition  $^1A_{1g} - ^1A_{1g} [(5s^2) - (5s6s)]$
- ii - a double band at energies close to those of the previous band, but with polarization properties corresponding to  $^1E_g$  symmetry. We tentatively assign this band to the Jahn-Teller split transition  $^1A_{1g} - ^1E_g [(5s^2) - (5s5d)]$
- iii - a small two-photon forbidden band corresponding to one-photon allowed C band  $^1A_{1g} - ^1T_{1u} [(5s^2) - (5s5p)]$  partially allowed by the coupling of  $^1T_{1g}$  with  $^1A_{1g}$

A schematic diagram of the  $\text{Ag}^-$  levels in RbCl is shown in the figure together with the one-photon (full line) and two-photon spectra (dots), the latter taken with parallel polarization of the two beams. The two photon spectrum clearly shows the features i) and iii) described above /2/.

Experiments are in progress to study the temperature dependence of the



Jahn-Teller splitting of the  $1E_g$  level and the analogous properties of  $Ag^+$  in other host lattices.

\* permanent address: Physik. Inst., Wilhelm-Klemm-Str., 4400 Munster, FRG

1) F.J.Lohmeier and K.Schmitt, Opt.Comm. 63, 49 (1987)

2) F.J.Lohmeier, R.Francini and U.M.Grassano to be published

# EPR STUDY OF JAHN-TELLER EFFECT IN $\text{Ag}^{2+}:\text{KLiSO}_4$ CRYSTALS

Y.Ravi Sekhar and H.Bill, Département de Chimie Physique  
University of Geneva, Sciences II, 30 quai E. Ansermet  
CH 1211 Geneva 4, SWITZERLAND

There have been few studies on the Jahn-Teller (JT) effects of  $d^9$  ions in trigonal or hexagonal symmetry<sup>1</sup>. We present here the EPR results of  $\text{Ag}^{2+}$  ions in potassium lithium sulphate (KLS) crystals in the temperature range 4.2-77K and subjected to external uniaxial stress applied along b and c axes of the crystal. KLS has a structure of hexagonal symmetry with space group  $P6_3$  ( $z=2$ ). The  $\text{K}^+$  ions occupy positions on the hexagonal c axis and are surrounded by nine oxygens. In order to obtain an unperturbed  $\text{Ag}^{2+}$  center in the high symmetry surrounding of the host, the crystals were doped with  $\text{Ag}^+$  ions. They were then irradiated at low temperatures to convert the silver ions into paramagnetic state without any associated defects.

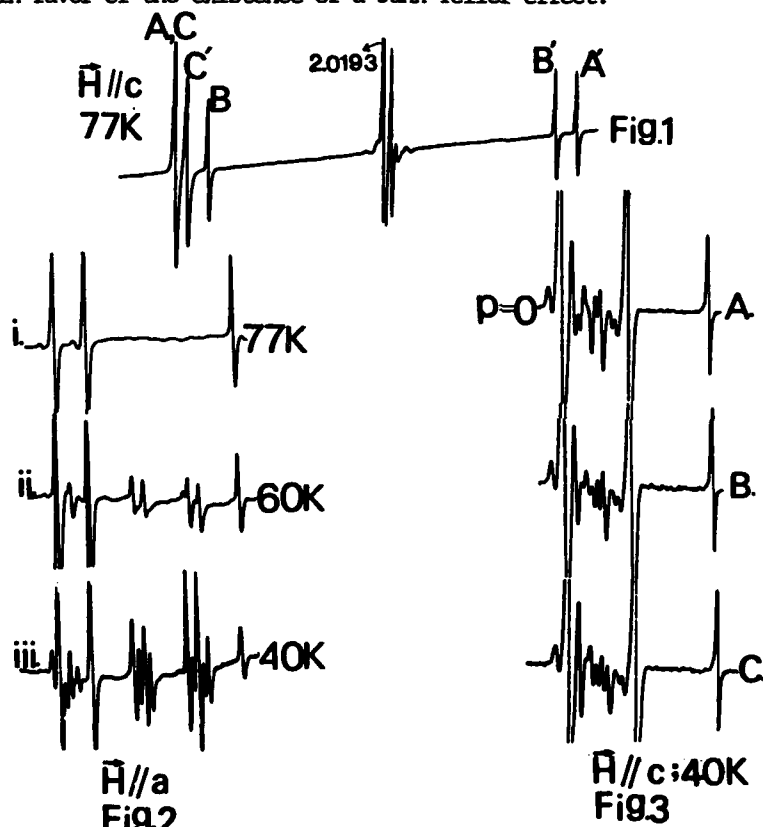
Fig.1 shows the EPR spectrum at 77K recorded with  $\vec{H}$  along the c-axis immediately after irradiation. One finds two doublets marked as AA', BB' with a separation of nearly 693,671G respectively and an additional doublet CC' with only about 20G splitting. Apart from these impurity related centers, there are other lines around  $g=2.0193$  due to host radicals. The doublets AA' and BB' have been identified as due to  $\text{Ag}^0$  centers ( $\text{Ag}$  has two isotopes  $^{107}\text{Ag}$  with 51% and  $^{109}\text{Ag}$  with 49% abundance and  $I=1/2$ ). The doublet CC' for  $\vec{H} // c$  arises from  $\text{Ag}^{2+}$  center created after irradiation at 77K. When the crystal is cooled slowly to temperatures below 77K, new lines begin to appear in the EPR spectra. As shown in Fig.2, three doublets are seen at about 60K when  $\vec{H}$  is parallel to a axis. Below 55K, the doublet CC' along c axis splits into two and similar effects are seen along a and b axes. When the crystal reaches about 40K, there are significant intensity redistributions among the split lines. These features remain unchanged down to 4.2K.

We also studied the uniaxial stress effects on the EPR spectra. When the stress is applied along the b axis of the crystal at about 40K, one observes the reorientational effects giving rise to intensity distributions different from those observed under unstressed conditions. Fig.3 shows these results where spectra B and C are recorded with stress applied along b axis in the increasing order.

The angular variation studies have been carried out at different temperatures to determine the principal g and A values and their orientation. For example,  $g_{xx}=2.4529, g_{yy}=2.0865, g_{zz}=2.0668, A_{xx}=78.1, A_{yy}=59.7$  and  $A_{zz}=50.7\text{MHz}$  at  $T=60\text{K}$ .

$\text{Ag}^{2+}$ , isoelectronic to  $\text{Cu}^{2+}$ , has  $4d^9$  ( $^2D$ ) ground state configuration. In trigonal field, this splits into two orbital doublets and an orbital

singlet with one of the doublets lowest. Thus the ground state is subject to JT effect and in the intermediate to strong coupling limit, gives rise to three distinguishable centers each having symmetry lower than axial. At low temperatures, these three equivalent distortions become "frozen-in" leading to the anisotropic g values while at high temperatures, the system may resonate between distortions of equivalent energy giving rise to a trigonal (in fact practically isotropic) g value. The observed changes in the EPR spectra between 4.2-77K and the effects under uniaxial stress are indeed in favor of the existence of a Jahn-Teller effect.



1. H. Bill, Chapter 13 in *The Dynamical Jahn-Teller Effect in Localized Systems*, edited by Yu.E. Perlin and M. Wagner, Elsevier Science Publishers B.V. (1984)

This research work was supported by the Swiss National Science Foundation. We thank Mr. D. Lovy for his help in the computations.

SIMULATION OF F-TYPE CENTERS AND  
HYDROGEN ANIONS IN MgO \*

Ravindra Pandey<sup>†</sup> and John M. Vail  
 Department of Physics, University of Manitoba  
 Winnipeg, Manitoba R3T 2N2, Canada

F-type centers in MgO have been studied extensively. The optical cycle of the two-electron F center involves electron capture and emission by a hydrogen center denoted  $(H_X^-)^+$ .<sup>1</sup> This process involves relaxed and unrelaxed states that provide a very severe test of simulation methods. While it is now known that electron capture by  $(H_X^-)^+$  does not result in an  $H^{2-}$  ion, the latter has itself been studied extensively.<sup>2</sup>

As a first step toward analysis of this system we have carried out simulations of the Hartree-Fock ground states of F and  $F^+$  centers, and of substitutional  $H^-$  and  $H^{2-}$  ions. Our method permits correlation correction, excited states, and both relaxed and unrelaxed states such as occur in electronic transitions, ionization, and electron capture. The simulations use the ICECAP program,<sup>3</sup> which solves a Hartree-Fock defect molecular cluster problem embedded in a shell-model lattice. The Hartree-Fock calculation is unrestricted, allowing for spin polarization, with explicit self-consistent field. The static shell-model lattice includes long-range polarization in the case of charged defects. For stationary states, the total energy of the defect lattice is automatically minimized to consistency among cluster and lattice configurations and Hartree-Fock wave function, for a given basis set. Cluster boundary conditions can incorporate Kunz-Klein potentials.<sup>4</sup>

We begin by determining a contracted basis set for  $O^{2-}$  in MgO. Optimal sets of primitive gaussians are then determined for F and  $F^+$  centers and for  $H^-$  and  $H^{2-}$  ions, all for nearest-neighbor clusters in the crystal. In these defect clusters, basis sets for free  $Mg^{2+}$  are improved upon by recontraction. The defect primitives and  $Mg^{2+}$  reconstructions are then incorporated in second-neighbor clusters. Kunz-Klein potentials are added to third and fourth neighbors, and the relaxed cluster configuration

is determined. This process is close to optimal at the Hartree-Fock level, except for the somewhat diffuse  $H^{2-}$  ion. A similar investigation is carried out for the  $F^+$  center unrelaxed excited state.

The defects studied here in strictly comparable calculations have an interesting variety: vacancy centered and nuclear centered, charged and uncharged, spin paired and unpaired. For the last,  $F^+$  and  $H^{2-}$ , spin densities are calculated and compared with experiment.<sup>5</sup> Finally, as a by-product, shell-model short-range interactions for  $H^-$  and  $H^{2-}$  with  $Mg^{2+}$  and with  $O^{2-}$  are determined from the energies of configurations that were investigated in finding the cluster relaxation.

\* Partially supported by NSERC Canada and University of Manitoba Faculty of Graduate Studies.

† Present address: Department of Physics, Michigan Technological University, Houghton, MI 49931, U.S.A.

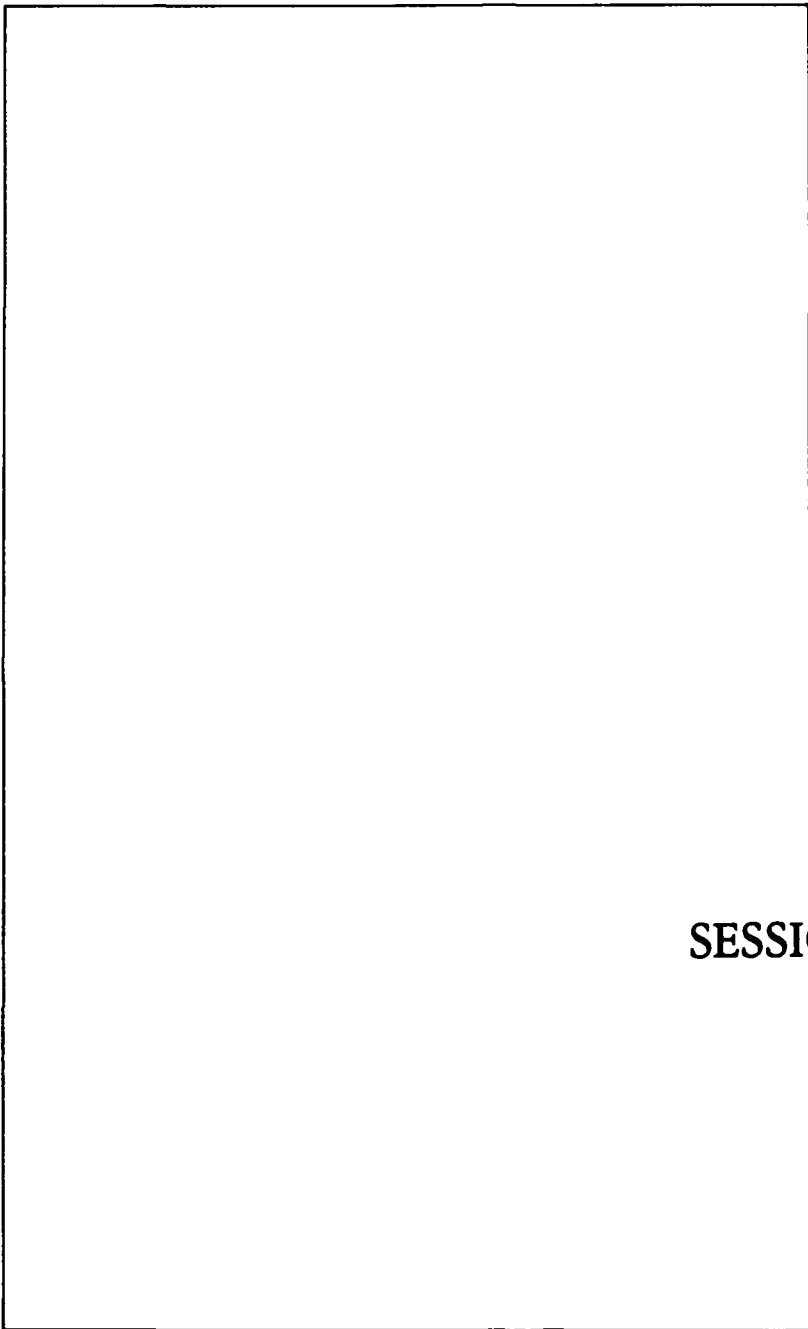
<sup>1</sup>V.M. Orera and Y. Chen, Phys. Rev. B36, 6120 (1987).

<sup>2</sup>J. Tombrello, H. Tohver, Y. Chen, and T.M. Wilson, Phys. Rev. B30, 7374 (1984).

<sup>3</sup>J.H. Harding, A.H. Harker, P.B. Keegstra, R. Pandey, J.M. Vail and C. Woodward, Physica B131, 151 (1985).

<sup>4</sup>A.B. Kunz and D.L. Klein, Phys. Rev. B17, 4614 (1978).

<sup>5</sup>L.E. Haliburton, D.L. Cowan, and L.V. Holroyd, Phys. Rev. B12, 3408 (1975); and ref. 2.



SESSION 9B

**PLASTIC ANISOTROPY IN CoO SINGLE CRYSTALS****F. Guilberterau\*, A. Dominguez - Rodriguez, J. Castaing\*\***Departamento de Optica - Facultad de Fisica, Apartado 1065,  
41080 Sevilla - Spain

Alkali halides with the rocksalt crystal structure are known to have very anisotropic plastic deformation properties. The  $\{110\}$  slip planes are much easier to activate than the  $\{001\}$  ones. This behaviour has received little attention in simple oxides. We have studied the compression of CoO single crystals along the  $\langle 111 \rangle$ , which does not allow  $\{110\}$  slip. Prior to deformation, the specimens were annealed at low oxygen pressure to avoid the formation of any  $\text{Co}_3\text{O}_4$  type precipitates. CoO could be deformed at a temperature as low as 293 K, with failure occurring after 3% strain. The yield stress was 1.000 MPa and decreased to 26 MPa at the temperature of 1273K. Transmission electron microscopy observations revealed long elongated screw dislocations. The whole set of results gives evidences that the  $\{001\}\langle 110 \rangle$  slip system has been activated: dislocation glide is controlled by the Peierls mechanism, the stress at 0 K being of the order of 1700 MPa.

\* Permanent address: Facultad de Ciencias; Universidad de Extremadura, Badajoz, Spain

\*\* C.N.R.S. - Bellevue, Laboratoire de Physique des Materiaux, Meudon, France.

ATOMISTIC CALCULATION OF POINT DEFECT INTERACTION WITH DISLOCATION IN  
NiO

J. RABIER and J. SOULLARD\*

Laboratoire de Métallurgie Physique, U.A. 131 au CNRS, Université de  
Poitiers

40, Avenue du Recteur Pineau, 86022 POITIERS, France

and M.P. PULS

Atomic Energy of Canada Limited, Whiteshell Nuclear Research  
Establishment, Pinawa, Manitoba R0E 1L0, Canada

Dislocation core structure of an  $a/2\langle 110 \rangle$  ( $1\bar{1}0$ ) edge dislocation has been computed in NiO using an atomistic description of the lattice. Point Ion Model (PIM) and Shell Model (SM) potentials were used to describe the ionic interactions. The binding energies of the dislocation with vacancies of different charge states are calculated by using the PDINT code which is based on a generalized Mott-Littleton procedure. Migration energies of vacancies inside the dislocation core are also computed. These results are analyzed with reference to possible change of stoichiometry in the dislocation core compared to the bulk crystal. Comparison with pipe diffusion measurements are also reported.

\* Permanent address : Instituto de Física UNAM, P.O. Box 20-364, 01000 MEXICO, D.F.

## A DIRECT EVIDENCE OF DISLOCATION DISSOCIATION IN THE NaCl-STRUCTURE

A. Foitzik, W. Skrotzki\* and P. Haasen

Institut für Metallphysik, Universität Göttingen, Hospitalstr. 3/5, 3400 Göttingen, FRG

\*Institut für Geologie und Dynamik der Lithosphäre, Universität Göttingen, Goldschmidt-Str. 3, 3400 Göttingen, FRG

Much attention has been focussed in the past on the fundamental question of dislocation dissociation in NaCl-type ionic crystals. According to calculations of FONTAINE (1968), FONTAINE AND HAASEN (1969) and HAASEN (1974)  $\langle 110 \rangle$ -dislocations in these crystals should be slightly dissociated on the  $\{110\}$  (in the order of a few Burgers vectors) and non-dissociated on the  $\{100\}$  slip plane. Support for this result is given indirectly by slip line observations on these slip systems. While slip on  $\{100\}$  planes is wavy at all temperatures (except for PbS; BARTHEL, 1984) slip on  $\{110\}$  is planar below a certain stress and temperature (SKROTZKI AND HAASEN, 1984). Wavy slip of screw dislocations is due to cross slip. This process becomes more difficult with increasing dissociation, a fact which is manifested in the dependence of the onset of dynamical recovery on temperature and hydrostatic pressure (ALADAG ET AL., 1970). So far weak beam transmission electron microscopy failed in resolving any dissociation in alkali halides (STRUNK, 1975). Taking the resolution limit of this method the upper bound for a dissociation in KI is 7b. Atomistic calculations of the core structure of  $\langle 110 \rangle$ -dislocations do not show any (PULS AND SO, 1980) or only slight dissociation (BELZNER AND GRANZER, 1977).

Having these results in mind the most promising method to resolve a possible dislocation dissociation in the NaCl-structure is high resolution transmission electron microscopy (HRTEM). To apply this method we used PbS single crystals which had been deformed in order to introduce a high enough dislocation density. The necessity to choose this material is given by the following reasons: (i) electron transparent foils can be produced by standard ion milling, (ii) the material is insensitive to electron irradiation and (iii) the lattice spacing  $d_{\{200\}} = 3\text{\AA}$  is large enough to be resolved easily in the Philips EM 420 ST.

The results of our HRTEM study are presented in Fig. 1 showing the core structure of two different types of dislocations viewed end-on. Type A is a  $45^\circ$ -dislocation with  $a/2 [101]$  Burgers vector. The edge component  $a/2 [100]$  determined by a Burgers circuit is seen in the image. Conventional TEM shows that this type of dislocation is typical for the dislocation microstructure on the  $\{010\}$  slip plane. The dissociation width on  $\{010\}$  is about 6b. Type B is an edge dislocation with  $a/2 [110]$  Burgers vector lying on the  $\{1\bar{1}0\}$  plane. This type of dislocation often arranged into dipoles characterizes the dislocation microstructure of the primary slip plane in alkali halides and oxides. The extended core of dislocation B is rather relaxed. Its dissociation width is estimated to about 1.5b. However, because of the small dissociation it is difficult to clearly define the  $\{1\bar{1}0\}$  stacking fault plane.

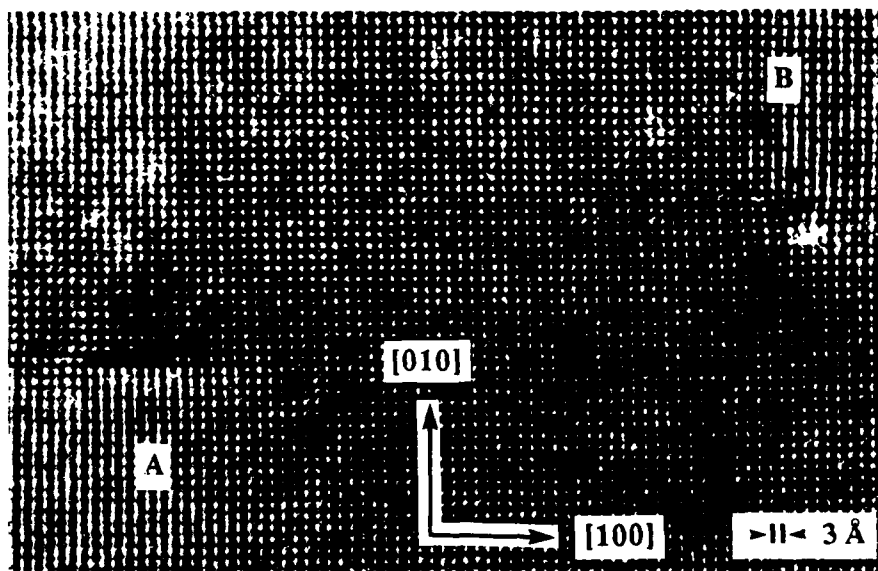


Fig. 1: HRTEM image of a  $[101]$ - (A) and  $[110]$ -dislocation (B) dissociated on the  $(010)$  and  $(1\bar{1}0)$  plane, respectively.

The results presented give a direct evidence of dislocation dissociation in the NaCl-structure. As expected  $\langle 110 \rangle$ -dislocations are only slightly dissociated on  $(110)$  planes. Surprising is the dissociation found on  $(100)$  planes. This observation may be explained by the low ionicity of the material used. Preliminary calculations show that with decreasing ionicity the dissociation width on  $(110)$  planes decreases while that on  $(100)$  increases from  $\approx 1b$  in alkali halides to about  $5b$  in PbS. An extended study on the dissociation in ionic crystals is in progress.

#### References

- ALADAG, E., DAVIS, L.A. AND GORDON, R.B., *Phil. Mag.* **21**, 469 (1970)
- BARTHEL, C., Diploma thesis, Göttingen 1984
- BELZNER, V. AND GRANZER, F., *phys. stat. sol. (a)* **29**, 183 (1977)
- FONTAINE, G., *J. Phys. Chem. Sol.* **29**, 209 (1968)
- FONTAINE, G. AND HAASEN, P., *phys. stat. sol.* **31**, K67 (1969)
- HAASEN, P., *J. de Physique* **35**, C7-167 (1974)
- PULS, M. AND SO, C.B., *phys. stat. sol. (b)* **98**, 87 (1980)
- SKROTZKI, W. AND HAASEN, P., *Mater. Sci. Res.* **18**, 429 (1984)
- STRUNK, H., *Proc. Quatrième Congrès Int. on Microscopie Électronique à Haute Tension*, Toulouse, 229 (1975)

# DISLOCATION INTERSECTION IN NaCl SINGLE CRYSTALS

F. Appel

Institute of Solid State Physics and Electron Microscopy  
Academy of Sciences of the GDR  
Halle/Saale, DDR-4050, GDR

Dislocation intersection is considered to be one of the most important mechanisms restricting the motion of gliding dislocations and contributing to work hardening. The process can involve several mechanisms such as an elastic interaction of the dislocation stress fields, the generation of kinks and jogs, and the formation of junctions. The character of the individual mechanisms is quite different and the resulting interaction forces depend on the geometrical details. Thus, the slip behaviour of dislocations gliding through forest dislocations can hardly be predicted. To get some direct information intersection processes of dislocations on oblique  $\langle 110 \rangle$   $\{110\}$  slip systems were initiated by latent hardening experiments on NaCl single crystals. The investigations were combined with electron microscope slip line studies by means of the heavy metal decoration technique [1]. The method images both, the forest screw dislocations introduced during the primary deformation and the slip lines of individual screw dislocations gliding through the forest dislocations during the secondary deformation. Thus, it was possible to study the processes occurring during dislocation intersection in detail. The evaluation of the micrographs yields the density of forest screw dislocations, the distributions of the lengths and orientations of cross-slip processes, the density of cross-slip events per slip line length, and the mean slip line length of individual gliding screw dislocations. The advantage of this method lies in the direct correlation of these parameters. The results can be summarized as follows.

Forest dislocations are highly capable of initiating extended cross-slip of the gliding screw dislocations. The cross-slip preferentially occurs on  $\{100\}$  planes. On an average the distance of cross-slip events per slip line length is equal to the distance of the forest screw dislocations. The cross-slip distances range up to a few microns, with the frequency distribution of the distances decreasing approximately exponentially. As a consequence of the cross-slip processes the screw dislocations get numerous jogs which are essentially higher than elementary intersection jogs.

In many cases gliding dislocations are immobilized by the forest dislocations. The mean slip line length was found to be proportional to the distance between the forest screw dislocations, which was calculated from the square root of the

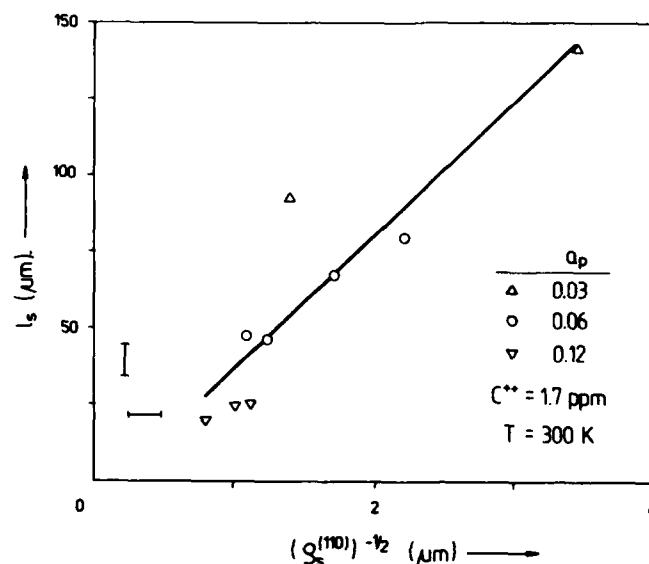


Fig. 1: Dependence of the mean slip line length  $l_s$  on the density of forest screw dislocations  $G_s^{(110)}$  on (110) planes.

forest dislocation density. The dependence is shown in Fig. 1. The slope of the regression line indicates that the slip path of the screw dislocations is about the twentyfold distance of the forest screw dislocations.

The experimental results were discussed in detail considering the elastic interaction of straight non-parallel dislocations [2]. Accordingly, strong long-range interaction forces occur in the direction of slip and cross-slip, which result in local stresses of about  $\mu/50$ .  $\mu$  is the shear modulus. Relative to the flow stress applied during the secondary deformation these stresses are very high, which may give rise to the observed cross-slip and immobilization processes. It is therefore assumed that dislocation intersection mainly results in an athermal contribution to the flow stress. The assumption is in agreement with the experimental observation that the activation volume for the thermally activated dislocation glide is not changed by latent hardening of the crystals.

[1] H. Bethge, phys. stat. sol. 2, 775, 1962

[2] R. Bullough and J.V. Sharp, Philos. Mag. 11, 605, 1965

DIFFUSION OF  $\text{Zn}^{2+}$  IN AgBr AND AgCl - EVIDENCE FOR  
NONLINEAR TEMPERATURE DEPENDENCE OF GIBBS FREE  
ENERGY FOR DEFECT FORMATION, ASSOCIATION AND MOTION

A. L. LASKAR, S. BETARBET AND J. LASKAR\*  
Department of Physics and Astronomy  
Clemson University, Clemson, SC 29631, USA

It is now established that the steep increase in the electrical conductivity and  $\text{Ag}^+$  diffusion in AgBr and AgCl from about 100° below the melting temperature is due to the creation of anomalously large concentration of cation Frenkel pairs caused by the nonlinear decrease of Gibbs free energy of formation ( $g_f$ ) with the increasing temperature. One effect of this phenomenon is that cations which diffuse via a vacancy exchange will also exhibit an anomalous increase in diffusivity. This was indeed observed as a positive curvature in the diffusion Arrhenius plots of  $\text{Na}^+$  and  $\text{K}^+$  in both AgCl and AgBr. The intrinsic curvature was accurately and numerically accounted for by the nonlinear decrease of  $g_f$  with temperature. Being homovalent with the host  $\text{Ag}^+$ , alkali ions do not perturb the thermal defect concentration and thus accurately probe the properties of intrinsic defects. Various theoretical approaches and computational techniques have been successful to provide excellent support to these experimental conclusion on the basis of an assumption that the entropy of formation ( $s_f$ ) is temperature-independent whereas enthalpy of formation ( $h_f$ ) is temperature dependent.<sup>1</sup>

It now appears that, in addition to  $g_f$ , Gibbs free energy for motion ( $g_m$ ) and that for association of the solutes with vacancies ( $g_a$ ) are also nonlinearly temperature dependent. Along with the temperature dependence of enthalpies such dependence, may be to a smaller degree, have to be assumed for entropy terms also. It is observed that is case of  $\text{Rb}^+$  and  $\text{Cs}^+$ , both alkali ions oversized with respect to  $\text{Ag}^+$  and thus introducing strain-induced binding between the solutes and vacancies, the nonlinear temperature dependence of  $g_f$ ,  $g_m$  and  $g_a$  compensates the overall effect resulting in perfectly linear Arrhenius plots for those solutes.<sup>2,3</sup> Moreover, the linear Arrhenius behavior for the diffusion of the large number of divalent solutes, so far reported, must be due to such compensation. Recent model calculations<sup>4</sup> also show the general trend: enthalpies and entropies of the defect parameters are temperatures dependent. Our present results of the study of the diffusion of  $\text{Zn}^{2+}$  in AgBr and AgCl provide additional support to the above view.

The diffusivity of  $\text{Zn}^{2+}$  in ultrapure single-crystalline AgBr and AgCl were measured by a standard tracer sectioning technique using a precision rotary microtome as described elsewhere<sup>2</sup>. The diffusivity of  $\text{Zn}^{2+}$  in AgBr accurately follows a linear Arrhenius relation  $D = D_0 \exp(-h/kT)$  with  $D_0 = 49.46 \text{ cm}^2 \text{ s}^{-1}$  and  $h = 0.97 \text{ eV}$  in the temperature range 240-414°C. Assuming that  $\text{Zn}^{2+}$  diffuses by a vacancy-association mechanism, if we use the relation  $h = h_f/2 + h_m - h_a$ , we get  $h_m - h_a = 0.39 \text{ eV}$ . The values for  $h_m$  and  $h_a$  in this system are not known independently. The reported values for the diffusion of other divalent ions in AgBr indicate  $h_m > 0.7 \text{ eV}$ . Taking this as a guide, for AgBr: $\text{Zn}^{2+}$   $h_a \geq 0.3 \text{ eV}$ . The linearity of Arrhenius diffusion plot strongly suggests that the nonlinearity of  $g_f(t)$  is compensated by the nonlinearity in  $g_a(t)$  and/or  $g_m(t)$ .

In contrast, our results for the diffusion of  $\text{Zn}^{2+}$  in AgCl exhibits an Arrhenius plot with positive curvature in the temperature range 192-445°C. The plot of  $\ln(D/x_0)$  vs  $1/T$  has almost zero slope. The implication of this surprising result is that  $g_m(t)$  and  $g_a(t)$  cancels out and the diffusion Arrhenius plot shows the positive curvature due to  $g_f(t)$ . Making an Arrhenius fit of the data (192-350°C), we obtain  $D_0 = 0.058 \text{ cm}^2 \text{ s}^{-1}$   $h = 0.76 \text{ eV}$ . This leads to an estimate:  $h_m - h_a = 0.04 \text{ eV}$ . Like other divalent ions, if we assume  $h_m = 0.6 \text{ eV}$ , then  $h_a$  for  $\text{Zn}^{2+}$  is 0.6 eV - an unusually large value. These results for AgCl: $\text{Zn}^{2+}$  and consequently the conclusions are in complete agreement with the earlier results of Batra and Slifkin<sup>5</sup>.

It thus appears that a detailed theoretical consideration is necessary to explore the nonlinear temperature dependence of the free energies for the defects and their transport.

#### References:

1. A. L. Laskar, in "Diffusion in Solids, pp. 59-74, edited by A. L. Laskar et al, Trans Tech. Publications, Switzerland, (1984).
2. P. A. Cardegna and A. L. Laskar, Phys. Rev. **B24**, 530 (1981).
3. A. P. Batra and L. M. Slifkin, J. Phys. Chem. Solids, **37**, 963 (1976).
4. C. R. A. Catlow, J. Corish, J. H. Herding and P. W. M. Jacobs, Phil. Mag. A, **55**, 481 (1987).
5. A. P. Batra and L. M. Slifkin, Phys. Stat. Sol (a), **19**, 171 (1973).

\* Present Address: Department of Electrical Computer Engineering, University of Illinois, Urbana, Illinois, 61801, USA.

# AUTHOR INDEX

## A

Abe H.	71	Ballesteros C.	579
Abraham M.M.	341, 579	Baranov P.G.	79, 145
Aegerter M.A.	15	Barriuso M.T.	163, 165
Agnew P.	275	Barsova L.I.	207
Agostinelli J.A.	397	Bartram R.H.	37, 151, 169, 333, 337
Aguirre de Cárcer I.	211	Bausá L.E.	115
Agulló-López F.	213, 381	Becker K.D.	515
Ahlers F.J.	201	Beersma J.	219
Akhtar M.J.	85	Beerwerth F.	69
Akiyama N.	229	Bellis J.A.	535
Albers J.	585	Bello A.	417
Alcalá R.	411, 413	Belskiy A.N.	429
AlGhamdi A.A.	473	Benci S.	21, 459
Alhäuser R.	509	Beregi E.	555
Allan N.L.	345, 521	Bernard M.	203
Alonso P.J.	411, 413	Betarbet S.	627
Amara A.	157, 159	Betzler K.	55
Andeen C.G.	25	Bill H.	613
Andraud C.	385	Bing-Kun Yu	35
Andreev B.V.	457	Blak A.R.	273, 467, 469
Antonini R.	469	Blanzat B.	385, 387, 389
Appel F.	625	Böhmer R.	281, 283
Aramburu J.A.	163, 165	Boiko S.A.	225, 227
Arimoto O.	73	Boris A.V.	561
Arivuoli D.	531	Borissov M.	93
Awano T.	191, 193, 601	Botti S.	9, 127

## B

Badalyan A.G.	145	Bouazi A.	133
Baetzold R.C.	83, 261, 427, 581	Boulon G.	171
Baldacchini G.	9, 33, 127, 131, 231, 405	Bourson P.	91, 243
Baldochi S.L.	439	Boyarskaya Yu.S.	527
		Bravo D.	423
		Brebec G.	501
		Bredikhin S.I.	109, 111, 561
		Breñosa A.G.	375
		Bridges T.	609

Brodin A.M.	225, 227
Buckley S.N.	275
Bunde A.	105
Burberry M.S.	407, 399
Burkel E.	29
Burki Y.	209
Butler E.P.	493
Butlers P.	443
Butvina L.N.	483

# C

Cabrera J.M.	381, 423
Cachei G.	395
Cain L.S.	331, 341
Caldas M.J.	161
Calmon P.	501
Capelletti R.	129, 135, 137, 285, 287, 297, 583
Carabatos-Nédelec C.	301
Carrol J.C.G.	523
Casalboni M.	611
Castaing J.	619
Catlow C.R.A.	57, 83, 85, 89, 255, 257, 355
Chadwick A.V.	249, 257, 563, 573
Chai B.H.T.	267
Chakrabarti K.	603
Chandler P.J.	471
Chang E.K.	491
Charpie J.C.	333
Chen C.Y.	341, 461
Chen R.	453, 455
Chen Y.	291, 331, 341, 371, 393, 461, 579
Chernov S.V.	425
Chiari A.	21
Chu A.X.	607

Cocquyt B.	139
Comins J.D.	27, 503
Consolati G.	43
Corish J.	83, 523
Cormack A.N.	57, 87, 253
Corradi G.	419
Costa da F.E.	439
Courtois B.	339
Cox A.C.	447
Cox P.A.	355
Cravero I.	137
Cremer G.	157
Cussó F.	211
Cvetkov A.	567
Cywiński R.	297, 431, 433
Czaja W.	209
Czapelski M.	545

# D

Dallacasa V.	349
Dalmau Garcia M.R.	537
Dameron M.	59
Dance J.M.	377
Davidson A.T.	27
Davoli I.	429
De Matteis F.	131, 405
Debrus S.	133
Denis J.P.	385, 387, 389
Derid Yu.O.	557
Derry T.E.	27
Diakonov V.V.	79
Dianov E.M.	245, 483
Dieckmann R.	353
Diéguez E.	381, 423

Dierolf V.	13, 435
Dominguez-Rodriguez A.	619
Donatti D.A.	15
Donnerburg H.	257
Dorembos P.	53
Driyaev D.G.	529
Dunn B.	25
Durán A.	115
Durand D.	91, 243
Durga Rani A.N.	475
Duval E.	569
Dwivedi A.	253
Dykman M.I.	225, 227, 485

# E

Eachus R.S.	223, 319, 397, 427
Edamatsu K.	193
Edwards G.J.	151, 337
Emura S.	409
Ernst L.	565

# F

Fabeni P.	241
Fang Rong	5
Fang Shugan	205
Farley T.W.D.	303
Fazzio A.	161
Feng Duan	299
Fengxiqi	463
Fermi F.	21, 459
Fernández Rodrigo G.	165
Fetter L.	555
Février H.	481
Finkernagel B.	51

Flack K.W.	249
Fleurent H.	403
Flórez M.	165
Fockele M.	37, 169
Foitzik A.	623
Földvári I.	135, 137, 151, 225, 583
Fontanella J.J.	25, 267
Fowler W.B.	129, 583, 607
Francini R.	611
Franke P.	353
Fredj E.	505
Fricke M.	153
Fritz S.	593
Fröhlich D.	69
Frongillo Y.	173

# G

Gabriagues J.M.	481
Galavis M.E.	417
Galustashvili M.V.	529
García Macedo J.	119, 121
García-Cabañes A.	381
García-Solé J.	115
Gash P.W.	247
Geatches R.M.	563
Gellermann W.	35, 239
Georgiev M.	93
Gerbredner V.	567
Ghosh S.	519
Gilliam O.R.	151, 337
Giovenale E.	131, 231, 405
Glasbeek M.	77

Gnanam F.D.	531, 533
Godefroy G.	281
Goer de, A.M.	499
Gomes L.	9, 269
Gonzales-Calbet J.M.	553
González R.	579
Goovaerts E.	141, 401
Göpel W.	315
Gorczyca G.	91, 243
Goswami K.	513
Gouskos N.	123
Grabko D.Z.	527
Grabs M.	55
Granzer F.	51, 507, 509
Grassano U.M.	9, 127, 131, 231, 405, 611
Grasser R.	79
Grenier J-C.	553
Grigorjeva L.G.	181
Grimes R.W.	89
Gromov V.V.	457
Groote J.C.	219
Gubański A.	289
Guiberteau F.	619
Gunsser W.	425

## H

Haasen P.	623
Hackmann A.	585
Halama G.	437
Halperin A.	599
Hanic F.	539
Harding J.H.	63, 249
Hartmanová M.	539
Hartog den, H.W.	53, 219, 251

Hayes W.	303
Healy F.M.	83
Heidinger R.	279
Henning J.	425
Higashimura T.	195
Hirai M.	71, 221
Hodgson E.R.	213, 321
Hofstaetter A.	79
Hong J.P.	133
Hooton I.E.	517
Hörsch G.	233
Hull S.	303
Hutchings M.T.	303, 575

## I

Ibarra A.	277
Iida T.	15, 195
Ikezawa M.	191, 193, 601
Ishiguro M.	409
Islam M.S.	255
Isotani S.	469
Ito H.	409
Itoh C.	99
Itoh N.	99
Ivankiv A.L.	307
Ivleva L.I.	547

## J

Jackson R.A.	85
Jacobs P.W.M.	83, 103, 351, 517
Jain H.	493
Jansons J.	183
Jaque F.	211
Jasiolek G.	305

Jassemnejad B. 49  
 Jiménez de Castro M. 277  
 Jingchen L. 463  
 Jones J. 257  
 Joosen W. 41, 139, 401, 403  
 Jordan M. 11  
 Jost M. 609  
 Jovanović A. 125

# K

Kaifu Y. 195  
 Kaizu I. 195  
 Kalinowski H.J. 587  
 Kanienskikh I.A. 429  
 Kan'no K. 73, 187, 189  
 Kanert O. 153, 155, 585  
 Kao C.T. 197  
 Kaplyanskii A. 97  
 Kappers L.A. 135, 151  
 Kapphan S. 55, 125  
 Karasawa T. 195  
 Karaseva L.G. 457  
 Karttunen K. 235  
 Kato R. 117  
 Kemmler-Sack S. 559  
 Ketolainen P. 17  
 Khasanov I.Sh. 109  
 Khramtsov V.A. 145  
 Kimura H. 221  
 Kirsh Y. 455  
 Kishigami T. 117  
 Knab G.G. 539  
 Köhler J. 441  
 Köhler P. 69  
 Kokta M.R. 341

Kolem H. 155, 585  
 Komatsu T. 195  
 Königer F. 279  
 Kosacki I. 497  
 Kosaka H. 73  
 Koschnick F.K. 149  
 Kotomin E. 443  
 Kotru P.N. 541, 543  
 Kovács L. 137, 583  
 Kovaleva N.N. 109, 111, 561  
 Krantz M. 435  
 Kricsanowits R. 507  
 Kristianpoller N. 455  
 Kristoffel N. 525  
 Kuchler R. 153  
 Kulis P. 183, 443  
 Kumar J. 533  
 Kunz A.B. 175  
 Kuz'minov Yu.S. 547

# L

Lama F.L. 471  
 Laredo E. 417  
 Laskar A.L. 627  
 Laskar J. 627  
 Lavanant G. 481  
 Lazar D.P. 143  
 Leblans M. 41, 401  
 Ledoux P. 481  
 Leeuwen van, P.A. 77  
 Lefrant S. 203  
 Leonhardt U. 421  
 Lépine Y. 173  
 Leslie M. 83, 255

Leung C.H.	75
Li Zhiqiang	205
Licci F.	541
Lichkova N.V.	109, 561
Lifante G.	115
Lima de, J.F.	271
Linarès C.	171
Linari R.	241
Ling S.	57
Lisitsa M.P.	225, 227
Litvinchuk A.P.	497
Lohmeier F.G.	611
Lohse F.	37, 169
Loidl A.	281, 283
López F.J.	423, 595
Lorenzo F.	265
Luff B.J.	447
Lumbreras M.	301
Lushington K.J.	261
Lüty F.	5, 9, 11, 13, 127, 237, 239, 269, 395, 435, 437

## M

Mac Dónaill D.A.	351
Macalik B.	293, 465
Mackrodt W.C.	345, 521, 523
Maeda H.	409
Maglione M.	281
Maï C.	569
Maiti A.K.	513
Makur M.	519
Maleev M.N.	551
Manfredi M.	113, 297, 367, 465
Mangelschots I.	597
Manson N.B.	415

Marchetti A.	407
Marco de Lucas C.	373
Mariotto G.	569
Martín A.	595
Martin-Brunetiere F.	157
Mathur V.K.	603
Matsuyama T.	193, 601
Matthews, Jr., G.E.	59
Matzke Hj.	593
May M.	133
McClure D.S.	339
McKeever S.W.S.	49, 453
Mehta A.	491
Meucci M.	231
Michel-Calendini F.M.	171, 335
Michiels L.	597
Mikhailin V.V.	429
Millers D.K.	181
Minić D.	495
Mitchell T.E.	347
Moine B.	339
Mondragon M.A.	119
Montagna M.	569
Monty C.	47
Morato S.P.	439
Morawska-Koval T.	545
Moreno M.	163, 165, 359, 373, 375, 377
Moretti P.	167, 335
Morháčová E.	539
Mori Y.	383, 229
Morlotti R.	559
Mugeńska I.	431
Mugeński E.	433
Mukai T.	187
Müller K.A.	585
Murata H.	117
Murata T.	409

Murin I.V. 425  
Murti Y.V.G.S. 479  
Müssig Th. 507

## N

Nagorny A. 459  
Nagy G. 555  
Nakai Y. 73, 187, 189  
Nanba T. 193, 601  
Ngoepe P.E. 503  
Nie W. 171  
Nierzewski K.D. 465  
Nihtianova D.D. 549, 551  
Nikl M. 113  
Niklas J. 421, 507  
Nistor L.C. 451  
Nistor S.V. 141, 143, 451  
Nomojev A.V. 181  
Nowak-Woźny D. 289  
Nowick A.S. 57  
Nunes R.A. 587  
Nuttall R.H.D. 223

## O

Ohkura H. 229, 383  
Okuno E. 271, 273  
Olm M.T. 319, 427  
Opyrchal H. 297, 465  
Orera V.M. 291  
Ortiz-Lopez J. 237  
Osten von der, W. 23, 395  
Ouroushev D. 259

## P

Paciornik S. 587  
Pajaczkowska A. 305  
Pál E. 555

Pandey R. 175, 615  
Paracchini C. 349, 511  
Park J.L. 341  
Parras M. 553  
Pashkevich V. 567  
Paus H.J. 13, 233, 435  
Pazzi G.P. 241  
Peacock S.J. 563  
Pedrini C. 339  
Peiponen K.-E. 235, 489  
Peisl J. 29  
Pellé F. 385, 387, 389  
Peña J.I. 413  
Peneva S.K. 549  
Pérez E. 379  
Péter Á. 337  
Pető A. 295  
Petranović N. 495  
Petrov L.L. 549  
Pilla O. 385, 387  
Pirogov F. 449  
Pischel B. 507  
Pogatschnik G.J. 331, 341, 371  
Polák K. 113  
Poletaev A.B. 111  
Polgár K. 137, 419  
Polozkov N.M. 547  
Pontuschka W.M. 469  
Pouchard M. 553  
Poulain M. 327  
Poumellec B. 481  
Poźniak J. 293  
Pueyo L. 165  
Puls M.P. 621

Puma M.	265	Salviati G.	541
Pyttel B.L.	177	Salvini L.	241
<b>Q</b>		Sanyal S.P.	263
Quernet B.	133	Saralidze Z.K.	529
<b>R</b>		Sardela Jr., M.R.	161
Rabier J.	621	Sathyanarayana N.	147
Rachko Z.	183	Scacco A.	131, 231, 405
Radautsan S.I.	557	Scavarda do Carmo L.C.	587
Radhakrishna S.	147, 475, 477	Scharmann A.	79
Ramasamy P.	531, 533	Schiller A.	65
Ranfagni A.	241	Schmid D.	65, 441
Ravi Sekhar Y.	613	Schmidt N.	55
Razdan A.K.	543	Schmidt T.	441
Rearinne P.	17	Schoemaker D.	41, 139, 141, 401, 403
Rebane I.	487	Schön F.	79
Reichardt J.	559	Schreiber E.	23
Rendell H.M.	215	Schrempel M.	239
Rimmington S.	521	Schulz H.	585
Rodríguez F.	373, 375, 377	Schwan L.O.	65
Rodríguez V.D.	379	Seggern von, H.	311
Romanov N.G.	79	Serruys Y.	501
Rosa J.	145	Shafer R.P.	461
Rosenblatt G.H.	393	Shannon R.D.	267
Rossi de, W.	439	Shidlovskaya E.K.	179
Rossman G.R.	267	Shluger A.L.	179
Rowan L.G.	197	Shmurak S.Z.	111
Roy T.	347	Shpak A.M.	227
Runciman W.A.	415	Sibley W.A.	119, 121
Rycerz Z.A.	351	Sieren C.	41
Rzepka E.	133, 203	Silfsten P.	235
<b>S</b>		Silin A.R.	589
Sainath Prasad P.S.	475, 477	Singh R.K.	263
Salce B.	499	Sinkovits R.S.	333
		Skrotzki W.	623
		Skuja L.N.	185
		Slifkin L.M.	197, 365



Vieira, Jr., N.D.	439
Viglienzoni A.	559
Vijayan C.	479
Vila R.	277
Viliani G.	569
Viry de, D.	389
Vitukhnovsky A.G.	177
Voszka R.	225, 337
Vrtis M.	303

## W

Wagner M.	199
Wanklyn B.M.	543
Watanabe K.	195
Watterich A.	135, 151, 337
Weerkamp J.R.W.	219
Williams R.T.	39, 75, 393, 461
Williams, Jr., G.P.	39, 393, 461
Winkler H.P.	125
Wintersgill M.C.	25, 267
Wochner P.	29
Wöhlecke M.	125
Wood R.A.	217
Woods A.M.	333
Wright J.D.	563
Wu A.	461
Wu G.	461
Wurmb v., V.	515

## Y

Yamaoka H.	193, 601
Yang D.L.	25
Yang X.H.	453
Yihong Yang	5
Ying Jifong	463
Yoshimura E.M.	271
Yurik T.K.	207

## Z

Zhang L.	471
Zhang Qiren	463
Zhitaru R.P.	527
Zorita E.	411